Evaluation of Nitrogen Utilisation for Improved Nitrogen Use Efficiencies in Maize

Joseph Noble Amoah

THE UNIVERSITY OF SYDNEY

A thesis submitted in fulfilment of
the requirements for the degree of
Doctor of Philosophy

School of Life and Environmental Science
Faculty of Science
The University of Sydney

2025

STATEMENT OF ORIGINALITY

This is to certify that the content of this thesis is my own work. This thesis has not been submitted for any other degree or purpose.

I certify that the intellectual content of this thesis is the product of my own work, and that all assistance received in preparing this thesis and all sources have been acknowledged.

Joseph Noble Amoah

December 1, 2025

AUTHOR ATTRIBUTION STATEMENT

This thesis contains seven research chapters which are the results of my own investigations.

Chapter 1 presents a general introduction and research aims.

Chapter 2 is under consideration with *Journal of Plant Growth Regulation*, with the title 'Nitrogen deficiency impacts growth and modulates nitrogen metabolism in maize'. All authors contributed to the method conceptualisation. Experimentation, data curation, formal analysis, and data analysis and visualisation was conducted by JNA. The original draft was written by JNA and reviewed and edited by CK and BNK.

Chapter 3 has been published in *Planta* and is titled 'Nitrogen deficiency impacts growth and modulates carbon metabolism in maize'. All authors contributed to the method conceptualisation. Experimentation, data curation, formal analysis, and data analysis and visualisation was conducted by JNA. The original draft was written by JNA and reviewed and edited by CK and BNK.

Chapter 4 has been published in *Physiology and Molecular Biology of Plants* and is titled 'Nitrogen deficiency identifies carbon metabolism pathways and root adaptation in maize'. All authors contributed to the method conceptualisation. Experimentation, data curation, formal analysis, and data analysis and visualisation was conducted by JNA. The original draft was written by JNA and reviewed and edited by CK and BNK.

Chapter 5 has been published in *Journal of Plant Growth Regulation* and is titled 'Nitrogen Form Substitution Enhances Growth and Carbon Accumulation in Maize'. All authors contributed to the method conceptualisation. Experimentation, data curation, formal analysis, and data analysis and visualisation was conducted by JNA. The original draft was written by JNA and reviewed and edited by CK and BNK.

Chapter 6 is under consideration with *Physiology and Molecular Biology of Plants* and is titled 'Nitrogen form substitution identifies nitrogen use efficiency management pathways in maize'. All authors contributed to the method conceptualisation. Experimentation, data curation, formal analysis, and data analysis and visualisation was conducted by JNA. The original draft was written by JNA and reviewed and edited by CK and BNK.

Chapter 7 is under consideration with *Journal of Plant Nutrition and Soil Science*, with the title 'Low ammonium enhances maize growth and reveals nitrogen efficiency pathways. All authors contributed to the method conceptualisation. Experimentation, data curation, formal analysis, and data

analysis and visualisation was conducted by JNA. The original draft was written by JNA and reviewed and edited by CK and BNK.

Chapter 8 has been published in *Journal of Plant Physiology* and is titled '<u>Ammonium (NH_4^+) regulates carbon metabolism and spatial–diurnal assimilate partitioning to improve growth and nitrogen use efficiency in maize.</u>'. All authors contributed to the method conceptualisation. Experimentation, data curation, formal analysis, and data analysis and visualisation was conducted by JNA. The original draft was written by JNA and reviewed and edited by CK and BNK.

Chapter 9 of this thesis focuses on the general discussion, conclusions, and suggestions for future research.

References for each chapter are consolidated at the end of the thesis to help decrease the thesis size.

Joseph Noble Amoah

December 1, 2025

Supervisor statement

As supervisor for the candidature upon which this thesis is based, I can confirm that the authorship attribution statements above are correct.

Prof. Brent Kaiser

Professor of Legume Biology and Molecular genetics

December 1, 2025

GENERATIVE AI ATTRIBUTION STATEMENT

During the preparation of thesis, the authors used Microsoft Copilot for the purposes of text enhancement. The use of this generative AI tool includes spelling corrections, minor sentence restructuring, and clarity enhancement. The author confirms that where text was modified by generative AI, the content was reviewed for possible errors, inaccuracies, and bias. The author takes full responsibility for the submitted thesis, confirms the work is their own, and has used generative AI in accordance with university guidelines and policies.

ABSTRACT

Ammonium (NH_4^+) and nitrate (NO_3^-) are the primary nitrogen (N) sources essential for plant growth, development, and metabolic function. While plants efficiently absorb both forms from the soil, their distinct roles in regulating physiological and biochemical processes are well-characterized. However, the impacts of N deficiency, nitrogen form substitution (NFS; NO_3^-→NH_4^+/NH_4^+→NO_3^-), and low ammonium (LA) supply on the integrated nitrogen and carbon (C) economy of maize is not well understood. This study examines how these N forms influence growth dynamics, assimilate partitioning, and metabolic plasticity in the maize inbred line TX-40J.

Under low nitrate (LN) conditions, maize exhibited pronounced stress-adaptive responses, including enhanced root biomass and increased root-to-shoot allocation, alongside a significant reduction in shoot growth and protein synthesis. LN treatment upregulated the activities of N assimilation enzymes, such as glutamine synthetase (GS) and glutamate synthase (GOGAT), while suppressing NO_3^- reduction enzymes (NR and NiR), thereby promoting efficient NH_4^+ assimilation. Furthermore, LN induced substantial accumulation of soluble sugars and starch in both leaves and roots, with transcriptional activation of genes involved in sugar and starch metabolism. C accumulation was spatially concentrated in leaf tips, sheaths, brace roots, and lateral roots, suggesting inefficient C utilization in sink tissues rather than impaired assimilation.

Furthermore, NFS (NO_3^-→NH_4^+) treatment significantly improved total biomass, photosynthetic performance, and N assimilation efficiency. Enhanced activities of NR, GS, and GOGAT facilitated the coordinated assimilation of both NO_3^- and NH_4^+. Transcriptional upregulation of NH_4^+ transporters and assimilation genes supported dynamic N partitioning across tissues. Notably, reduced sucrolytic activity under NFS was associated with more efficient sucrose utilization, improved root-to-shoot biomass allocation, and diminished C accumulation in leaves, indicating optimized assimilate distribution under fluctuating N conditions.

LA supply further stimulated photosynthesis, cob development, and overall growth, primarily through elevated GS-GOGAT activity and gene expression, despite concurrent downregulation of nitrate reduction pathways. LA treatment promoted carbohydrate accumulation, with increased activities of sucrose- and starch-metabolizing enzymes and transcriptional activation of their corresponding transport and metabolism genes. Spatial and diel analyses revealed dynamic N and C partitioning between shoots and roots, underscoring the significant contribution of LA to nutrient assimilation and metabolic regulation. Collectively, these findings demonstrate the remarkable metabolic flexibility of maize in response to diverse N forms. They offer mechanistic insights into how N availability and form modulate C and N assimilation, allocation, and utilization, providing a foundation for enhancing nitrogen use efficiency (NUE) and crop productivity under variable nutrient environments.

ACKNOWLEDGEMENT

I extend my deepest and most reverent gratitude to God Almighty for His unwavering faithfulness, boundless mercy, and divine grace, which enabled me to pursue my academic journey at the University of Sydney. Without His guidance, none of this would have been possible.

I am profoundly grateful to my supervisor, Professor Brent Kaiser, whose mentorship has been instrumental in shaping both my academic path and personal growth. From the moment you welcomed me at the Sydney airport, your generosity and steadfast support have meant everything. Brent, you are truly second to none. Thank you for always keeping your door open, even during your busiest days, and for your patience through the highs and lows of my PhD, especially when I was still finding my footing. Your critical insights, thoughtful discussions, and steady encouragement during experimental setbacks were invaluable. I am especially thankful for the many opportunities you created for me throughout this journey, which broadened my perspective and deepened my sense of purpose. More than a mentor, you have been a true friend. Thank you for believing in me and walking beside me every step of the way.

I would also like to express my sincere appreciation to my auxiliary supervisor, Dr. Claudia Keitel, for her patience and guidance throughout my PhD. Her unwavering support was a true blessing, and I was fortunate to have her as my co-supervisor. Many thanks to Dr. Sonam Tashi for your exceptional assistance and support, particularly with the procurement of consumables and the comprehensive training on laboratory equipment at the Centre. I am equally grateful to Mr. Ralf Faux for your steadfast support, especially in setting up the semi-hydroponic system for all my experiments.

My heartfelt thanks go to Mrs. Lynne Gardner for your kind support and availability, especially during times when Brent was unavailable. Thank you for the incredible opportunities you offered and directed me toward, I cannot thank you enough, Lynne. I deeply appreciate the support from all BNK lab members, colleagues at the Centre for Carbon, Water and Food (CCWF), and the Peer Learning Advisory (PLA) Team.

I gratefully acknowledge the financial support provided by the University of Sydney International Scholarship, the Australian Research Training Program (RTP) Scholarship, which covered my tuition, overseas health insurance, and living expenses, the Francis Henry Loxton Supplementary Scholarship (Agriculture), the Australian Research Council (ARC) for funding my research, and the Postgraduate Research Support Scheme (PRSS) for conference and travel assistance.

Finally, I am profoundly thankful to my wife, Esi Fafa Letsa, for your unwavering support and sacrifices for our family. To my girls, Stephanie Boatemaa Amoah, Sika Elinam Amoah, and Adwoa Obrempomaa Amoah, my mother, Doris Boateng, and my siblings, Emmanuel Boateng and Philipa Boateng, thank you all for your love, encouragement, and motivation throughout this journey.

DEDICATION

This thesis is lovingly dedicated to the memory of my father, Godfred Kofi Boateng, whose enduring legacy of wisdom, humility, and faith continues to guide my steps. Though you are no longer here, your spirit has been a constant source of strength throughout this journey, and to my supervisor, Professor Brent Norma Kaiser, whose extraordinary mentorship, generosity, and belief in me transformed this academic pursuit into a deeply personal journey of growth. Without your guidance and unwavering support, this PhD would not have been possible.

ABBREVIATIONS

AGPase	ADP-glucose pyrophosphorylase
AMT	Ammonium transporter
AMY	α-amylase
ANOVA	Analysis of variance
ATP	Adenosine Triphosphate
BAM	β-amylase
C	Carbon
C/N	Carbon/Nitrogen interaction
cDNA	Complementary Deoxyribonucleic Acid
cHATS	Constitutive high-affinity transport system
CINV	Cytoplasmic invertase
CWINV	Cell wall invertase
DAT	Days after seedling transfer
DW	Dry weight
EDTA	Ethylene Diamine Tetracetic Acid
EGTA	Egtazic acid
FW	Fresh weight
GHA	L-glutamic acid γ-monohydroxymate
GOGAT	Glutamate synthase
GS	Glutamine synthase
H/S	Hexose sucrose ratio
HATS	High-affinity transport system
HEPES	4-(2-hydroxyethyl)-1-piperazineethanesulfonic acid
HN	High nitrogen
iHATS	Inducible high-affinity transport system
LA	Low ammonium
LATS	Low-affinity transport system
LN	Low nitrogen
MN	Moderate nitrogen
N	Nitrogen
NFS	Nitrogen form substitution

NiR	Nitrite reductase
NO_2^-	Nitrite
NO_3^-	Nitrate
NPF	Nod Factor Perception
NR	Nitrate reductase
NRT	Nitrate transporter
NT	Nitrogen treatment
NUE	Nitrogen use efficiency
NupE	Nitrogen uptake efficiency
NutE	Nitrogen utilization efficiency
NH_4^+	Ammonium
NH_4NO_3	Ammonium nitrate
PGS	Plant growth stage
PGS × NT	Plant growth stage and nitrogen treatment interaction
Pn	Net photosynthetic rate
qPCR	Quantitative real-time polymerase chain reaction
R/S ratio	Root-to-shoot ratio
RNA	Ribonucleic acid
Rubisco	Ribulose-1,5-bisphosphate carboxylase/oxygenase
SPS	Sucrose phosphate synthase
SS	Starch synthase
STP	Sugar transporters
SuSy	Sucrose synthase
SUTs	Sucrose Transporters
SWEETs	Sugars Will Eventually be Exported Transporters
UDP-glucose	Uridine Diphosphate Glucose
v/v	Volume/volume
VINV	Vacuolar invertase
w/v	Weight/volume
w.w	Weight/weight
YEB	Youngest fully expanded blade

TABLE OF CONTENTS

LIST OF FIGURES

LIST OF TABLES

SUPPLEMENTARY FIGURES

SUPPLEMENTARY TABLES

CHAPTER 1: GENERAL INTRODUCTION AND LITERATURE REVIEW

1.1. Introduction

Nitrogen (N) is an essential macronutrient required for plants for growth and development. It is a primary constituent of key biomolecules such as amino acids, proteins, chlorophyll, and nucleic acids. Beyond its structural role, N also functions as a signalling molecule in various physiological processes, including abiotic stress resistance, seed germination, and hormone signalling (Ahmad et al. 2023; Grubb et al. 2025). N deficiency inhibits growth and causes chlorosis, leading to a substantial reduction in harvestable yield. Despite N abundance in the soils, its availability to plants is often inadequate for optimal growth and productivity. Consequently, growers often resort to heavy nitrogen fertilization to compensate for the deficiency. However, the efficiency of crop uptake of applied N fertiliser is typically low (less than 50%), resulting in increased production costs and environmental risks (George et al. 2016; Dechorgnat et al. 2018).In addition, plants acquire N from the soil primarily as nitrate (NO_3^-) and ammonium (NH_4^+). Of these, NO_3^- is generally more prevalent across diverse soil types, making it the dominant form available for plant uptake (George et al. 2016). N requirements and preferences vary among plant species; while many favour a combination of NO_3^- and NH_4^+, the optimal balance between these forms is influenced by environmental factors such as soil temperature and pH (Peng et al. 2023a). Additionally, the energetic costs and rhizosphere pH changes associated with the uptake and assimilation of each N form play a significant role in determining plant preference. This issue is further complicated by evidence that NO_3^- can inhibit NH_4^+ uptake, adding another factor that impact plant N acquisition (Jakob et al. 2007; Miller and Hawkins 2007; George et al. 2016; Wang et al. 2019). Given the lower concentration of NH_4^+ compared to NO_3^- in soils, it is important to evaluate the contribution of NH_4^+, especially at low concentrations, to the N economy of crops.

While N forms (NH_4^+, NO_3^-, or their combination as NH_4NO_3) at various ratios have been studied, little is known about the impacts of dynamically switching between these forms. In both natural and agricultural systems, the availability of NO_3^- and NH_4^+ fluctuates due to microbial activity, fertilization practices, and environmental factors (Norton and Ouyang 2019; Hui et al. 2024). Prolonged fluctuations can induce stress responses that may compromise crop productivity. However, previous studies have examined N supply under static conditions or with single N forms, failing to reflect the dynamic nature of field environments (Garnett et al. 2013; George et al. 2016; Plett et al. 2016; Dechorgnat et al. 2019; Wang et al. 2019; Peng et al. 2023a). This has left a critical gap in our understanding of how plants respond to shifting N sources. The present study addresses this gap by investigating how changes in N form affect the growth and metabolism of maize (*Zea mays* L.), with a particular focus on carbon (C) and nitrogen (N) metabolic pathways. It further explores diurnal patterns of C and N assimilates in leaves, their spatial distribution across maize tissues, and how these are influenced by different N treatments.

1.2.1. Nitrogen in the soil

Nitrogen gas (N_2) constitutes about 78% of the Earth's atmosphere; however, it is largely inaccessible to most plants in this inert form. Majority of plants can absorb N after it has been converted or fixed into reactive forms such as NO_3^- and NH_4^+, through lightning or biological fixation by microorganisms (Chanway et al. 2014; Zayed et al. 2023). N supply in an agricultural system depends on synthetic fertilizers produced via the energy-intensive Haber–Bosch process (Chanway et al. 2014; Zayed et al. 2023). While N fertilizer inputs are essential for crop productivity, excessive application of these fertilizers causes serious environmental concerns, such as water contamination and increased greenhouse gas emissions (Follett and Delgado 2002). While NH_4^+ and NO_3^- are the primary N forms absorbed by most crops, evidence indicates that some plant species in the artic and forest ecosystems can absorb simple amino acid under limited-N availability conditions, indicating that organic N plays an essential role in natural ecosystem than previously thought (Finzi and Berthrong 2005).

Furthermore, about 90% of soil N exists in organic matter resulting from microbial decomposition of plant and animal residues (Chen et al. 2023b). This decomposition process modulates N availability, and is impacted by climate, vegetation, and topography (Viancelli and Michelon 2024). During this process, N is mineralized to NH_4^+, then nitrified to NO_3^- by bacteria. Due to its positive charge, NH_4^+ binds to clay particles and resists leaching, whereas NO_3^-, existing as free anions, is highly mobile and more susceptible to leaching and runoff (Tunlid et al. 2022). In most agricultural soils, NO_3^- is the preferred nitrogen source for many crop species, owing to the rapid nitrification of NH_4^+. In contrast, NH_4^+ remains the primary N source in ecosystems with limited microbial nitrification, such as the Arctic tundra, where plants exhibit a strong preference for NH_4^+ and glycine uptake during early developmental stages (Zheng et al. 2021).

Interestingly, studies in the boreal forests revealed that mycorrhizal plants utilize organic N as their primary N source, as it constitutes the major N reserve in these soils. In contrast, wetland soils, such as those supporting paddy rice cultivation, are typically rich in NH_4^+, which serves as the principal N source for rice under flooded conditions (Whiteside et al. 2012; Alam et al. 2023). Plant adaptation to diverse environmental influences their preference for N form. Across ecosystems, varying environmental factors leads to distinct proportion of these N forms, and native species have evolved accordingly (Ye et al. 2022). NH_4^+ and NO_3^- levels in the soil are affected by management practices such as grazing, fertilization and soil pH (Qin et al. 2023). Despite the abundance of NO_3^- than NH_4^+ in agricultural soils, NH_4^+ is available in small amount, typically about 10% of NO_3^- level (George et al. 2016). Consequently, most agricultural crops show a preference for NO_3^- as N source, particularly under well-aerated and neutral to alkaline soil condition (Zhang et al. 2022). In contrast, forest soils, often acidic and rich in NH_4^+, favour NH_4^+ uptake, and many native plant species in these ecosystems have

adapted accordingly (Zhao and Shen 2018). Additionally, species-specific preferences for N form have been observed in certain grassland and alpine plant communities, where long-term nitrogen deposition has driven shifts in phylogenetic structure and nutrient acquisition strategies, underscoring the role of ecological adaptation (Liu et al. 2024)

1.2.2. Impacts of N fertilization: productivity gains versus environmental costs

The rapid growth of the world's population has intensified the demand for food, necessitating increased reliance on N fertilizers to sustain cereal production (Mulvaney et al. 2009; Govindasamy et al. 2023). However, current fertilization practices remain inefficient, with cereals typically absorbing only ~50% of the applied N, while the remainder is lost to the environment (Ladha et al. 2005). A substantial fraction volatilizes into the atmosphere or is transported via surface runoff into aquatic ecosystems, where it promotes excessive algal proliferation. This eutrophication process depletes dissolved oxygen, resulting in hypoxic 'dead zones' that compromise aquatic biodiversity and ecosystem integrity (Owens and Karlen 2020; Govindasamy et al. 2023). Furthermore, the release of nitrous oxide (N_2O) from N fertilizers, contributes significantly to greenhouse gas emission, given its high global warming potential (Reay et al. 2012; Filonchyk et al. 2024). Economically, inefficient N utilization raises production costs for growers, as fertilizer prices are closely tied to fluctuations in natural gas prices.(Ladha et al. 2005) Currently, N fertilizers represent the second-largest input cost in many agricultural production systems (Rodríguez-Espinosa et al. 2023). Given the global importance of cereal production, it is essential to enhance nitrogen use efficiency (NUE) through sustainable practices to ensure continued supply (Omara et al. 2019; Salim and Raza 2020). NUE in crops is defined as the grain yield produced per unit of N supplied. It reflects both N uptake efficiency (NupE) and N utilization efficiency (NutE) (Lea and Azevedo 2006; Gallais and Coque 2005). Interestingly, current research efforts are focused on enhancing NUE through the optimization of agronomic practices, such as fertilizer, irrigation management, and the development of hybrid crops with superior NUE traits (Govindasamy et al. 2023; Reddy et al. 2025; Ali et al. 2025b).

1.2.3. Plant nitrate and ammonium uptake

1.2.3.1. NO_3^- and NH_4^+ uptake mechanism

In plants, NO_3^- and NH_4^+ first diffuse into the root apoplast before being actively transported across the plasma membrane into the symplast(Muratore et al. 2021). NO_3^- movement across membranes is primarily mediated by proton-coupled symport mechanisms (Kronzucker et al. 1995b). Three distinct transport systems facilitate NO_3^- uptake: the inducible high-affinity transport system (iHATS), the constitutive high-affinity transport system (cHATS), and the low-affinity transport system (LATS).

iHATS is induced under NO_3^- availability, whereas cHATS remain functional even in the absence of external NO_3^- (Crawford and Glass 1998; Forde 2002; Glass et al. 2002). LATS is activated when the external NO_3^- concentration exceeds 250 μM, and its transport activity exhibits a linear relationship with the ambient NO_3^- level (Glass et al. 2002). Although iHATS is upregulated upon NO_3^- provision, continuous NO_3^- supply has been reported to downregulate LATS activity (Kronzucker et al. 1995b). As a cation, NH_4^+ is absorbed by plant roots along an electrochemical gradient (Smith and Walker 1978). NH_4^+ absorption follows a biphasic model, with HATS mediating uptake at low concentrations and LATS contributing under higher NH_4^+ availability (Ullrich et al. 1984; Kronzucker et al. 1996). At elevated NH_4^+ levels, the electrochemical gradient becomes energetically favourable (downhill), facilitating passive uptake (Ullrich et al. 1984).

1.2.3.2. Nitrogen (N) transporters in plants

1.2.3.2.1. NO_3^- transport system

Nitrate uptake in plants is primarily mediated by two gene families: NPF and NRT2. In *Arabidopsis thaliana* (*Arabidopsis*), 53 genes belong to the NPF family, yet only 16 have been experimentally validated as nitrate transporters (Krapp et al. 2014; Aluko et al. 2023b). NPF proteins are integral membrane transporters predicted to contain 12 transmembrane helices linked by short peptide loops (Léran et al. 2014; Parker and Newstead 2014). In maize, 87 NRT genes have been identified that contribute to both high- and low-affinity nitrate transport systems (HATS and LATS), including 78 NPF (NRT1/PTR) genes, 7 NRT2 genes, and 2 NRT3 genes (Jia et al. 2023).

CHL1 was the first nitrate (NO_3^-) transporter identified in plants, discovered in a chlorate-resistant *Arabidopsis* mutant produced via T-DNA tagging (Crawford and Glass 1998). This gene, now known as NRT1.1 (or NPF6.3), was originally classified as a LAT. However, studies have also shown that NRT1.1 displays dual-affinity kinetics, functioning as a high-affinity transporter under low external NO_3^- conditions via phosphorylation at Thr-101, and as a LAT under high NO_3^- availability. Unlike most NRT1/NPF transporters, which generally mediate low-affinity (LATS) uptake, NRT1.1 uniquely switches between LATS and HATS according to phosphorylation status (Liu et al. 1999; Parker and Newstead 2014). Phosphorylation at Thr101 switches NRT1.1/NPF6.3 between its low- and high-affinity NO_3^- transport modes. This mechanism was first discovered by Liu & Tsay and was recently linked to stomatal regulation and drought tolerance under low NO_3^- conditions (Liu and Tsay 2003; Kou et al. 2025). Functioning as a "transceptor," NRT1.1 not only facilitates NO_3^- uptake but also modulates the primary NO_3^- response gene network based on external NO_3^- availability (Ho et al. 2009; Krouk et al. 2010). Long-distance NO_3^- transport involves multiple NPF members. NRT1.5/NPF7.3 exports NO_3^- from pericycle cells to the xylem, whereas NRT1.8/NPF7.2 retrieves NO_3^- from the xylem sap. NRT1.7/NPF2.13 remobilizes NO_3^- from source (older) leaves to sink (younger) leaves via the

phloem. NRT1.9/NPF2.9 loads NO_3^- into the root phloem, while NRT1.11/NPF2.11 and NRT1.12/NPF2.12 mediate xylem-to-phloem transfer in petioles (Lin et al. 2008). Beyond NO_3^-, several NPF proteins possess expanded substrate profiles. NPF4.6/NRT1.2 and its homologs import abscisic acid, while GTR1/2/3 (NPF2.10/2.11/2.9) function as key glucosinolate transporters (Corratgé-Faillie and Lacombe 2017; Chiba et al. 2015). Collectively, these findings highlight the multifunctional nature of the NPF family and confirms its active roles in NO_3^- allocation.

In plants, high-affinity NO_3^- uptake is facilitated by a dual-component transport system involving proteins from the NRT2 and NRT3 (also known as NAR2) families (Zoghbi-Rodríguez et al. 2021). The first NRT2-type high-affinity nitrate transporters were cloned nearly three decades ago from *Chlamydomonas reinhardtii* and *Aspergillus nidulans (Quesada et al. 1997)*, highlighting the evolutionary origins of HATS NO_3^- transporters outside higher plants. Plant genome analysis has identified seven NRT2s in Arabidopsis (*AtNRT2*), seven in maize (*ZmNRT2*), ten in barley (*HvNRT2*) and 49 in hexaploidy wheat (*TaNRT2*), demonstrating a lineage-specific expansion (Xu et al. 2024a; Deng et al. 2023). Most NRT2 proteins require the accessory subunit NRT3/NAR2 to form a functional HATS NO_3^- (Feng et al. 2011; Feng et al. 2023a). However, exceptions exist, for instance, *AtNRT2.4* in Arabidopsis and several rice isoforms, such as *OsNRT2.4* have been shown to function independently, highlighting isoform-specific flexibility in transporter regulation (Feng et al. 2023b; Zhang et al. 2025). Furthermore, in *Arabidopsis*, *AtNRT2.1* remains the principal HATS component and its activity has been shown to be fine-tuned by multi-site phosphorylation, such as Ser 21/Ser 28 in the N terminus as well as the classic Thr101 switch in its partner transceptor NRT1.1 (Chaput et al. 2023). High external NO_3^- availability repress the expression of *AtNRT2.1*, 2.4 and 2.5 via feedback pathways that involves NRT1.1/NLP7 signalling, whereas NH_4^+ allows their re induction under low N conditions (Chaput et al. 2023). Additionally, in maize, *ZmNRT2.5* was highly up-regulated under prolonged N starvation and natural variation in this gene shapes husk-leaf architecture, highlighting a dual role in nutrition and development (Wu et al. 2024a; Wang et al. 2025a). Collectively, this reinforces earlier discussion that NRT2.1 and its orthologues play a crucial role in high affinity NO_3^- uptake, whereas NRT2.4 and NRT2.5 in Arabidopsis, or NRT2.5 in maize, function as specialist transporters under N deficiency.

1.2.3.2.2. NH_4^+ transport system

Plant NH_4^+ transporters are categorized into two distinct families, AMT1 and AMT2 (Yang et al. 2023; Von Wittgenstein et al. 2014). Yeast and Xenopus assays show that both clades encode high-affinity NH_4^+ transporters (Gazzarrini et al. 1999; Sohlenkamp et al. 2002; Bindel and Neuhäuser 2021). The first NH_4^+ transporter gene identified in plants was AMT1 in *Arabidopsis*, encoding a high-affinity transporter (Ninnemann et al. 1994). Since then, several studies have isolated homologues of AMT1 and AMT2 from Arabidopsis thaliana (Gazzarrini et al. 1999), 3 in tomato and 10 in rice. Furthermore,

in rice, AMT2 family consists of three subfamilies namely AMT2, AMT3 and AMT4 (Suenaga et al. 2003), and the transporters appear to be functioning as HATS in plants. Interestingly, previous studies have shown that low NO_3^- availability suppressed the expression of *AtAMT2* in the roots of Arabidopsis, while the shoot transcript expression levels remained unchanged, demonstrating that NH_4^+ uptake is modulated by internal N status through various regulatory mechanisms (Gansel et al. 2001; Sohlenkamp et al. 2002). In maize, functional analyses of *ZmAMT1.1A* and *ZmAMT1.3* confirmed their active role in high affinity NH_4^+uptake (Gu et al. 2013; Zhao et al. 2018).

1.2.4. Nitrogen (N) assimilation

During N assimilation, inorganic N entering the plant roots is first incorporated into organic N before undergoing further metabolism. NO_3^-, a primary N form, may be reduced either in the roots or transported via the xylem to the shoots for assimilation. NO_3^- assimilation occurs in the leaves of herbaceous plants and in the roots of woody plants (Andrews and Raven 2022). In contrast, NH_4^+ is assimilated directly in the roots (Liu and von Wirén 2017). NH_4^+ in plants arises from multiple sources beyond direct uptake. Nitrate reduction, amino acid catabolism, and photorespiration contribute to NH_4^+ production (Yamaya and Oaks 2004; Lea and Azevedo 2007). Studies have identified the epidermal and exodermal cells a major site of primary NH_4^+ assimilation in rice and barley (Tobin and Yamaya 2001). Moreover, NH_4^+ assimilation is modulated by environmental factors such as pH, carbon (C) availability and stress-related signals (Sarasketa et al. 2016; Ye et al. 2022)

Nitrate reductase (NR), nitrite reductase (NiR), glutamine synthetase (GS), and glutamate synthase (GOGAT) are the key enzymes involved in N assimilation. While NR and NiR catalyse the assimilation of NO_3^-, GS and GOGAT are actively involved in NH_4^+ assimilation (Kishorekumar et al. 2020). During this process, NO_3^- is first reduced to NO_2^- by NR. The NO_2^- produced in the cytosol is then transported to the roots or chloroplasts, where it is converted into NH_4^+ by NiR. Subsequently, NH_4^+ enters the GS/GOGAT cycle to form glutamine and glutamate. Plants possess two primary GS isoforms: cytosolic GS1 and chloroplastic/plastidic GS2. These enzymes facilitate NH_4^+ assimilation either through direct uptake or via photorespiration, with GS2 also contributing to the reduction of NO_3^- to NH_4^+ (Betti et al. 2012; Moreira et al. 2022). Notably, about 95% of the NH_4^+ taken up by plant roots is assimilated via the GS1/GOGAT cycle. In contrast, NH_4^+ produced from NO_3^- reduction in the plastids or chloroplasts is incorporated into glutamine and glutamate predominantly through the GS2/GOGAT pathway, which serves as a precursor pool for amino acid biosynthesis (Yoneyama and Suzuki 2019; Hirel and Lea 2002). Compared to NH_4^+ uptake, NO_3^- assimilation incurs a significantly higher energy cost (Glass et al. 2002; Bloom 2015a). This is because NO_3^- reduction to NO_2^- requires the transfer of two ATP molecules, followed by a further reduction to NH_4^+ that demands an additional six ATP (Bloom et al. 1992; George et al. 2016).

1.2.4.1. Regulation of N uptake

Being sessile, plants have evolved intricate regulatory networks to cope with fluctuations in soil N availability (Kraiser et al. 2011). These networks integrate signals from both external N supply and internal N status through coordinated local and systemic signalling pathways that regulate uptake, metabolism, and resource allocation (Krouk et al. 2010). NO_3^- uptake is influenced by a regulated mechanism that is activated in response to the N demand of plants and overall N status (Ruffel et al. 2014). Interestingly, when plants experience N fluctuations, they exhibit an increased NO_3^- uptake compared to those under sustained NO_3^- supply (Zhao et al. 2020). This uptake capacity varies temporally, highlighting dynamic interaction between plant demand and external N availability in the nutrient medium (Plett et al. 2016). A notable example is the 'primary NO_3^- response,' triggered when plants experience N starvation followed by re-supply. This transient signalling event persisting for hours, stimulates high affinity NO_3^- uptake and induces NRT2 protein accumulation in the roots (Kiba et al. 2012; George et al. 2016).

Moreover, specific amino acids such as glutamine, glutamate (Glu) and asparagine (Asn) act as central regulators of N uptake, reflecting the overall N status and C/N balance of plants (Miller et al. 2008). Amino acids transported via the phloem from shoots to roots function as mobile signals reflecting the N nutritional status of plants, thereby modulating NO_3^-uptake from external medium (Miller et al. 2008; Muratore et al. 2021). For example, glutamine has been shown to downregulate NO_3^- and NH_4^+ influx and transporter genes expression in root tissues (Miller and Hawkins 2007).). This feedback regulation involves alterations in transporter gene regulation and post-translational modifications, highlighting the essential role of plant amino acids in modulating N acquisition (Quesada et al. 1997; Miller and Hawkins 2007)

NO_3^- and NH_4^+ uptake in plants are modulated by analogous feedback regulatory mechanisms (Gansel et al. 2001). In *Arabidopsis*, for example, NH_4^+ uptake capacity is upregulated during N starvation but markedly suppressed following N resupply. This dynamic adjustment is driven by a negative feedback loop, wherein elevated glutamine levels in plant tissues act as internal signals to downregulate NH_4^+ transport activity (Yuan et al. 2007). Furthermore, feedback control of NO_3^- and NH_4^+ uptake is stronger in HATS than LATS that dominates at higher external N levels (Kronzucker et al. 1996). Studies have shown that transcript levels of NRT2 and AMT genes respond differentially to N availability, with upregulation under N starvation and repression upon NH_4^+ or glutamine accumulation (Ostria-Gallardo et al. 2024).

The uptake of NO_3^- and NH_4^+ is regulated by diel rhythms (Hayes et al. 2010), with uptake rates rising during the light period, peaking towards the end of the photoperiod, and declining during the night (Gazzarrini et al. 1999; Glass et al. 2002). In wheat, sucrose supplementation under dark

conditions significantly enhanced NO_3^- uptake, by up to 7 times, demonstrating that sugar availability can substitute for light in activating nitrate transport mechanisms (Li et al. 2021a). Studies have also shown that the regulation of *NRT2* and *AMT1* families exhibited circadian and light-responsive regulation (von Wirén et al. 2000). This transcriptional regulation may coordinate N acquisition with C metabolism and energy status, optimizing nutrient uptake relative to metabolic demand (Liu et al. 2025), highlighting the need to integrate temporal dynamics into models of nutrient transport and nitrogen use efficiency (NUE).

Furthermore, soil temperature significantly influences nitrogen (N) uptake in plants (Scholberg et al. 2002). Evidence from different studies indicates that nitrate uptake is highly sensitive to low temperatures, often exhibiting substantial inhibition, whereas NH_4^+ uptake remains relatively stable under the same conditions (Reay et al. 1999; Clarkson and Warner 1979; Tang et al. 2015). For instance, in *Lolium perenne*, approximately 85% of the N absorbed at low temperatures was in the form of NH_4^+, indicating a shift toward preferential NH_4^+ assimilation when NO_3^- transport is restricted (Clarkson et al. 1986). The differential response may be due to the higher energy requirement and transport sensitivity associated with NO_3^- uptake and reduction, making NH_4^+ a more favourable N source in cooler soils. These findings underscore the importance of temperature-dependent N-form preference in plant nutrition, further suggesting that NH_4^+-based fertilization may be more effective in low-temperature environments or early-season applications (Hu et al. 2017).

Root-zone pH exerts a significant influence on the uptake of nitrate and ammonium, with optimal ranges varying across species (Tylova-Munzarova et al. 2005). Studies have shown that NH_4^+ uptake decreases while NO_3^- uptake increases as root-zone pH declines (Vessey et al. 1990; Ruan et al. 2007). Similarly, in conifers and soybean, net NO_3^- uptake is greatest at neutral pH, while NH_4^+ uptake in soybean is reduced at pH 4 (Hawkins and Robbins 2010). While barley seedlings showed maximum NO_3^- uptake at pH 4, in wheat, NO_3^- uptake was significantly inhibited at pH 4, with optimal absorption occurring around 6.5 (Zsoldos et al. 1999), highlighting the influence between N form and pH dynamics.

Soil temperature impacts plant NO_3^- and NH_4^+ uptake. Studies have shown that soil temperature influences the uptake of NO_3^- and NH_4^+ in plants. Comparatively, NO_3^- uptake tends to be more sensitive to temperature fluctuations than NH_4^+ uptake (Frota and Tucker 1972). This is because NO_3^- uptake increases more rapidly than NH_4^+ uptake as temperatures rise increase (Vaast et al. 1998). For example, in rice and lettuce seedlings, higher temperatures enhance NO_3^- uptake, whereas low temperatures significantly suppress it. In contrast, at low temperatures, up to 85% of nitrogen absorbed by *Lolium perenne* was in the form of NH_4^+ (Clarkson et al. 1986).

1.2.5. Sugar metabolism in plants

Plant sugars play an essential role in regulating growth, development, metabolism, and stress responses. Sugars such as glucose, sucrose, and fructose are not only involved in photosynthesis, primary C

metabolism and starch synthesis but also act as dynamic signalling molecules (Jeandet et al. 2022). They influence a wide range of physiological processes by interacting with hormonal pathways, regulating gene expression, and activating signalling cascades. Through these mechanisms, sugars help control cell division, flowering, and plant responses to environmental cues (Van den Ende 2014; Afzal et al. 2021). Similar to sugars, starch serves as both a vital energy reserve and a key regulator of plant physiology, participating in diurnal C balance, growth regulation, and adaptation to environmental stresses (Prathap and Tyagi 2020).

Different N forms, whether NO_3^-, NH_4^+ or mixed sources, contributes to shaping C metabolism and partitioning in plants. These N sources influence not only nutrient uptake but also the regulation of sugar synthesis, transport, and utilization. Studies have shown that NH_4^+ nutrition increases soluble sugar level, whiles inhibiting starch synthesis in maize (Fan et al. 2025). Elevated NH_4^+ levels trigger rapid changes in gene expression and protein post-translational modifications, affecting key enzymes involved in sugar metabolism. This often leads to cytosolic acidification and oxidative stress, impairing sugar utilization and disrupting energy balance (Liu and von Wirén 2017; Di 2023). In *Arabidopsis* and rice, high NH_4^+ supply has been associated with increased glutamine and proton accumulation, contributing to acidic stress and metabolic dysfunction (Liu and von Wirén 2017; Di 2023). In contrast, NO_3^- nutrition enhances photosynthetic capacity by promoting chlorophyll synthesis and activating enzymes that drive sugar accumulation (Cerqueira et al. 2019; Zhang et al. 2021). For instance, in sweet potato and apple, moderate NO_3^- supply significantly increased soluble sugar and starch levels, boosted the activity of sugar- and starch-metabolizing enzymes, and upregulated genes involved in sucrose and starch metabolism (Zhao et al. 2020; Dong et al. 2025). Recent studies further highlight that mixed N sources at optimized ratios can outperform sole NO_3^- or NH_4^+ treatments in promoting plant growth and enhancing carbon metabolism. Mixed N nutrition improves sugar accumulation, chlorophyll content, and the expression of carbohydrate metabolism genes in crops, such as grapevine, tomato, and maize (Yin et al. 2020; Sun et al. 2023; Wang et al. 2019; Peng et al. 2023a; Wang et al. 2024b). However, these responses are highly species-specific and influenced by developmental stage and environmental conditions, underscoring the need for tailored N management strategies in crop production (Foyer et al. 2001; Lawlor 2002; Baslam et al. 2020)

1.2.6. Plants preferences for N sources

Plant N uptake preferences are influenced by various factors, including plant species, climate, and soil conditions. In the soil, the availability of nitrogen in the form of either NO_3^- or NH_4^+ largely depends on the nitrification process (Subbarao et al., 2007). Some plants have the capacity to modulate this process, thereby soil N composition. Studies have shown that species with a higher capacity to inhibit nitrification tend to prefer NH_4^+ over NO_3^- (Boudsocq et al. 2012; Ardichvili et al. 2024). From an

energetic perspective, NO_3^- assimilation is more costly, requiring about 12 ATP molecules compared to only 2 ATP for NH_4^+ assimilation, suggesting that growth under NO_3^- nutrition may be more constrained (Bloom et al. 1992). Despite its lower energy cost and rapid assimilation potential, excessive NH_4^+ supply has been associated with toxicity, which can impair plant growth and metabolism (Kong et al. 2022). Moreover, NH_4^+ uptake and assimilation result in the release of H^+ ions, acidifying the rhizosphere and potentially inhibiting root growth (Feng et al. 2020), whereas NO_3^- uptake and assimilation release hydroxyl ions, generally increasing rhizosphere pH (Andrews et al. 2013).

Furthermore, studies have shown that NO_3^- uptake in NO_3^--nourished plants is often facilitated by the concurrent absorption of cations such as calcium (Ca^{2+}), potassium (K^+), and magnesium (Mg^{2+}), which help maintain ionic balance and support translocation to aerial tissues. In contrast, plants grown under NO_3^--deprived conditions tend to accumulate alternative anions such as sulphate (SO_4^{2-}), phosphate (PO_4^{3-}), and various trace elements to compensate for the reduced NO_3^- availability and maintain charge equilibrium (Fang et al. 2020). The enhanced uptake of cations in NO_3^--nourished plants is attributed to the increased rhizosphere pH associated with NO_3^- assimilation. As NO_3^- is reduced within plant cells, organic anions such as malate and citrate are produced as intermediates. To maintain ionic balance, plants absorb inorganic cations, particularly K^+, Ca^{2+}, and Mg^{2+}, which serve as counterions to both the NO_3^- and the organic anions formed during assimilation (Feng et al. 2020; Islam 2022). This coordinated ion uptake stabilizes cellular pH and supports efficient N metabolism and translocation (Sun et al. 2020a).

NH_4^+ uptake influences nutrient dynamics in distinct ways. It facilitates the absorption of anions such as PO_4^{3-} and SO_4^{2-}, while often suppressing the uptake of K^+, Ca^{2+}, and Mg^{2+}. This suppression is partly due to ionic competition and the acidification of the rhizosphere resulting from H^+ release during NH_4^+ assimilation (Coleto et al. 2023) . The lowered pH enhances the solubility and availability of several micronutrients, such as Mn^{2+} and Zn^{2+}, thereby promoting their uptake from the soil solution. However, the competitive inhibition of cation uptake becomes more pronounced under elevated NH_4^+ concentrations (Rengel 2015; Naeem et al. 2023). In soybean seedlings, for instance, a moderate NH_4^+ supply (e.g., 500 μM) enhance the uptake of K^+, Ca^{2+}, and Mg^{2+}, but higher concentrations tend to restrict their absorption due to intensified ionic competition and rhizosphere acidification (Rayar and Van Hai 1977; Noor et al. 2024). Similarly, in maize, enhanced phosphorus (P) uptake under NH_4^+ nutrition has been linked to dynamic shifts in rhizosphere pH, which modulate P solubility and availability (Jing et al. 2010; Sun et al. 2020a).

Although NO_3^- and NH_4^+ are widely used as the primary N sources to support plant growth and metabolism, there is growing interest in supplying N as a mixture of both forms, commonly applied as ammonium nitrate (NH_4NO_3), in varying ratios. This mixed N strategy has been shown to improve NUE, enhance root development, and optimize C/N coordination, particularly in various crop species

(Yang et al. 2025; Wang et al. 2019; Peng et al. 2023b; Wang et al. 2024b). By balancing the physiological advantages and limitations of each form, mixed nitrogen supply can mitigate toxicity risks, stabilize rhizosphere pH, and promote more robust nutrient uptake.

1.2.7. Regulatory inhibition of NH_4^+ on NO_3^- uptake

NH_4^+ has been shown to inhibit NO_3^-uptake in plants, though the underlying mechanisms vary. Studies have demonstrated that short-term exposure to NH_4^+ reduces NO_3^- influx, particularly in NO_3^--induced plants and under low external NO_3^- levels (Kronzucker et al. 1995a). This inhibition has been attributed to NH_4^+-induced depolarization of the plasma membrane, which compromises the function of the inducible high-affinity NO_3^- transport system (Lee and Drew 1989). In Arabidopsis and rice, NH_4^+ exposure primarily suppressed NO_3^- uptake by reducing influx, with minimal contribution from efflux (Feng et al. 2020), reflecting a conserved inhibitory mechanism across species. Moreover, elevated root N status suppresses NO_3^- uptake through feedback inhibition of NO_3^- transporters, reflecting a reduced N demand by the plant (Kumar et al. 2020). NH_4^+ toxicity, characterized by rhizosphere acidification, ionic imbalance, and disruption of C/N metabolism, has also been shown to systemically suppress NO_3^- uptake even in the presence of NO_3^-, as observed in both rice and *Arabidopsis* (Kumar et al. 2020; Xie et al. 2025). Additionally, the long-term accumulation of glutamine and other amino acids, inhibits NR activity and NO_3^- influx, indicating a tightly regulated feedback loop between N assimilation and uptake (Dubey et al. 2021). Phloem-translocated amino acids, including arginine, glutamate, asparagine, and alanine, further act as systemic signals of N sufficiency, directly suppressing NO_3^- uptake at the root level (Forde and Clarkson 1999; Feng et al. 2020). These findings highlight the complexity of NO_3^- uptake regulation, which integrates local root conditions with the plant's overall N status and metabolic feedback mechanisms.

1.3. Aims and objectives

Although NO_3^- and NH_4^+ are the predominant N sources in agricultural soils, plants often exhibit a physiological preference for NH_4^+ due to its lower energy cost for assimilation (Hachiya and Sakakibara 2017). However, the impact of dynamically switching between these N forms, referred to as nitrogen form substitution (NFS), on plant growth and metabolism is not well understood and its mechanistic contribution to the integrated N and C budget has not been elucidated.

This thesis aims to investigate the physiological and metabolic consequences of NFS in maize, with a particular focus on the inbred line TX-40J. By examining how N form transitions influence growth, N assimilation, and C metabolism, this study seeks to uncover adaptive strategies that may enhance nutrient use efficiency and stress resilience.

1.3.1 Specific objectives

i. To examine the impact of different N forms (NO_3^- vs. NH_4^+) on growth, as well as C and N metabolism in maize inbred line TX-40J.

ii. To quantify the influence of substituting N form ($NO_3^- \rightarrow NH_4^+$) on biomass accumulation and C partitioning.

iii. To understand how low NH_4^+ supply affects growth and the coordination of N and C metabolism in maize.

1.3.2. Thesis structure and chapter overview

Chapter 2: Assesses the impact of varying N levels and forms on N assimilation and metabolic profiles.

Chapter 3: Investigates how different N regimes influence C metabolism, including sucrose and starch dynamics.

Chapter 4: Explores root morphological adaptations and their relationship to C metabolism under distinct N forms.

Chapter 5: Elucidates the effects of N form substitution on N assimilation pathways and transporter activity.

Chapter 6: Examines the contribution of NFS to C accumulation, focusing on spatial distribution and utilization efficiency.

Chapter 7: Evaluates the impact of low NH_4^+ supply on N uptake, assimilation, and related enzymatic activities.

Chapter 8: Investigates how low NH_4^+ availability modulates C metabolism, including changes in sugar partitioning and enzyme regulation.

Chapter 9: Synthesizes key findings, discusses broader implications for nutrient management, and proposes future research directions.

CHAPTER 2: NITROGEN DEFICIENCY IDENTIFIES NITROGEN USE EFFICIENCY MANAGEMENT PATHWAYS IN MAIZE[1]

Abstract

Nitrogen (N) is an essential macronutrient for plant growth, development, and metabolic processes. However, the regulatory mechanisms governing N assimilate allocation and utilization under different N forms remain unclear. This study examines N metabolism, utilization and spatial distribution in hydroponically grown maize seedlings subjected to three N treatments: 1 mM NO_3^- (low N, LN), 2 mM NO_3^- (medium N) and 10 mM NO_3^- (high N). LN treatment induced significant physiological and molecular adaptations, such as enhanced root biomass and root/shoot (R/S) ratio, which prioritized N acquisition efficiency under a N deficiency condition. LN-treated plants exhibited significantly ($P \leq 0.05$) reduced shoot biomass, protein synthesis, as well as NO_3^- and NO_2^- content, alongside increased NH_4^+ levels. The activities of key N metabolism enzymes, such as nitrate reductase (NR) and nitrite reductase (NiR) were decreased, while glutamine synthetase (GS) and glutamate synthase (GOGAT) activities were upregulated, facilitating efficient NH_4^+ assimilation. Molecular analysis revealed transcriptional reprogramming under LN condition, with downregulation of NO_3^- metabolism-related genes, *ZmNR1* and *ZmNiR1*, and upregulation of NO_3^- and NH_4^+ transporter genes, *ZmNPF6.2*, *ZmNRT2.1*, *ZmNRT3.1*, *ZmAMT1.1* and *ZmAMT2.1*, as well as GS-GOGAT pathway genes *ZmGS1* and *ZmGOGAT1*. Spatial and diurnal analysis highlighted dynamic N partitioning and adaptive regulation, with LN-treated plants exhibiting consistently higher NH_4^+ levels and reduced NO_3^- concentrations in leaves, roots, and sheath tissues. These findings underscore the robust plasticity of maize N metabolism under LN conditions, providing useful insights into optimizing N use efficiency (NUE) for sustainable agriculture. Future research may explore these adaptive mechanisms in diverse maize varieties and field conditions to enhance NUE and crop productivity under nutrient-limited condition.

Keyword: Assimilated partitioning, Diurnal assimilates accumulation, Maize adaptation, Nitrogen deficiency Nitrogen metabolism, Nitrogen use efficiency

---

[1]This chapter is currently under review in the Journal of Plant Growth Regulation, with the title 'Nitrogen deficiency impacts growth and modulates nitrogen metabolism in maize' (Manuscript ID: JPGR-D-25-00669).

2.1. INTRODUCTION

Nitrogen (N) is an essential macronutrient crucial for plant growth and development. It plays a vital role in the synthesis of nucleotides, amino acids, proteins, enzymes, and chlorophyll, which are indispensable for maintaining physiological and biochemical processes in plants (Duan et al. 2023b;

Mu and Chen 2021). N availability is often a significant limiting factor for crop productivity due to its vulnerability to adsorption, leaching, and transformation processes within the soil (Masclaux-Daubresse et al. 2010). To address this limitation, growers frequently apply substantial amounts of N fertilizers. However, less than 50% of the applied N is efficiently utilized by crops, with the remainder lost through processes such as NO_3^- leaching, often triggered by excessive rainfall or irrigation (Govindasamy et al. 2023). This loss results in dynamic changes in N supply conditions, alternating between periods of deficiency, sufficiency, and excess. These variations can occur naturally in agricultural soils due to environmental factors or arise as a direct outcome of agricultural practices (Nacry et al. 2013). These unpredictable nutrient dynamics adversely affect crucial metabolic processes in plants, ultimately limiting growth and reducing productivity (Govindasamy et al. 2023). Therefore, understanding crop growth and development under different N conditions, especially under a N deficiency condition is crucial for defining pathways to improved nitrogen use efficiencies that can help ensure global food security and sustainability (Penuelas et al. 2023).

N deficiency in plants arises when the available N supply is insufficient to support optimal growth, leading to substantial reductions in growth, yield, and crop quality. To adapt to low N availability, plants have evolved morphological and physiological strategies that enhance N uptake and allow them to adjust to fluctuations in soil N levels (Kiba and Krapp 2016; Dechorgnat et al. 2018). Studies have shown that N deficiency significantly reduces photosynthesis and growth by lowering chlorophyll content, impairing photosynthetic efficiency, altering thylakoid membrane structures, and diminishing yield across various crops (Mu and Chen 2021; Cetner et al. 2017). In apple leaves, N deficiency causes irreversible cell morphology damage, decreases the activity of N-related enzymes, and downregulates the expression of N metabolism-related genes (Wen et al. 2019). Similar effects have been observed in mung bean (Zhou et al. 2023) and pepper seedlings (Costa et al. 2024). Despite extensive research on maize responses to varying N levels, comparative studies specifically examining the effects of low N treatments have remain limited, leaving significant gaps in our understanding of NUE responses under N-limited conditions. Our recent findings reveal that N deficiency significantly inhibits growth, reallocates assimilates (carbon) toward roots at the expense of shoot growth, and increases sucrolytic activity in maize seedlings (Amoah and Kaiser, 2025). Despite these insights, our understanding of N metabolic alterations under low N conditions remains relatively limited.

Plants utilize organic N, NH_4^+, and NO_3^- as primary N sources. However, organic N uptake is often limited by competition with soil microorganisms, making NH_4^+ and NO_3^- the predominant N forms available to roots. NO_3^- availability is influenced by soil type and microbial activity (Bloom 2015b). NO_3^- uptake in roots functions through two transport systems: the low-affinity, high-capacity transport system (LATS) active at N concentrations >250 μM, and the high-affinity, low-capacity transport system (HATS) dominant at concentrations <250 μM (Glass et al. 2002). Furthermore, NO_3^- uptake is regulated by the NPF (NRT1/PTR) and NRT2 families of transporter genes, encoding proteins

for LATS and HATS, respectively (Dechorgnat et al. 2018). Similarly, NH_4^+ uptake at low external concentrations (HATS) is mediated by the AMT (ammonium transporter) gene family (Yuan et al. 2007). Currently, no specific AMT transporter has been identified for NH_4^+ LATS activity, though AMF1 proteins in soybean, *Medicago* and yeast show promise as a potential candidates (Chiasson et al. 2014; Dechorgnat et al. 2018; Ovchinnikova et al. 2023). Once inside root cells, NO_3^- and NH_4^+ ions can either be directly assimilated or stored within the vacuole or cytoplasm (Dechorgnat et al. 2011). These ions may also undergo radial transport to the xylem via symplastic and apoplastic pathways, supporting their translocation within the plant.

NO_3^- assimilation, involves its reduction to NO_2^- by the cytosolic enzyme nitrate reductase (NR) (Wany et al. 2020). NO_2^- is subsequently reduced to NH_4^+ by plastid-localized nitrite reductase (NiR) (Vidal et al. 2020). NH_4^+ generated from NO_3^- reduction, along with NH_4^+ absorbed via direct root uptake, is primarily assimilated in the plastid through the glutamine synthetase-glutamate synthase (GS-GOGAT) cycle. In this cycle, glutamine synthetase (GS) catalyses the amination of glutamate to form glutamine (Tabuchi et al. 2007). Glutamine then reacts with 2-oxoglutarate to produce two molecules of glutamate via glutamate synthase (GOGAT) (Hirel and Lea 2002). After the production of glutamine and glutamate through the GS-GOGAT cycle, assimilated N participates in various amination and deamination processes, contributing to amino acid biosynthesis.

Maize (*Zea mays* L.) was selected for this study due to its prominence as a staple food crop and its suitability as a model for studying N management (Simons et al. 2014). Its well-characterized growth patterns, responsiveness to environmental factors, and adaptability to varying N conditions make it an ideal candidate for exploring the impacts of N availability on N metabolism and distribution (Dong et al. 2023b). Moreover, the global economic significance of maize underscores the importance of optimizing nutrient management to enhance productivity (Begam et al. 2024). This study focuses on elucidating the mechanisms governing N metabolism between the shoot and root in maize. Specifically, we examined the effects of varying NO_3^- levels on the activity of N metabolism enzymes involved in N utilization and transport within the shoot and root sinks of the maize inbred line TX-40J. Additionally, we investigated diurnal fluctuations in NO_3^- and NH_4^+ levels in leaves, as well as their distribution across different maize tissues, such as upper and middle leaves, leaf sheaths, and roots, during vegetative and reproductive growth stages under varying N treatments. The findings of this study aim to deepen our understanding of how different N forms regulate allocation and metabolism, providing critical insights for optimizing crop production and nitrogen use efficiencies under diverse N conditions, particularly in plants grown under N deficiency.

2.2. Materials and methods

2.2.1. Plant materials and experimental site

The experiment was conducted at the Centre for Carbon Water and Food, The University of Sydney, Australia. Seeds of the fast-flowering, short-cycle inbred mini-maize line TX-40J (McCaw et al. 2016) were used in this study. This maize line offers significant advantages, including a uniform genetic background, a shorter lifecycle, and early flowering, which enable efficient and targeted research in various areas of plant biology. The traits observed in this variety serve as valuable references for breeders, facilitating the development of hybrids with enhanced performance and improved nitrogen use efficiency (Șuteu et al. 2014; Ghosh et al. 2014; McCaw and Birchler 2017; McCaw et al. 2021). The seeds were germinated in Oasis Horticube Propagation Slabs (Aqua Gardening, Brisbane, Australia) placed in germination trays. The trays were transferred to a climate-controlled growth room, set to a 14/10 day-night cycle, with temperatures of 25°C during the day and 22°C at night, and 80% relative humidity for 5 d to allow for seed germination. Once the seedlings had germinated uniformly, they were transferred to a temperature controlled glasshouse for the subsequent experiments (Amoah and Kaiser 2025).

2.2.2. Experimental treatment, set up and sampling

Seedlings were divided into three treatment groups and grown in 3 L pots, with their roots supported by inorganic expanded clay pellets (Aqua Gardening, Brisbane, Australia). Each group received a specific nitrogen (N) source: 1 mM NO_3^- (low N; LN), 2 mM NO_3^- (medium N; MN) and 10 mM NO_3^- (high N; HN). These nutrient levels were selected based on previous studies (Zhao et al. 2020; Amoah and Kaiser 2025). The seedlings were grown for 40 d, allowing data collection at both the vegetative (V6; 20 days after treatment, DAT) and reproductive (R1; 40 DAT) growth stages. The system was set up in a climate-controlled glasshouse, with conditions matching those of the growth room used for seed germination, but with supplemental LED lighting providing 1000 µmol m^{-2} s^{-1} at pot level. Each system was designed to accommodate 40 pots, with one plant per pot. Plants were drip-irrigated with the respective nutrient solution, which was circulated through a hydroponic pump system. Irrigation occurred twice daily for 1 min, at 12:00 PM and 5:00 PM.

The nutrient solution comprised the following concentrations (in mM): 1.0 $MgSO_4$, 1.0 KH_2PO_4, 0.05 H_3BO_3, 0.005 $MnSO_4$, 0.001 $ZnSO_4$, 0.001 $CuSO_4$, 0.001 Na_2MoO_4, 0.1 KCl, 0.1 Fe-EDTA, 0.1 Fe-EDDHA, 0.25 $Ca(NO_3)_2$, 0.25 K_2SO_4, 0.25 $CaCl_2$, and 1.75 $CaSO_4$ (Amoah and Kaiser 2025) and were stored in 162 L Brute Containers with lids (Rubbermaid, USA). The solution was changed weekly, with daily pH adjustments with 1 M H_2SO_4 or 1 M NaOH to maintain a stable pH of 5.9. The treatment solution was delivered to the system by an Eden 140G FL submersible water pump (Creative Pumps, Australia). Plants were uniquely identified and randomized into blocks using R statistical software (v4.4.2). Sampling was done at 20 (vegetative, V6 stage) and 40 (reproductive, R1 stage) days after seedling transfer (DAT). Fresh leaf and root tissues for biochemical analysis were

collected, immediately frozen in liquid nitrogen (N_2), and stored at -80°C. Shoot and root samples for biomass analysis were oven-dried at 70°C for 48 h to determine dry weights (DW). The shoot and root biomass values were summed to calculate the total plant biomass in grams (g DW).

2.2.3. Spatial distribution and diurnal changes determination

To examine the spatial distribution of NO_3^- and NH_4^+, the youngest emerging leaf at 20 and 40 DAT was sampled and divided into upper and middle sections. Additional samples included the corresponding leaf sheath and root. Sampling was done at 22:00 and again at 7:00 the following morning on 20 and 40 DAT. For diurnal analysis, the middle sections of the youngest fully expanded leaves were collected at 7:00, 12:00, 17:00, 22:00, and 7:00 (the next day) on 20 and 40 DAT. All samples were immediately frozen in liquid N_2 and stored at -80 °C for subsequent biochemical analysis.

2.2.4. Net photosynthetic rate and chlorophyll and nitrogen (N) measurement

The net photosynthetic rate (Pn) was measured on the young emerging leaf of each treatment using the portable LI-6400 photosynthetic system (LI-COR Inc., Lincoln, NE, USA). Measurements were taken at 9:00 AM and 11:00 AM. Cuvette conditions included a light level of 1000 µmol m^{-2} s^{-1}, CO_2 concentration of 400 ppm, flow rate of 500 µmol m^{-2} s^{-1}, and relative humidity between 60% and 65%. Chlorophyll pigment was extracted from approximately 0.1 g of leaf tissue using 100% methanol on a shaker at 25°C until the tissue was completely bleached (Amoah and Seo 2021). The extract was then centrifuged at 10,000 × *g* for 10 min, and the absorbance of the supernatant was measured at 646, 470, and 663 nm using a UV-vis spectrophotometer (Shimadzu, Tokyo, Japan). The concentration of chlorophyll was calculated following the method described by (Amoah and Adu-Gyamfi 2024).

N content was determined using the Kjeldahl method as described by (Amoah and Kaiser 2025), with minor modifications. A 0.2 g dry sample was digested with 0.5 mL of concentrated H_2SO_4 and 0.5 mL of a catalyst mixture consisting of 10 g of K_2SO_4 and 1 g of $CuSO_4$. The mixture was heated at 100°C for 60 min on a heating block in a fume hood. After digestion, the samples were allowed to cool, and 0.5 mL of 40% NaOH solution was slowly added, followed by 0.5 mL of distilled water. Subsequently, 1 mL of the resulting mixture was combined with 1 mL of Nessler's reagent and incubated for 10 min at room temperature. The absorbance was measured at 420 nm using a UV-vis spectrophotometer (Shimadzu, Tokyo, Japan). Nitrogen content was determined from a standard curve generated with $(NH_4)_2SO_4$ standards.

2.2.5. Sucrose and starch content determination

Soluble sugar and sucrose content were measured as described by Amoah and Adu-Gyamfi (2024). Briefly, 100 mg of ground samples were homogenized in 1 mL of 80% (v/v) ethanol, and the mixture was heated at 80°C for 30 min. After cooling for 5 min, the mixture was centrifuged at 12,000 × *g* for 10 min. The supernatants were collected, and soluble sugar and sucrose contents were determined by measuring absorbance at 620 nm and 480 nm, respectively, using a spectrophotometer UV-vis spectrophotometer (Shimadzu, Tokyo, Japan). The ethanol-insoluble residue was used for starch extraction following the procedure outlined by Amoah et al. (2024). After evaporating the ethanol, 2 mL of distilled water was added to the samples, which were then incubated at 100°C for 15 min. Starch was hydrolysed using separate treatments of 9.2 M $HClO_4$. The starch content was quantified spectrophotometrically using the anthrone reagent, and absorbance was measured at 620 nm.

2.2.6. Total amino acid and protein quantification

Total amino acids content was determined using the methods outlined by Bates et al. (1973). Frozen leaf tissues (100 mg) were homogenized in 10 mL of 3% (v/v) aqueous sulfosalicylic acid. After filtering the homogenate, 1 mL of filtrate was combined with 1 mL of glacial acetic acid and 1 mL of acidic ninhydrin. The resulting mixture was incubated at 100°C for 1 h and then cooled on ice for 20 min before being extracted with 1 mL of toluene. The concentrations of amino acids were measured using a spectrophotometer at A580 nm. Leaf and root total protein contents were extracted from 100 mg of fresh material in 1 mL chilled extraction buffer [50 mM HEPES pH 7.5, 20% glycerol, 1 mM EDTA, 1 mM EGTA, 0.1% Triton X-100, 1 mM Benzamidine, 1 mM 6-Aminohexanoic acid and 1% Protease Inhibitor Cocktail (Sigma-Aldrich cat#P9599)]. After centrifugation, the clean supernatant was used to test the enzyme activities.

2.2.7. Nitrate (NO_3^-), nitrite (NO_2^-) and ammonium (NH_4^+) determination

NO_3^-, NO_2^- and NH_4^+ were extracted from 100 mg of dried plant material using 1 mL of water. NO_3^- content was quantified using a colorimetric method based on the reduction of NO_3^- to NO_2^- by Vanadium (III), as adapted from (Miranda et al. 2001). NO_2^- contents were detected using the Griess assay (Dechorgnat et al. 2018). NH_4^+ levels were measured using the 'Ammonium Assay Kit' from Sigma-Aldrich (St. Louis, MO, USA, cat#AA0100), in accordance with the manufacturer's instruction.

2.2.8. Nitrate reductase (NR), nitrite reductase (NiR), glutamine synthase (GS) and glutamate synthase (GOGAT) activities assay

NR activity was evaluated using the method described by Baki et al. (2000), with 300 mg of fresh plant material extracted in 1 mL of extraction buffer. Proteins were extracted from 200 mg of fresh material using 1 mL of chilled extraction buffer, which included 50 mM HEPES (pH 7.5), 20% (v/v) glycerol, 1 mM EDTA, 1 mM EGTA, 0.1% (v/v) Triton X-100, 1 mM benzamidine, 1 mM 6-aminohexanoic acid, and 1% Protease Inhibitor Cocktail (Sigma-Aldrich, cat#P9599). After centrifugation, the resulting clear supernatant was used for enzyme activity assays. Nitrite reductase (NiR) activity was measured by mixing 10 µL of extracted protein solution with 90 µL of reaction buffer containing 130 mM K_2HPO_4, 70 mM KH_2PO_4, 0.5 mM KNO_2, and 2 mM methyl viologen. To initiate the reaction, 10 µL of a sodium-based solution (20 mg/mL Na_2CO_3 and $Na_2S_2O_4$) was added. The reaction mixture was incubated at 30°C for 15 min, after which the reaction was terminated by vortexing. Nitrite content was subsequently quantified using the Griess assay (Dechorgnat et al. 2018). GS and GOGAT activities were quantified by mixing 20 µL of extracted protein with 80 µL of a reaction buffer containing 100 mM hydroxylamine, 125 mM MOPS, 0.5 mM ADP, 12.5 mM sodium arsenate, 37.5 mM glutamine, and 1.25 mM $MnCl_2$. The reaction was allowed to proceed for 30 min at room temperature. Subsequently, 100 µL of detection buffer, which included 370 mM $FeCl_3$, 576 mM HCl, and 157 mM TCA, was added to the mixture. The optical density was then measured at 540 nm. L-glutamic acid γ-monohydroxymate (GHA) was used as the reference standard.

2.2.9 RNA isolation, cDNA synthesis and qPCR analysis

Total RNA was isolated from leaf and root tissues using the Trizol RNA Isolation Reagents (Invitrogen, Carlsbad, CA, USA) following the manufacturer's protocol. RNA quantity and integrity were assessed by measuring the optical density at 260 nm and through 1.0% (w/v) agarose gel electrophoresis, respectively. Subsequently, 1 µg of total RNA was reverse-transcribed into single-stranded cDNA using the iScript™ RT Reagent Kit (Bio-Rad, Hercules, CA, USA) according to the manufacturer's instructions. Quantitative real-time polymerase chain reaction (qPCR) was performed using the CFX 96 Real-Time System (Bio-Rad, Richmond, CA, USA) with SYBR Green fluorescence (Bio-Rad, Richmond, CA, USA). The $^{\Delta\Delta}$CT method was used for data analysis. The list of genes studied are provided in Table S2.1. The thermal cycling conditions consisted of an initial denaturation step at 95 °C for 5 min, followed by 40 cycles of 95 °C for 15 s, 55 °C for 15 s, and 72 °C for 30 s. All experiments were conducted with three biological replicates, and relative transcript levels were normalized using *ZmActin1* and *ZmUBQ1* as internal controls.

2.2.10. Statistical analysis

The study was repeated twice, with tissue samples collected in triplicate. Data were analysed using a two-way analysis of variance (ANOVA) with Tukey's multiple comparison test in R statistical software (v4.4.2). Growth stage (S) and N treatments were considered fixed and variable factors, respectively. Results are presented as the mean ± standard error (SE) of six independent plants (n=6). Different letters on the error bars indicate statistically significant differences at a probability level of $p \leq 0.05$. Graphical charts were made with GraphPad Prism (v10.4.0). Pearson's correlation plots were made with the R statistical software (v4.4.2).

2.3. Results

2.3.1. Biomass accumulation and N content under different N forms

LN treatment led to a significant reduction ($P \leq 0.05$) in shoot biomass, which in turn affected the overall total biomass (Fig. 2.1A-B). The concentrations of total protein, amino acids, NO_3^-, and NO_2^- were markedly lower in the LN-treated plants, resulting in a reduced total N content (Fig. 2.1C-F). Interestingly, the LN-treated plants demonstrated a higher NH_4^+ content compared to other treatments (Fig. 2.1G). Furthermore, LN treatment significantly ($P \leq 0.05$) increased root biomass, leading to an enhanced R/S ratio relative to other treatments (Fig. 2.2A-B). In contrast, the total protein, amino acids, NO_3^-, and NO_2^-, and overall N content decreased significantly ($P \leq 0.05$) under LN treatment (Fig. 2.2C-G), whereas NH_4^+ concentrations were significantly elevated in the LN-treated plants (Fig. 2.2H).

2.3.2. N metabolism enzyme activities under different N forms

The activities of N metabolism enzymes, including NR, NiR, GS, and GOGAT, were differentially regulated in plants under varying N treatment conditions. In the leaf, LN treatment significantly ($P \leq 0.05$) reduced NR and NiR activities while increasing ($P \leq 0.05$) GS and GOGAT activities (Figs.2.3A, C, E, and G). Similarly, in the roots, LN treatment significantly ($P \leq 0.05$) decreased NR and NiR activities but enhanced GS and GOGAT activities after 20 and 40 d of N treatment (Figs. 2.3B, D, F, and H).

2.3.3. Expression pattern of N metabolism-related transcripts

To understand the molecular mechanisms associated with N metabolism under different N forms, the expression levels of N metabolism-related genes, *ZmNR1*, *ZmNiR1*, *ZmGS1*, and *ZmGOGAT1*, were analysed in the leaves and roots of plants subjected to LN, MN, and HN treatment conditions. As shown in Fig. 4, the transcripts related to N metabolism were differentially ($P \leq 0.05$) regulated in both leaves

and roots under these treatments. For instance, the NO_3^- and NO_2^- metabolism-related transcripts, *ZmNR1* and *ZmNiR1*, were significantly ($P \leq 0.05$) downregulated in the leaves (Fig. 2.4A and C) and roots (Fig. 2.4B and D). In contrast, the NH_4^+ metabolism-related transcripts, *ZmGS1* and *ZmGOGAT1*, were significantly ($P \leq 0.05$) upregulated in the leaves (Fig. 2.4E and H) and roots of plants under LN treatment compared to plants under increasing N treatments (Fig. 2.4F and I). Additionally, the expression patterns of NO_3^- and NH_4^+ transporter genes were examined in the leaves and roots under different N treatments. LN treatment significantly ($P \leq 0.05$) upregulated the expression levels of *ZmNPF6.2*, *ZmNRT2.1*, *ZmNRT3.1*, *ZmAMT1.1*, and *ZmAMT2.1* in both the leaves (Figs. 2.5A, C, E, G, and I) and roots (Figs. 2.5B, D, F, H, and J) of maize seedlings. Notably, the fold expression of these genes was relatively ($P \leq 0.05$) higher in the roots of plants under LN treatment compared to their leaves (Fig. 2.5).

2.3.4. Analysis of variance of growth, N metabolism and transporter gene expression in maize under different N treatments

Analysis of variance (ANOVA) was conducted to identify patterns, variabilities, and relationships among plant growth stage (PGS), N treatment (NT), and their interaction (PGS × NT). In the leaves, PGS significantly ($P \leq 0.05$) influenced shoot biomass, total biomass, total protein, amino acids, NO_3^-, NO_2^-, NH_4^+, NiR, GOGAT, and the expression levels of *ZmNR1*, *ZmNiR1*, and *ZmNRT2.1*. NT significantly affected all measured indicators, while PGS × NT had no significant impact on any of these indicators. In the roots, PGS significantly influenced root biomass, total biomass, total protein, amino acids, NO_3^-, NO_2^-, N, GS, GOGAT, and the expression levels of *ZmNR1*, *ZmGS1*, *ZmNRT2.1*, and *ZmNRT3.1*. NT significantly affected all indicators as well. However, PGS × T significantly impacted NO_3^- concentration and *ZmNRT3.1* expression (Table 2.1).

2.3.5. Correlations between physio-biochemical and molecular indicators analysed

Analysis of variance (ANOVA) was conducted to identify patterns, variabilities, and relationships among plant growth stage (PGS), N treatment (NT), and their interaction (PGS × NT). In the leaves, PGS significantly ($P \leq 0.05$) influenced shoot biomass, total biomass, total protein, amino acids, NO_3^-, NO_2^-, NH_4^+, NiR, GOGAT, and the expression levels of *ZmNR1*, *ZmNiR1*, and *ZmNRT2.1*. NT significantly affected all measured indicators, while PGS × NT had no significant impact on any of these indicators. In the roots, PGS significantly influenced root biomass, total biomass, total protein, amino acids, NO_3^-, NO_2^-, N, GS, GOGAT, and the expression levels of *ZmNR1*, *ZmGS1*, *ZmNRT2.1*, and *ZmNRT3.1*. NT significantly affected all indicators as well. However, PGS × T significantly impacted NO_3^- concentration and *ZmNRT3.1* expression (Table 2.1).

2.3.6. Diurnal changes of NO_3^- and NH_4^+ under different forms

LN-treated plants consistently exhibited decreased ($P \leq 0.05$) NO_3^- concentrations and increased ($P \leq 0.05$) NH_4^+ concentrations throughout the day. The levels of NO_3^- and NH_4^+ were significantly ($P \leq 0.05$) different from those observed in other treatment groups at both sampling stages (Fig. 2.7). The diurnal pattern of NO_3^- levels showed a peak in the early morning (7:00 AM), followed by a decline at 12:00 PM, and a rapid increase after 5:00 PM, lasting until the following morning (7:00 AM) (Figs. 2.7A-C). Conversely, NH_4^+ levels were lowest in the morning (7:00 AM), increased after 12:00 PM, peaked at 10:00 PM, and declined again by 7:00 AM the next day (Figs. 2.7B-D). Notably, these diurnal patterns for NO_3^- and NH_4^+ were consistent across both 20 and 40 DAT (Figs. 2.7A-D). At 20 DAT, significant differences ($P \leq 0.05$) in NO_3^- and NH_4^+ levels were recorded among the treatment groups, with LN-treated plants consistently demonstrating lower NO_3^- but higher NH_4^+ concentrations throughout the day. These levels exhibited distinct daily rhythms: NO_3^- concentrations initially rose after 7:00 AM, declined at 12:00 PM, and increased again by the next morning. Similarly, NH_4^+ levels rose after 12:00 PM, peaked at 10:00 PM, and declined by 7:00 AM the next day. Furthermore, after overnight transport, LN-treated plants retained significantly lower NO_3^- but higher NH_4^+ concentrations compared to plants in other treatment groups (Fig. 2.7).

2.3.7. Spatial distribution of NO_3^- and NH_4^+ under different forms

The spatial distribution of NO_3^- and NH_4^+ across different parts of the maize plant, including the upper, middle, and basal leaves, the leaf sheath, and the roots, was analysed. LN-treated plants exhibited significantly ($P \leq 0.05$) lower NO_3^- but higher NH_4^+ contents across various maize tissues compared to other treatment groups. Specifically, at 22:00, the upper, middle, and basal leaves, as well as the leaf sheath, displayed elevated NH_4^+ levels. In contrast, plants under HN treatment showed increased ($P \leq 0.05$) NO_3^- accumulation by the end of the day (Fig. 2.8A). By 07:00 the next morning, LN-treated plants retained lower residual NO_3^- levels in the upper and basal leaves and the leaf sheath, with concentrations comparable to those recorded at 22:00 (Fig. 2.8A–C). Conversely, LN-treated plants accumulated higher NH_4^+ levels in the leaves by 22:00 and retained elevated NH_4^+ concentrations following overnight remobilization. NH_4^+ content in the roots (sink tissues) was relatively higher and exhibited significant ($P \leq 0.05$) variation among treatment groups at both 22:00 and 07:00 (Fig. 28B–D).

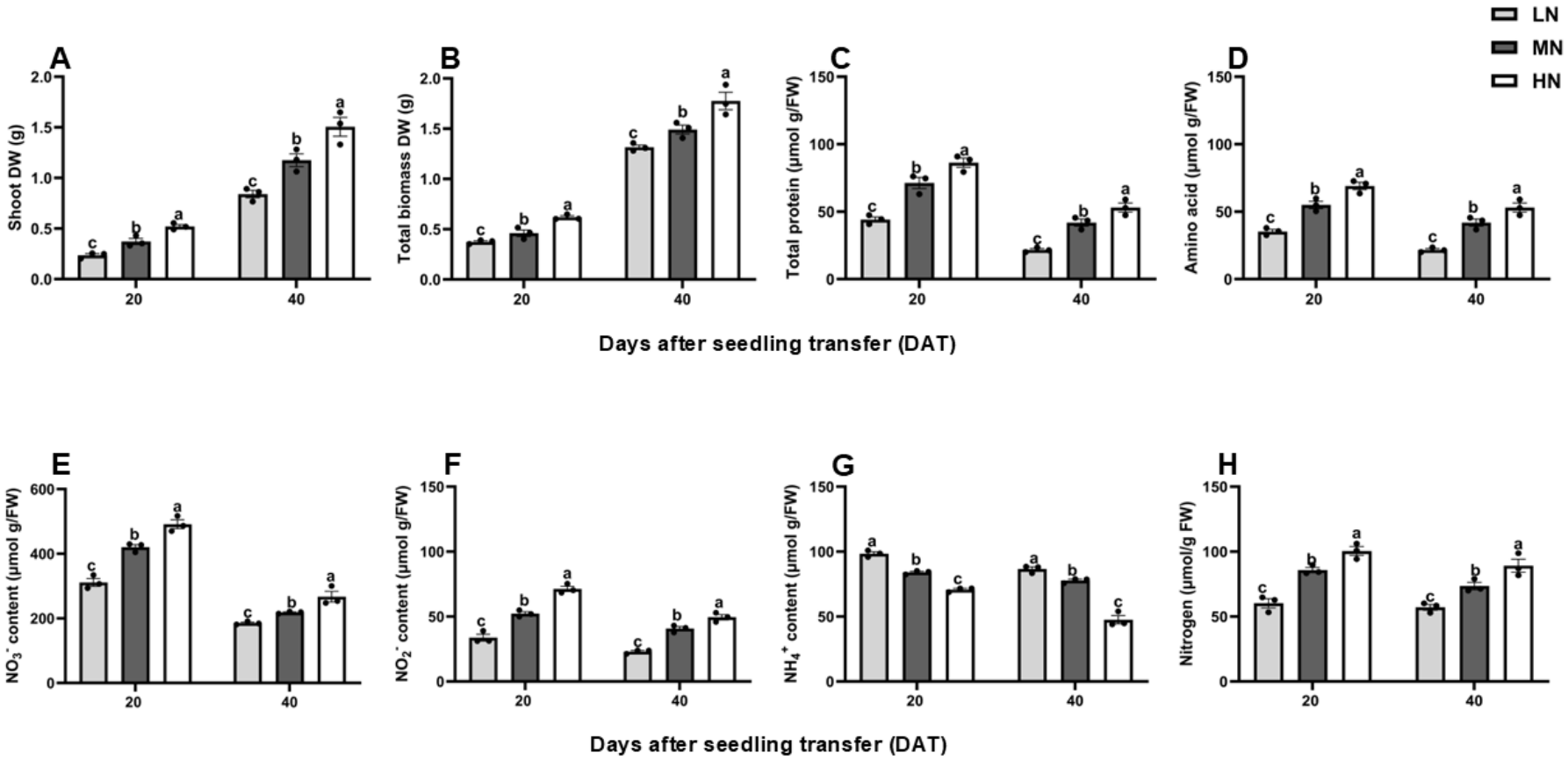

Fig. 2.1 Shoot biomass (**A**), total biomass (**B**), leaf total protein (**C**), leaf amino acid content (**D**), leaf nitrate (**E**), leaf nitrite (**F**), leaf ammonium (**G**), and leaf total nitrogen content (**H**) in maize inbred line TX-40J were measured under varying nitrogen treatments. Data are expressed as mean ± standard deviation (n = 6). Statistical significance was analysed using Tukey's multiple range test ($P < 0.05$), with different letters denoting significant differences among treatments. FW and DW represent fresh and dry weights, respectively; LN indicates low nitrogen (N deficiency), MN represents moderate nitrogen, and HN denotes high nitrogen

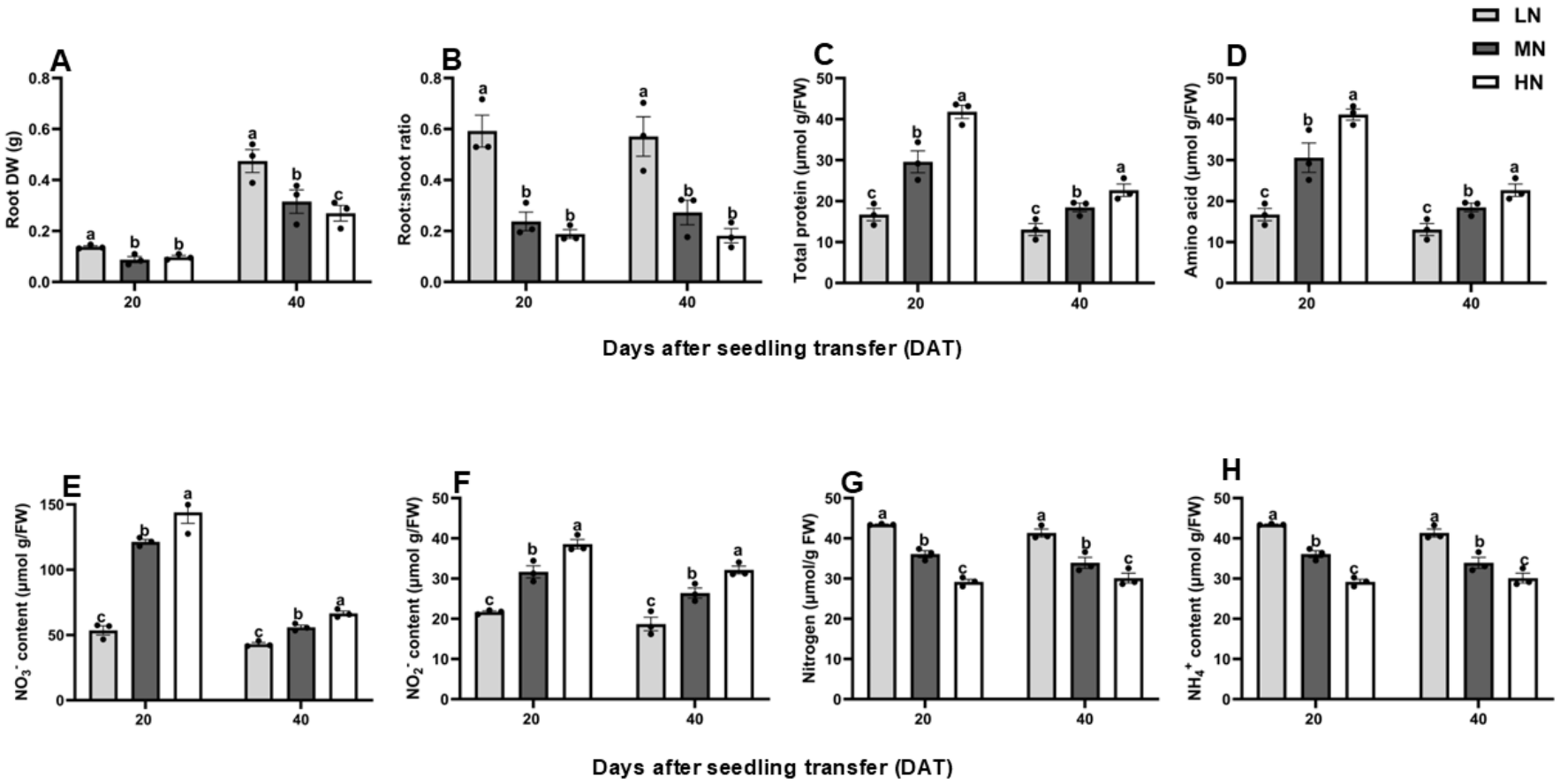

Fig. 2.2 Root biomass (**A**), root/shoot ratio (**B**), root total protein (**C**), root amino acid content (**D**), root nitrate (**E**), root nitrite (**F**), root ammonium (**G**), and root total nitrogen content (**H**) in maize inbred line TX-40J were measured under varying nitrogen treatments. Data are expressed as mean ± standard deviation (n = 6). Statistical significance was analysed using Tukey's multiple range test ($P < 0.05$), with different letters denoting significant differences among treatments. FW and DW represent fresh and dry weights, respectively; LN indicates low nitrogen (N deficiency), MN represents moderate nitrogen, and HN denotes high nitrogen.

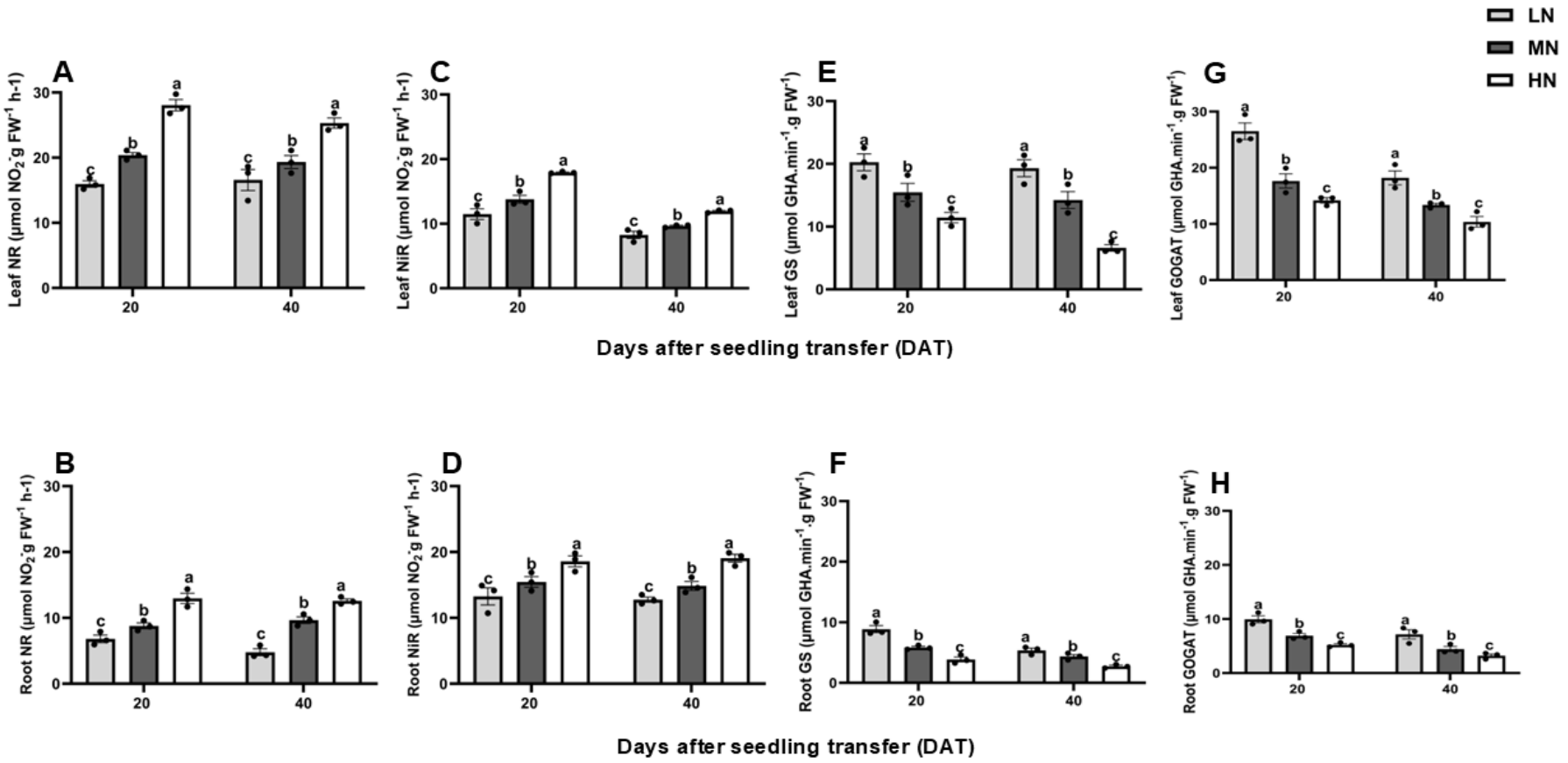

Fig. 2.3 Leaf nitrate reductase (**A**), nitrite reductase (**C**), glutamine synthetase (**E**), glutamate synthase (**G**), and root nitrate reductase (**B**), nitrite reductase (**D**), glutamine synthetase (**F**), and glutamate synthase (**H**) activities were measured in maize inbred line TX-40J under different nitrogen treatments. Data are presented as mean ± standard deviation (n = 6). Statistical significance was determined using Tukey's multiple range test ($P < 0.05$), with distinct letters indicating significant differences among treatments. FW denotes fresh weights; LN corresponds to low nitrogen (N deficiency), MN to moderate nitrogen, and HN to high nitrogen.

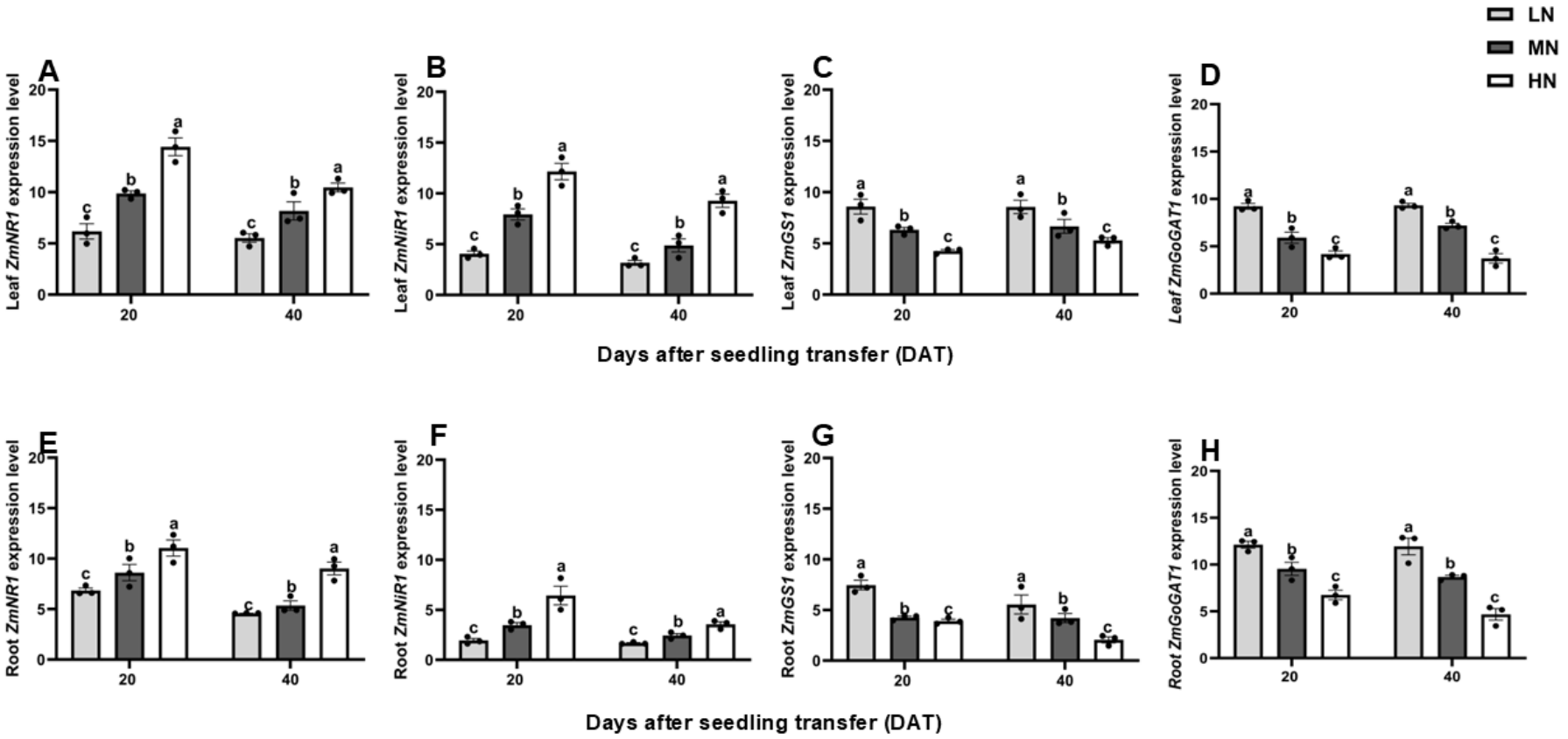

Fig. 2. 4 Relative expression of nitrogen metabolism-related genes in maize inbred line TX-40J under different nitrogen treatments. Expression levels of *ZmNR1* (**A**), *ZmNiR1* (**C**), *ZmGS1* (**E**), *ZmGOGAT1* (**H**) in the leaves, and *ZmNR1* (**B**), *ZmNiR1* (**D**), *ZmGS1* (**F**), *ZmGOGAT1* (**I**) in roots. Data are presented as mean ± standard deviation (n = 6). Statistical significance was determined using Tukey's multiple range test ($P < 0.05$), with distinct letters indicating significant differences among treatments. LN corresponds to low nitrogen (N deficiency), MN to moderate nitrogen, and HN to high nitrogen.

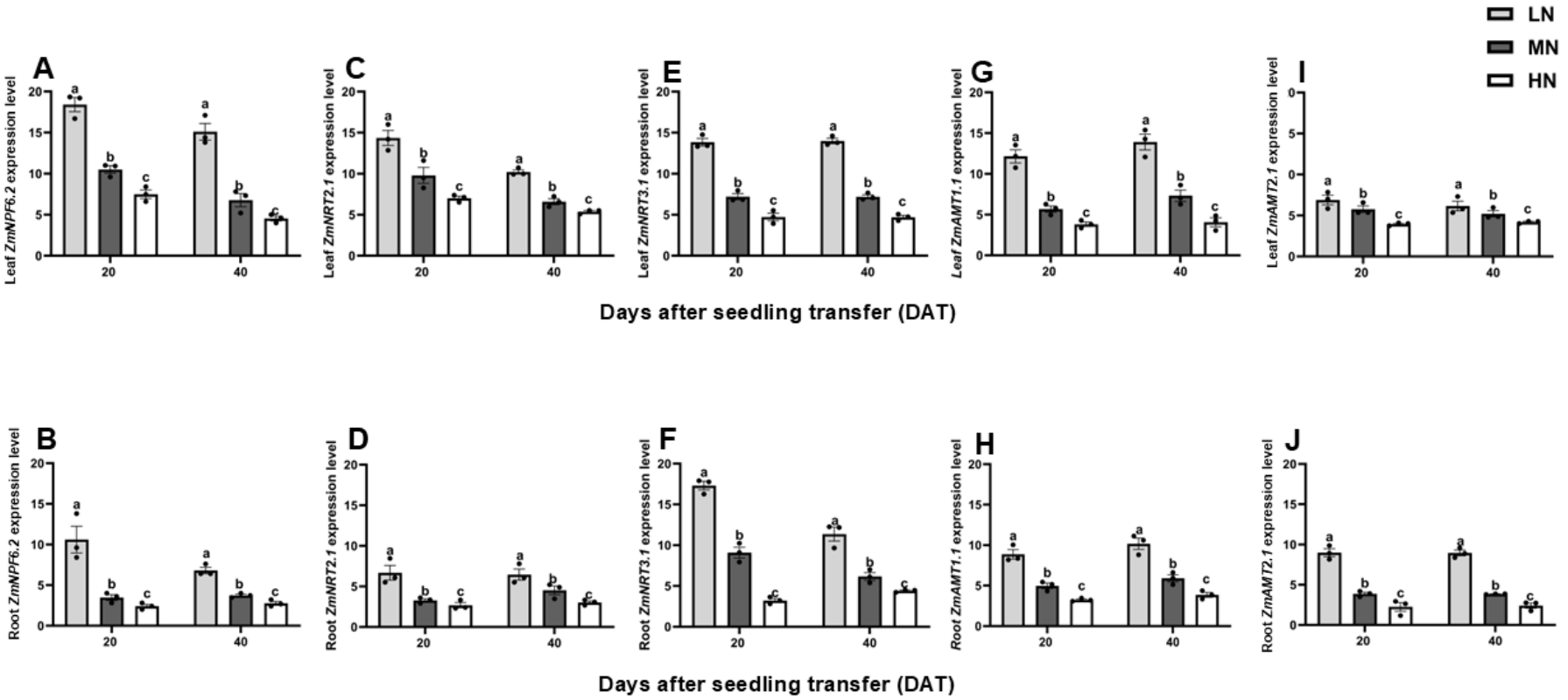

Fig. 2.5 Relative expression of nitrate and ammonium transporter genes in maize inbred line TX-40J under different nitrogen treatments. Expression levels of *ZmNPF6.2* (**A**), *ZmNRT2.1* (**C**), *ZmNRT3.1* (**E**), *ZmAMT1.1* (**G**) and *ZmAMT2.1* (**I**) in the leaves, and *ZmNPF6.2* (**B**), *ZmNRT2.1* (**D**), *ZmNRT3.1* (**F**), *ZmAMT1.1* (**H**) and *ZmAMT2.1* (**J**) in the roots. Data are presented as mean ± standard deviation (n = 6). Statistical significance was determined using Tukey's multiple range test ($P < 0.05$), with distinct letters indicating significant differences among treatments. LN corresponds to low nitrogen (N deficiency), MN to moderate nitrogen, and HN to high nitrogen.

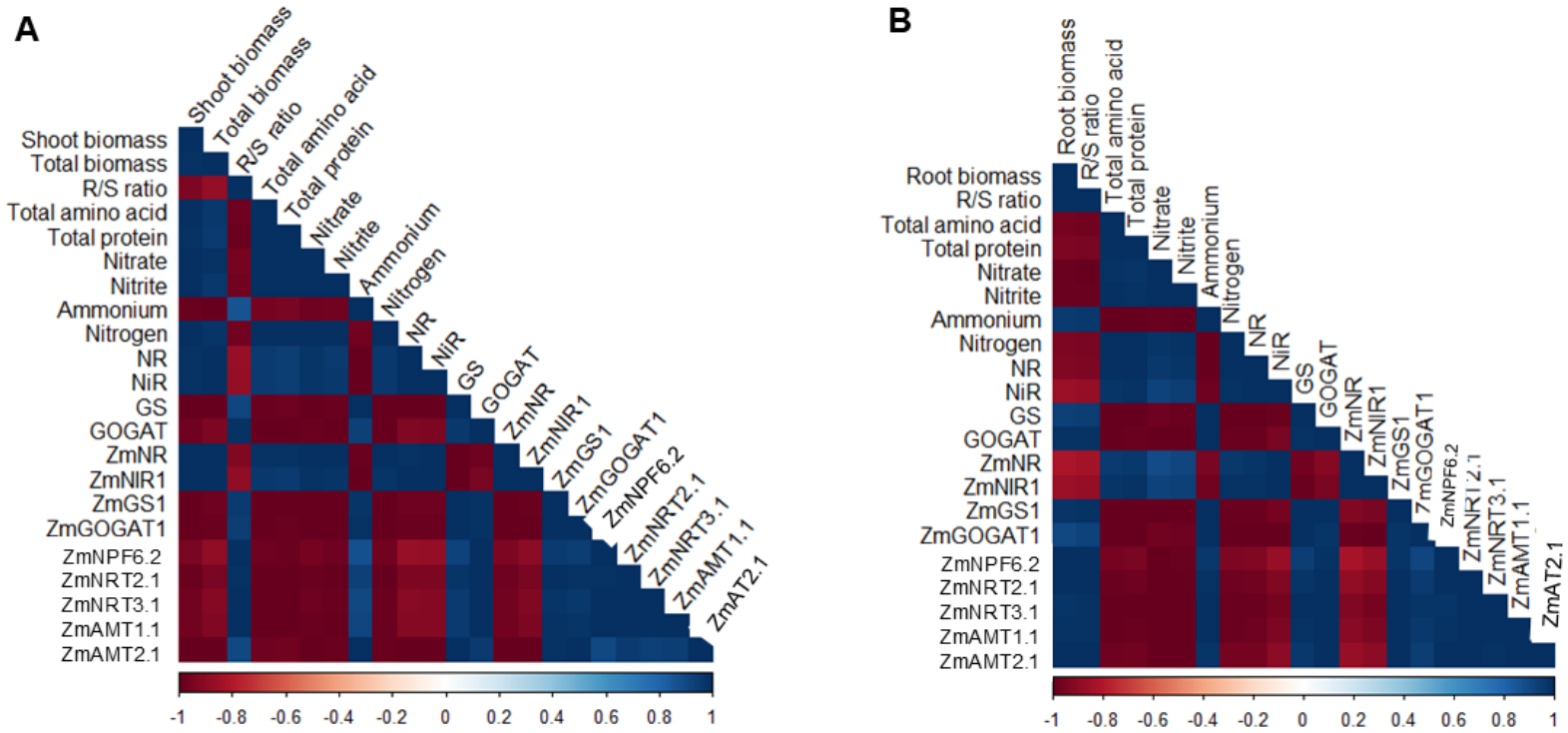

Fig. 2.6. Pearson's correlation plot between physio-biochemical and molecular indicators under different NO_3^- levels in maize leaves (**A**) and roots (**B**). The plot was constructed using mean values at 20 and 40 days after seedling transfer (DAT). NR/*ZmNR1*: nitrate reductase, NiR/*ZmNiR1*: nitrite reductase, GS/*ZmGS1*: glutamine synthase, GOGAT/*ZmGOAT1*: glutamate synthase, *ZmNPF6.2*/*ZmNRT2.1*/*ZmNRT3.1*: nitrate transporter genes and *ZmAMT1.1*/*ZmAMT2.1*: ammonium transporter genes

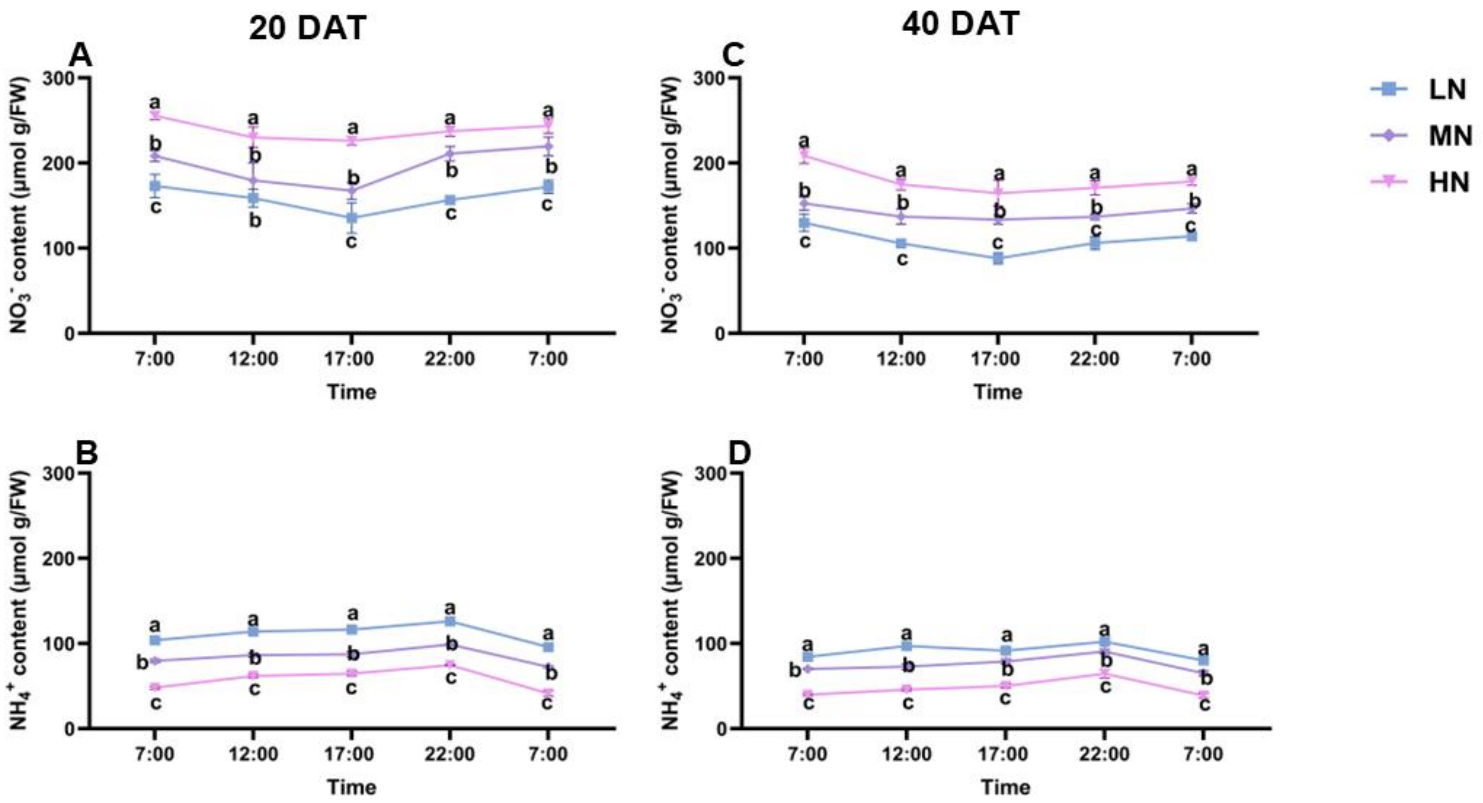

Fig. 2.7 Diurnal changes in leaf NO_3^- (**A**) and NH_4^+ (**B**) at 20 days after transfer (DAT) and leaf sucrose NO_3^- (**C**) and NH_4^+ (**D**) at 40 DAT under different nitrogen treatments. Samples were collected at 7:00, 12:00, 17:00, 22:00, and 7:00 on the second day. Data are presented as mean ± standard deviation (n = 6). Statistical significance was determined using Tukey's multiple range test ($P < 0.05$), with different letters indicating significant differences among treatments. FW denotes fresh weight of tissue samples. LN: low nitrogen (N deficiency), MN: moderate nitrogen and HN: high nitrogen treatment.

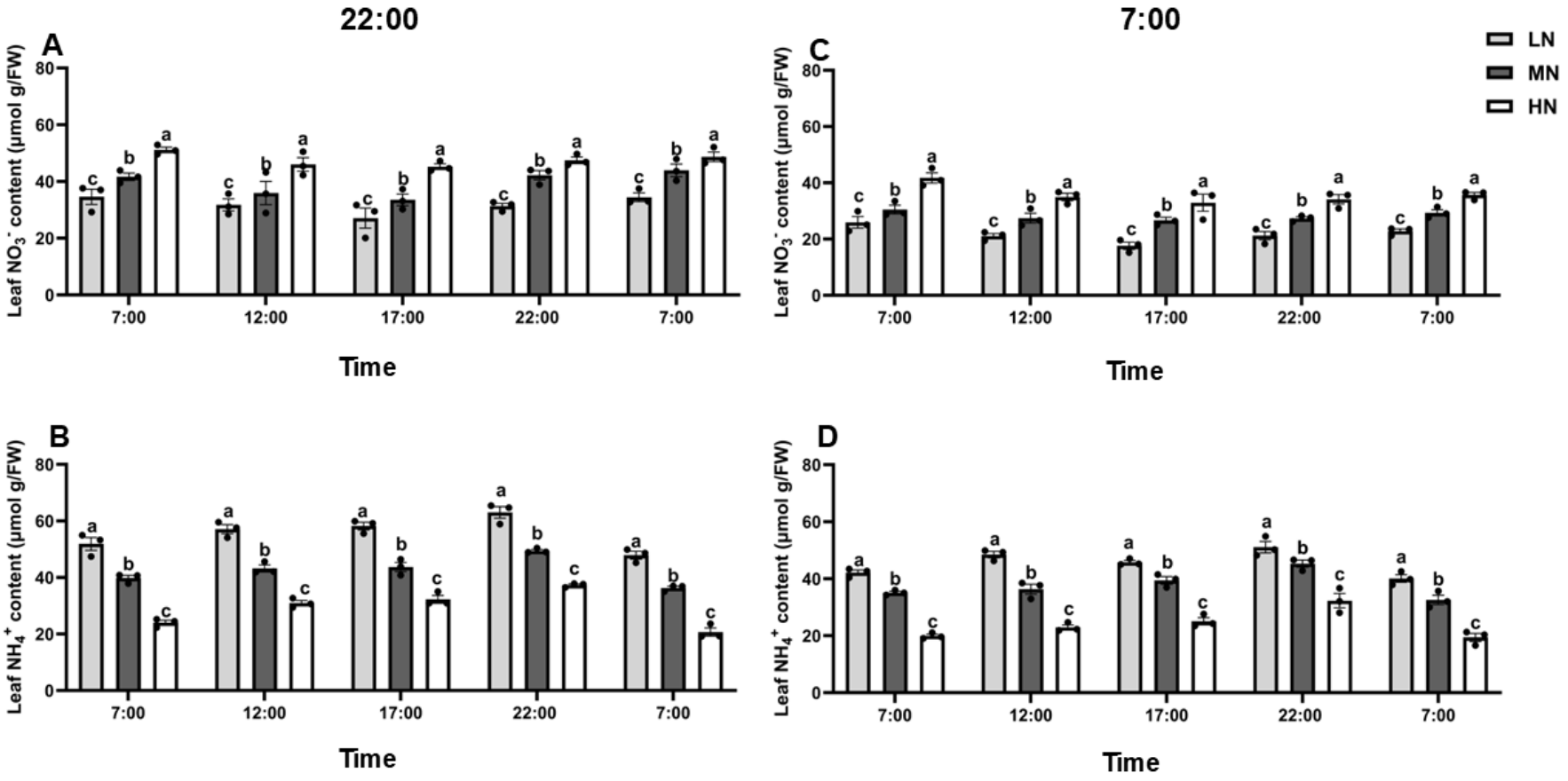

Fig. 2.8 Leaf NO_3^- (**A**) and NH_4^+ (**B**) at 20 DAT and leaf NO_3^- (**C**) and NH_4^+ (**D**) at 40 DAT in different tissues under various nitrogen form treatments. Data are presented as mean ± standard deviation (n = 6). Statistical significance was determined using Tukey's multiple range test ($P < 0.05$), with different letters indicating significant differences among treatments. FW denotes fresh weight of tissue samples. LN: low nitrogen (N deficiency), MN: moderate nitrogen and HN: high nitrogen treatment.

Table 2.1: Two-way analysis of variance (ANOVA) of physio-biochemical and molecular indicator studied in the leaves and root of maize.

Traits/(plants)	**Sources of variation**					
	Shoot/leaf			**Root**		
	Growth stage (S) (df=1)	**Treatment (T) (df=2)**	**S x T (df=2)**	**Growth stage (S) (df=1)**	**Treatment (T) (df=2)**	**S x T (df=2)**
Biomass	0.0058**	0.012*	0.079ns	0.0041**	0.0466*	0.2018ns
Total biomass	0.002**	0.0126*	0.2306ns	0.9705ns	0.0168*	0.7566ns
Total protein	0.0117*	0.0065**	0.3745ns	0.0248*	0.0073**	0.0675ns
Total amino acids	0.0238*	0.0006***	0.7791ns	0.0273*	0.0191*	0.1027ns
NO_3^-	0.0016**	0.0065**	0.0538ns	0.0039***	0.0074***	0.0177*
NO_2^-	0.0281*	0.001***	0.0953ns	0.0351*	0.0021**	0.6133ns
NH_4^+	0.0009***	0.0077**	0.0689ns	0.2171ns	0.0078**	0.1965ns
Nitrogen	0.0946ns	0.0092**	0.2832ns	0.0125*	0.0172*	0.2421ns
NR	0.2832ns	0.0035**	0.2967ns	0.1702ns	0.0099**	0.2125ns
NiR	0.019*	0.0015**	0.179ns	0.8014ns	0.005**	0.7486ns
GS	0.2055ns	0.0021**	0.3247ns	0.0231*	0.0022**	0.1724ns
GOGAT	0.0122*	0.0076**	0.0612ns	0.0114*	0.0018**	0.7875ns
ZmNR1	0.0176*	0.0066**	0.0807ns	0.0336*	0.0334*	0.5833ns
ZmNIR1	0.0398*	0.0043**	0.2928ns	0.0541ns	0.0123*	0.0808ns
ZmGS1	0.4518ns	0.0071**	0.6038ns	0.0069**	0.0175*	0.3238ns
ZmGOGAT1	0.1419ns	0.0032**	0.2498ns	0.2418ns	0.0122*	0.3035ns
ZmNPF6.2	0.053ns	0.0048**	0.2546ns	0.1895ns	0.0171*	0.1864ns
ZmNRT2.1	0.0498*	0.0057**	0.259ns	0.0057**	0.0408*	0.2294ns
ZmNRT3.1	0.8836ns	0.0037**	0.8347ns	0.007**	0.0018**	0.0043**
ZmAMT1.1	0.2565ns	0.0005***	0.4689ns	0.1579ns	0.0008***	0.7335ns
ZmAMT2.1	0.4543ns	0.0197*	0.5446ns	0.9493ns	0.0035**	0.9296ns

NR/*ZmNR1*: denotes nitrate reductase activity, NIR/*ZmNiR*: nitrite reductase activity, GS/*ZmGS1*: glutamine synthase activity, GOGAT/*ZmGOGAT1*/: glutamate synthase activity, *ZmNPF6.2*/ *ZmNRT2.1*/ *ZmNRT3.1*: nitrate transporter genes and *ZmAMT1.1*/*ZmAMT2.1*: ammonium transporter genes. ***, **, *, ns denotes significance at 0.001, 0.01, 0.05 and non-significance, respectively.

2.4. Discussion

2.4.1. LN severely inhibits shoot growth while promoting root growth, thereby increasing the root-to-shoot ratio

The mechanism underlying assimilate allocation that supports a higher root-to-shoot (R/S) ratio under LN conditions is not well understood. In this study, shoot growth was significantly inhibited, while root growth was enhanced after 40 days of LN treatment. As a result, the R/S ratio increased markedly (Figs. 2.1A and 2.2A–B). These findings suggest that roots received a relatively greater share of N despite its limited availability under LN treatment, consistent with previous reports (Zhao et al. 2020; Amoah and Kaiser 2025). This allocation pattern reflects an adaptive strategy employed by plants to enhance N uptake efficiency under N-deficient conditions. Furthermore, N is a vital component of chlorophyll (Qiang et al. 2019). In LN-treated plants, reduced N availability led to a significant decline in chlorophyll synthesis (Fig. S2.1A), impairing the plant's ability to capture light energy and fix CO_2 efficiently (Fig. S2.1B and Fig. S2.2A-D) (Evans and Clarke 2019). Consequently, the reduced photosynthetic output indicates a decrease in photosynthate production, thereby limiting the energy available for overall plant growth, particularly shoot biomass accumulation (Mengesha 2021; Mu and Chen 2021). These findings support previous observations on how LN conditions influence plant growth patterns, emphasizing the critical role of sufficient N availability in modulating root-shoot dynamics and overall productivity.

2.4.2. LN significantly inhibited protein and amino acid synthesis, leading to a decreased total plant biomass and N content

Sufficient N significantly influences amino acid and protein synthesis and regulation in plants, ensuring efficient physiological function and growth (Batista-Silva et al. 2019; Heinemann and Hildebrandt 2021). Previous studies have demonstrated that higher NO_3^- levels enhance the accumulation of amino acids, proteins, and total N content in plants (Garnett et al. 2013; George et al. 2016; Zhao et al. 2020). This aligns with the present study, where plants under HN treatment exhibited increased amino acid, protein, and total N accumulation, along with enhanced growth (Fig. 2.1A–B). These findings underscore the vital role of adequate N supply in optimizing N metabolism, which supports key physiological and biochemical processes, ultimately promoting plant growth and productivity. In contrast, LN treatment caused a significant reduction in amino acid, protein, and total N content (Fig. 2.1C, D, and H). These deficiencies inhibited shoot growth and led to reduced total biomass (Fig. 2.1B), highlighting the importance of sufficient N availability. Furthermore, a negative correlation was observed between the R/S ratio and total protein, amino acid, and N content (Fig. 2.6A–B). This suggests that LN-treated plants experienced a substantial decline in amino acid and protein synthesis while allocating more resources to root development (Figs. 2.2A–B) (Zhao et al. 2020; Liu et al. 2020).

This negative correlation reflects a physiological trade-off, where plants can prioritize N acquisition through root expansion at the expense of protein and amino acid biosynthesis (Andrews et al. 2001). Although this adaptive response may support survival under N deficiency, it can negatively impact plant growth and productivity as well as effective nitrogen use efficiencies (Figueroa-Bustos et al. 2018; Xu et al. 2015).

2.4.3. LN impaired NO_3^- assimilation but upregulated the expression of NO_3^- transporter genes

NO_3^- is a vital form of N that is highly accessible to plants, serving as a key nutrient to support their growth, development, and metabolic functions (Hachiya and Sakakibara 2017). Previous studies have shown that NO_3^- availability strongly influences its uptake and regulation within plants (Kiba and Krapp 2016; Wen et al. 2019). In this study, LN treatment significantly reduced NO_3^- content, which, in turn, led to a reduction in NO_2^- content across various growth stages compared to MN or HN treatments (Figs. 2.1 and 2.2E-F). The trends in NO_3^- and NO_2^- content was closely associated with their corresponding enzyme activities, namely NR and NiR involved in the coupled regulatory process of reducing NO_3^- to NH_4^+, a critical step in N assimilation (Peng et al. 2023) (Figs. 2.3A-D). NR activity is induced by NO_3^-, and its activity is primarily dependent on NO_3^- (Carillo et al. 2005; Kovács et al. 2015). In this study, LN treatment significantly reduced NR and NiR activities (Figs. 2.3A-D), and decreased tissue NO_3^- and NO_2^- content (Fig. 2.6A-B). These findings are consistent with previous studies showing that the activity of N-related isozymes and their associated gene expression levels are closely linked to available NO_3^- concentrations (Wen et al. 2019; Peng et al. 2023a; Dechorgnat et al. 2018). Under LN conditions, NR and NiR activities were reduced by 10% and 15% in the leaves and by 42% and 13% in the roots, respectively, after 40 d of treatment (Figs. 2.3A-D). Furthermore, the relative expression levels of *ZmNR1* and *ZmNiR1*, which encode NR and NiR, decreased significantly by 1.9 and 1.7 fold in the leaves, respectively and by 1.1 fold and 1.98 fold in the roots, respectively, after 40 d of treatment (Fig. 2.4A-D). The NO_3^- and NO_2^- content, NR and NiR activities, and the expression of *ZmNR1* and *ZmNiR1* were positively correlated, suggesting an integrated regulatory network. These results highlight the plant's adaptive strategy to optimize N assimilation and maintain essential metabolic functions under N-deficient conditions.

Furthermore, LN treatment significantly upregulated the expression of *ZmNPF6.2*, *ZmNRT1.2*, and *ZmNRT3.1*. The expression of these genes increased by 1.6-fold, 1.4-fold, and 1.10-fold in the leaves, and by 1.6-fold, 1.2-fold, and 1.6-fold in the roots, respectively, under LN conditions compared to the higher N treatments (Figs. 2.5A-E and B-F). The *ZmNPF6.2* transporter has been functionally characterized as playing a dual role in NO_3^- uptake and signalling. It mediates high-affinity NO_3^- transport and facilitates root-to-shoot NO_3^- translocation (Dechorgnat et al. 2018; Cao et al. 2024). Similarly, as a member of the *NRT1* family, *ZmNRT2.1* contributes to NO_3^- uptake and transport under

N-deficient conditions, ensuring efficient NO_3^- acquisition even at low external NO_3^- concentrations (Dechorgnat et al. 2018; Dechorgnat et al. 2019). Additionally, *ZmNRT3.1* has been reported to function as an accessory protein, enhancing the activity of high affinity NO_3^- transporters such as *ZmNRT2.1*. The upregulation of *ZmNRT3.1* under various N treatment conditions has been shown to improve maize's ability to scavenge NO_3^- from the soil (Dechorgnat et al. 2018; Wu et al. 2024). In this study, the upregulation of these genes under LN treatment conditions underscores their crucial role in steps to improve NUE. By enhancing NO_3^- uptake through N-linked signalling, these transporters help maize seedlings adapt to N-deficient conditions, ensuring survival and maintaining growth (Figs. 2.1 and 2.2A-B). These findings align with previous studies (Wang et al. 2018; Cao et al. 2024; Dechorgnat et al. 2019), emphasizing the significance of these transporters in optimizing N acquisition and utilization under LN conditions.

2.4.4. LN increased NH_4^+ assimilation and upregulated the expression of AMTs

Plants subjected to LN treatment exhibited a higher NH_4^+ concentration than those under MN or HN treatment (Figs. 2.1–2G). This increase in NH_4^+ content may result from limited NO_3^- availability causing a reduction in NR and NiR activity and subsequent impacts on C-skeleton availability (Figs. 2.3A–D) (Zhu et al. 2021). Studies have demonstrated that plants shift their N uptake to alternative sources, such as NH_4^+, under conditions of limited NO_3^- availability (Chalk and Smith 2021; Amoah and Kaiser 2025). Although NO_3^- is the dominant N form in most aerobic, pH balanced soils, NH_4^+ in many plants is more favourable for assimilation due to its lower energy requirement for uptake, assimilation, and incorporation into amino acids compared to NO_3^- (Liu and von Wirén 2017). For instance, while NO_3^- assimilation requires 12 ATP molecules, NH_4^+ assimilation only needs 2 ATP (Bloom 1997; George et al. 2016). The higher NH_4^+ accumulation in LN-treated plants may also be attributed to enhanced NH_4^+ uptake, reduced assimilation due to limited carbon skeleton availability, or increased internal recycling through low N induced protein degradation (Figs. 2.1-2C) and elevated photorespiration (Melino et al. 2022; Marmagne et al. 2022). Furthermore, the GS-GOGAT cycle plays a central role in NH_4^+ assimilation by converting NH_4^+ into glutamine and glutamate, which serve as N donors for amino acid biosynthesis (Kojima et al. 2021). Studies have shown that increased NH_4^+ levels can induce the upregulation of GS and GOGAT activities, enhancing NH_4^+ assimilation and mitigating potential toxicity (Jian et al. 2018; Yamaya and Oaks 2004; Peng et al. 2023a; Liao et al. 2025). We found that, LN-treated plants exhibited increased NH_4^+ accumulation alongside elevated GS and GOGAT activities (Figs. 2.2G, 2.3E–H), demonstrating a compensatory mechanism aimed at detoxifying excess NH_4^+. However, the continued NH_4^+ accumulation suggests that assimilation capacity may be constrained under LN conditions, potentially due to limited availability of C skeletons or energy resources (Feng et al. 2020). Nonetheless, this enzymatic response plays a crucial role in

mitigating NH_4^+ toxicity, which can disrupt cellular metabolism (Hachiya and Sakakibara 2017; Feng et al. 2020).

Additionally, *ZmGS1* (Figs. 2.4E-F) and *ZmGOGAT1* (Figs. 2.4H-I) were highly upregulated in LN-treated plants, and their expression positively correlated with NH_4^+ content as well as GS and GOGAT activities (Figs. 2.6A-B). This correlation indicates an increased demand for NH_4^+ under N-deficient conditions, ensuring that NH_4^+ is rapidly converted into amino acids to support growth and metabolic function (Wang et al. 2019; George et al. 2016; Peng et al. 2012). Furthermore, LN treatment also upregulated the expression levels of *AMT1.1* and *AMT2.1*, highlighting an adaptive transcriptional regulation to enhance high-affinity NH_4^+ uptake (Yuan et al. 2007). Studies have shown that these genes are induced under low NO_3^- availability to compensate for reduced NO_3^- uptake in various plant species (Glass et al. 2002; Dechorgnat et al. 2019; Leng et al. 2024; Gansel et al. 2001). This aligns with our findings in maize seedlings under LN treatment (Figs. 2.5G-J). The upregulation of *ZmAMT1.1* and *ZmAMT2.1* under LN conditions demonstrates maize's adaptive response to enhance NUE. This enables plants to efficiently assimilate and utilize NH_4^+ despite N limitation, ensuring their survival and continued growth.

2.4.5. Diurnal variations in NO_3^- and NH_4^+ accumulation under different N forms

Diurnal fluctuations in the pool sizes of NO_3^- and NH_4^+ were analysed to profile potential plant N regulatory mechanisms. LN treated plants consistently exhibited lower NO_3^- and higher NH_4^+ levels throughout the day, highlighting the role of N type and availability in modulating key metabolic pathways. However, similar diurnal trends were observed across all treatments, suggesting that these patterns may not be exclusively driven by N status but rather reflect a broader regulatory framework that regulate N assimilation (Macduff et al. 1997) (Figs. 2.7A–D). The diurnal changes were not immediate responses to fertigation events. Instead, the rhythmic pattern of NO_3^-, which peaked in the early morning (7:00 AM), declined by midday (12:00 PM), and rose again in the evening (5:00 PM), may reflect periodic shifts in root uptake and assimilation rates rather than direct fertilization effects (Pearson and Steer 1977; Macduff et al. 1997) (Fig. 2.8A). Similarly, the gradual increase in NH_4^+ levels throughout the day, peaking at night (10:00 PM), suggests a circadian driven regulatory mechanism that operates independently of short-term N supply (Fig. 2.8B). Importantly, LN treated plants retained significantly altered N profiles, characterized by reduced NO_3^- and elevated NH_4^+ levels, even after overnight transport. This persistence indicates that the metabolic adjustments induced by N deficiency are stable across environmental transitions and are not readily compensated by external changes in transport. The sustained impact of LN treatment on N storage and regulation underscores the adaptive capacity of plants under N limited conditions (Macduff et al. 1997) (Figs. 2.9A–B). These findings provide valuable insights into the complex interplay between N availability, metabolic regulation, and

diurnal rhythms, advancing our understanding of plant adaptation strategies under nutrient limited environments (Hasan et al. 2022).

2.4.6. N availability shapes NO_3^- and NH_4^+ dynamics across maize tissues

The spatial distribution of NO_3^- and NH_4^+ across maize tissues provides valuable insights into their adaptive responses under different N forms (Fang et al. 2007). In this study, maize plants showed differential responses to N forms, consistent with previous findings suggesting that different N forms enhance NO_3^- and NH_4^+ accumulation in leaves to improve N assimilation, partitioning, and storage (Duan et al. 2023a; Duan et al. 2023c; Amoah and Kaiser 2025). LN-treated plants exhibited increased NH_4^+ levels in aboveground tissues (upper, middle, basal leaves, and leaf sheath) at 22:00, in contrast to consistently lower NO_3^- levels (Figs. 2.8A-B). NH_4^+ content was relatively higher and varied significantly across treatments at both 22:00 and 07:00, demonstrating the role of roots as a N sink during N deficiency (Zhao et al. 2020). Furthermore, at 07:00, residual NO_3^- levels in the leaves and sheath of LN-treated plants remained unchanged from 22:00 (Figs. 2.8A-D), highlighting limited NO_3^- replenishment overnight, as demonstrated previously (Huanosto Magaña et al. 2009). The tissue-specific N distribution reflects adaptive strategies to sustain metabolic function during N deficiency (Zhao et al. 2024; Amoah and Kaiser 2025). In summary, these findings underscore the critical role of N allocation and metabolism in maize under LN conditions, offering valuable strategies to improve crop productivity under N deficiency (Schlüter et al. 2012a; Asibi et al. 2019). Future studies will investigate molecular and enzymatic pathways regulating these spatial patterns, particularly the mechanisms underlying remobilization between source and sink tissues.

2.5. Conclusion

The study highlights the important role of N form and availability in shaping the physiological, molecular, and metabolic adaptations of maize seedlings growth. Under low nitrogen (LN) conditions, maize exhibited pronounced physiological responses, such as increased root biomass and R/S ratio, to enhance N uptake efficiency. LN-treated plants demonstrated reduced NO_3^- assimilation capacity and elevated NH_4^+ accumulation responses, indicating a metabolic shift towards NH_4^+ as a primary N source. The data also highlights a potential incapability of utilising NH_4^+, an outcome which could further impact the LN growth response. The shift towards NH_4^+ assimilation was driven by the apparent upregulation of key NH_4^+ assimilatory enzymes (*ZmGS1* and *ZmGOGAT1*) and NH_4^+ transporter genes (*ZmAMT1.1* and *ZmAMT2.1*). Additionally, the diurnal and spatial patterns of NO_3^- and NH_4^+ dynamics revealed maize's ability to fine-tune N assimilation and storage, maintaining metabolic balance even during nutrient limitations. The differential regulation of N metabolism-related transcripts, including

ZmNR1, *ZmNiR1*, *ZmGS1*, and *ZmGOGAT1*, highlighted robust transcriptional plasticity under LN stress conditions. These findings provide insight into the molecular, enzymatic, and physiological mechanisms driving maize adaptation to N deficiency. The integration of these mechanisms offers a foundation for improving NUE in crops, with significant implications for sustainable agriculture under nutrient-limited conditions.

It is important to note that this study focused on maize seedlings cultivated under controlled growth conditions for a specific duration of up to 40 d (R1 stage). To validate these findings and fully comprehend the complexity of N deficiency responses in agriculturally relevant settings, further research under field conditions and across diverse maize varieties is essential. While this study provides valuable insights into gene expression, additional functional characterization of the identified genes is needed to elucidate their precise role in N metabolism under LN stress. Future studies can explore several key areas to build upon these findings: (a) Investigating the specific signalling pathways that regulate the observed changes in gene expression and enzyme activities under LN, including the role of transcription factors and hormonal signals; (b) Assessing the long-term effects of LN treatment on maize yield, grain quality, and overall plant development; (c) Examining the interactions between different N forms and their combined impacts on maize growth and metabolism under N deficiency conditions and (e) Evaluating the genetic variation in these adaptive responses across different maize genotypes to identify potential targets for breeding N-efficient crops; (f) Elucidate how rot microbial profiles changes in responds to the N status.

2.6. Supplementary data

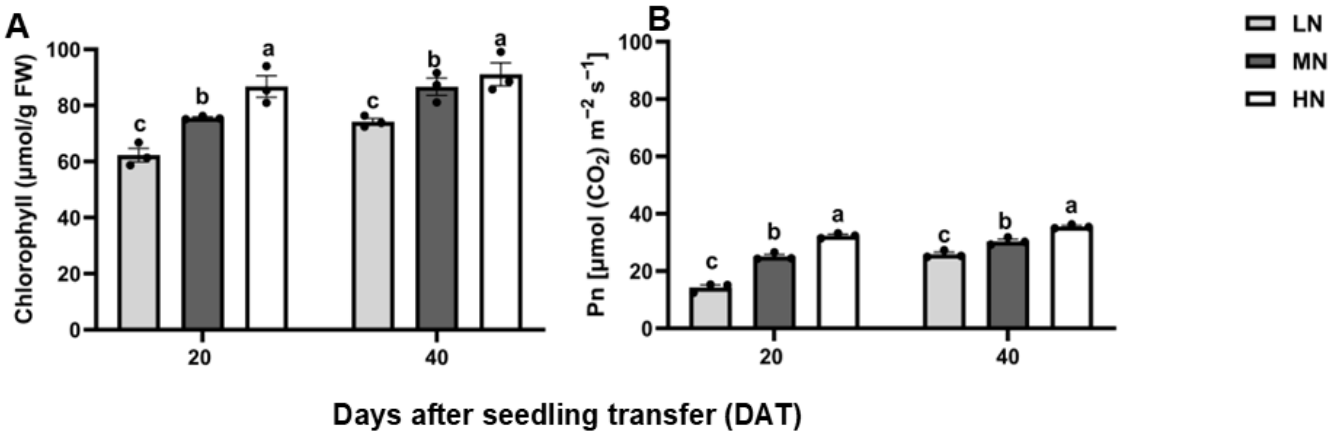

Fig. S2.1 Leaf chlorophyll content (**A**) and leaf net photosynthesis rate (**B**) measured in maize inbred line TX-40J under different nitrogen treatments. Data are presented as mean ± standard deviation (n = 6). Statistical significance was determined using Tukey's multiple range test ($P < 0.05$), with distinct letters indicating significant differences among treatments. FW denotes fresh weights; LN corresponds to low nitrogen (N deficiency), MN to moderate nitrogen, and HN to high nitrogen.

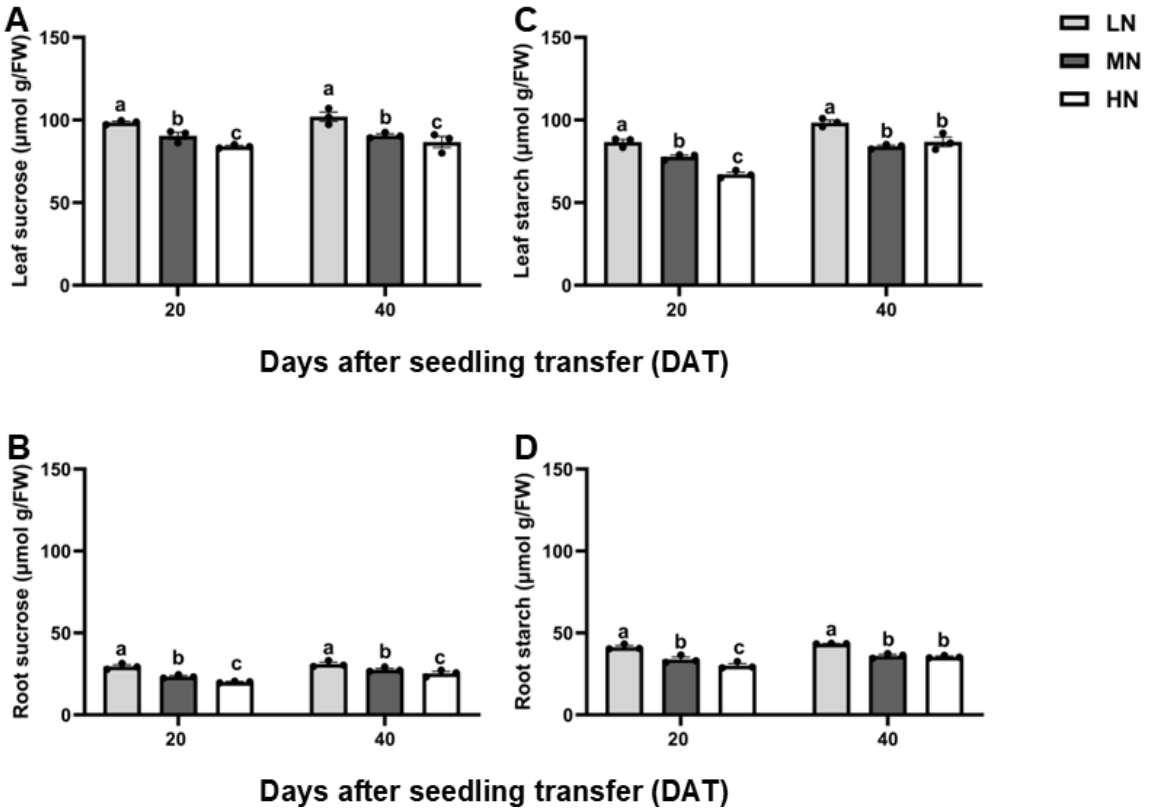

Fig. S2.2 Leaf sucrose (**A**), root sucrose (**B**), leaf starch (**C**) and root starch content (**D**) in maize inbred line TX-40J under different nitrogen treatments. Data are presented as mean ± standard deviation (n = 6). Statistical significance was determined using Tukey's multiple range test ($P < 0.05$), with distinct letters indicating significant differences among treatments. FW denotes fresh weights; LN corresponds to low nitrogen (N deficiency), MN to moderate nitrogen, and HN to high nitrogen.

Table S2.1 List of genes studied

Gene name	NCBI Locs
ZmNR	LOC103654219
ZmNiR	LOC103627781
ZmGS	LOC542746
ZmGOGAT	LOC103651348
ZmNRT2	LOC542092
ZmNPF6.2	LOC100383494
ZmNRT3.1	LOC778428
ZmAMT1.1	LOC100272903
ZmAMT2.1	LOC100191554
ZmUBQc	LOC100279740
ZmActin	LOC100282267

CHAPTER 3: NITROGEN DEFICIENCY IMPACTS GROWTH AND MODULATES CARBON METABOLISM IN MAIZE[2]

Abstract

Soluble sugars are vital for plant development, with nitrogen (N) availability playing a key role in their distribution across plant organs, ultimately shaping growth patterns. However, the regulatory mechanisms governing carbon (C) assimilate allocation and utilization under different N forms remain unclear. This study examined C fixation, utilization, and spatial distribution in hydroponically grown maize seedlings subjected to four N treatments: 1 mM NO_3^- (low N, LN), 2 mM NO_3^- (medium N), 10 mM NO_3^- (high N), and 1 mM NH_4^+ (low ammonium, LA). LN treatment significantly increased soluble sugar and starch contents while promoting greater root biomass at the expense of shoot biomass, leading to a higher root-to-shoot assimilate allocation. The activities of sugar and starch metabolism enzymes were more tightly regulated in both shoots and roots under LN, indicating enhanced C utilization and increased competition for assimilates, particularly in the root. Key genes involved in above-ground sugar and starch metabolism, *ZmSPS1*, *ZmSuSy1*, *ZmCINV1*, *ZmVINV1*, *ZmCWINV1*, *ZmSTP2*, *ZmSUC2*, *ZmSWEET14*, *ZmSS1*, *ZmAMY1*, *ZmBAM1*, and *ZmAGPase1*, were upregulated under LN, correlating with enhanced enzyme activity and resulting increased sugar and starch accumulation. Starch and sucrose accumulated more in LN-treated leaves than in other N treatments, with starch primarily stored in leaf tips and sucrose concentrated in the leaf sheath. This pattern suggests that excess C accumulation results from inefficient C utilization in sink tissues rather than impaired C assimilation. These findings provide new insights into how LN modulates C partitioning between leaves and roots for stress adaptation, highlighting the importance of improving C utilization in sink tissues to mitigate N deficiency and enhance plant growth.

Keywords: Carbon partitioning and accumulation, Low nitrogen, Root-to-shoot ratio, Sink-source dynamics, Sugar and starch metabolism

---

[2]This chapter is published as: Amoah JN, Keitel C, Kaiser BN (2025) Nitrogen deficiency impacts growth and modulates carbon metabolism in maize. Planta 262 (4):94. doi:10.1007/s00425-025-04814-x

3.1. Introduction

Nitrogen (N) is an essential nutrient for plant growth and development, serving as a fundamental component of biomolecules such as nucleic acids, amino acids, and proteins. It also serves as a crucial signalling molecule, influencing numerous plant processes, including lateral root growth, resistance to biotic and abiotic stresses, regulation of seed germination, and mediation of hormone signalling (Ahmad et al. 2014). Due to its susceptibility to adsorption, leaching, and transformation in the soil, N availability is often a major limiting factor for crop productivity. Hence growers apply large quantities of N fertilizers to mitigate N limitations. However, less than 50% of the applied N is effectively utilized by crops, with the remainder lost due to excessive rainfall or irrigation, which leads to significant nitrate leaching from the soil profile (Govindasamy et al. 2023). This loss creates a fluctuating N supply characterized by alternating periods of N deficiency, sufficiency, or excess, which can arise in agricultural soils due to environmental factors or as a consequence of agricultural practices. This unpredictable nutrient dynamic negatively impacts various metabolic functions in plants, ultimately hindering growth and productivity (Govindasamy et al. 2023). Thus, understanding crop growth and development under different N treatments, particularly under nitrogen-deficient conditions, is crucial for ensuring food security and promoting sustainable crop production.

N forms differentially regulate N metabolism, affecting protein and amino acid dynamics (Yang et al. 2020). Studies have shown that NO_3^- treatment improves N assimilation and stimulates glutamine synthetase (GS)-related gene expression, enhancing amino acid biosynthesis and production of structural and functional proteins (Zhang and Wu 2023). While NO_3^- promotes amino acid and protein synthesis, NH_4^+ treatment triggers distinct catabolic responses by activating proteolytic enzymes, such as cysteine and aspartic proteases. These enzymes accelerate protein degradation, leading to shifts in amino acid composition and redistribution, which reflect a characteristic metabolic adaptation to NH_4^+ exposure (González-Moro et al. 2021). These proteolytic activity under NH_4^+ conditions significantly influence C/N interactions. In particular, excessive NH_4^+ supply can disrupt C balance by diverting C skeletons toward N assimilation and stress-related pathways, thereby impairing carbohydrate metabolism and energy homeostasis (Li et al. 2023). Although protein degradation is a general response to NH_4^+ presence, the disruption of C balance is more pronounced under high NH_4^+ concentrations, underscoring the dose-dependent nature of NH_4^+-induced metabolic reprogramming.

To mitigate the detrimental effects of N deficiency-induced stress, plants have evolved various adaptive mechanisms, including reduced biomass accumulation and photosynthesis, decreased N uptake, and regulating shoot and root growth (Zhao et al. 2020). Specifically, under LN condition, reduced root biomass and even further reduced shoot biomass resulting in an elevated root-to-shoot (R/S) ratio have been identified as key traits of N-efficient crops (Lopez et al. 2023). While some insights have been gained into the molecular mechanisms regulating root growth in response to LN (Lai

et al. 2023), these studies have primarily focused on root architecture without addressing C allocation between the root and shoot under different N forms, particularly under LN conditions. Importantly, root response is closely linked to the supply of assimilates, which not only serve as source of energy but also act as signalling molecules and enhance root adaptation to LN stress. Hence, numerous studies have observed C accumulation in roots under LN conditions (Zhao et al. 2020). However, the regulation of assimilate partitioning between root and shoot under LN poorly understood. The critical initial step in assimilate utilisation is the breakdown of sucrose, after long-distance transport from source to sink into hexoses by sucrose synthase or invertase (Lemoine et al. 2013). Interestingly, elevated root invertase activity has been associated with higher R/S ratio in soybean under drought stress (Du et al. 2020a), suggesting a link between sucrose metabolism and root growth under stress conditions. In this context, we hypothesize that sucrose-degrading enzymes play a crucial role in regulating assimilate allocation between root and shoot under LN conditions.

N deficiency reduces photosynthesis; however, studies have shown that sugars and starch accumulate in leaves under LN conditions despite a decline in the photosynthetic rate, a response that appears to be conserved across many plant species (Mu and Chen 2021). To date, the mechanism underlying LN-induced C accumulation in leaves remains unclear. Research suggests that LN reduced sink demand limits the translocation of photo-assimilates, despite enhanced export capacity from source leaves. Consequently, excess C accumulates in source tissues such as leaves and sheaths, primarily due to the imbalance between C supply through photosynthesis and its limited utilization by sink organs (Huang et al. 2022). Given the contradictory findings on C accumulation in source and sink tissues, it is crucial to elucidate the physiological basis of N deficiency-induced C accumulation. Similar to modulating the activities of C metabolism in sink tissue, sucrose and starch metabolism enzymes were induced in LN leaves, demonstrating an increase in starch and sucrose synthesis, that improved C accumulation. Conversely, sucrose synthase activity in root tissues has been shown to increase under LN conditions, particularly in the elongation and maturation zones, where it supports root growth by facilitating sucrose cleavage and promoting C partitioning to structural and storage compounds (Zhao et al. 2020). This enhanced activity contributes to increased starch accumulation and localized utilization of sugars in roots, aiding in root expansion under N-limited conditions. The C pool in plant leaves is determined by the balance between C fixation, which generally follow a diurnal rhythm, making the C pool dynamic throughout the day (Amoah and Kaiser 2025). Hence, examining the diurnal fluctuations and spatial distribution of assimilates can provide valuable insights into the mechanisms driving LN-induced C accumulation in leaves.

Maize (*Zea mays* L.) was chosen for this study due to its significance as a staple food crop and its role as an ideal model for understanding N metabolism and C allocation. Its well-documented growth patterns, responsiveness to environmental factors, and ability to adapt to various N conditions make it an excellent crop for studying the effects of N form substitution on C distribution (Dong et al. 2023).

Furthermore, the economic importance of maize in global agriculture highlights the potential impact of optimizing nutrient management to enhance crop productivity. This study aims to unravel the mechanism underpinning C allocation between the shoot and root of maize. To achieve this, we investigated the effects of different N (mainly NO_3^- and NH_4^+) forms on the activities of sucrose metabolism enzymes involved in sucrose utilization within the shoot and root sinks of the maize inbred line TX-40J and their relationship with C accumulation during photosynthesis. We examined the diurnal fluctuations of assimilates in source leaves and their distribution across various maize tissues, including upper and middle leaves, leaf sheaths, and roots, during both vegetative and reproductive growth stages under different N treatments. Additionally, the total protein and amino acid content was quantified to understand N assimilation and remobilization under different N treatments. The findings of this study will enhance our understanding of how N forms regulate C partitioning and serve as a valuable reference for optimizing crop production under varying N conditions, particularly, under N deficiency conditions.

3.2.1. Materials and methods

3.2.2. Plant materials and experimental site

Seeds of the fast-flowering, short-cycle inbred mini-maize line TX-40J were used in this study (Amoah and Kaiser, 2025). This maize line offers significant advantages, including a uniform genetic background, a shorter lifecycle, and early flowering, which enable efficient and targeted research in various areas of plant biology. The traits observed in this variety serve as valuable references for breeders, facilitating the development of hybrids with enhanced performance and improved nitrogen use efficiency (McCaw et al. 2021). The seeds were germinated in Oasis Horticube Propagation Slabs (Aqua Gardening, Brisbane, Australia) placed in germination trays. The trays were transferred to a climate-controlled growth room, set to a 14/10 day-night cycle, with temperatures of 25°C during the day and 22°C at night, and 80% relative humidity for 5 d to allow for seed germination. Once the seedlings had germinated uniformly, they were transferred to a temperature controlled glasshouse for the subsequent experiments (Amoah and Kaiser 2025).

3.2.3. Experimental treatment, set up and sampling

Seedlings were divided into four treatment groups and cultivated in 3 L pots, with their roots supported by inorganic expanded clay pellets (Aqua Gardening, Brisbane, Australia). Each group received a specific nitrogen (N) source: 1 mM NO_3^- (low N; LN), 2 mM NO_3^- (medium N; MN), 10 mM NO_3^- (high N; HN), and 1 mM NH_4^+ (low NH_4^+; LA). These nutrient levels were selected based on previous studies (Amoah and Kaiser 2025). The seedlings were grown for 40 days.

The system was set up in a climate-controlled glasshouse, with conditions matching those of the growth room used for seed germination, but with supplemental LED lighting providing 1000 μmol m^{-2} s^{-1} at pot level. Each system was designed to accommodate 40 pots, with one plant per pot. Plants were drip-irrigated with the respective nutrient solution, which was circulated through a hydroponic pump system. Irrigation occurred twice daily for 1 min, at 12:00 PM and 5:00 PM. The nutrient solution comprised the following concentrations (in mM): 1.0 $MgSO_4$, 1.0 KH_2PO_4, 0.05 H_3BO_3, 0.005 $MnSO_4$, 0.001 $ZnSO_4$, 0.001 $CuSO_4$, 0.001 Na_2MoO_4, 0.1 KCl, 0.1 Fe-EDTA, 0.1 Fe-EDDHA, 0.25 $Ca(NO_3)_2$, 0.25 K_2SO_4, 0.25 $CaCl_2$, and 1.75 $CaSO_4$ (Table S1) and were stored in 162 L Brute Containers with lids (Rubbermaid, USA). The solution was changed weekly, with daily pH adjustments with 1 M H_2SO_4 or 1 M NaOH to maintain a stable pH of 5.9. The treatment solution was delivered to the system by an Eden 140G FL submersible water pump (Creative Pumps, Australia). Plants were uniquely identified and randomized into four blocks using the 'agricolae' package of the R statistical software (v4.4.2).

Sampling was conducted at 20 (vegetative, V6 stage) and 40 (reproductive, R1 stage) days after treatment (DAT). Fresh leaf, root and ear tissues for biochemical analysis were collected, immediately frozen in liquid nitrogen (N_2), and stored at -80°C. Shoot and root samples for biomass analysis were oven-dried at 70°C for 48 h to determine dry weights. The shoot and root biomass values were summed to calculate the total plant biomass in grams (g DW).

3.2.4. Spatial distribution and diurnal changes determination

To examine the spatial distribution of sugars and starch, the youngest emerging leaf at 20 and 40 DAT was sampled and divided into three equal segments. Additional samples included the corresponding leaf sheath, root, basal 5 cm of expanded leaves, root, and ear. Sampling was conducted at 22:00 and again at 6:00 the following morning on 20 and 40 DAT. For diel analysis, the middle sections of the youngest fully expanded leaves were collected at 7:00, 12:00, 17:00, 22:00, and 7:00 (the next day) on 20 and 40 DAT. All samples were immediately frozen in liquid N_2 and stored at −80 °C for subsequent biochemical analysis. To further investigate the diurnal variations in sugar metabolism under different N forms, the rates of leaf sucrose and starch synthesis and degradation and net sucrose and starch accumulation were calculated based on the diurnal sucrose and starch data, using the formulas in Table S3.1.

3.2.5. Net photosynthetic rate and chlorophyll and nitrogen (N) measurement

The net photosynthetic rate (Pn) was measured on the young emerging blade (YEB) of each treatment using a portable LI-6400 photosynthetic system (LI-COR Inc., Lincoln, USA). Measurements were

taken at 9:00 AM and 11:00 AM. Cuvette conditions included a light level of 1000 µmol m^{-2} s^{-1}, CO_2 concentration of 400 ppm, flow rate of 500 µmol m^{-2} s^{-1}, and relative humidity between 60% and 65%. Chlorophyll pigment was extracted from the youngest fully expanded blade (YEB) following Licor measurements. The YEB samples were harvested and ground into a fine powder, and 0.2 g of the ground tissue was extracted with 100% methanol on a shaker at 25 °C until complete bleaching occurred (Amoah et al. 2019). The extract was then centrifuged at 10,000 × *g* for 10 min, and the absorbance of the resulting supernatant was measured at 470, 646, and 663 nm using a UV-vis spectrophotometer (Shimadzu, Tokyo, Japan). Chlorophyll concentration was calculated based on the equations described by (Amoah and Kaiser 2025).

N content was determined using the Kjeldahl method as described by (Rizvi et al. 2022), with minor modifications. A 0.2 g samples of YEB was digested with 0.5 mL of concentrated H_2SO_4 and 0.5 mL of a catalyst mixture consisting of 10 g of K_2SO_4 and 1 g of $CuSO_4$. The mixture was heated at 100ºC for 60 min on a heating block in a fume hood. After digestion, the samples were allowed to cool, and 0.5 mL of 40% NaOH solution was slowly added, followed by 0.5 mL of distilled water. Subsequently, 1 mL of the resulting mixture was combined with 1 mL of Nessler's reagent and incubated for 10 min at room temperature. The absorbance was measured at 420 nm using a UV-vis spectrophotometer (Shimadzu, Tokyo, Japan). Total N content was determined from a standard curve generated with $(NH_4)_2SO_4$ standards.

3.2.6. Soluble sugar, starch, glucose and sucrose content determination

Soluble sugar and sucrose content were measured as described by Amoah and Adu-Gyamfi (2024). Briefly, 100 mg of ground samples were homogenized in 1 mL of 80% (v/v) ethanol, and the mixture was heated at 80 °C for 30 min. After cooling for 5 min, the mixture was centrifuged at 12,000 × *g* for 10 min. The supernatants were collected, and total soluble sugars were determined using the anthrone reagent, with absorbance measured at 620 nm. Sucrose content was determined by the resorcinol-HCl method, which forms a pink complex measured at 480 nm using a UV-vis spectrophotometer (Shimadzu, Tokyo, Japan). The ethanol-insoluble residue was used for starch extraction following the procedure outlined by Du et al. (2020a) After evaporating the ethanol, 1 mL of distilled water was added to the samples, which were then incubated at 100 °C for 15 min. Starch was hydrolysed using separate treatment of 9.2 M perchloric acid ($HClO_4$). The resulting glucose units were quantified using the anthrone reagent, and absorbance was measured at 620 nm using a UV-vis spectrophotometer (Shimadzu, Tokyo, Japan). Glucose and fructose content were determined using the anthrone colorimetry method as described by Dong et al. (2023b). A mixture of 1 mL of supernatant and 5 mL of anthrone diluted sulfuric acid reagent was boiled for 10 min. A blank was prepared similarly, using 1 mL of distilled Milli-Q water instead of the supernatant. After cooling, the solution's absorbance was

measured at 620 nm using a spectrophotometer, with the blank adjusted to zero. For fructose content, 1 mL of extract, 1 mL of 0.1% (v/v) hydroquinone, and 3.5 mL of 30% (v/v) HCl were combined in a test tube, thoroughly mixed, and heated at 80°C for 10 min in a water bath. After cooling, the solution's absorbance was measured at 480 nm using a spectrophotometer, with the blank adjusted to zero. The measured absorbance was used to calculate fructose content based on a standard curve.

3.2.7. Sugar metabolism enzymes activity assays

Enzymes were extracted following the method described by Chen et al. (2019), with slight modifications. A 100 mg plant tissue. sample was ground to a fine powder using liquid N_2 and homogenized in 1 mL of ice-cold extraction buffer. The buffer contained 50 mM HEPES-NaOH (pH 7.5), 5 mM $MgCl_2$, 0.1% (v/v) β-mercaptoethanol, 0.05% (v/v) Triton-X100, 0.05% (w/v) BSA, 2% (w/v) polyvinylpyrrolidone, and 1 mM EDTA. The homogenate was centrifuged at 12,000 × *g* for 10 min at 4°C, and the supernatant was used for the assays of sucrose synthase (SuSy), vacuolar invertase (VINV), and cytoplasmic invertase (CINV) activities. The pellet was washed twice with 0.5 mL of extraction buffer and then resuspended in 1.8 mL of salt extraction buffer. Samples were extracted overnight at 4°C and centrifuged at 12 000 × *g* for 10 min at 4°C. The resulting supernatant was used for the assay of cell wall invertase activity (CWINV).

SuSy and CINV activities were determined following the method by (Li et al. 2021b), while VINV activity was assayed according to (Chen et al. 2019). For SuSy activity, 100 µL of enzyme extract was mixed on ice with 200 µL of a reaction solution containing 80 mM MES-NaOH (pH 5.5), 5 mM NaF, 100 mM sucrose, and 5 mM UDP. The reaction was incubated at 30°C for 30 min and terminated by boiling for 2 min. A control reaction lacking UDP was included. For VINN, CINV and CWIN assays, the procedure was similar, but with variations in the reaction mixtures. VIN activity was measured using 200 mM acetic acid-sodium acetate buffer (pH 4.5 or 4.8) with 100 mM sucrose. CINV activity utilized 100 mM HEPES-NaOH buffer (pH 7.5) with 100 mM sucrose. For sucrose phosphate synthase (SPS) activity measurement, 0.1 g of frozen tissue was homogenized in an extraction buffer containing 50 mM Tris-HCl (pH 7.5), 1 mM EDTA, 1 mM $MgCl_2$, 12.5% (v/v) glycerine, 10% polyvinylpyrrolidone (PVP), and 10 mM mercaptoethanol. For SPS activity, 200 µL of supernatant was mixed with reaction buffer containing 200 mM Tris-HCl (pH 7.0), 40 mM $MgCl_2$, 12 mM UDP-glucose, 40 mM fructose-6-P, and 200 µL extract. Another reaction buffer containing 12 mM UDP, 40 mM sucrose, 200 mM Tris-HCl (pH 7.0), and 40 mM $MgCl_2$ was prepared. The mixture was incubated at 30 °C for 30 min and terminated using 100 µL of 2 M of NaOH. The mixture was incubated at 100 °C for 10 min to destroy untreated hexose and hexose phosphates, cooled to room temperature, and mixed with 1 mL of 0.1% (w/v) resorcin in 95% (v/v) ethanol and 3.5 mL of 30% (w/v) HCl. The solution was incubated for 10

min at 80 °C. Sucrose content in the SPS reaction was calculated using a standard curve measured at A480 nm using anthrone reagent.

3.2.8. Starch metabolism enzymes activity assay

For starch synthase (SS) activity, 100 mg of tissue samples were homogenized in an extraction buffer containing 50 mM Tris-HCl (pH 7.0), 10% glycerol, 10 mM EDTA, 5 mM DTT, 1 mM PMSF, and 50 µL/g tissue of 10× Protease Inhibitor Cocktail (Sigma-Aldrich, Cat# P9599). The homogenate was centrifuged at 12,000 × *g* for 10 minutes, and the supernatant was collected. A reaction mixture was prepared by mixing 0.1 mL of the supernatant with 0.9 mL of a solution containing 50 mM Tris-HCl (pH 7.0), 5 mM ADP-glucose, 1 mg/mL glycogen, and 10 mM $MgCl_2$. The reaction mixture was incubated at 30 °C for 30 min. To stop the reaction, 0.1 M HCl was added to denature the enzymes. To detect inorganic phosphate (Pi) consumption, 1% (w/v) ammonium molybdate was added. The mixture was incubated at room temperature for 30 min, and the absorbance was recorded at a wavelength of 620 nm using a UV-vis spectrophotometer (Shimadzu, Tokyo, Japan). A standard curve was prepared using known Pi concentrations, and starch synthase activity was calculated as the amount of Pi released, expressed in $\mu molg^{-1}FW$.

The activities of α-and β-amylase was measured according to the methods by Du et al. (2020) with minor modifications. Briefly, tissue samples were homogenized in 1 mL of chilled distilled water and centrifuged at 12,000 x *g* for 15 min. The supernatants were separated and used for quantifying α- and β-amylase. For α-amylase activity, 0.5 mL of supernatant was mixed with 3 mM $CaCl_2$, heated at 70 °C for 5 min to inactivate β-amylase, cooled to room temperature, followed by the addition of 2% starch solution in 0.1 M citrate buffer. The mixture was incubated at 30 °C for 5 min and stopped by adding 1 mL of colour reagent dinitro salicylic acid (DNS. The mixture was heated at 50 °C for 5 min, cooled down, and the α-amylase activity was determined by recording absorbance at 540 nm wavelength with a UV-vis spectrophotometer (Shimadzu, Tokyo, Japan). β-amylase activity (BAM) was assayed by initially inactivating α-amylase (AMY) with 0.1 M EDTA. After, a 1 mL solution containing 0.1 M EDTA, 2% starch solution, and 0.1 mM citrate buffer were mixed with 0.5 mL enzyme extract. The mixture was incubated at 30 °C for 5 min. The reaction was stopped by adding 1 mL of colour reagent (dinitro salicylic acid). The β-amylase activity was measured by recording absorbance at 540 nm wavelength with a UV-vis spectrophotometer (Shimadzu, Tokyo, Japan).

ADP-glucose pyrophosphorylase (AGPase) activity was determined using previously described methods by Amoah et al. (2025), with minor modifications. Briefly, 100 mg of fresh samples were homogenized in 1 mL of ice-cold extraction buffer containing 0.1 M Tris-HCl (pH 7.9), 5 mM glutathione, and 1 mM EDTA. The homogenate was centrifuged at 15,000 × *g* for 20 min at 4 °C, and the supernatant was collected. Subsequently, 0.1 mL of the supernatant was mixed with 0.9 mL of a

reaction mixture containing 0.4 M Tris-HCl buffer (pH 7.9), 0.06 M $MgSO_4$, 48 mM cysteine, 2.4 mg/mL BSA, 4 mM ADP-glucose, 20 mM sodium pyrophosphate, 30 mM 3-phosphoglycerate, and 4 units each of glucose-6-phosphate dehydrogenase and phosphoglucomutase. Afterwards, 0.1 mL of enzyme extract was added to $NADP^+$ as the final component. The absorbance was measured at 340 nm using a UV-vis spectrophotometer (Shimadzu, Tokyo, Japan). The AGPase activity was expressed as μmol min^{-1} g^{-1} FW.

3.2.9. Total amino acid quantification

Total amino acids content was determined using the methods outlined by (Bates et al. 1973). Frozen leaf tissues (100 mg) were homogenized in 10 mL of 3% (v/v) aqueous sulfosalicylic acid. After filtering the homogenate, 1 mL of filtrate was combined with 1 mL of glacial acetic acid and 1 mL of acidic ninhydrin. The resulting mixture was incubated at 100°C for 1 h and then cooled on ice for 20 min before being extracted with 1 mL of toluene. The concentrations of amino acids were measured using a UV-vis spectrophotometer (Shimadzu, Tokyo, Japan) at A580 nm. Leaf and root total protein content was estimated using the Bradford Protein Assay (Bradford 1976) following manufacturer's protocol (Bio-Rad, South Granville, Australia).

3.2.10. RNA isolation, cDNA synthesis and qPCR analysis

Total RNA was isolated from leaf and root tissues using the TRIzol RNA Isolation Reagents (Invitrogen, Carlsbad, CA, USA) following the manufacturer's protocol. RNA quantity and integrity were assessed by measuring the optical density at 260 nm and through 1.0% agarose (v/w) gel electrophoresis, respectively. Subsequently, 1 μg of total RNA was reverse-transcribed into single-stranded cDNA using the iScript™ RT Reagent Kit (Bio-Rad, Hercules, CA, USA) according to the manufacturer's instructions. Quantitative real-time polymerase chain reaction (qPCR) was performed using the CFX 96 Real-Time System (Bio-Rad, Richmond, CA, USA) with SYBR Green fluorescence (Bio-Rad, Richmond, CA, USA). The ΔΔCT method was used for data analysis. The list of genes studied are provided in Table S3.2. The thermal cycling conditions consisted of an initial denaturation step at 95 °C for 5 min, followed by 40 cycles of 95 °C for 15 s, 55 °C for 15 s, and 72 °C for 30 s. All experiments were conducted with four analytical replicates, and relative transcript levels were normalized using *ZmActin1* and *ZmUBQ1* as internal controls.

3.2.11. Statistical analysis

Data were analysed using a two-way analysis of variance (ANOVA) in R statistical software (v4.4.2), considering growth stage (S) and nitrogen (N) treatment as fixed factors. Tukey's multiple comparison test was used for post hoc analysis, with significance set at $P \leq 0.05$. Results are presented as the mean ± standard error (SE) of four biological replicates. Different letters above error bars indicate statistically significant differences. Graphs were generated using GraphPad Prism (v10.4.0), and Pearson's correlation plots were produced in R (v4.4.2).

3.3. Results

3.3.1. Plant photosynthesis, total shoot and root biomass, tissue N, total amino acid, and protein contents

The tissue biomass, N, total amino acid, total protein, and leaf net photosynthetic rate (Pn) differed among plants in the different treatment groups. Specifically, at 40 DAT, shoot biomass increased significantly ($P \leq 0.05$) by 56%, 72%, 66%, and 67% under LN, MN, HN, and LA treatments, respectively, while root biomass rose by 69%, 71%, 47%, and 68% under the same conditions (Table 1). Plants grown under HN treatment exhibited significantly ($P \leq 0.05$) increased shoot biomass, N content, total amino acids, protein contents, and leaf Pn. However, plants treated with LN showed a significantly ($P \leq 0.05$) increased root biomass and R/S ratio compared to plants in the other treatment groups (Table 1). Growth stage (S) significantly influenced ($P \leq 0.05$) shoot and root biomass, as well as leaf and root N, total amino acid, and total protein contents (Table 3.2). The type and amount of N supplied nitrogen treatment (T) had a significant impact on shoot and root biomass, R/S ratio, and leaf and root total amino acid and protein content. Comparatively, plants grown under NO_3^- treatment, particularly MN and HN, showed higher accumulation of total protein and amino acids in both the leaves and the roots, whereas LA-treated plants exhibited increased levels of these compounds compared to LN plants (Table 3.1). However, the interaction between growth stage and treatment (S x T) significantly ($P \leq 0.05$) affected only root biomass (Table 3.2).

3.3.2. Soluble sugars and starch accumulation under different N forms

The glucose, fructose, sucrose, starch and soluble sugar contents in the leaves (Figs. 3.1A, C, E, G and S1A) and roots (Figs. 3.1B, D, F, H and S3.1B) were significantly ($P \leq 0.05$) higher in LN-treated plants . This resulted in a significantly ($P \leq 0.05$) increased hexose content (sum of glucose and fructose), total non-structural carbohydrate (TNC) content (sum of sucrose, glucose, fructose and starch) and hexose: sucrose (H/S) ratio in both the leaves (Figs. S3.1C, E and G) and roots (Figs. S3.1D, F and H). S affected leaf soluble sugar, starch, and TNC, as well as root soluble sugar, sucrose, fructose, starch, TNC, and

H/S ratio. T affected the leaf and root soluble sugar, sucrose, fructose, glucose, hexose, TNC, and H/S ratios. In contrast, the S x T impacted only the root soluble sugar and H/S ratio (Table 3.2).

3.3.4. Sugar and starch metabolism enzymes activity

SPS and SuSy activities were significantly ($P \leq 0.05$) higher in the leaves (Fig. 3.2A, C) and roots (Fig. 3.2B, D) of LN-treated plants . Similarly, CINV, VINV, and CWINV activities increased significantly ($P \leq 0.05$) in the leaves (Fig. S3.2A, C, E) and root (Fig. S3.2B, D, F) of LN-treated plants, resulting in higher total sucrolytic activity in the leaves (Fig. S3.2G) and root (Fig. S3.2H) in LN plants compared to plants in other treatment groups. Additionally, plants under LN treatment showed enhanced AGPase, SS, AMY and BAM activity in the leaves (Figs. 3.2E, G and S3.3A, C) and roots (Figs. 3.2E, G and S3B, D), which supported the higher starch accumulation in LN-nourished plants. Both S and T significantly ($P \leq 0.05$) influenced leaf and root SPS, SuSy, AGPase, SS, AMY, BAM, CINV, VINV, CWINV, and total sucrolytic activity, while S x T interaction was found for leaf AMY and BAM activities, as well as root SPS, SuSy, AGPase, and total sucrolytic activity (Table 3.2).

3.3.5. Expression pattern of sugar and starch metabolism-related gene activity

To understand the molecular mechanisms associated with C accumulation under different N forms, the expression levels of sucrose and starch metabolism-related genes *ZmSuSy1, ZmSPS1*, *ZmCINV1*, *ZmVINV1, ZmCWINV1*, *ZmSTP2*, *ZmSUC2*, *ZmSWEET14*, *ZmSS1*, *ZmAMY1*, *ZmBAM1* and *ZmAGPase1* were analysed in the leaves and roots of maize plants under LN, MN, HN, and LA treatments. As shown in Figs. 3.3, 3.4 and 3.5, the sugar and starch metabolism-related genes were differentially regulated in the leaves and roots of maize plants. For example, *ZmSuSy1*, *ZmSPS1*, *ZmCINV1*, *ZmVINV1*, *ZmSTP2*, *ZmSUC2*, and *ZmSWEET14* were highly upregulated in the leaves (Figs. 3.3, 3.4A, C, E) and roots (Figs.3. 3, 4B, D, F, H). In contrast, the starch metabolism-related genes; *ZmSS1*, *ZmAMY1* and *ZmBAM1* and *ZmAGPase1* were highly upregulated in both the leaves (Figs. 3.5A, C, E, G) and roots (Fig. 3.5B, D, F, H) of maize plant under LN treatment. Additionally, S greatly influenced the expression of *ZmCWINV1*, *ZmCINV1*, and *ZmSTP2*, *ZmSS1, ZmAMY1* and *ZmBAM1* in the leaves and *ZmSUC2* and *ZmSWEET14* in the roots. T affected the expression of all genes in the leaves and roots, except for *ZmSWEET14* in the leaves. However, S x T had no influence on the expression of any genes in both the leaves and roots of maize plants (Table 3.2).

3.3.6. Diurnal changes of sugars and starch under different N forms

The diurnal pattern of sucrose, starch, fructose, and glucose levels showed the lowest values in the early morning (7:00 AM), followed by an increase at 12:00 PM, peaking at 5:00 PM, and declining overnight to reach their lowest levels again at 7:00 AM the next day. This pattern was consistent across both 20 DAT and 40 DAT (Figs. 3.6A-D and S3.4A-D). At 20 DAT, significant differences ($P \leq 0.05$) in sucrose and starch contents were recorded among the treatment groups. Plants subjected to LN treatment consistently exhibited elevated concentrations of leaf sucrose, starch, fructose, and glucose throughout the day. These sugar levels were significantly different ($P \leq 0.05$) from those observed in other treatment groups during both sampling stages (Figs. 3.6A-D and S3.4A-D). Furthermore, after overnight transport, plants under LN treatment retained significantly ($P \leq 0.05$) higher leaf sucrose and starch concentrations than those in other treatment groups (Fig. 3.6A-D).

3.3.7. Leaf sucrose and starch synthesis and degradation under different nitrogen forms

Starch synthesis significantly increased in the leaves of LN-treated plants at 20 DAT (Fig. 3.7). However, MN-treated plants exhibited higher leaf sucrose and starch synthesis rates, which were comparable to those observed in LN-, HN-, and LA-treated plants (Fig. 3.7A–B). Furthermore, sucrose and starch degradation rates were consistently higher at both 20 and 40 DAT in plants subjected to LN treatment compared to other treatments (Fig. 3.7C–D). Plants under MN treatment showed significantly higher net sucrose accumulation. Meanwhile, net starch accumulation was comparable between LN and MN-treated plants at 20 DAT, and between LN and HN-treated plants at 40 DAT (Fig. S3.5A–B).

3.3.8. Diurnal and spatial distribution of soluble sugars and starch under different forms

Plants subjected to LN treatment exhibited significantly higher sucrose and starch contents across various maize tissues (upper, middle, and basal leaves, the leaf sheath, and the roots) compared to other treatment groups. Specifically, at 21:00, the upper, middle, and basal leaves, as well as the leaf sheath, demonstrated elevated sucrose levels. In contrast, plants under HN treatment displayed reduced sucrose accumulation by the end of the day (Fig. 3.8A). By 07:00 the following morning (end of the night), LN-treated plants retained higher residual sucrose levels in the upper and basal leaves and the leaf sheath, with concentrations comparable to those recorded at 21:00 (Fig. 3.8A–C). Similarly, LN-treated plants accumulated greater starch levels in the leaves by 21:00 and retained higher starch concentrations following overnight remobilization. Starch content in the roots (sink tissues), however, was relatively lower and showed significant variation among treatment groups at both 21:00 and 07:00 (Fig. 3.8B–D).

As shown in Fig. S3.6, LN-treated plants exhibited higher glucose and fructose levels across all examined maize tissues. The upper, middle, basal, and sheath regions, which constitute the leaf tissues, accumulated significantly higher fructose levels, particularly at 21:00 compared to 07:00. In

contrast, LA-treated plants displayed lower glucose and fructose concentrations at 21:00 (Fig. S3.6A–D). By 07:00, LN-treated plants retained greater residual glucose and fructose in the leaves, mirroring the concentrations observed at 21:00. Interestingly, fructose and glucose levels were consistently lower in root tissues (sink tissues) compared to leaves (source tissues), with notable variation among treatment groups at both sampling times (Fig. S3.6A–D). This pattern underscores the influence of N availability on carbohydrate storage and redistribution. LN treatment notably enhanced the retention of sucrose, starch, glucose, and fructose in source tissues, even after overnight remobilization.

3.3.9. Correlations of R/S ratio with physio-biochemical and molecular indicators

To investigate the relationship between the R/S ratio and various indicators in maize leaves and roots under different nitrogen (N) conditions, a Pearson correlation analysis was conducted (Table 3.3). In maize leaves, the R/S ratio exhibited significant positive or negative correlations with the majority of the indicators, with the exception of H/S ratio and TNC. Similarly, in maize roots, the R/S ratio significantly correlated (positively or negatively) with most indicators. However, no significant correlations were observed with Pn, total protein, glucose, fructose, hexose, H/S ratio, TNC, or the expression levels of *ZmCINV1* and *ZmSWEET14* (Table 3.3).

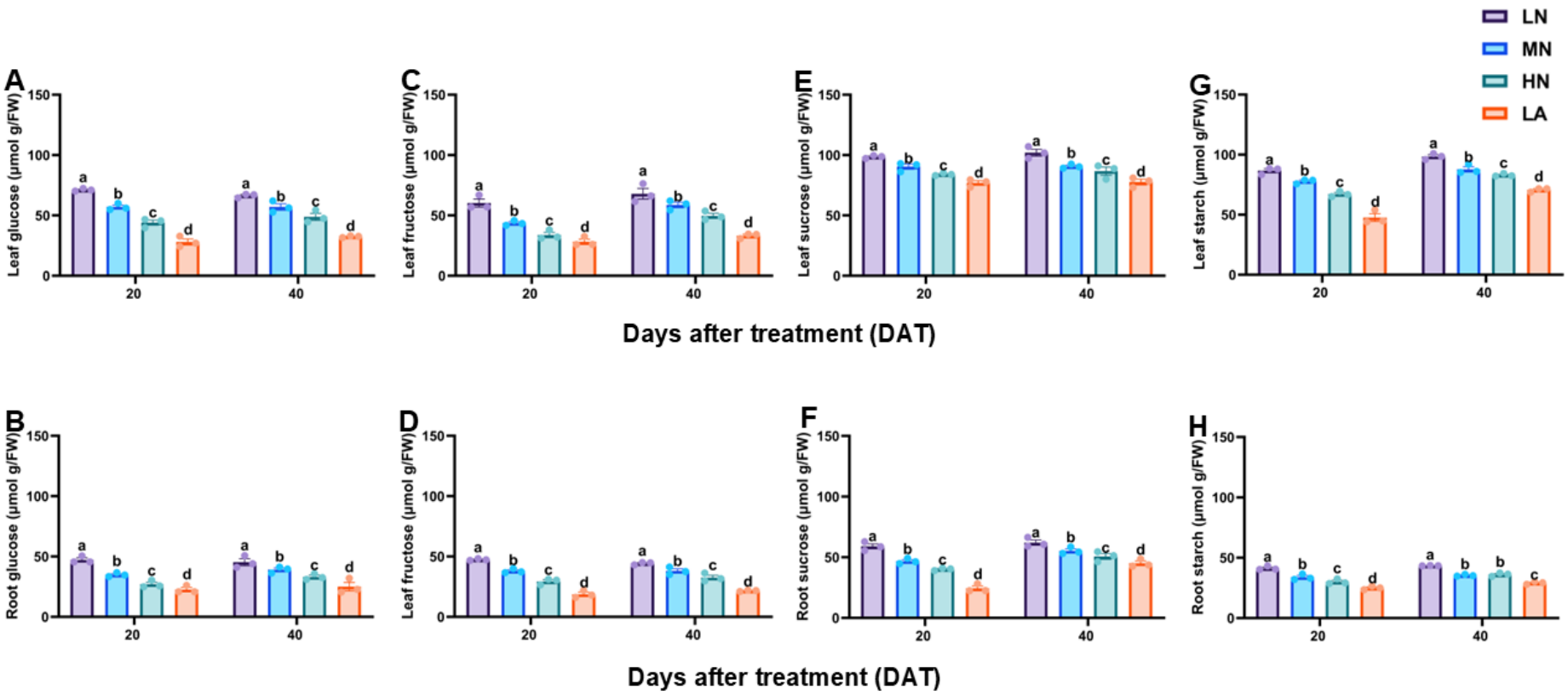

Fig. 3.1 Effect of different nitrogen forms on glucose, fructose, sucrose and starch content in the leaves (**A**, **C**, **E**, **G**) and roots (**B**, **D**, **F**, **H**) of maize inbred line TX-40J. Data are presented as mean ± SE (n = 6). Statistical significance was determined using Tukey's multiple range test ($P \leq 0.05$), with different letters indicating significant differences between treatments. FW, fresh weight; LN, low nitrogen (N deficiency); MN, moderate nitrogen; HN, high nitrogen; LA, low ammonium treatment.

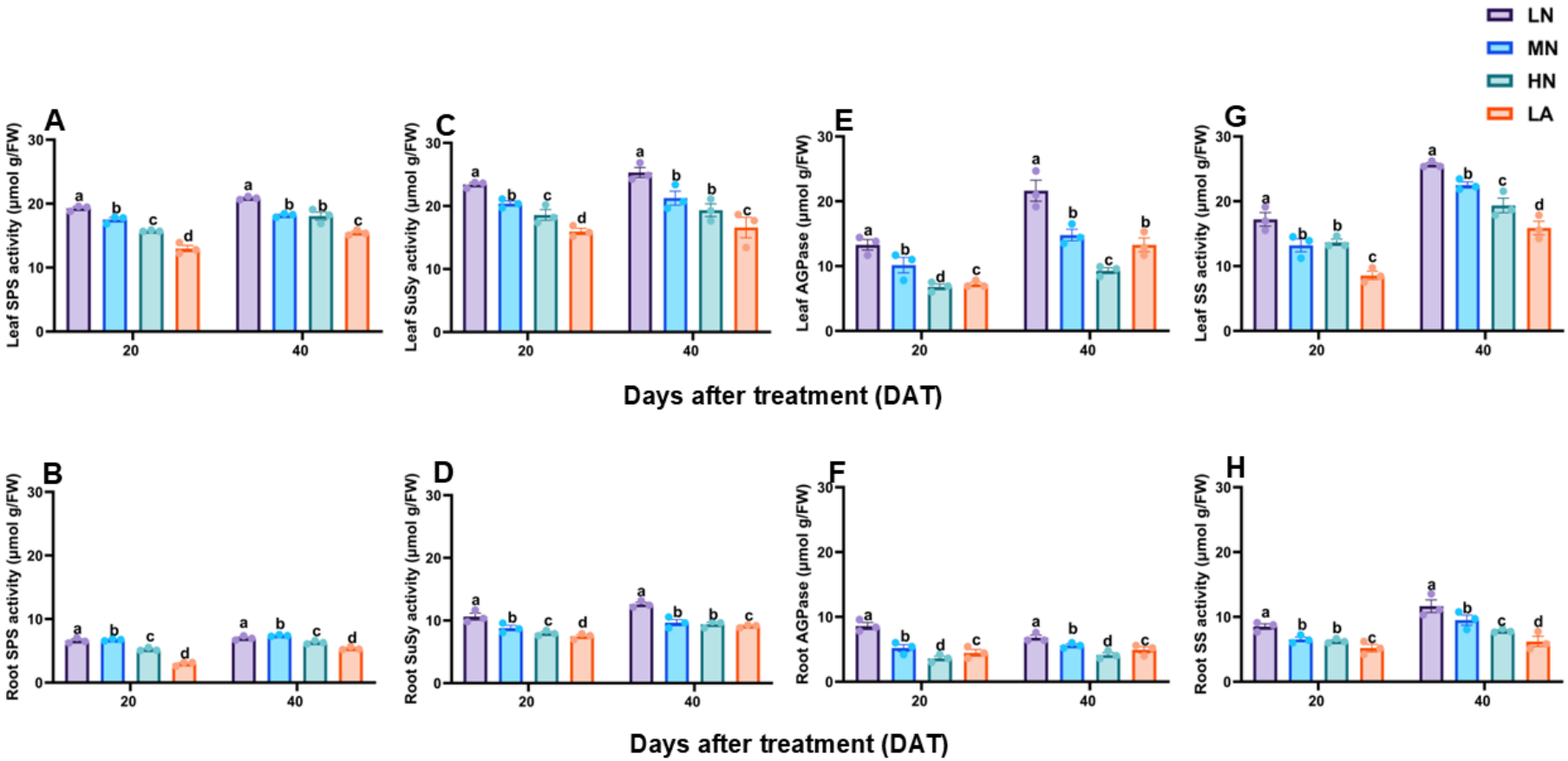

Fig. 3.2 Effect of different nitrogen forms on sucrose phosphate synthase, sucrose synthase, sucrose synthase, ADP-glucose pyrophosphorylase and starch synthase activity in the leaves (**A**, **C**, **E**, **G**) and roots (**B**, **D**, **F**, **H**) of maize inbred line TX-40J. Data are presented as mean ± SE ($n = 6$). Statistical significance was determined using Tukey's multiple range test ($P \leq 0.05$), with different letters indicating significant differences between treatments. FW, fresh weight; LN, low nitrogen (N deficiency); MN, moderate nitrogen; HN, high nitrogen; LA, low ammonium treatment.

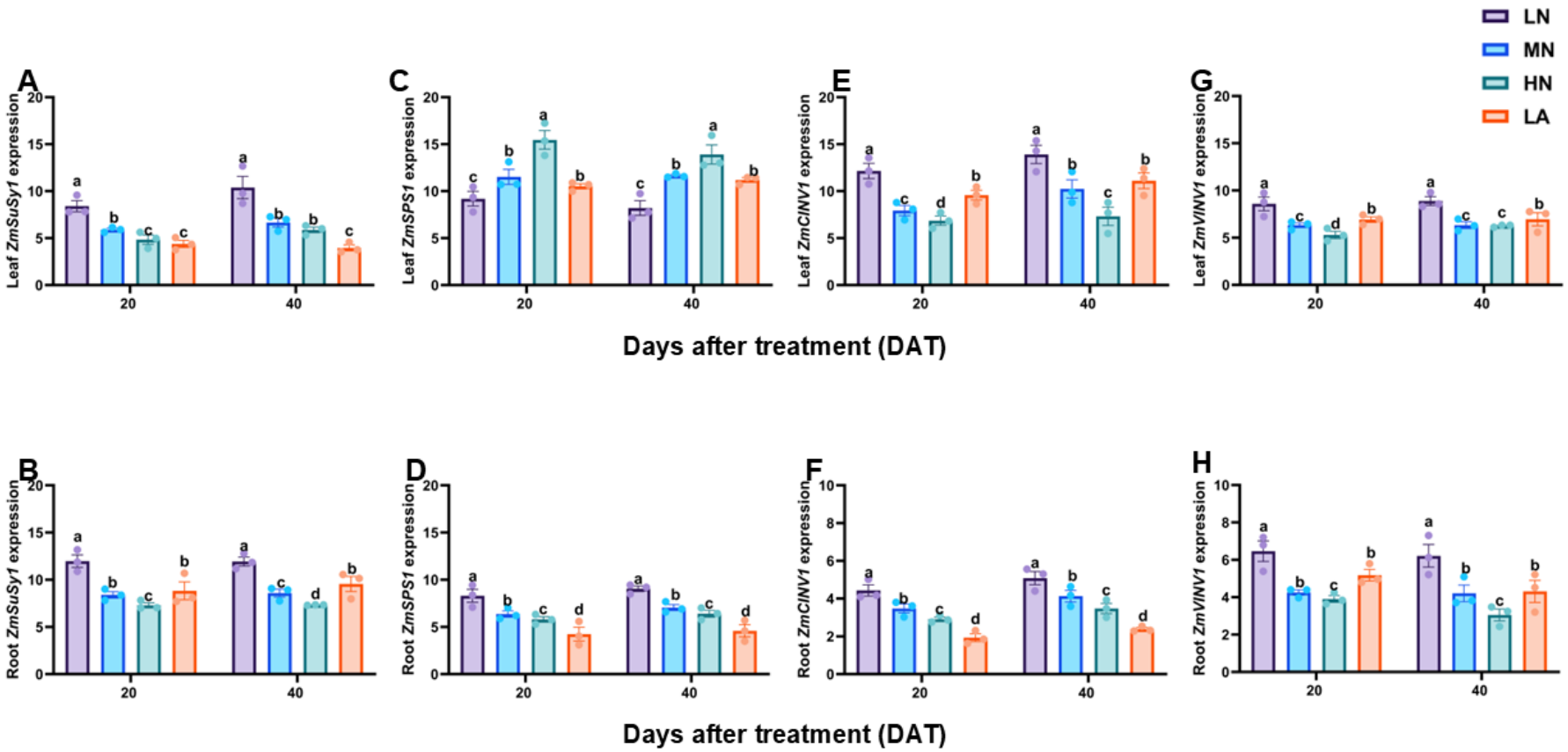

Fig. 3.3 Effect of different nitrogen forms on the expression pattern of sugar metabolizing genes. Expression level of *ZmSuSy1*, *ZmSPS1*, *ZmCINV1* and *ZmVINV1* in the leaves (**A**, **C**, **E**, **G**) and roots (**B**, **D**, **F**, **H**) of maize inbred line TX-40J. Data are presented as mean ± SE (n = 6). Statistical significance was determined using Tukey's multiple range test ($P \leq 0.05$), with different letters indicating significant differences between treatments. FW, fresh weight; LN, low nitrogen (N deficiency); MN, moderate nitrogen; HN, high nitrogen; LA, low ammonium treatment.

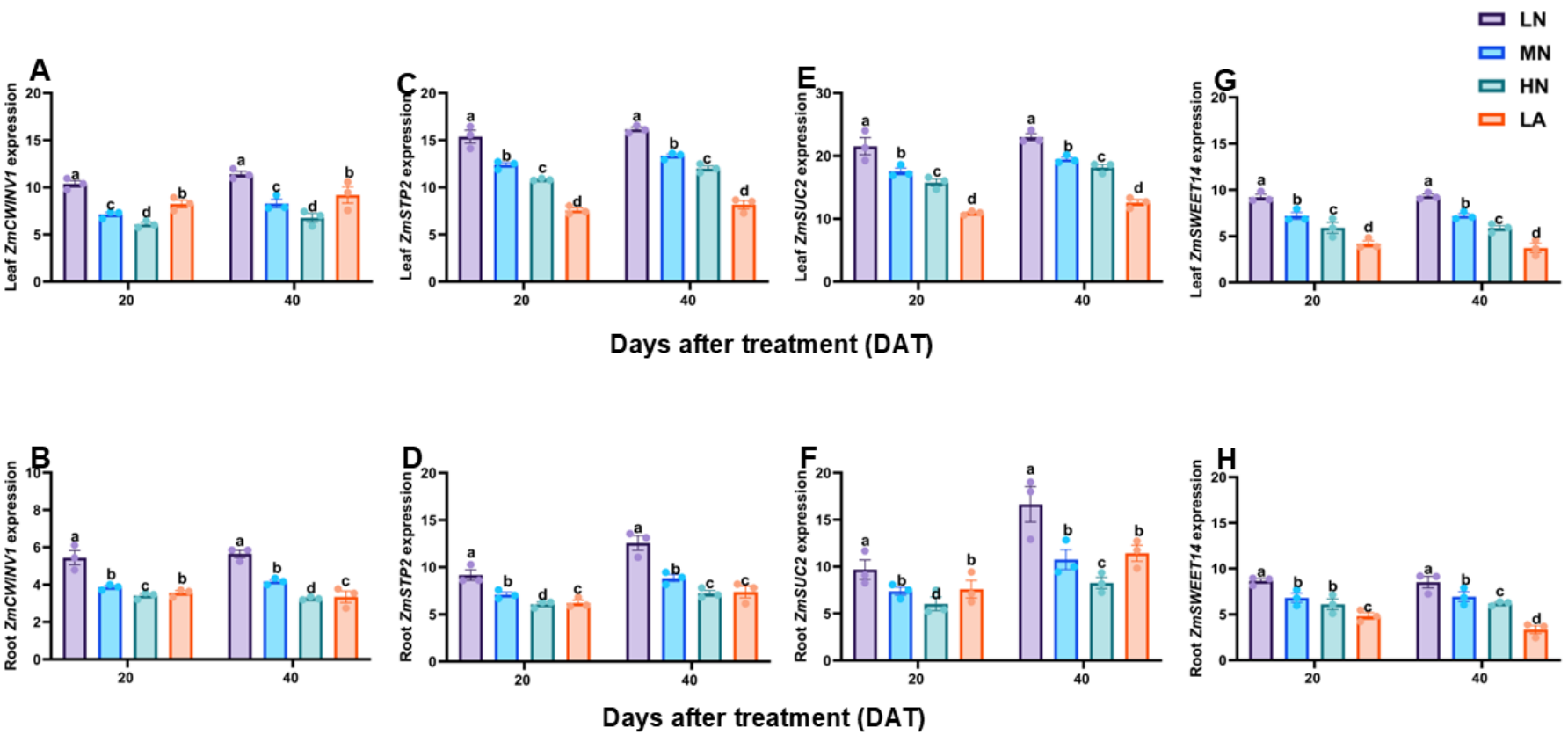

Fig. 3.4 Effect of different nitrogen forms on the expression pattern of sugar metabolizing and sucrose transporter genes. Expression level of *ZmCWINV1*, *ZmSTP2*, *ZmSUC2* and *ZmSWEET14* in the leaves (**A**, **C**, **E**, **G**) and roots (**B**, **D**, **F**, **H**) of maize inbred line TX-40J. Data are presented as mean ± SE (n = 6). Statistical significance was determined using Tukey's multiple range test ($P \leq 0.05$), with different letters indicating significant differences between treatments. FW, fresh weight; LN, low nitrogen (N deficiency); MN, moderate nitrogen; HN, high nitrogen; LA, low ammonium treatment.

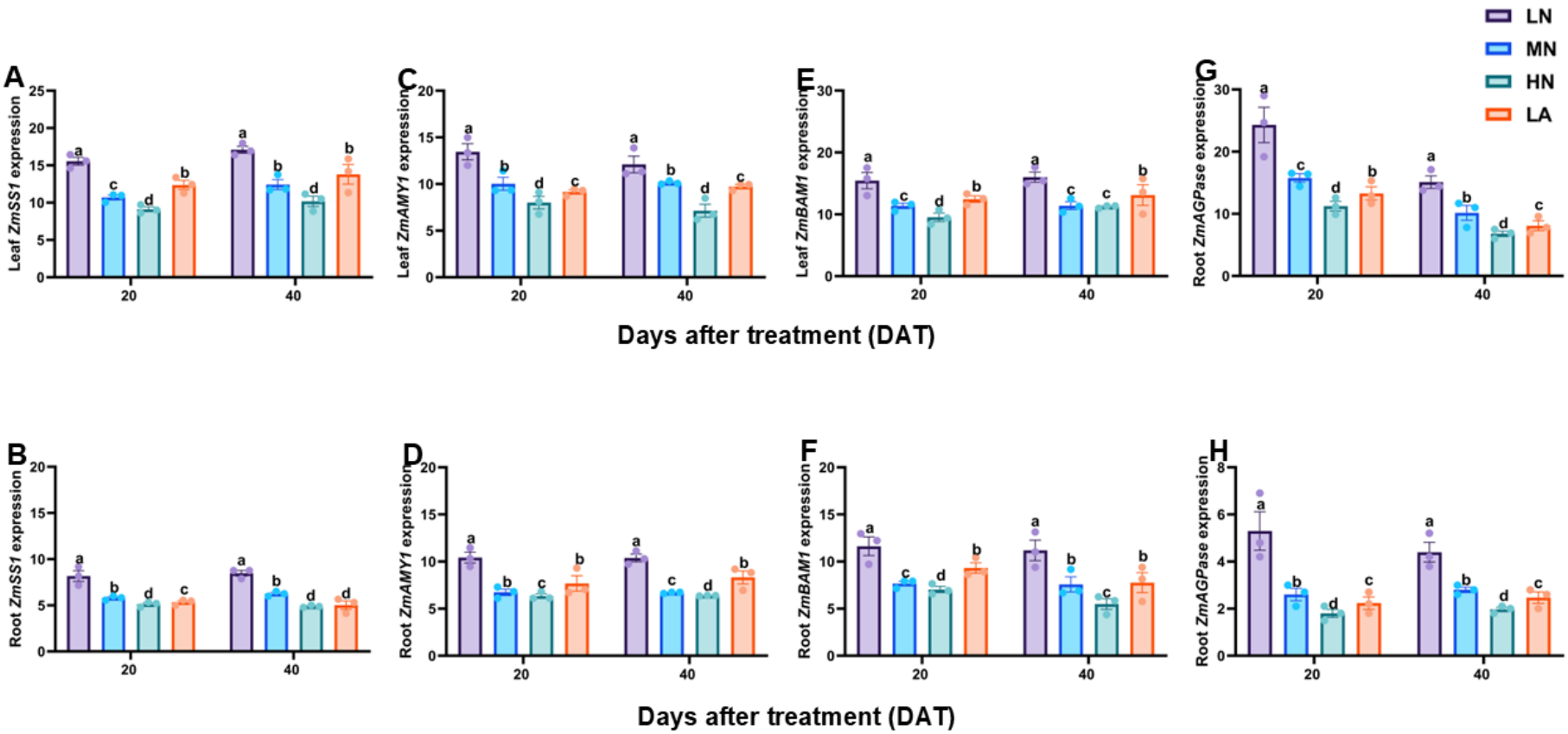

Fig. 3.5 Effect of different nitrogen forms on the expression pattern of starch metabolizing genes. Expression level of *ZmSS1*, *ZmAMY1*, *ZmBAM1* and *ZmAGPase1* in the leaves (**A**, **C**, **E**, **G**) and roots (**B**, **D**, **F**, **H**) of maize inbred line TX-40J. Data are presented as mean ± SE (n = 6). Statistical significance was determined using Tukey's multiple range test ($P \leq 0.05$), with different letters indicating significant differences between treatments. FW, fresh weight; LN, low nitrogen (N deficiency); MN, moderate nitrogen; HN, high nitrogen; LA, low ammonium treatment.

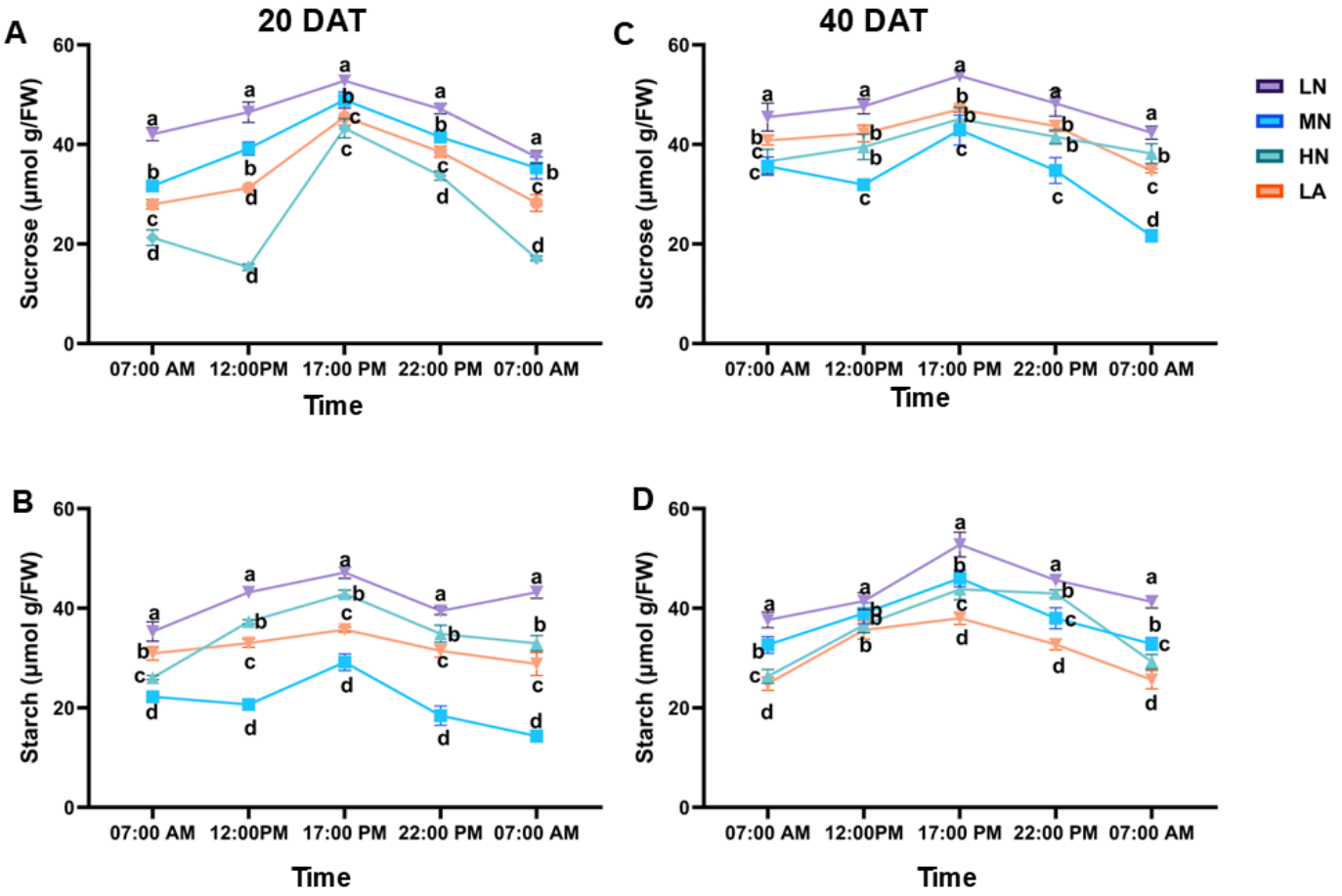

Fig. 3.6 Diurnal changes in leaf sucrose (**A**) and starch (**B**) at 20 days after treatment (DAT) and leaf sucrose (**C**) and starch (**D**) at 40 DAT under different nitrogen treatments. Samples were collected at 7:00, 12:00, 17:00, 22:00, and 7:00 on the second day. Data are presented as mean ± SE (n = 6). Statistical significance was determined using Tukey's multiple range test ($P \leq 0.05$), with different letters indicating significant differences between treatments. FW, fresh weight; LN, low nitrogen (N deficiency); MN, moderate nitrogen; HN, high nitrogen; LA, low ammonium treatment.

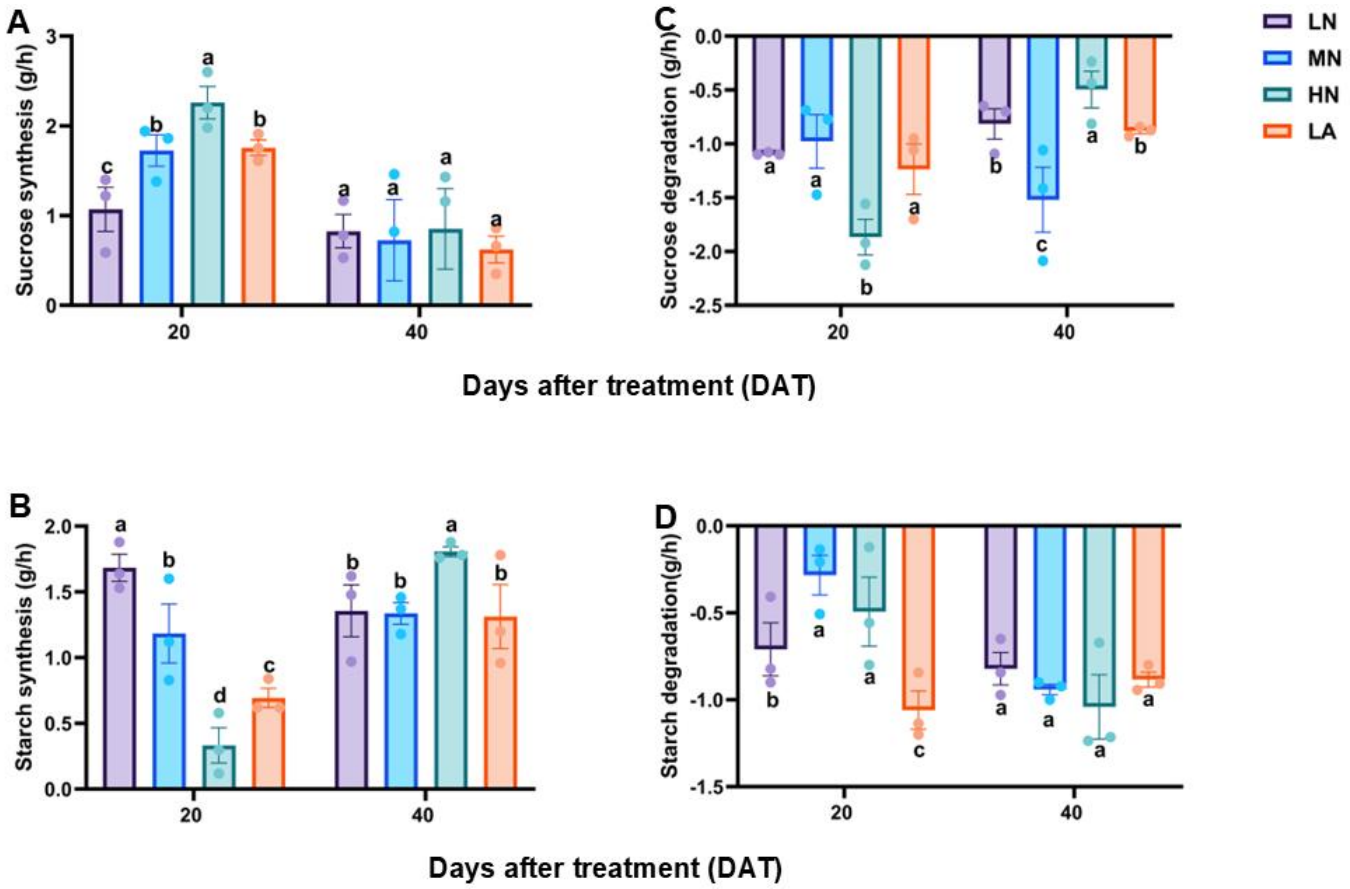

Fig. 3.7 Sucrose (**A**) and starch (**B**) synthesis and sucrose (**C**) and starch (**D**) degradation in the leaves of maize inbred line TX-40J grown under varying nitrogen treatments. Data are presented as mean ± SE (n = 6). Statistical significance was determined using Tukey's multiple range test ($P \leq 0.05$), with different letters indicating significant differences between treatments. FW, fresh weight; LN, low nitrogen (N deficiency); MN, moderate nitrogen; HN, high nitrogen; LA, low ammonium treatment.

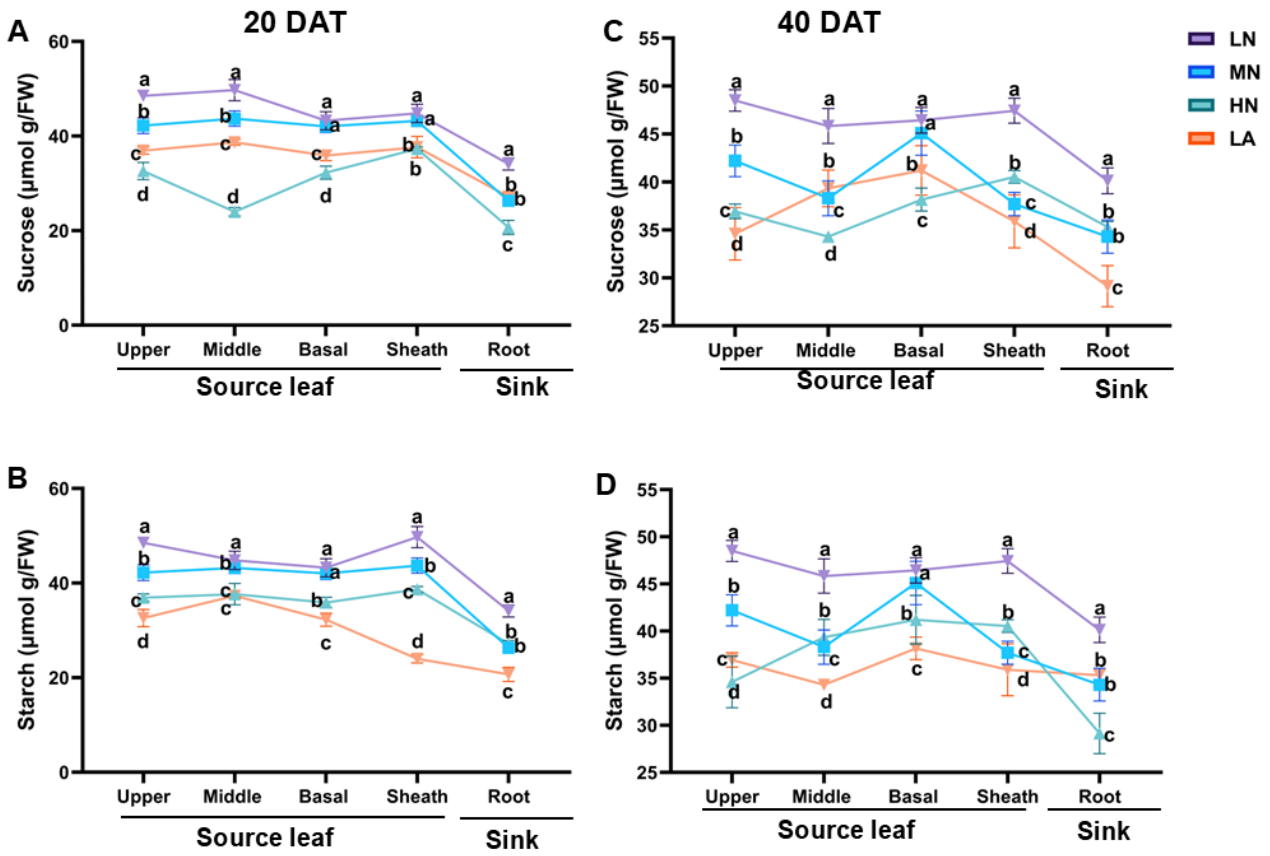

Fig. 3.8 Leaf sucrose (**A**) and starch (**B**) at 20 DAT, and leaf sucrose (**C**) and starch (**D**) at 40 DAT in different tissues under various nitrogen form treatments. Data are presented as mean ± SE (n = 6). Statistical significance was determined using Tukey's multiple range test ($P \leq 0.05$), with different letters indicating significant differences between treatments. FW, fresh weight; LN, low nitrogen (N deficiency); MN, moderate nitrogen; HN, high nitrogen; LA, low ammonium treatment.

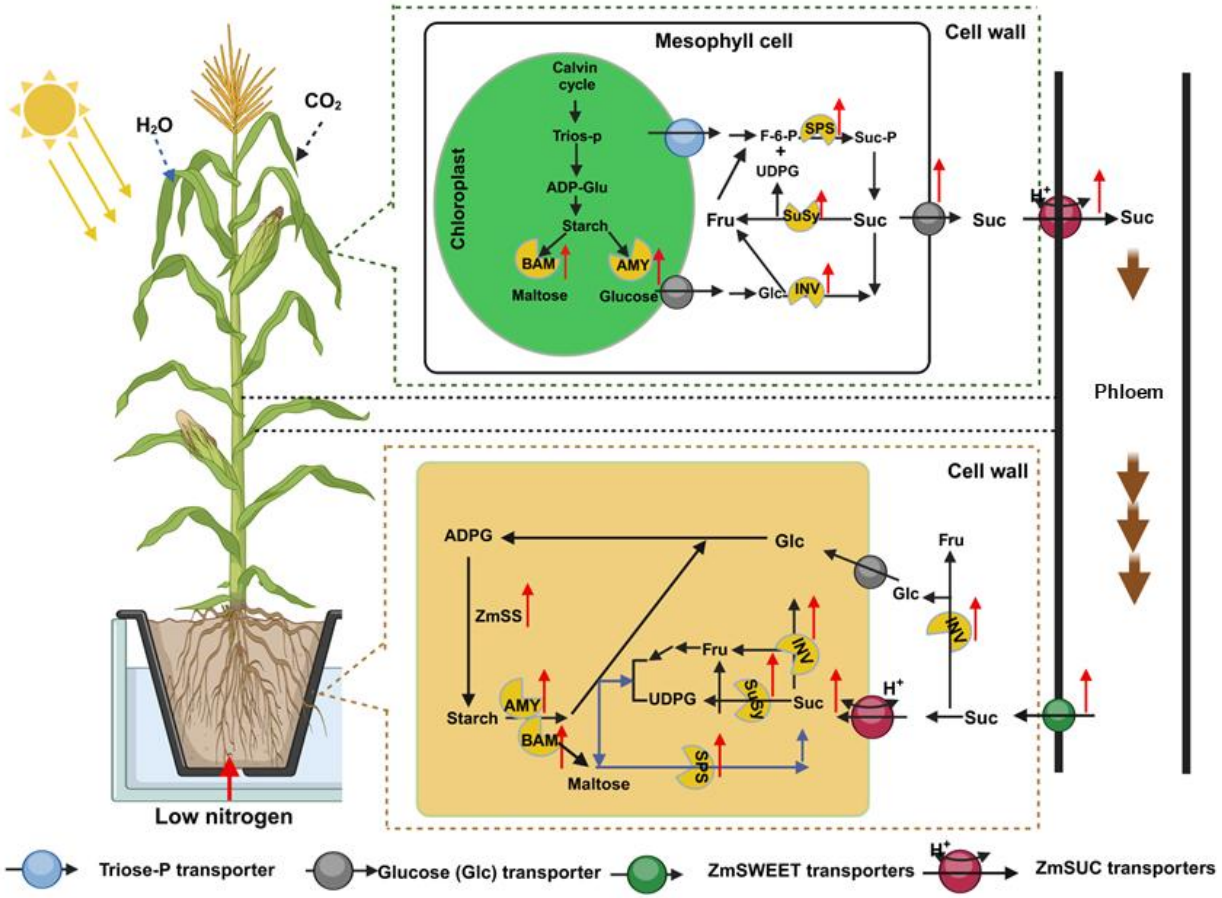

Fig. 3.9 A proposed model of sugar regulation in maize seedlings in response to N deficiency (low nitrogen; LN). LN triggers a sugar-mediated tandem reaction, enhancing maize tolerance to N deficiency. N limitation stress modifies the expression of key regulatory metabolic genes and the activities of sugar metabolism enzymes. This modulation influences sugar accumulation and activates sugar transporter transcription, thereby regulating sugar allocation for environmental adaptation. Upward red arrows represent upregulated components.

Table 3.1 Effect of different Nitrogen forms on growth, photosynthesis, total amino acid and protein content in the leaf and root of maize.

	20 DAT				40 DAT			
Shoot/leaf	**LN**	**MN**	**HN**	**LA**	**LN**	**MN**	**HN**	**LA**
Biomass	0.23 ± 0.02c	0.31 ± 0.04b	0.51 ± 0.02a	0.24 ± 0.03b	0.551 ± 0.02c	1.15 ± 0.04b	1.57 ± 0.14a	0.86 ± 0.08c
R/S ratio	0.59 ± 0.06a	0.28 ± 0.05b	0.13 ± 0.01c	0.31 ± 0.04b	0.772 ± 0.06a	0.26 ± 0.03c	0.09 ± 0.0s1d	0.37 ± 0.04b
T. biomass	0.31 ± 0.02c	0.40 ± 0.04c	0.69 ± 0.02a	0.42 ± 0.04c	0.77 ± 0.03d	1.46 ± 0.05b	1.98 ± 0.16a	1.19 ± 0.08c
Pn	20.06 ± 0.53d	27.11 ± 0.99b	32.08 ± 1.22a	23.02 ± 0.95c	22.18 ± 2.31d	31.20 ± 1.24b	35.27 ± 0.80a	27.10 ± 1.10c
Nitrogen	61.16 ± 4.50d	83.19 ± 2.86b	99.28 ± 4.39a	74.50 ± 3.81c	66.98 ± 3.19d	99.75 ± 1.32b	112.05 ± 3.72a	85.82 ± 1.99c
Amino acid	14.73 ± 0.64d	22.95 ± 1.12b	28.77 ± 1.16a	18.63 ± 1.27c	10.80 ± 0.52d	20.99 ± 1.32b	26.52 ± 1.68a	13.55 ± 0.78c
Protein	29.46 ± 1.28d	47.55 ± 2.78b	57.30 ± 2.31a	37.26 ± 2.58c	21.61 ± 1.05d	41.90 ± 2.64b	53.06 ± 3.35a	27.13 ± 1.56c

	20 DAT				40 DAT			
Root	**LN**	**MN**	**HN**	**LA**	**LN**	**MN**	**HN**	**LA**
Biomass	0.14 ± 0.04a	0.07 ± 0.02c	0.05 ± 0.01d	0.11 ± 0.04b	0.49 ± 0.03a	0.38 ± 0.01c	0.14 ± 0.02d	0.32 ± 0.02b
R/S ratio	0.59 ± 0.06a	0.22 ± 0.05b	0.13 ± 0.01c	0.35 ± 0.04b	0.77 ± 0.06a	0.25 ± 0.03c	0.09 ± 0.01d	0.37 ± 0.04b
Nitrogen	23.73 ± 0.77d	35.99 ± 1.60b	49.55 ±3.45a	29.36 ± 2.10c	24.54 ± 0.71d	32.41 ± 0.96b	41.09 ± 1.81a	30.15 ± 0.55c
Amino acid	8.36 ± 0.75d	15.35 ± 1.79b	20.58 ± 0.64a	12.30 ± 0.81c	6.55 ± 0.72d	9.33 ± 0.52b	11.33 ± 0.75a	8.55 ± 0.64c
Protein	16.79 ± 1.50d	30.67 ± 3.59b	41.89 ± 1.60a	24.63 ± 1.62c	13.06 ± 1.44d	18.47 ± 1.03b	22.69 ± 1.51a	17.06 ± 1.28c

Data are presented as mean ± SEM (n = 6). Statistical significance was determined using Tukey's multiple range test ($P < 0.05$), with different letters indicating significant differences between treatments. FW and DW denotes fresh and dry weights; LN: low nitrogen (N deficiency), MN: moderate nitrogen, HN: high nitrogen, and LA: low ammonium treatment; DAT: days after transfer, Pn; net photosynthesis, R/S ratio; root-shoot ratio and T. biomass; total biomass.

Table 3.2 Two-way analysis of variance (ANOVA) for the indicators studied in the shoot/leaf and root of maize inbred-line TX-40J under different N treatments.

Trait/(plants)	Sources of variations					
	Shoot/leaf			Root		
	S (df=1)	**T (df=3)**	**S x T (df=3)**	**S (df=1)**	**T (df=3)**	**S x T (df=3)**
Biomass	0.0046**	0.0017**	0.5867ns	0.0079**	0.0053**	0.0168*
T. biomass	0.0024**	0.0469*	0.1272ns	0.4841ns	0.0069**	0.0933ns
Pn	0.0828ns	0.0057**	0.6957ns	n/a	n/a	n/a
Sucrose	0.3649ns	0.00478**	0.6724ns	0.001**	0.0065**	0.0761ns
Nitrogen	0.0066**	0.0146*	0.5013ns	0.0724ns	0.0022**	0.2929ns
S. sugar	0.0084**	0.0031**	0.1439ns	0.0029**	0.0081**	0.0093**
Sucrose	0.3649ns	0.0047**	0.6724ns	0.001**	0.0065**	0.0761ns
Starch	0.0021**	0.0032**	0.0677ns	0.004**	0.0047**	0.3294ns
Fructose	0.0522ns	0.0125*	0.1901ns	0.0381*	0.0086**	0.5235ns
Glucose	0.5173ns	0.0044**	0.1753ns	0.2566ns	0.0158*	0.3824ns
Hexose	0.1592ns	0.0008***	0.1495ns	0.1522ns	0.0007***	0.1695ns
TNC	0.002**	0.0005***	0.1207ns	0.0065**	0.0023**	0.1237ns
H/S ratio	0.3255ns	0.0101*	0.4445ns	0.0151*	0.1462ns	0.0469*
SPS	0.0084**	0.0031**	0.1439ns	0.0147*	0.0062**	0.0315*
SuSy	0.0355*	0.0087**	0.7709ns	0.0032**	0.0152*	0.5101ns
AGPase	0.0064**	0.0563ns	0.2363ns	0.438ns	0.0063**	0.2436ns
CINV	0.1131ns	0.003**	0.7025ns	0.1801ns	0.0073**	0.0445*
VINV	0.0438*	0.0115*	0.1266ns	0.019*	0.0003***	0.0605ns
CWINV	0.0005***	0.0162*	0.1512ns	0.0011**	0.0057**	0.4607ns
Amino acid	0.0209*	0.0005***	0.6194NS	0.0199*	0.0131*	0.1075ns
Total protein	0.031*	0.0023**	0.7153ns	0.0236*	0.0092**	0.0999ns
TSUC	0.0201*	0.0036**	0.5331ns	0.0078**	0.003**	0.0184*
ZmSuSy1	0.2054ns	0.0195*	0.3628ns	0.1572ns	0.0154*	0.8374ns
ZmSPS1	0.6194ns	0.0183*	0.4934ns	0.4353ns	0.0384*	0.8592ns
ZmCINV1	0.0387*	0.0169*	0.645ns	0.673ns	0.0011**	0.8434ns
ZmVINV1	0.6256ns	0.0097**	0.6616ns	0.1943ns	0.0482*	0.1635ns
ZmCWINV1	0.0428*	0.009**	0.8617ns	0.7135ns	0.0074**	0.2518ns
ZmAGPase1	0.0215*	0.0121*	0.3896ns	0.3421ns	0.0407*	0.1725ns
ZmSUC2	0.0602ns	0.0026**	0.7507ns	0.0049**	0.0169*	0.6381ns
ZmSWEET14	0.9827ns	0.0582ns	0.9378ns	0.0119*	0.0225*	0.3619ns
ZmSS1	0.0428*	0.009**	0.8617ns	0.7137ns	0.0074**	0.2518ns
ZmAMY1	0.04644*	0.0183*	0.4934ns	0.6441ns	0.0016**	0.8302ns
ZmBAM1	0.0253*	0.0074**	0.4297ns	0.1206ns	0.0370*	0.1709ns
SS	0.0004***	<0.0001****	0.0632ns	0.01801**	0.0017**	0.1221ns
AMY	0.0047**	<0.0001***	0.0413*	0.011*	<0.0001****	0.0919ns
BAM	0.0449*	0.001**	0.0061**	0.0277*	0.0021**	0.5368ns

R/S ratio, root-to-shoot ratio; T. biomass, total biomass; S, growth stage; T, treatment; S x T, growth stage and treatment interaction; S. sugar; soluble sugar; Pn, net photosynthetic rate; H/S ratio, hexose/sucrose ratio; SuSy, sucrose synthase activity; CINV/*ZmCINV1*, cytoplasmic invertase activity; VINV/*ZmVINV1*, vacuolar invertase activity; SPS/ZmSPS1, sucrose phosphate synthase; AGPase/ZmAGPase1, ADP-glucose pyrophosphorylase; TSUC, total sucrolytic activity; TNC, total non-structural carbohydrate; ns, non-significant; na, non-applicable. Additionally, *, **, and ***: denote significance at probability levels of 0.05, 0.01, and 0.001, respectively. Tissue biomasses were quantified as g DW, net photosynthesis was quantified as [μmol (CO_2) m^{-2} s^{-1}], while other indicators were quantified as (μmol/g DW).

Table 3.3 Pearson's correlation analysis of R/S ratio with physio-biochemical and molecular indicators in the leaves and root of maize.

Traits/(plant)	Leaf	Root
Shoot biomass	-0.941**	0.968***
Total biomass	-0.921**	-0.921**
Nitrogen	-0.978**	-0.921**
Net photosynthetic rate	-0.957**	-0.924**
Soluble sugar	0.548**	0.235**
Sucrose	0.641**	0.574**
Total amino acid content	-0.926**	-0.967**
Total protein content	-0.926**	-0.959**
Starch content	0.788**	0.948**
Fructose content	0.638**	0.544**
Glucose content	0.544**	0.678**
Hexose content	0.583**	0.583**
Hexose/sucrose ratio	0.482**	0.657**
Non-structured carbohydrates	0.341ns	0.404**
Sucrose phosphate synthase	0.548**	0.235**
Sucrose synthase	0.658**	0.850**
Cytoplasmic invertase	0.876**	0.896**
Vacuolar inveretase	0.999**	0.980**
Cell wall invertase	0.981**	0.963**
Total sucrolytic activity	0.937**	0.963**
AGPase activity	0.935**	0.947**
Starch synthase	0.807**	0.871**
α-amylase	0.856**	0.998**
β-amylase	0.871**	0.958**
ZmSuSy1	0.772**	0.624**
ZmSPS1	-0.948**	0.986**
ZmCINV1	0.990**	0.585**
ZmVINV1	0.996**	1.000**
ZmCWNV1	0.995**	0.908*
ZmSTP2	0.996**	1.000**
ZmSUC2	0.511**	0.997**
ZmSWEET14	0.617**	0.955**
ZmAGPase1	0.934**	0.547**
ZmSS1	0.995**	0.576**
ZmAMY1	0.959**	0.558**
ZmBAM1	0.994**	0.640**

*, **, ***, ns denotes $P < 0.05$, 0.01, 0.001 and not significant, respectively.

3.4. Discussion

Maize depends greatly on N for growth and development, and studies have shown that different N forms distinctly influence plant physiological responses (Nematpour and Eshghizadeh 2024). In this study, LN treatment significantly ($P \leq 0.05$) reduced total biomass due to suppressed photosynthesis and C fixation. Despite overall biomass reduction, the enhanced root growth resulted in a R/S ratio (Table 3.1). This shift reflects an adaptive strategy to allocate limited C toward root systems to improve nutrient acquisition under N deficiency (Zhao et al. 2020). Moreover, plants grown under MN and HN treatments accumulated more amino acids, proteins, and total N, correlating with enhanced growth (Table 3.1). These findings highlight the essential role of adequate NO_3^- supply in promoting N assimilation and physiological performance (Wang et al. 2021b). In contrast, LN impaired amino acid and protein synthesis, further limiting shoot development. Our findings underscore the strong interaction between N and C metabolism, as reduced N availability disrupted photosynthesis and led to altered biomass partitioning (Wang et al. 2021a). The findings emphasize the role of LN in maintaining the balance between N and C metabolism, which is essential for maximizing plant growth, NUE, and overall productivity under N deficiency condition (Aluko et al. 2023a).

3.4.1. LN increased sugars and starch accumulation in leaves, optimizing C allocation and sustaining growth under N deficiency

Efficient coordination between C fixation and downstream metabolism is essential for plant growth and development. LN inhibited photosynthetic C assimilation, resulting in metabolic disruption that constrained growth (Table 3.1). However, maize leaves under LN accumulated higher sugars and non-structured carbohydrates (Figs. 3.1A, C, E and S3.1A, C, E, G). The observed sugar accumulation reflects and adaptive shift in C metabolism, supported by enhanced activities and upregulation of sucrose metabolism enzymes, SPS, SuSy, CINV, VINV and CWIN and their associated genes, *ZmSPS1*, *ZmSuSy1*, *ZmCINV1*, *ZmVINV1* and *ZmCWINV1* (Figs. 3.2A, C. E, G and 3.4A). Although sucrolytic enzymes activity and their corresponding genes were upregulated under LN, sucrose level remained higher in the leaves, which may be due to enhanced biosynthesis and turnover, as indicated by elevated SPS and SuSy activities and simultaneous synthesis and degradation (Figs. 3.2A, B, C, D) supporting energy demands while maintaining sucrose for osmotic and signalling functions (Bilska-Kos et al. 2020). Furthermore, a positive correlation was observed between R/S ratio and the level of sugars in LN plants (Table 3.3), indicating a preferential partitioning of C to the root systems as a strategic adaptation to N limitation. LN upregulated the expression of sucrose transporter genes, *ZmSUC2*, *ZmSTP2* and *ZmSWEET14* in both the leaves (Fig. 3.4C, E, G) and roots (Fig. 3.4D, F, H) of maize seedlings, indicating enhanced source-to-sink movement, improved phloem loading and unloading efficiency, and C partitioning to the roots to support growth during N stress (Lemoine et al. 2013;

Saddhe et al. 2021). Furthermore, the significantly increased root sugar and starch metabolism, along with increased root ratios in maize seedlings under LN can be attributed to the CO_2-concentrating mechanism in C_4 plants, which enables reduced abundance of Ribulose-1,5-bisphosphate carboxylase/oxygenase (Rubisco) and enhances NUE (Evans and Clarke 2019). Unlike C_4 species such as maize, C_3 plants like wheat depends greatly on Rubisco to maintain efficient photosynthesis, requiring greater N investment in the photosynthetic apparatus. In contrast, maize can strategically allocate more N toward root development and stress adaptation (Lemaire et al. 2008). This suggests that the reduced leaf N content observed in LN-treated maize likely facilitated increased N investment in root biomass and sink strength. C_3 plants, by comparison, may experience greater constraints under N limitation due to the higher N demands associated with maintaining photosynthetic capacity (Gao et al. 2015; Mu and Chen 2021). Future research will explore the mechanistic links between N investment in Rubisco and belowground resource allocation under varying N regimes across photosynthetic types. Comparative analyses between C_3 and C_4 species will provide a comprehensive insight into N budgeting strategies and their implications for root development, stress adaptation, and overall NUE.

Starch metabolism responds dynamically to N availability, reflecting it role in adaptive C storage under N limited conditions (Zhao et al. 2020). LN induced starch accumulation (Fig. 3.1G-H), with upregulation of starch biosynthetic (*ZmSS1*, *ZmAGPase1*,) (Fig. 3.5A-B, G-H) and degradative (*ZmAMY1*, *ZmBAM1*) (Fig. 3.4C-D, E-F) genes and their corresponding enzymes (Figs. 3.2E-H, S3.3A-D). These dynamic responses reflect a tightly regulated starch turnover system that adjusts to N deficiency by balancing energy storage and mobilization (Smith and Zeeman 2020). A positive correlation was observed between R/S ratio, starch levels, metabolizing enzymes activity, and their associated genes (Table 3.3), which reinforces the central role of starch metabolism in the adaptive response of maize to N limitation (Kumar et al. 2023).

3.4.2. LN stimulates root carbohydrate metabolism for adaptive growth

Sugar metabolism is crucial for root development under N deficiency (Zhao et al. 2020). LN increase root SPS, SuSy and INVs activities (Figs. 3.2 and S3.2B, D, F, H), along with upregulation of *ZmSPS1*, *ZmSuSy1*, *ZmCINV1*, *ZmVINV1* and *ZmCWINV1* (Figs. 3.3B, D, F, H and 3.4B), promoting sucrose breakdown and re-synthesis cycle. This led to an increased root sucrose content, correlating with increased enzyme activity and gene expression. Furthermore, starch metabolism was enhanced under LN, evidenced by increased SS, AGPase, AMY and BAM activities (Figs. 3.2F, H and S3.3B, D), and expression of *ZmSS1*, *ZmAGPase1*, *ZmAMY1* and *ZmBAM1* (Fig. 3.5B, D, F and H). These dynamic changes increased root starch and sugar content (Fig. 3.1), supporting stress resilience and improved root growth, as highlighted by (Du et al. 2020b). Increased root sink strength likely enhanced sucrose export from the leaves, supporting shoot-to-root C allocation. Interestingly, the R/S ratio correlated

positively with sugar content, sugar-metabolizing enzyme activities, and the expression of related genes (Table 3.3), emphasizing that the intensified recycling and storage of sucrose and starch contributed to an increased R/S ratio and improved adaptation to N limitation.

3.4.3. Diurnal regulation of carbohydrate metabolism by N form and availability

Carbohydrate levels followed diel rhythms, with LN plants exhibiting consistently higher sugar and starch levels across the photoperiods (Fig. 3.6A-D). Peak accumulation of sucrose and starch occurred by 17:00, followed by overnight declines, corresponding with photosynthetic accumulation and nighttime utilisation via respiration (Amoah and Kaiser 2025). LN plant maintained elevated sucrose and starch levels even after nocturnal export, indicating robust storage and mobilization. Furthermore, starch synthesis peaked under LN (Fig. 3.7B), demonstrating an adaptive mechanism for C storage when growth is limited by N (Zhao et al. 2020). Interestingly, MN-treated plants showed the highest overall sucrose and starch synthesis rates (Figs. 3.7A–B), reflecting a more balanced C/N status. Furthermore, starch and sucrose degradation was enhanced under LN (Figs. 3.8C–D), promoting rapid energy mobilization (Ma et al. 2024). Although MN increases sucrose accumulation, LN and HN plants showed comparable net starch accumulation at 40 DAT (Fig. S3.5A–B), revealing distinct metabolic priorities under different N regimes. LN promoted a dynamic turnover, while MN emphasized storage. These patterns highlight the importance of considering both N form and availability in regulating C metabolism.

3.4.4. N form and availability modulate tissue-specific carbohydrate distribution

Maize plants exhibited differential response to N availability, with LN showing the sugar and starch accumulation (Figs. 3.8A-D and S3.6A-D), particularly in the upper leaves at both 20 and 40 DAT. These plants also showed lower N content and distinct diurnal and spatial carbohydrate dynamics (Figs. 3.8 and S3.6 and Table 3.1). While significant variations in C accumulation in the leaves of plants under different N forms have been documented in some species (Lv et al. 2021), this study confirms that the sugar and starch profile in maize is influenced by N treatments, growth stage, and tissue type (Table 3.2), which is consistent with previous findings (Amoah and Kaiser 2025) and enhanced our understanding of N management in maize. Specifically, (a) N treatment induced distinct sucrose and starch pattern across stages. (b) LN boosted starch in the upper leaves and (c) LN plants maintained higher carbohydrates levels than other N treatment plants. These results emphasizes that N forms and availability shape carbohydrate partitioning strategies. LN-treated plants retained more carbohydrates, indicating a shift toward energy conservation under stress. Future studies will examine the molecular and enzymatic mechanisms controlling sugar and starch redistribution between source and sink tissues.

3.5. Conclusion

This study demonstrated that low-nitrogen (LN) treatment increased the root-to-shoot (R/S) ratio in maize seedlings. This increase was attributed to a greater inhibition of shoot biomass accumulation compared to root biomass. Under LN treatment, maize growth was predominantly regulated by sugar metabolism, allocation, and transport (Fig. 9). LN conditions enhanced the activities of sucrose and starch metabolism enzymes and upregulated the expression of genes such as *ZmSPS1*, *ZmSuSy1*, *ZmVINV1*, *ZmCINV1*, *ZmCWINV1*, *ZmAMY1*, *ZmAGPase1*, and *ZmBAM1*. These changes improved the efficiency of sucrose and starch utilization. Furthermore, LN treatment upregulated the expression of sugar transporter genes, including *ZmSWEET14*, *ZmSUC2*, and *ZmSTP2*, in both the leaves and roots of maize seedlings. This facilitated the transport of sucrose from leaves to roots. In summary, nitrogen deficiency elevated the levels of soluble sugars and starch in maize by regulating sugar metabolism and transport. This mechanism appears to be a preferred strategy for sustaining root growth and metabolism under N-limited conditions. Future studies will explore the effects of various N forms through several approaches. (a) conducting field trials across diverse agricultural soils and environmental conditions would help validate these findings and provide practical insights. (b) examining different genotypes and crop species is essential to assess the broader implications for NUE, as this study focused on the high-performing maize inbred line TX-40J, which may limit the applicability of the results to other maize varieties and crops. (c), incorporating detailed anatomical and transcriptomic analyses would offer deeper insights into the physiological and molecular impacts of N availability on maize growth and development.

3.6. Supplementary data

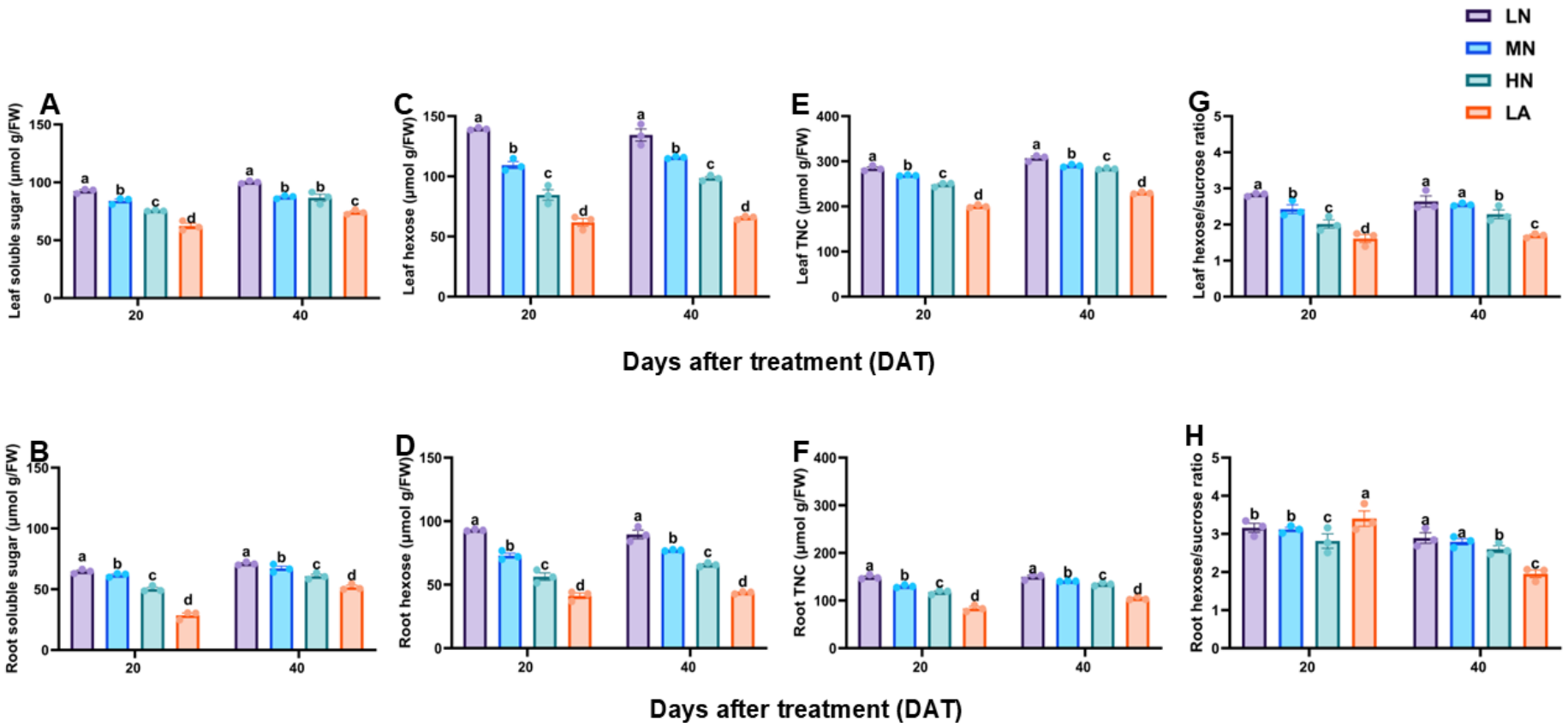

Fig. S3.1 Effect of different nitrogen forms on soluble sugar, hexose, total non-structural carbohydrate and hexose: sucrose ratio in the leaves (**A**, **C**, **E**, **G**) and roots (**B**, **D**, **F**, **H**) of maize inbred line TX-40J. Data are presented as mean ± SE (n = 6). Statistical significance was determined using Tukey's multiple range test ($P \leq 0.05$), with different letters indicating significant differences between treatments. FW, fresh weight; LN, low nitrogen (N deficiency); MN, moderate nitrogen; HN, high nitrogen; LA, low ammonium treatment.

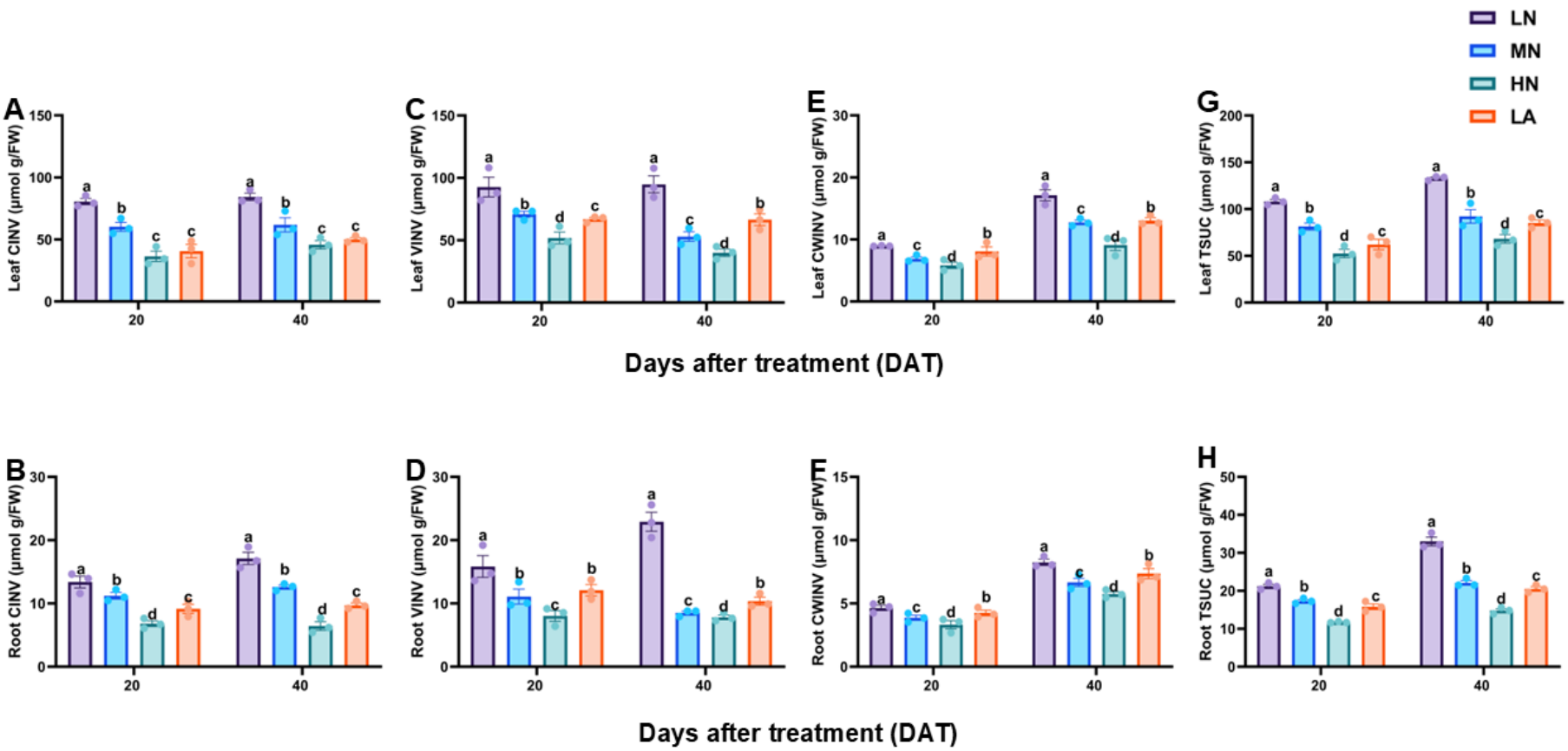

Fig. S3.2 Effect of different nitrogen forms on cytoplasmic invertase, vacuolar invertase, cell wall invertase, total sucrolytic activity in the leaves (**A**, **C**, **E**, **G**) and roots (**B**, **D**, **F**, **H**) of maize inbred line TX-40J. Data are presented as mean ± SE (n = 6). Statistical significance was determined using Tukey's multiple range test ($P \leq 0.05$), with different letters indicating significant differences between treatments. FW, fresh weight; LN, low nitrogen (N deficiency); MN, moderate nitrogen; HN, high nitrogen; LA, low ammonium treatment.

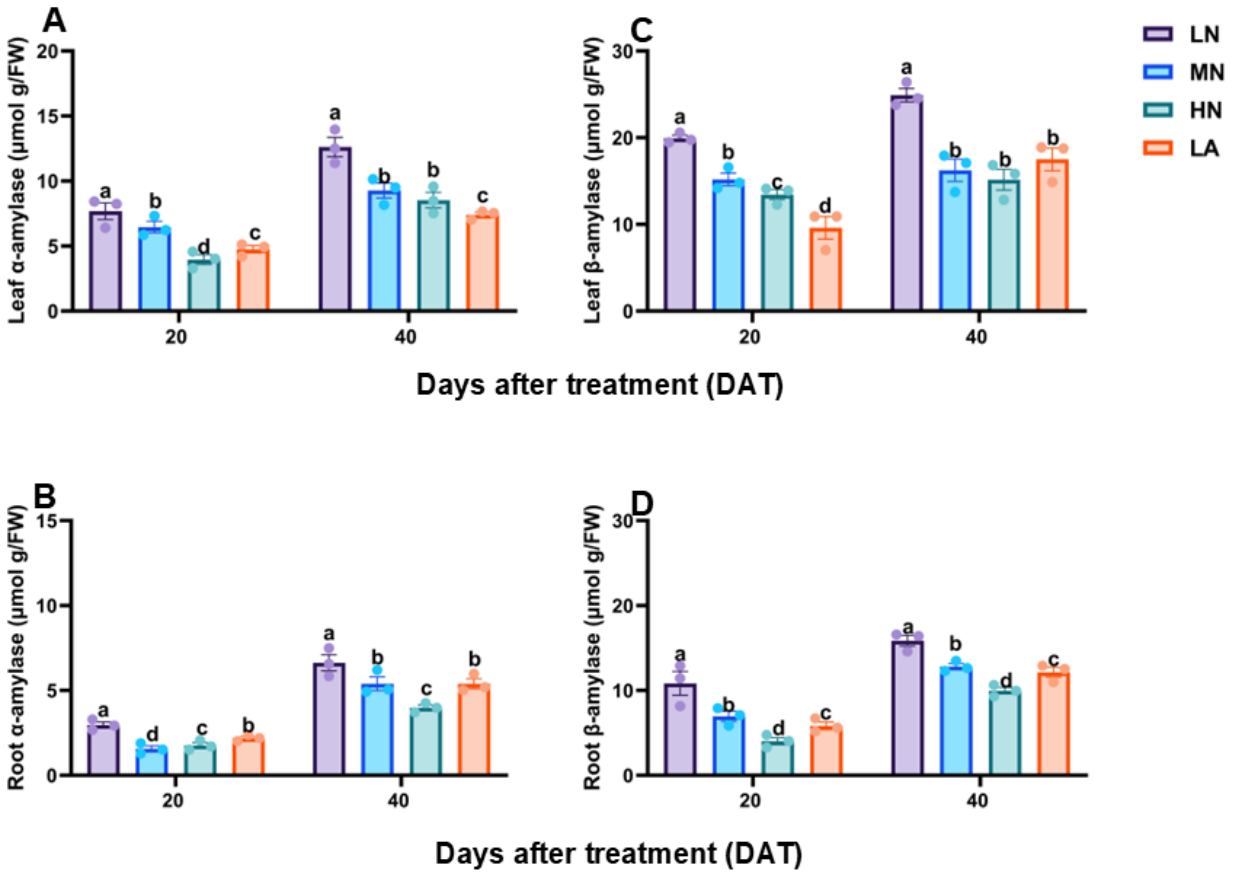

Fig. S3.3 Effect of different nitrogen forms on starch metabolizing enzymes activity. Leaf (A) and root (**B**) α-amylase and leaf (**C**) and root (**D**) β-amylase activity. Data are presented as mean ± SE (n = 6). Statistical significance was determined using Tukey's multiple range test ($P \leq 0.05$), with different letters indicating significant differences between treatments. FW, fresh weight; LN, low nitrogen (N deficiency); MN, moderate nitrogen; HN, high nitrogen; LA, low ammonium treatment.

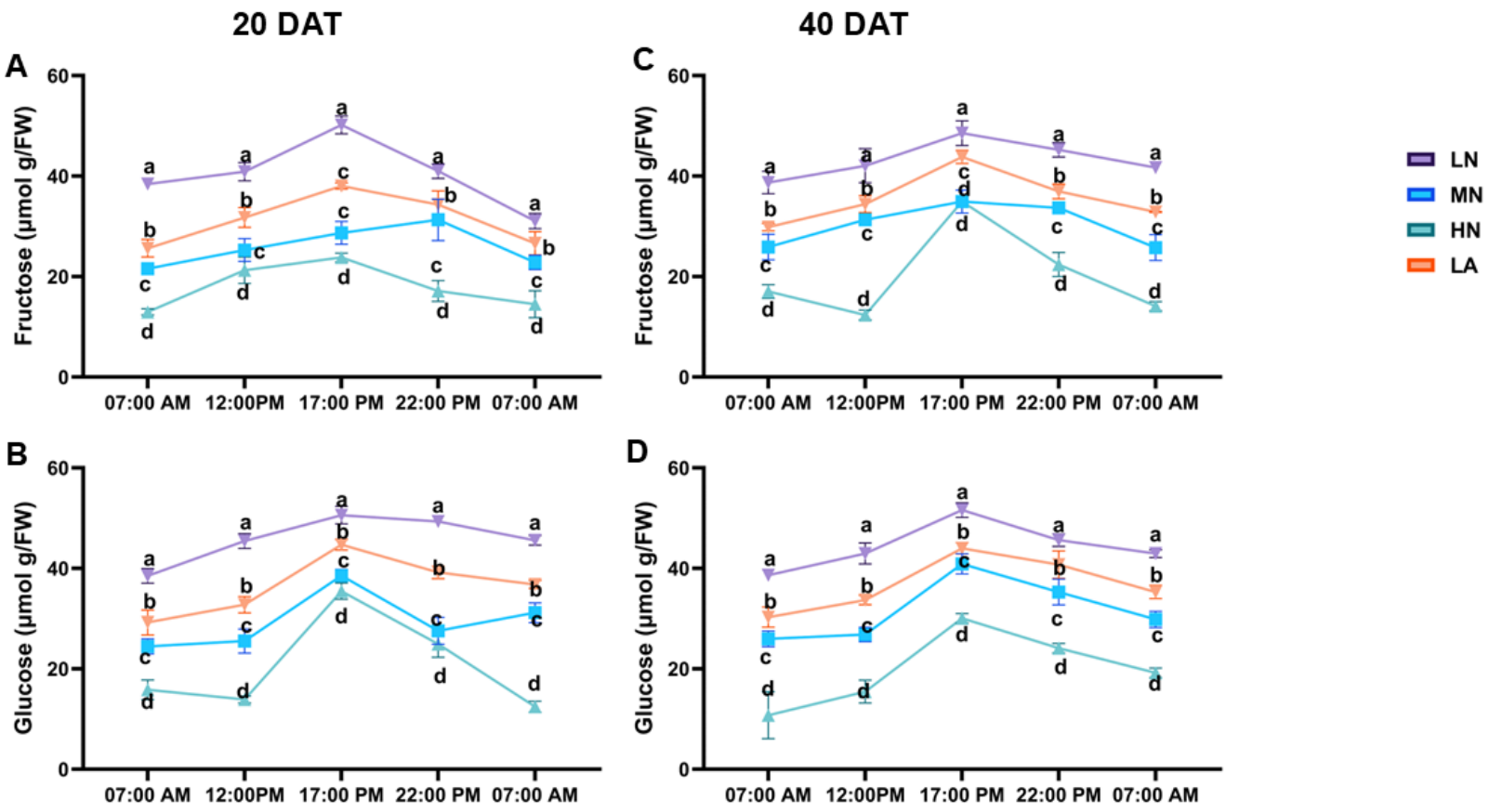

Fig. S3.4 Diurnal changes in leaf fructose (**A**) and glucose (**B**) at 20 days after treatment (DAT) and leaf fructose (**C**) and glucose (**D**) at 40 DAT under different nitrogen treatments. Samples were collected at 7:00, 12:00, 17:00, 22:00, and 7:00 on the second day. Data are presented as mean ± SE (n = 6). Statistical significance was determined using Tukey's multiple range test ($P \leq 0.05$), with different letters indicating significant differences between treatments. FW, fresh weight; LN, low nitrogen (N deficiency); MN, moderate nitrogen; HN, high nitrogen; LA, low ammonium treatment.

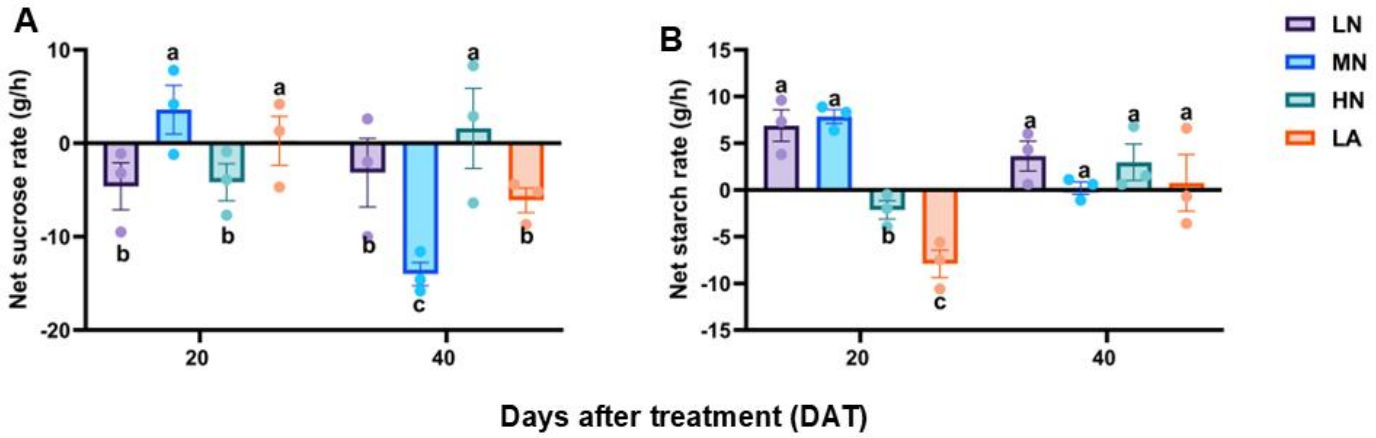

Fig. S3.5 Net sucrose (**A**) and net starch (**B**) accumulation rate in maize inbred line TX-40J grown under varying nitrogen treatments. Data are presented as mean ± SE (n = 6). Statistical significance was determined using Tukey's multiple range test ($P \leq 0.05$), with different letters indicating significant differences between treatments. FW, fresh weight; LN, low nitrogen (N deficiency); MN, moderate nitrogen; HN, high nitrogen; LA, low ammonium treatment.

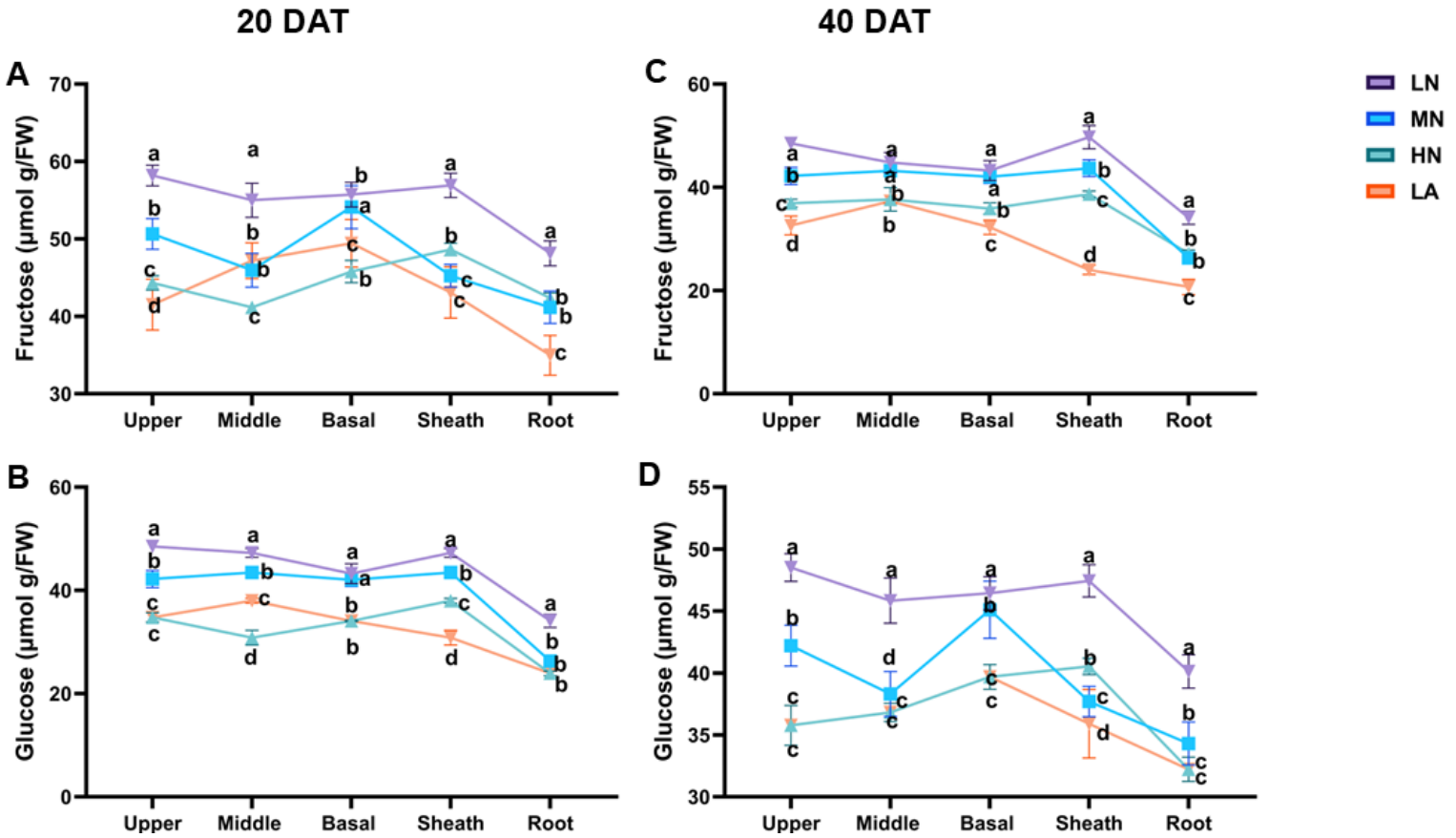

Fig. S3.6 Leaf fructose (**A**) and glucose (**B**) at 20 DAT, and leaf fructose (**C**) and glucose (**D**) at 40 DAT in different tissues under various nitrogen form treatments. Data are presented as mean ± SE (n = 6). Statistical significance was determined using Tukey's multiple range test ($P \leq 0.05$), with different letters indicating significant differences between treatments. FW, fresh weight; LN, low nitrogen (N deficiency); MN, moderate nitrogen; HN, high nitrogen; LA, low ammonium treatment.

Table S3.1 List of equations used for estimating sucrose and starch synthesis, degradation and net accumulations rates

1. Sucrose and starch degradation equations:

$$\text{Sucrose synthesis rate} = \frac{\text{Sucrose at 12:00 PM} - \text{Sucrose at 07:00 AM}}{5\text{h}}$$

$$\text{Starch synthesis rate} = \frac{\text{Starch at 12:00 PM} - \text{Starch at 07:00 AM}}{5\text{h}}$$

2. Sucrose and starch degradation equations:

$$\text{Sucrose degradation rate} = \frac{\text{Sucrose at 10:00 PM} - \text{Sucrose at 07:00 AM (Next day)}}{9\text{ h}}$$

$$\text{Starch degradation rate} = \frac{\text{Starch at 10:00 PM} - \text{Starch at 07:00 AM (Next day)}}{9\text{ h}}$$

3. Net sucrose and starch accumulation rates:

Net sucrose accumulation = Sucrose synthesis value – Sucrose degradation value

Net starch accumulation = Starch synthesis – Starch degradation values

Table S3.2 List of genes studied

Gene name	NCBI LOCs
LOC542247	*ZmSuSy*
LOC542711	*ZmSPS*
LOC541615	*ZmSUC2*
LOC542737	*ZmAGPase*
LOC541669	*ZmSS*
LOC100273083	*ZmSTP2*
LOC100280251	*ZmSUT2*
LOC100273029	*ZmAMY1*
LOC542472	*ZmBAM1*
LOC542324	*ZmVINV*
LOC100382511	*ZMCINV*
LOC100282267	*ZmActin*
LOC541665	*ZmUBQc*
LOC542314	*ZmCWINV*

CHAPTER 4: NITROGEN DEFICIENCY IDENTIFIES CARBON METABOLISM PATHWAYS AND ROOT ADAPTATION IN MAIZE[3]

Abstract

Sugars are essential for plant development, with nitrogen (N) availability playing a critical role in their distribution across plant organs, ultimately shaping growth patterns. However, the regulatory mechanisms governing carbon (C) assimilate allocation and utilization under different N forms is not well understood. This study examined C fixation, utilization, and spatial re-distribution in the roots of hydroponically grown maize seedlings subjected to four N treatments: 1 mM NO_3^- (low N; LN), 2 mM NO_3^- (medium N; MN), 10 mM NO_3^- (high N; HN), and 1 mM NH_4^+ (low ammonium; LA). LN treatment significantly increased soluble sugar, sucrose, and starch contents while promoting greater root biomass at the expense of shoot biomass, leading to a higher root to shoot assimilate allocation. The activities of sugar and starch metabolism enzymes were more tightly regulated under LN, indicating enhanced C utilization and increased competition for assimilates. Key genes involved in sugar (*ZmSPS*, *ZmSuSy*, *ZmSWEET6*, *ZmSUC2*, *ZmSTP2*, and *ZmAINV1*) and starch (*ZmAGPASE* and *ZmSS*) metabolism were upregulated under LN, correlating with increased root sucrose and starch accumulation and enhanced enzyme activity. Sucrose and starch accumulated predominantly in the brace and lateral roots. This pattern suggests that excess C accumulation results from inefficient C utilization in sink tissues rather than impaired C assimilation. These findings provide new insights into how LN modulates C partitioning in roots for stress adaptation, highlighting the importance of improving C utilization in sink tissues to mitigate N deficiency and enhance plant growth.

Keywords: Adaptation, Root development, Root system architecture, Nitrogen use efficiency, *Zea mays*

---

[3]This chapter is published as: Amoah JN, Keitel C, Kaiser BN (2025) Nitrogen deficiency identifies carbon metabolism pathways and root adaptation in maize. Physiology and Molecular Biology of Plants. doi:10.1007/s12298-025-01631-0

4.1. Introduction

Nitrogen (N) is a vital macronutrient, and its forms, nitrate (NO_3^-) or ammonium (NH_4^+), are integral to various plant metabolic processes, including growth, development, and the production of harvestable yields. Carbon (C) is equally important to plant function, serving as both structural component and primary energy source (Artins et al. 2024). C is captured and assimilated through photosynthesis and distributed across various organs to support metabolism and contribute to biomass accumulation (Cui et al. 2025). The intricate coordination between C and N metabolism is essential for plant productivity (Nunes Pires et al. 2024). N availability not only impact photosynthetic efficiency and C assimilation but also modulate C portioning among plant organs. Conversely, C supply to roots support N uptake by promoting root growth and metabolic activity. This dynamic interplay between C and N modulates various developmental and physiological processes, playing an important role in plant adaptation, particularly under limited-N conditions (Zhao et al. 2020).

Plant roots serve as the primary organs for nutrient and water acquisition from the soil, facilitating plant growth and development. The availability and form of N significantly influence root system architecture, affecting both primary root (PR) and lateral root (LR) development (Sun et al. 2017; Kiba and Krapp 2016; Zhao et al. 2024). For instance, previous studies have shown that N deficiency enhances PR and LR growth, whereas high N availability results in shorter PR and reduced LR numbers (Zhao et al. 2020; Xue et al. 2021; Huang et al. 2018). The plant root system consists of various components, such as LR, seminal roots (SR), PR, crown roots (CR), brace roots (BR), each playing a distinct role in N uptake to support plant growth and development (Zhang and Wu 2023). Root growth is rightly linked to the distribution of carbohydrates, especially under N deficient conditions. Source leaf-derived carbohydrates serve as intermediary substrates for metabolism, providing the necessary C for root growth and development (Schlüter et al. 2012b; Wang and Ruan 2015; Zhao et al. 2020). Understanding the mechanisms influencing carbohydrate distribution in roots in response to different N forms is crucial for elucidating the interplay between C and N, as well as the adaptive responses of plant roots to varying soil N conditions.

Roots, as sink organs, require carbohydrates provided by leaves to grow and develop. Carbohydrate allocation depends on sink strength, which is related to the ability to unload and metabolize translocated carbohydrates (Prescott 2022). Sucrose is the predominant carbohydrate transported from source to sink organs in plants. This process relies on the efficient phloem transport system, which includes the symplastic and apoplastic pathways (Chen et al. 2017). Phloem loading or unloading of sucrose in roots involves a symplastic pathway through plasmodesmata, while the apoplastic pathway requires sucrose transporters, such as *SUTs*, *SWEETs*, and *SUCs* (Braun 2022). Following sucrose unloading in the apoplastic pathway, sucrose is converted into glucose and fructose by cell wall invertase and transported to root cells by SUTs on the plasma membrane. Sucrose unloading

regulates sink strength and root cell growth. In sink cells, sucrose is converted to fructose and glucose by neutral invertase or to fructose and UDP-glucose by sucrose synthase (SuSy). Sucrose is also transported to the vacuole, where it is converted to glucose and fructose by vacuolar acid invertase. In vacuoles, sucrose concentration regulates cell turgor and expansion, promoting root growth. N forms and levels can affect the activity and expression of enzymes involved in sugar metabolism, as shown in various plants (Wang et al. 2006; Ruan et al. 2007; Zhang et al. 2021; Zhao et al. 2020; Huang et al. 2022). Previous studies have associated N deficiency with increased carbohydrate and nutrient ion allocation to roots (Terashima and Evans 1988), while N levels affect root sugar concentration (Dzamic and Stevanovic 1996). This finding has been confirmed in maize and citrus seedlings under varying NO_3^- concentrations (Zhao et al. 2020; Huang et al. 2022). In contrast, NH_4^+ nutrition inhibited root development but promoted photosynthesis in Arabidopsis and wheat (Guo et al. 2007b; Chen et al. 2020). However, there are few studies on sugar metabolism changes in roots under different N forms and levels. It remains unclear how root systems improve sugar metabolism efficiency to meet carbon requirements for growth under varying N forms.

Maize (*Zea mays* L.) was chosen for this study due to its significance as a staple food crop and its suitability as a model for investigating N metabolism and C allocation (Simons et al. 2014). Its growth patterns, responsiveness to environmental factors, and adaptability to various N conditions make it ideal for examining the effects of N forms and levels on carbon distribution (Dong et al. 2023b). Optimizing N management in maize can significantly enhance global agricultural productivity (Begam et al. 2024). To elucidate the mechanisms underlying C allocation in different root systems, we examined the effects of various N forms on sucrose metabolism enzyme activities and transcript expression levels in maize seedlings. This study provides valuable insights into how different N forms influence C allocation and accumulation in the maize root system, aiding crop improvement strategies to address N deficiency or fluctuations. In this study, NO_3^- levels were chosen based on (Zhao et al. 2020), while NH_4^+ concentration followed (George et al. 2016). Seedlings exposed to varying NO_3^- levels, LN, MN, and HN, exhibited differential root growth, development and sugar accumulation. Zhao et al. (2020) showed that LN treatment promotes root growth and enhances C metabolism more effectively than MN and higher NO_3^- levels. Conversely, small amounts of NH_4^+ were associated with improved root growth and photosynthesis in maize (George et al. 2016), whereas elevated NH_4^+ levels inhibited plant growth due to toxicity. High NH_4^+ concentrations can disrupt intracellular pH, osmotic balance, and nutrient absorption, leading to reduced growth and poor root development (Shilpha et al. 2023; Wang et al. 2022a; Zhu et al. 2021). Therefore, using low NH_4^+ concentrations is essential for investigating C metabolism in maize root systems while avoiding the effects associated with higher levels of NH_4^+ nutrition.

This study aims to elucidate the impact of N deficiency on carbohydrate metabolism and root system architecture in maize, with a specific focus on how different N forms regulate sucrose utilization

and partitioning, starch accumulation, and root plasticity. Through an integrative approach encompassing physiological, biochemical, and transcriptional analyses, the research seeks to unravel the mechanisms governing N-mediated C partitioning in maize roots. By evaluating these regulatory pathways, the findings will advance our understanding of nitrogen use efficiency (NUE), offering valuable insights into optimizing maize growth and resilience under N-deficient conditions. Ultimately, this research contributes to the development of sustainable agricultural practices and low input farming strategies, fostering improved crop productivity while minimizing environmental impact.

4.2. . Materials and methods

4.2.1. Plant materials and seed treatment

Seeds of the fast-flowering, short-cycle inbred mini-maize line TX-40J (McCaw et al. 2016), which were used in our previous experiment (Amoah et al. 2025), were also used in this study. Seeds were disinfected with 5% sodium hypochlorite for 5 min and wash with ultrapure water, 5 times at 3 min each. Sterilized maize seeds were germinated in Oasis Horticube Propagation Slabs (Aqua Gardening, Australia), an inorganic and pH-neutral growing foam medium, placed in germination trays.

4.2.2. Experimental treatment and growth conditions

The germination trays were transferred to a climate-controlled growth room, set to a 14/10 day-night cycle, with temperatures of 25°C during the day and 22°C at night, and 80% relative humidity for 5 d to allow for seed germination. After 5 d, the uniformly germinated seedlings were selected and divided into four treatment (T1-T4) groups and grown in 3L pots, which has root supported by organic expanded clay pellets (Aqua Gardening, Australia). Each treatment group received specific N sources. Plants in T1 received 1 mM NO_3^- (low N; LN), T2 received 2 mM NO_3^- (medium N; MN), T3 had 10 mM NO_3^- (High N; HN) and T4 received 1 mM NH_4^+ (low NH_4^+; LA). The NO_3^- concentrations were chose based on previous studies (Zhao et al. 2020; Amoah and Kaiser 2025) and the NH_4^+ concentration was selected based on previous study (George et al. 2016; Peng et al. 2023a; Amoah and Kaiser 2025). The hydroponic system was set-up in a climate-controlled glasshouse, with conditions similar to those of the growth room, where the seeds were germinated but supplemented with LED lighting which provided 1000 µmol m^{-2} s^{-1} above pot level (Amoah and Kaiser 2025). Four systems were set-up, and each system accommodated 40 pots, with each pot, containing one plant. Plants were drip-irrigated specified nutrient solutions (LN, MN, HN and LA), which was circulated through a hydroponic pump system. Irrigation occurred twice daily for 1 min, at 12:00 PM and 5:00 PM. Plants in each treatment groups were treated under hydroponic condition for 30 d before samples were harvested (Dechorgnat et al. 2018).

4.2.3. Nutrient composition

The treatment solutions contained 1 mM $(NH_4)_2SO_4$ (LA), 1 mM KNO_3 (LN), 2 mM KNO_3 (MN), or 10 mM KNO_3 (HN), along with 1 mM, 2 mM, or 10 mM of $MgSO_4$, KH_2PO_4, KCl, K_2SO_4, $CaCl_2$, $CaSO_4$, Fe-EDTA, Fe-EDDHA, H_3BO_3, $MnSO_4$, $ZnSO_4$, $CuSO_4$, and Na_2MoO_4. Solutions were stored in 162 L Brute Containers with lids (Rubbermaid, USA) and were replaced weekly, with daily pH adjustments to maintain a stable pH of 5.9, using 1 M H_2SO_4 or 1 M NaOH. The treatment solution was delivered to the system via an Eden 140G FL submersible water pump (Creative Pumps, Australia). Plants were uniquely identified and randomized into blocks using the agricolae package R statistical software (v4.5.0).

4.2.4. Photosynthesis and N content measurement

The net photosynthetic rate (Pn) was measured on the young emerging leaf of each treatment using the portable LI-6400 photosynthetic system (LI-COR Inc., Lincoln, NE, USA). Measurements were taken at 9:00 AM and 11:00 AM. Cuvette conditions included a light level of 1000 μmol m^{-2} s^{-1}, CO_2 concentration of 400 ppm, flow rate of 500 μmol m^{-2} s^{-1}, and relative humidity between 60% and 65%. Total chlorophyll pigment was extracted from approximately 0.1 g of leaf tissue using 100% methanol on a shaker at 25°C until the tissue was completely bleached. The extract was then centrifuged at 10,000 × g for 10 min, and the absorbance of the supernatant was measured at 652 and 663 nm using a UV-vis spectrophotometer (Shimadzu, Japan). The concentration of chlorophyll was calculated following the method described by (Amoah et al. 2023). N content was determined using a modified Kjeldahl method (Zhao et al. 2020). A 0.2 g dry sample was digested with 0.5 mL concentrated H_2SO_4 and a catalyst mixture (10 g K_2SO_4, 1 g $CuSO_4$) at 100°C for 60 min. After cooling, 0.5 mL of 40% NaOH and 0.5 mL distilled water were added. The mixture was then combined with 1 mL Nessler's reagent and incubated for 10 min. Absorbance at 420 nm was measured using a UV-vis spectrophotometer (Shimadzu, Tokyo, Japan), and N content was calculated from a standard curve of $(NH_4)_2SO_4$.

4.2.5. Root measurements

At 30 DAT under hydroponic conditions, uniformly grown maize seedlings were sampled and divided into two sets (Set I and Set II), each comprising 12 individual plants per treatment group (T1–T4). In Set I, whole roots were carefully separated from shoots, rinsed with potable water, and processed as follows: roots from six plants were floated in water in a transparent plastic tray and scanned using an Epson Perfection V700 photo scanner (Epson Australia Pty. Ltd., Australia) for morphological analysis. Subsequently, the roots were blotted with tissue paper and oven-dried at 70 °C for 48 h to determine total root biomass. The remaining six plants were immediately frozen in liquid nitrogen and stored at

−80 °C for subsequent biochemical and molecular analyses. In Set II, roots were dissected into distinct types: brace roots (BR), crown roots (CR), lateral roots (LR), primary roots (PR), and seminal roots (SR). Roots from six plants were scanned as described above, then oven-dried at 70 °C for 48 h to assess individual root-type biomass. The remaining six plants were used for biochemical and molecular analyses, with each root type frozen separately in liquid nitrogen and stored at −80 °C. Image analysis was performed using RhizoVision Explorer software (version 2.0.3) (Seethepalli et al. 2021).

4.2.6. Quantification of soluble sugar and starch

Soluble sugar and sucrose contents were determined following the method described by (Xiao et al. 2024). Ground samples (0.1 g) were homogenized in 1 mL of 80% (v/v) ethanol and heated at 80°C for 30 min. After cooling for 5 min, the mixture was centrifuged at 12,000 × g for 10 min. The supernatants were collected to determine soluble sugar and sucrose contents using a UV-vis spectrophotometer (Shimadzu, Tokyo, Japan), with absorbance recorded at 620 nm and 480 nm, respectively. For starch content, 1 mL of distilled water was added to the ethanol-insoluble residues and incubated for 30 min. Starch was hydrolyzed with 9.2 M and 4.6 M perchloric acid solutions. The starch content was quantified using anthrone reagent, and absorbance was measured at 620 nm (Du et al. 2020).

4.2.7. Starch metabolism enzymes activity assay

For starch synthase (SS) activity, 100 mg of tissue samples were homogenized in an extraction buffer containing 50 mM Tris-HCl (pH 7.0), 10% glycerol, 10 mM EDTA, 5 mM DTT, 1 mM PMSF, and 50 µL/g tissue of 10× Protease Inhibitor Cocktail (Sigma-Aldrich, Cat# P9599) (Cao et al. 1999). The homogenate was centrifuged at 12,000 × g for 10 min, and the supernatant was collected. A reaction mixture was prepared by mixing 0.1 mL of the supernatant with 0.9 mL of a solution containing 50 mM Tris-HCl (pH 7.0), 5 mM ADP-glucose, 1 mg/mL glycogen, and 10 mM $MgCl_2$. The reaction mixture was incubated at 30 °C for 30 min. To stop the reaction, 0.1 M HCl was added to denature the enzymes. To detect inorganic phosphate (Pi) consumption, 1% (w/v) ammonium molybdate was added. The mixture was incubated at room temperature for 30 min, and the absorbance was recorded at a wavelength of 620 nm using a UV-vis spectrophotometer (Shimadzu, Tokyo, Japan). A standard curve was prepared using known Pi concentrations, and starch synthase activity was calculated as the amount of Pi released, expressed in $\mu molg^{-1}FW$.

ADP-glucose pyrophosphorylase (AGPase) activity was determined using previously described methods by Amoah et al. (2025), with minor modifications. Briefly, 100 mg of fresh samples were homogenized in 1 mL of ice-cold extraction buffer containing 0.1 M Tris-HCl (pH 7.9), 5 mM glutathione, and 1 mM EDTA. The homogenate was centrifuged at 15,000 × g for 20 minutes at 4 °C,

and the supernatant was collected. Subsequently, 0.1 mL of the supernatant was mixed with 0.9 mL of a reaction mixture containing 0.4 M Tris-HCl buffer (pH 7.9), 0.06 M $MgSO_4$, 48 mM cysteine, 2.4 mg/mL BSA, 4 mM ADP-glucose, 20 mM sodium pyrophosphate, 30 mM 3-phosphoglycerate, and 4 units each of glucose-6-phosphate dehydrogenase and phosphoglucomutase. Afterwards, 0.1 mL of enzyme extract was added to $NADP^+$ as the final component. The absorbance was measured at 340 nm using a UV-vis spectrophotometer (Shimadzu, Tokyo, Japan). The AGPase activity was expressed as μmol min^{-1} g^{-1} FW.

To determine SPS and SuSy activity, a 0.1 g of frozen tissue samples were homogenized in an extraction buffer containing 50 mM Tris-HCl (pH 7.5), 1 mM EDTA, 1 mM $MgCl_2$, 12.5% (v/v) glycerine, 10% polyvinylpyrrolidone (PVP), and 10 mM mercaptoethanol to ascertain the activities of sucrose metabolism-related enzymes. The SPS and SuSy activities were measured using the extract (Liu et al. 2013). Briefly, 200 μL of supernatant was mixed with reaction buffer containing 200 mM Tris-HCl (pH 7.0), 40 mM $MgCl_2$, 12 mM UDP-glucose, 40 mM fructose-6-P, and 200 μL extract. Another reaction buffer containing 12 mM UDP, 40 mM sucrose, 200 mM Tris-HCl (pH 7.0), and 40 mM $MgCl_2$ was also prepared. The mixture was incubated at 30 °C for 30 min and terminated using 100 μL 2 mol L^{-1} of NaOH. The mixture was then heated at 100 °C for 10 min to destroy untreated hexose and hexose phosphates, cooled to room temperature, and mixed with 1 mL of 0.1% (w/v) resorcin in 95% (v/v) ethanol and 3.5 mL of 30% (w/v) HCl. The solution was incubated for 10 min at 80 °C. Sucrose content in the SPS reaction and fructose content in the SuSy reaction were calculated using a standard curve measured at A480 nm and A540 nm wavelengths, respectively.

4.2.8. RNA isolation, cDNA synthesis and qPCR analysis

Total RNA was isolated from whole root and the different root types (BR, CR, LR, PR and SR) using the Trizol RNA Isolation Reagents (Invitrogen, Carlsbad, CA, USA) following the manufacturer's protocol. RNA quantity and integrity were assessed by measuring the optical density at 260 nm and through 1.0% (w/v) agarose gel electrophoresis, respectively. Subsequently, 1 μg of total RNA was reverse-transcribed into single-stranded cDNA using the iScript™ RT Reagent Kit (Bio-Rad, Hercules, CA, USA) according to the manufacturer's instructions. Quantitative real-time polymerase chain reaction (qPCR) was performed using the CFX 96 Real-Time System (Bio-Rad, Richmond, CA, USA) with SYBR Green fluorescence (Bio-Rad, Richmond, CA, USA). The ΔΔCT method was used for data analysis. The list of genes studied are provided in Table S4.1. The thermal cycling conditions consisted of an initial denaturation step at 95 °C for 5 min, followed by 40 cycles of 95 °C for 15 s, 55 °C for 15 s, and 72 °C for 30 s. All experiments were conducted with three biological replicates, and relative transcript levels were normalized using *ZmActin1* and *ZmUBQ1* as internal controls.

4.2.9. Statistical analysis

The study was repeated twice, with tissue samples collected in triplicate at 30 DAT. Data were analysed using a one-way analysis of variance (ANOVA) to assess overall differences among groups, followed by post-hoc Turkey's honest significant difference (HSD) test for pairwise comparison using Prism software (v10.0). Quantified data points represent the mean ± standard error (SE) of six independent plants (n = 6). Different letters on the error bars denote statistically significant differences at a probability level of $p \leq 0.05$, determined via Tukey's HSD test. Graphical charts were generated using GraphPad Prism (v10.4.0), and Pearson's correlation plots were created using R statistical software (v4.5.0).

4.3. Results

4.3.1. Phenotypic response, biomass and photosynthesis under different N forms

At 30 DAT, maize plants grown under HN conditions exhibited enhanced shoot growth, whereas LN-treated plants showed increased root growth (Figs. S4.1A-B). Consistent with these phenotypic changes, LN treatment significantly ($P \leq 0.05$) inhibited shoot biomass while promoting root biomass accumulation, leading to a higher total biomass and an increased root-to-shoot (R/S) ratio in maize seedlings (Figs. S4.2A-C and S4.3A). Furthermore, LN treatment was associated with reduced N concentration, Pn, and chlorophyll content in both the leaves and roots of maize seedlings (Figs. S4.2D and S4.2B, S4.3C-D). Additionally, N treatments (NT) significantly ($P \leq 0.05$) affected root and shoot biomass, N content, and the R/S ratio (Table S4.2).

4.3.2. Changes in root morphology under different N treatment forms

The morphological changes associated with LN, MN, HN, and LA treatment conditions were examined after 30 d. As shown in Fig. S4.2, LN-treated plants exhibited significantly increased total root length, a higher number of root tips, greater root volume, and an expanded total root surface area (Fig. S4.2E-H). These traits corresponded with a significant increase in root biomass compared to other treatment groups (Fig. S4.2B). All measured root morphological traits were significantly ($P \leq 0.05$) affected by the different nitrogen treatments (Table S4.2).

4.3.3. Soluble sugars and sucrose metabolism enzymes activities under different N forms

LN treatment significantly ($P \leq 0.05$) increased total soluble sugar, sucrose, and starch contents in the roots of maize seedlings compared to other nitrogen-treated plants (Fig. 4.1A-C). Similarly, the activities of sugar metabolism enzymes (SPS and SuSy) and starch metabolism enzymes (AGPASE and

SS) were markedly ($P \leq 0.05$) higher in the roots of LN-treated plants than in those under MN, HN, and LA treatments (Figs. 4.2A-D). Additionally, soluble sugar, sucrose, starch, and the activities of SPS, SuSy, AGPASE, and SS were all significantly ($P \leq 0.05$) influenced by NT (Table S4.2).

4.3.4. Transcriptional regulation of sucrose-metabolism genes under different N forms

The expression patterns of sucrose metabolism and transporter-related genes (*ZmSPS1*, *ZmSuSy1*, *ZmAINV1* and *ZmSUC2*) were analysed in the roots of maize plants under LN, MN, HN, and LA treatment conditions. As seen in Fig. 4.3, LN treatment significantly ($P \leq 0.05$) upregulated the expression of *ZmSPS1*, *ZmSuSy1*, *ZmSWEET6*, *ZmSUC2*, and *ZmAINV1*), with greater fold changes compared to other treatment groups (Figs. 4.3A, B, E, F, G and H). Similarly, the expression of starch metabolism genes (*ZmAGPASE1* and *ZmSS1*) was also markedly upregulated in the roots of LN-treated plants compared to those in other treatment groups (Figs. 4.3C-D). Interestingly, N T significantly influenced the expression of all genes analysed (Table S4.2).

4.3.5. Diurnal changes of sugars and starch under different forms

Plants subjected to LN treatment consistently exhibited increased sucrose and starch levels throughout the day. These sucrose and starch levels were significantly different ($P \leq 0.05$) from those observed in other treatment groups (Fig. 4.4A-B). The diurnal pattern of sucrose level showed the lowest values in the early morning (7:00 AM), followed by an increase at 12:00 PM, peaking at 5:00 PM, and declining overnight to reach their lowest levels again at 7:00 AM the next day. The diurnal starch level was also lower in the early morning, increased at 12:00 PM and peaked at 22:00 PM and reach the lowest again at 7:00 AM the next day. Furthermore, after overnight transport, plants under LN treatment retained significantly ($P \leq 0.05$) higher root sucrose and starch concentrations than those in other treatment groups (Fig. 4.4A-B).

4.3.6. Biomass and morphology of different root types under different N condition

To evaluate the effects of LN, MN, HN, and LA treatments, whole roots were categorized into five primary types: BR, CR, PR, LR and SR. As shown in Fig. S4.4, HN treatment significantly promoted the biomass accumulation of BR, CR, PR, and SR in maize seedlings. However, LR growth was strongly influenced by LA treatment (Fig. 4.6C). The magnitude of biomass accumulation was highest in CR, LR, and SR, but lower in BR and PR. In contrast, LN treatment inhibited BR, CR, PR, and SR growth. Furthermore, LN treatment significantly ($P \leq 0.05$) increased the length of all root types (Figs. S4.5A-D), enhanced LR tip number (Figs. S4.5E-F), and increased the volume of CR, LR, and PR (Figs.

S4.6A-D), as well as the surface area of CR, PR, and LR (Figs. S4.6E-F). MN treatment stimulated CR and LR tip number and increased PR volume and LR surface area (Figs. S4.5 and S4.6). However, HN treatment concurrently significantly inhibited the morphological development of various root types , leading to reduced total root length, number of root tips, root volume and root surface area. NT significantly impacted CR, LR, PR, and SR growth in maize seedlings (Table S4.2).

4.3.7. Soluble sugars and sucrose metabolism enzyme activities in different root types

LN treatment significantly ($P \leq 0.05$) increased soluble sugar, sucrose, and starch contents in BR and PR (Figs. 4.5). In contrast, MN treatment enhanced sugar, sucrose, and starch accumulation in CR, LR and SR (Figs. S4.5). Consistent with these changes in sugar and starch content, LN treatment significantly increased the activities of sucrose and starch metabolism enzymes (SPS, SuSy, AGPASE, and SS) in BR and SR, whereas MN treatment enhanced the activities of these enzymes in CR, LR, and PR, respectively (Table S4.3). Additionally, soluble sugar, sucrose, starch content, and the activities of SPS, SuSy, AGPASE, and SS were all significantly affected by N T (Table S4.2).

4.3.8. Expression of sucrose and starch metabolism-related genes in different root types

LN treatment significantly ($P \leq 0.05$) upregulated the expression of *ZmSPS1*, *ZmSuSy1, ZmAGPASE1*, *ZmSS1*, *ZmSWEET6*, *ZmSUC2*, *ZmSTP2*, and *ZmAINV1* in BR (Figs. 4.6-4.9A and F) and SR (Figs. 4.6-4.9 E-F). In contrast, the expression of these genes was highly upregulated in CR (Figs. 4.6-9B and G), as well as LR and PR (Figs. 4.6-4.9D and I) in plants under MN treatment. Additionally, NT significantly affected the expression levels of *ZmSPS1, ZmSuSy1*, *ZmAGPASE1*, *ZmSS1*, *ZmSWEET6*, *ZmSUC2*, *ZmSTP2*, and *ZmAINV1* (Table S4.2).

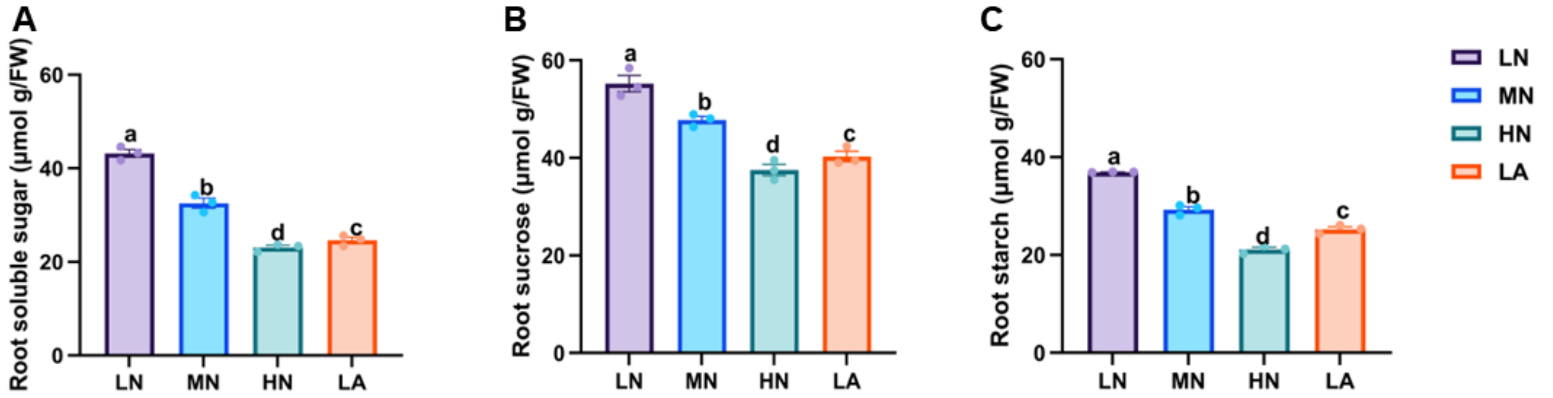

Fig. 4.1 Effects of different nitrogen (N) treatments on soluble sugar (**A**), sucrose (**B**), and starch (**C**) contents in the whole roots of maize inbred line TX-40J. Data represent mean ± standard error (SE) of six plants (n = 6). Different letters on error bars indicate statistically significant differences at $P \leq 0.05$. FW fresh weight, LN low nitrate, MN moderate nitrate, HN high nitrate and LA low ammonium.

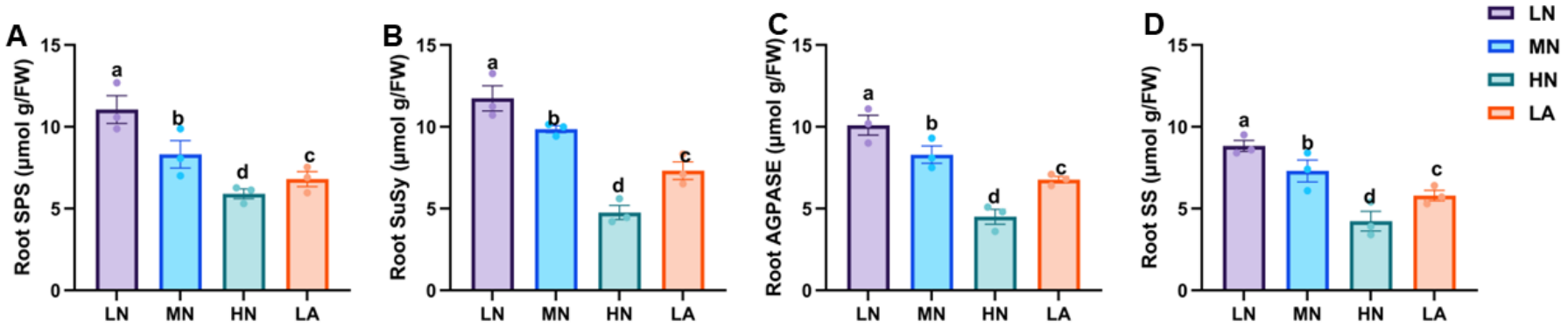

Fig. 4.2 Activities of sucrose phosphate synthase (**A**), sucrose synthase (**B**), ADP-glucose pyrophosphorylase (**C**), and starch synthase (**D**) in the whole roots of maize seedlings under different nitrogen (**N**) treatments. Data represent mean ± standard error of the mean (SEM) of six plants (n = 6). Statistical significance was assessed using Tukey's multiple range test ($P < 0.05$); different letters indicate significant differences between treatments. FW fresh weight, LN low nitrate, MN moderate nitrate, HN high nitrate and LA low ammonium.

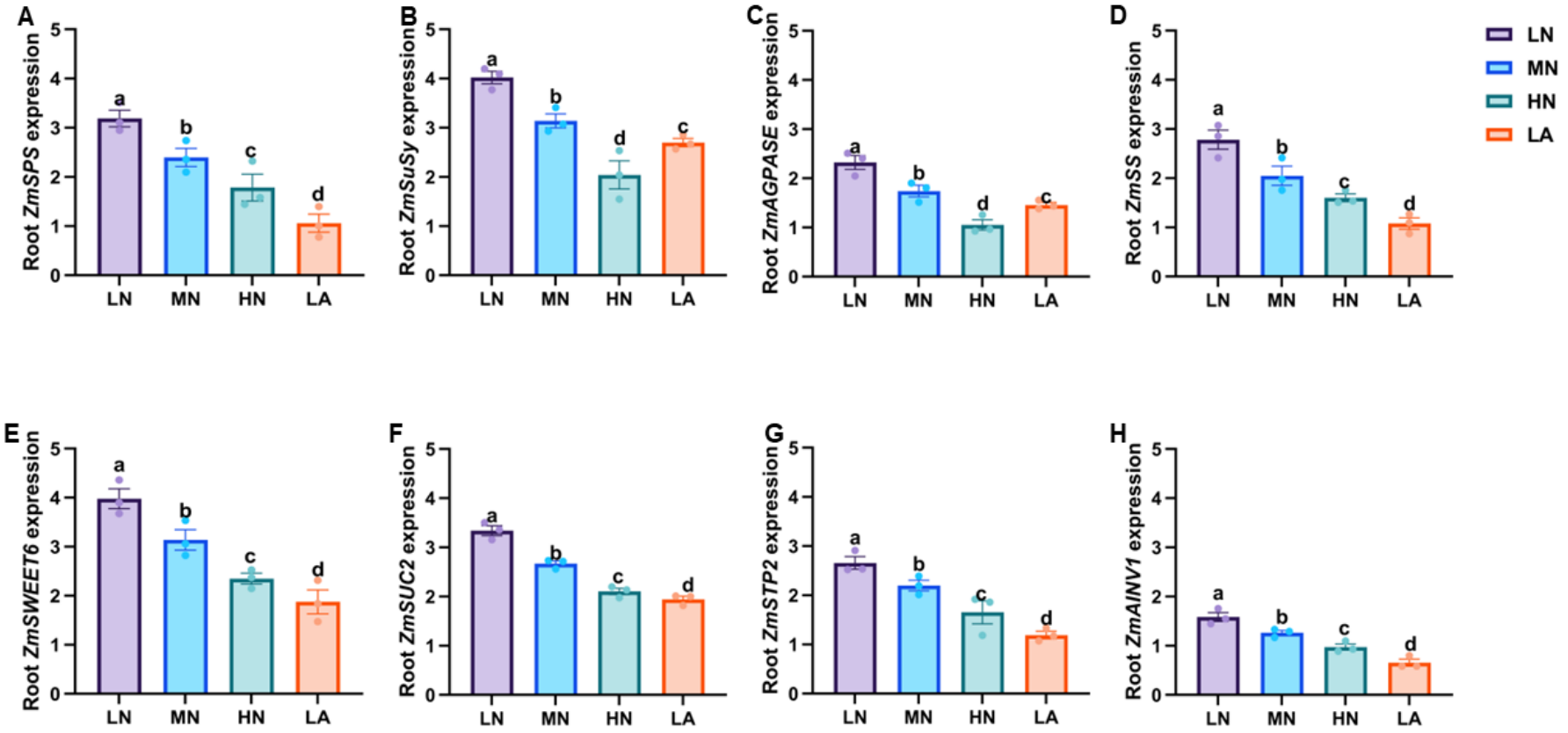

Fig. 4.3 Effects of different nitrogen (N) treatments on the expression patterns of sugar and starch metabolism-related genes in the whole roots of maize inbred line TX-40J. Expression levels of *ZmSPS* (**A**), *ZmSuSy* (**B**), *ZmAGPASE* (**C**), *ZmSS* (**D**), *ZmSWEET6* (**E**), *ZmSUC2* (**F**), *ZmSTP2* (**G**), and *ZmAINV1* (**H**). Data represent mean ± standard error of the mean (SEM) of six plants (n = 6). Statistical significance was determined by Tukey's multiple range test ($P < 0.05$); different letters indicate significant differences among treatments. LN low nitrate, MN moderate nitrate, HN high nitrate and LA low ammonium.

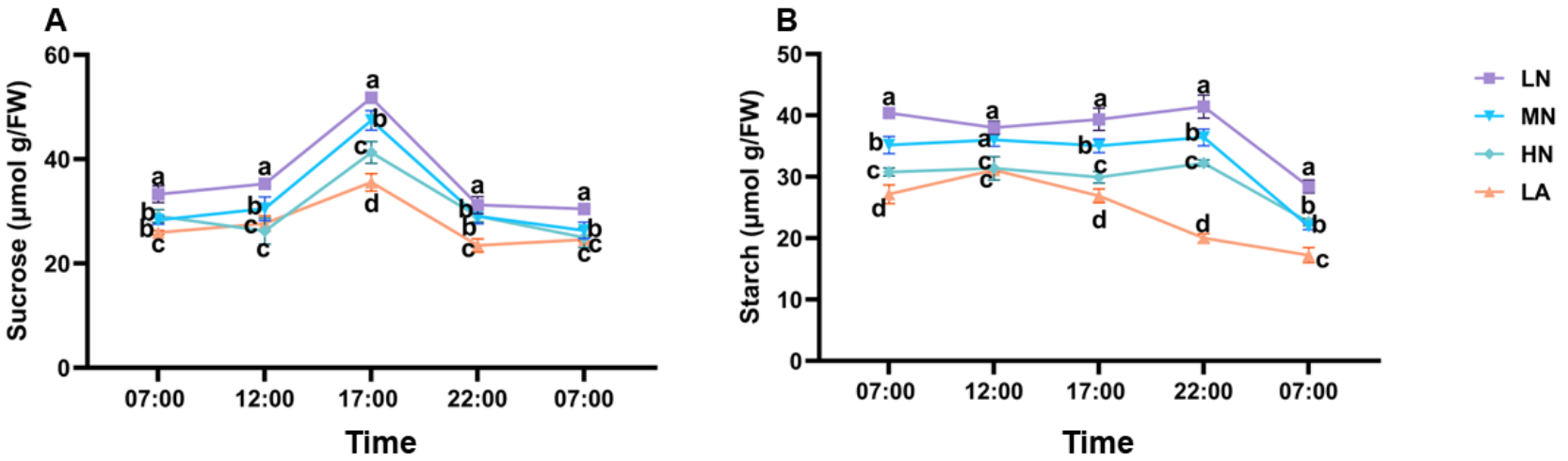

Fig. 4.4 Impact of different nitrogen (N) forms on the diurnal patterns of sucrose (**A**) and starch (**B**) contents in the whole roots of maize seedlings. Samples were collected at 7:00, 12:00, 17:00, 22:00, and 7:00 on the following day. Data represent mean ± standard error of the mean (SEM) of six plants (n = 6). Statistical significance was determined by Tukey's multiple range test ($P < 0.05$); different letters indicate significant differences among treatments. FW fresh weight, LN low nitrate (N deficiency), MN moderate nitrate, HN high nitrate and LA low ammonium.

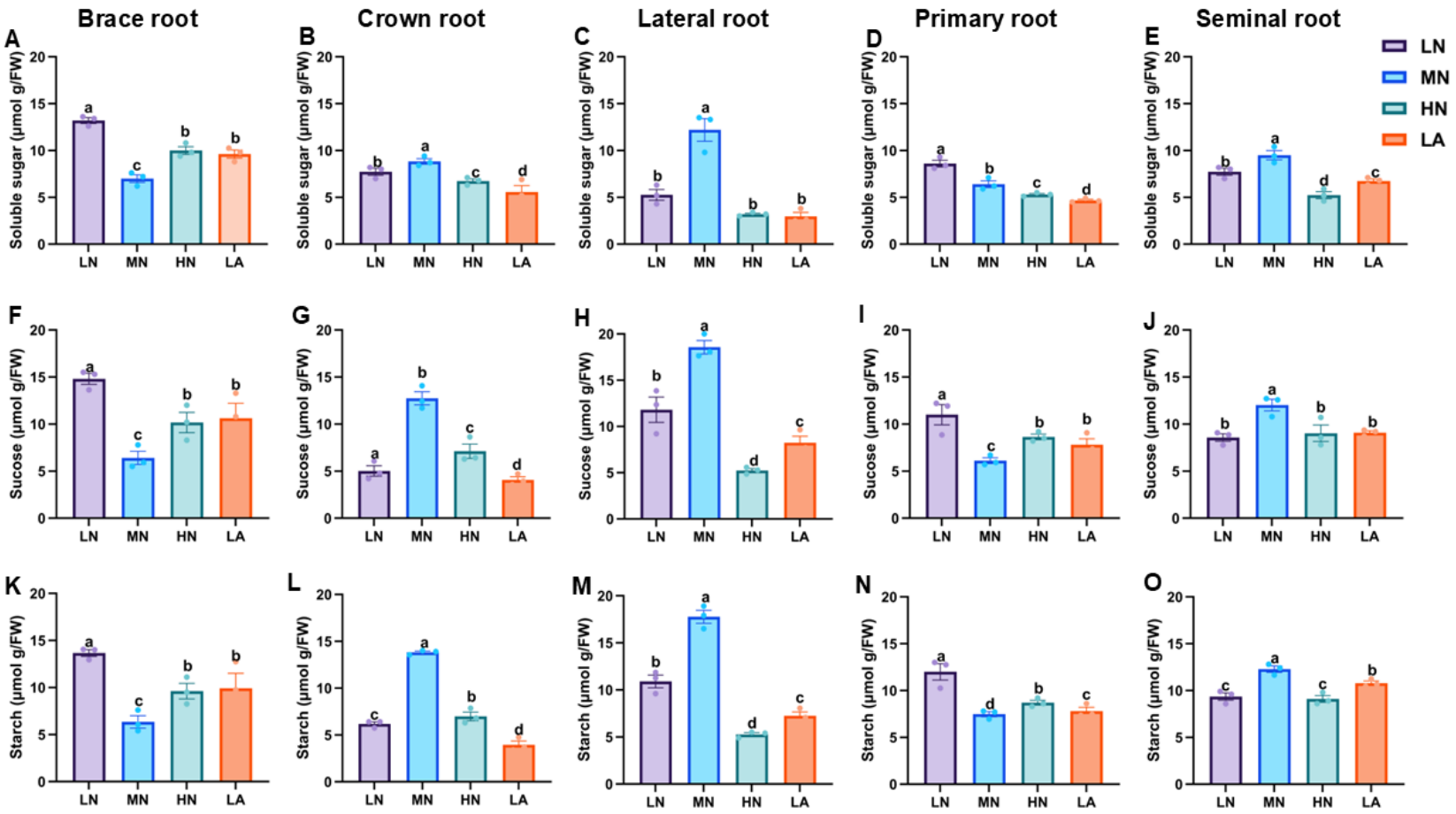

Fig. 4.5 Effect of different nitrogen (N) forms on sugars and starch content in different root types of maize inbred line TX-40J. Soluble sugar content in brace (**A**), crown (**B**), lateral (**C**), primary (**D**) and seminal root (**E**). Sucrose content in brace (**F**), crown (**G**), lateral (**H**), primary (**I**) and seminal root (**J**), and starch content in brace (**K**), crown (**L**), lateral (**M**), primary (**O**) and seminal root (**P**). Data represent mean ± standard error of the mean (SEM) of six plants (n = 6). Statistical significance was determined by Tukey's multiple range test ($P < 0.05$); different letters indicate significant differences among treatments. LN low nitrate, MN moderate nitrate, HN high nitrate and LA low ammonium.

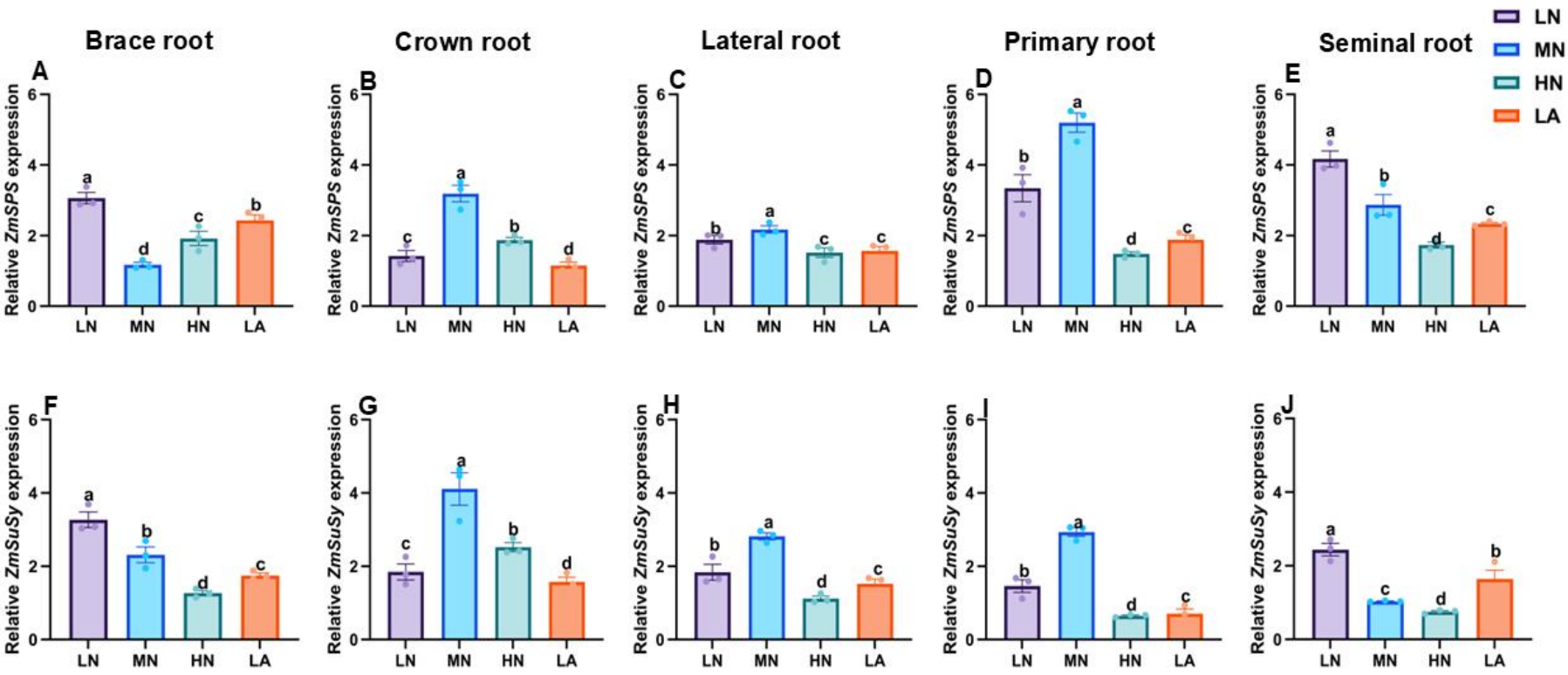

Fig. 4.6 Effects of different nitrogen (N) treatments on the expression patterns of sugar metabolism-related genes in different root types of maize inbred line TX-40J. Expression levels of *ZmSPS1* in brace, crown, lateral, primary, and seminal roots (**A–E**), and *ZmSuSy1* in brace, crown, lateral, primary, and seminal roots (**F–J**) are shown. Data represent mean ± standard error of the mean (SEM) of six plants (n = 6). Statistical significance was determined by Tukey's multiple range test ($P < 0.05$); different letters indicate significant differences among treatments. LN low nitrate, MN moderate nitrate, HN high nitrate and LA low ammonium.

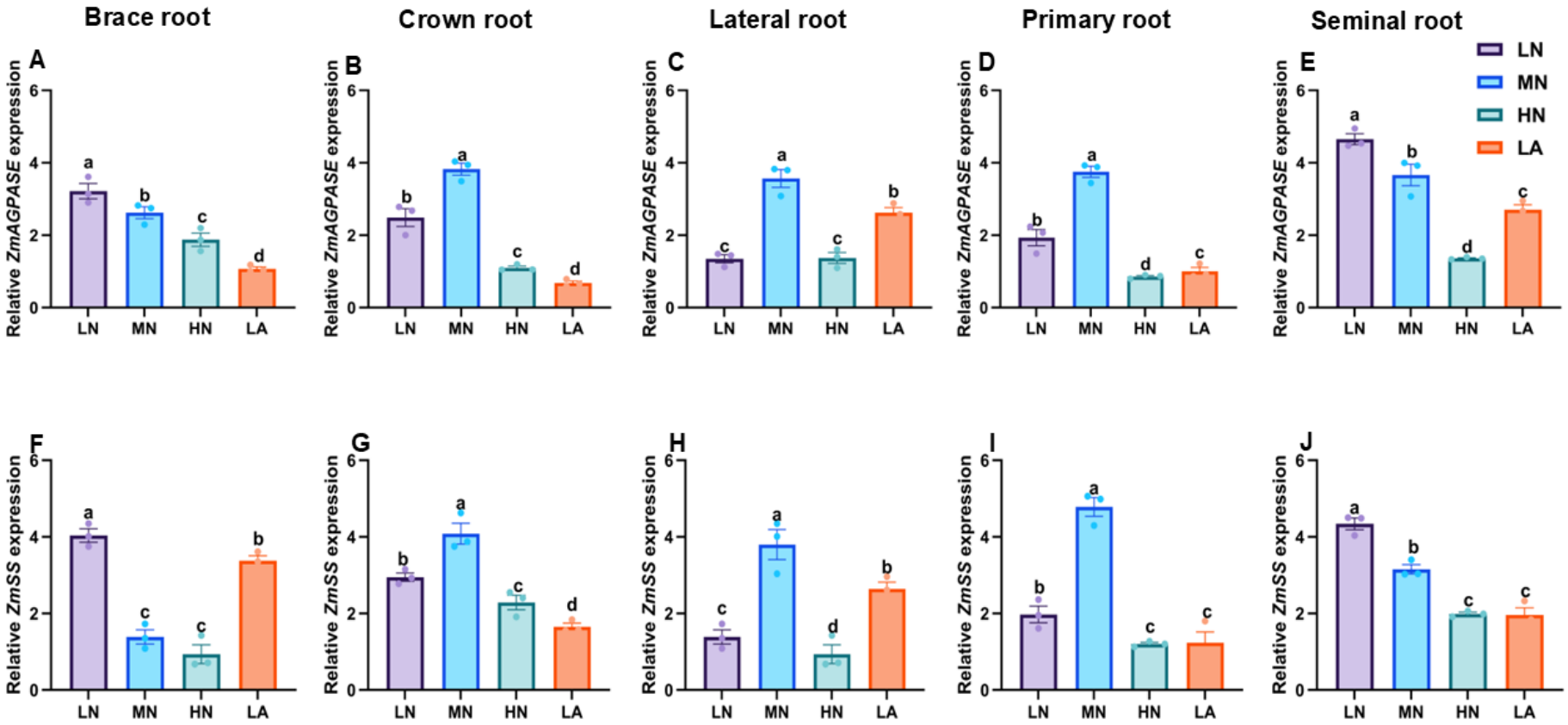

Fig. 4.7 Effects of different nitrogen (N) treatments on the expression patterns of starch metabolism-related genes in different root types of maize inbred line TX-40J. Expression levels of *ZmAGPASE1* in brace, crown, lateral, primary, and seminal roots (**A–E**), and *ZmSS1* in brace, crown, lateral, primary, and seminal roots (**F–J**) are shown. Data represent mean ± standard error of the mean (SEM) of six plants (n = 6). Statistical significance was determined by Tukey's multiple range test ($P < 0.05$); different letters indicate significant differences among treatments. LN low nitrate, MN moderate nitrate, HN high nitrate and LA low ammonium.

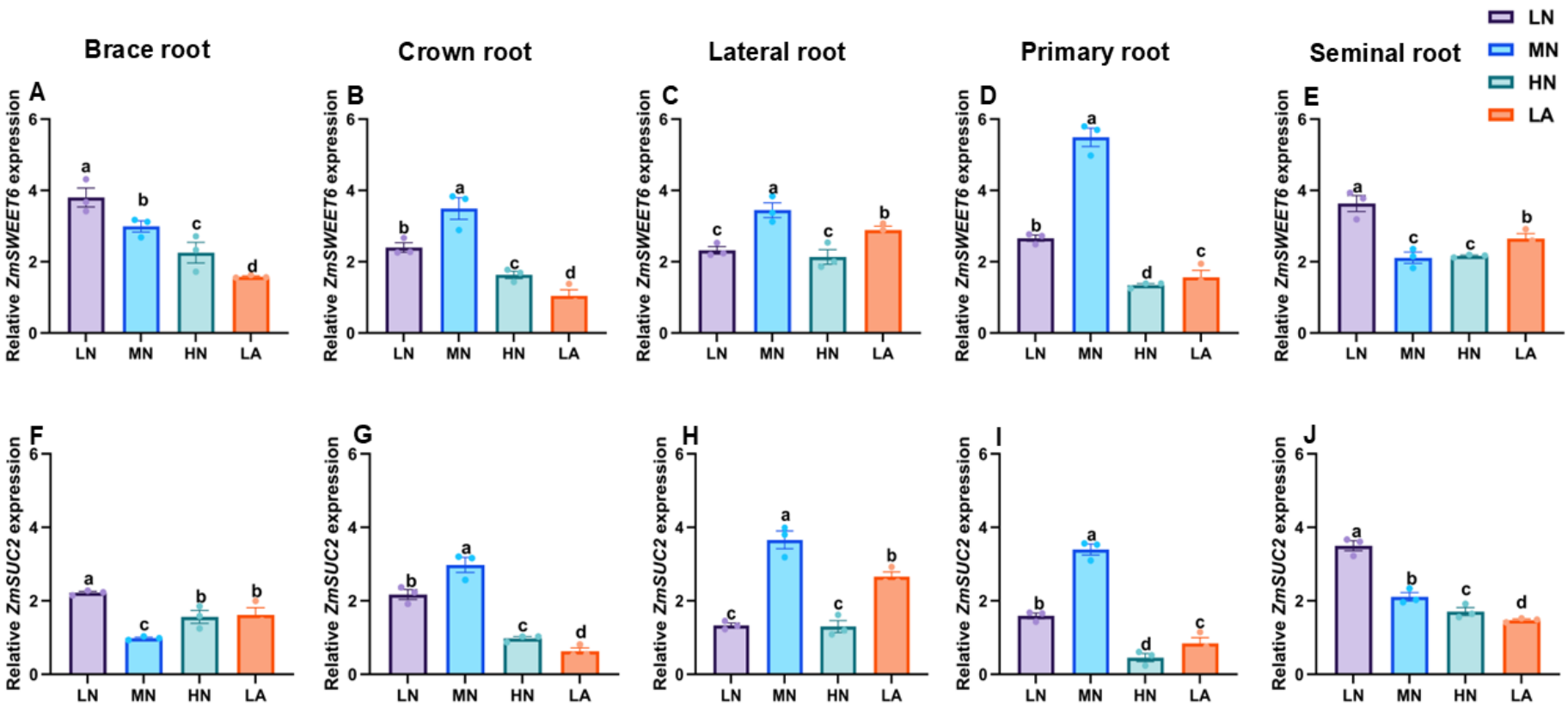

Fig. 4.8 Effects of different nitrogen (N) treatments on the expression patterns of sucrose metabolism-related genes in different root types of maize inbred line TX-40J. Expression levels of *ZmSWEET6* in brace, crown, lateral, primary, and seminal roots (**A–E**), and *ZmSUC2* in brace, crown, lateral, primary, and seminal roots (**F–J**) are shown. Data represent mean ± standard error of the mean (SEM) of six plants (n = 6). Statistical significance was determined by Tukey's multiple range test ($P < 0.05$); different letters indicate significant differences among treatments. LN low nitrate, MN moderate nitrate, HN high nitrate and LA low ammonium.

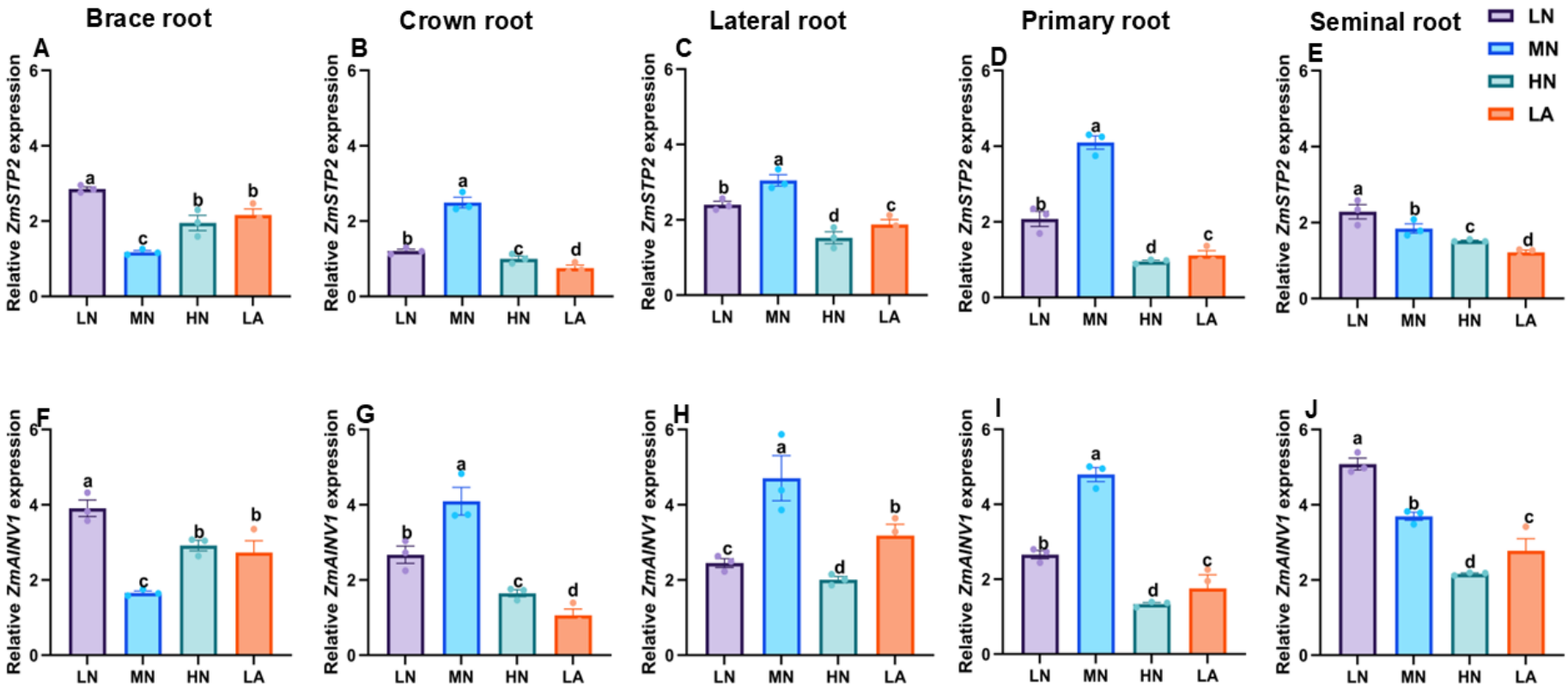

Fig. 4.9 Effects of different nitrogen (N) treatments on the expression patterns of sucrose transporter (*ZmSTP2*) and sugar metabolism (*ZmAINV1*) genes in different root types of maize inbred line TX-40J. Expression levels of *ZmSTP2* in brace, crown, lateral, primary, and seminal roots (**A–E**), and *ZmAINV1* in brace, crown, lateral, primary, and seminal roots (**F–J**) are shown. Data represent mean ± standard error of the mean (SEM) of six plants (n = 6). Statistical significance was determined by Tukey's multiple range test ($P < 0.05$); different letters indicate significant differences among treatments. LN low nitrate, MN moderate nitrate, HN high nitrate and LA low ammonium.

Table 4.1. One-way analysis of variance (ANOVA) for indicators measured in roots of maize plants under different nitrogen conditions.

Traits/(plants)	Sources of variations					
	Treatment (df=3)					
	Whole root	**Brace root**	**Crown root**	**Lateral root**	**Primary root**	**Seminal root**
Root length	0.0021**	NA	0.0045**	<0.0001****	<0.0001****	0.0001***
Root tip number	0.0034**	NA	0.0011**	0.0006***	0.0025**	<0.0001****
Root volume	0.0225*	NA	0.0022**	0.0023**	0.0002***	0.0004***
Root surface area	<0.0001****	NA	0.0001***	<0.0001****	<0.0001****	<0.0001****
Shoot biomass	0.0028**	NA	NA	NA	NA	NA
Root biomass	<0.0001****	<0.0001****	<0.0001****	0.0009***	0.1955ns	<0.0001****
Root-to-shoot ratio	<0.0001***	NA	NA	NA	NA	NA
Nitrogen	<0.0001***	NA	NA	NA	NA	NA
Soluble sugar	<0.0001***	0.0356*	0.0001***	0.0001***	<0.0001****	0.004**
Sucrose	<0.0001***	0.0038**	0.0001***	<0.0001****	0.0052**	0.0105*
Starch	<0.0001***	0.0051**	0.0198*	<0.0001****	<0.0001****	0.0006***
SPS activity	0.0026**	0.0001***	0.0017**	0.0102*	<0.0001****	0.0002***
SuSy activity	0.006**	0.0029**	0.0006***	0.1037ns	<0.0001****	0.001**
AGPASE activity	<0.0001****	0.0007***	0.0002***	0.0095**	0.0046**	<0.0001****
Starch synthase	0.0011**	0.0107*	0.0016**	0.0069**	0.0001***	0.0013**
ZmSPS1	0.0005***	0.0002***	<0.0001****	0.0156*	<0.0001****	0.0138*
ZmSuSy1	0.0003***	0.0029**	0.0006***	0.0035**	<0.0001****	0.0019**
ZmAGPASE1	0.0002***	<0.0001****	0.0002***	0.0443*	<0.0001****	0.0095**
ZmSS1	0.0019**	0.0041**	0.0058**	<0.0001****	<0.0001****	0.0004***
ZmSWEET6	0.0003***	0.0004***	0.0003***	0.002**	<0.0001****	0.0459*
ZmSUC2	0.0006***	0.0013**	0.0005***	0.0129*	<0.0001****	0.0012**
ZmSTP2	<0.0001****	0.0002***	0.0001***	0.0008***	0.0026**	0.0011**
ZmAINV1	<0.0001****	0.0035**	<0.0001****	<0.0001****	<0.0001****	0.0028**

SPS/*ZmSPS1* (sucrose phosphate synthase), SuSy/*ZmSuSy1* (sucrose synthase), and AGPASE/*ZmAGPASE1* (ADP-glucose pyrophosphorylase). The symbols *, **, ***, and **** indicate significant differences at probability levels of 0.5, 0.1, 0.001, and 0.0001, respectively. NA, ns, and df denote not applicable, non-significant, and degree of freedom, respectively.

Table 4.2. Biomass and morphological indicators in maize root types under different N forms

Traits/(plants)	Treatments			
	LN (1 mM NO_3^-)	MN (2 mM NO_3^-)	HN (1 mM NO_3^-)	LA (10 mM NH_4^+)
	Biomass DW (g)			
Brace root	0.013 ± 0.001c	0.018 ± 0.001	0.035 ± 0.002a	0.035 ± 0.002a
Crown root	0.018 ± 0.001d	0.058 ± 0.003b	0.081 ± 0.002a	0.081 ± 0.002a
Lateral root	0.021 ± 0.001b	0.028 ± 0.003a	0.031 ± 0.003a	0.031 ± 0.003a
Primary root	0.022 ± 0.004d	0.047 ± 0.003b	0.083 ± 0.002a	0.083 ± 0.002a
Seminal root	0.148 ± 0.006b	0.101 ± 0.008c	0.070 ± 0.003d	0.070 ± 0.003d
	Root length (cm)			
Crown root	95.064 ± 9.36a	63.061 ± 1.84c	42.381 ± 3.06d	68.815 ± 3.06b
Lateral root	20.198 ± 36.09a	16.295 ± 3.15b	7.809 ± 3.15d	14.429 ± 1.97c
Primary root	108.564 ± 36.09a	32.545 ± 1.42c	20.384 ± 8.33d	59.689 ± 12.41b
Seminal root	100.353 ± 7.81a	64.264 ± 7.36c	46.383 ± 4.99d	75.919 ± 3.52b
	Root tip number			
Crown root	752.334 ± 58.63b	1045.668 ± 77.45a	354.335 ± 27.18d	598.666 ± 107.73c
Lateral root	812.668 ± 24.88a	567.668 ± 52.83c	417.663 ± 43.54d	676.332 ± 27.95b
Primary root	248.435 ± 28.67c	313.234 ± 11.35b	150.338 ± 25.64d	390.897 ± 43.21a
Seminal root	492.510 ± 33.43b	753.160 ± 42.32a	302.765 ± 20.46d	436.505 ± 35.27c
	Root volume (cm^3)			
Crown root	11.288 ± 1.04a	4.790 ± 0.52c	4.248 ± 0.89c	8.449 ± 1.15b
Lateral root	16.627 ± 1.21a	12.069 ± 1.03b	7.185 ± 0.86c	12.623 ± 1.27b
Primary root	19.755 ± 1.22b	25.502 ± 1.92a	9.581 ± 1.15d	16.530 ± 0.54c
Seminal root	13.052 ± 0.95a	10.708 ± 0.55b	5.716 ± 0.58c	10.798 ± 0.50b
	Root surface area (cm^2)			
Crown root	322.390 ± 19.97a	157.730 ± 20.91c	113.039 ± 12.06d	206.496 ± 12.41b
Lateral root	397.537 ± 42.02b	610.485 ± 29.81a	212.620 ± 8.44d	336.215 ± 28.74c
Primary root	530.308 ± 7.81a	138.758 ± 12.50c	126.498 ± 36.64c	321.887 ± 16.15b
Seminal root	250.357 ± 33.55a	241.656 ± 51.87b	141.748 ± 5.63d	224.143 ± 19.16c

The data represent the mean (±SE) of six independent plants (n=6). Different letters attached to the standard error indicate significant differences among treatments at a probability level of 0.05, as determined by one-way analysis of variance (ANOVA) followed by post-hoc comparisons. LN (low nitrate), MN (medium nitrate), HN (high nitrate), and LA (low ammonium nutrition), and DW (dry weight of samples).

Table 4.3: Soluble sugar, sucrose and starch contents in maize root types under different N forms

Traits/(plants)	Treatments			
	LN (1 mM NO_3^-)	MN (2 mM NO_3^-)	HN (1 mM NO_3^-)	LA (10 mM NH_4^+)
	Soluble sugar (µmol g^{-1} FW)			
Brace root	6.689 ± 0.15a	3.700 ± 0.35c	5.100 ± 0.21b	4.967 ± 0.99b
Crown root	5.139 ± 0.54b	9.801 ± 1.01b	4.902 ± 0.31c	2.201 ± 0.35d
Primary root	12.200 ± 1.21b	5.290 ± 0.58b	3.290 ± 0.12c	2.907 ± 0.42d
Seminal root	6.401 ± 0.36b	8.600 ± 0.37a	5.340 ± 0.12c	4.500 ± 0.12d
Lateral root	8.809 ± 0.29a	7.7300 ± 0.37b	5.589 ± 0.69d	6.765 ± 0.23c
	Sucrose (µmol g^{-1} FW)			
Brace root	20.733 ± 0.82a	8.971 ± 0.9bc	14.230 ± 1.50b	14.869 ± 2.23b
Crown root	7.030 ± 0.78c	17.830 ± 0.97a	9.904 ± 1.07b	5.710 ± 0.47d
Primary root	16.5331 ± 1.92b	30.100 ± 1.34a	7.000 ± 0.29d	11.501 ± 0.99c
Seminal root	15.495 ± 1.50a	8.567 ± 0.43d	12.180 ± 0.42b	10.930 ± 0.89c
Lateral root	11.998 ± 0.56c	16.831 ± 0.87a	12.643 ± 1.22b	12.700 ± 0.28b
	Starch (µmol g^{-1} FW)			
Brace root	13.001 ± 0.36a	6.351 ± 0.65c	9.610 ± 0.82b	9.919 ± 1.59b
Crown root	6.181 ± 0.22b	13.812 ± 0.14a	6.980 ± 0.46b	3.951 ± 0.42c
Primary root	10.901 ± 0.67b	21.408 ± 1.28a	5.269 ± 0.19d	7.251 ± 0.42c
Seminal root	7.483 ± 0.27c	12.100 ± 0.88a	8.734 ± 0.26b	7.800 ± 0.40c
Lateral root	9.365 ± 0.39c	12.280 ± 0.34a	9.105 ± 0.36c	10.785 ± 0.24b

LN (low nitrate), MN (medium nitrate), HN (high nitrate), LA (low ammonium nutrition), and FW (fresh weight of samples). The data represent the mean (±SE) of six independent plants (n=6). Different letters attached to the standard error indicate significant differences among treatments at a probability level of 0.05, as determined by one-way analysis of variance (ANOVA) followed by post-hoc comparisons.

Table 4.4: Sugars and starch metabolism enzymes activity in maize root types under different N forms

Traits/(plants)	Treatments			
	LN (1 mM NO_3^-)	MN (2 mM NO_3^-)	HN (1 mM NO_3^-)	LA (10 mM NH_4^+)
SPS activity (µmol g^{-1} FW)				
Brace root	8.97 ± 0.41a	3.45 ± 0.17d	5.62 ± 0.51c	6.80 ± 0.27b
Crown root	3.66 ± 0.12b	5.89 ± 0.67a	2.77 ± 0.26c	2.25 ± 0.16d
Lateral root	5.52 ± 0.30b	6.37 ± 0.26a	4.92 ± 0.04c	4.44 ± 0.34d
Primary root	6.53 ± 0.66b	12.11 ± 0.45a	2.89 ± 0.09c	3.13 ± 0.47c
Seminal root	4.94 ± 0.08b	7.87 ± 0.63a	4.56 ± 0.06c	3.38 ± 0.15c
SuSy activity (µmol g^{-1} FW)				
Brace root	11.36 ± 0.41a	4.89 ± 0.22c	8.94 ± 0.72b	8.05 ± 1.06b
Crown root	3.57 ± 0.36c	7.95 ± 0.74a	4.879 ± 0.21b	3.04 ± 0.22d
Lateral root	7.11 ± 0.72b	8.40 ± 0.35a	6.23 ± 0.68c	5.88 ± 0.44d
Primary root	8.84 ± 0.58b	17.03 ± 0.59a	3.77 ± 0.10c	4.11 ± 0.62d
Seminal root	6.98 ± 0.42b	7.92 ± 0.48a	6.00 ± 0.06c	4.36 ± 0.15d
AGPASE activity (µmol g^{-1} FW)				
Brace root	6.35 ± 0.29a	2.81 ± 0.23c	3.25 ± 0.48b	4.62 ± 0.25b
Crown root	2.75 ± 0.22b	7.62 ± 0.68a	2.77 ± 0.32b	1.87 ± 0.42c
Lateral root	5.53 ± 0.24b	6.60 ± 0.30a	3.97 ± 0.50c	4.575 ± 0.33c
Primary root	6.45 ± 0.23a	4.97 ± 0.52b	3.97 ± 0.07c	3.92 ± 0.32c
Seminal root	3.95 ± 0.37b	9.56 ± 0.43a	2.41 ± 0.07c	2.47 ± 0.48c
SS activity (µmol g^{-1} FW)				
Brace root	7.73 ± 0.17a	4.50 ± 0.39c	5.92 ± 0.52b	6.45 ± 0.52b
Crown root	3.59 ± 0.45b	6.59 ± 0.56a	4.00 ± 0.05b	2.93 ± 0.17c
Lateral root	6.58 ± 0.29b	8.01 ± 0.66a	4.79 ± 0.45c	5.02 ± 0.23c
Primary root	10.87 ± 0.40a	7.30 ± 0.98b	3.47 ± 0.15d	3.69 ± 0.25c
Seminal root	5.18 ± 0.25b	6.49 ± 0.26a	4.24 ± 0.22d	4.84 ± 0.04c

SPS (sucrose phosphate synthase), SuSy (sucrose synthase), AGPASE (ADP-glucose pyrophosphorylase), SS (sucrose synthase), LN (low nitrate), MN (medium nitrate), HN (high nitrate), LA (low ammonium nutrition), and FW (fresh weight of samples). The data represent the mean (±SE) of six independent plants (n=6). Different letters attached to the standard error indicate significant differences among treatments at a probability level of 0.05, as determined by one-way analysis of variance (ANOVA) followed by post-hoc comparisons.

4.4. Discussion

Nitrogen (N) is an essential nutrient that shapes biomass distribution between shoots and roots. Its various forms and concentrations elicit distinct plant responses with LN and NH_4^+ supply often inhibiting shoot growth while promoting root development (Sun et al. 2021). While extensive studies have examined N responses different crop species, research in maize has primarily remains limited in focused on single N form , leaving gaps in understanding how different N forms influences growth and C metabolism. Evaluating the impact of various N forms is essential for elucidating plant adaptation mechanisms. Studies indicate that NO_3^- and NH_4^+, differentially affect maize root architecture and nutrient uptake efficiency (The et al. 2021), while fluctuations in N availability influences C partitioning, starch accumulation and sucrose metabolism (Zhang et al. 2020). A comprehensive evaluation of N effects enhances our understanding of maize growth dynamics, root C metabolism, and NUE, offering valuable insight for optimizing fertilization strategies and improving crop productivity.

4.4.1. Physiological Adaptations to Different Nitrogen Forms in Maize Roots

In this study, LN treatment inhibited aerial growth, as evidenced by a reduction in shoot biomass, lower Pn, and decreased chlorophyll and total N content in both the leaves and roots of maize seedlings (Figs. S4.1A, S4.2A-D and S4.3A-D). These findings align with previous studies demonstrating that N deficiency impairs growth and photosynthetic efficiency, limiting C assimilation and shoot expansion (Zhao et al. 2020). Conversely, LN treatment stimulated overall root growth at the whole root system level, increasing the R/S ratio and enhancing total biomass accumulation (Figs. S4.2B-C). The increased overall root development expands the root system, improving the plant's ability to absorb N from the soil under N-deficient conditions (Kiba and Krapp 2016). A higher R/S ratio indicates that maize seedlings prioritize C allocation to the roots, strengthening resilience to N stress and supporting overall growth (Lopez et al. 2023). Despite the inhibition of shoot growth, the increase in total biomass in LN-treated plants highlights their compensatory response, expanding root structures to enhance root development and N acquisition (Zhao et al. 2020). At the whole root levels, maize plants grown under LN treatment exhibited greater root length, higher root number, increased root volume, and expanded root surface area (Fig. S4.2E-H). These overall root architectural modifications are presumed to enhance N uptake efficiency, thereby offering a potential advantage for LN-treated plants to better adapt and survive under N-deficient conditions, consistent with previous findings (Sun et al. 2021). Furthermore, these results emphasize the critical role of root plasticity in maintaining plant growth and development under suboptimal N availability (Nacry et al. 2013; Awasthi and Laxmi 2021). The findings also highlight the importance of root system modulation as a strategic adaptation to N deficiency, providing valuable insights into resource allocation optimization for improved plant resilience and productivity.

Moreover, examining the distinct physiological and architectural traits of different maize root types offers valuable insight into the mechanisms driving the overall whole-root response (Protto et al. 2024). While the whole root system showed overall promotion of growth and architecture, the mechanism underlying assimilate allocation in different root types under various N forms shows distinct growth patterns and developmental responses across specific root types in response to varying N treatments. LN treatment inhibited the growth of BR, CR, SR and PR, while promoting LR development (Figs. S4.5 and S4.6). This demonstrates a strategic shift in root architecture under N-limited conditions. The decreased biomass of BR, CR, PR, and SR under LN suggests that LN plants prioritize assimilate allocation away from these root types, which may be due to their high metabolic cost and lower efficiency in N uptake under N-limited conditions (Khan et al. 2019). Conversely, the enhanced LR proliferation under LN treatment represents an adaptive response to increase surface area for nutrient absorption (Pélissier et al. 2021). Contributing to the overall increase in whole-root length, plants grown under LN treatment exhibited increased root length across all root types (Figs. S4.5A-D). This was supported by a higher number of LR tips and expanded CR, PR, and LR volume and surface area. These specific morphological adaptations in root types, particularly the extensive development of lateral roots and expansion of surface areas (Figs. S4.5 and S4.6), contributed significantly to the enhanced N acquisition capacity observed at the whole root level under conditions of LN condition (Giehl et al. 2014).

Furthermore, as a signalling molecule, NO_3^- has been shown to regulate root system architecture (RSA) (Asim et al. 2020). In this study, LN treatment promoted LR elongation, improving their ability to explore a larger soil volume for N uptake (Figs. S4.5 and S4.6). This observation is consistent with previous findings (Gruber et al. 2013), suggesting that maize seedlings actively remodel their RSA to compensate for LN supply. The expansion of CR, PR, and LR under LN conditions demonstrates a coordinated developmental response aimed at increasing the absorptive interface between the root system and the soil matrix (López-Bucio et al. 2003). This dynamic shift toward a more extensively branched root network may contribute to improved NUE and enhanced adaptation to N-deficient conditions observed at the whole plant level (Figs. S4.2E-H).

4.4.2. Effects of different N forms on C-N coordination in maize roots and specific root types

N availability plays a crucial role in root formation, and this process is closely linked to C metabolism (Zhao et al. 2020). The observed physiological and architectural adaptations under N deficiency are underpinned by coordinated biochemical and molecular changes in C metabolism throughout the root system, with distinct patterns across different root types (Fig. 4.5). At the whole root level, N forms led to differential sugar and starch accumulation in maize seedlings. While LN plants consistently accumulated higher levels of soluble sugar and sucrose (Figs. 4.1A-B), indicating a strong allocation of

photosynthetic assimilates to roots under N deficiency (The et al. 2021; Ruan et al. 2007). LA treatment also influenced C metabolism, although with distinct pattern (Fig. 4.1). The activities of SPS and SuSy were significantly elevated at the whole root level (Figs. 4.2A-B), alongside the upregulated expression of *ZmSPS1*, *ZmSuSy1*, *ZmAINV1*, *ZmSWEET6*, *ZmSUC2*, and *ZmSTP2* in the whole roots (Figs. 4.3A-B, E-H). The enhanced accumulation of carbohydrates in roots may be attributed to an increased capacity for unloading photosynthetic assimilates, thereby facilitating root growth and adaptation to N deficiency. These findings emphasize the critical role of N availability in regulating C partitioning and root development, which is vital for improving NUE (Amoah and Kaiser 2025).

Sucrose loading in the phloem at the source and its unloading at the sink create a turgor pressure difference, driving the mass flow of assimilates (Lalonde et al. 2003). To maintain this pressure gradient and ensure continuous sucrose unloading into the roots, sucrose must be degraded (Ruan 2014). Under LN treatment, enhanced maize root growth and development depended on sucrose as an energy source, with increased SuSy activity alongside upregulated expression of *ZmSPS1*, *ZmSuSy1* and *ZmAINV1* (Fig. 4.3), aligning with previous findings (Zhao et al. 2020). Given the role of SuSy as a marker of sink strength (Kortstee et al. 2007), its elevated activity and expression suggests a key function in enhancing whole-root sink strength under LN conditions. *STPs* facilitates sucrose transport from source tissues, promoting root growth and development (Wu et al. 2024b). In this study, *ZmSTP2* expression was significantly higher at the whole-root level under LN , indicating its strong induction in response to N deficiency and its role in efficient sucrose transport to the roots, ensuring an adequate energy supply for growth. *SUCs* contribute to sucrose breakdown into glucose and fructose, providing energy and C skeletons for various metabolic processes (Ruan, 2012). This expression is often upregulated under N deficiency, accelerating sucrose degradation to support root cell division and expansion (Wang et al., 2020). Here, *ZmSUC2* was upregulated at whole-root level under LN treatment (Fig. 4.3), reinforcing its role in sucrose degradation and energy supply for root development in N-limited conditions (Zhu et al. 2022).

LN treatment increased root starch content, indicating a shift in C metabolism under N deficiency (Fig. 4.1C). Starch a crucial energy and C storage compound , is strongly influenced by N availability (Amoah and Kaiser 2025). The increased whole-root starch content observed in LN-treated plants suggests enhanced C storage, demonstrating a strategy where LN plants prioritize starch accumulation in roots when shoot growth is inhibited due to N limitation (Zhao et al., 2020). Under N deficient conditions, reduced shoot growth may lower assimilate demand, consequently decreasing carbohydrate allocation to developing tissues and leading to starch accumulation in the roots. This buildup may be attributed to reduced sink strength (Sun et al. 2020b; Aluko et al. 2023b). Furthermore, N deficiency can impose metabolic constraints, particularly on enzymatic activities involved in C partitioning, thereby affecting starch metabolism and

utilization efficiency in plants (MacNeill et al. 2017; Liu et al. 2025). Thus, starch accumulation under LN conditions may not solely indicate improved stress adaptation but rather reflect reduced sink strength or metabolic constraints. Consistent with whole-root starch accumulation, LN significantly increased AGPASE and SS activities while upregulated the expression of *ZmAGPASE1* and *ZmSS1* at the whole-root level (Figs. 4.3C-D, 4.4C-D, and S4.3). The Increased AGPASE and SS activities and the upregulation of *ZmAGPASE1* and *ZmSS1* at the whole-root highlight enhanced starch synthesis, ensuring a stable energy supply for root expansion and adaptation under N-deficient conditions, as previously demonstrated (Li et al. 2018)

The differential effects of N treatments on soluble sugar, sucrose, and starch accumulation across maize root types illustrate dynamic C partitioning in response to N availability (Zhao et al. 2020). Under LN, sugar and starch contents increased specifically in BR and PR, suggesting a strategic allocation of C reserves to enhance deep-rooted structural stability and nutrient acquisition (Fig. 4.5). This aligns with previous findings demonstrating that N availability modulates carbohydrate metabolism to optimize root function (Khan et al. 2019; Wang et al. 2021b). Conversely, MN treatment led to higher sugar and starch accumulation in CR, LR, and SR, directing C toward root types associated with increased proliferation and exploration under MN availability (Yu et al. 2016). Additionally, SPS, SuSy, AGPASE, and SS activities correlated with these changes in sugar accumulation, reinforcing the role of N in regulating carbohydrate metabolism to optimize specific root-type development (Fig. S4.8). Under LN conditions, elevated enzymatic activity in BR and SR likely enhances C utilization in structural and absorptive root segments (Table S4.3). Meanwhile, increased enzyme activity in CR, LR, and PR under MN suggests a metabolic adaptation favouring LR expansion and N acquisition in those conditions (Lemoine et al. 2013). These findings underscore the intricate interplay between N availability and C partitioning across maize root types, shaping the overall C status observed at the whole-root level (Fig. 4.1). At the molecular level, LN upregulated genes involved in sucrose transport (*ZmSWEET6*, *ZmSUC2*), starch synthesis (*ZmAGPASE1*, *ZmSS1*), and sink strength (*ZmAINV1*) specifically in BR and SR, suggesting enhanced C turnover to sustain growth under N deficiency. In contrast, MN predominantly induced these genes in CR, LR, and PR, aligning with increased sugar accumulation and enzymatic activity in those root types (Liu et al. 2022).

4.4.3. A coherent model of C–N coordination in maize roots under varying N availability

The integration of physiological, biochemical, and molecular responses reveals a coherent model of C–N coordination in maize roots under varying N availability. Under LN conditions, maize plants exhibit a strategic physiological adaptation by prioritizing root over shoot growth, resulting in a higher R/S ratio (Fig. S4.2A–C). This shift is achieved through precise architectural remodelling of the root system, in which the growth of BR, CR, PR, and SR is suppressed, while LR development is significantly

promoted (Figs. S4.4-S4.6). This differential root-type growth lead to an extensive, branched network optimized for N exploration and uptake, contributing to increased total root length, number, volume, and surface area observed at the whole-root level (Figs. S4.2E–H) (Dechorgnat et al. 2018; Wu et al. 2024a). This physiological and architectural plasticity is driven by a coordinated biochemical and molecular program (Wang et al. 2025b). Under LN, enhanced C allocation from shoots to roots results in higher levels of soluble sugars, sucrose, and starch in the whole root system (Fig. 4.1A–C and Fig. S4.7). This increased C supply provides essential energy and metabolic precursors for adaptive root growth. Notably, C is not distributed uniformly but is strategically allocated to specific root types based on N status (Fig. 4.5). Under LN, C reserves accumulate primarily in BR and PR, reinforcing structural integrity and deep rooting. In contrast, under MN conditions, C is preferentially directed to CR, LR, and SR to support active exploration and nutrient uptake (Fig. 4.5). The utilization and storage of C within each root type are tightly regulated by interconnected biochemical and molecular networks involving key enzymes and transporters (Wang and Ruan 2015; Wang et al. 2025b).

At the molecular level, sucrose transporters (*ZmSWEET6*, *ZmSTP2*) and starch biosynthesis genes (*ZmAGPASE1*, *ZmSS1*) are broadly upregulated in whole roots under LN conditions (Fig. 4.7-4.9). However, their expression varies across root types (Figs. 4.7-4.9). Under LN, genes facilitating C turnover, such as *ZmSWEET6*, *ZmSUC2*, *ZmAGPASE1*, *ZmSS1*, and *ZmAINV1*, are predominantly induced in BR and SR, supporting metabolic activity in these structural and absorptive roots (Fig. 4.6-4.9). Under MN, these genes are primarily expressed in CR, LR, and PR, aligning with observed root-type growth dynamics (Figs. 4.4, 4.6-4.9). This differential molecular regulation ensures that the metabolic machinery for sucrose degradation and starch synthesis is active in root segments strategically favoured under each N condition. Enzymes such as SuSy and SUCs, supported by transporters, such as *ZmSTP2* and *ZmSWEET6*, facilitate sucrose breakdown, supplying energy and C skeletons for root cell division, elongation, and maintenance of the expanded root system. Starch accumulation serves as a critical energy reserve (Liang et al. 2023b; Tian et al. 2024).

Temporal dynamics further underscore this coordination. Diurnal patterns show that LN-treated plants consistently maintain elevated sugar and starch levels throughout day and night cycles (Fig. 4.4), reflecting enhanced capacity for carbohydrate storage and utilization under N stress. Collectively, these findings support a coherent model in which N deficiency triggers a cascade of responses from the whole plant to the molecular level. Physiological adaptation involves resource reallocation and root architectural remodelling, particularly through differential growth of specific root types (Calleja-Cabrera et al. 2020; Ranjan et al. 2022). This is reinforced by enhanced C allocation and strategic partitioning across the root system (Fig. 5). The metabolic fate of this C is modulated by differential enzyme activities and the expression of genes involved in sucrose and starch metabolism, precisely regulated within each root type to match its functional role in the adaptive root architecture (Figs. 4.6–4.9). This multi-layered, root-type-specific coordination of C and N metabolism enables maize to

optimize root plasticity and improve NUE, which is essential for survival and productivity under N-limited conditions (Amoah and Kaiser 2025). These insights deepen our understanding of N-induced metabolic and molecular adaptations in maize roots, offering a valuable framework for crop improvement and sustainable agriculture. Ultimately, this model can inform N management strategies aimed at optimizing root function and enhancing resilience in low-input farming systems.

4.5. Conclusion

The study examined the intricate relationship between N availability and C metabolism in maize roots, analysing responses at multiple levels: biomass accumulation, root morphology, and sugars and starch metabolism at both biochemical and transcriptional scales. Under LN conditions, maize seedlings exhibited significant adaptive responses. In terms of biomass accumulation and phenotypic adaptation, shoot growth was inhibited, while root growth was promoted, resulting in an increased R/S ratio. This enhancement in root development, characterized by greater root length, number, volume, and surface area, represents a strategic shift in resource allocation to improve N acquisition under N-limited conditions. Notably, LN treatment suppressed the growth of BR, CR, PR, and SR, while promoting LR development. These architectural modifications enhance maize plant's ability to absorb N from the soil. Supporting these physiological adaptations, biochemical analyses revealed significant metabolic shifts. LN treatment induced higher sugar and starch levels in maize roots, indicating increased transport of photosynthetic assimilates to the roots to provide essential energy and carbon skeletons for root growth and adaptation. These dynamic changes were driven by enhanced activities of key enzymes involved in sugar and starch metabolism, including SPS, SuSy, AGPASE, and SS. Furthermore, transcriptional analysis demonstrated a coordinated upregulation of genes associated with sucrose metabolism (*ZmSPS1*, *ZmSuSy1*, *ZmAINV1*, *ZmSWEET6*, *ZmSUC2*, and *ZmSTP2*) and starch biosynthesis (*ZmAGPASE1* and *ZmSS1*) under LN conditions. This suggests an active molecular program facilitating sucrose transport (*ZmSTP2*, *ZmSWEET6*, *ZmSUC2*), root sink strength (*ZmSuSy1*, *ZmAINV1*), and C storage (*ZmAGPASE1*, *ZmSS1*). Notably, these responses varied across different root types, indicating an enhanced regulatory network that modulates sucrose allocation and metabolic pathways to optimize maize adaptation to LN conditions. Collectively, these findings at morphological, biochemical, and molecular levels illustrate how maize coordinates a cohesive response to N deficiency. Molecular signals trigger metabolic adjustments that provide essential resources for adaptive root architectural modifications, ultimately enhancing NUE under N-limited conditions. These insights hold valuable implications for optimizing fertilization strategies and improving crop performance. Future studies will consider field validation across diverse genotypes and explore the anatomical, transcriptomic, and proteomic responses of maize roots to varying N levels to better understand root development and plasticity under N-deficient conditions.

4.6. Supplementary data

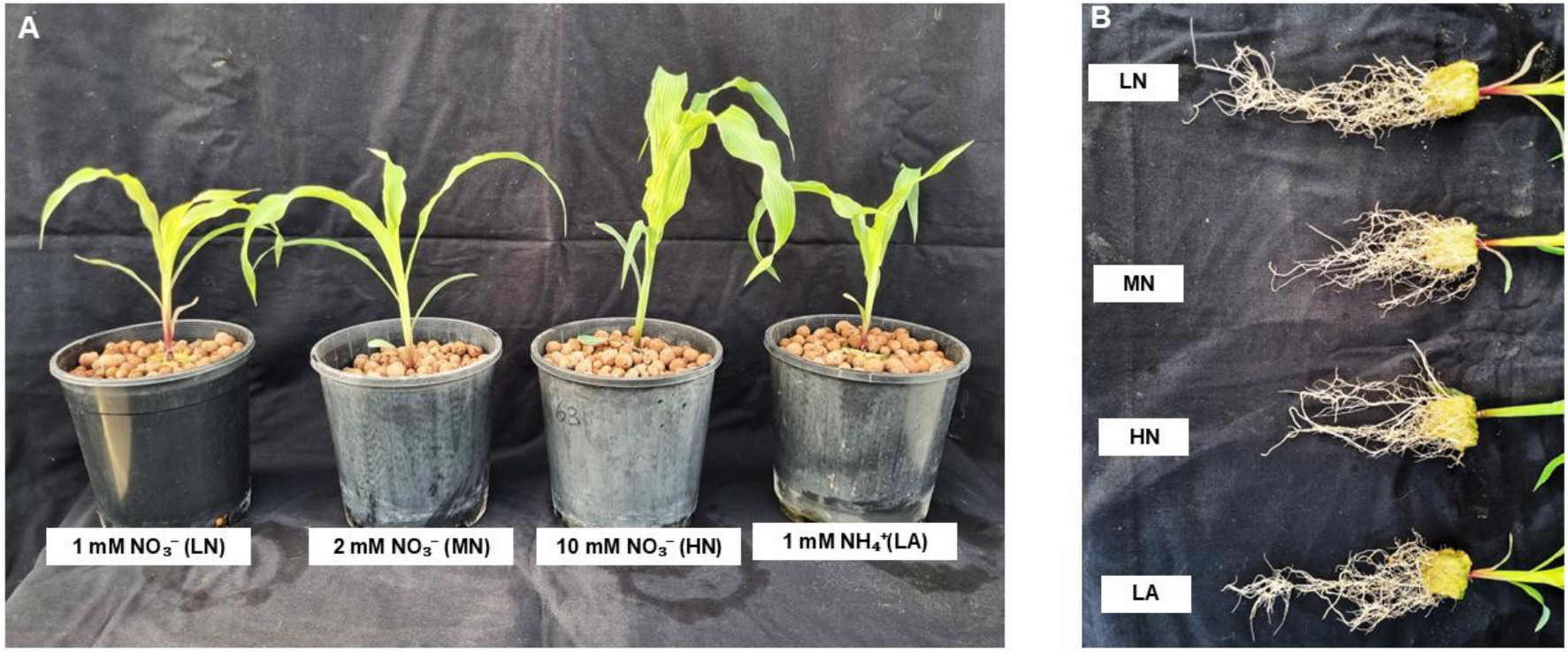

Fig. S4.1 Representative photos of shoot (**A**) and root (**B**) phenotypic response of maize seedlings to different N treatment conditions. LN: low nitrogen (N deficiency), MN: moderate nitrogen, HN: high nitrogen, and LA: low ammonium treatment.

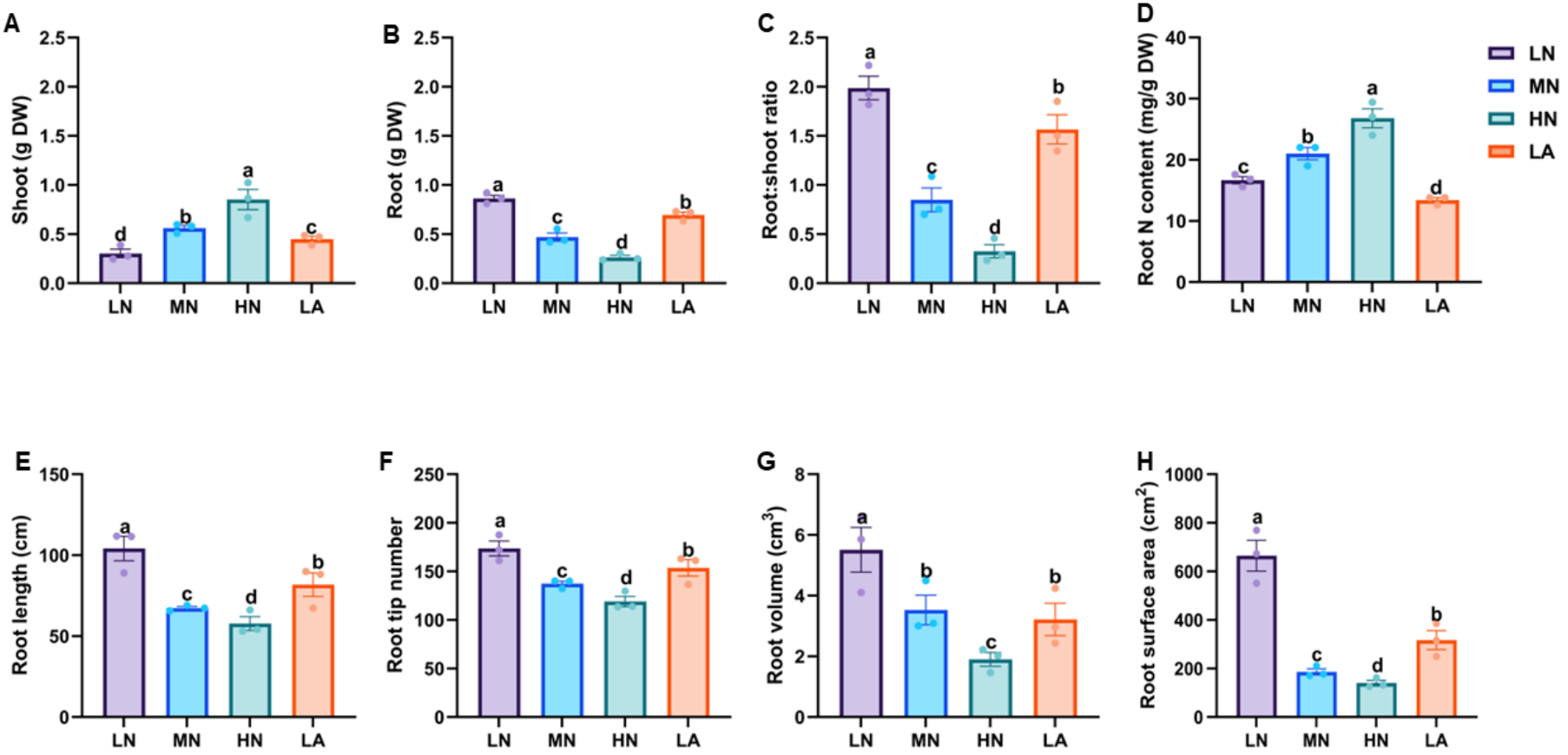

Fig S4.2 Effects of different nitrogen (N) treatments on (**A**) shoot biomass, (**B**) whole-root biomass, (**C**) whole-root-to-shoot ratio, (**D**) whole-root nitrogen content, (**E**) whole-root length, (**F**) whole-root tip number, (**G**) whole-root volume, and (**H**) whole-root surface area in maize inbred line TX-40J. Data represents mean ± standard error (SE) of six independent plants (n = 6). Different letters on error bars indicate statistically significant differences at $P \leq 0.05$. DW dry weight, LN low nitrate, MN moderate nitrate, HN high nitrate and LA low ammonium.

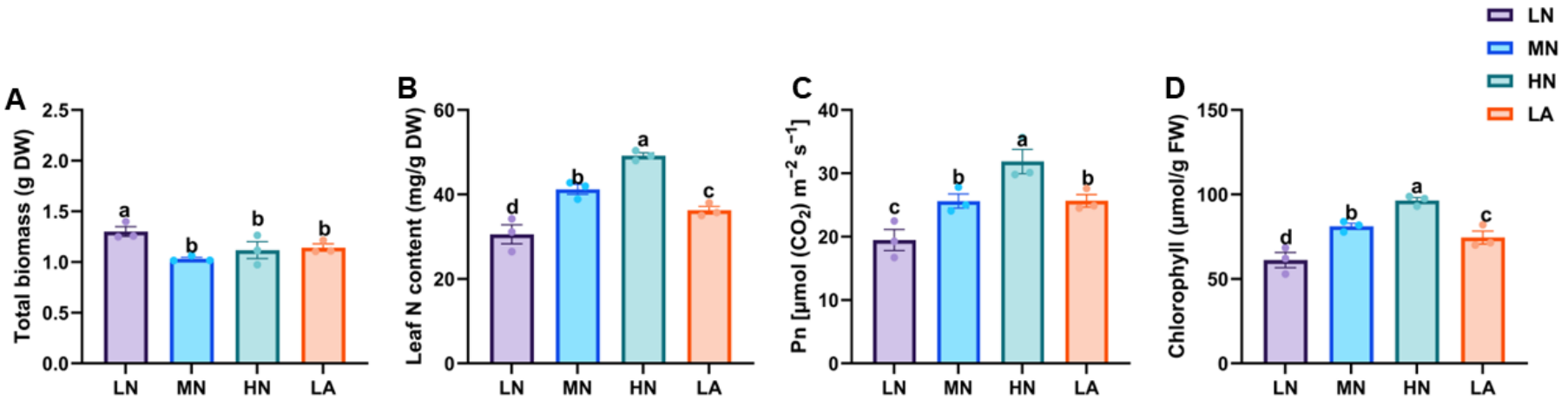

Fig. S4.3 Total biomass (**A**), leaf nitrogen content (**B**), leaf net photosynthetic rate (**C**) and leaf chlorophyll content (**D**) of maize seedlings grown under different nitrogen (N) treatments. Data represents the mean ± SEM (n = 6). Statistical significance was determined using Tukey's multiple range test ($P< 0.05$), with different letters indicating significant differences between treatments. DW denotes dry weights; LN: low nitrogen (N deficiency), MN: moderate nitrogen, HN: high nitrogen, and LA: low ammonium treatment

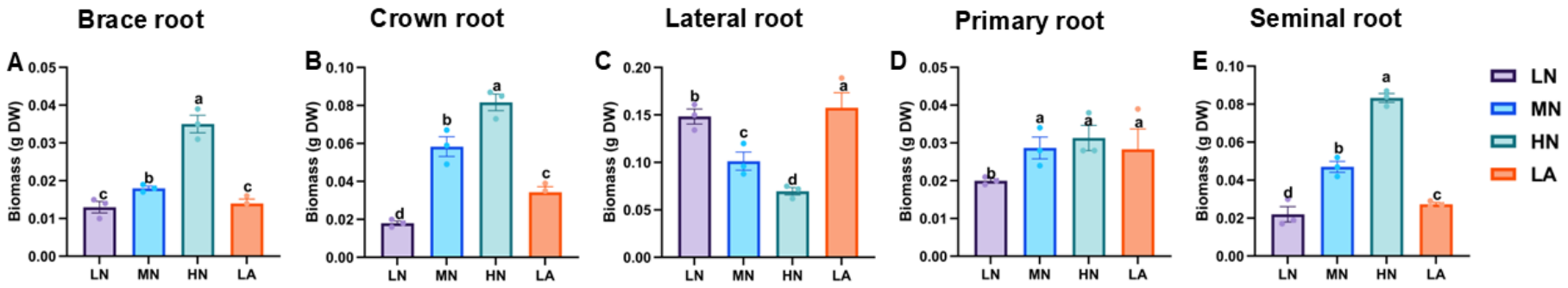

Fig. S4.4 Effect of different N forms on root biomass accumulation. Brace (**A**), crown (**B**), lateral (**C**), primary (**D**) and seminal (**E**) root biomass after 30 days of seedling transfer. Data are presented as the mean ± SEM (n = 6). Statistical significance was determined using Tukey's multiple range test ($P< 0.05$), with different letters indicating significant differences between treatments. DW denotes dry weights; LN: low nitrogen (N deficiency), MN: moderate nitrogen, HN: high nitrogen, and LA: low ammonium treatment.

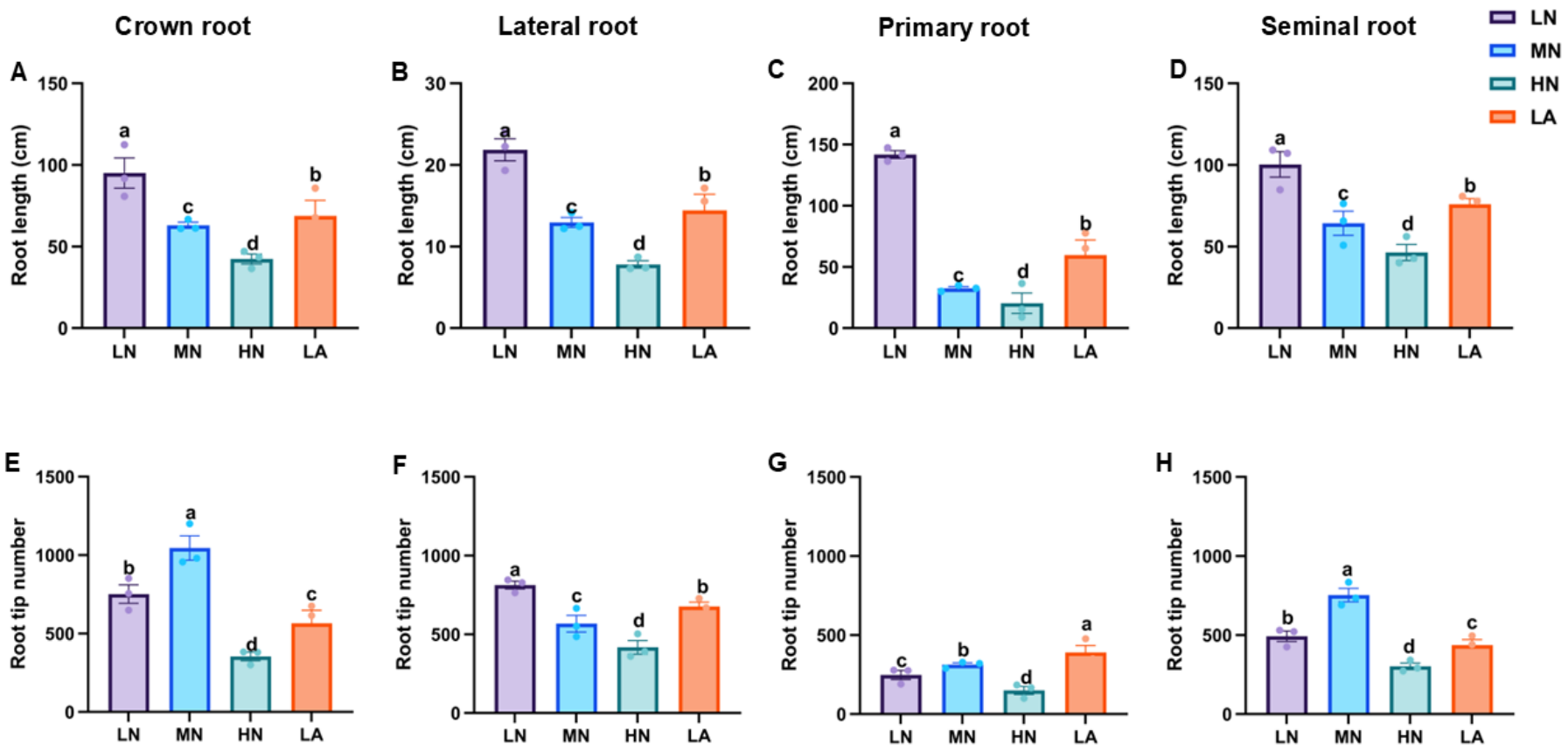

Fig. S4.5 Effect of different N forms on morphological response of different root types. Crown (**A**), lateral (**B**), primary (**C**) and seminal (**D**) root length (cm) and crown (**A**), lateral (**B**), primary (**C**) and seminal (**D**) root tip numbers. Data are presented as mean ± SEM (n = 6). Statistical significance was determined using Tukey's multiple range test ($P< 0.05$), with different letters indicating significant differences between treatments. LN: low nitrogen (N deficiency), MN: moderate nitrogen, HN: high nitrogen, and LA: low ammonium treatment.

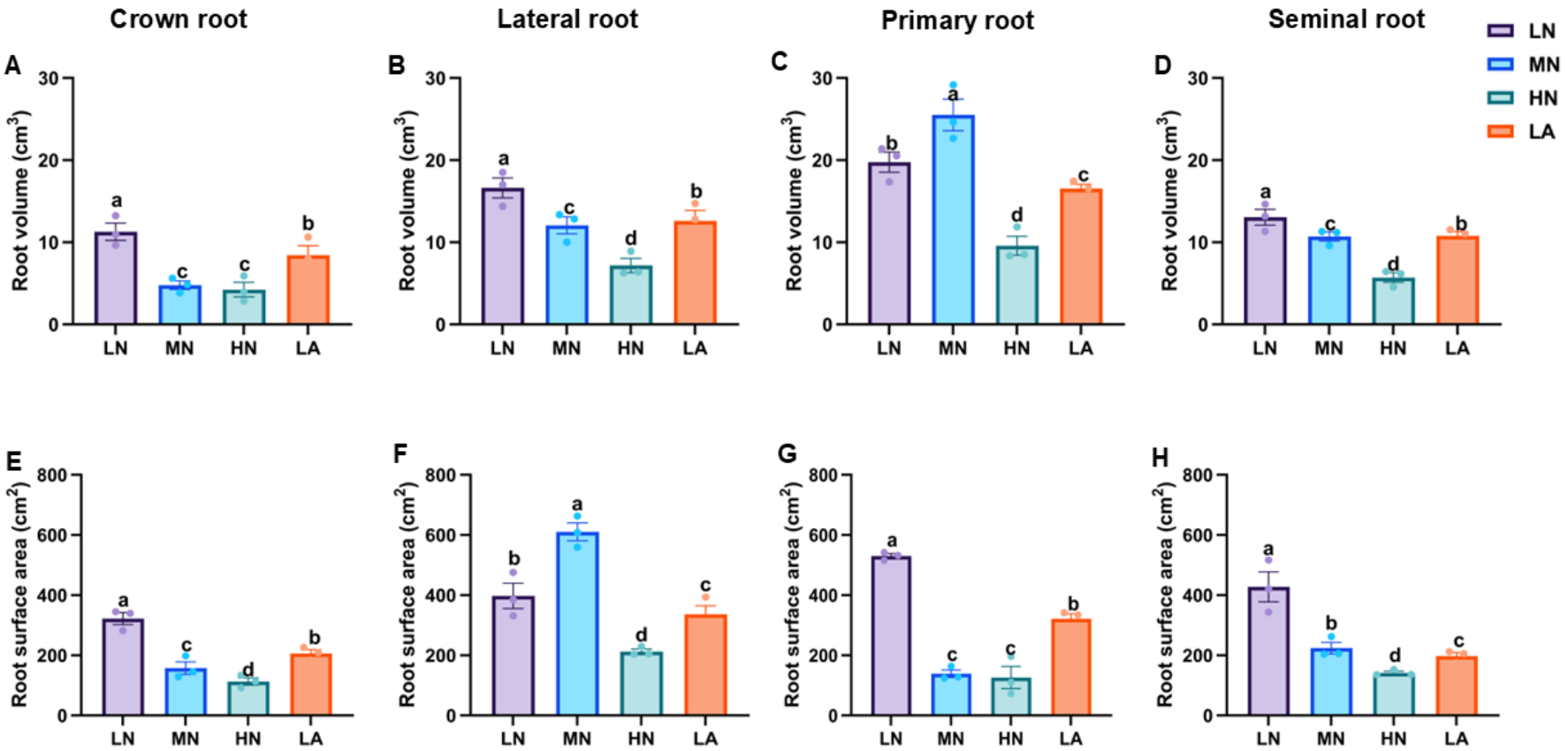

Fig. S4.6 Effect of different N forms on morphological response of different root types. Crown (**A**), lateral (**B**), primary (**C**) and seminal (**D**) root length and Crown (**A**), lateral (**B**), primary (**C**) and seminal (**D**) root surface area (cm^{-2}). Data are presented as mean ± SEM (n = 6). Statistical significance was determined using Tukey's multiple range test ($P< 0.05$), with different letters indicating significant differences between treatments. LN: low nitrogen (LN), MN: moderate nitrogen, HN: high nitrogen, and LA: low ammonium treatment.

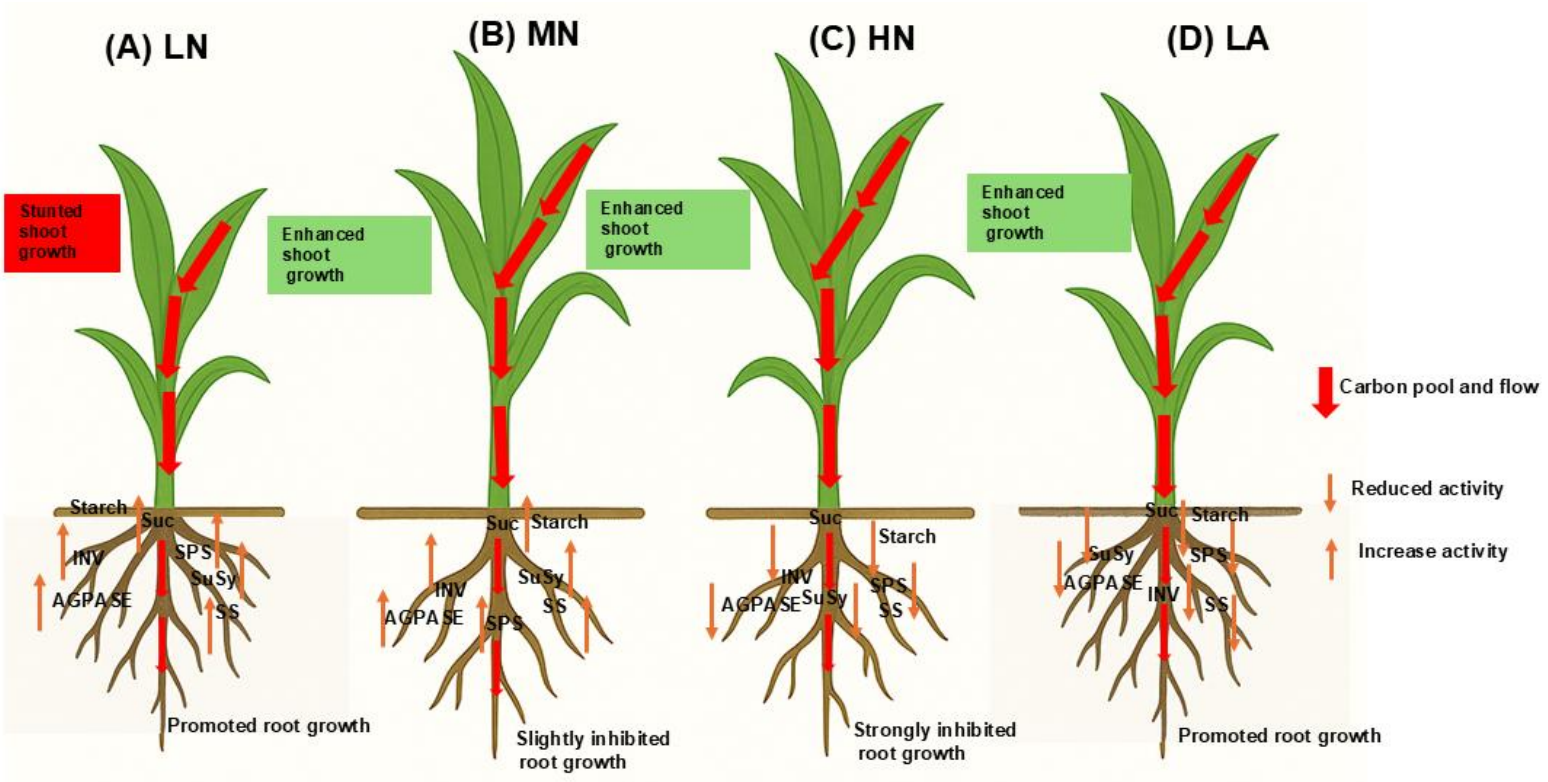

Fig. S4.7 Schematic diagram summarizing the changes occurring in maize due to different N treatments. Shoot and root growth, as well as carbon partitioning, varied markedly across treatments. Low nitrate (LN) reduced shoot growth while promoting root development, accompanied by diminished SPS activity and starch accumulation. Medium nitrate (MN) and high nitrate (HN) enhanced shoot growth with elevated SPS, SuSy, and AGPASE activities, though root growth was slightly or strongly inhibited, respectively. Low ammonium (LA) stimulated both shoot and root growth, suggesting enhanced coordination of sucrose metabolism and carbon flow, with increased INV, SuSy, AGPASE, and SPS activities. Abbreviations: Suc – sucrose, INV – invertase, SuSy – sucrose synthase, SS – starch synthase, AGPASE – ADP-glucose pyrophosphorylase, SPS – sucrose phosphate synthase, LN – low nitrate, MN – medium nitrate, HN – high nitrate, LA – low ammonium treatment. Suc: sucrose, INV: invertase, SuSy: sucrose synthase, SS: starch synthase, AGPASE: ADP-glucose pyrophosphorylase, SPS: sucrose phosphate synthase, LN: low nitrate, MN: medium nitrate, HN: high nitrate and LA: low ammonium treatment.

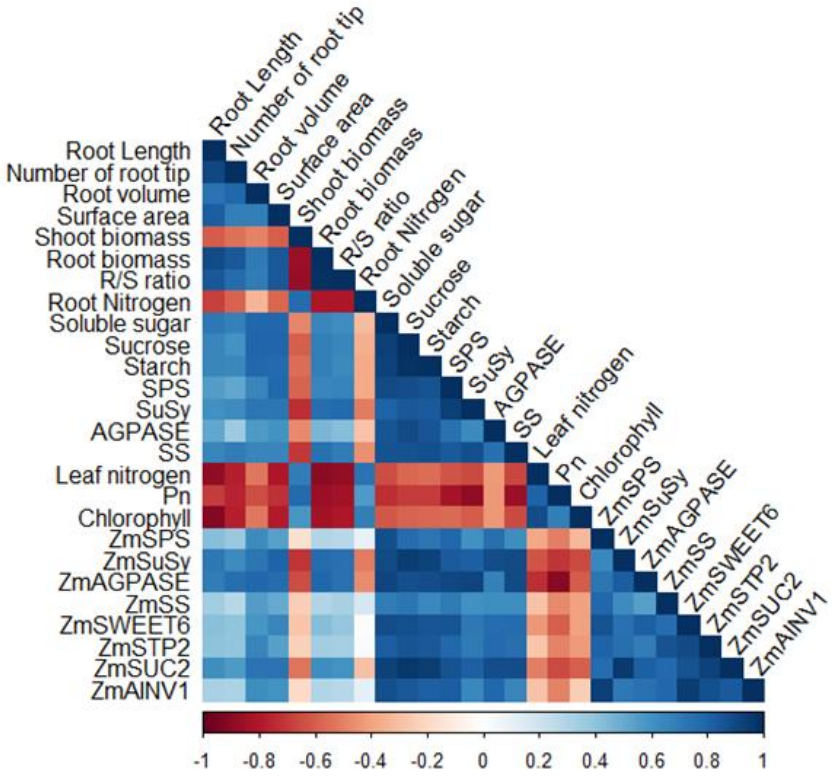

Fig. S4.8 Pearson's correlation plot between physio-biochemical and molecular indicators under different nitrogen forms in maize roots. The plot was constructed using mean values of samples. SuSy/*ZmSuSy1:* sucrose synthase, , *ZmAINV1*: acid/alkaline invertase, SPS/*ZmSPS1*: sucrose phosphate synthase, SS/*ZmSS1*: starch synthase, AGPase/*ZmAGPase1*, ADP-glucose pyrophosphorylase , Pn: net photosynthetic rate, correlations are represented by colour gradients, ranging from blue (positive correlation) to red (negative correlation).

Table S1: List of genes studied

Name	NCBI LOCs
ZmSuSy	LOC542247
ZmSPS	LOC542711
ZmSUC	LOC541615
ZmAGPase	LOC542737
ZmSTP	LOC100273083
ZmSWEET	LOC100282708
ZmVINV	LOC542324
ZmActin	LOC100282267
ZmUBQc	LOC541665
ZmSS	LOC541669

Table S4.2 One-way analysis of variance (ANOVA) for indicators measured in roots of maize plants under different nitrogen conditions

Traits/(plants)	Sources of variations					
	Treatment (df=3)					
	Whole root	**Brace root**	**Crown root**	**Lateral root**	**Primary root**	**Seminal root**
Root length	0.0021**	NA	0.0045**	<0.0001****	<0.0001****	0.0001***
Root tip number	0.0034**	NA	0.0011**	0.0006***	0.0025**	<0.0001****
Root volume	0.0225*	NA	0.0022**	0.0023**	0.0002***	0.0004***
Root surface area	<0.0001****	NA	0.0001***	<0.0001****	<0.0001****	<0.0001****
Shoot biomass	0.0028**	NA	NA	NA	NA	NA
Root biomass	<0.0001****	<0.0001****	<0.0001****	0.0009***	0.1955ns	<0.0001****
Root:shoot ratio	<0.0001***	NA	NA	NA	NA	NA
Nitrogen	<0.0001***	NA	NA	NA	NA	NA
Soluble sugar	<0.0001***	0.0356*	0.0001***	0.0001***	<0.0001****	0.004**
Sucrose	<0.0001***	0.0038**	0.0001***	<0.0001****	0.0052**	0.0105*
Starch	<0.0001***	0.0051**	0.0198*	<0.0001****	<0.0001****	0.0006***
SPS activity	0.0026**	0.0001***	0.0017**	0.0102*	<0.0001****	0.0002***
SuSy activity	0.006**	0.0029**	0.0006***	0.1037ns	<0.0001****	0.001**
AGPASE activity	<0.0001****	0.0007***	0.0002***	0.0095**	0.0046**	<0.0001****
Starch synthase	0.0011**	0.0107*	0.0016**	0.0069**	0.0001***	0.0013**
ZmSPS1	0.0005***	0.0002***	<0.0001****	0.0156*	<0.0001****	0.0138*
ZmSuSy1	0.0003***	0.0029**	0.0006***	0.0035**	<0.0001****	0.0019**
ZmAGPASE1	0.0002***	<0.0001****	0.0002***	0.0443*	<0.0001****	0.0095**
ZmSS1	0.0019**	0.0041**	0.0058**	<0.0001****	<0.0001****	0.0004***
ZmSWEET6	0.0003***	0.0004***	0.0003***	0.002**	<0.0001****	0.0459*
ZmSUC2	0.0006***	0.0013**	0.0005***	0.0129*	<0.0001****	0.0012**
ZmSTP2	<0.0001****	0.0002***	0.0001***	0.0008***	0.0026**	0.0011**
ZmAINV1	<0.0001****	0.0035**	<0.0001****	<0.0001****	<0.0001****	0.0028**

SPS/*ZmSPS1* (sucrose phosphate synthase), SuSy/*ZmSuSy1* (sucrose synthase), and AGPASE/*ZmAGPASE1* (ADP-glucose pyrophosphorylase). The symbols *, **, ***, and **** indicate significant differences at probability levels of 0.5, 0.1, 0.001, and 0.0001, respectively. NA, ns, and df denote not applicable, non-significant, and degree of freedom, respectively.

Table S4.3 Sugars and starch metabolism enzymes activity in maize root types under different N forms

Traits/(plants)	Treatments			
	LN (1 mM NO_3^-)	MN (2 mM NO_3^-)	HN (1 mM NO_3^-)	LA (10 mM NH_4^+)
SPS activity (µmol g^{-1} FW)				
Brace root	8.97 ± 0.41a	3.45 ± 0.17d	5.62 ± 0.51c	6.80 ± 0.27b
Crown root	3.66 ± 0.12b	5.89 ± 0.67a	2.77 ± 0.26c	2.25 ± 0.16d
Lateral root	5.52 ± 0.30b	6.37 ± 0.26a	4.92 ± 0.04c	4.44 ± 0.34d
Primary root	6.53 ± 0.66b	12.11 ± 0.45a	2.89 ± 0.09c	3.13 ± 0.47c
Seminal root	4.94 ± 0.08b	7.87 ± 0.63a	4.56 ± 0.06c	3.38 ± 0.15c
SuSy activity (µmol g^{-1} FW)				
Brace root	11.36 ± 0.41a	4.89 ± 0.22c	8.94 ± 0.72b	8.05 ± 1.06b
Crown root	3.57 ± 0.36c	7.95 ± 0.74a	4.879 ± 0.21b	3.04 ± 0.22d
Lateral root	7.11 ± 0.72b	8.40 ± 0.35a	6.23 ± 0.68c	5.88 ± 0.44d
Primary root	8.84 ± 0.58b	17.03 ± 0.59a	3.77 ± 0.10c	4.11 ± 0.62d
Seminal root	6.98 ± 0.42b	7.92 ± 0.48a	6.00 ± 0.06c	4.36 ± 0.15d
AGPASE activity (µmol g^{-1} FW)				
Brace root	6.35 ± 0.29a	2.81 ± 0.23c	3.25 ± 0.48b	4.62 ± 0.25b
Crown root	2.75 ± 0.22b	7.62 ± 0.68a	2.77 ± 0.32b	1.87 ± 0.42c
Lateral root	5.53 ± 0.24b	6.60 ± 0.30a	3.97 ± 0.50c	4.575 ± 0.33c
Primary root	6.45 ± 0.23a	4.97 ± 0.52b	3.97 ± 0.07c	3.92 ± 0.32c
Seminal root	3.95 ± 0.37b	9.56 ± 0.43a	2.41 ± 0.07c	2.47 ± 0.48c
SS activity (µmol g^{-1} FW)				
Brace root	7.73 ± 0.17a	4.50 ± 0.39c	5.92 ± 0.52b	6.45 ± 0.52b
Crown root	3.59 ± 0.45b	6.59 ± 0.56a	4.00 ± 0.05b	2.93 ± 0.17c
Lateral root	6.58 ± 0.29b	8.01 ± 0.66a	4.79 ± 0.45c	5.02 ± 0.23c
Primary root	10.87 ± 0.40a	7.30 ± 0.98b	3.47 ± 0.15d	3.69 ± 0.25c
Seminal root	5.18 ± 0.25b	6.49 ± 0.26a	4.24 ± 0.22d	4.84 ± 0.04c

SPS (sucrose phosphate synthase), SuSy (sucrose synthase), AGPASE (ADP-glucose pyrophosphorylase), SS (sucrose synthase), LN (low nitrate), MN (medium nitrate), HN (high nitrate), LA (low ammonium nutrition), and FW (fresh weight of samples). The data represent the mean (±SE) of six independent plants (n=6). Different letters attached to the standard error indicate significant differences among treatments at a probability level of 0.05, as determined by one-way analysis of variance (ANOVA) followed by post-hoc comparisons.

CHAPTER 5: NITROGEN FORM SUBSTITUTION ENHANCES GROWTH AND CARBON ACCUMULATION IN MAIZE[4]

Abstract

Sugars are essential for plant development, and nitrogen (N) availability regulates their distribution, influencing overall growth. However, the mechanisms underlying carbon (C) assimilate allocation and utilization in response to different N forms remain unclear. This study examined the effects of nitrogen form substitution (NFS) on C accumulation and utilization in hydroponically grown inbred mini-maize (TX-40J). Maize seedlings were divided into three treatment groups: T1 (1 mM NO_3^-), T2 (1 mM NH_4^+), and T3, where 1 mM NO_3^- was substituted with 1 mM NH_4^+ (NFS) at 10 days after seedling transfer (DAT). The results showed that NFS led to a significant reduction in total sucrolytic activity by 27% in leaves and 21% in roots, resulting in a lower hexose-to-sucrose ratio. Despite this, NFS enhanced shoot biomass by 30%, root biomass by 24%, and total plant biomass by 28%, suggesting improved sucrose utilization and increased competition for assimilates. Root-to-shoot biomass allocation was particularly enhanced under NFS conditions. Additionally, starch and sucrose accumulated at lower levels in leaves under NFS compared to other N treatments. Starch was predominantly stored in the leaf tips, whereas sucrose accumulated in the leaf sheath. This spatial distribution suggests that C buildup was not due to impaired C assimilation but rather inefficient C utilization in sink tissues. These findings provide new insights into how NFS influences C allocation between leaves and roots, promoting stress adaptation. Understanding the role of C partitioning under NFS conditions may help optimize plant growth and improve nutrient use efficiency under N deficiency.

Keywords: nitrogen form substitution (NFS), plant growth, nitrogen allocation and assimilation, nitrogen use efficiency, nitrogen fluctuation

---

[4]This chapter is published as: Amoah JN, Kaiser BN (2025) Nitrogen Form Substitution Enhances Growth and Carbon Accumulation in Maize. Journal of Plant Growth Regulation. doi:10.1007/s00344-025-11713-8

5.1. Introduction

Nitrogen (N) is an essential macro-nutrient required for plant development, serving as a structural component of essential biomolecules such as nucleic acids, amino acids, and proteins. Additionally, N functions as a key signalling molecule, influencing various plant metabolic processes, including photosynthesis, seed regulation, responses to abiotic stress, and hormone signalling pathways (Vidal et al. 2014; da Silva et al. 2024). However, in most agricultural systems, plant productivity is often constrained limited availability of N in the soil. N deficiency greatly impacts total biomass and harvestable yield, which directly affects grower's profitability (Navarro-Morillo et al. 2024; Lopez et al. 2023). Growers often apply large quantities of nitrogen (N) fertilizers to mitigate N limitations. However, less than 50% of the applied N is effectively utilized by crops, with the remainder lost due to excessive rainfall or irrigation, which leads to significant nitrate leaching from the soil profile. This loss creates a fluctuating N supply condition characterized by alternating periods of N deficiency, sufficiency, or excess. Such fluctuations can arise naturally in agricultural soils due to environmental factors or as a consequence of agricultural practices (Nacry et al. 2013). This unpredictable nutrient dynamic negatively impacts various metabolic functions in plants, ultimately hindering growth and productivity (Lassaletta et al. 2014; Govindasamy et al. 2023).

Previous studies have demonstrated that different nitrogen (N) supplies can significantly affect plant growth, photosynthesis, and carbon metabolism, with excessive N generally inhibiting growth and metabolic functions (Dong et al. 2019). Nitrate (NO_3^-) and ammonium (NH_4^+) are the primary forms of nitrogen available to plants, each having distinct impacts on growth and development (Glass et al. 2002). Research has shown that plants tend to grow better when supplied with NO_3^- rather than NH_4^+ (Boschiero et al. 2019; Chen Wei et al. 2005). However, in maize, NH_4^+ nutrition has been shown to enhance growth, as well as carbon and nitrogen assimilation (George et al. 2016). Additionally, recent studies indicate that maize plants supplied with both NH_4^+ and NO_3^- sources are more productive than those fed with either NO_3^- or NH_4^+ alone (Banik et al. 2016; Peng et al. 2023a; Wang et al. 2019). In Arabidopsis, when NH_4^+ was the predominant nitrogen source, biomass and chlorophyll content decreased, and cellular stress symptoms appeared (M'rah Helali et al. 2010). A similar trend was observed in maize, where plants fed only NH_4^+ showed lower dry biomass yields compared to those fed with NO_3^- alone, with the highest nitrogen use efficiency seen in plants receiving only NO_3^- (Peng et al. 2023a). However, the underlying mechanisms related to changes in nitrogen forms, such as switching from NO_3^- to NH_4^+ nutrition, and their effects on growth, photosynthesis, and carbon metabolism in maize remain marginally unclear.

Given that both under-application and over-application of nitrogen (N) fertilizers negatively impact plant growth, metabolic processes, the environment, and human health (Nacry et al. 2013; Zhang et al. 2021; Zhao et al. 2020), it is essential to explore alternative strategies that support plant

development under variable environmental conditions. Such approaches could provide critical insights for developing crops with higher yields and improved nitrogen use efficiency (NUE), addressing food security challenges posed by the growing global population (Nacry et al. 2013). In this context, we propose that substituting the nitrogen form, such as switching from NO_3^- to NH_4^+, during plant growth may enhance growth and productivity compared to plants grown on sole NO_3^- or NH_4^+ nutrition. Additionally, we suggest that nitrogen form substitution (NFS) treatment may facilitate a shift in nitrogen supply and availability during the transition from periods of limited nitrogen (Zhao et al. 2020; Sun et al. 2022). This adaptive mechanism is anticipated to improve resource allocation and utilization, thereby promoting growth and enhancing photosynthesis in plants.

Maize (*Zea mays*) was chosen for this study due to its significance as a staple food crop and its role as an ideal model for understanding N metabolism and C allocation (Simons et al. 2014). Its well-documented growth patterns, responsiveness to environmental factors, and ability to adapt to various nitrogen conditions make it an excellent crop for studying the effects of nitrogen form substitution on carbon distribution (Dong et al. 2023b). Furthermore, the economic importance of maize in global agriculture highlights the potential impact of optimizing nutrient management to enhance crop productivity (Begam et al. 2024). This study explores the mechanisms underlying altered carbon allocation in maize under nitrogen form substitution (NFS) conditions. Specifically, we examined the effects of NFS on growth, photosynthesis, and the metabolism of sugars and starch in maize leaves and roots. Additionally, we investigated the diurnal changes in assimilates within source leaves and their distribution among various tissues, including the source leaf, sheath, root, and ear, at 20 (vegetative stage) and 40 (reproductive stage) days after seedling transfer (DAT). The findings of this study contribute to a deeper understanding of how NFS influences carbon allocation and accumulation, offering valuable insights for crop production strategies in environments with fluctuating nitrogen availability.

5.2. Materials and methods

5.2.1. Plant materials and treatments

Seeds of the fast-flowering, short-cycle inbred mini-maize line TX-40J (McCaw et al. 2016) were used in this study. This maize line offers significant advantages, including a uniform genetic background, a shorter lifecycle, and early flowering, which enable efficient and targeted research in various areas of plant biology. The traits observed in this variety serve as valuable references for breeders, facilitating the development of hybrids with enhanced performance and improved nitrogen use efficiency (Șuteu et al. 2014; Ghosh et al. 2014; McCaw and Birchler 2017; McCaw et al. 2021). The seeds were disinfected with 8% (v/v) sodium hypochlorite for 5 min and then rinsed five times with distilled water, each rinse lasting 5 min. The seeds were subsequently germinated in Oasis Horticube Propagation Slabs (Aqua

Gardening, Brisbane, Australia), an inorganic and pH-neutral growing foam medium, placed in germination trays. The trays were transferred to a climate-controlled growth room, set to a 14/10 day-night cycle, with temperatures of 25°C during the day and 22°C at night, and 80% relative humidity for 5 d to allow for seed germination. Once the seedlings had germinated uniformly, they were transferred to a glasshouse for the subsequent experiments.

Uniformly grown seedlings were selected and divided into three treatment groups (T1–T3) (Fig. S5.1) and were grown in 3 L pots with their roots supported by inorganic expanded clay pellets (Aqua Gardening, Brisbane, Australia). Initially, plants in T1 and T2 were grown with 1 mM NO_3^-, while T3 was grown with 1 mM NH_4^+. At 10 days after transfer (DAT), when the seedlings reached the fully expanded third leaf stage (Zadoks et al. 1974), T1 and T3 plants continued with the same nutrient solutions (1 mM NO_3^-), whereas in T2, 1 mM NO_3^- was substituted with 1 mM NH_4^+. Thus, T2 served as the primary treatment for evaluating the effect of nitrogen form substitution (NFS) on carbohydrate accumulation in maize, while T1 and T3 acted as control groups for comparison. These nutrient levels were chosen based on previous studies (Plett et al. 2016; Dechorgnat et al. 2018). The plants were grown for a total of 40 days, with tissue sampling performed at 20 and 40 DAT to capture data for both vegetative and reproductive growth stages.

The system was set up in a climate-controlled glasshouse, with conditions matching those of the growth room used for seed germination, but with supplemental LED lighting providing 1000 µmol m^{-2} s^{-1} at the pot level. Each system was designed to accommodate 40 pots, with one plant per pot. Plants were drip-irrigated with the respective nutrient solution, which was circulated through a hydroponic pump system. Irrigation occurred twice daily for 1 minute, at 12:00 PM and 5:00 PM. The treatment solutions containing 1 mM $(NH_4)_2SO_4$, 1 mM KNO_3, 0.5 mM $MgSO_4$, 0.5 mM KH_2PO_4, 1.05 mM KCl, 1.25 mM K_2SO_4, 0.25 mM $CaCl_2$, 1.75 mM $CaSO_4$, 0.1 mM Fe-EDTA, 0.1 mM Fe-EDDHA, 25 µM H_3BO_3, 2 mM $MnSO_4$, 2 mM $ZnSO_4$, 0.5 mM $CuSO_4$, and 0.5 mM Na_2MoO_4 were stored in 162 L Brute Containers with lids (Rubbermaid, USA). The solution was changed weekly, with daily pH adjustments to maintain a stable pH of 5.9. The treatment solution was delivered to the system by an Eden 140G FL submersible water pump (Creative Pumps, Australia). Plants were uniquely identified and randomized into blocks using R statistical software (v2.3.4).

Sampling was conducted at 20 (vegetative, V6 stage) and 40 (reproductive, R1 stage) days after seedling transfer (DAT). Fresh leaf, root and ear tissues for biochemical analysis were collected, immediately frozen in liquid nitrogen (N_2), and stored at -80°C. Shoot and root samples for biomass analysis were oven-dried at 70°C for 48 h to determine dry weights. The shoot and root biomass values were summed to calculate the total plant biomass in grams (g).

5.2.2. Net photosynthetic rate and chlorophyll and nitrogen (N) measurement

The net photosynthetic rate (Pn) was measured on the young emerging leaf of each treatment using the portable LI-6400 photosynthetic system (LI-COR Inc., Lincoln, NE, USA). Measurements were taken at 9:00 AM and 11:00 AM. Cuvette conditions included a light level of 1000 μmol m^{-2} s^{-1}, CO_2 concentration of 400 ppm, flow rate of 500 μmol m^{-2} s^{-1}, and relative humidity between 60% and 65%. Chlorophyll pigment was extracted from approximately 0.1 g of leaf tissue using 100% methanol on a shaker at 25°C until the tissue was completely bleached (Amoah and Seo 2021). The extract was then centrifuged at 10,000 × g for 10 min, and the absorbance of the supernatant was measured at 646, 470, and 663 nm using a UV-vis spectrophotometer (Shimadzu, Japan). The concentration of chlorophyll was calculated following the method described (Calderon Flores et al. 2021).

Total nitrogen (N) was determined using the Kjeldahl method as described by (Rizvi et al. 2022), with minor modifications. A 0.2 g dry sample was digested with 0.5 mL of concentrated H_2SO_4 and 0.5 mL of a catalyst mixture consisting of 10 g of K_2SO_4 and 1 g of $CuSO_4$. The mixture was heated at 100^{o}c for 60 min on a heating block in a fume hood. After digestion, the samples were allowed to cool, and 0.5 mL of 40% NaOH solution was slowly added, followed by 0.5 mL of distilled water. Subsequently, 1 mL of the resulting mixture was combined with 1 mL of Nessler's reagent and incubated for 10 min at room temperature. The absorbance was measured at 420 nm using a UV-vis spectrophotometer (Shimadzu, Tokyo, Japan). Total nitrogen content was determined from a standard curve generated with $(NH_4)_2SO_4$ standards.

5.2.3. Soluble sugar, starch, glucose and sucrose content determination

Soluble sugar and sucrose content were measured as described by Amoah and Adu-Gyamfi (2024). Briefly, 100 mg of ground samples were homogenized in 1 mL of 80% (v/v) ethanol, and the mixture was heated at 80°C for 30 minutes. After cooling for 5 min, the mixture was centrifuged at 12,000 × g for 10 min. The supernatants were collected, and soluble sugar and sucrose contents were determined by measuring absorbance at 620 nm and 480 nm, respectively, using a UV-vis spectrophotometer (Shimadzu, Tokyo, Japan). The ethanol-insoluble residue was used for starch extraction following the procedure outlined by (Amoah et al. 2024). After evaporating the ethanol, 2 mL of distilled water was added to the samples, which were then incubated at 100°C for 15 min. Starch was hydrolysed using separate treatments of 9.2 M $HClO_4$. The starch content was quantified spectrophotometrically using the anthrone reagent, and absorbance was measured at 620 nm.

Glucose and fructose content were determined using the anthrone colorimetry method as described by (Dong et al. 2023b). A mixture of 1 mL of supernatant and 5 mL of anthrone diluted sulfuric acid reagent was boiled for 10 min. A blank was prepared similarly, using 1 mL of distilled Milli-Q water instead of the supernatant. After cooling, the solution's absorbance was measured at 620 nm using a spectrophotometer, with the blank adjusted to zero. For fructose content, 1 mL of extract, 1

mL of 0.1% (v/v) hydroquinone, and 3.5 mL of 30% (v/v) HCl were combined in a test tube, thoroughly mixed, and heated at 80°C for 10 min in a water bath. After cooling, the solution's absorbance was measured at 480 nm using a spectrophotometer, with the blank adjusted to zero. The measured absorbance was used to calculate fructose content based on a standard curve.

5.2.4. Spatial distribution and diurnal changes determination

To examine the spatial distribution of sugars and starch, the youngest emerging leaf at 20 and 40 DAT was sampled and divided into three equal segments. Additional samples included the corresponding leaf sheath, root, basal 5 cm of expanded leaves, root, and ear. Sampling was conducted at 22:00 and again at 6:00 the following morning on 20 and 40 DAT. For diurnal analysis, the middle sections of the youngest fully expanded leaves were collected at 6:00, 12:00, 17:00, 22:00, and 6:00 (the next day) on 20 and 40 DAT. All samples were immediately frozen in liquid nitrogen and stored at −80 °C for subsequent biochemical analysis.

5.2.5. Enzyme activity assays

Enzymes were extracted following the method described by Chen et al. (2019) , with slight modifications. A 100 mg plant tissues was ground to a fine powder using liquid nitrogen and homogenized in 1 mL of ice-cold extraction buffer. The buffer contained 50 mM HEPES-NaOH (pH 7.5), 5 mM $MgCl_2$, 0.1% (v/v) β-mercaptoethanol, 0.05% (v/v) Triton-X100, 0.05% (w/v) BSA, 2% (w/v) polyvinylpyrrolidone, and 1 mM EDTA. The homogenate was centrifuged at 12,000 × *g* for 10 min at 4°C, and the supernatant was used for the assays of sucrose synthase, vacuolar invertase, and cytoplasmic invertase (CIN) activities. The pellet was washed twice with 0.5 mL of extraction buffer and then resuspended in 1.8 mL of salt extraction buffer. Samples were extracted overnight at 4°C and centrifuged at 12 000 × *g* for 10 min at 4°C. The resulting supernatant was used for the assay of cell wall invertase activity.

Sucrose synthase and cytoplasmic invertase activities were determined following the method by (Li et al. 2021b), while vacuolar invertase activity was assayed according to (Chen et al. 2019). For sucrose synthase activity, 100 μL of enzyme extract was mixed on ice with 200 μL of a reaction solution containing 80 mM MES-NaOH (pH 5.5), 5 mM NaF, 100 mM sucrose, and 5 mM UDP. The reaction was incubated at 30°C for 30 min and terminated by boiling for 2 min. A control reaction lacking UDP was included. For vacuolar and cytoplasmic invertase assays, the procedure was similar, but with variations in the reaction mixtures. Vacuolar invertase activity was measured using 200 mM acetic acid-sodium acetate buffer (pH 4.5 or 4.8) with 100 mM sucrose. Cytoplasmic invertase activity utilized 100 mM HEPES-NaOH buffer (pH 7.5) with 100 mM sucrose.

5.2.6. Statistical analysis

Differences between means were assessed using Tukey's multiple range test ($P< 0.05$). Bar charts were generated using GraphPad Prism software v10.1. The experiment was repeated twice, with all treatments and sampling conducted in triplicate.

5.3. Results

5.3.1. Phenotypic response to different N forms

Maize plants respond differently to N treatment conditions. For instance, at 20 DAT, plants grown under 1 mM NO_3^- exhibited growth inhibition compared to NFS-treated plants or those under 1 mM NH_4^+ treatment. However, by 40 DAT, NFS-treated plants showed enhanced growth, producing larger cobs than plants under 1 mM NH_4^+ or 1 mM NO_3^- (Fig. S5.2A-B). Furthermore, at 20 DAT, NFS-treated plants developed longer roots than those under other treatments (Fig. S5.3A). However, by 40 DAT, plants treated with 1 mM NH_4^+ had larger roots than those under 1 mM NO_3^-, with no significant difference compared to NFS-treated plants (Fig. S5.3B).These findings indicate that different nitrogen forms influence maize growth dynamics at various developmental stages, with NFS treatment being the most favourable treatment, supporting maize development.

5.3.2. NFS increased growth and photosynthesis

The N content in NFS-treated plants increased significantly ($P \leq 0.05$) in both the leaf and root compared to plants under the 1 mM NO_3^- treatment. However, it was lower than the N content observed in plants grown under 1 mM NH_4^+. Notably, the N content in the leaves of NFS-treated plants was similar to that observed in plants grown under 1 mM NH_4^+ (Fig. 5.1A-B). Compared to plants under 1 mM NO_3^- and 1 mM NH_4^+ treatments, NFS-treated plants exhibited ($P \leq 0.05$) increased shoot and root biomass, enhanced overall plant biomass, higher photosynthetic activity, and elevated ($P \leq 0.05$) chlorophyll content (Fig. 5.1C-G). However, the root-to-shoot biomass (R/S) ratio was inhibited ($P \leq 0.05$) in NFS-treated plants (Fig. 5.1H).

5.3.3. NFS treatment improved the accumulation of total sugars in plants

At 20 DAT, no significant differences ($P \leq 0.05$) in sucrose content were observed in either the leaf or root of plants across all treatments (Fig. 5.2A-B). Plants treated with 1 mM NO_3^- and 1 mM NH_4^+ exhibited higher leaf and root starch content, respectively (Fig. 5.2C-D), while NFS-treated plants showed a significant ($P \leq 0.05$) reduced in both leaf and root soluble sugar content (Fig. 5.2E-F). NFS-

treated plants had reduced root glucose, fructose, and hexose contents (Fig. 5.3B, D, and F), while the leaf glucose content was higher in plants under 1 mM NO_3^- treatment. Conversely, the fructose and hexose contents were comparably higher in plants treated with 1 mM NO_3^- and 1 mM NH_4^+, respectively (Fig. 5.3A-E). In contrast, at 40 DAT, NFS-treated plants exhibited lower ($P \leq 0.05$) leaf and root sucrose, starch, soluble sugar, glucose, fructose, and leaf hexose content, but higher root hexose content, when compared to control plants (those under 1 mM NO_3^- and 1 mM NH_4^+ treatments) (Fig. 5.3). Furthermore, the hexose/sucrose (H/S) ratio was significantly higher ($P \leq 0.05$) in the leaves of plants treated with 1 mM NO_3^- at both 20 and 40 DAT (Fig. 5.4A). In contrast, NFS-treated plants exhibited a reduced root H/S ratio at 20 DAT, while at 40 DAT, the root H/S ratio was lower than plants in other treatment groups (Fig. 5.4B).

5.3.4. Sucrose-degrading enzyme activities were reduced in both the leaves and roots of NFS-treated plants

Sucrose synthase (SuSy) activity was lower in the leaf than in the root. NFS treatment significantly ($P \leq 0.05$) increased SuSy activity in the leaf but reduced it in the root (Fig. 5.5A-B). Plants treated with 1 mM NO_3^- and 1 mM NH_4^+ showed no significant differences ($P \leq 0.05$) in leaf and root cytoplasmic invertase (CIN) activity at 40 DAT. However, NFS-treated plants exhibited reduced root and leaf CIN activity at both 20 and 40 DAT (Fig. 5.5C-D). Similarly, plants under 1 mM NO_3^- demonstrated significantly ($P \leq 0.05$) reduced leaf and root vacuolar invertase (VIN) activity, whereas NFS-treated plants showed lowered ($P \leq 0.05$) root VIN activity only at 20 DAT (Fig.5. 5E-F). Corresponding to the observed SuSy, CIN, and VIN activities, total sucrolytic activity (TSA) was higher in the leaf than in the root. Plants under 1 mM NO_3^- displayed higher leaf TSA at 20 DAT and higher root TSA at 40 DAT, while NFS-treated plants exhibited significantly ($P \leq 0.05$) lower TSA at 20 DAT (Fig. 5.5G-H).

5.3.5. Diurnal changes of sucrose and starch under NFS

Sucrose and starch contents varied significantly among the treatment groups at 20 and 40 DAT across most time points (Fig. 5.6A-D). Notably, sucrose and starch levels were lowest at 6:00, gradually increased from 12:00, peaked at 5:00, and then declined until 6:00 the following day. Plants treated with 1 mM NH_4^+ consistently exhibited higher sucrose and starch contents across all sampling times. However, in NFS-treated plants, no significant differences were observed compared to plants under 1 mM NH_4^+ in sucrose content at 6:00 (both initial and following day) at 20 DAT, or in starch content at 6:00 at 40 DAT (Fig. 5.6A-D). After overnight transport, approximately half of the starch and sucrose remained in the leaves of plants under 1 mM NO_3^-, a level significantly lower than in other treatments (Fig. 5.6A-D).

5.3.6. Spatial distribution of sucrose and starch under NFS

Sucrose and starch levels were differentially regulated among the treatment groups. NFS-treated plants exhibited lower sucrose and starch contents at both 20 and 40 DAT compared to plants in other treatments (Fig. 5.7A-D). In contrast, plants grown under 1 mM NO_3^- and 1 mM NH_4^+, particularly those under 1 mM NO_3^-, accumulated higher sucrose levels, with more pronounced accumulation in leaves than in the sheath. Notably, the elevated sucrose content was consistent across 20 and 40 DAT (Fig. 5.7A-C). At 6:00, NFS-treated plants had lower residual sucrose levels in leaves compared to those under 1 mM NO_3^- treatment, with residual sucrose levels comparable to those observed at 22:00. A similar trend was observed for starch content, where plants under 1 mM NO_3^- accumulated more starch in leaves by the end of the day (Fig. 5.7B-D). Following overnight remobilization, nearly half of the starch remained. Root starch content was considerably lower than that in source leaves, with no significant difference between NFS-treated plants and those grown with 1 mM NH_4^+ (Fig. 5.7B-D). Additionally, dynamic changes in sucrose and starch content were analysed in ear tissues at 40 DAT (Fig. S5.4). NFS-treated plants accumulated higher sucrose levels, comparable to those in plants under 1 mM NH_4^+ treatment, with similar sucrose levels at 22:00 and 6:00. Conversely, NFS-treated plants exhibited lower starch content than other treatment groups, with no significant differences observed between plants under 1 mM NO_3^- and 1 mM NH_4^+ (Fig. S5.4A-B).

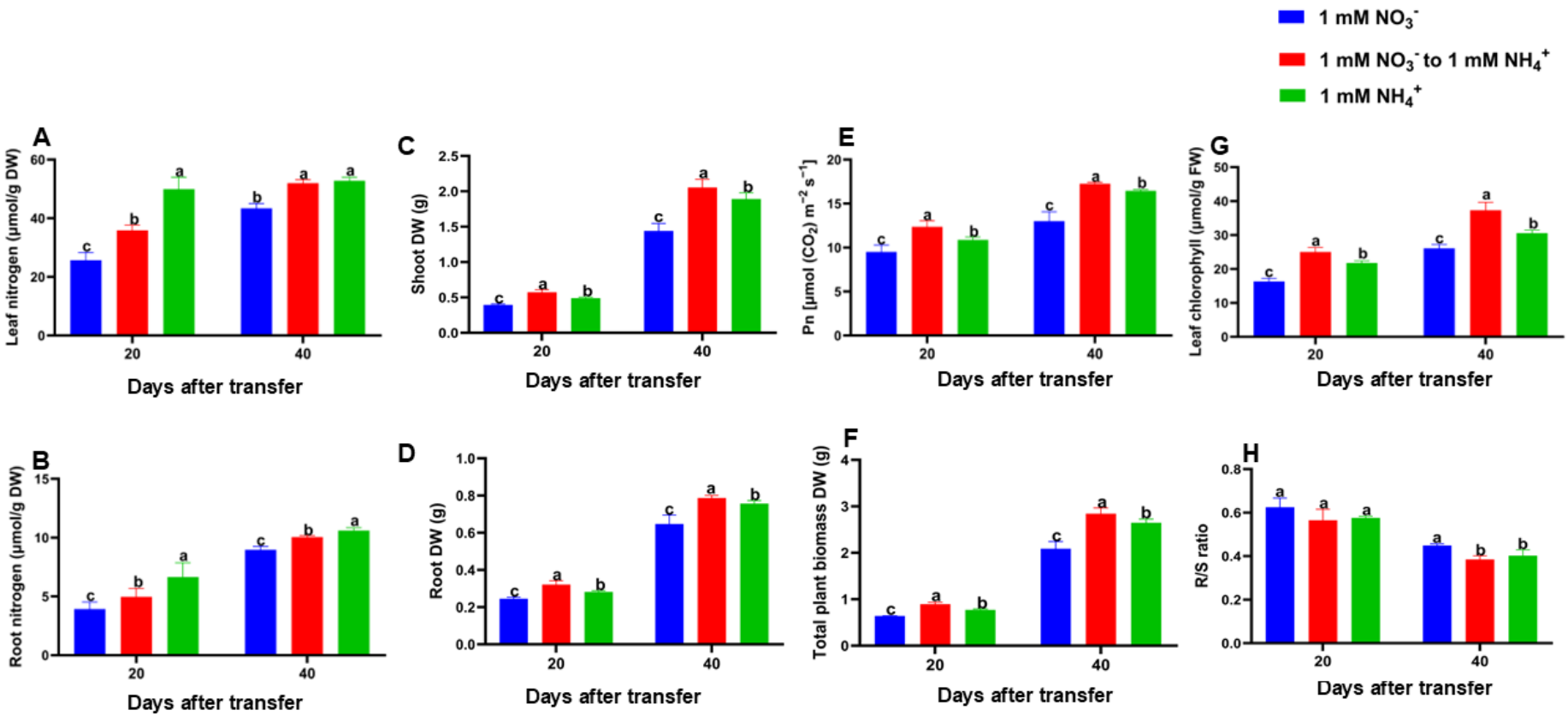

Fig. 5.1 Leaf (**A**) and root (**B**) nitrogen content, shoot (**C**) and root (D) biomass, leaf net photosynthetic rate (**E**), total plant biomass (**F**), leaf chlorophyll content (**G**), and root-to-shoot ratio (**H**) in maize inbred line TX-40J plants grown under varying nitrogen concentrations. Data are expressed as mean ± SEM (n = 6). Statistical analysis was conducted using Tukey's multiple range test *(P*<0.05), with different letters on error bars denoting significant differences among treatments. DW and FW represents the dry and fresh weight of tissue samples.

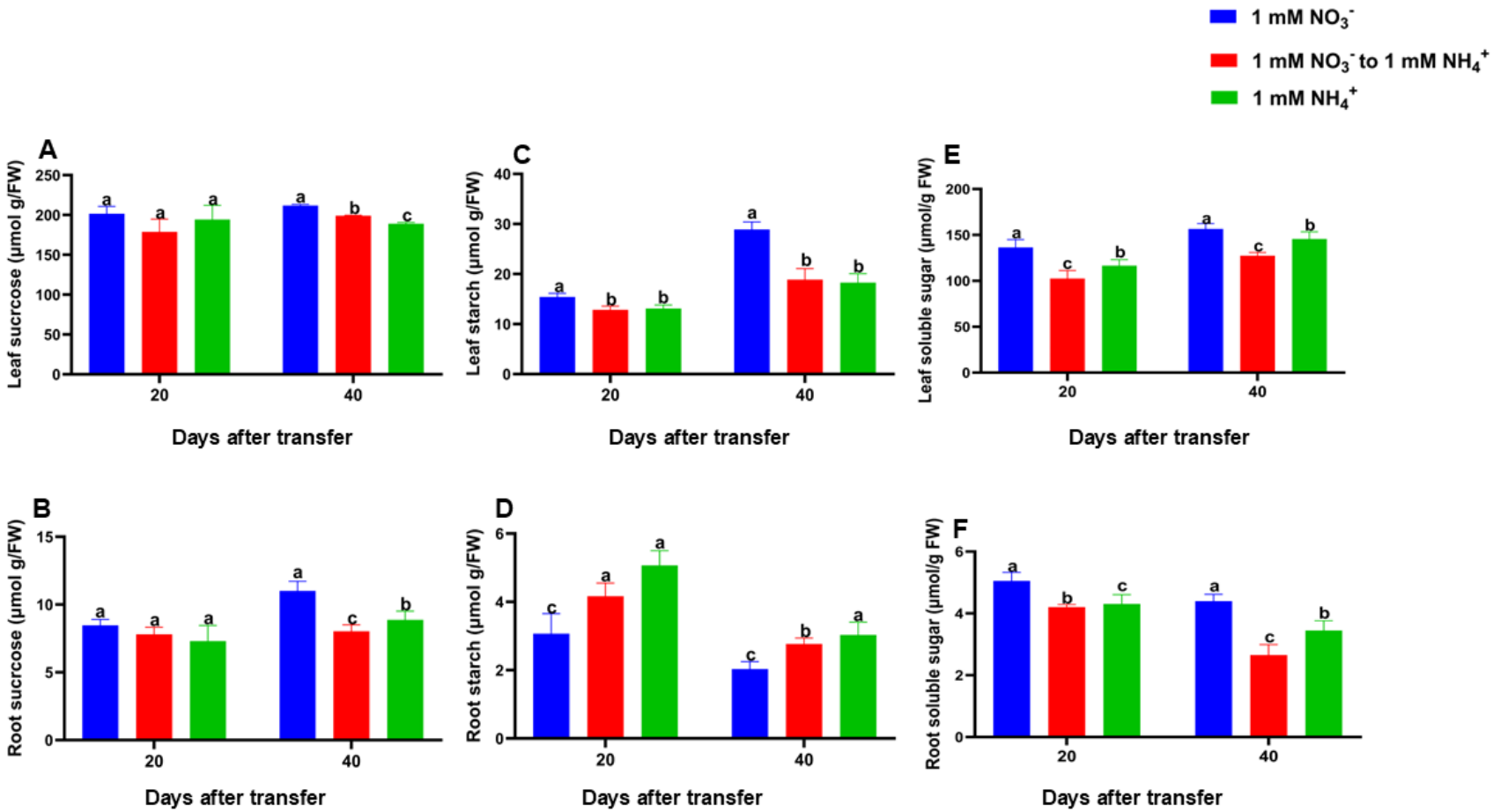

Fig. 5.2 Leaf (A) and root (B) sucrose content, leaf (C) and root (D) starch, leaf (E) and root (F) soluble sugar content in maize inbred line TX-40J plants grown under different N forms. Data are expressed as mean ± SEM (n = 6). Statistical analysis was conducted using Tukey's multiple range test (P<0.05), with different letters on error bars denoting significant differences among treatments. DW represents the dry weight of tissue samples.

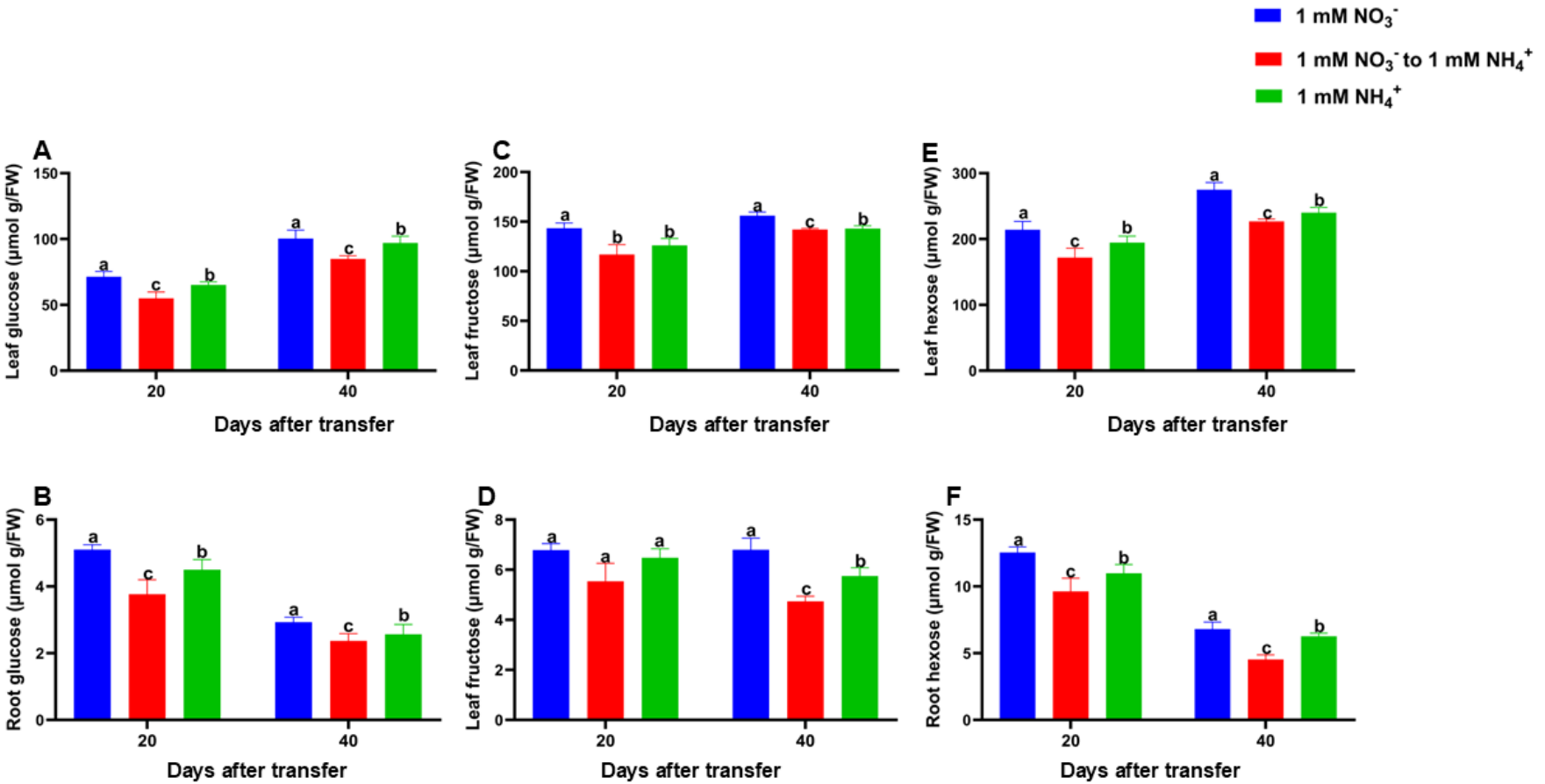

Fig. 5.3 Leaf (**A**) and root (**B**) glucose content, leaf (**C**) and root (**D**) fructose, leaf (**E**) and root (**F**) hexose content in maize inbred line TX-40J plants grown under different N forms. Hexose content was calculated as the sum of sucrose and glucose contents. Data are expressed as mean ± SEM (n = 6). Statistical analysis was conducted using Tukey's multiple range test (P<0.05), with different letters on error bars denoting significant differences among treatments. DW represents the dry weight of tissue samples.

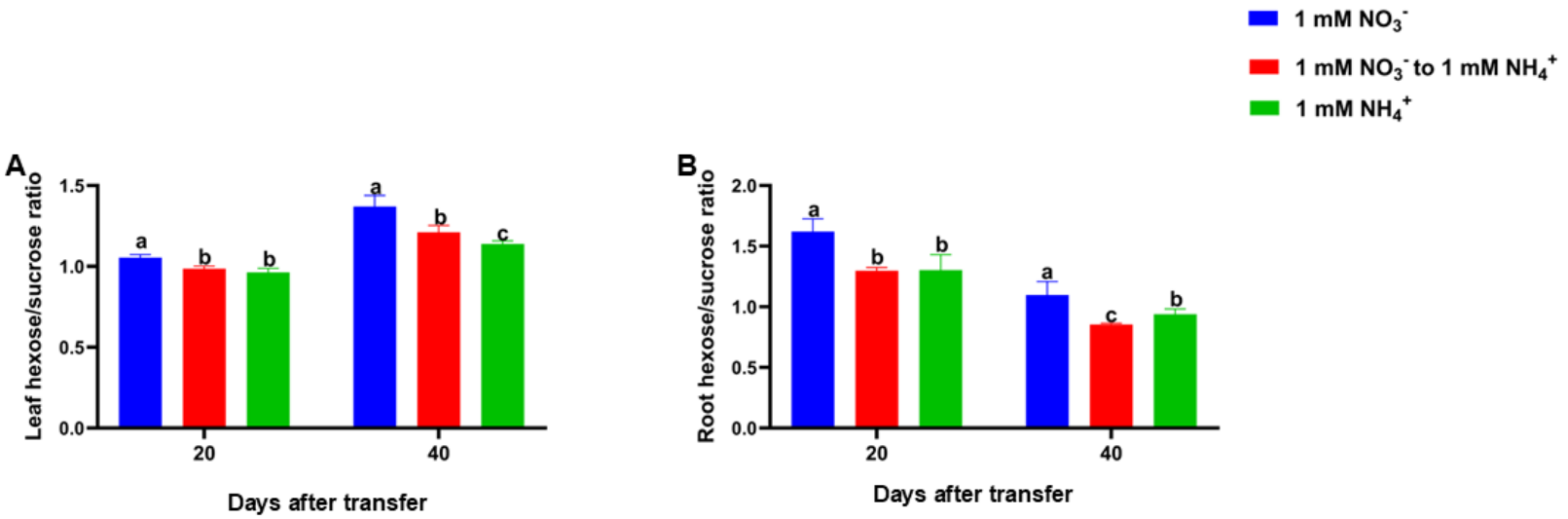

Fig. 5.4 Leaf (**A**) and root (**B**) hexose/sucrose ratio in maize inbred line TX-40J plants grown under different nitrogen forms. Data are expressed as mean ± SEM (n = 6). Statistical analysis was conducted using Tukey's multiple range test (P<0.05), with different letters on error bars denoting significant differences among treatments. DW represents the dry weight of tissue samples.

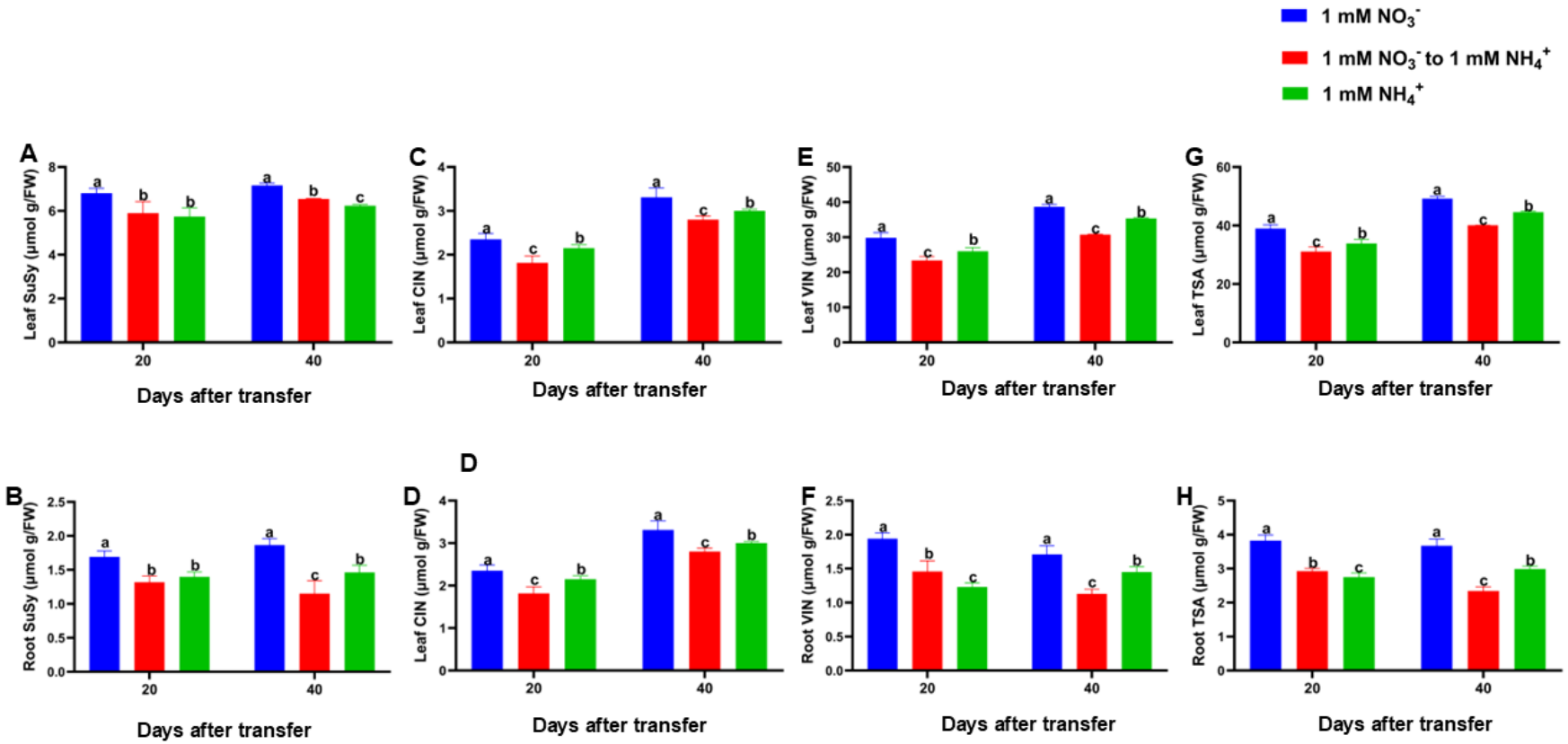

Fig. 5.5 Leaf (**A**) and root (**B**) sucrose synthase activity, leaf (**C**) and root (**D**) cytoplasmic invertase activity, leaf (**E**) and root (**F**) vacuolar invertase activity, leaf (**G**) and root (**H**) total sucrolytic activity in maize inbred line TX-40J plants grown under different nitrogen forms. Total sucrolytic activity was calculated as the sum of SuSy, CIN and VIN activities. Data are expressed as mean ± SEM (n = 6). Statistical analysis was conducted using Tukey's multiple range test (*P<0.05*), with different letters on error bars denoting significant differences among treatments. FW represents the fresh weight of tissue samples.

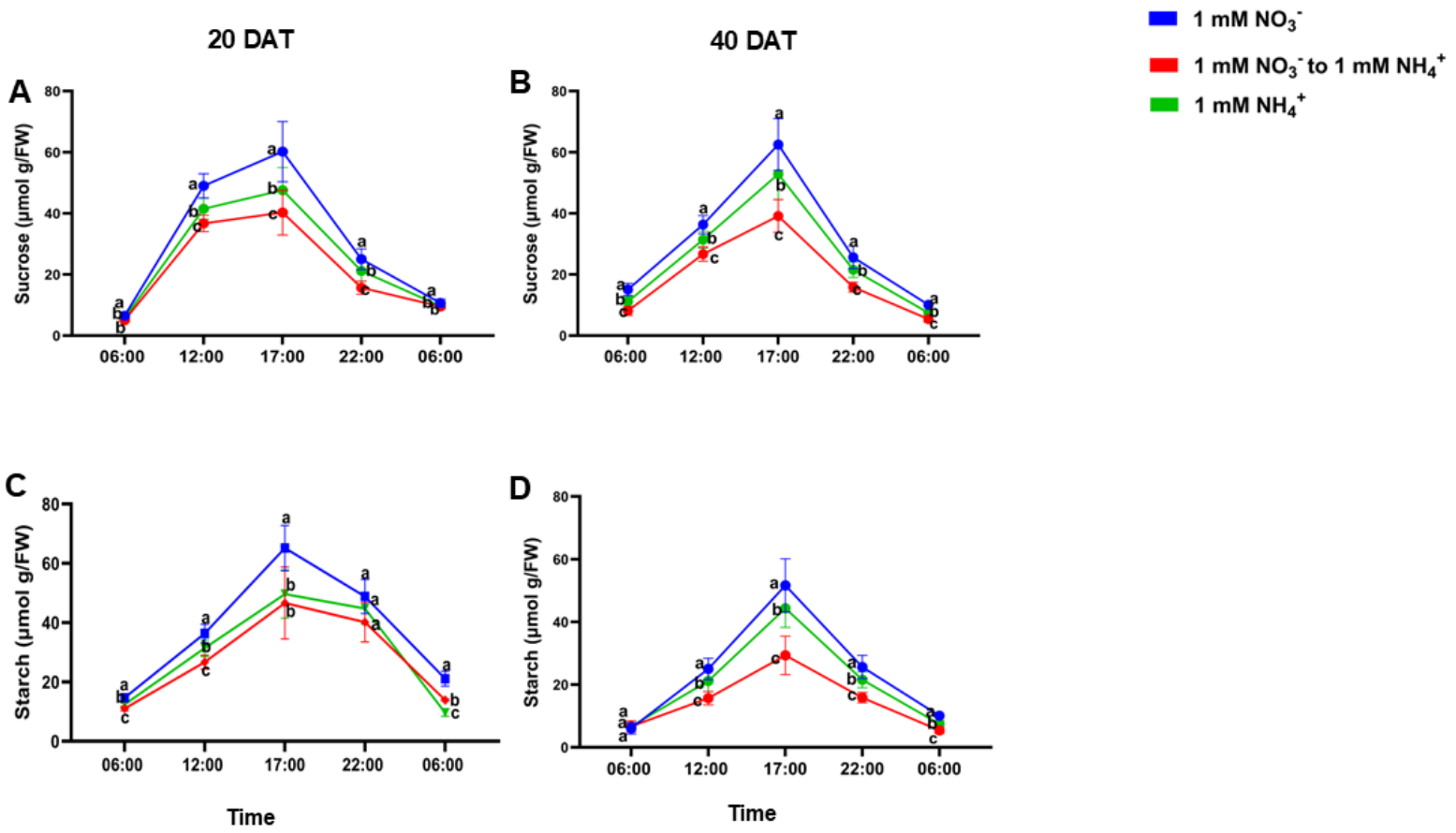

Fig. 5.6 Diurnal changes in leaf sucrose content at 20 days after transfer (DAT) (**A**), leaf sucrose content at 40 DAT (**B**), leaf starch content at 20 DAT (**C**), and leaf starch content at 40 DAT (**D**) under nitrogen form substitution (NFS) conditions. Samples were collected at 6:00, 12:00, 17:00, 22:00, and 6:00 on the second day. Data are presented as mean ± SEM (n = 6). Statistical significance was determined using Tukey's multiple range test ($P < 0.05$), with different letters on error bars indicating significant differences among treatments. FW represents fresh weight of tissue samples.

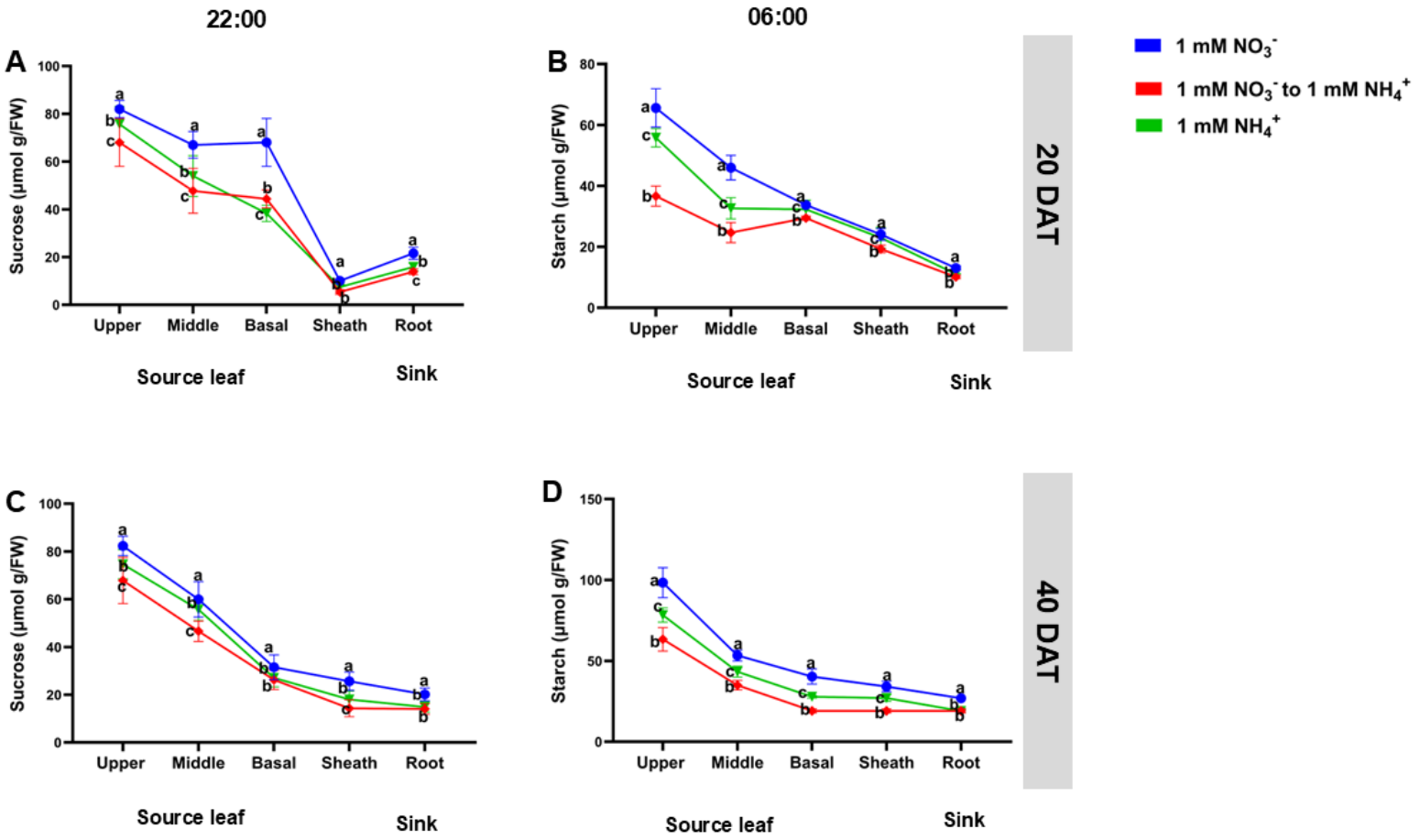

Fig. 5.7 Spatial and temporal analysis of sucrose and starch in different tissues of maize**.** Leaf sucrose (**A**) and starch (**B**) at 20 DAT, and leaf sucrose (**C**) and starch (**D**) at 40 DAT in different tissues under various nitrogen form treatments. FW represents the fresh weight of tissue samples. Data are presented as mean ± SEM (n = 6). Statistical significance was determined using Tukey's multiple range test ($P < 0.05$), with different letters on error bars indicating significant differences among treatments. FW represents fresh weight of tissue samples.

5.4. Discussion

5.4.1. NFS enhances sucrose utilization while promoting carbon allocation to shoot but R/S ratio

Nitrogen (N) is essential for plant growth and survival. Plants exhibit varying growth responses to different nitrogen forms. Previous studies have shown that N, whether supplied as sole NO_3^-, sole NH_4^+, or as a mixed form (NH_4NO_3), influences plant growth and metabolic processes in distinct ways (Peng et al. 2023a; Wang et al. 2019; George et al. 2016) . However, the effects on plant growth and metabolism when N sources, such as NO_3^- and NH_4^+, are substituted remain unexplored. In this study, both shoot and root growth were significantly enhanced under NFS treatment at 40 DAT (Fig. 5.1C-D, S5.2A-B and S5.3A-B). However, the R:S ratio was comparable across all treatment groups (Fig. 5.1H). This reduction in the R/S ratio at 40 DAT coincided with reduced carbon fixation, leading to a more pronounced increase in plant biomass in NFS-treated plants compared to other treatment groups (Fig. 5.1E-G). The observed trend suggests that a greater proportion of carbon was allocated to the shoot when NO_3^- and NH_4^+ nutrition was substituted. This could be attributed to enhanced N availability and assimilation in the shoot, which likely stimulated shoot growth, photosynthesis, and chlorophyll content (Fig. 5.1A-C, E, G, S5.2A-B and S5.3A-B). These findings align with previous studies showing that relatively small concentrations of NH_4^+ can enhance growth and N assimilation (George et al. 2016; Peng et al. 2023a). Sucrose unloading into roots leaves occurred via the symplasmic pathway, facilitated by plasmodesmata-driven sugar gradients (Baker et al. 2016). This mechanism supports the observed synchronous growth of both shoots and roots, greatly observed in NFS-treated plants (Fig. 5.1A-C), reflecting efficient assimilate utilization by maize seedlings under NFS-treatment conditions. The balanced allocation of assimilates to both shoots and roots underscores the dual sink function of these organs under NFS-treatment, enhancing overall plant growth (Fig. 5.1 and S5.2-5.3). Sucrose-degrading enzymes play a pivotal role in sugar utilization within sink tissues and in regulating symplasmic unloading (Chen et al. 2017; Shen et al. 2023). The differential activities of sucrose synthase and invertases observed in NFS-treated plants suggest their potential involvement in modulating carbon allocation between roots and shoots under NFS-treatment conditions. In this study, sucrolytic activity was lower in the leaf and the root of NFS treated plants (Fig. 5.5), suggesting that sucrose synthase and invertases may play a key role in carbon modulation between root and shoot sinks under NFS conditions. Enhanced sucrolytic activity in the roots of NFS treated plants indicates improved root sink strength, facilitating allocation of assimilates from shoots to roots and promoting nutrient uptake and overall plant growth. Sucrose synthases and invertases are also involved in regulating the hexose/sucrose ratio (Shen et al. 2023). The improved hexose/sucrose ratio observed in NFS treated plants (Fig. 4) supported enhanced sucrolytic activity (Fig. 5.5), which facilitated carbon allocation and synchronized root and shoot development. This aligns with previous findings that enhanced hexose/sucrose ratio promotes cell division and expansion (Koch 2004). The findings suggest that the regulation of carbon allocation between roots and leaves under NFS treatment conditions may be driven

by modulating source activity, achieved through the inhibition of sucrose utilization in the root (Fig. 5.3). These observations in plants treated with 1 mM NO_3^- are consistent with previous studies (Zhao et al. 2020) but offer new insights into shoot and root modulation when N sources are alternated.

5.4.2. NFS enhanced the utilization of sucrose in sink tissues and improved source productivity, leading to increased growth and C accumulation

Under NFS condition, N content was increased in both source and sink tissues, resulting in improved plant growth (Figs. 5.1A-D, F and Fig. S5.2-5.3). This indicates that alternating N sources ensured a balanced supply, preventing N depletion in both source and sink tissues, and maintaining higher N content across tissues. Furthermore, sucrose-degrading enzymes, such as sucrose synthase (SuSy) and invertases, serve as key indicators of sink activity (Liang et al. 2023c). Our examination of SuSy and invertase activities revealed a decrease in total sucrolytic activity in both the leaf and root under NFS (Fig. 5.5G-H), indicating a reduced capacity for sucrose utilization in these tissues. Interestingly, sucrose content in the leaf sheath was lower under NFS, with a gradual decline from the sheath to the leaf tip (Fig. 5.7A–C and S5.5), suggesting that sucrose loading and export in the source leaf remained functional. These findings suggest that reduced sink activity, characterized by diminished sucrose degradation and utilization under NFS, leads to carbon accumulation in the source leaves. Consistent with studies on plants under 1 mM NO_3^-, a recent study reported increased sugar and starch contents in plants alongside reduced SuSy activity in roots under N deficiency (Zhao et al. 2020). Starch content was higher in plants grown under 1 mM NO_3^-, aligning with previous findings (Zhao et al. 2020). In contrast, NFS-treated plants showed reduced starch accumulation, particularly in the roots (Fig. 5.2), suggesting an improved source-sink balance (Dong and Beckles 2019). The enhanced starch storage in leaves under NFS conditions likely serves as a temporary reserve, maintaining balance between source activity and sink demand, and ensuring a continuous energy supply for growth and development (MacNeill et al. 2017; Smith and Zeeman 2020). The lower starch content in NFS-treated plants may result from decreased sucrolytic activity, highlighting the roles of SuSy and invertases in converting sucrose into glucose and fructose, key substrates for starch biosynthesis (Koch 2004; Granot et al. 2013). These findings underscore the importance of enhancing carbohydrate utilization efficiency as a strategy for developing nitrogen-efficient plant varieties. Optimizing carbon distribution and utilization under NFS conditions could significantly improve plant growth and performance, particularly in N-limited environments.

5.4.3. Temporal and spatial patterns of NFS-induced carbon accumulation

Maize plants exhibited differential responses to NFS treatment at 20 DAT; and 40 DAT. NFS treatment significantly increased N content at both stages, reflected in marked diurnal changes and spatial carbon distribution. Notably, at 20 DAT, significant carbon accumulation was observed in the leaves (Fig. 5.6). This is consistent with findings that N deficiency enhances sucrose and starch accumulation in leaves due to reduced nitrogen assimilation and increased carbon partitioning toward storage compounds (Schlüter et al. 2012a; Wang and Tillberg 1996; Shah et al. 2024; Zhang et al. 2021). However, carbon dynamics under NFS conditions remain less understood. Studies have suggested that N availability influences C allocation and diurnal starch turnover, impacting plant metabolism and growth responses (Cooke et al. 2005; Brauner et al. 2018; Pokhilko et al. 2014; Smith and Zeeman 2020). Our observations indicate that the duration of NFS treatment, sampling times, and sampling positions significantly influence carbon accumulation patterns. For instance, at 20 DAT, no significant differences in sucrose and starch content were observed at the start (6:00) and end (22:00) of sampling between NFS-treated plants and those under 1 mM NH_4^+ treatments (Fig. 6). However, at 6:00, starch content in the upper parts of NFS-treated plants was lower than in plants under 1 mM NO_3^-or NH_4^+ treatments, but by 22:00, levels became similar (Fig. 5.7). These results align with previous research demonstrating that N form affects the timing and magnitude of starch degradation and sucrose translocation in maize and other crops (Ning et al. 2018a; Geiger et al. 2000; Si et al. 2018; Stitt and Zeeman 2012). Furthermore, sucrose and starch content were not uniformly distributed within leaves across treatments, supporting earlier reports that N supply influences spatial carbohydrate partitioning and metabolism (Cooke et al. 2005; Brauner et al. 2018; Pokhilko et al. 2014; Smith and Zeeman 2020; Slewinski and Braun 2010). Similar findings have been reported in maize and *Arabidopsis*, where N treatments altered the compartmentalization of sugars within leaves, affecting both source–sink dynamics and growth efficiency (Ning et al. 2018b; Wang et al. 2021b; Santiago and Tegeder 2017). These findings on temporal and spatial sugar and starch dynamics under NFS conditions provide valuable insights for understanding N-C interactions and optimizing N management strategies in maize production.

5.5. Conclusion

The study revealed that NFS enhances maize growth by optimizing carbon allocation among shoots, roots, and ears. NFS-treated plants exhibited reduced sucrolytic activity in both shoot and root sinks, enabling roots to compete more effectively for assimilates while maintaining vigorous shoot growth, as evidenced by a decreased root-to-shoot (R/S) ratio (Fig. 5.4-5.5). Additionally, enhanced sink activity in the leaves facilitated more efficient assimilate utilization, leading to greater carbon accumulation in leaves and sheaths. This adaptive mechanism underpins maize growth and development, offering a strategic advantage in breeding nutrient-efficient cultivars for resource-limited environments. These findings highlight the potential of NFS as a promising strategy for improving NUE and promoting

sustainable agricultural practices. To maximize its impact, future research should explore the broader practical implications of NUE in other crops and agricultural systems. Investigating species-specific responses in key staple crops such as wheat, rice, and soybean could provide valuable insights into the generalizability of nitrogen form substitution strategies. Additionally, field trials across diverse soil types and environmental conditions would enhance the applicability of these findings for real-world agricultural settings. Since this study focused on the high-performing inbred maize line TX-40J, testing a wider range of genotypes could offer a deeper understanding of genetic variability in nitrogen responses. Furthermore, exploring a broader spectrum of nitrogen concentrations would help refine our knowledge of plant adaptability to different nutrient regimes, ultimately guiding precision nutrient management strategies for optimized crop productivity. Exploring a broader range of N concentrations and incorporating additional control treatments could provide deeper insights into the underlying mechanisms of plant responses under varying N conditions. Additionally, future studies may incorporate transcriptomic approach or gene expression analyses at specific developmental stages and under different treatments to gain deeper insights into the molecular mechanisms underlying NF

5.6. Supplementary data

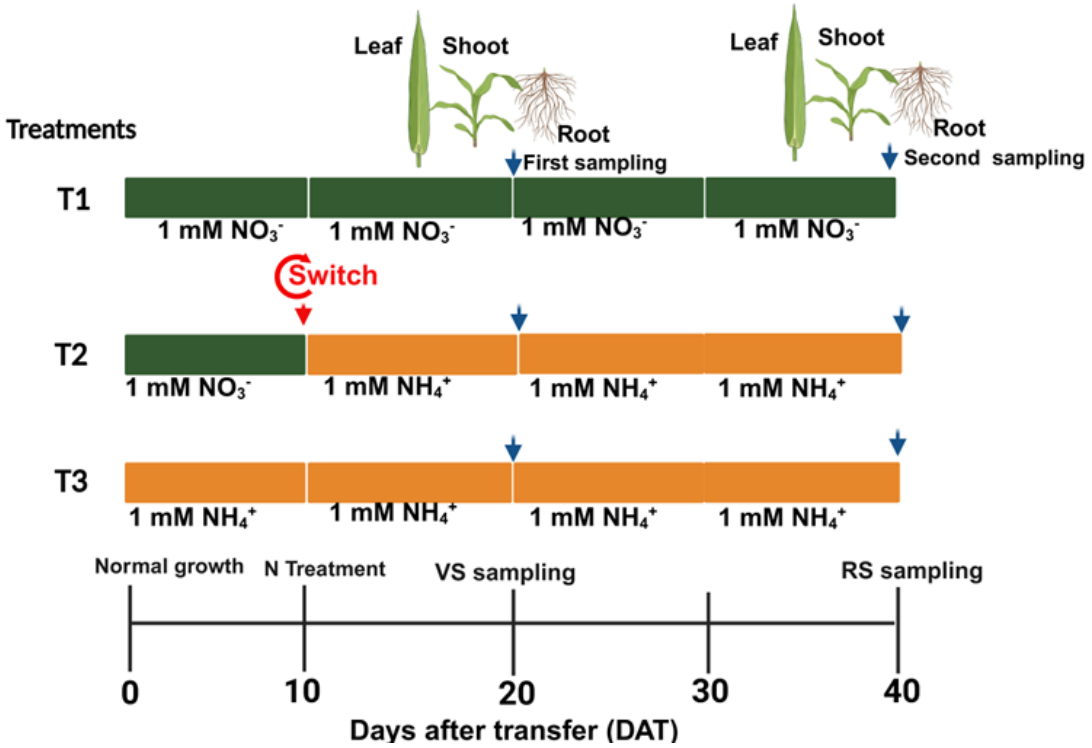

Fig. S5.1 Illustrates the experimental setup for the maize inbred line TX-40J. Maize seedlings were divided into three treatment groups (T1–T3), with T1 and T2 receiving 1 mM NO_3^- and T3 supplied with 1 mM NH_4^+ from 0 DAT to 10 DAT. At 10 DAT, T1 and T3 plants continued growing under 1 mM NO_3^- and 1 mM NH_4^+, respectively, while T2 plants were switched from 1 mM NO_3^- to 1 mM NH_4^+. Plants were then grown for an additional 30 days (until 40 DAT), with tissue sampling conducted at 20 DAT and 40 DAT for shoot, root, and leaf tissues. Normal growth refers to conditions without a nutrient switch, while N treatment indicates different nitrogen forms. The vegetative stage (VS, V6) and reproductive stage (RS, R1) are represented accordingly. In the diagram, green and yellow blocks denote 1 mM NO_3^- and 1 mM NH_4^+, respectively, while blue downward arrows indicate tissue sampling, and red downward arrows represent the nutrient switch (1 mM NO_3^- → 1 mM NH_4^+).

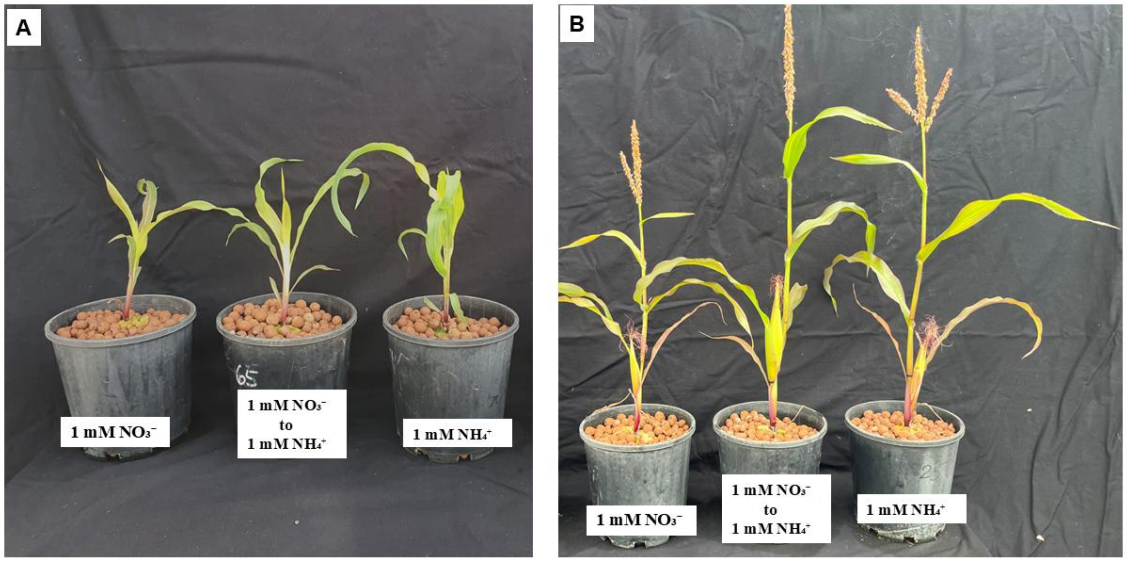

Fig. S5.2 Phenotypic response of the maize inbred line TX-40J to different nitrogen (N) forms. Representative images of shoot morphology at 20 days (**A**) and 40 days (**B**) after nitrogen treatments (DAT).

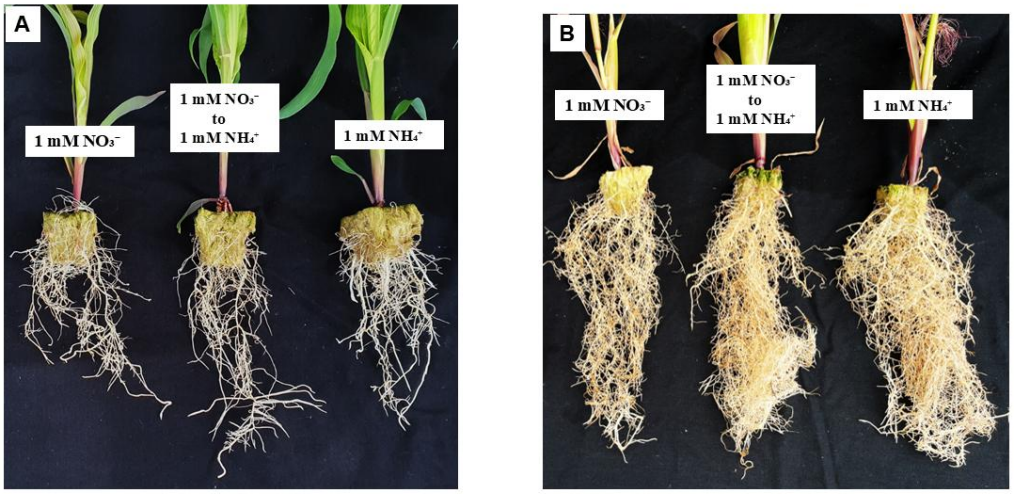

Fig. S5.3 Phenotypic response of the maize inbred line TX-40J to different nitrogen (N) forms. Representative images of root morphology at 20 days (**A**) and 40 days (**B**) after nitrogen treatments (DAT).

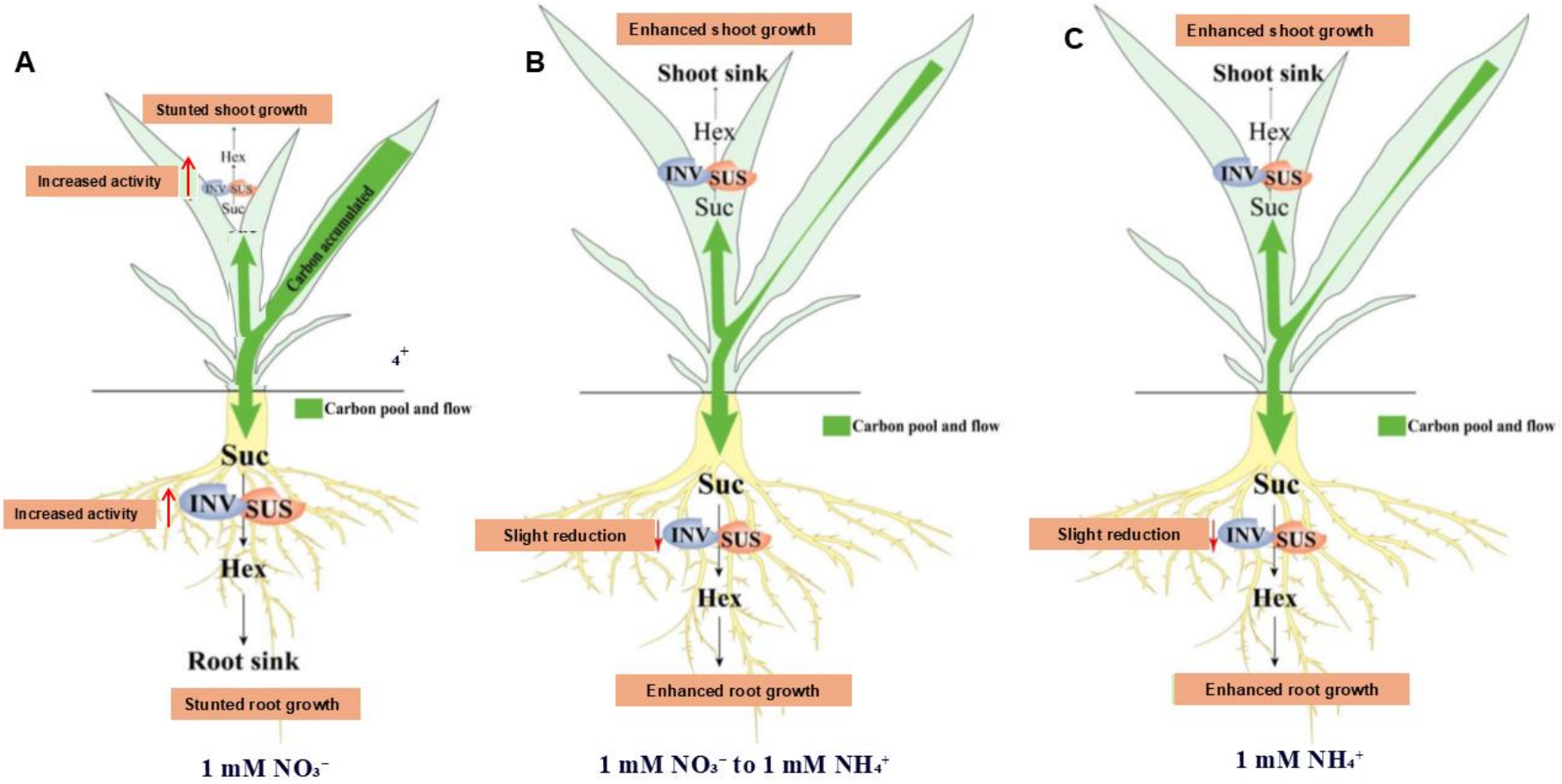

Fig. S5.4 A conceptual model illustrating the regulation of sugars, sucrose, and the activity of sucrose metabolism enzymes in the leaves and roots of maize plants under different nitrogen forms. Abbreviations: Suc – sucrose, Hex – hexose, INV – invertases, SUS – sucrose synthase.

CHAPTER 6: NITROGEN FORM SUBSTITUTION IDENTIFIES NITROGEN USE EFFICIENCY MANAGEMENT PATHWAYS IN MAIZE[5]

Abstract

Plants rely on nitrogen (N) for their growth, development, and metabolic functions. However, the regulatory mechanisms modulating N assimilate allocation under varying N forms is unclear. This study examines N metabolism and spatial distribution in maize seedlings subjected to four N treatments (T1 to T4): T1, 1 mM NO_3^- (sole NO_3^-); T2, substitution of 1 mM NO_3^- with 1 mM NH_4^+ (N form substitution, NFS); T3, 1 mM NH_4^+ (sole NH_4^+); and T4, 0.5 mM NH_4NO_3 (mixed N supply). The NFS treatment induced significant physiological and molecular adaptations, such as enhanced growth and total biomass under fluctuating N conditions. NFS-treated plants exhibited improved photosynthesis, increased protein and amino acid synthesis, and increased NO_3^- and NH_4^+ accumulation. Activities of key N metabolism enzymes, such as nitrate reductase (NR), nitrite reductase (NiR), glutamine synthetase (GS), and glutamate synthase (GOGAT), were significantly upregulated, supporting efficient assimilation of both NO_3^- and NH_4^+. Molecular analysis revealed transcriptional reprogramming under NFS, marked by the upregulation of genes related to NH_4^+ metabolism (*ZmGS1* and *ZmGOGAT1*) and transport (*ZmAMT1.1* and *ZmAMT2.1*). Furthermore, spatial and diurnal analyses revealed dynamic N partitioning and adaptive regulation, with NFS-treated plants maintaining consistently higher NO_3^- and NH_4^+ levels in leaves, roots, sheaths, and developing ears. These findings highlight the robust plasticity of maize N metabolism under NFS conditions and provide valuable insights into optimizing N use efficiency (NUE) for sustainable crop production. Future studies will focus on exploring these adaptive mechanisms across different maize genotypes and under field conditions to improve NUE and productivity in varying N environments.

Keywords: Nitrogen assimilation, nitrogen source dynamics, nitrogen transporter activity, maize growth response, diurnal nitrogen allocation

---

[5]This chapter has been accepted for publication in Physiology and Molecular Biology of Plants, with the title 'Nitrogen form substitution identifies nitrogen use efficiency management pathways in maize' (Manuscript ID: PMBP-D-25-00703).

6.1. Introduction

Nitrogen (N) is an important macro-nutrient nutrient required for the growth, development, and yield of crops. In agricultural soils, nitrate (NO_3^-) and ammonium (NH_4^+) are the two primary forms of N available to plants, with NO_3^- typically being the predominant source due to its higher concentration (George et al. 2016). The positive impact of NO_3^- on plant growth and metabolism has been widely documented across various species. For instance, NO_3^- treatment has been associated with enhanced growth (Yan et al. 2023; Li et al. 2023), increased N accumulation, and improved N use efficiency (NUE) (Sinha et al. 2020; Peng et al. 2023a; Aluko et al. 2023b). It also leads to higher total amino acid and protein content (Yin et al. 2020; Liang et al. 2023a), contributing to better quality, increased harvestable yields (Cui et al. 2023; Wei et al. 2024; Heuermann et al. 2021) and improved sugar metabolism (Peng et al. 2023a; Yin et al. 2020; Liu et al. 2023; Xu et al. 2023). The activity of nitrate reductase (NR), a crucial enzyme for NO_3^- assimilation, is also tightly regulated, further optimizing N assimilation in plants (Dechorgnat et al. 2018; Fu et al. 2023; Peng et al. 2023a).

NH_4^+ nutrition has been a nutrition form associated with mixed effects on plant growth and metabolism. While it can positively influence certain physiological and biochemical processes, its adverse impacts often outweigh the benefits in many crop species, although these effects are highly dependent on various factors including plant species, growth stage, soil pH, nutrient concentration, and environmental conditions. Documented positive effects of NH_4^+ include increased growth, improved N assimilation, and enhanced NUE in maize (George et al. 2016; Jing et al. 2010), improved salinity tolerance in sorghum (de Souza Miranda et al. 2016), improved grain quality in wheat (Fuertes-Mendizábal et al. 2013), enhanced photosynthesis in rice (Guo et al. 2007a), as well as enhanced N metabolism and amino acid synthesis in tomato (González-Hernández et al. 2019). However, excessive NH_4^+ supply can negatively affect plant performance due to its toxicity, leading to metabolic imbalances and increased energy demand for detoxification (Hachiya et al. 2021). Studies have shown that NH_4^+ reduces growth and NO_3^- accumulation (Chen et al. 2020; Coleto et al. 2023; Podgórska et al. 2017; Wang et al. 2024a), reduces N assimilation (Xu et al. 2023; Peng et al. 2023a; Wang et al. 2019), inhibits photosynthesis and reduces yield quality (Chen et al. 2023a; Cui et al. 2023).

Although the comparative effects of NH_4^+ and NO_3^- on various metabolic processes are well-documented, studies show that combining these N forms in varying ratios enhances plant growth and improves N uptake and utilization more effectively than supplying either form alone. This enhanced growth is attributed to the synergistic interaction between NO_3^- and NH_4^+ (Wang et al. 2019; Peng et al. 2023a; Chen et al. 2024a). While plants generally prefer NH_4^+ due to its lower energy requirement for assimilation (Hachiya and Sakakibara 2017), little is known about the impacts of dynamically switching between these nutrient forms. In natural and agricultural settings, NO_3^- and NH_4^+ availability fluctuates due to microbial activity, fertilization practices, and environmental changes (Norton and Ouyang 2019;

Hui et al. 2024). Prolonged fluctuations can trigger stress responses that may impair overall productivity. However, static studies fail to fully capture these dynamic conditions. Previous research on plant N management has primarily focused on static N supply or single N forms (Garnett et al. 2013; George et al. 2016; Plett et al. 2016; Dechorgnat et al. 2019; Wang et al. 2019; Peng et al. 2023a). This approach overlooked the complexity of changing N availability, leaving a gap in understanding plant responses to dynamic N conditions.

Nitrogen Form Substitution (NFS) treatments tackle this limitation by integrating alternating N sources rather than maintaining a constant N environment. By simulating natural N fluctuations, NFS provides new perspective into how plants adapt to varying N conditions and optimize their growth. Unlike static studies, which capture only responses to unchanging N supply, NFS offers a more comprehensive understanding of nutrient adaptation mechanisms. In our recent study, NFS treatments significantly promoted growth, enhanced photosynthesis, and stimulated carbon metabolism in maize. The observed growth responses and metabolic adjustments highlight adaptive strategies and synergistic interactions that were not evident in plants exposed to a single N form (Amoah and Kaiser 2025). These findings underscore the importance of dynamic nitrogen availability in shaping plant performance and reinforce the value of NFS as an approach for investigating nutrient adaptation mechanisms. Building on these insights, the present study was designed to explore how NFS influences N metabolism in maize. By integrating changes in both N form and supply, we aimed to elucidate the regulatory mechanisms modulating N uptake, assimilation, and utilization under fluctuating N conditions, thereby advancing our understanding of plant adaptive responses to dynamic N environments and provide valuable insights for breeding crops with improved nitrogen use efficiency (NUE).

6.2. Materials and methods

6.2.1. Plant materials and experimental site

Seeds of the fast-flowering, short-cycle inbred mini-maize line TX-40J (McCaw et al. 2016), which were used in our previous experiment (Amoah et al. 2025), were also used in this study. Seeds were disinfected with 5% sodium hypochlorite for 5 min and wash with ultrapure water, 5 times at 3 min each. Sterilized maize seeds were germinated in Oasis Horticube Propagation Slabs (Aqua Gardening, Australia), an inorganic and pH-neutral growing foam medium, placed in germination trays.

6.2.2. Experimental treatment, set up and sampling

Seedlings were categorized into four treatment groups (T1–T4) and cultivated in 3 L pots, with their roots stabilized using inorganic expanded clay pellets (Aquaponics, Perth, Australia). At the fully

expanded third leaf stage (Fig. 1), plants in T1 and T2 were initially provided with 1 mM NO_3^-, whereas those in T3 and T4 received 1 mM NH_4^+ and 0.5 mM NH_4NO_3, respectively. While T1, T3, and T4 continued under the same nutrient conditions, T2 underwent the Nitrogen Form Substitution (NFS) treatment, in which 1 mM NO_3^- was substituted with 1 mM NH_4^+ (Amoah & Kaiser, 2025). Consequently, T2 served as the primary group for evaluating NFS effects on N uptake, assimilation, and utilization in maize, whereas T1, T3, and T4 functioned as reference groups for comparative analysis, aligned with prior investigations (Amoah & Kaiser, 2025). Low concentrations of NO_3^-, NH_4^+, and NH_4NO_3 were employed to better reflect field conditions, mitigate NH_4^+ toxicity, and enable a more precise evaluation of N assimilation. This approach facilitates the assessment of NUE, highlights key physiological and molecular adaptations, and allows for a detailed analysis of NO_3^- and NH_4^+ interactions (George et al. 2016; Ye et al. 2022). Plants were cultivated for 40 d after seedling transfer (DAT), with tissue sampling conducted at 20 (vegetative: V6 stage) and 40 (reproductive: R1 stage) DAT (Amoah & Kaiser, 2025). The system was established in a climate-controlled glasshouse under environmental conditions identical to those of the seed germination growth room, with supplemental LED lighting delivering 1000 µmol m^{-2} s^{-1} at pot level. Each system accommodated 40 pots, with one plant per pot. Nutrient solutions were delivered via a drip-irrigation system integrated with a hydroponic pump to ensure circulation. Irrigation was administered twice daily for 1 min, at 12:00 and 17:00 (Amoah & Kaiser, 2025).

The nutrient solution contained the following concentrations (mM): 1.0 KNO_3, 1.0 $(NH_4)_2SO_4$, 0.5 NH_4NO_3, 1.0 $MgSO_4$, 1.0 KH_2PO_4, 0.05 H_3BO_3, 0.005 $MnSO_4$, 0.001 $ZnSO_4$, 0.001 $CuSO_4$, 0.001 Na_2MoO_4, 0.1 KCl, 0.1 Fe-EDTA, 0.1 Fe-EDDHA, 0.25 $Ca(NO_3)_2$, 0.25 K_2SO_4, 0.25 $CaCl_2$, and 1.75 $CaSO_4$ (Amoah & Kaiser, 2025). The solution was stored in 162 L Brute Containers with lids (Rubbermaid, USA) and replaced weekly, with daily pH adjustments using 1 M H_2SO_4 or 1 M NaOH to maintain a stable pH of 5.9. The treatment solution was delivered via an Eden 140G FL submersible water pump (Creative Pumps, Australia). Plants were uniquely identified and randomized into blocks using R statistical software (v4.4.5). Fresh leaf, root, and ear tissues designated for biochemical analysis were immediately frozen in liquid nitrogen (N_2) and stored at -80°C. Shoot and root samples for biomass analysis were oven-dried at 70°C for 48 h to determine biomass accumulation (DW). Total plant biomass (g) was calculated by summing shoot and root biomass values.

6.2.3. Determination of spatial distribution and diurnal variations

To investigate the spatial distribution of NO_3^- and NH_4^+, as well as NR and GS activities, the youngest emerging leaf was sampled at 20 and 40 DAT and segmented into upper and middle sections. Additional samples were taken from the corresponding leaf sheath, root, and developing ear. At 40 DAT, sampling was conducted at 22:00 and again at 7:00 the following morning. For diel analysis, the middle sections

of the youngest fully expanded leaves were collected at five time points, at 7:00, 12:00, 17:00, 22:00, and again at 7:00 the next day, at both 20 and 40 DAT. All samples were immediately frozen in liquid nitrogen (N_2) and stored at -80°C for subsequent biochemical analysis.

6.2.4. Photosynthetic rate, chlorophyll, and Nitrogen determination

Photosynthetic rate (Pn) was measured on the youngest emerging leaf of each treatment using a LI-6400 portable photosynthetic system (LI-COR Inc., Lincoln, NE, USA). Measurements were recorded at 10:00 AM and 12:00 PM under cuvette conditions of 1000 µmol m^{-2} s^{-1} light intensity, 400 ppm CO_2 concentration, a flow rate of 500 µmol m^{-2} s^{-1}, and RH maintained between 60% and 65%. For chlorophyll content pigment extraction, 100 mg of leaf tissue was mixed with 100% methanol and centrifuged at 5,000 × g for 5 min. The absorbance of the supernatant was measured at 646, 470, and 663 nm using a spectrophotometer (Shimadzu, Japan). N content was quantified using the Kjeldahl method (Amoah & Kaiser, 2025), with slight modifications. A 0.1 g dry sample was digested with 0.5 mL concentrated H_2SO_4 and 0.5 mL of a catalyst mix containing 10 g K_2SO_4 and 1 g $CuSO_4$ and heated at 90°C for 1 h. The mixture was cooled, and 0.5 mL of 40% NaOH was gradually added, followed by 500 µL distilled water. Next, 1 mL of the solution was added to 1 mL of Nessler's reagent and incubated for 10 min at room temperature. Absorbance was measured at 420 nm using a UV-vis spectrophotometer (Shimadzu, Tokyo, Japan), and N content was determined using a standard curve generated from $(NH_4)_2SO_4$ standards.

6.2.5. Total amino acid and protein quantification

Tissue amino acid content was assayed following the method outlined by Bates et al. (1973). Frozen leaf tissues (100 mg) were homogenized in 10 mL of 3% (v/v) aqueous sulfosalicylic acid. After filtration, 1 mL of the filtrate was mixed with 1 mL of glacial acetic acid and 1 mL of acidic ninhydrin, then incubated at 100°C for 1 h. The solution was cooled for 20 min, followed by the addition of 1 mL of toluene. Amino acid concentrations were measured at 580 nm using a spectrophotometer. Total protein content in leaf and root tissues was extracted from 100 mg of fresh material using the phenol approach outlined by (Dechorgnat et al. 2018). After centrifugation, the supernatant was used for enzyme activity assays.

6.2.6. Nitrate (NO_3^-), nitrite (NO_2^-) and ammonium (NH_4^+) determination

NO_3^-, NO_2^-, and NH_4^+ were extracted from 100 mg of dried plant material using 1 mL of water. NO_3^- content was quantified using a colorimetric assay based on the reduction of NO_3^- to NO_2^- by Vanadium

(III) (Dechorgnat et al. 2018). NO_2^- levels were determined using the Griess assay (Dechorgnat et al. 2011), while NH_4^+ concentrations were measured using the Ammonium Assay Kit (Sigma-Aldrich, St. Louis, MO, USA, cat# AA0100), following the manufacturer's instructions.

6.2.7. Nitrate reductase (NR), nitrite reductase (NiR), glutamine synthase (GS) and glutamate synthase (GOGAT) activities assay

NR activity was assayed using the method described by Dechorgnat et al. (2018), with minor modifications. A 10 µL aliquot of extracted protein solution was mixed with 90 µL of reaction buffer containing 130 mM K_2HPO_4, 70 mM KH_2PO_4, 0.5 mM KNO_2, and 2 mM methyl viologen. The reaction was initiated by adding 10 µL of a sodium-based solution (20 mg/mL Na_2CO_3 and $Na_2S_2O_4$) and incubated at 30°C for 20 min. The reaction was terminated by vortexing, and NO_2^- content was quantified using the Griess assay (Dechorgnat et al., 2018). GS and GOGAT activities were determined by mixing 20 µL of extracted protein with 80 µL of reaction buffer containing 100 mM hydroxylamine, 125 mM MOPS, 0.5 mM ADP, 12.5 mM sodium arsenate, 37.5 mM glutamine, and 1.25 mM $MnCl_2$. The reaction was incubated at room temperature for 30 min, followed by the addition of 100 µL of detection buffer comprising 370 mM $FeCl_3$, 576 mM HCl, and 157 mM TCA. Optical density was measured at 540 nm, with L-glutamic acid γ-monohydroxymate (GHA) serving as the reference standard (Dechorgnat et al., 2018). NiR activity was assessed by combining 10 mL of extracted protein solution with 90 mL of reaction buffer (130 mM K_2HPO_4, 70 mM KH_2PO_4, 0.5 mM KNO_2, and 2 mM methyl viologen), followed by the addition of 10 mL of a sodium-based reaction solution containing 20 mg/mL Na_2CO_3 and $Na_2S_2O_4$. After incubation at 30 °C for 15 min, the reaction was stopped by vertexing, and nitrite concentration was quantified using the Griess assay (Wang et al. 2007).

6.2.8. RNA isolation, cDNA synthesis and qPCR analysis

Total RNA was isolated from leaf and root tissues using the Trizol RNA Isolation Reagents (Invitrogen, Carlsbad, CA, USA) following the manufacturer's protocol. RNA quantity and integrity were assessed by measuring the optical density at 260 nm and through 1.0% (w/v) agarose gel electrophoresis, respectively. Subsequently, 1 µg of total RNA was reverse-transcribed into single-stranded cDNA using the iScript™ RT Reagent Kit (Bio-Rad, Hercules, CA, USA) according to the manufacturer's instructions. Quantitative real-time polymerase chain reaction (qPCR) was performed using the CFX 96 Real-Time System (Bio-Rad, Richmond, CA, USA) with SYBR Green fluorescence (Bio-Rad, Richmond, CA, USA). The $^{\Delta\Delta}$CT method was used for data analysis. The list of gene studied are provided in Table S6.1. The thermal cycling conditions consisted of an initial denaturation step at 95 °C for 5 min, followed by 40 cycles of 95 °C for 15 s, 55 °C for 15 s, and 72 °C for 30 s. All experiments

were conducted with three biological replicates, and relative transcript levels were normalized using *ZmActin1* and *ZmUBQc* as internal controls.

6.2.9. Statistical analysis

The study was independently conducted twice, with tissue samples collected in triplicate for each experiment. All quantitative data represent the mean ± deviation (SD) of six (6) independent plants (n = 6). Data were analysed using a two-way analysis of variance (ANOVA) to assess the effects of treatment and developmental stage. Post-hoc pairwise comparisons were subsequently performed in GraphPad Prism (version 10) to identify statistically significant differences between groups. In the ANOVA model, plant growth stage (PGS) was designated as a fixed factor, while N treatments (NT) were treated as variable factors. Statistical significance was determined at a probability of $p \leq 0.05$, with differing lowercase letters used to denote significant differences in graphical representations. Graphical visualizations were generated using GraphPad Prism (version 10.4.0), and Pearson's correlation matrices were constructed using R statistical software (version 4.4.5).

6.3. Results

6.3.1. Phenotypic performance and biomass accumulation under dynamic N forms

Maize seedlings showed distinct growth responses to the various N treatments. By 20 DAT, seedlings plants subjected to the NFS treatment displayed significantly improved shoot and root growth, resulting in superior overall phenotypic performance compared to those grown under other N treatments (Fig. S6.1A–B). This enhanced growth trend continued at 40 DAT, with NFS-treated plants displaying vigorous shoot development and produced larger cobs. Conversely, plants grown solely with NH_4^+ developed more extensive root systems than those under other N regimes (Fig. S6.1C–D), highlighting the differential effects of N sources on maize growth dynamics. Furthermore, NFS treatment significantly enhanced total N accumulation in both leaf and root tissues at 20 and 40 DAT (Figs. 6.2–3C). This increase was accompanied by a substantial rise in shoot, root, and total biomass compared to plants supplied with sole NO_3^-, NH_4^+, or mixed (NH_4NO_3) N sources. Notably, despite this increase in biomass, the R/S ratio remained stable across all treatments and time points (Figs. 6.2–6.3A, B, and D), suggesting proportionally coordinated growth. In parallel, NFS-treated plants exhibited elevated chlorophyll content and higher Pn relative to other N treatment (Fig. S6.2A–B). Two-way ANOVA revealed that both plant growth stage (PGS) and nitrogen treatment (NT) significantly influenced biomass partitioning, N content, chlorophyll concentration, and Pn. Moreover, a significant PGS × NT interaction was observed for total biomass, root biomass, and root N content, whereas the R/S ratio remained unaffected by either factor or their interaction (Table 6.1).

6.3.2. NFS enhances amino acid and protein synthesis and N metabolite accumulation

The dynamic NFS treatment significantly increased the total amino acid and protein contents in both leaves and roots of maize seedlings at 20 and 40 DAT (Figs. 6.2–3D–E). Similarly, NFS-treated plants accumulated higher levels of NO_3^-, NO_2^- and NH_4^+ in both leaves and roots at both time points compared to all other N treatments (Figs. 6.2–6.3F–H). The accumulation of these N metabolites in leaf and root tissues was significantly influenced by PGS, NT, and PGS × NT.

6.3.3. Promotion of N Assimilation enzyme activities by NFS

Consistent with the increased accumulation of N metabolites, the activities of key N assimilation enzymes, such as NR, NiR, GS and GOGAT, were significantly higher in the leaves and roots of NFS-treated plants compared to other N treatments (Fig. 6.4A–H). In leaves, the activities of NR, NiR, GS, and GOGAT were all significantly influenced by PGS, NT, and PGS × NT (Table 6.1). Additionally, in roots, NR, NiR, and GS activities were similarly affected by PGS, NT, and PGS × NT, while GOGAT activity was influenced solely by PGS and NT, with no significant interaction effect (Table 6.1).

6.3.4. Transcriptional regulation of N metabolism genes under dynamic N conditions

The expression patterns of N metabolism enzyme-related genes, such as *ZmNR1*, *ZmNiR1*, *ZmGS1*, and *ZmGOGAT1*, varied distinctly across N treatments. While NO_3^- metabolism-related transcripts (*ZmNR1* and *ZmNiR1*) were significantly upregulated under sole NO_3^- treatment, NH_4^+ metabolism-related genes (*ZmGS1* and *ZmGOGAT1*) showed elevated expression in both leaves and roots of NFS-treated plants compared to other N treatments (Figs. 6.5–6.6A–D). Similarly, NO_3^- transporter genes (*ZmNPF6.2* and *ZmNRT2.1*) were highly induced in NO_3^--treated plants, but NH_4^+ transporter genes (*ZmAMT1.2* and *ZmAMT2.1*) exhibited a three- to four-fold higher expression in NFS-treated plants compared to other treatments (Figs. 6.5–6.6E–F). Both the enzyme-related genes (*ZmNR1*, *ZmNiR1*, *ZmGS1*, *ZmGOGAT1*) and the transporter genes (*ZmNPF6.2*, *ZmNRT2.1*, *ZmAMT1.2*, *ZmAMT2.1*) were significantly influenced by PGS, NT, and PGS × NT in both maize leaves and roots (Table 6.1).

6.3.5. Diurnal patterns of N metabolites and enzyme activities

We observed consistent diurnal patterns of NO_3^- and NH_4^+ accumulation and enzyme activities across treatments. Diurnal NO_3^- levels increased in the early morning (7:00 AM), peaked at midday (12:00 PM), and then declined until the following morning (Figs. 6.7A–B). Conversely, NH_4^+ levels were

lowest at 7:00 AM, increased after 12:00 PM, peaked at 10:00 PM, and then dropped by 7:00 AM the next day (Figs. 6.7B–D). These diurnal fluctuations were consistent at both 20 and 40 DAT (Figs. 6.7A–D). At 20 DAT, NFS-treated plants consistently exhibited significantly higher ($P \leq 0.05$) accumulation of both NO_3^- and NH_4^+ throughout the day compared to other treatment groups. Even after overnight transport, NFS-treated plants retained higher NO_3^- and NH_4^+ levels (Fig. 6.7). Correspondingly, NR activity was high at 7:00 AM, peaked at 12:00 PM, and then rapidly decreased until the next morning (Fig. 6.8A–C). GS activity followed a similar pattern, increasing after 7:00 AM, peaking at 12:00 PM, and declining afterwards. At 20 DAT, NFS-treated plants consistently showed significantly higher ($P \leq 0.05$) NR activity throughout the day compared to other treatments (Fig. 6.8).

6.3.6. Spatial distribution of N forms across maize tissues

Spatial analysis revealed differential distribution of NO_3^- and NH_4^+ across various maize tissues, such as upper, middle, and basal leaves, leaf sheath, roots, and developing ear. NFS-treated plants exhibited significantly ($P \leq 0.05$) higher concentrations of both NO_3^- and NH_4^+ across these tissues compared to other N treatments. At 22:00, elevated NO_3^- and NH_4^+ levels were observed in the upper, middle, and basal leaves, along with the roots, suggesting enhanced N uptake and retention under NFS. Notably, NFS-treated plants maintained elevated NH_4^+ concentrations following overnight remobilization and increased NO_3^- accumulation in leaves by 22:00. In sink tissue, such as the roots, NO_3^- and NH_4^+ levels were comparatively higher and showed significant variation ($P \leq 0.05$) among N treatments at both 22:00 and 07:00 (Fig. 6.9A-D), suggesting differential N dynamics throughout the diurnal cycle.

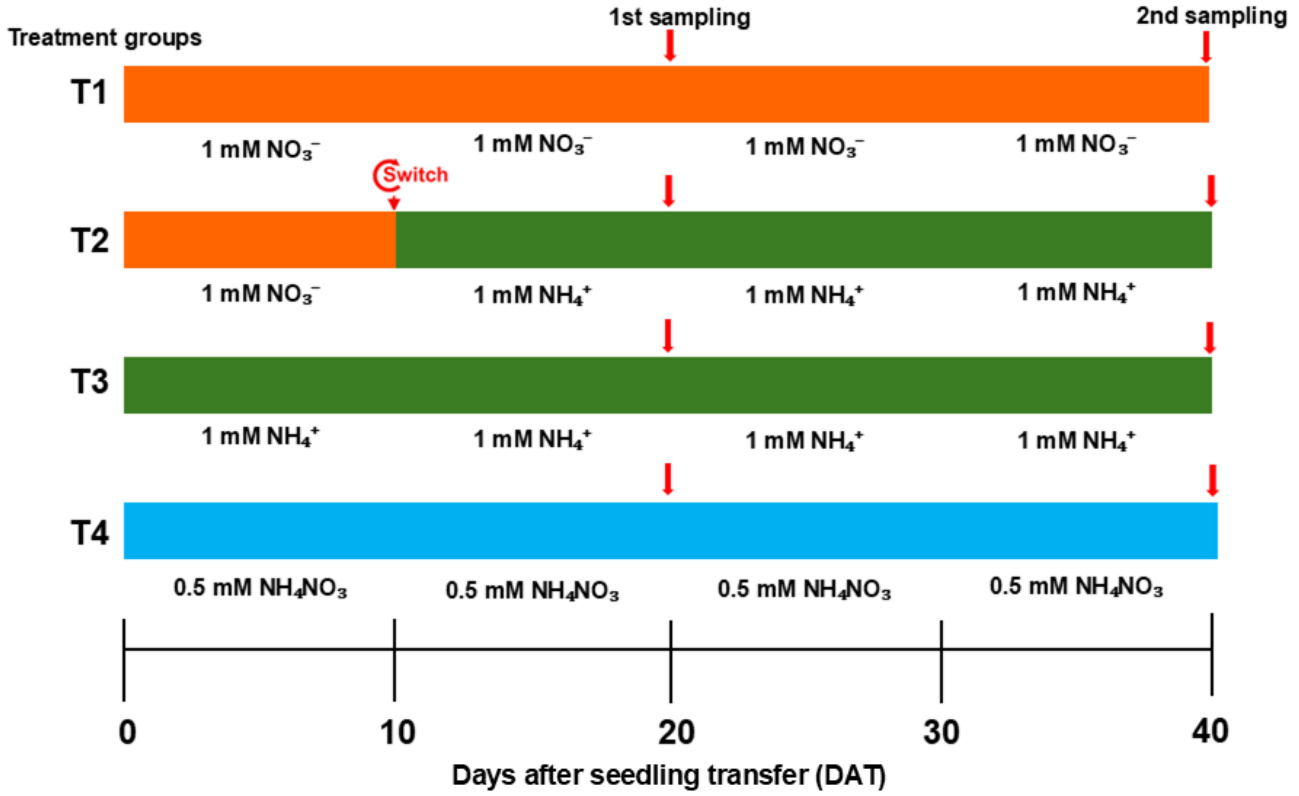

Fig. 6.1 Schematic representation of the experimental setup for the maize inbred line TX-40J. Maize seedlings were assigned to four nitrogen (N) treatment groups (T1 to T4): T1, 1 mM NO_3^- (sole nitrate supply); T2, substitution of 1 mM NO_3^- with 1 mM NH_4^+ at 10 days after transfer (DAT) (nitrogen form substitution, NFS); T3, 1 mM NH_4^+ (sole ammonium supply); and T4, 0.5 mM NH_4NO_3 (combined nitrate and ammonium supply). Plants were subsequently grown for an additional 30 days (up to 40 DAT), with shoot, root, and leaf samples collected at 20 DAT and 40 DAT. In the diagram, orange, green, and blue blocks represent 1 mM NO_3^-, 1 mM NH_4^+, and 0.5 mM NH_4NO_3, respectively. Red downward arrows indicate the nitrogen form switch (from 1 mM NO_3^- to 1 mM NH_4^+), while black downward arrows denote tissue sampling time points.

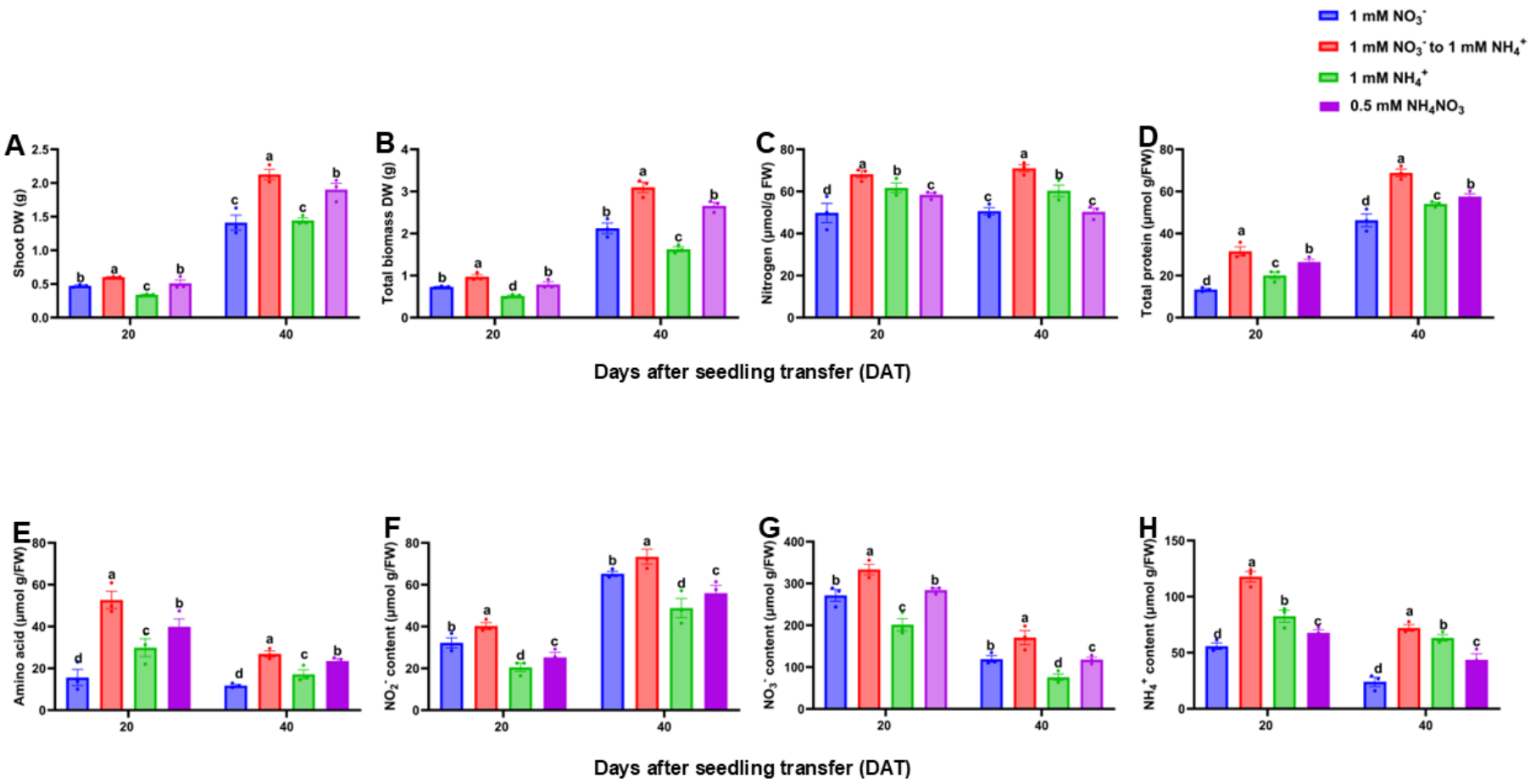

Fig. 6.2 Shoot biomass (**A**), total biomass (**B**), leaf nitrogen content (**C**), leaf total protein content (**D**), leaf total amino acids (**E**), leaf nitrate (**F**), leaf nitrite (**G**), and leaf ammonium content (**H**) under different nitrogen forms. Data points represent the mean ± standard deviation (SD) of six independent biological replicates (n = 6). Different letters above the error bars indicate statistically significant differences at $p \leq 0.05$. Abbreviations: DAT – days after seedling transfer; FW – fresh weight; DW – dry weight.

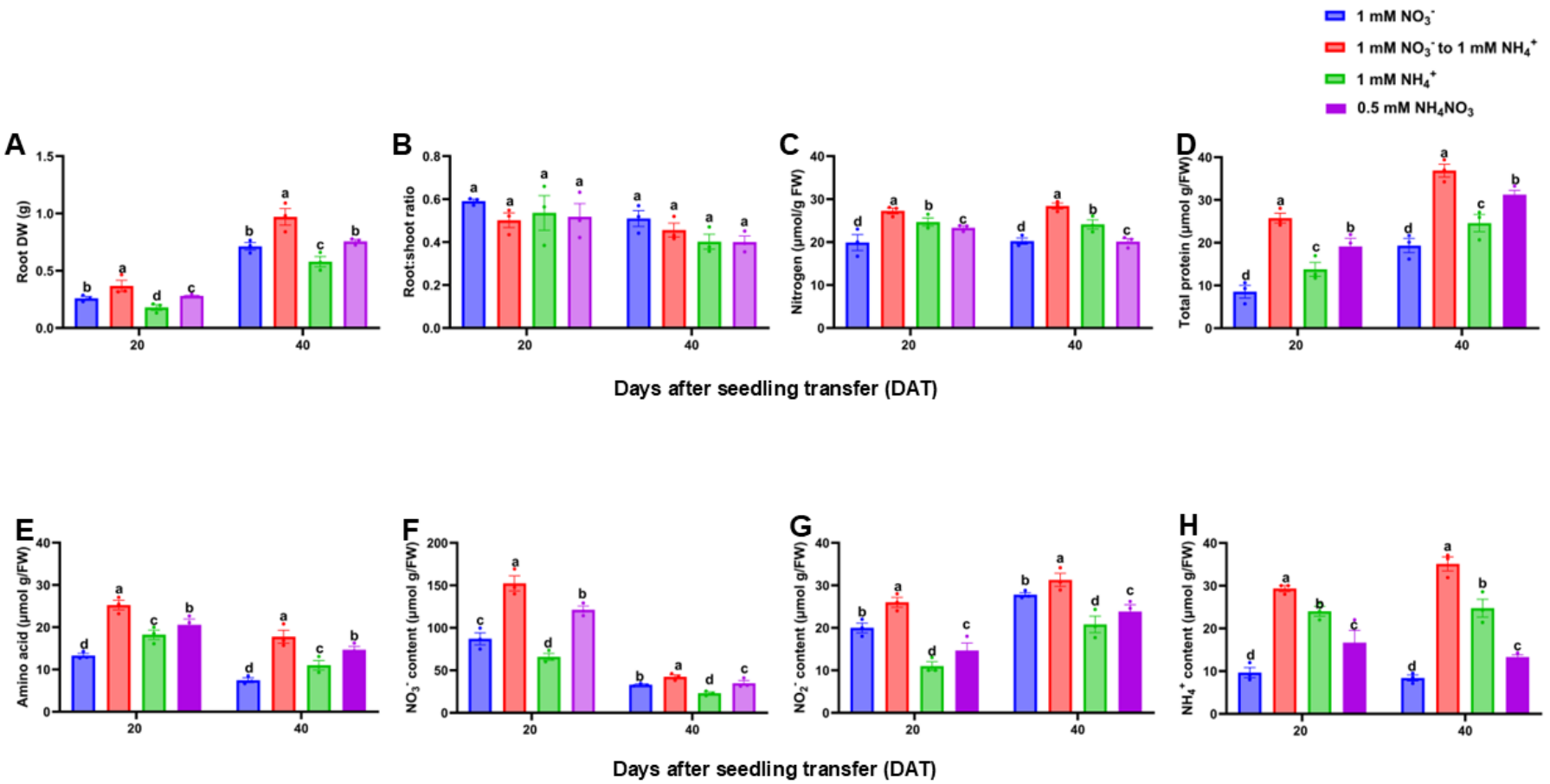

Fig. 6.3 Root biomass (A), root: shoot biomass ratio (B), root nitrogen content (C), root total protein content (D), root total amino acids (E), root nitrate (F), root nitrite (G), and root ammonium content (H) under different nitrogen forms. Data points represent the mean ± standard deviation (SD) of six independent biological replicates (n = 6). Different letters above the error bars indicate statistically significant differences at $p \leq 0.05$. Abbreviations: DAT – days after seedling transfer; FW – fresh weight; DW – dry weight.

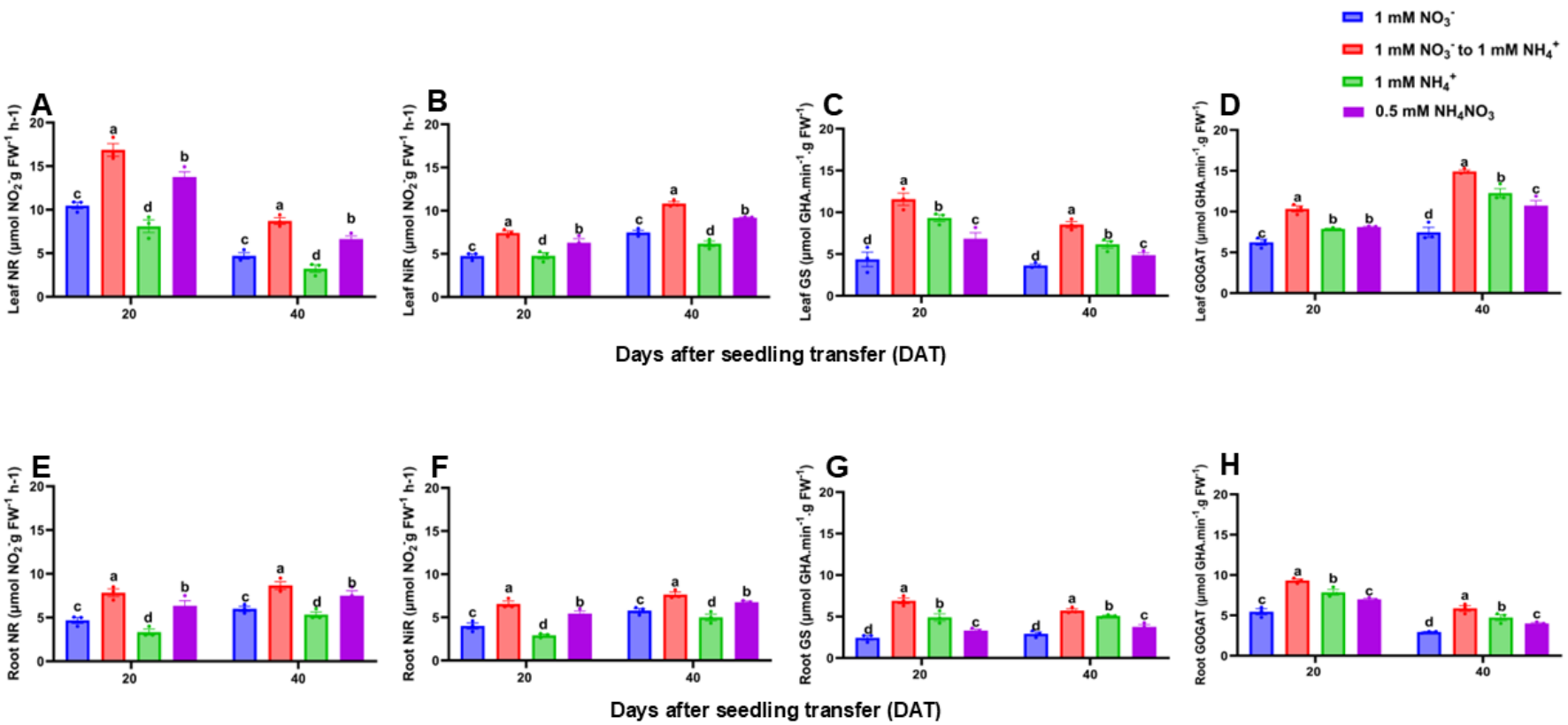

Fig. 6.4 Nitrate reductase (**A, E**), nitrite reductase (**B, F**), glutamine synthetase (**C, G**), and glutamate synthase (**D, H**) activities in the leaves (**A–D**) and roots (**E–H**) of the maize inbred line TX-40J. Data are presented as mean ± standard deviation (SD) from six independent biological replicates (n = 6). Different letters above the error bars indicate statistically significant differences at $p \leq 0.05$. Abbreviations: DAT – days after seedling transfer; FW – fresh weight.

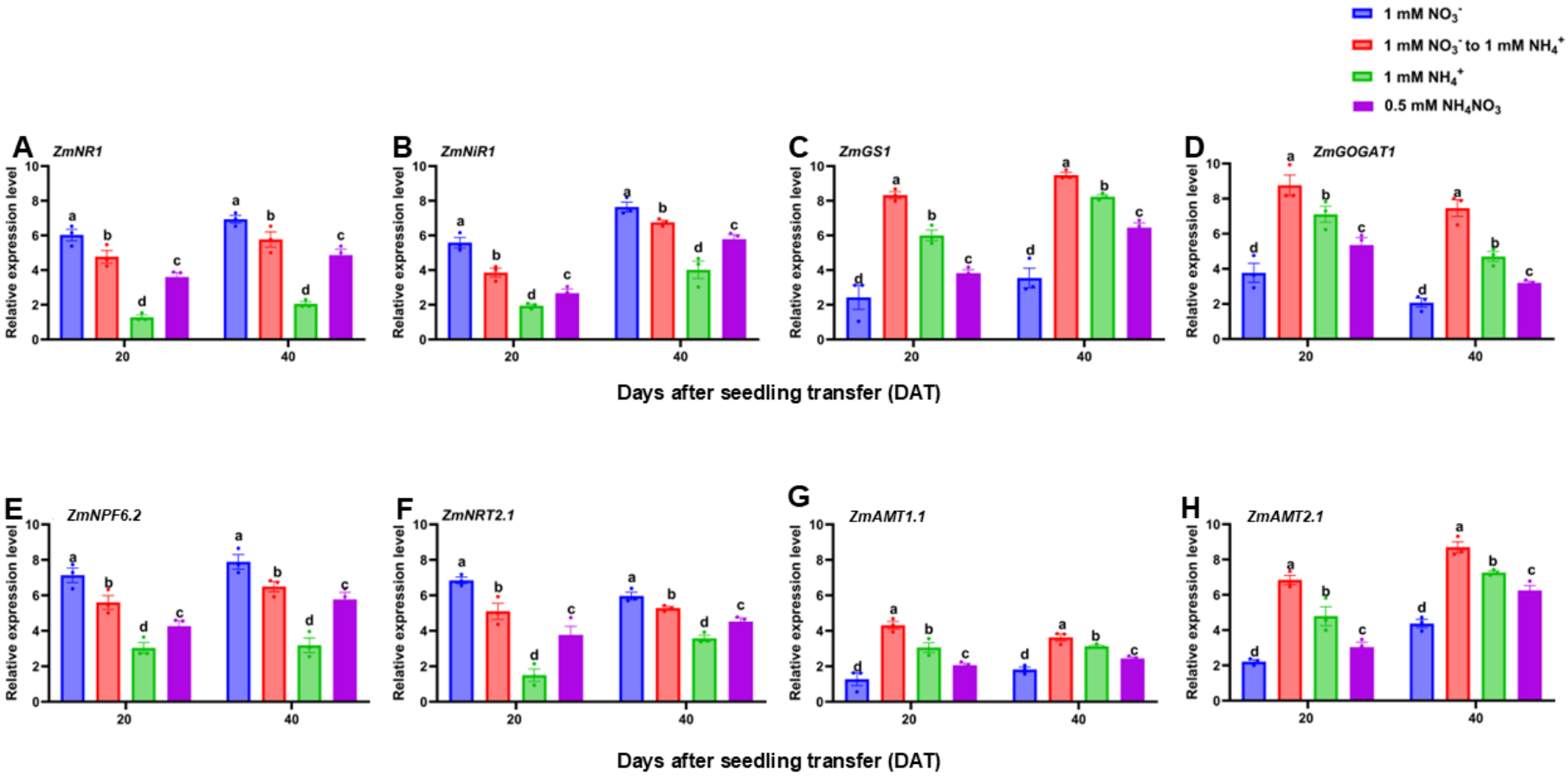

Fig. 6.5. Expression patterns of nitrogen (N) assimilation and transporter genes under different N forms. Relative expression levels of *ZmNR1* (**A**), *ZmNiR1* (**B**), *ZmGS1* (**C**), *ZmGOGAT1* (**D**), *ZmNPF6.2* (**E**), *ZmNRT2.1* (**F**), *ZmAMT1.1* (**G**), and *ZmAMT2.1* (**H**) in the root of the maize inbred line TX-40J. Data are presented as mean ± standard deviation (SD) from six independent biological replicates (n = 6). Different letters above the error bars indicate statistically significant differences at $p \leq 0.05$.

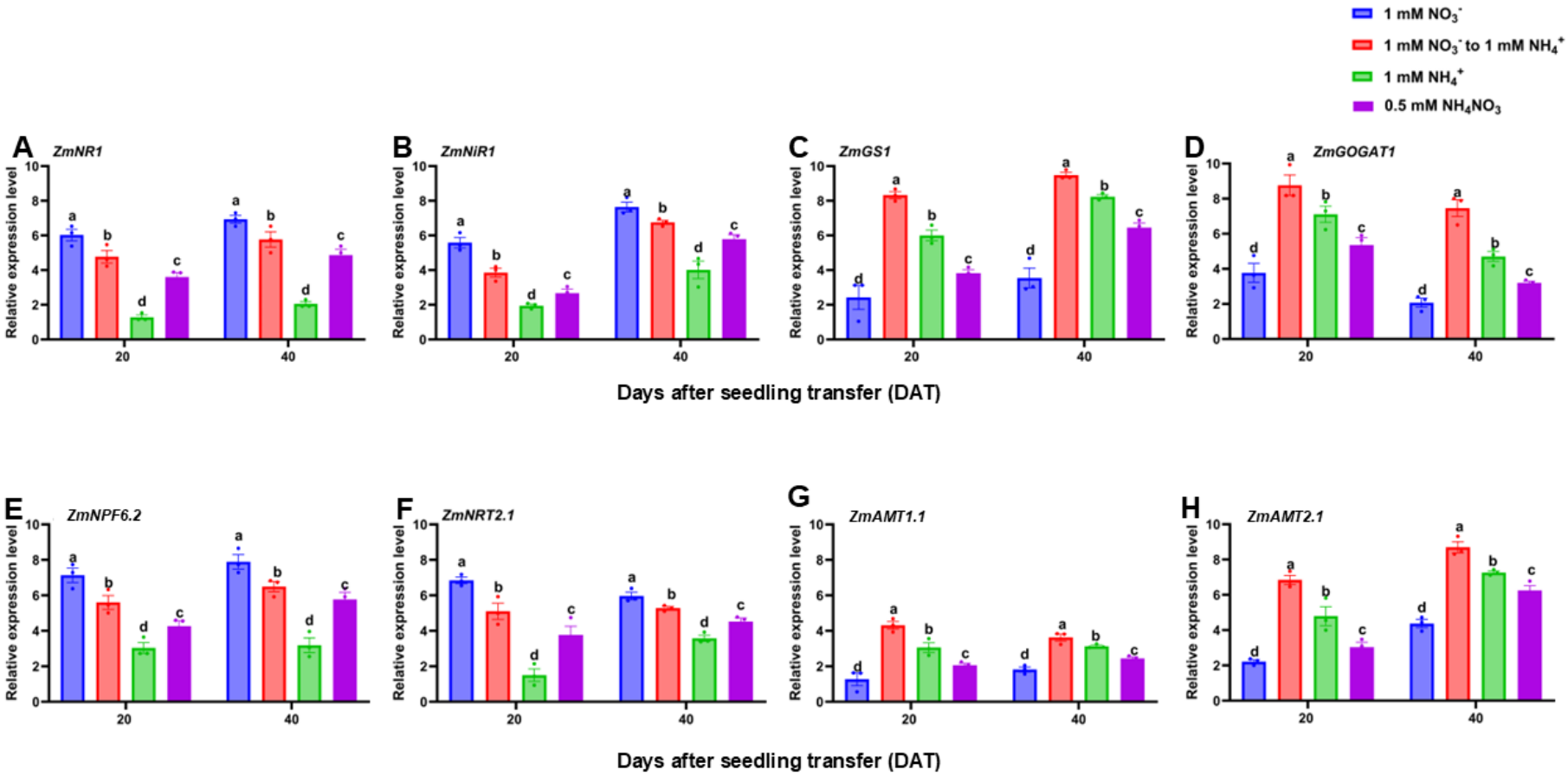

Fig. 6.6. Expression patterns of nitrogen (N) assimilation and transporter genes under different N forms. Relative expression levels of *ZmNR1* (**A**), *ZmNiR1* (**B**), *ZmGS1* (**C**), *ZmGOGAT1* (**D**), *ZmNPF6.2* (**E**), *ZmNRT2.1* (**F**), *ZmAMT1.1* (**G**), and *ZmAMT2.1* (**H**) in the root of the maize inbred line TX-40J. Data are presented as mean ± standard deviation (SD) from six independent biological replicates (n = 6). Different letters above the error bars indicate statistically significant differences at $p \leq 0.05$.

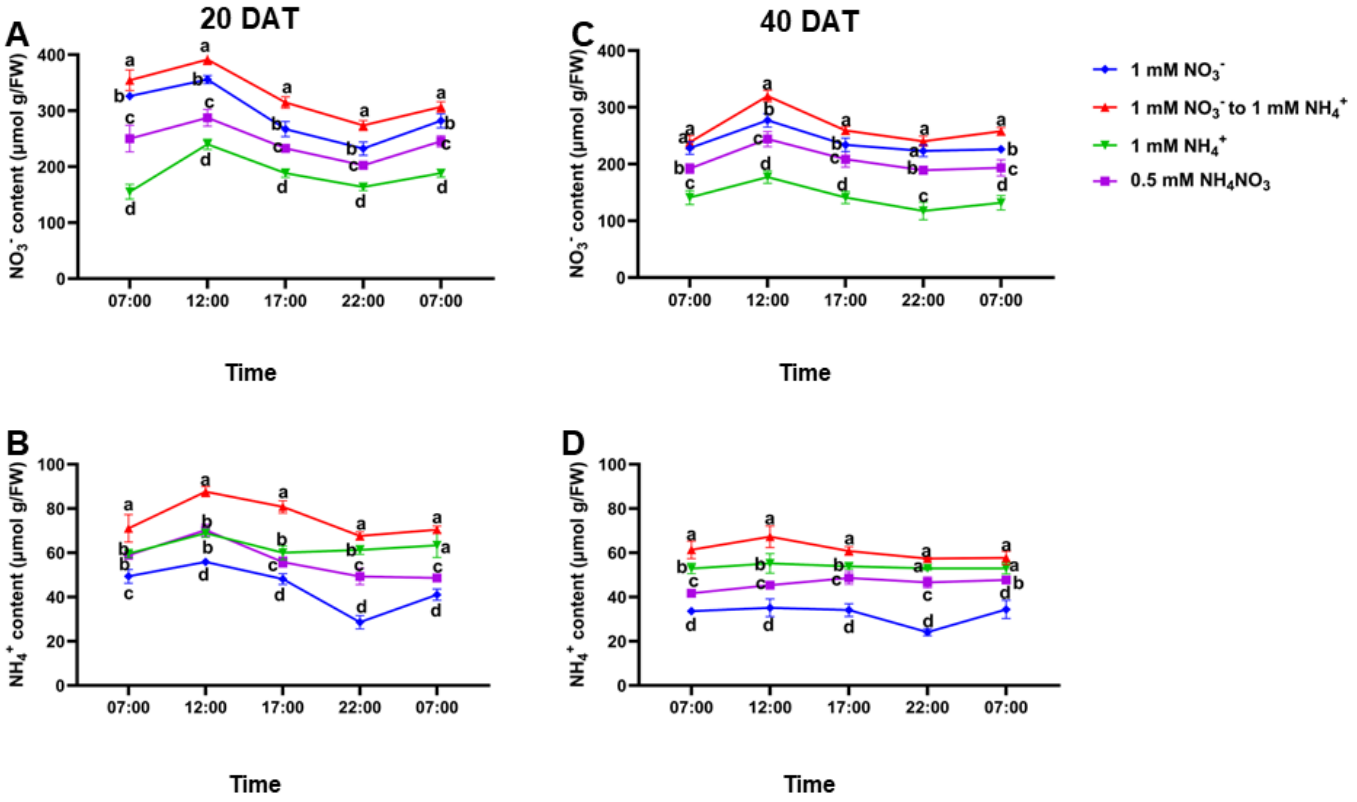

Fig. 6.7 Diurnal changes in leaf nitrate and ammonium content under nitrogen form substitution (NFS) conditions. Leaf nitrate content at 20 days after transfer (DAT) (**A**) and 40 DAT (**B**), and leaf ammonium content at 20 DAT (**C**) and 40 DAT (**D**). Samples were collected at five time points: 7:00, 12:00, 17:00, 22:00, and 7:00 on the following day. Data are presented as mean ± standard deviation (SD) from six independent biological replicates (n = 6). Different letters above the error bars indicate statistically significant differences at $p \leq 0.05$. Abbreviations: DAT – days after seedling transfer; FW – fresh weight

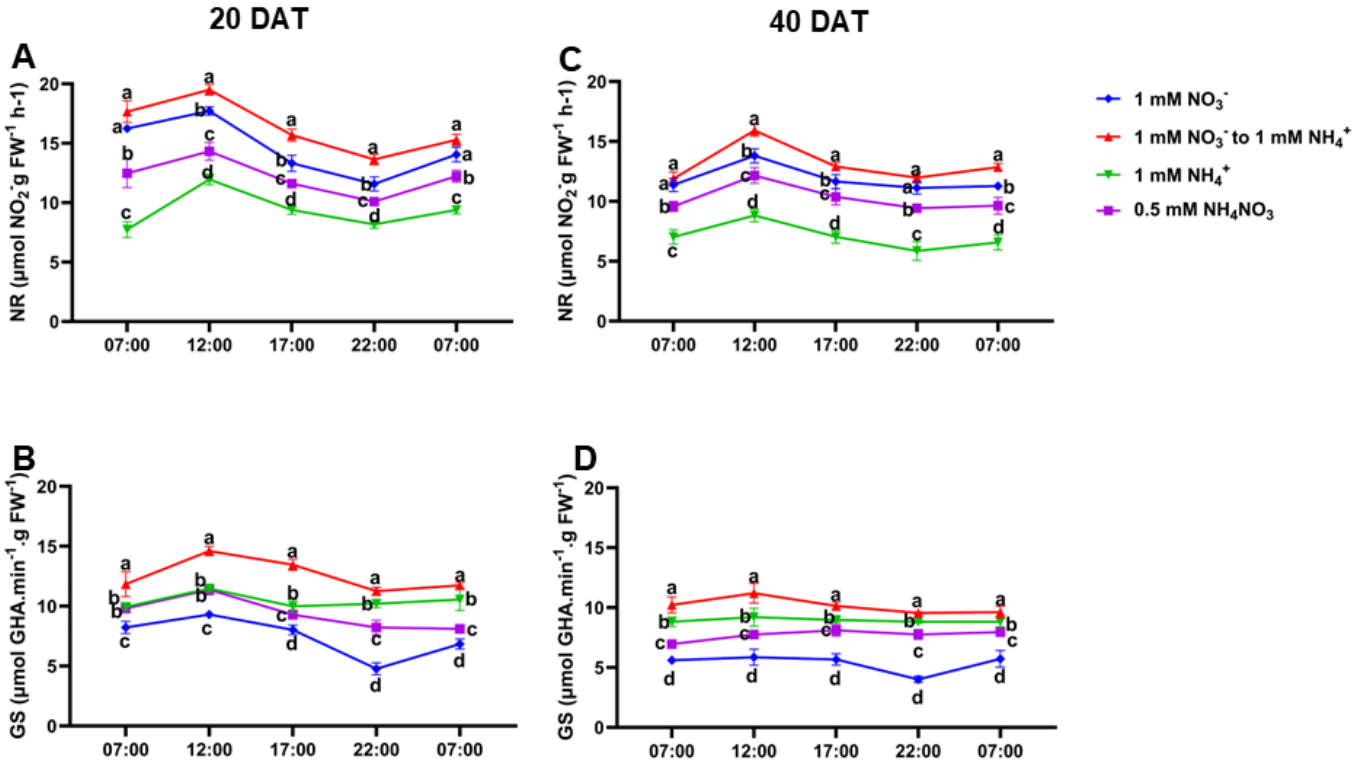

Fig. 6.8 Diurnal changes in leaf nitrate reductase and glutamine synthase activity under nitrogen form substitution (NFS) conditions. Leaf nitrate reductase activity at 20 days after transfer (DAT) (**A**) and 40 DAT (**B**), and leaf glutamine synthase activity at 20 DAT (**C**) and 40 DAT (**D**). Samples were collected at five time points: 7:00, 12:00, 17:00, 22:00, and 7:00 on the following day. Data are presented as mean ± standard deviation (SD) from six independent biological replicates (n = 6). Different letters above the error bars indicate statistically significant differences at $p \leq 0.05$. Abbreviations: DAT – days after seedling transfer; FW – fresh weight.

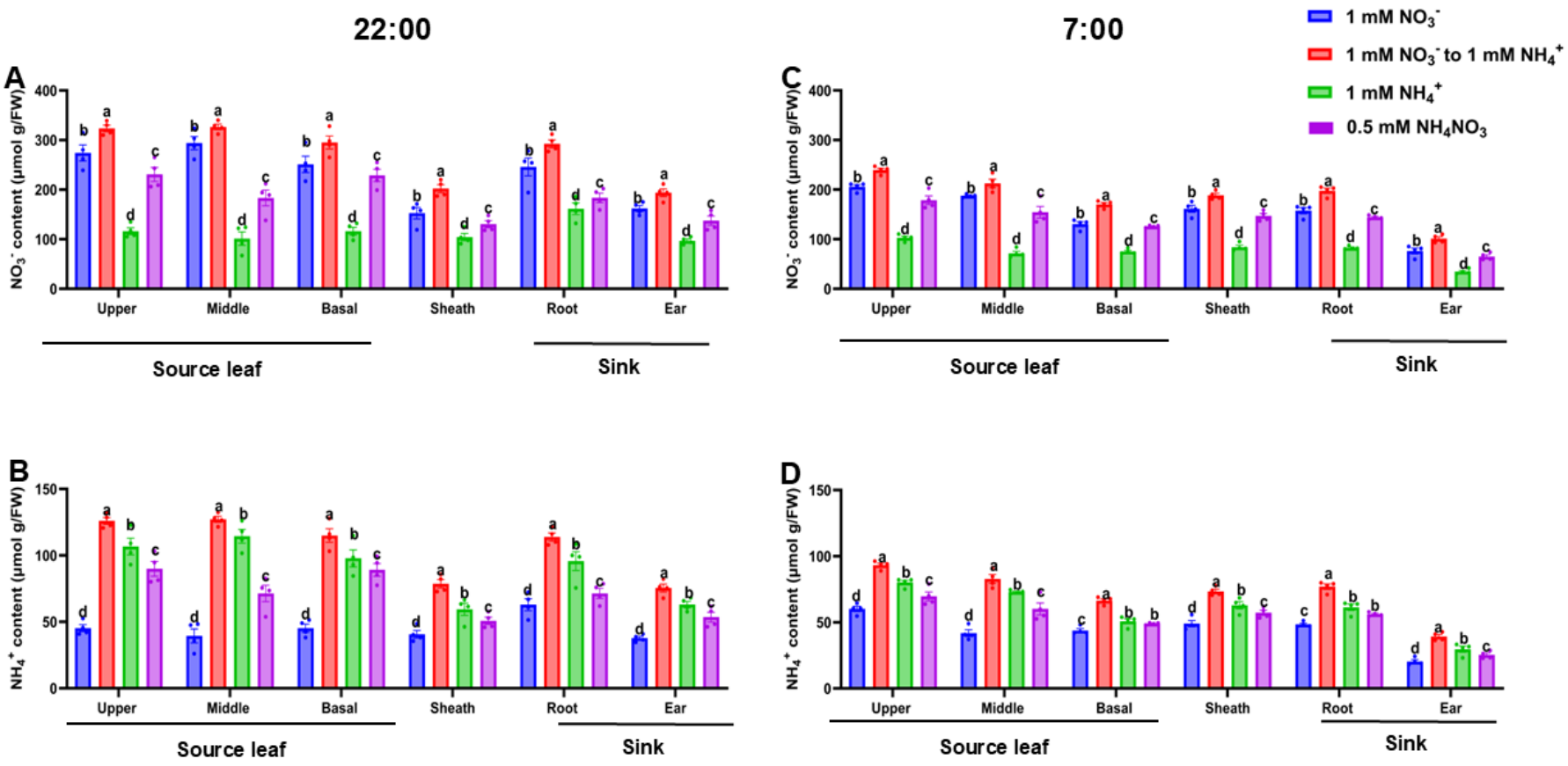

Fig. 6.9 Spatial and temporal analysis of nitrate and ammonium content in maize tissues at 40 DAT. Leaf nitrate (**A**) and ammonium (**B**) levels at 22:00, and leaf nitrate (**C**) and ammonium (**D**) levels at 07:00, measured under different nitrogen form treatments. FW indicates the fresh weight of tissue samples. Data are presented as mean ± standard deviation (SD) from six independent biological replicates (n = 6). Different letters above the error bars denote statistically significant differences at $p \leq 0.05$. Abbreviations: DAT – days after seedling transfer; FW – fresh weight.

Table 6.1 Two-way analysis of variance (ANOVA) for the indicators in the shoot/leaf and root of maize inbred-line TX-40J under different N treatments

Trait/(plants)	Sources of variation					
	Shoot/leaf			Root		
	PGS (df=1)	NT (df=3)	PGS x NT (df=3)	PGS (df=1)	NT (df=3)	PGS x NT (df=3)
Biomass	0.0004***	0.0462*	0.0651ns	0.0075**	0.0051**	0.0847ns
Total biomass	0.0005***	0.0275*	0.0367*	0.0005***	0.0275*	0.0367*
Root: shoot ratio	0.1615ns	0.3714ns	0.8599ns	0.1615ns	0.3714ns	0.8599ns
Chlorophyll	0.017*	0.0454*	0.2045ns	n/a	n/a	n/a
Pn	0.02921*	0.0487*	0.2679ns	n/a	n/a	n/a
Nitrogen	0.02474*	0.0286*	0.3226ns	0.03474ns	0.0286*	0.2226ns
Total protein	0.0003***	0.0094**	0.0898ns	0.01293*	<0.0001****	<0.0001****
Total amino acid	0.0034**	<0.0001****	<0.0001****	0.0099**	<0.0001***	<0.0001*****
Nitrate	0.0318*	<0.0001****	<0.0001****	<0.0001****	<0.0001****	<0.0001****
Nitrite	0.02739ns	<0.0001****	<0.0001****	0.0106*	<0.0001****	0.0001***
Ammonium	0.0004***	<0.0001****	<0.0001****	0.0015**	0.0073**	<0.0001****
NR	0.0294*	<0.0001****	<0.0001****	0.0116*	0.0004***	<0.0001***
NiR	0.0051**	<0.0001****	<0.0001****	0.0197*	<0.0001****	<0.0001****
GS	0.0003***	<0.0001****	<0.0001****	0.001***	0.0867ns	<0.0001****
GOGAT	0.0009***	<0.0001****	<0.0001****	0.0001***	<0.0001****	<0.0001****
ZmNR1	0.0294*	<0.0001****	<0.0001****	0.9147ns	0.0022**	<0.0001***
ZmNiR1	0.0051**	<0.0001****	<0.0001****	0.003***	<0.0001****	<0.0001****
ZmGS1	0.0412*	<0.0001****	<0.0001****	0.0323*	<0.0001****	<0.0001****
ZmGOGAT	0.0094**	0.01906*	<0.0001****	0.015774*	<0.0001****	<0.0001****
ZmNPF6.2	0.03539*	<0.0001****	<0.0001****	0.0264*	0.0057**	<0.0001***
ZmNRT2.1	0.0294*	<0.0001****	<0.0001****	0.0041**	<0.0001****	<0.0001****
ZmNRT3.1	0.0449*	0.0001***	<0.0001****	0.0015**	0.025*	<0.0001***
ZmAMT1.1	0.0109*	<0.0001****	<0.0001****	0.0355*	0.0073**	<0.0001****
ZmAMT2.1	0.04171*	<0.0001****	<0.0001****	0.03522*	<0.0001****	<0.0001****

PGS: plant growth stage, NT: nitrogen treatment, PGS x NT: interaction between plant growth stage and nitrogen treatments, Pn: net photosynthetic rate, NR: nitrate reductase activity, GS: glutamine synthase activity, GOGAT: glutamate synthase activity, ns: non-significant, n/a: non-applicable. Additionally, *, **, and ***: denote significance at probability levels of 0.05, 0.01, and 0.001, respectively.

6.4. Discussion

6.4.1. NFS promotes maize growth by optimizing N allocation and mitigating stress

Our findings demonstrate that NFS significantly promotes shoot, root, and total plant biomass accumulation in maize compared to static single or mixed N forms (Fig. 6.2A-B and Fig. 6.3A). This aligns with our recent study showing enhanced growth under NFS (Amoah and Kaiser 2025). While it has been shown that mixed NO_3^- and NH_4^+ supply generally improves N uptake and utilization due to synergistic interactions, our study provides an insight into how the dynamic and alternating nature of NFS specifically modulate this synergy to optimize plant performance and nutrient homeostasis under fluctuating conditions (Peng et al. 2023a; Chen et al. 2024b). The enhanced growth under NFS may be attributed to a complementary N uptake mechanism that mitigates stress and toxicity associated with sole N forms (Fang et al. 2021). The addition of NH_4^+, which has a lower energy requirement for uptake and assimilation than NO_3^-, contributes to optimized resource partitioning (George et al. 2016). For example, NH_4^+ uptake can reduce the demand for NO_3^- assimilation, allowing greater carbohydrate retention in shoots and promoting shoot dry matter accumulation (Peng et al. 2023a). This optimized resource partitioning and conservative growth is reflected in the lower R/S ratio observed in NFS plants (Fig. 6.3B), indicating a more efficient allocation of resources toward shoot development (Zhao et al. 2020). Furthermore, NH_4^+ treatment is known to stimulate root proton extrusion, which lowers rhizosphere pH and can improve NO_3^- availability, uptake and accumulation (Zhao et al. 2020; Amoah and Kaiser 2025; Hachiya and Sakakibara 2017). This physiological adjustment provides a mechanistic basis for the observed synergistic uptake effect under NFS, leading to higher NO_3^- accumulation in leaves and roots. The dynamic shift in N supply under NFS appears to play a crucial role in modulating N assimilation pathways. We observed that *ZmNPF6.2*, *ZmNRT2.1*, and *ZmNRT3.1*, genes encoding NO_3^- transporters, while highly induced in sole NO_3^--treated plants, also showed distinct expression patterns in NFS-treated plants compared to those under sole NH_4^+ or mixed N supply (Figs. 6.5–6.6E–F). This suggests that the alternating N supply in NFS may prime or maintain the plant's capacity for efficient NO_3^- uptake and assimilation even when NH_4^+ is introduced, rather than completely downregulating NO_3^- pathways as might occur under prolonged NH_4^+ exposure. This dynamic modulation of N transporter gene expression, combined with changes in NR and NiR activities, underpins the enhanced N uptake, assimilation and overall growth observed with NFS (Figs. S6.1, S6.2A–B).

6.4.2. NFS optimizes N assimilation through coordinated enzyme activity and gene expression

Our results demonstrate that NFS treatment increased NO_3^- and NO_2^- accumulation (Figs. 6.2–3F–G), which has not been previously observed under alternating N forms. While enhanced accumulation of these assimilated is known under different N treatment forms, the dynamic switch in NFS likely

stimulated NO_3^- accumulation beyond its metabolic demand, facilitating greater storage capacity. This observation aligns with studies demonstrating that combining NO_3^- and NH_4^+ enhances N uptake and efficiency, and our data demonstrate that the dynamic switch between N sources further amplified this synergistic effect (George et al. 2016; Peng et al. 2023a). Notably, NFS plants accumulated even higher NH_4^+ levels than plants under NH_4^+ treatment (Figs. 6.2–6.3H). This increased NH_4^+ pool mechanistically linked to enhanced amino acid biosynthesis and significantly enhanced GS and GOGAT activities (Figs. 6.4C–D and G–H). Furthermore, the induced expression of *ZmGS1*, *ZmGOGAT1* and NH_4^+ transporter genes (*ZmAMT1.2*, *ZmAMT2.1*) in NFS plants provides molecular evidence for a robust and highly efficient NH_4^+ assimilation via the GS-GOGAT pathway. This rapid conversion of NH_4^+ into amino acids, triggered by the alternating N supply, serves as an adaptive strategy or detoxification mechanism to mitigate potential NH_4^+ toxicity, which is a common physiological challenge under sole NH_4^+ nutrition (Cánovas et al. 2007; Liu and von Wirén 2017). The strong positive correlation between NR, NiR, GS, and GOGAT activities further substantiate that N switching promotes rapid and coordinated N conversion and prevents toxic accumulation, ensuring sustained growth even under high NH_4^+ conditions.

6.4.3. Diurnal regulation of N metabolism under dynamic N availability

Although diurnal fluctuations in N pools and enzyme activities are well-documented in plant physiology, our study highlights how NFS distinctly modulates these rhythms and their underlying regulatory mechanisms beyond simple N status. NFS plants consistently maintained elevated NO_3^- and NH_4^+ concentrations both during the day and overnight (Figs. 6.7A–D), suggesting that the dynamic N supply enhances the capacity for N storage and may modulate the amplitude of these fluctuations, potentially through circadian-regulated signalling or nutrient-sensing pathways (Macduff et al. 1997). The rhythmic patterns observed, such as NO_3^- peaking in the morning and declining by midday, and NR activity mirroring this trend, indicate a coordinated regulation of NO_3^- reduction and accumulation that is maintained or even enhanced under NFS (Fig. 6.8). In contrast, the gradual increase of NH_4^+ levels throughout the day, peaking at night, and the corresponding increase in GS activity reaching maximum levels at night, suggest a circadian-driven regulatory mechanism that ensures sustained NH_4^+ assimilation into organic molecules, particularly when NO_3^- availability may be lower (Tucker et al. 2004; Shanks et al. 2024). The ability of NFS plants to maintain altered N profiles, characterized by increased NO_3^- and NH_4^+ levels even after overnight transport, underscores the plant's robust adaptive responses to modified N sources (Amoah and Kaiser 2025; Hasan et al. 2022). These findings provide insights into the intricate interplay between N availability, metabolic regulation, enzymatic activity, and diurnal rhythms, advancing our understanding of plant adaptation mechanisms under dynamic nutrient conditions.

6.4.4. N availability shapes N assimilated dynamics across maize tissues: implications for allocation and remobilization

The spatial distribution of NO_3^- and NH_4^+ provides insights into how maize adapts to varying N forms (Fang et al. 2007), particularly under dynamic NFS conditions. Our results demonstrate that NFS-treated plants exhibited significantly increased NO_3^- and NH_4^+ levels across all sampled aboveground tissues (leaves and leaf sheath) and roots, particularly at 22:00 (Fig. 6.9). This highlights enhanced N accumulation and retention throughout plants under NFS. The significant variation in NO_3^- and NH_4^+ levels in roots at different time points (22:00 and 07:00) demonstrates the active role of roots as N sinks during dynamic N changes. This suggests that under *NFS*, specific *NRT* and *AMT* transporters are likely upregulated to facilitate rapid N acquisition and storage (Dechorgnat et al. 2019; Duan et al. 2023c). Furthermore, the consistent residual NO_3^- in the leaves and sheath of NFS-treated plants between 22:00 and 07:00 indicates a strategy of NO_3^- retention as a temporary storage pool for subsequent remobilization during periods of metabolic demand. This tissue-specific N distribution under NFS reflects adaptive strategies that sustain metabolic function, such as maintaining nutrient uptake capacity in roots and providing N reserves in leaves capacity (Krapp 2015; Tegeder and Masclaux-Daubresse 2018; Peng et al. 2023a). The enhanced GS activity, peaking at night, likely contributes to the observed increased NH_4^+ levels in aboveground tissues and roots at 22:00, supporting N status during the dark period when photosynthesis is not active (Miflin and Habash 2002). Understanding these spatial patterns of N partitioning patterns and their underlying regulatory mechanisms, such as diurnal rhythms and coordinated enzyme regulation, is essential for guiding crop improvement strategies. Future studies will delve into the molecular and enzymatic pathways specifically modulating these spatial patterns, particularly focusing on the mechanisms underlying N remobilization between source and sink tissues under more complex, continuous N fluctuations to better reflect natural field conditions.

6.5. Conclusion

This study demonstrates that NFS significantly enhances overall maize performance, including shoot and root development, biomass accumulation, and photosynthetic capacity, outperforming static single or mixed nitrogen treatments. NFS plants exhibited increased total N levels and increased accumulation of NO_3^-, NO_2^-, and NH_4^+ in both leaves and roots, with these concentrations sustained across diel cycles. Importantly, NFS improves NUE by leveraging the alternating supply of NH_4^+ and NO_3^- to modulate a synergistic interaction. This dynamic regime optimizes N acquisition while mitigating the stress and toxicity typically associated with prolonged exposure to a single N form. It promotes nutrient homeostasis and induces adaptive metabolic adjustments not observed under static conditions. Mechanistically, NFS enhances NH_4^+ assimilation via the GS-GOGAT pathway, facilitating amino acid biosynthesis and efficient N incorporation. Elevated activities of NR, NiR, GS, and GOGAT, along with

the coordinated upregulation of key genes involved in NH_4^+ metabolism (*ZmGS1*, *ZmGOGAT1*) and N transport (*ZmAMT1.1*, *ZmAMT2.1*, *ZmNPF6.2*, *ZmNRT2.1*, *ZmNRT3.1*), underscore the plant's capacity to fine-tune its N metabolic machinery in response to fluctuating availability. Tissue-specific analyses further revealed that under NFS, roots act as dynamic N sinks, while leaves retain elevated NO_3^- levels overnight, serving as temporary storage pools for subsequent remobilization. These spatial patterns, coupled with diurnal shifts in N metabolites and enzyme activities, suggest that NFS modulates the amplitude and efficiency of circadian-regulated N processes, ultimately enhancing N utilization. Collectively, these findings highlight the significant advantages of dynamic NH_4^+–NO_3^- interactions over static nitrogen regimes, offering a promising strategy to improve NUE and support sustainable agriculture by better mimicking natural N fluctuations. Future research will focus on validating these results through field trials across different maize varieties and exploring the effects of more complex, continuous N fluctuations to truly simulate natural environments, thereby maximizing their applicability and impact. Additionally, integrative anatomical and transcriptomic analyses will offer deeper insights into the physiological adaptations and molecular mechanisms underpinning NFS responses, enabling a more comprehensive understanding of how dynamic N supply shapes plant function at multiple biological levels.

6.6. Supplementary data

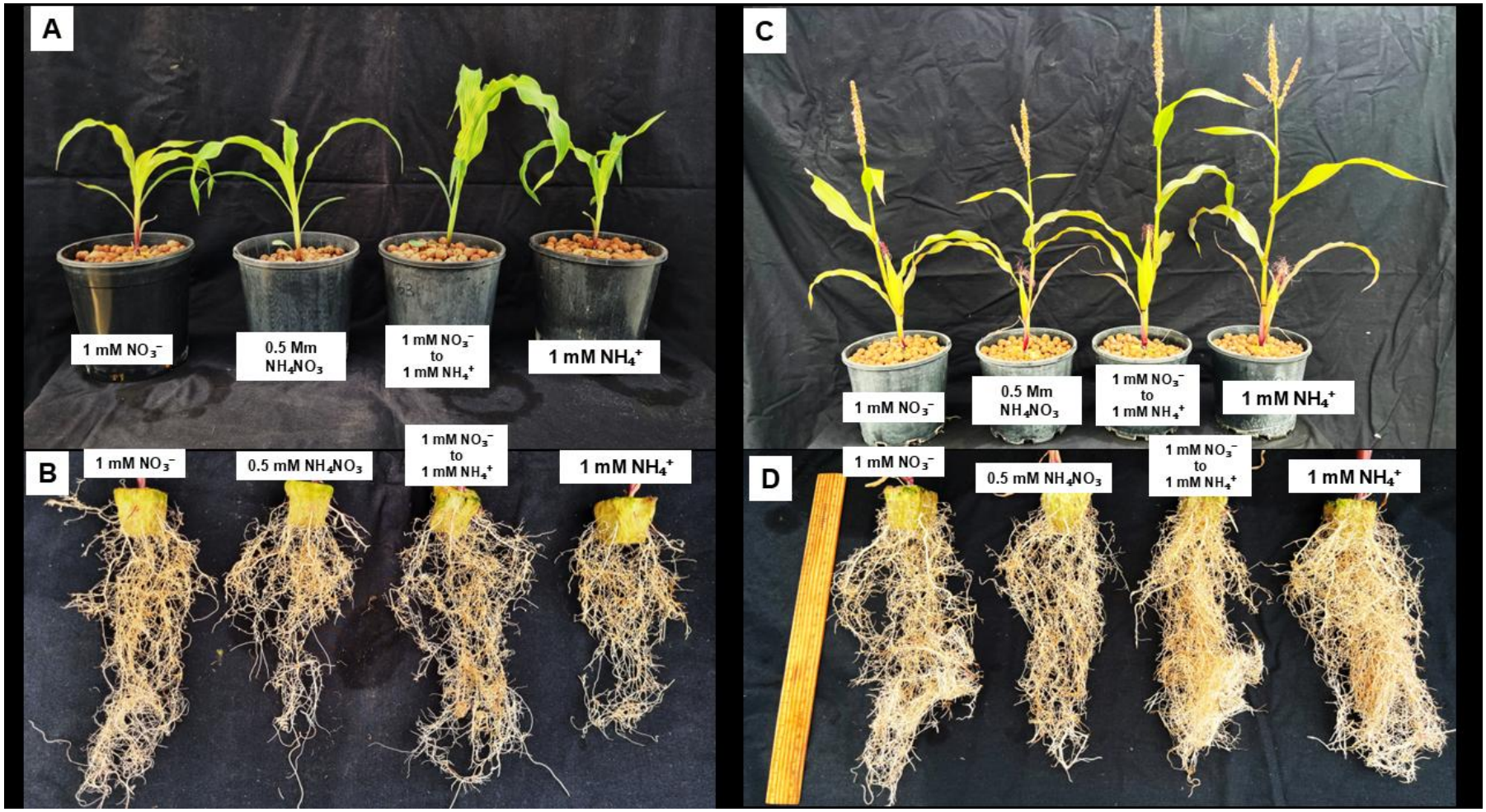

Fig. S6.1 Phenotypic response of the maize inbred line TX-40J to different nitrogen (N) forms. Representative imaged of shoot morphology at (**A,C**) and root morphology at 20 and 40 (**B, D**) days after nitrogen treatments (DAT).

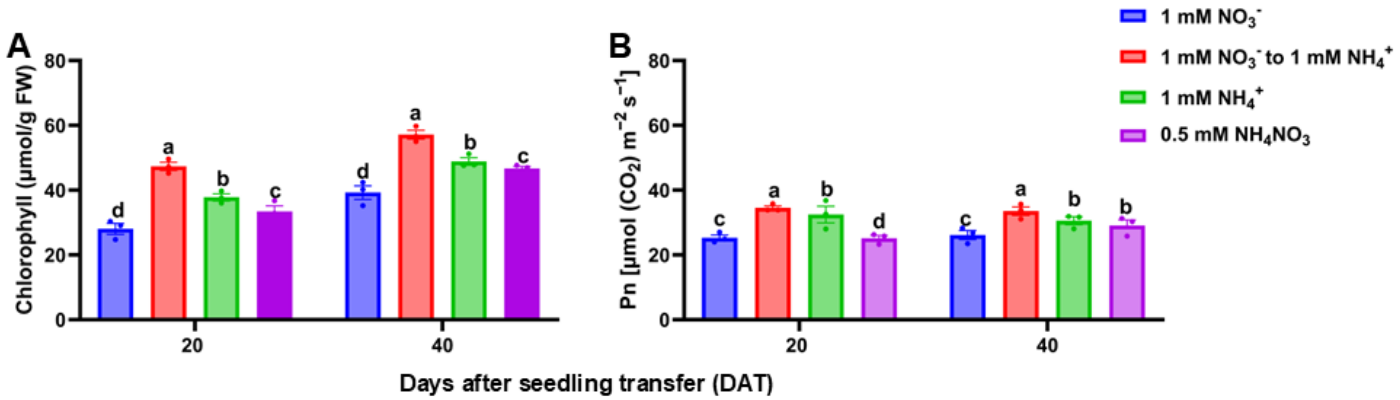

Fig. S6.2 Leaf chlorophyll content (**A**) and net photosynthetic rate (**B**) under different nitrogen forms. Data points represent the mean ± standard deviation (SD) of six independent biological replicates (n = 6). Different letters above the error bars indicate statistically significant differences at $p \leq 0.05$. Abbreviations: DAT – days after seedling transfer; FW – fresh weight.

Table S6.1 List of primers used for quantitative polymerase chain reaction (qPCR) analysis

Gene name	**NCBI LOCs**
ZmNR	LOC103654219
ZmNiR	LOC103627781
ZmGS	LOC542746
ZmGOGAT	LOC103651348
ZmNRT2	LOC542092
ZmNPF6.2	LOC100383494
ZmAMT1.1	LOC100272903
ZmAMT2.1	LOC100191554
ZmUBQc	LOC100279740
ZmActin	LOC100282267

CHAPTER 7: LOW AMMONIUM ENHANCES MAIZE GROWTH AND REVEALS NITROGEN EFFICIENCY PATHWAYS[6]

Abstract

Nitrogen (N) is an essential macronutrient for plant growth and metabolism. Nitrate (NO_3^-) and ammonium (NH_4^+) are the predominant forms of N available to plants in agricultural soils. NO_3^- concentrations are generally higher than those of NH_4^+, and this ratio remains consistent across various soil types. However, the potential contribution of low concentrations of NH_4^+ (low ammonium, LA) to the overall N budget of crop plants is often overlooked. This study explores how LA influences N metabolism, utilization, and spatial distribution in maize. The primary objective is to examine the physiological and molecular responses that enhance N use efficiency (NUE) under LA conditions. Maize seedlings were hydroponically grown under five N treatments: T1 – control N, T2 – 1 mM NO_3^-, T3 – 1 mM NH_4^+ (LA), T4 – 0.5 mM NH_4NO_3 (mixed N), and T5 – substitution of 1 mM NH_4^+ with 1 mM NO_3^- at 10 days after transfer (DAT). Physiological, biochemical, and gene expression analyses were performed to assess N assimilation and allocation. LA treatment induced notable adaptations, including improved growth, enhanced photosynthesis, and well-developed cobs. These responses were associated with increased activities of N assimilation enzymes, glutamine synthetase (GS) and glutamate synthase (GOGAT), and the upregulation of *ZmGS1* and *ZmGOGAT1*. In contrast, *ZmNR1* and *ZmNiR1* were downregulated. Spatial and diel analyses showed dynamic N distribution, indicating efficient root-to-shoot assimilate partitioning under LA. LA supply stimulates key molecular and physiological responses that optimize N utilization in maize. These findings offer insights into adaptive strategies for NUE. Future studies will explore this mechanism in diverse maize genotypes under field conditions.

Keywords: Nitrogen assimilation, Nitrogen source dynamics**,** Nitrogen transporter activity**,** Root system architecture**,** Maize growth response

---

[6] This chapter has been accepted for publication in Journal of Plant Nutrition and Soil Science, with the title 'Low ammonium enhances maize growth and reveals nitrogen efficiency pathways' (Manuscript ID: 9102614).

7.1. Introduction

Plants require nitrogen (N), an essential macronutrient critical for growth and development. It serves as a primary constituent of key biomolecules, including amino acids, proteins, and nucleic acids. It also plays an active role in numerous metabolic processes (Grubb et al. 2025). Although N is abundant in soils, it often becomes a limiting factor in crop production due to significant losses from leaching, volatilization, and denitrification, as well as its relatively low uptake efficiency by plants (Reddy et al. 2025; Alami et al. 2025). N deficiency can reduce total plant biomass and harvestable yield, directly affecting the profitability of seed growers (Amoah and Kaiser 2025). To mitigate this, growers often apply large quantities of inorganic nitrogen fertilizers. However, crops typically absorb only 45–50% of the applied N, with the remainder lost through volatilization, leaching, and denitrification (Whetton et al. 2022). Plants absorb N in the inorganic forms of nitrate (NO_3^-) and ammonium (NH_4^+), as microbial competition in soils often limits access to organic N sources. The availability of NH_4^+ is variable, depending on soil properties and microbial activity (Ali et al. 2025a; Mao et al. 2025). Understanding crop performance under different N regimes is thus essential for enhancing N use efficiency (NUE) and contributing to global food security (Yang et al. 2025).

Studies on N nutrition have focused on NO_3^-, largely due to its chemical stability and consistent agronomic performance. However, recent evidence highlights a distinct and potentially beneficial role for NH_4^+, particularly at low concentrations (LA) (Marino et al. 2016; Gao et al. 2022). These LA regimes remain relatively underexplored, despite their potential to enhance plant growth, modulate carbon (C) allocation, improve NUE, and act as a stress signal that initiates metabolic reprogramming and confers greater stress resilience. Despite this potential, NO_3^- continues to dominate fertilizer strategies, a trend often attributed to the challenges of maintaining low NH_4^+ concentrations in the root zone. These challenges arise primarily from rapid nitrification and microbial competition (Bollmann et al. 2002). Moreover, high NH_4^+ concentrations can be phytotoxic, resulting in what is commonly referred to as 'NH_4^+ syndrome,' characterized by reduced photosynthesis, stunted growth, and disrupted metabolic profiles (Horchani et al. 2010; Peng et al. 2023a). To mitigate such toxicity, plants have evolved compensatory mechanisms, such as the redirection of assimilates toward root development, thereby increasing the root-to-shoot biomass ratio (Dechorgnat et al. 2018; Zhao et al. 2020; Amoah and Kaiser 2025; Éva et al. 2019).

Interestingly, although extensive research has examined plant responses to various nitrogen (N) forms, a significant knowledge gap persists regarding nitrogen use efficiency (NUE) under N-limited conditions. Comparative studies exploring the potential benefits of low ammonium (NH_4^+) supply in crops such as maize are especially scarce. Addressing this gap is essential for deepening our understanding of nutrient signaling and for developing integrated N management strategies that enhance crop performance and promote agricultural sustainability. We hypothesize that LA supply exerts a

distinct influence on maize growth and N metabolism compared to other N forms. This potential benefit may stem from the reduced energy requirement associated with NH_4^+ assimilation. Through LA supply, we aim to uncover the regulatory mechanisms modulating growth, N assimilation, and resource allocation under fluctuating N conditions. These insights will contribute to advancing our knowledge of plant adaptive responses and inform the development of crop systems with enhanced NUE.

Maize (*Zea mays* L.) was selected for this study due to its global significance as a staple food crop and its established utility as a model system for investigating N metabolism dynamics (Dong et al. 2023a). The fast-flowering, short-cycle inbred mini-maize line TX-40J offers distinct advantages for controlled, high-throughput experimentation, enabling precise dissection of fundamental metabolic and regulatory processes during early developmental stages (McCaw et al. 2021). This study aims to elucidate the mechanisms modulating N assimilation between the shoot and root in maize LA regimes. Specifically, we investigated how LA treatment influences key enzymatic activities associated with N metabolism in the leaf and root tissues. In addition, we examined diel fluctuations in assimilate levels within source leaves and tracked their distribution across various plant organs during both vegetative and reproductive phases under LA treatments. By integrating temporal dynamics with metabolic profiling, this research provides novel insights into the regulatory effects of LA on N assimilate partitioning source–sink coordination. Ultimately, these findings will provide the basis for optimizing N management strategies and enhancing crop performance through improved nutrient assimilation and allocation efficiency.

7.2. Materials and methods

7.2.1. Plant materials and seed treatment

Seeds of TX-40J were disinfected with 5% (v/v) sodium hypochlorite for 5 min and washed with ultrapure water, 5 times for 3 min. Sterilized seeds were germinated in Oasis Horticube Propagation Slabs (Aqua Gardening, Australia) and placed in germination trays.

7.2.2. Experimental treatment and growth conditions

Germination trays were moved to a climate-controlled growth room with a 14/10 day-night cycle, 25°C day/22°C night temperatures, and 80% relative humidity for 5 d to allow for seed germination. After 5 d, uniformly germinated seedlings were selected and divided into five treatment groups (T1–T5), then grown in 3 L pots with roots supported by organic expanded clay pellets (Aqua Gardening, Australia). Each treatment group received a specific N source: T1: NO_3^- ($CaNO_3^-$), T2: received 1 mM NO_3^- (sole NO_3^-), T3: received 1 mM NH_4^+ (sole NH_4^+), and T4: received 0.5 mM NH_4NO_3 (mixed N supply). For

T5, 1 mM NH_4^+ was replaced with 1 mM NO_3^- (1 mM NH_4^+→1 mM NO_3^- substitution) at 10 d after seedling transfer, and plants were grown until 40 d after transplanting (DAT). T5 served as the primary group for evaluating the effects of NH_4^+ treatment on maize growth and C metabolism, while T1 through T4 functioned as reference groups for comparative analysis, in alignment with a previous study (Amoah and Kaiser 2025). The use of low, physiologically relevant concentrations of N forms was deliberate and strategic to reflect dynamic field conditions and mitigate NH_4^+ toxicity (Horchani et al. 2010; George et al. 2016; Amoah and Kaiser 2025). This approach enables precise evaluation of N assimilation dynamics and the complex interplay between N forms and C metabolism, facilitating accurate assessment of NUE and highlighting physiological adaptations where N assimilation is not saturated. Plants were cultivated for 40 DAT, with tissue sampling at 20 and 40 DAT (Amoah and Kaiser 2025). The system was established in a climate-controlled glasshouse under environmental conditions identical to those of the seed germination growth room, with supplemental LED lighting delivering 1000 µmol m^{-2} s^{-1} at pot level. Each system accommodated 40 pots, with one plant per pot. Nutrient solutions were delivered via a drip-irrigation system integrated with a hydroponic pump to ensure circulation. Irrigation was administered twice daily for 1 min at 12:00 and 17:00 (Amoah and Kaiser 2025).

7.2.3. Nutrient composition and tissue sampling

The base N nutrient solution contained 1.0 $MgSO_4$, 1.0 KH_2PO_4, 0.05 H_3BO_3, 0.005 $MnSO_4$, 0.001 $ZnSO_4$, 0.001 $CuSO_4$, 0.001 Na_2MoO_4, 0.1 KCl, 0.1 Fe-EDTA, 0.1 Fe-EDDHA, 0.25 $Ca(NO_3)_2$, 0.25 K_2SO_4, 0.25 $CaCl_2$, 1.75 $CaSO_4$ and trace elements, supplemented with three N treatments (1.0 KNO_3, 1.0 $(NH_4)_2SO_4$ or 0.5 NH_4NO_3) (Amoah & Kaiser, 2025). The solution was stored in 162 L Brute Containers with lids (Rubbermaid, USA) and replaced weekly, with daily pH adjustments using 1 M H_2SO_4 or 1 M NaOH to maintain a stable pH of 5.9. The treatment solution was delivered via an Eden 140G FL submersible water pump (Creative Pumps, Australia). Plants were uniquely identified and randomized into blocks using the agricolae package R statistical software (v4.5.0). Fresh leaf and root tissues for biochemical analysis were immediately frozen in liquid N_2. Shoot and root samples for biomass analysis were oven-dried to determine dry weight (DW). Total plant biomass was calculated by summing shoot and root biomass values. For whole-root morphological assessment, uniformly grown maize seedlings from each treatment group (T1–T5) were sampled at 40 days after transplanting (DAT), carefully separated from the shoots, and rinsed with potable water. The entire root systems of six plants per treatment were floated in water in a transparent plastic tray and scanned using an Epson Perfection V700 photo scanner (Epson Australia Pty. Ltd., Australia). Image analysis was performed using The RhizoVision Explorer software (version 2.0.3) (Seethepalli et al. 2021).

7.2.4. Photosynthesis, N, total amino acid and protein content determination

The net photosynthetic rate (Pn) was measured on the young emerging leaf of each treatment using the portable LI-6800 photosynthetic system (LI-COR Inc., Lincoln, NE, USA). Measurements were taken at 9:00 AM and 11:00 AM. Cuvette conditions included a light level of 1000 µmol m^{-2} s^{-1}, CO_2 concentration of 400 ppm, flow rate of 500 µmol m^{-2} s^{-1}, and relative humidity between 60% and 65%. Total chlorophyll pigment was extracted from approximately 0.1 g of leaf tissue using 100% methanol on a shaker at 25°C until the tissue was completely bleached. The extract was then centrifuged at 10,000 × *g* for 10 min, and the absorbance of the supernatant was measured at 652 and 663 nm using a UV-vis spectrophotometer (Shimadzu, Tokyo, Japan). The concentration of chlorophyll was calculated following the method described by (Amoah et al. 2023). N content was determined using a modified Kjeldahl method (Zhao et al. 2020). A 0.2 g dry sample was digested with 0.5 mL concentrated H_2SO_4 and a catalyst mixture (10 g K_2SO_4, 1 g $CuSO_4$) at 100°C for 60 min. After cooling, 0.5 mL of 40% NaOH and 0.5 mL distilled water were added. The mixture was then combined with 1 mL Nessler's reagent and incubated for 10 min. Absorbance at 420 nm was measured using a UV-vis spectrophotometer (Shimadzu, Tokyo, Japan), and leaf total N concentration was calculated from a standard curve of $(NH_4)_2SO_4$ estimated with the same assay.

Total amino acids content was determined using the methods outlined by (Bates et al. 1973). Frozen leaf tissues (100 mg) were homogenized in 10 mL of 3% (v/v) aqueous sulfosalicylic acid. After filtering the homogenate, 1 mL of filtrate was combined with 1 mL of glacial acetic acid and 1 mL of acidic ninhydrin. The resulting mixture was incubated at 100°C for 1 h and then cooled on ice for 20 min before extracting with 1 mL of toluene. The concentrations of amino acids were measured using a spectrophotometer at A580 nm. Leaf and root total protein content was estimated using the Bradford Protein Assay (Bradford 1976), by following manufacturer's protocol (Bio-Rad, South Granville, Australia).

7.2.5. Nitrate (NO_3^-), nitrite (NO_2^-) and ammonium (NH_4^+) determination

NO_3^-, NO_2^-, and NH_4^+ were extracted from 100 mg of dried plant material using 1 mL of water. NO_3^- content was quantified using a colorimetric assay based on the reduction of NO_3^- to NO_2^- by Vanadium (III) (Dechorgnat et al. 2018). NO_2^- levels were determined using the Griess assay (Dechorgnat et al. 2011), while NH_4^+ concentrations were measured using the Ammonium Assay Kit (Sigma-Aldrich, St. Louis, MO, USA, cat# AA0100), following the manufacturer's instructions.

7.2.6. Nitrate reductase (NR), nitrite reductase (NiR), glutamine synthase (GS) and glutamate synthase (GOGAT) activities assay

NR activity was assayed using the method described by Dechorgnat et al. (2018), with minor modifications. A 10 µL aliquot of extracted protein solution was mixed with 90 µL of reaction buffer containing 130 mM K_2HPO_4, 70 mM KH_2PO_4, 0.5 mM KNO_2, and 2 mM methyl viologen. The reaction was initiated by adding 10 µL of a sodium-based reducing solution (20 mg/mL Na_2CO_3 and $Na_2S_2O_4$) and incubated at 30°C for 20 min. The reaction was terminated by vortexing, and NO_2^- content was quantified using the Griess assay (Dechorgnat et al., 2018). GS and GOGAT activities were determined by mixing 20 µL of extracted protein with 80 µL of reaction buffer containing 100 mM hydroxylamine, 125 mM MOPS, 0.5 mM ADP, 12.5 mM sodium arsenate, 37.5 mM glutamine, and 1.25 mM $MnCl_2$. The reaction was incubated at room temperature for 30 min, followed by the addition of 100 µL of detection buffer comprising 370 mM $FeCl_3$, 576 mM HCl, and 157 mM TCA. Optical density was measured at 540 nm, with L-glutamic acid γ-monohydroxymate (GHA) serving as the reference standard (Dechorgnat et al., 2018). NiR activity was assessed by combining 10 mL of extracted protein solution with 90 mL of reaction buffer (130 mM K_2HPO_4, 70 mM KH_2PO_4, 0.5 mM KNO_2, and 2 mM methyl viologen), followed by the addition of 10 mL of 20 mg/mL (Na_2CO_3 and $Na_2S_2O_4$). After incubation at 30 °C for 15 min, the reaction was stopped by vortexing, and NO_2^- concentration was quantified using the Griess assay (Wang et al. 2007).

7.2.7. RNA isolation, cDNA synthesis and qPCR analysis

Total RNA was isolated from leaf and root tissues using the Trizol RNA Isolation Reagents (Invitrogen, Carlsbad, CA, USA) following the manufacturer's protocol. RNA quantity and integrity were assessed by measuring the optical density at 260 nm and through size separation using 1.0% (w/v) agarose gel electrophoresis, respectively. Subsequently, 1 µg of total RNA was reverse-transcribed into single-stranded cDNA using the iScript™ RT Reagent Kit (Bio-Rad, Hercules, CA, USA) according to the manufacturer's instructions. Quantitative real-time polymerase chain reaction (qPCR) was performed using the CFX 96 Real-Time System (Bio-Rad, Richmond, CA, USA) with SYBR Green fluorescence (Bio-Rad, Richmond, CA, USA). The $^{\Delta\Delta}$CT method was used for data analysis. The list of genes studied are provided in Table S7.1. The thermal cycling conditions consisted of an initial denaturation step at 95 °C for 5 min, followed by 40 cycles of 95 °C for 15 s, 55 °C for 15 s, and 72 °C for 30 s. All experiments were conducted with three biological replicates, and relative transcript levels were normalized using *ZmActin1* and *ZmUBQ1* as internal controls.

7.2.8. Statistical analysis

The study was independently conducted twice, with tissue samples collected in triplicate for each experiment. All quantitative data represent the mean ± standard deviation (SD) of six (6) independent

plants (n = 6). Data was analysed using a two-way analysis of variance (ANOVA) to assess the effects of treatment and developmental stage. Post-hoc pairwise comparisons were subsequently performed in GraphPad Prism (version 10) to identify statistically significant differences between groups. In the ANOVA model, plant growth stage (PGS) was designated as a fixed factor, while N treatments (NT) were treated as variable factors. Statistical significance was determined at a probability of $p \leq 0.05$, with differing lowercase letters used to denote significant differences in graphical representations. Graphical visualizations were generated using GraphPad Prism (version 10.4.0), and Pearson's correlation matrices were constructed using R statistical software (version 4.4.5).

7.3. Results

7.3.1. LA promoted root: shoot biomass accumulation and enhanced photosynthesis

At 40 DAT, plants grown with LA treatment exhibited enhanced shoot and root performance, producing larger, well-developed cobs (Figs. S7.1A-B). Furthermore, LA-treated maize plants exhibited significantly ($P \leq 0.05$) increased nitrogen (N) content in both leaf and root tissues at 20 and 40 DAT (Table 7.1). Compared to other nitrogen treatments (NT), LA application increased shoot and root biomass, root-to-shoot (R/S) ratio, net photosynthetic rate (Pn), and chlorophyll content. Additionally, LA-treated plants accumulated higher total protein and amino acid levels in both leaves and roots. Root morphological traits, such as total root length (TRL), root volume (RV), and root surface area (RSA), were also significantly ($P \leq 0.05$) enhanced under LA treatment, contributing to improved root development and an elevated R/S ratio (Table 7.1). Plant growth stage (PGS) and NT independently influenced all assessed parameters, such as biomass, N content, protein and amino acid concentrations, chlorophyll content, Pn, and root morphology. Notably, the interaction between PGS and NT significantly affected all shoot and leaf indicators, as well as the root biomass, R/S ratio, RSA, and TRL (Table S7.2).

7.3.2. LA enhanced both N accumulation and its subsequent assimilation pathways

Plants grown under the different NTs exhibited distinct patterns of NO_3^-, NO_2^-, and NH_4^+ accumulation in both leaves and roots of maize seedlings at 20 and 40 DAT. Notably, NFS ($NH_4^+ \rightarrow NO_3^-$)-treated plants showed significantly ($P \leq 0.05$) higher levels of NO_3^- and NO_2^- in both tissues, whereas LA-treated plants accumulated greater amounts of NH_4^+ in leaves and roots (Fig. 7.1). Corresponding to these patterns, NO_3^- and NO_2^- assimilation enzyme activities (NR and NiR) were significantly upregulated in the leaves and roots of NFS plants (Figs. 7.2A–B, E–F), while NH_4^+ assimilation enzymes (GS and GOGAT) displayed elevated activity in LA plants (Figs. 7.2C–D, G–H). As shown in

Table S7.2, PGS, NT, and their interaction (PGS × NT) significantly influenced NO_3^-, NO_2^-, and NH_4^+ contents, along with their associated enzyme activities in both leaf and root tissues.

7.3.3. Diurnal changes of NO_3^- and NH_4^+ under different N forms

The diurnal patterns of NO_3^- and NH_4^+ levels increased during the early morning (7:00 AM), peaked at midday (12:00 PM), and declined sharply thereafter, with low levels persisting until the following morning (Figs. 7.3A–B). These fluctuations were consistent across both 20 and 40 DAT (Figs. 7.3A–D). At 20 DAT, significant differences ($P \leq 0.05$) in NO_3^- and NH_4^+ concentrations were observed among treatments: NFS-treated plants consistently exhibited elevated NO_3^- levels, while LA-treated plants accumulated higher NH_4^+ throughout the day. Following the initial morning rise, NO_3^- and NH_4^+ levels declined by midday and subsequently increased overnight. Notably, after overnight transport, NFS-treated plants retained higher NO_3^-, whereas LA-treated plants maintained elevated NH_4^+ concentrations relative to other treatments (Fig. 7.3).

7.3.4. Spatial distribution of NO_3^- and NH_4^+ under different forms

The spatial distribution of NO_3^- and NH_4^+ across various maize tissues, including upper, middle, and basal leaves, leaf sheaths, and roots, was analyses. NFS-treated plants exhibited significantly ($P \leq 0.05$) higher NO_3^- concentrations, whereas LA-treated plants showed elevated NH_4^+ levels. At 22:00, the leaves (upper, middle, and basal) and roots displayed increased NO_3^- and NH_4^+ levels, indicating enhanced nitrogen accumulation and retention. Notably, by 22:00, NFS-treated plants maintained elevated NO_3^- concentrations, while LA-treated plants exhibited higher NH_4^+ accumulation in the leaves, reflecting sustained metabolite levels following overnight remobilization. Additionally, in the sink tissues (roots), both NO_3^- and NH_4^+ concentrations were comparatively higher and differed significantly ($P \leq 0.05$) among NTs at both 22:00 and 07:00 (Fig. 7.4A–D), highlighting distinct nitrogen dynamics across the diurnal cycle.

7.3.5. Expression pattern of N assimilation and transporter gene under different N conditions

Furthermore, the NO_3^-- (*ZmNR1* and *ZmNiR*1) and NH_4^+-related (*ZmGS1* and *ZmGOGAT1*) genes were differentially expressed in the leaves and roots of maize seedlings. Notably, *ZmNR1* and *ZmNiR1* were strongly upregulated in both tissues of NFS-treated plants, while LA treatment significantly enhanced the expression of *ZmGS1* and *ZmGOGAT1* (Figs. 7.5A–H). Consistent with the expression profiles of *ZmNR1* and *ZmNiR1*, the nitrate transporter genes *ZmNPF6.2* and *ZmNRT2.1* were significantly induced in the leaves and roots of NFS-treated seedlings (Figs. 7.6A–B, E–F). In contrast, the

ammonium transporter genes *ZmAMT1.1* and *ZmAMT2.1* were highly expressed in seedlings subjected to LA treatment (Figs. 7.6C–D, G–H). Additionally, the expression levels of *ZmNR1*, *ZmNiR1*, *ZmGS1*, *ZmGOGAT1*, *ZmNPF6.2*, *ZmNRT1.1*, *ZmAMT1.1*, *and ZmAMT2.1* were significantly influenced by PGS, NT, and their interaction (PGS × NT (Table S7.2).

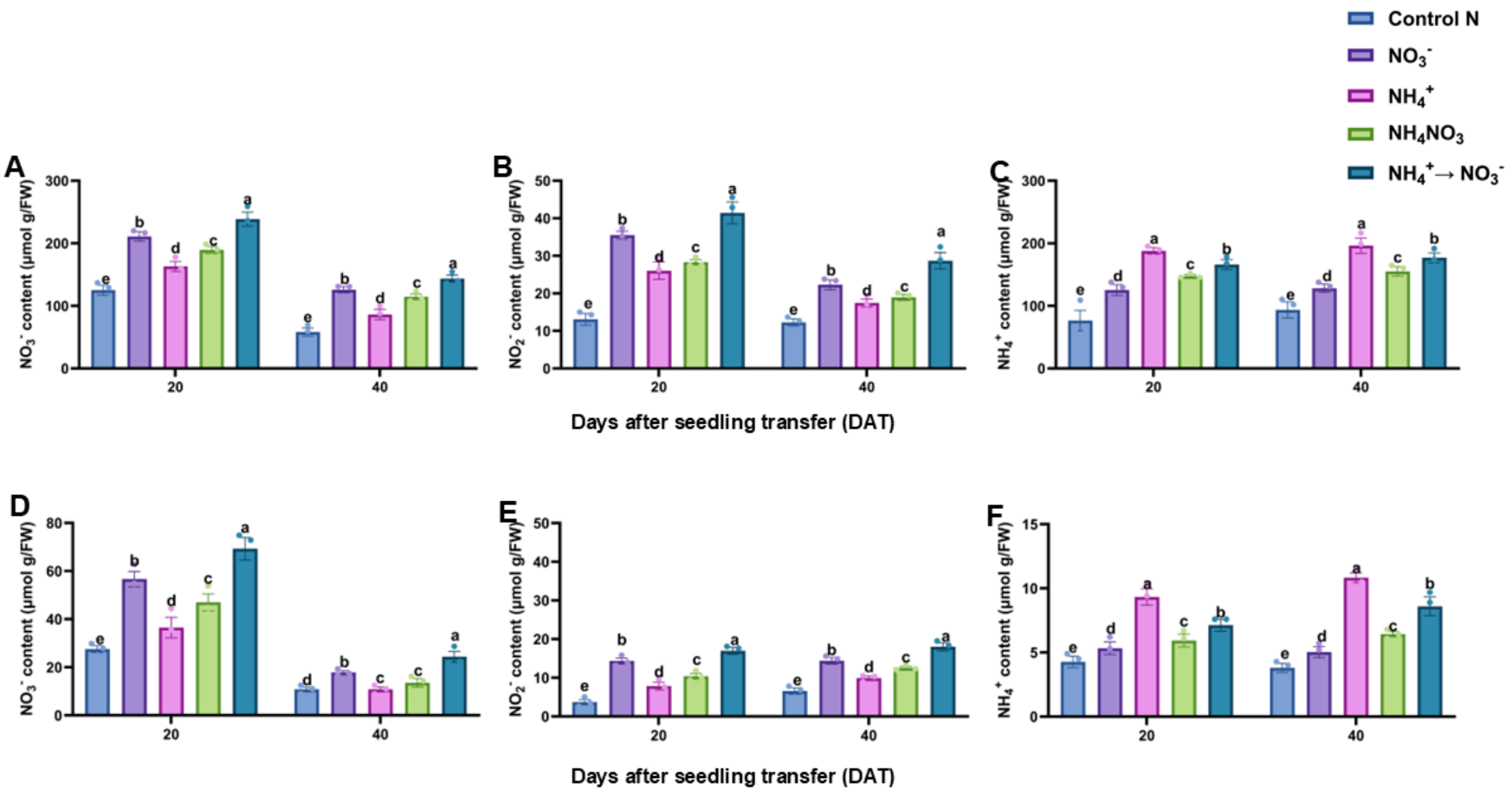

Fig. 7.1 Effect of different nitrogen (N) treatment on N assimilate accumulation in maize. Nitrate, nitrite and ammonium concentration in the leaves (**A-C**) and root (**C-F**) of maize seedlings. Data points represent the mean ± standard (SD) from six independent biological replicates (n = 6). Different letters above the error bars indicate statistically significant differences at $p \leq 0.05$. Abbreviation: FW, fresh weight.

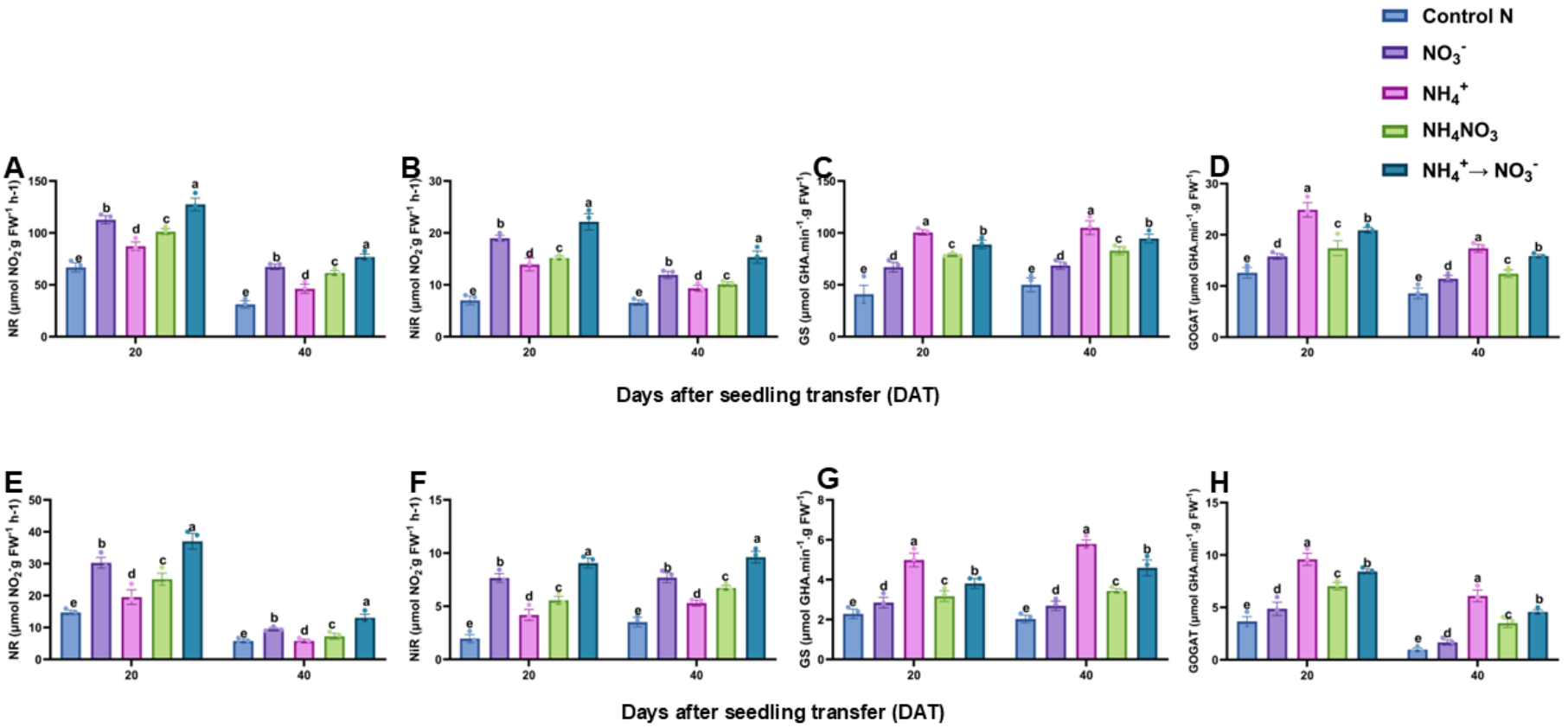

Fig. 7.2 Impact of nitrogen forms on the activity of nitrogen (N) assimilation enzymes. Nitrate reductase, nitrite reductase, glutamine synthase and glutamate synthase activity in the leaves (**A-D**) and root (**E-H**) tissues of maize. Data points represent the mean ± standard (SD) from six independent biological replicates (n = 6). Different letters above the error bars indicate statistically significant differences at $p \leq 0.05$. Abbreviation: FW, fresh weight.

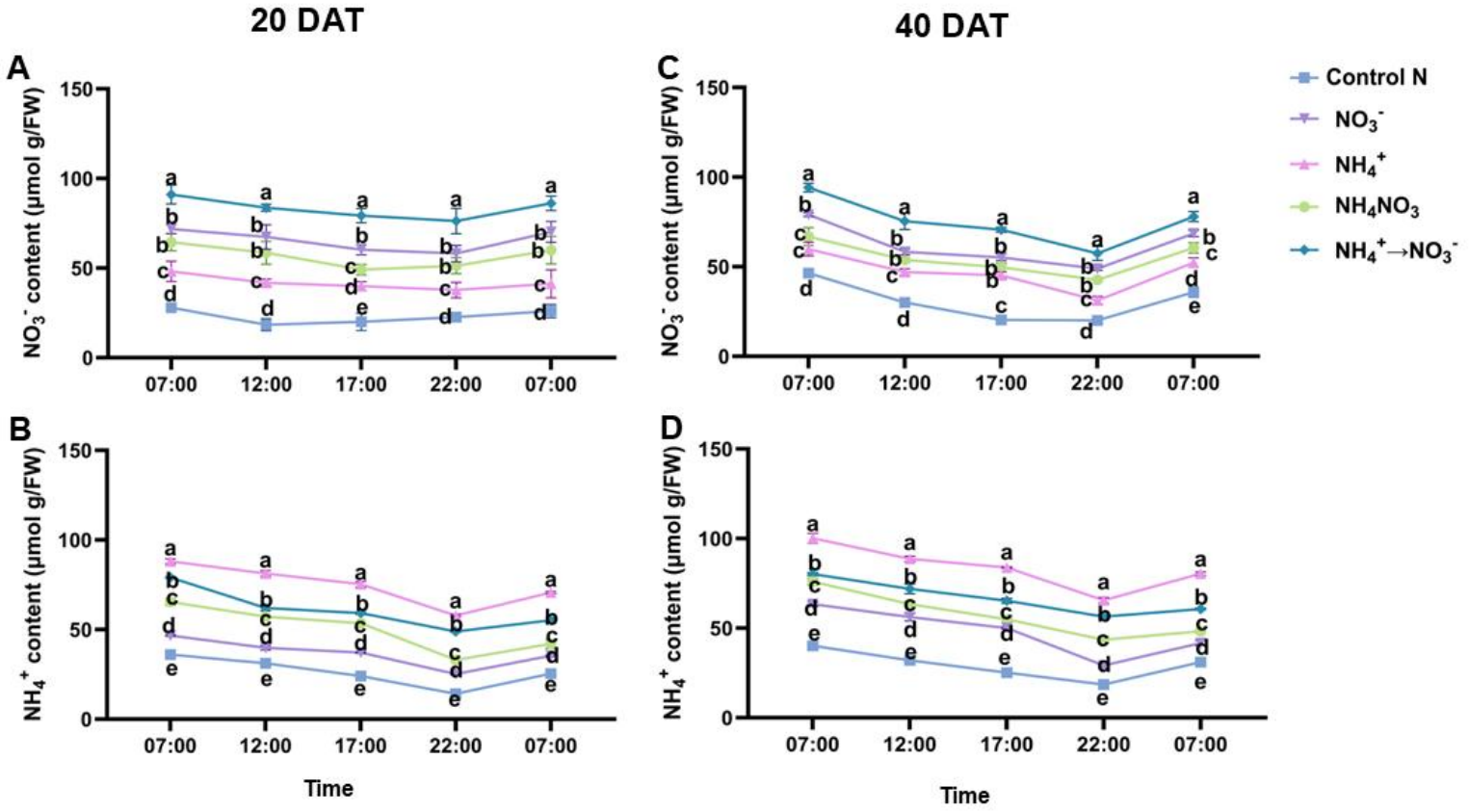

Fig. 7.3 Diurnal changes in leaf NO_3^- (**A**) and NH_4^+ (**B**) at 20 days after transfer (DAT) and leaf sucrose NO_3^- (**C**) and NH_4^+ (**D**) at 40 DAT under different nitrogen treatments. Samples were collected at 7:00, 12:00, 17:00, 22:00, and 7:00 on the second day. Data are presented as mean ± standard deviation (n = 6). Statistical significance was determined using Tukey's multiple range test ($P < 0.05$), with different letters indicating significant differences among treatments. FW denotes fresh weight of tissue samples.

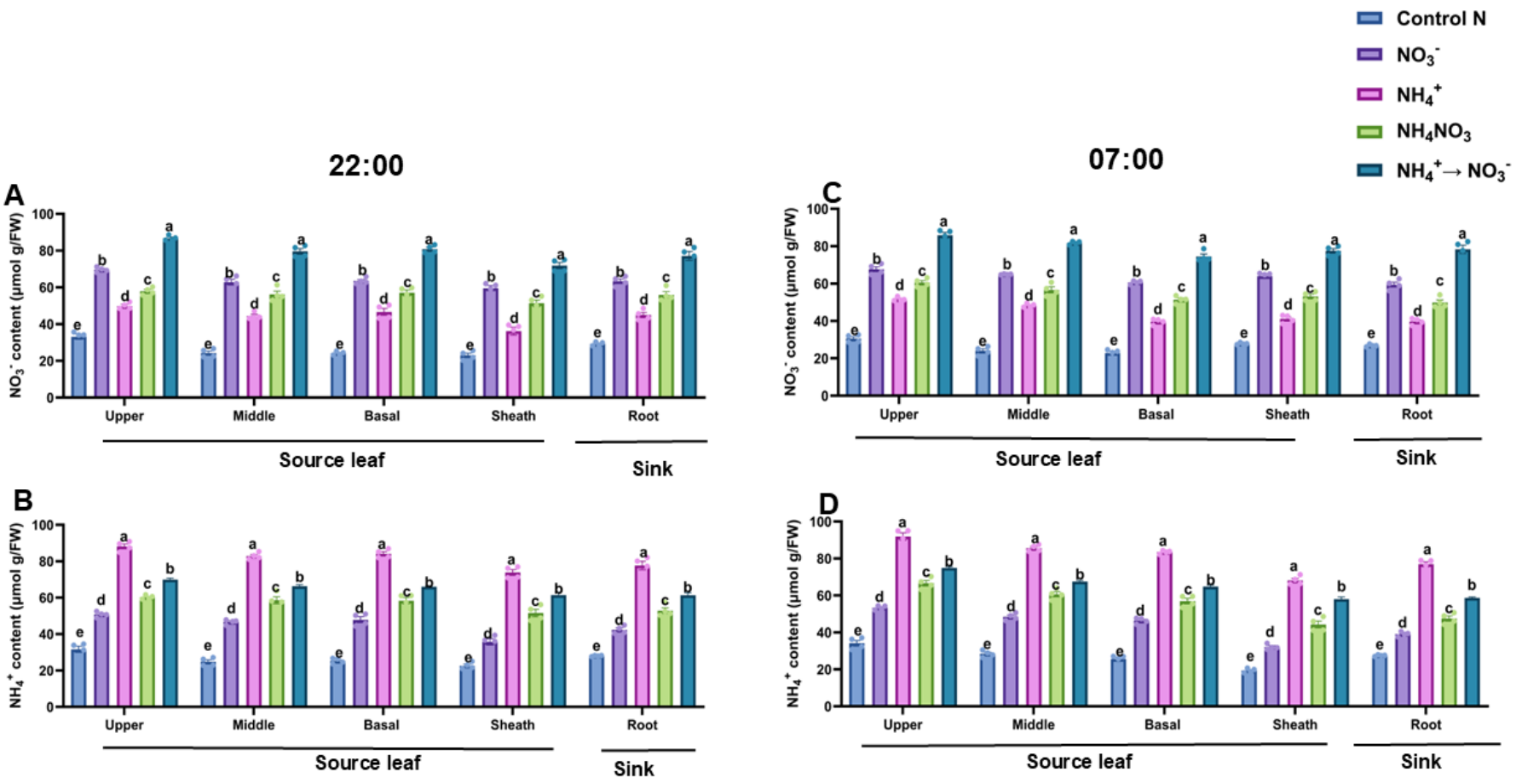

Fig. 7.4 Leaf NO_3^- (**A**) and NH_4^+ (**B**) at 20 DAT and leaf NO_3^- (**C**) and NH_4^+ (**D**) at 40 DAT in different tissues under various nitrogen form treatments. Data are presented as mean ± standard deviation (n = 6). Statistical significance was determined using Tukey's multiple range test ($P < 0.05$), with different letters indicating significant differences among treatments. FW denotes fresh weight of tissue samples.

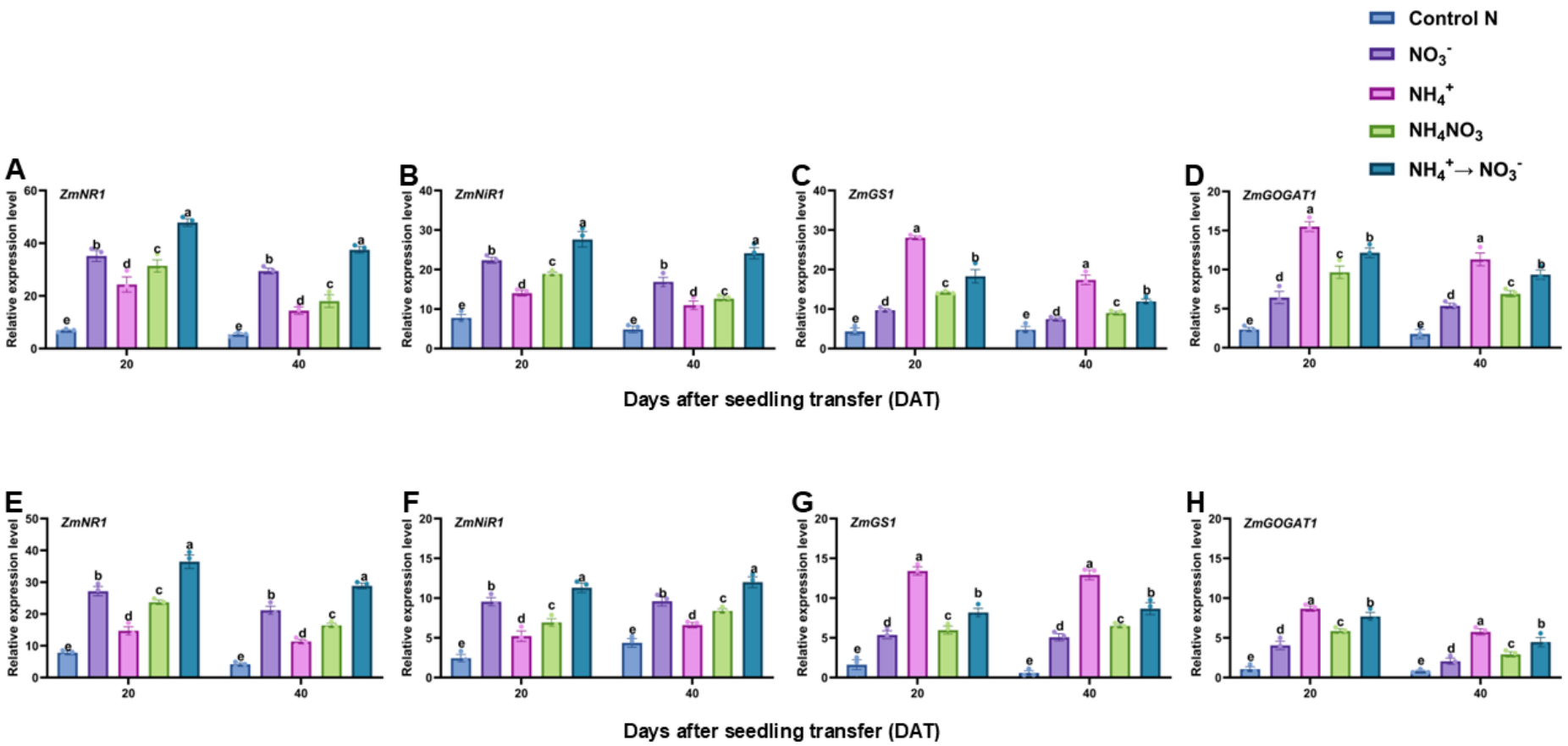

Fig. 7.5 Transcriptional regulation of nitrogen (N) assimilation genes. Expression level of *ZmNR1*, *ZmNiR1*, *ZmGS1* and *ZmGOGAT1* in the leaves (**A-D**) and roots (**E-H**) of maize seedlings exposed to different nitrogen forms. Data points represent the mean ± standard deviation (SD) of six independent biological replicates (n = 6). Different letters above the error bars indicate statistically significant differences at $p \leq 0.05$.

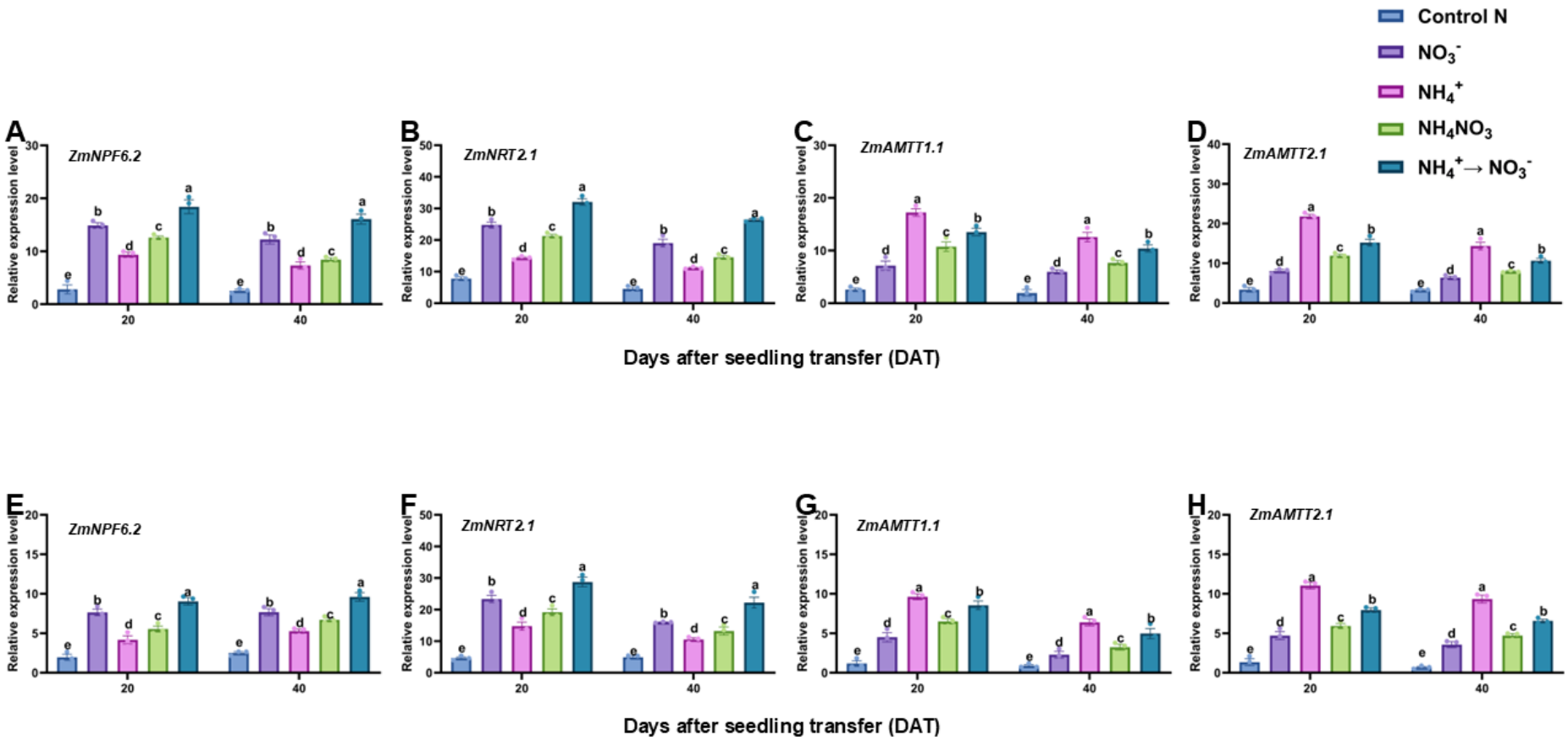

Fig. 7.6. Transcriptional regulation of nitrate (NO_3^-) and ammonium (NH_4^+) transporter genes. Expression level of *ZmNPF6.2*, *ZmNRT2.1*, *ZmAMT1.1* and *ZmAMT2.1* in the leaves (**A-D**) and roots (**E-H**) of maize seedlings exposed to different nitrogen forms. Data points represent the mean ± standard deviation (SD) of six independent biological replicates (n = 6). Different letters above the error bars indicate statistically significant differences at $p \leq 0.05$.

Table 7.1 Effect of different nitrogen forms on biomass, photosynthesis, root morphology, total protein and total amino acid contents

Shoot	20 DAT					40 DAT				
	Control N	**NO_3^-**	**NH_4^+**	**NH_4NO_3**	**$NH_4^+ \rightarrow NO_3^-$**	**Control N**	**NO_3^-**	**NH_4^+**	**NH_4NO_3**	**$NH_4^+ \rightarrow NO_3^-$**
Biomass	0.17 ± 0.01e	0.24 ± 0.01d	0.57 ± 0.03a	0.35 ± 0.02c	0.45 ± 0.03b	0.57 ± 0.04e	1.09 ± 0.10d	2.09 ± 0.09a	1.35 ± 0.14bc	1.74 ± 0.09b
TB	0.25 ± 0.02e	0.38 ± 0.04d	0.79 ± 0.04a	0.46 ± 0.02c	0.63 ± 0.04b	0.78 ± 0.04e	1.34 ± 0.09d	2.69 ± 0.12a	1.73 ± 0.15c	2.18 ± 0.09b
Pn	17.37 ± 1.23e	22.70 ± 1.65d	38.21 ± 1.63a	27.27 ± 1.55c	31.77 ± 1.20b	21.15 ± 1.20d	29.77 ± 1.54c	39.87 ± 2.31a	35.10 ± 0.99b	34.25.53b
Chl	30.10 ± 3.57e	62.32 ± 3.19d	91.95 ± 2.31a	74.81 ± 5.36c	75.60 ± 5.50b	28.75 ± 4.37e	57.97 ± 1.96d	92.25 ± 5.83a	62.49 ± 1.63c	79.15 ± 3.42b
TN	27.15 ± 3.14d	50.39 ± 4.73cc	76.35 ± 3.08a	52.55 ± 1.34b	59.21 ± 5.34b	35.59 ± 2.61e	50.11 ± 3.66d	78.10 ± 1.47a	58.10 ± 4.41c	68.36 ± 3.53b
Protein	1.86 ± 0.13e	2.53 ± 0.24d	4.91 ± 0.23a	3.330 ± 0.12c	3.73 ± 0.18b	7.23 ± 0.80d	17.35 ± 1.46c	41.30 ± 2.29a	17.33 ± 1.46c	29.20 ± 1.45b
AA	2.96 ± 0.32e	5.23 ± 0.15d	9.90 ± 0.59a	5.81 ± 0.45c	7.06 ± 0.28b	4.10 ± 0.32e	17.41 ± 2.25d	34.93 ± 2.34a	24.49 ± 1.69c	28.490 ± 1.27b

Root	20 DAT					40 DAT				
	Control N	**NO_3^-**	**NH_4^+**	**NH_4NO_3**	**$NH_4^+ \rightarrow NO_3^-$**	**Control N**	**NO_3^-**	**NH_4^+**	**NH_4NO_3**	**$NH_4^+ \rightarrow NO_3^-$**
Biomass	0.073 ± 0.01d	0.14 ± 0.01c	0.25 ± 0.02a	0.11 ± 0.01c	0.18 ± 0.01b	0.11 ± 0.01e	0.28 ± 0.04d	0.54 ± 0.03a	0.35 ± 0.02c	0.43 ± 0.03b
R/S	0.78 ± 0.04e	1.34 ± 0.09d	2.639 ± 0.12a	1.73 ± 0.15c	2.18 ± 0.09b	0.28 ± 0.045e	0.25 ± 0.18d	0.323 ± 0.02a	0.25 ± 0.02c	0.28 ± 0.03b
NR	259.45 ± 22.15d	233.10 ± 11.70e	326.31 ± 41.37a	244.85 ± 27.43c	315.05 ± 25.66b	352.31 ± 62.65e	594.12 ± 35.34d	1177.55 ± 61.42a	695.7±52.55c	926.05 ±65.07b
TRL	77.67 ± 7.92b	12.93 ± 2.05e	108.46 ± 8.74a	41.16 ± 3.33d	45.39 ± 3.23c	89.33 ± 11.7ce	98.16 ± 14.35d	309.46 ± 29.35a	148.07±19.57c	209.30 ± 28.06b
RV	2.29 ± 0.42d	2.57 ± 0.24c	4.28 ± 1.87b	1.85 ± 0.49e	4.38 ± 0.67a	36.08 ± 3.28e	43.47 ± 5.23d	169.27 ± 14.16a	78.77 ± 14.88c	118.03 ± 11.30b
RSA	135.09 ± 45.89e	221.99 ± 89.82d	427.58 ± 11.44a	262.47 ± 24.67c	316.64 ± 33.02b	291.09 ± 32.59e	440.64 ± 66.61d	1420.49 ±115.23a	581.79±147.81c	876.29 ± 53.77b
Protein	1.06 ± 0.09e	1.96 ± 0.15d	3.23 ± 0.09a	2.26 ± 1.15c	2.81 ± 1.17b	1.79 ± 0.15e	2.36 ± 0.22d	4.31 ± 0.21a	2.86 ± 0.12c	3.75 ± 0.15b
AA	1.710 ±0.25e	2.56 ±0.08d	6.11 ±0.52a	3.03 ±0.29c	4.36 ±0.41b	1.30 ±0.15e	2.36 ±0.22d	4.38 ±0.21a	2.86 ±0.12c	3.70 ±0.15b

Data points represent the mean ± standard error (SE) from six independent biological replicates (n = 6). Different letters attached to standard error values indicate statistically significant differences at $p \leq 0.05$. Abbreviations: -N, treatment without nitrogen (nitrogen free); DAT, days after seedling transfer; TB, total biomass; Pn, net photosynthetic rate; Chl, chlorophyll content; TN, total nitrogen; AA, total amino acid content; R/S, root-shoot-ratio; NR, number of roots; TRL, total root length (cm); RV, root volume (cm^{-3}); RSA, root surface area (cm^{-3}); and $NH_4^+ \rightarrow NO_3^-$, a change of nutrition from ammonium to nitrate.

7.4. Discussion

Nitrogen (N) is an essential macronutrient for plant growth and development, primarily present in soils as NO_3^- and NH_4^+, the two main inorganic forms absorbed by plant roots (Peng et al. 2023a). The influence of N forms on plant physiology has been extensively studied across various species. However, a significant gap remains in understanding the complex mechanisms by which dynamic shifts between N forms (NFS) differentially affect plant growth and N metabolism. Our recent study demonstrated that substituting NO_3^- with NH_4^+ (NO_3^-→NH_4^+) enhanced maize growth, improved photosynthetic performance, and optimized C metabolism, highlighting the potential of NFS in promoting plant growth and metabolic activity (Amoah and Kaiser, 2025). Building on these findings, the present study investigates the reverse transition from NH_4^+ to NO_3^- (NH_4^+→NO_3^-), specifically focusing on its impact on N assimilation, which remains largely unexplored. Understanding this mechanism will offer valuable insight into the differential efficacy of these N shift strategies in maize, contributing to a more comprehensive understanding of plant responses to varying N availability. Given the preferential uptake of NH_4^+ over NO_3^- in maize (Dechorgnat et al. 2018; Zhang et al. 2019b; Amoah and Kaiser 2025), we hypothesize that plants treated with LA may exhibit superior growth and N metabolism compared to those exposed to NH_4^+→NO_3^-, potentially due to the inherent metabolic advantages of NH_4^+ assimilation (Zhang et al. 2019b)

7.4.1. LA treatment enhanced N allocation and utilization, promoting growth in maize

LA-treated plants exhibited significantly enhanced growth, as evidenced by increased root and shoot development, larger and well-formed cobs, and greater overall biomass accumulation (Fig. S7.1). These physiological improvements were accompanied by elevated photosynthetic activity, increased chlorophyll content, improved root morphology, and higher total nitrogen content (Table 7.1). These findings align with our previous study, which reported enhanced shoot and root growth, an increased root-to-shoot ratio, and greater total biomass in maize plants treated solely with NH_4^+ (Amoah and Kaiser, 2025). Furthermore, in our previous study, plants supplied with either NH_4^+ or subjected to an N form shift (NO_3^-→NH_4^+) displayed significantly greater growth and net photosynthetic rates compared to those grown under a sole NO_3^- regime. This supports the notion that NH_4^+-induced metabolic adjustments play a critical role in optimizing N remobilization. This may be attributed to the lower energy cost associated with NH_4^+ assimilation (2 ATP) compared to the 12 ATP required for NO_3^- assimilation (George et al. 2016), thereby enabling more energy-efficient N utilization and maintaining an optimal C-N balance through enhanced N assimilation and efficient protein and amino acid biosynthesis (Liu et al. 2025). Beyond biomass and photosynthetic performance, LA treatment significantly increased root tip number, total root length, root volume, and surface area (Fig. S7.1; Table 7.1). These improvements in root morphology reinforce the concept that NH_4^+ promotes root expansion

and enhances nutrient acquisition efficiency, ultimately supporting greater nitrogen uptake and contributing to increased shoot, root, and total biomass accumulation (Reddy et al. 2025). Notably, LA-treated plants also exhibited elevated total protein and amino acid levels in both leaves and roots, indicating that NH_4^+ directly supports protein biosynthesis via enhanced N assimilation, further reinforcing the metabolic advantages of NH_4^+-based nutrition (Zhang et al. 2019c).

7.4.2. LA treatment suppressed NO_3^- assimilation while promoting NH_4^+ assimilation in maize

LA-treated plants exhibited significantly reduced NO_3^- and NO_2^- accumulation (Fig. 7.1A–B, D–E), consistent with previous findings (Amoah and Kaiser, 2025; Peng et al., 2023; Wang et al., 2019). This likely reflects the substantial energy and reduced investment required for enzymatic conversion of NO_3^- to NH_4^+ during assimilation (George et al., 2016). In contrast, LA-treated plants accumulated markedly higher levels of NH_4^+ in both leaves and roots (Fig. 7.1C–D). Unlike NO_3^-, which requires reduction prior to incorporation into organic compounds, NH_4^+ can be directly absorbed and assimilated by plant roots, explaining its greater accumulation relative to other N treatments (Dechorgnat et al. 2019). These observations align with previous studies reporting enhanced NH_4^+ uptake and tissue retention under NH_4^+ nutrition (Wang et al. 2019; Peng et al. 2023a). Interestingly, the increased NH_4^+ accumulation in LA-treated plants was consistent with elevated total amino acid and protein levels in both leaves and roots, increased GS and GOGAT activities, and higher expression levels of *ZmGS1*, *ZmGOGAT1*, *ZmAMT1.1*, and *ZmAMT2.1* (Table 7.1; Fig. 7.2 and Fig. 7.3C–D, G–H). These results indicate that LA treatment enhanced NH_4^+ assimilation into amino acids via the GS-GOGAT pathway. This rapid conversion, triggered by sustained NH_4^+ supply, likely facilitated the safe storage of excess NH_4^+, promoting its accumulation compared to plants under other nitrogen treatments. The enhanced amino acid synthesis observed in LA-treated plants may serve as an adaptive strategy or detoxification mechanism to counteract the potential toxicity of elevated NH_4^+ levels (Cánovas et al. 2007; Liu and von Wirén 2017). Conversely, the lower NO_3^- content in LA plants were consistent with reduced NR and NiR activities and lower expression of *ZmNR1*, *ZmNiR1*, *ZmNPF6.2*, and *ZmNRT2.1* (Fig. 7.2–7.3A–B, E–F). This suppression reflects a constrained capacity for NO_3^- acquisition and assimilation under LA conditions. Such limitations may result from feedback regulation due to reduced NO_3^- uptake and availability, which is known to downregulate NR and NiR expression (O'Brien et al. 2016; Wang et al. 2018a). Additionally, the downregulation of *ZmNPF6.2* and *ZmNRT2.1* aligns with the repression of NO_3^- transporters under N-limited conditions (Fan et al. 2017; Wang et al. 2022b), while the reduced NR and NiR activities under diminished NO_3^- supply suggest possible post-transcriptional inhibition in response to substrate scarcity (Krapp 2015; Plett et al. 2016).

7.4.3. Diurnal variations in NO_3^- and NH_4^+ accumulation

Diurnal changes in NO_3^- and NH_4^+ pools were examined to investigate potential nitrogen regulatory mechanisms. LA-treated plants consistently exhibited higher NH_4^+ and lower NO_3^- levels throughout the day, highlighting the influence of N availability on metabolic pathways. Interestingly, N-treated plants showed similar diurnal trends, suggesting that these fluctuations may be governed by broader regulatory mechanisms beyond N status alone (Fig. 7.4A–D). Such regulation may be driven by circadian rhythms or light/dark cycles, which modulate enzyme activity and metabolite accumulation independently of short-term N fluctuations (Amoah and Kaiser, 2025). The observed diurnal changes in NH_4^+ and NO_3^- levels did not correspond directly to fertigation events. Instead, the rhythmic pattern, with peaks in the early morning (7:00 AM), declines by midday (12:00 PM), and rises again in the evening (5:00 PM), likely reflects periodic adjustments in root uptake and N assimilation rather than immediate fertilization effects (Hasan et al. 2022). Moreover, LA-treated plants maintained distinct N profiles, characterized by elevated NH_4^+ and reduced NO_3^- accumulation even after overnight transport. The sustained effects of LA treatment on N storage and regulation underscore the plant's adaptive response to N availability (Hasan et al. 2022; Amoah and Kaiser 2025). These findings offer new insights into the complex interplay between N availability, metabolic regulation, and diurnal rhythms, advancing our understanding of how plants adapt to dynamic nutrient conditions.

7.4.4. N availability shapes NO_3^- and NH_4^+ dynamics across maize tissues

The spatial distribution of NO_3^- and NH_4^+ in maize tissues provides critical insights into adaptive responses to different N forms (Fang et al. 2007). In this study, maize plants exhibited differential responses to N sources, consistent with findings that various N forms enhance NO_3^- and NH_4^+ accumulation in leaves, facilitating assimilation, partitioning, and storage (Duan et al. 2023c; Amoah and Kaiser 2025). LA plants displayed elevated NH_4^+ contents across aboveground tissues (upper, middle, basal leaves, and leaf sheath) and roots at 22:00 (Fig. 7.5). Notably, NH_4^+ concentrations were significantly higher and varied across treatments at both 22:00 and 07:00, demonstrating the role of roots as N sinks under LA treatment conditions (Zhao et al. 2020; Amoah and Kaiser 2025). The residual NH_4^+ in the leaves and sheath of NFS-treated plants remained unchanged between 22:00 and 07:00 (Fig. 7.4A–D), integrating diurnal variations with tissue-specific N allocation (Figs. 7.4 and 7.5). This pattern reinforces previous findings that NH_4^+ accumulates overnight (Huanosto Magaña et al. 2009). Tissue-specific N distribution suggests adaptive strategies that sustain metabolic function under LA treatment, including higher NH_4^+ retention in leaves and sheath as a temporary storage pool for remobilization, and roots acting as N sinks to maintain nutrient uptake capacity (Krapp 2015; Masclaux-Daubresse et al. 2008). These results underscore the critical role of N allocation and metabolic processes in maize subjected to LA conditions, suggesting avenues to boost productivity amid variable N supply. Insight into tissue-specific N distribution and key regulatory factors, such as diurnal rhythms and enzymatic

dynamics, can guide targeted breeding and genetic engineering for improved performance in N-limited settings. Ongoing research focuses on elucidating the molecular and enzymatic networks driving these spatial patterns, particularly those controlling N remobilization between source and sink organs.

7.5. Conclusion

The findings of the study show that LA treatment improved overall performance of maize, evidenced by enhanced shoot and root development, biomass accumulation and photosynthesis capacity. LA plants exhibited increased total N levels and accumulation of N assimilates in both the leaves and roots, with these levels sustained across diel cycles. Notably, LA enhanced NUE by leveraging the supply of sustained NH_4^+ to modulate metabolic processes. It enhanced NH_4^+ assimilation via the GS-GOGAT pathways, facilitating amino acid biosynthesis and efficient N incorporation. Increased NR, NiR, GS and GOGAT activities, along with upregulation of *ZmGS1*, *ZmGOGAT1*, *ZmAMT1.1* and *ZmAMT2.1*, highlights the ability of maize plants to fine-tune its N metabolic machinery in response to fluctuating N availability. Spatial analysis further showed that under LA, roots serve as a dynamic N sink, while leaves retain higher NH_4^+ levels overnight, serving as a temporary storage pool for subsequent remobilization. These spatial patterns, coupled with diurnal shifts in N metabolites and enzyme activities, suggest that LA modulates the amplitude and efficiency of circadian-regulated N processes, ultimately enhancing N utilization. These findings highlight the significant advantages of sustained LA regimes, offering a promising strategy to improve NUE and support sustainable agriculture by better mimicking natural N fluctuations. Future research will focus on validating these results through field trials across different maize varieties and exploring the effects of more complex, continuous N fluctuations to truly simulate natural environments, thereby maximizing their applicability and impact. Additionally, integrative anatomical and transcriptomic analyses will offer deeper insights into the physiological adaptations and molecular mechanisms underpinning LA responses, enabling a more comprehensive understanding of how dynamic N supply shapes plant function at various levels.

7.6. Supplementary data

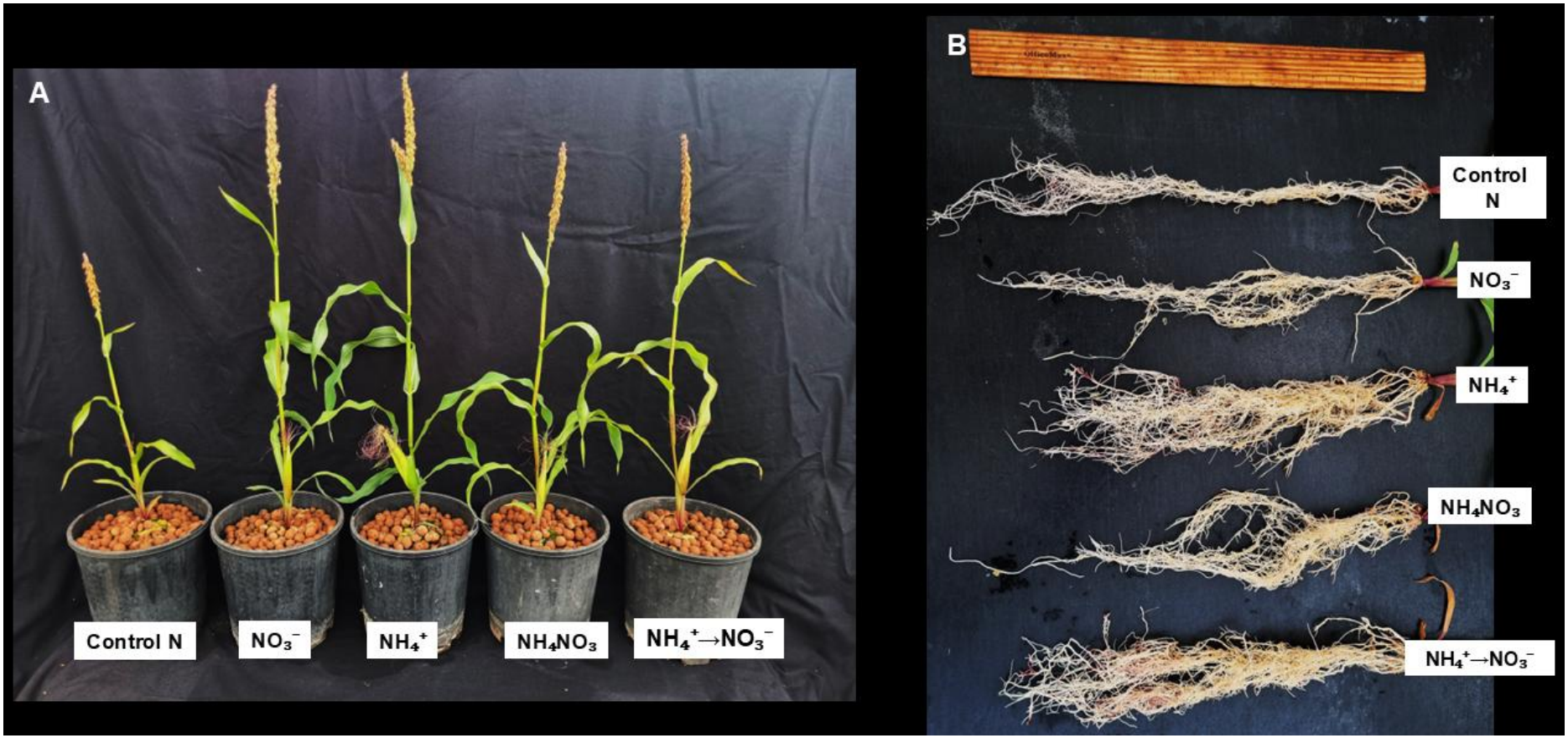

Fig. S7.1 Phenotypic response of the maize inbred line TX-40J to different nitrogen (N) forms. Representative images of shoot morphology (**A**) and root morphology (**B**) at 40 days after nitrogen treatments (DAT).

Table S7.1 List of primers used for quantitative polymerase chain reaction (qPCR) analysis

Gene name	NCBI LOCs
ZmNR	LOC103654219
ZmNiR	LOC103627781
ZmGS	LOC542746
ZmGOGAT	LOC103651348
ZmNRT2	LOC542092
ZmNPF6.2	LOC100383494
ZmAMT1.1	LOC100272903
ZmAMT2.1	LOC100191554
ZmNRT3.1	LOC778428
ZmUBQc	LOC100279740
ZmActin	LOC100282267

Table S7.2 Two-way ANOVA for indicators in the leaves and root of maize

Traits/(plants)	Sources of variation					
	Shoot/leaf			Root		
	PGS (df=1)	NT (df=4)	PGS x NT (df=4)	PGS (df=1)	NT (df=4)	PGS x NT (df=4)
Biomass	0.0003***	0.002**	0.0075**	0.0002***	0.0026**	0.0476*
Total biomass	0.0003***	0.0004***	0.0018**	0.0115*	0.0035**	0.3071ns
Amino acid	0.0009***	0.0068**	0.0107*	0.0287*	0.0125*	0.2208ns
Total protein	0.0005***	0.0007	0.0024**	0.0116*	0.004**	0.1215ns
Ammonium	0.0211*	0.00153**	0.0034**	0.0043**	0.0197*	0.0025**
Nitrogen	0.026*	0.0022**	0.0343*	0.0475*	0.0036**	0.0548ns
Nitrate	0.0123*	0.0103*	0.0242*	0.0352*	0.0004***	0.0218*
RSA	0.0206*	N/A	N/A	0.0475*	0.0019**	0.032*
RV	0.0165*	N/A	N/A	0.0206*	0.0052**	0.0478*
TRL	0.0175*	N/A	N/A	0.0112*	0.0006***	0.1215ns
R/S ratio	0.0214*	N/A	N/A	0.0004***	0.0004***	0.0076**
Chl	0.0052**	0.0002***	0.0344*	N/A	N/A	N/A
NR	0.0214*	<0.0001****	0.0271*	0.0003***	<0.0001****	0.0035**
Pn	0.0017**	<0.0001****	0.0031**	N/A	N/A	N/A
NiR	0.0114*	0.0101*	0.0028**	0.0367*	0.0004***	0.0012**
NR	0.0259*	<0.0001****	0.0016**	0.0109*	0.0039**	0.0005***
GS	0.0008***	<0.0001****	0.0137*	0.8211ns	<0.0001****	0.0109*
GOGAT	0.0441*	0.0001***	0.0172*	0.0017**	0.0002***	0.0031**
ZmNR1	0.8582ns	0.0002***	0.0011**	0.0251*	<0.0001****	0.0157*
ZmNiR1	0.0109*	<0.0001****	0.0005***	0.2598ns	<0.0001****	0.0016**
ZmGS1	0.0151*	<0.0001****	0.0012**	0.2598ns	<0.0001****	0.0016**
ZmGOGAT1	0.0211*	0.0004***	0.0008***	0.0109*	<0.0001****	0.0005***
ZmNPF6.2	0.0025**	<0.0001****	0.0011**	0.0043**	<0.0001****	0.0011**
ZmNRT2.1	0.0044**	0.0002***	0.0101*	0.0197*	<0.0001****	0.0025**
ZmAMT1.1	0.0152*	0.0003***	0.019*	0.0027**	<0.0001****	<0.0001****
ZmAMT2.1	0.0105*	<0.0001****	<0.0001****	0.0081**	<0.0001****	0.0031**

Abbreviations: total biomass; Pn, net photosynthetic rate; Chl, chlorophyll content; R/S, root-shoot-ratio; NR, number of roots; TRL, total root length (cm); RV, root volume (cm^{-3}); RSA, root surface area (cm^{-3}); and $NH_4^+ \rightarrow NO_3^-$, a change of nutrition from ammonium to nitrate. *, **, ***, ****, NS, and NA denotes significance at a probability of 0.05, 0.01, 0.001, 0.0001, not significant and not applicable, respectively. PGS, plant growth stage; NT, nitrogen treatment and PGS x NT, plant growth stage and nitrogen treatment interaction.

CHAPTER 8: AMMONIUM (NH_4^+) REGULATES CARBON METABOLISM AND SPATIAL–DIURNAL ASSIMILATE PARTITIONING TO IMPROVE GROWTH AND NITROGEN USE EFFICIENCY IN MAIZE[7]

Abstract

Nitrogen (N) is primarily taken up by most plant species in the form of nitrate (NO_3^-) and ammonium (NH_4^+) to support growth and metabolic functions. However, the regulatory mechanisms modulating carbon (C) assimilate allocation under varying N forms remain unclear. This study investigated C metabolism and its spatial distribution in maize seedlings subjected to five N treatments (T1–T5): T1, nitrogen-free (control N); T2, 1 mM NO_3^- (sole NO_3^-); T3, 1 mM NH_4^+ (sole NH_4^+); T4, 0.5 mM NH_4NO_3 (mixed N supply); and T5, substitution of 1 mM NH_4^+ with 1 mM NO_3^- ($NH_4^+ \rightarrow NO_3^-$) at 10 days after seedling transfer (DAT). NH_4^+ treatment triggered significant physiological and molecular adaptations, such as enhanced growth, improved photosynthetic performance, and increased sucrose and starch accumulation. These elevated carbohydrate levels were closely associated with increased activity of sucrose-metabolizing enzymes (SuSy, SPS, and INVs) and starch-metabolizing enzymes (AGPase, SS, AMY, and BAM), alongside the upregulation of key genes involved in sucrose metabolism (*ZmSPS1*, *ZmSuSy1*, and *ZmINVs*), sucrose transport (*ZmSWEET14*, *ZmSUT2*, and *ZmSTP2*), and starch metabolism (*ZmSS1*, *ZmAGPase1*, *ZmAMY1*, and *ZmBAM1*). Spatial and diurnal analyses revealed dynamic patterns of C partitioning across the leaves, roots, and leaf sheaths. These findings advance our understanding of how different N forms, particularly NH_4^+, regulate C metabolism and shoot–root allocation to facilitate carbon utilization in sink tissues to improve plant resilience to N fluctuations. Future research will focus on exploring these adaptive mechanisms across diverse maize genotypes under field conditions, with the goal of improving nitrogen use efficiency (NUE) and productivity in variable N environments.

Keyword: *Zea mays*, assimilate allocation, sucrose transport regulation, energetic efficiency, nitrogen use efficiency, root morphology

---

[7]This chapter is published as: Amoah JN, Keitel C, Kaiser BN (2025a) Ammonium (NH_4^+) regulates carbon metabolism and spatial–diurnal assimilate partitioning to improve growth and nitrogen use efficiency in maize. Journal of Plant Physiology 314:154607. doi:10.1016/j.jplph.2025.154607

8.1. Introduction

Nitrogen (N) is an essential macronutrient required for plant growth and development, acting as a primary constituent of biomolecules, such as amino acids, proteins and nucleic acids. It also plays an essential role in various physiological processes, such as photosynthesis, respiration, signal transduction, resistance to abiotic and biotic stress and regulation of seed germination (Dechorgnat et al. 2018; Xu et al. 2024). Despite its abundance in the soil as mineralized N, available N often becomes a limiting factor in crop production due to its high potential for loss (leaching, volatilisation, consumption) and relatively low use efficiency by the intended crop (Mahmud et al. 2021; Govindasamy et al. 2023). N deficiency can inhibit total plant biomass and harvestable yield, impacting the profitability of seed growers (Dechorgnat et al. 2019). This condition compels growers to apply large amounts of inorganic N fertilizers, yet only 45–50% is taken up by crops, with the rest subjected to losses to the environment through volatilization, leaching, and denitrification (Mahmud et al. 2021). Plants primarily utilize nitrate (NO_3^-) and ammonium (NH_4^+) as inorganic N sources, as competition with soil microbes often limits access to organic N. NH_4^+ availability itself can vary with soil type and microbial activity (Mao et al. 2025; Pausch et al. 2024). Understanding crop growth and development under different N forms is therefore crucial for enhancing food security (Amoah et al. 2025a).

Although NO_3^- supply is known to support plant growth, its assimilation requires more energy than NH_4^+. Consequently, relatively few plant species perform well when NH_4^+ is the sole N source, and high NH_4^+ level can even induce toxicity symptoms such as "NH_4^+ syndrome" (Britto and Kronzucker 2002; Horchani et al. 2010; Britto and Kronzucker 2013). This syndrome is characterized by reduced net photosynthesis, appearance of leaf chlorosis, stunted growth, and altered metabolite profiles (Horchani et al. 2010; Peng et al. 2023). Plants often mitigate this toxicity by allocating more assimilates to roots rather than shoots, increasing the root-to-shoot biomass ratio (George et al. 2016; Hachiya and Sakakibara 2017; Amoah and Kaiser 2025; Pélissier et al. 2021). Although molecular mechanisms regulating growth in response to NH_4^+ supply have been elucidated, most studies have focused on root architecture and N assimilation, with limited attention given to C allocation between roots and shoots under NH_4^+ supply conditions (Horchani et al. 2010; Hachiya et al. 2021). The adaptive response of plant roots to NH_4^+ is closely linked to assimilate supply, which serves a signalling role in modulating root responses to NH_4^+ availability (Walch-Liu et al. 2005; Pélissier et al. 2021).

While several studies have examined the comparative effects of NH_4^+ and NO_3^- on plant metabolic processes, and others have investigated dynamic changes in N forms across different plant species, most of these studies included an intervening period of N deficiency before assessing plant responses to a new N source. For instance, Arabidopsis plants previously supplied with NO_3^- nutrition showed enhanced responses to NH_4^+ following N deprivation, suggesting a priming effect that

facilitated NH_4^+ acquisition and assimilation (Ishiyama et al. 2004). Similarly, NH_4^+ transport studies often involved pre-culturing in NH_4NO_3 followed by N deficiency before evaluation (Loqué et al. 2006; Yuan et al. 2007; Wang et al. 2013). These findings highlighted important aspects of N form dynamics and plant acclimation to N fluctuations, particularly in relation to N uptake and transport mechanisms. Despite these advances, little is known about how plants respond to a direct, dynamic and continuous transition between N forms without an intervening deficiency period, especially with regard to C metabolism and its spatial distribution.

The cultivation method of dynamically switching between NO_3^- and NH_4^+ without imposing N deficiency represents a unique feature of our study. This approach enables the evaluation of overlapping effects of N forms while retaining the influence of the preceding N supply, which would otherwise be masked by deficiency treatment. In our previous study, we demonstrated that the NO_3^-→NH_4^+ transition synergistically enhanced maize growth, photosynthesis, and C metabolism, revealing adaptive strategies and synergistic effects absent in plants grown under a single N form (Amoah and Kaiser 2025). Building on these findings, the present study was designed to evaluate the less explored but equally important NH_4^+→NO_3^- transition, with the aim of providing mechanistic insights into its influence on C metabolism in maize. We hypothesize that the NH_4^+→NO_3^- transition may exert a weaker impact on growth and C metabolism compared with the previously observed NO_3^-→NH_4^+ transition, due to the lower energy requirement of NH_4^+ assimilation and the stronger synergistic effects associated with the latter. By integrating dynamic switches between N forms, we aim to elucidate the regulatory mechanisms that modulate growth, C metabolism, and resource utilization under fluctuating N conditions. This will advance our understanding of plant adaptation and contribute to the development of crops with improved nitrogen use efficiency (NUE).

Maize (*Zea mays* L.) was selected due to its importance as a staple food crop and its suitability as a model for N metabolism and C allocation studies (Dong et al. 2023). The fast-flowering, short-cycle inbred mini-maize line TX-40J offers advantages for controlled, high-throughput experiments, enabling a precise dissection of fundamental metabolic and regulatory mechanisms at early developmental stages (McCaw et al. 2016; McCaw et al. 2021). This study aims to elucidate the mechanisms modulating C allocation between shoot and root tissues in maize. Specifically, we examined the effects of different N forms, primarily NO_3^- and NH_4^+, on key enzymes involved in sucrose metabolism in shoot and root sinks. Additionally, we examined diurnal changes in assimilate levels in source leaves and tracked their distribution across various tissues during vegetative and reproductive stages under different N treatments. The findings will advance our understanding of how N form influences C allocation and provide valuable insights for improving crop performance.

8.2. Materials and methods

8.2.1. Plant materials and seed treatment

Seeds of the fast-flowering, short-cycle inbred mini-maize line TX-40J were used in this study (Amoah et al. 2025b). They were disinfected with 5% (v/v) sodium hypochlorite for 5 min and washed with ultrapure water for 5 times (3 min each). Sterilized seeds were then germinated in Oasis Horticube Propagation Slabs (Aqua Gardening, Australia), an inorganic and pH-neutral growing foam and placed in germination trays.

8.2.2. Experimental treatment and growth conditions

Germination trays were moved to a climate-controlled growth room with a 14/10 day-night cycle, 25°C day/22°C night temperatures, and 80% relative humidity for 5 d to allow for seed germination. After 5 d, uniformly germinated seedlings were selected and divided into five treatment groups (T1–T5), then grown in 3 L pots with roots supported by organic expanded clay pellets (Aqua Gardening, Australia). Each treatment group received a specific N source: T1: received no nitrogen (Control N or N free), T2: received 1 mM NO_3^- (sole NO_3^-), T3: received 1 mM NH_4^+ (sole NH_4^+), and T4: received 0.5 mM NH_4NO_3 (mixed N supply). For T5, 1 mM NH_4^+ was replaced with 1 mM NO_3^- (1 mM $NH_4^+ \rightarrow$1 mM NO_3^- substitution) at 10 d after seedling transfer, and plants were grown until 40 d after transplanting (DAT) (Fig. S8.1). T3 and T5 served as the primary groups for assessing the effects of N form substitution and NH_4^+ treatment, respectively, on maize growth and C metabolism, while T1, T2, and T4 acted as reference groups for comparative analysis, in line with our previous studies (Amoah & Kaiser, 2025). The use of low, physiologically relevant concentrations of N forms was deliberate and strategic to reflect dynamic field conditions and mitigate NH_4^+ toxicity (George et al. 2016; Amoah and Kaiser 2025). This approach enables precise evaluation of N assimilation dynamics and the complex interplay between N forms and C metabolism, facilitating accurate assessment of NUE and highlighting physiological adaptations where N assimilation is not saturated. Plants were cultivated for 40 DAT, with tissue sampling at 20 and 40 DAT (Amoah & Kaiser, 2025). The system was established in a climate-controlled glasshouse under environmental conditions identical to those of the seed germination growth room, with supplemental LED lighting delivering 1000 µmol $m^{-2}s^{-1}$ at pot level. Each system accommodated 40 pots, with one plant per pot. Nutrient solutions were delivered via a drip-irrigation system integrated with a hydroponic pump to ensure circulation. Irrigation was administered twice daily for 1 min, at 12:00 and 17:00 (Amoah & Kaiser, 2025). To minimize nitrification and ensure NH_4^+-specific effects, all hydroponic systems were sterilized prior to use, with nutrient solutions replaced weekly and pH adjusted daily to maintain stability. Although complete suppression of microbial activity may not be guaranteed, the low microbial load and tightly controlled conditions likely reduced NO_3^-

formation to minimal levels. We acknowledge the possibility of partial nitrification and its potential influence on interpreting NH_4^+-related physiological responses.

8.2.3. Nutrient composition and tissue sampling

The nutrient solution contained the specific concentrations (mM) of various minerals, such as 1.0 KNO_3, 1.0 $(NH_4)_2SO_4$, 0.5 NH_4NO_3, 1.0 $MgSO_4$, 1.0 KH_2PO_4, 0.05 H_3BO_3, 0.005 $MnSO_4$, 0.001 $ZnSO_4$, 0.001 $CuSO_4$, 0.001 Na_2MoO_4, 0.1 KCl, 0.1 Fe-EDTA, 0.1 Fe-EDDHA, 0.25 $Ca(NO_3)_2$, 0.25 K_2SO_4, 0.25 $CaCl_2$, and 1.75 $CaSO_4$ and trace elements (Amoah & Kaiser, 2025). The elemental composition of all treatments is provided in Table S3. The solution was stored in 162 L Brute Containers with lids (Rubbermaid, USA) and replaced weekly, with daily pH adjustments using 1 M H_2SO_4 or 1 M NaOH to maintain a stable pH of 5.9. The treatment solution was delivered via an Eden 140G FL submersible water pump (Creative Pumps, Australia). Plants were uniquely identified and randomized into blocks using the *agricolae* package R statistical software (v4.5.0). Fresh leaf and root tissues for biochemical analysis were immediately frozen in liquid N_2. Shoot and root samples for biomass analysis were oven-dried to determine dry weight. Total plant biomass was calculated by summing shoot and root biomass values. For whole-root morphological assessment, uniformly grown maize seedlings from each treatment group (T1–T5) were sampled at 40 d after transplanting (DAT), carefully separated from the shoots, and rinsed with potable water. The entire root systems of 6 plants per treatment were floated in water in a transparent plastic tray and scanned using an Epson Perfection V700 photo scanner (Epson Australia Pty. Ltd., Australia). Image analysis was performed using The RhizoVision Explorer software (version 2.0.3) (Seethepalli et al. 2021).

8.2.4. Photosynthesis, N, total amino acid and protein content determination

The net photosynthetic rate (Pn) was measured on the young emerging leaf of each treatment using the portable LI-6400 photosynthetic system (LI-COR Inc., Lincoln, NE, USA). Measurements were taken at 9:00 AM and 11:00 AM. Cuvette conditions included a light level of 1000 µmol m^{-2} s^{-1}, CO_2 concentration of 400 ppm, flow rate of 500 µmol m^{-2} s^{-1}, and relative humidity between 60% and 65%. Total chlorophyll pigment was extracted from approximately 0.1 g of leaf tissue using 100% methanol on a shaker at 25°C until the tissue was completely bleached. The extract was then centrifuged at 10,000 × g for 10 min, and the absorbance of the supernatant was measured at 652 and 663 nm using a Uv-vis spectrophotometer (Shimadzu, Tokyo, Japan). The concentration of chlorophyll was calculated following the method described by Amoah et al. (2023).

Total N content was determined using a modified Kjeldahl method. A 0.2 g dry sample was digested with 0.5 mL concentrated H_2SO_4 and a freshly prepared catalyst mixture consisting of 10 g

K_2SO_4 and 1 g $CuSO_4 \cdot 5H_2O$. Each component was finely ground separately using a porcelain mortar and pestle, then thoroughly mixed and passed through a mesh sieve to ensure homogeneity, following standard protocols (Bremner and Mulvaney 1982; Jones 2001). The mixture was stored in a dry, airtight container at room temperature until use. Digestion was carried out at 100°C for 60 minutes. After cooling, 0.5 mL of 40% (v/v) NaOH and 0.5 mL distilled water were added. The mixture was then combined with 1 mL Nessler's reagent and incubated for 10 minutes. Absorbance at 420 nm was measured using a UV-vis spectrophotometer (Shimadzu, Tokyo, Japan), and leaf total nitrogen concentration was calculated from a standard curve generated using $(NH_4)_2SO_4$.

Total amino acids content was determined using the methods outlined by Bates et al. (1973). Frozen leaf tissues (100 mg) were homogenized in 10 mL of 3% (v/v) aqueous sulfosalicylic acid. After filtering the homogenate, 1 mL of filtrate was combined with 1 mL of glacial acetic acid and 1 mL of acidic ninhydrin. The resulting mixture was incubated at 100°C for 1 h and then cooled on ice for 20 min before being extracted with 1 mL of toluene. The concentrations of amino acids were measured using a spectrophotometer at A580 nm. Leaf and root total protein content was estimated using the Bradford Protein Assay (Bradford 1976), by following manufacturer's protocol (Bio-Rad, South Granville, Australia).

8.2.5. Quantification of soluble sugar and starch

Soluble sugar and sucrose contents were determined following the method described by Xiao et al. (2024). Ground samples (0.1 g) were homogenized in 1 mL of 80% (v/v) ethanol and heated at 80°C for 30 min. After cooling for 5 min, the mixture was centrifuged at 12,000×*g* for 10 min. The supernatants were collected to determine soluble sugar and sucrose contents using a UV-Vis spectrophotometer (Shimadzu, Tokyo, Japan), with absorbance recorded at 620 nm and 480 nm, respectively. For starch content, 1 mL of distilled water was added to the ethanol-insoluble residues and incubated for 30 min. Starch was hydrolysed with 9.2 M and 4.6 M perchloric acid solutions. The starch content was quantified using anthrone reagent, and absorbance was measured at 620 nm (Du et al. 2020). The hexose concentration was calculated as the summation of the concentration of fructose and sucrose (Amoah and Kaiser 2025).

8.2.6. Sucrose phosphate synthase (SPS), sucrose synthase (SuSy), cell wall invertase (CWIN), cytoplasmic invertase (CIN), and vacuolar invertase (VIN) activity

To assay SPS and SuSy activities, 0.1 g of frozen tissue was homogenized in an extraction buffer containing 50 mM Tris-HCl (pH 7.5), 1 mM EDTA, 1 mM $MgCl_2$, 12.5% (v/v) glycerol, 10% polyvinylpyrrolidone (PVP), and 10 mM β-mercaptoethanol. Enzyme activities related to sucrose

metabolism were subsequently measured using the resulting extract, following the method described by Du et al. (2020). Briefly, 200 μL of the supernatant was mixed with a reaction buffer containing 200 mM Tris-HCl (pH 7.0), 40 mM $MgCl_2$, 12 mM UDP-glucose, 40 mM fructose-6-phosphate, and 200 μL of the extract. An additional reaction buffer was prepared for SuSy activity, consisting of 12 mM UDP, 40 mM sucrose, 200 mM Tris-HCl (pH 7.0), and 40 mM $MgCl_2$. The mixtures were incubated at 30 °C for 30 min and the reactions were terminated by adding 100 μL of 2 mol L^{-1} NaOH. To eliminate unreacted hexose and hexose phosphates, the mixture was heated at 100 °C for 10 min, cooled to room temperature, and then reacted with 1 mL of 0.1% (w/v) resorcinol in 95% (v/v) ethanol and 3.5 mL of 30% (w/v) HCl. The solution was incubated at 80 °C for 10 min. Sucrose content (for SPS activity) and fructose content (for SuSy activity) were quantified using standard curves, with absorbance measured at 480 nm and 540 nm, respectively.

For cytoplasmic invertase (CIN), vacuolar invertase (VIN), and cell wall invertase (CWIN) activities, 0.1 g of ground tissue was homogenized in 1 mL of ice-cold extraction buffer containing 50 mM HEPES-NaOH (pH 7.5), 5 mM $MgCl_2$, 0.1% (v/v) β-mercaptoethanol, 0.05% (v/v) Triton X-100, 0.05% (w/v) BSA, 2% (w/v) PVP, and 1 mM EDTA. The homogenate was centrifuged at 12,000 × g for 10 min at 4 °C, and the supernatant was used to assay CIN and VIN activities. For CWIN activity, the pellet was washed twice with 0.5 mL of extraction buffer, resuspended in 1.8 mL of salt extraction buffer, and extracted overnight at 4 °C. The mixture was then centrifuged again at 12,000 × g for 10 minutes at 4 °C, and the resulting supernatant was used for CWIN activity determination (Xiao et al. 2024). CIN activity was assayed by mixing 200 μL of the supernatant on ice with a reaction buffer containing 80 mM MES-NaOH (pH 5.5), 5 mM NaF, and 100 mM sucrose. VIN activity was measured using a buffer composed of 200 mM acetic acid–sodium acetate (pH 4.5 or 4.8) and 100 mM sucrose (Xiao et al., 2024). Total sucrolytic activity was calculated as the summation of SPS, SuSy, CWIN, CIN and VIN activities.

8.2.7. Starch metabolism enzymes activity assay

For starch synthase (SS) activity, 100 mg of tissue samples were homogenized in an extraction buffer containing 50 mM Tris-HCl (pH 7.0), 10% glycerol, 10 mM EDTA, 5 mM DTT, 1 mM PMSF, and 50 μL/g tissue of 10× Protease Inhibitor Cocktail (Sigma-Aldrich, Cat# P9599) (Dechorgnat et al. 2018). The homogenate was centrifuged at 12,000 × g for 10 min, and the supernatant was collected. A reaction mixture was prepared by mixing 0.1 mL of the supernatant with 0.9 mL of a solution containing 50 mM Tris-HCl (pH 7.0), 5 mM ADP-glucose, 1 mg/mL glycogen, and 10 mM $MgCl_2$. The reaction mixture was incubated at 30 °C for 30 min. To stop the reaction, 0.1 M HCl was added to denature the enzymes. To detect inorganic phosphate (Pi) consumption, 1% (w/v) ammonium molybdate was added. The mixture was incubated at room temperature for 30 min, and the absorbance was recorded at a

wavelength of 620 nm using a UV-Vis spectrophotometer (Shimadzu, Tokyo, Japan). A standard curve was prepared using known Pi concentrations, and starch synthase activity was calculated as the amount of Pi released, expressed in $\mu molg^{-1}FW$.

ADP-glucose pyrophosphorylase (AGPase) activity was determined using previously described methods by Amoah et al. (2025a), with minor modifications. Briefly, 100 mg of fresh samples were homogenized in 1 mL of ice-cold extraction buffer containing 0.1 M Tris-HCl (pH 7.9), 5 mM glutathione, and 1 mM EDTA. The homogenate was centrifuged at 15,000 × g for 20 minutes at 4 °C, and the supernatant was collected. Subsequently, 0.1 mL of the supernatant was mixed with 0.9 mL of a reaction mixture containing 0.4 M Tris-HCl buffer (pH 7.9), 0.06 M $MgSO_4$, 48 mM cysteine, 2.4 mg/mL BSA, 4 mM ADP-glucose, 20 mM sodium pyrophosphate, 30 mM 3-phosphoglycerate, and 4 units each of glucose-6-phosphate dehydrogenase and phosphoglucomutase. Afterwards, 0.1 mL of enzyme extract was added to $NADP^+$ as the final component. The absorbance was measured at 340 nm using a UV-vis spectrophotometer (Shimadzu, Tokyo, Japan). The AGPase activity was expressed as $\mu mol\ min^{-1}\ g^{-1}$ FW.

The α (AMY)- and β (BAM)- amylase activities was measured according to the methods by Du et al. (2020) with minor modifications. Briefly, tissue samples were homogenized in 1 mL of chilled distilled water and centrifuged at 12,000 x *g* for 15 min. The supernatants were separated and used for quantifying α-and β-amylase. For α-amylase activity, 0.5 mL of supernatant was mixed with 3 mM $CaCl_2$, heated at 70 °C for 5 min to inactivate β-amylase, cooled to room temperature, followed by the addition of 2% starch solution in 0.1 M citrate buffer. The mixture was incubated at 30 °C for 5 min and stopped by adding 1 mL of color reagent (dinitro salicyclic acid). The mixture was heated at 50 °C for 5 min, cooled down, and the α-amylase activity was determined by recording absorbance at 540 nm wavelength with a UV-vis spectrophotometer (Shimadzu, Tokyo, Japan). β-amylase activity was assayed by initially inactivating α-amylase with 0.1 M EDTA. After, a 1 mL solution containing 0.1 M EDTA, 2% starch solution, and 0.1 mM citrate buffer were mixed with 0.5 mL enzyme extract. The mixture was incubated at 30 °C for 5 min. The reaction was stopped by adding 1 mL of colour reagent (dinitro salicylic acid). The β-amylase activity was measured by recording absorbance at 540 nm wavelength with a UV-vis spectrophotometer (Shimadzu, Tokyo, Japan).

8.2.8. Diurnal and spatial sucrose and starch pattern determination

To investigate the spatial distribution of sucrose and starch, the youngest emerging leaf at 20 and 40 days after transplanting (DAT) was sampled and divided into upper and middle segments. Additional samples included the corresponding leaf sheath and root. On 40 DAT, sampling was conducted at 22:00 and again at 7:00 the following morning to assess nighttime dynamics. For diurnal analysis, the middle sections of the youngest fully expanded leaves were collected at six time points: 7:00, 10:00, 12:00,

17:00, 22:00, and 7:00 the next day, on both 20 and 40 DAT. All samples were immediately frozen in liquid nitrogen and stored at −80 °C until further biochemical analysis, following the procedures described previously. Sucrose and starch concentrations obtained from the diurnal sampling were used to calculate synthesis, degradation, and net accumulation rates, using the equations outlined below:

$$\text{Sucrose synthesis rate} = \frac{\text{Sucrose at 12:00 PM} - \text{Sucrose at 07:00 AM}}{5\text{h}}$$

$$\text{Starch synthesis rate} = \frac{\text{Starch at 12:00 PM} - \text{Starch at 07:00 AM}}{5\text{h}}$$

$$\text{Sucrose degradation rate} = \frac{\text{Sucrose at 10:00 PM} - \text{Sucrose at 07:00 AM (Next day)}}{9\text{ h}}$$

$$\text{Starch degradation rate} = \frac{\text{Starch at 10:00 PM} - \text{Starch at 07:00 AM (Next day)}}{9\text{ h}}$$

Net sucrose accumulation = Sucrose synthesis value – Sucrose degradation value

Net starch accumulation = Starch synthesis – Starch degradation values

8.2.8. RNA isolation, cDNA synthesis and qPCR analysis

Total RNA was isolated from the leaves and root tissue using the TRIzol RNA Isolation Reagents (Invitrogen, Carlsbad, CA, USA) following the manufacturer's protocol. RNA quantity and integrity were assessed by measuring the optical density at 260 nm and through 1.0% (w/v) agarose gel electrophoresis, respectively. Subsequently, 1 µg of total RNA was reverse-transcribed into single-stranded cDNA using the iScript™ RT Reagent Kit (Bio-Rad, Hercules, CA, USA) according to the manufacturer's instructions. Quantitative real-time polymerase chain reaction (qPCR) was performed using the CFX 96 Real-Time System (Bio-Rad, Richmond, CA, USA) with SYBR Green fluorescence (Bio-Rad, Richmond, CA, USA). The ΔΔCT method was used for data analysis. Gene-specific primers (Table S8.4) were employed to assess their expression patterns under different N (control N, NO_3^-, NH_4^+, NH_4NO_3 and $NH_4^+ \rightarrow NO_3^-$) treatment conditions. The thermal cycling conditions consisted of an initial denaturation step at 95 °C for 5 min, followed by 40 cycles of 95 °C for 15 s, 55 °C for 15 s, and 72 °C for 30 s. All experiments were conducted with three biological replicates, and relative transcript levels were normalized using *ZmActin1* and *ZmUBQ1* as internal controls.

8.2.9. Statistical analysis

The study was repeated twice, with tissue samples collected in triplicate at 20 and 40 DAT. Data were analysed using a two-way analysis of variance (ANOVA) to assess overall differences among groups, followed by post-hoc Turkey's honest significant difference (HSD) test for pairwise comparison using Prism software (v10.0). Quantified data points represent the mean ± standard error (SE) of six independent plants (n = 6). Different letters on the error bars denote statistically significant differences at a probability level of $P \leq 0.05$, determined via Tukey's HSD test. Graphical charts were generated using GraphPad Prism (v10.4.0), and Pearson's correlation plots were created using R statistical software (v4.5.0).

8.3. Results

8.3.1. Response of maize seedlings to different N forms

At 10 DAT, an initial assessment showed that maize seedlings grown with continuous NH_4^+ (T3) or mixed N (T4) exhibited significantly enhanced shoot growth (Fig. S8.2A). While root morphology was comparable across all treatments at this early stage (Fig. S2B), NH_4^+ supply resulted in the highest root biomass and a higher R/S ratio (Table S8.1), suggesting a proactive shift in resource allocation. Notably, NH_4^+-treated plants exhibited early and significantly increased soluble sugars, sucrose, starch, fructose, and glucose in both leaves and roots (Fig. S8.3).

8.3.2. Phenotypic response, biomass accumulation and photosynthesis

At 40 DAT, plants grown with sustained NH_4^+ treatment exhibited enhanced shoot and root performance, producing larger, well-developed cobs (Figs. S8.3A-B). This phenotypic superiority was corroborated by a significant increase in shoot, root, and total biomass (Fig. 8.1A-D). Moreover, NH_4^+-treated plants displayed enhanced photosynthetic activity, along with increased total leaf N content and chlorophyll synthesis (Fig. 8.1E, F, and S8.5A). The observed growth responses were consistently influenced by plant growth stage (PGS), nitrogen treatment (NT), and their interaction (PGS × NT), highlighting the dynamic interplay between N supply and developmental processes (Table 8.1).

8.3.3. Sugars and starch and metabolizing enzymes activities

NH_4^+-treated plants exhibited significantly elevated levels of soluble sugars, sucrose, fructose, glucose, hexose, and starch in both leaves (Fig. 8.2A–F) and roots (Fig. 8.3A–F), resulting in a higher hexose-to-sucrose ratio in both organs (Figs. S8.5B-C). PGS significantly influenced starch, glucose, hexose,

and root soluble sugar levels, while NT affected all measured indicators in leaves. Additionally, the PGS × NT interaction significantly impacted leaf and root hexose levels, as well as leaf soluble sugar and sucrose content (Table 8.1). Similarly, sucrose-metabolizing enzyme activities (SPS, SuSy, CINV, VINV, and CWINV) were markedly elevated in the leaves (Figs. 8.4A–E) and roots of plants grown under sole NH_4^+ treatment (Figs. 8.5A–E). In line with the observed enzymatic trends, total sucrolytic activity was higher in NH_4^+-treated plants in both leaves and roots (Figs. 8.4–5F). Furthermore, as shown in Table 1, PGS significantly affected leaf SPS and SuSy activity, as well as root SPS and CINV activity. NT influenced the activity of all sucrose-metabolizing enzymes in both leaves and roots, whereas the PGS × NT interaction specifically impacted leaf SPS, SuSy, CINV, VINV, and CWINV activities.

Furthermore, the activities of starch-metabolizing enzymes (SPS, AGPase, AMY, and BAM) followed a trend similar to starch content, with NH_4^+-treated plants exhibiting higher enzyme activities than other NT plants (Figs. 8.6A–H). Additionally, PGS significantly influenced the activities of leaf SS, AGPase, AMY, and BAM, as well as root AGPase. NT treatments affected all starch-metabolizing enzyme activities in both leaves and roots, while the interaction between PGS and NT (PGS × NT) significantly impacted only root AMY activity (Table 8.1).

8.3.4. Diurnal sucrose and starch pattern

To investigate how plants regulate C partitioning in response to N availability, we examined sucrose and starch dynamics in leaves under different N conditions. As shown in Fig. 8.7, NH_4^+-treated plants consistently exhibited elevated sucrose and starch levels throughout the day at both 20 and 40 DAT (Figs. 8.7A–D). Sucrose and starch levels were lowest in the morning (07:00), increased in the mid-morning (10:00), peaked at 17:00, and declined overnight, returning to lower levels at 07:00 the following day. After overnight transport, plants grown under NH_4^+ conditions retained significantly higher leaf sucrose and starch levels at both 20 and 40 DAT.

To further elucidate the mechanisms of C partitioning, energy storage, and metabolic regulation under the different N treatment conditions, we quantified sucrose and starch synthesis and degradation rates, as well as net sucrose and starch accumulation. As shown in Fig. S8.6, plants grown under mixed N supply exhibited a non-significant increase in sucrose synthesis rate, whereas those supplied with sole NO_3^- showed enhanced starch synthesis at 20 DAT. At 40 DAT, plants grown under Control N and $NH_4^+ \rightarrow NO_3^-$ conditions exhibited a higher sucrose synthesis rate; however, this rate was not significantly different from other N treatments. The rate of starch synthesis was markedly inhibited in control N plants at 40 DAT (Figs. S8.6A, D). Furthermore, by 40 DAT, NH_4^+-treated plants demonstrated a higher rate of sucrose degradation, whereas starch degradation was significantly pronounced in N-free plants (Figs. S8.6B, E). Collectively, at 40 DAT, $NH_4^+ \rightarrow NO_3^-$-treated plants

exhibited higher net sucrose accumulation, while starch was more highly accumulated in the leaves of plants grown under sole NO_3^-, NH_4^+, and mixed nitrogen supply (Figs. S8.6C, F).

8.3.5. Spatial distribution of sucrose and starch

The spatial distribution of sucrose and starch in source tissues, such as the upper leaf, middle leaf, leaf blade, and leaf sheath, and the sink tissue (root) was analysed to understand carbon partitioning and metabolic regulation between source and sink tissues. Sucrose and starch accumulated predominantly in the upper leaves but were lower in the leaf sheath (Fig. 8.8). Their spatial distribution remained consistent between 22:00 and 07:00, aligning with the relatively stable sucrose and starch levels observed in the diurnal change analysis (Figs. 8.7A–D). Sucrose and starch concentrations varied significantly among nitrogen treatments . The leaves and leaf sheaths of NH_4^+-treated plants contained significantly higher sucrose and starch levels both at the end of the day (22:00) and during the early morning (07:00). Additionally, NH_4^+-treated plants retained more residual sucrose across all tissues (Figs. 8.8A–D).

8.3.6. Transcriptional regulation of sucrose and starch metabolism and transporter genes

The expression patterns of sucrose metabolism genes (*ZmSPS1*, *ZmSuSy1*, *ZmCINV1*, *ZmCWINV1*, and *ZmVINV1*) and sucrose transporter genes (*ZmSWEET14*, *ZmSUC2*, *ZmSUT2*, and *ZmSTP2*) were analysed in the leaves and roots of maize seedlings grown under different NTs. At 20 DAT, these genes were highly upregulated in the leaves and roots of NH_4^+-treated plants compared to other NT plants (Figs. 8.9–8.10A–I). Similarly, at 40 DAT, plants grown under NH_4^+ treatment exhibited a greater fold change in the expression of these genes (Figs. 8.9–8.10A–I). Starch metabolism-related genes (*ZmSS1*, *ZmAGPase1*, *ZmAMY1*, and *ZmBAM1*) were significantly upregulated at both 20 and 40 DAT in the leaves and roots of NH_4^+-treated plants (Figs. S8.8E–H). Additionally, PGS significantly affected the expression of all genes except *ZmSWEET14* and *ZmSTP2* in the leaves, and *ZmCWINV1*, *ZmSUC2*, and *ZmSUT2* in the roots. NT and the PGS × NT interaction significantly influenced the expression of all genes in both the leaves and roots of the maize seedlings (Table 8.1)

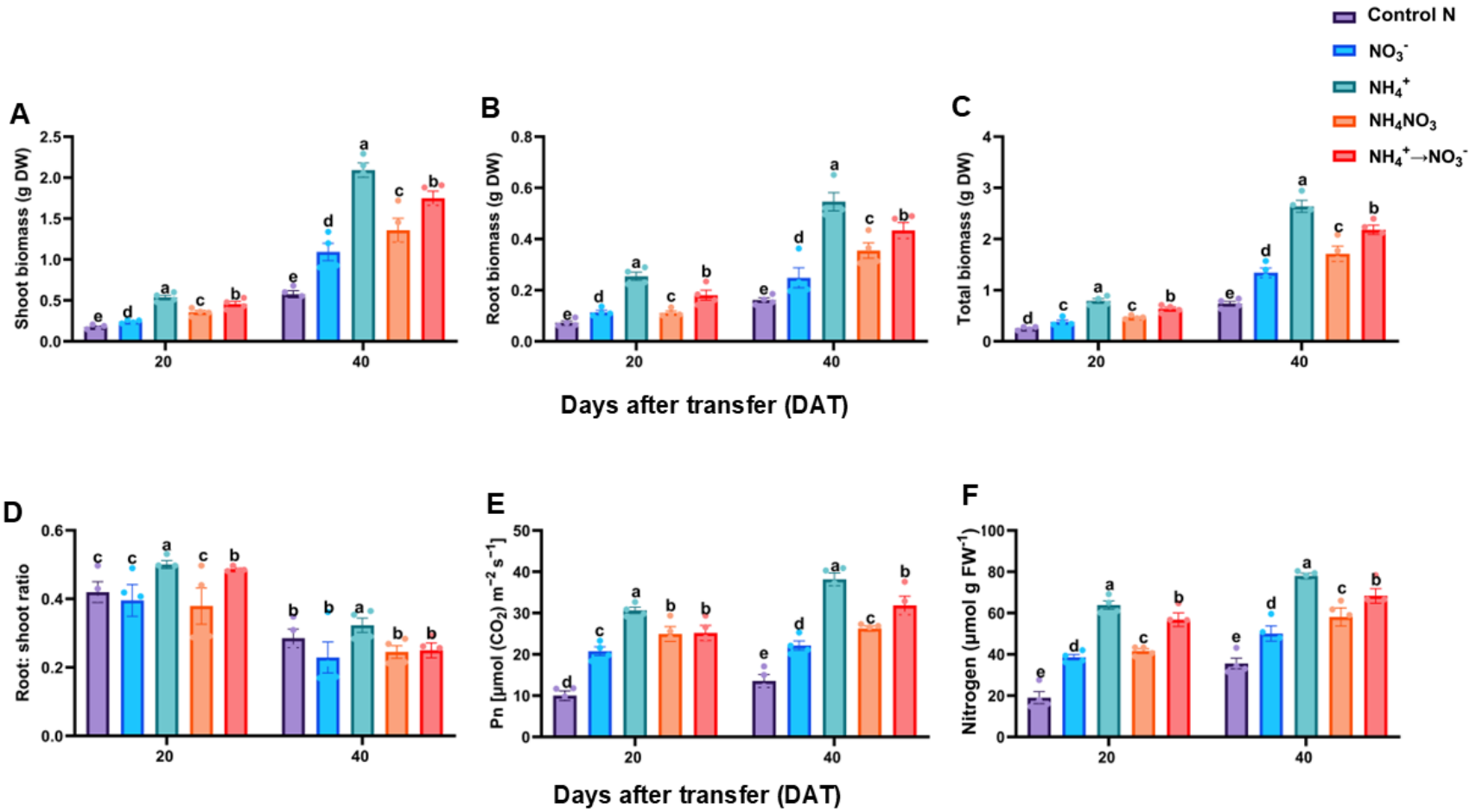

Fig. 8.1 Effect of different nitrogen treatments on biomass, photosynthesis and nitrogen accumulation. Shoot (**A**), root (**B**), and total biomass (**C**), root-to-shoot ratio (**D**), net photosynthetic rate (**E**), and leaf total nitrogen content (**F**). Data points represent the mean ± standard deviation (SD) of six independent biological replicates (n = 6). Different letters above the error bars indicate statistically significant differences at $P \leq 0.05$. Abbreviations: DAT – days after seedling transfer; FW – fresh weight; DW – dry weight.

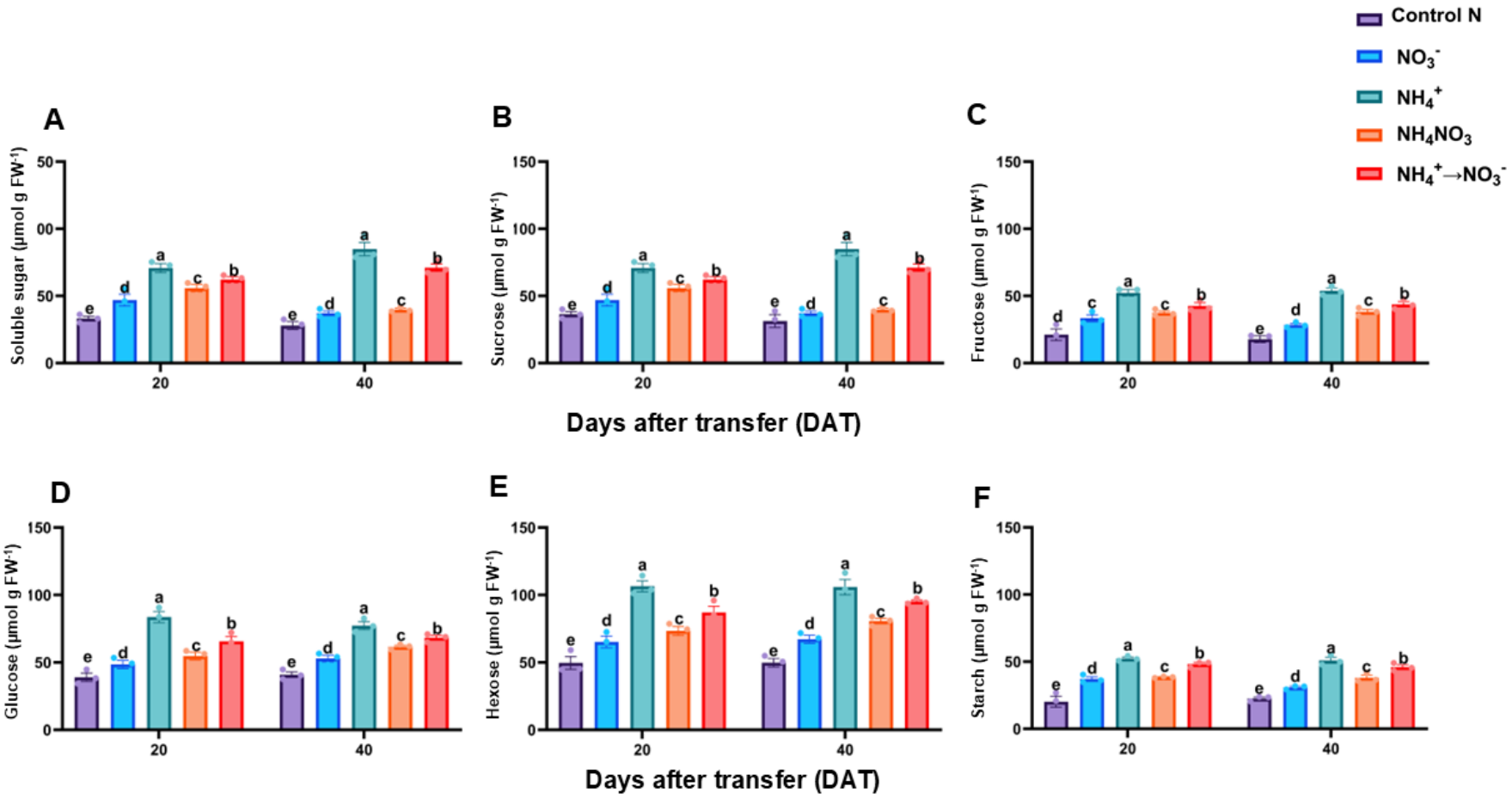

Fig. 8.2 Effect of different nitrogen forms on carbohydrates and starch accumulation. Soluble sugar (**A**), sucrose (**B**), fructose (**C**), glucose (**D**), hexose (**E**) and starch contents in the leaves of maize seedlings. Data points represent the mean ± standard deviation (SD) of six independent biological replicates (n = 6). Different letters above the error bars indicate statistically significant differences at $P \leq 0.05$. Abbreviations: DAT – days after seedling transfer; FW – fresh weight.

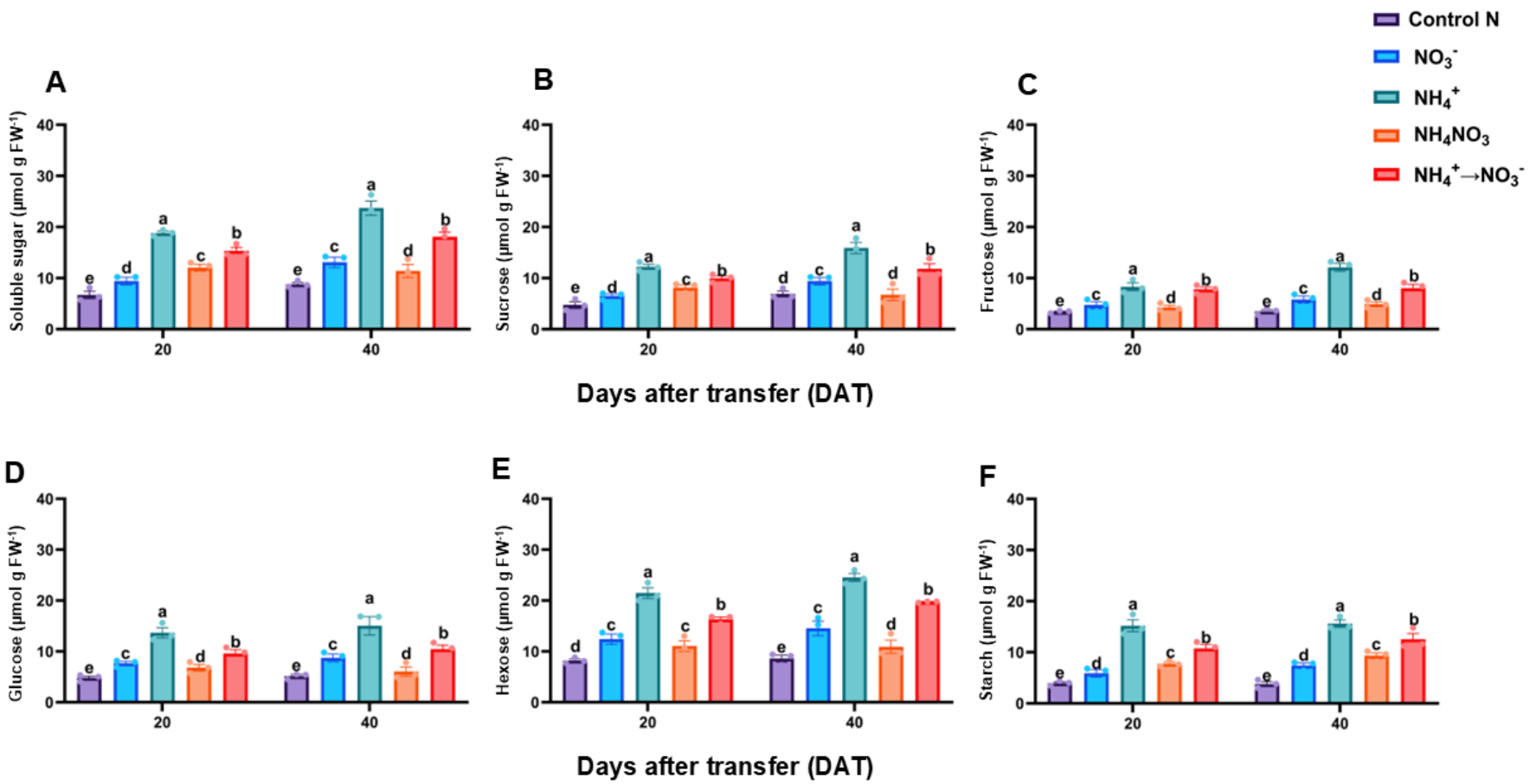

Fig. 8.3 Effect of different nitrogen forms on carbohydrates and starch accumulation. Soluble sugar (**A**), sucrose (**B**), fructose (**C**), glucose (**D**), hexose (**E**) and starch contents in the roots of maize seedlings. Data points represent the mean ± standard deviation (SD) of six independent biological replicates (n = 6). Different letters above the error bars indicate statistically significant differences at $P \leq 0.05$. Abbreviations: DAT – days after seedling transfer; FW – fresh weight.

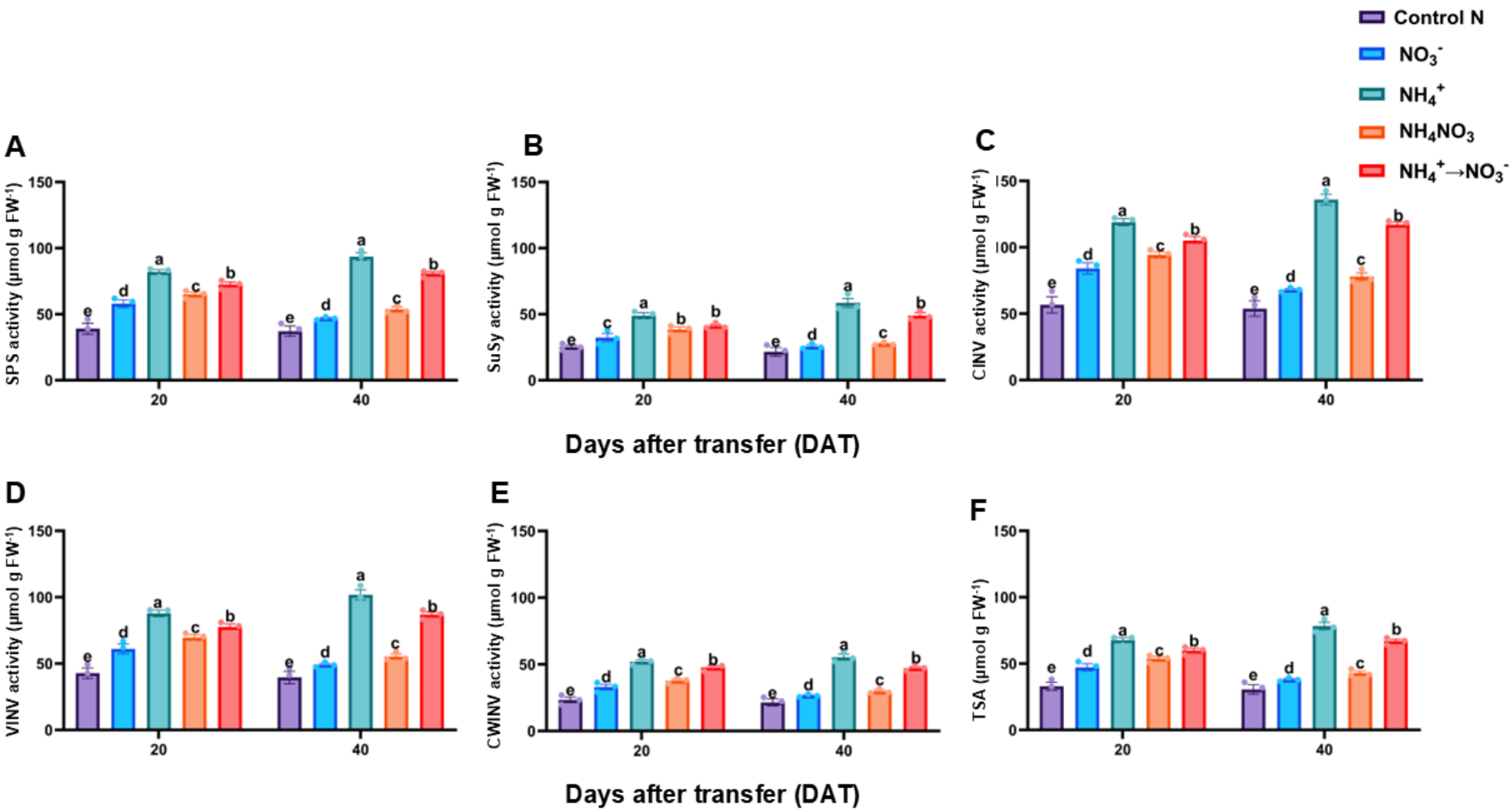

Fig. 8.4 Sucrose metabolizing enzymes activity in the leaves of maize seedlings under different nitrogen forms. Sucrose phosphate synthase (**A**), sucrose synthase (**B**), cytoplasmic invertase (**C**), vacuolar invertase (**D**), cell wall invertase (**E**) and total sucrolytic (**F**) activity. Data points represent the mean ± standard deviation (SD) of six independent biological replicates (n = 6). Different letters above the error bars indicate statistically significant differences at $P \leq 0.05$. Abbreviations: DAT – days after seedling transfer; FW – fresh weight

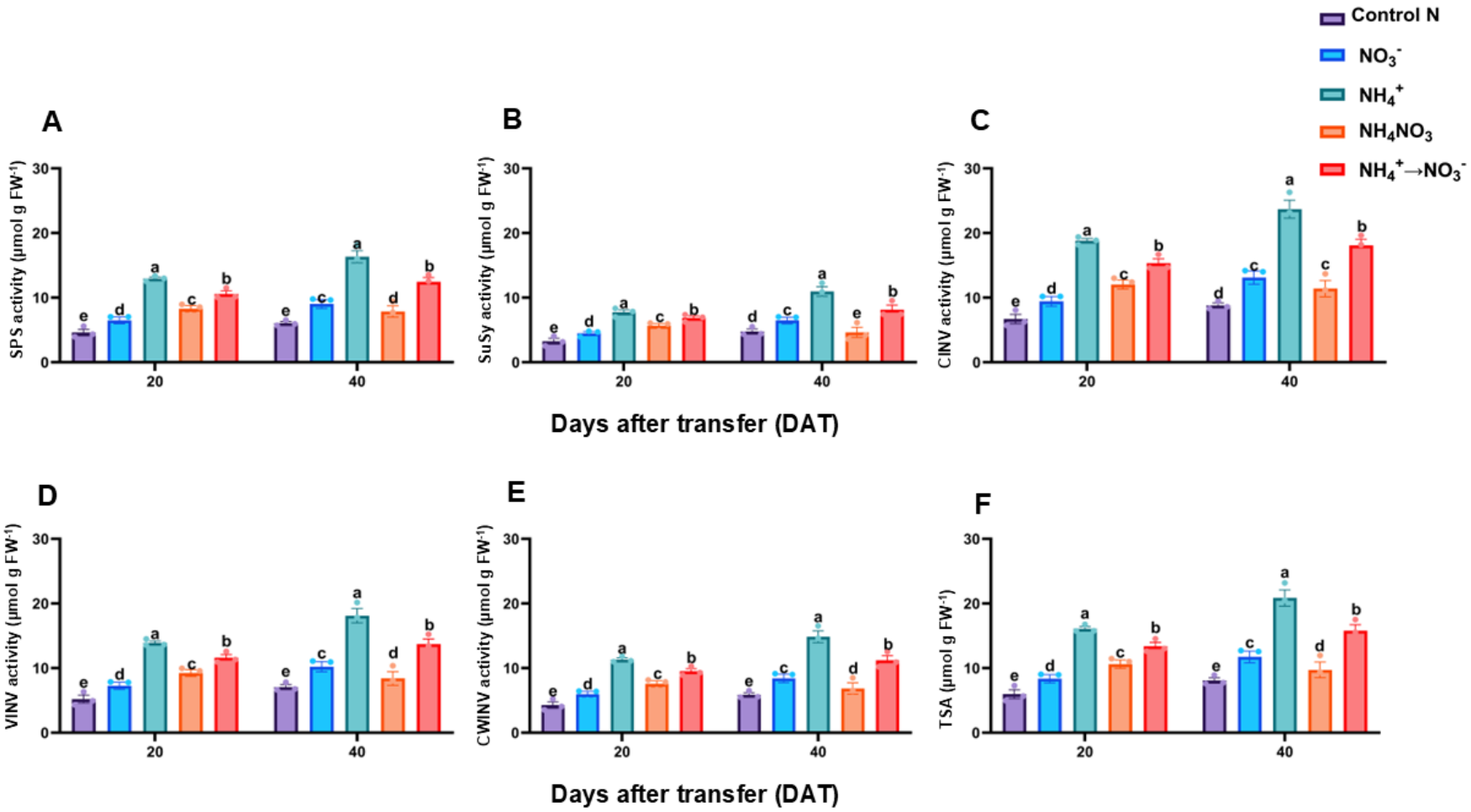

Fig. 8.5 Sucrose metabolizing enzymes activity in the roots of maize seedlings under different nitrogen forms. Sucrose phosphate synthase (**A**), sucrose synthase (**B**), cytoplasmic invertase (**C**), vacuolar invertase (**D**), cell wall invertase (**E**) and total sucrolytic (**F**) activity. Data points represent the mean ± standard deviation (SD) of six independent biological replicates (n = 6). Different letters above the error bars indicate statistically significant differences at $P \leq 0.05$. Abbreviations: DAT – days after seedling transfer; FW – fresh weight.

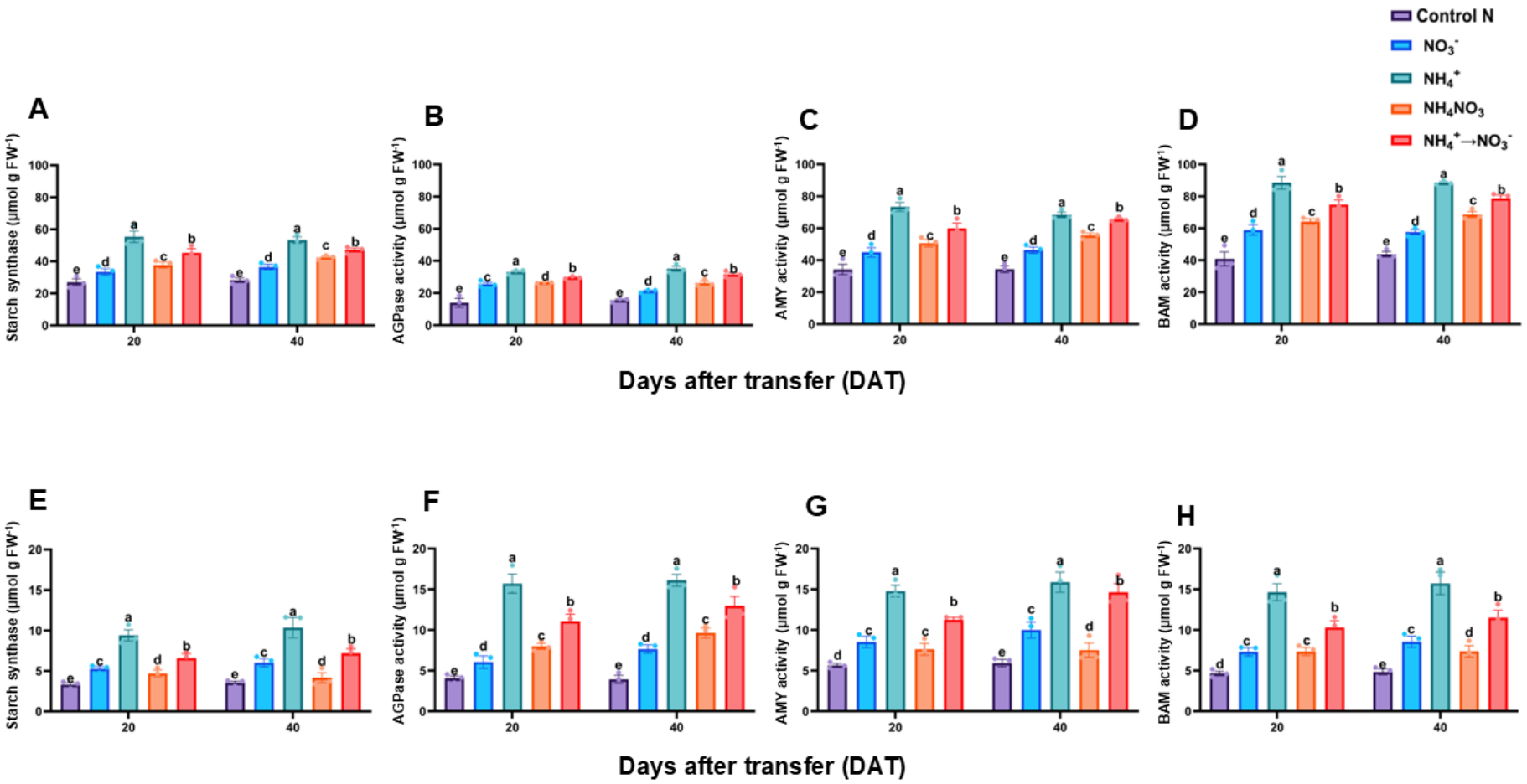

Fig. 8.6 Starch-metabolizing enzyme activities in maize seedlings under different nitrogen forms. Activities of starch synthase, ADP-glucose pyrophosphorylase, α-amylase, and β-amylase in leaves (**A–D**) and roots (**E–H**) are presented. Data points represent the mean ± standard deviation (SD) from six independent biological replicates (n = 6). Different letters above the error bars indicate statistically significant differences at $P \leq 0.05$. Abbreviations: DAT, days after seedling transfer; FW, fresh weight.

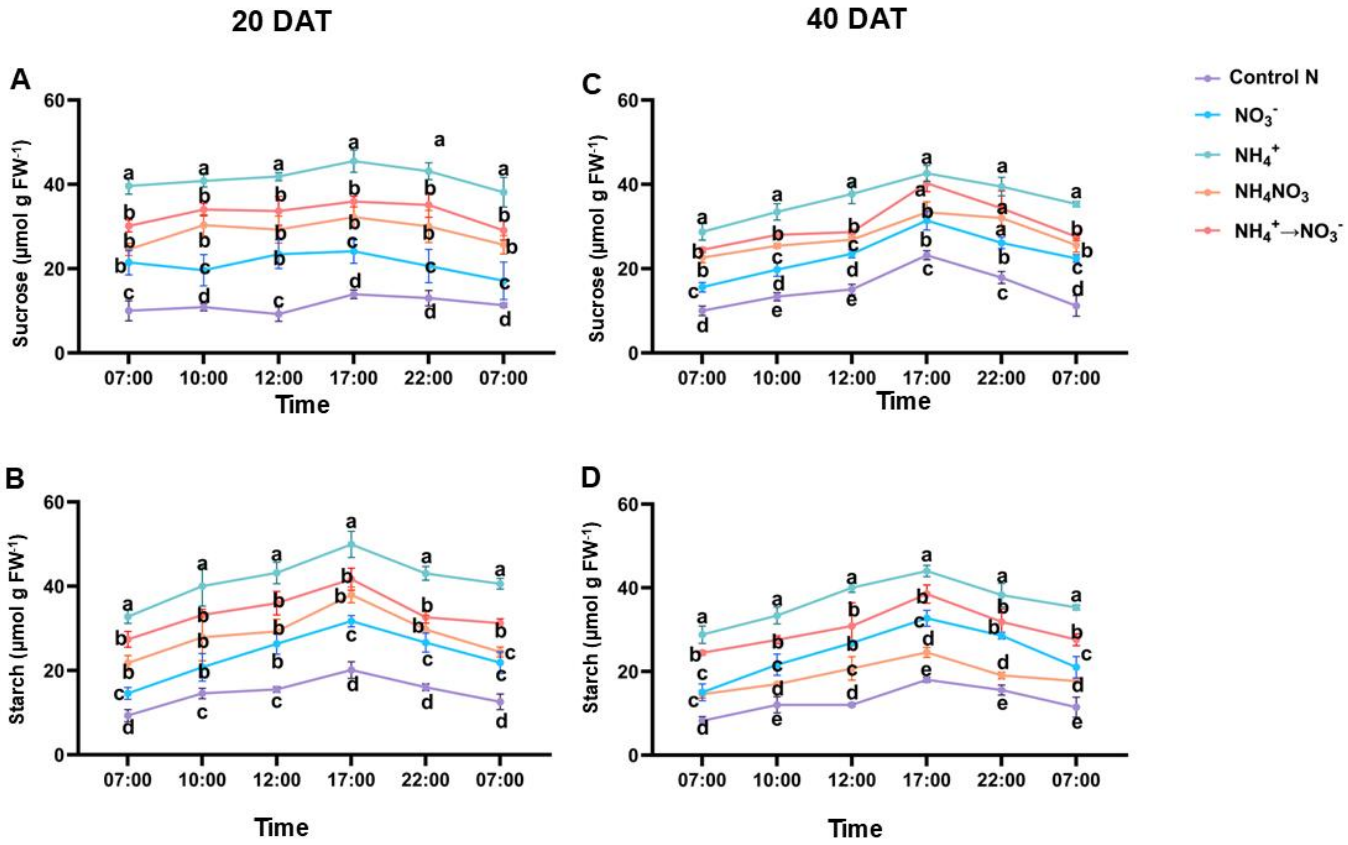

Fig. 8.7 Diurnal changes in leaf sucrose (**A**) and starch (**B**) at 20 days after treatment (DAT) and leaf sucrose (**C**) and starch (**D**) at 40 DAT under different nitrogen treatments. Leaf tissues were sampled at 07:00, 12:00, 17:00, 22:00, and 07:00 on the second day. Data are expressed as mean ± standard deviation (SD). Statistical differences were assessed using Tukey's multiple range test ($P \leq 0.05$); different letters above bars indicate significant differences among treatments. FW, fresh weight of tissue samples.

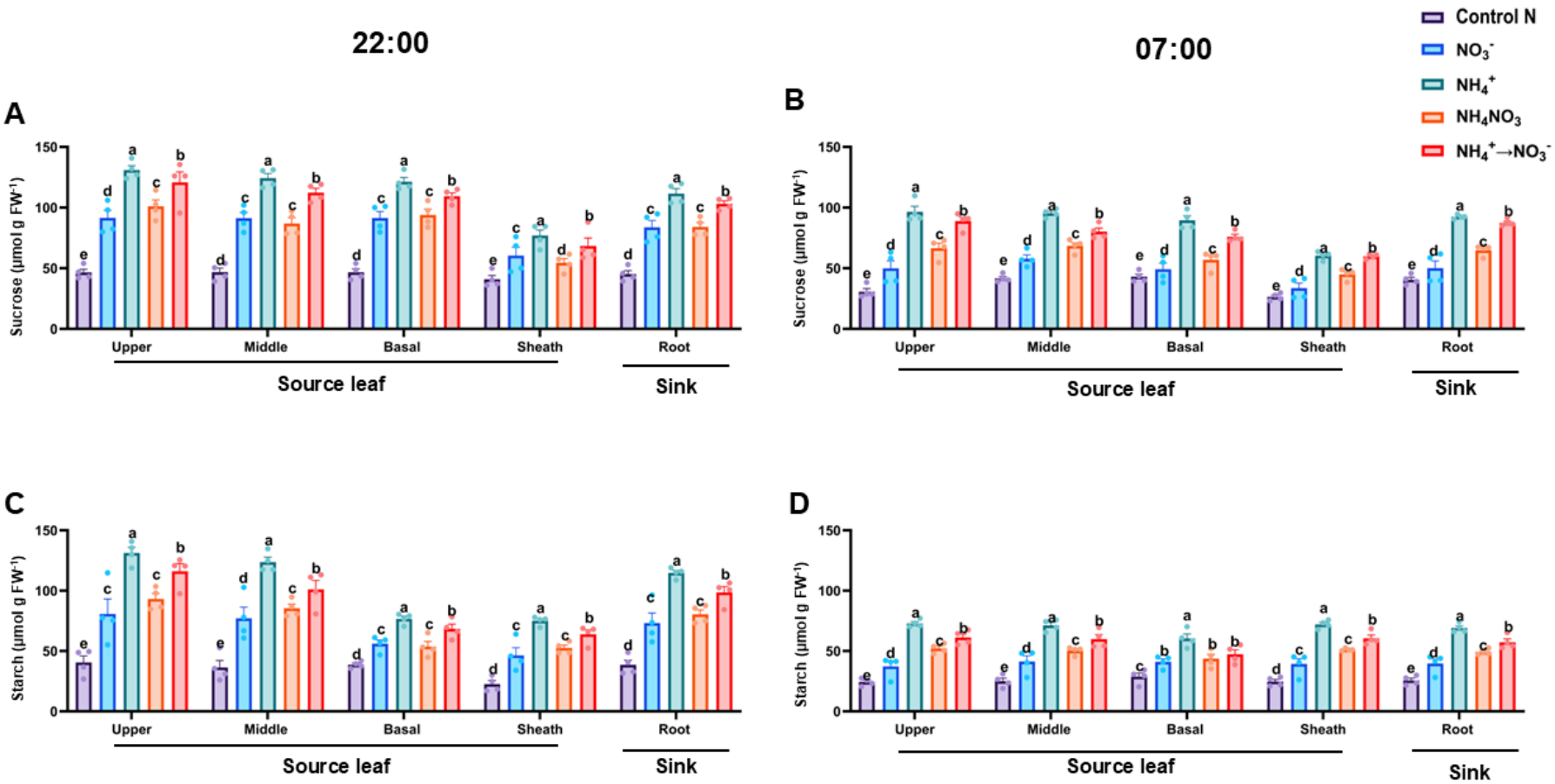

Fig. 8.8 Sucrose (**A–B**) and starch (**C–D**) contents in different maize tissues at 40 days after seedling transfer (DAT). The upper, middle, basal, sheath, and root tissues were sampled at 21:00 and 07:00 the next day. Data are presented as mean ± SEM (n = 6). Statistical significance was determined using Tukey's multiple range test ($P \leq 0.05$), with different letters indicating significant differences among treatments. FW and DAT represent the fresh weight and days after seedling transfer.

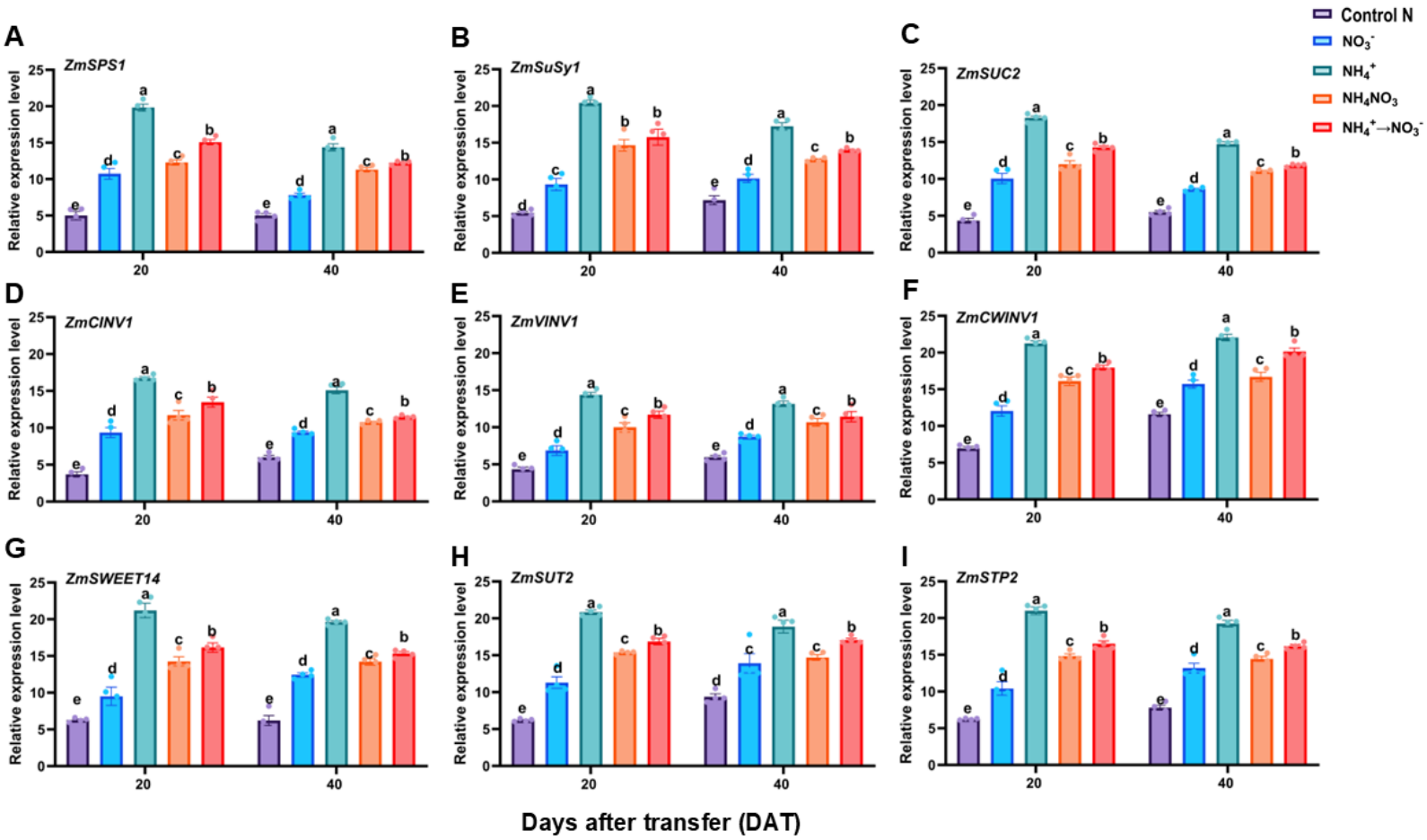

Fig. 8.9 Expression level of *ZmSPS1* (**A**), *ZmSuSy1* (**B**), *ZmSUC2* (**C**), *ZmCINV1* (**D**), *ZmVINV1* (**E**), *ZmCWINV1* (**F**), *ZmSWEET14* (**G**), *ZmSUT2* (**H**) and *ZmSTP2* (**I**) in the leaves of maize seedlings exposed to different nitrogen forms. Data points represent the mean ± standard deviation (SD) of six independent biological replicates (n = 6). Different letters above the error bars indicate statistically significant differences at $P \leq 0.05$.

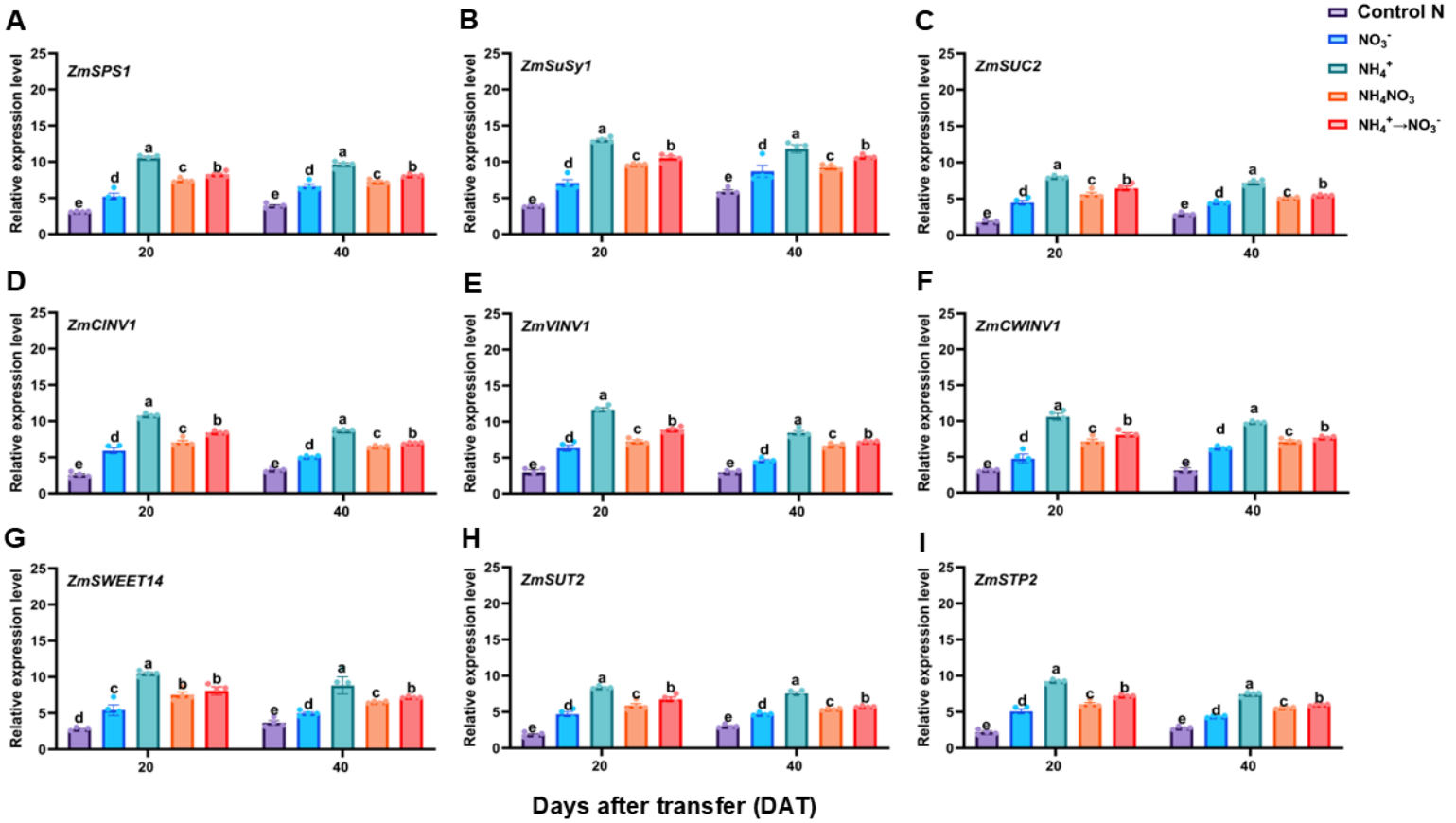

Fig. 8.10 Transcriptional regulation of sucrose metabolism and transporter genes. Expression level of *ZmSPS1* (**A**), *ZmSuSy1* (**B**), *ZmSUC2* (**C**), *ZmCINV1* (**D**), *ZmVINV1* (**E**), *ZmCWINV1* (**F**), *ZmSWEET14* (**G**), *ZmSUT2* (**H**) and *ZmSTP2* (**I**) in the roots of maize seedlings exposed to different nitrogen forms. Data points represent the mean ± standard deviation (SD) of six independent biological replicates (n = 6). Different letters above the error bars indicate statistically significant differences at $P \leq 0.05$.

Table 8.1 Two-way ANOVA for indicators in the leaves and root of maize.

Traits/(plants)	Sources of variation					
	Shoot/leaf			Root		
	PGS (df=1)	NT (df=4)	PGS x NT (df=4)	PGS (df=1)	NT (df=4)	PGS x NT (df=4)
Biomass	0.0003***	0.002**	0.0075**	0.0002***	0.0026**	0.0476*
Total biomass	0.0003***	0.0004***	0.0018**	0.0115*	0.0382*	0.3071ns
Amino acid	0.0009***	0.0068**	0.0107*	0.1587ns	0.0035**	0.2208ns
Total protein	0.0005***	0.0007	0.0024**	0.0116*	0.0125*	0.1215ns
Soluble sugar	0.463ns	0.0022**	0.0343*	0.0475*	0.004**	0.0548ns
Sucrose	0.2553ns	0.0103*	0.0242*	0.0752ns	0.0036**	0.1185ns
Starch	0.0405*	0.0052**	0.0867ns	0.0206*	0.0004***	0.1613ns
Fructose	0.657ns	0.0057**	0.2398ns	0.0131*	0.0142*	0.2935ns
Glucose	0.0171*	0.0049**	0.088ns	0.3317ns	0.0215*	0.1152ns
Hexose	0.0165*	0.0026**	0.0103*	0.0873ns	0.0019**	0.032*
H/S ratio	0.0165*	0.0026**	0.1031ns	0.0667ns	0.0052**	0.049**
SPS	0.046*	0.0022**	0.0343*	0.0475*	0.004**	0.0548ns
SuSy	0.0255*	0.0103*	0.0242*	0.0676ns	0.0006***	0.0602ns
CINV	0.463ns	0.0022**	0.0343*	0.0475*	0.004**	0.0548ns
VINV	0.2207ns	0.0033**	0.0289*	0.059ns	0.0037**	0.0754ns
CWINV	0.2348ns	0.0031**	0.0295*	0.0579ns	0.0037**	0.0728ns
TSA	0.2639ns	0.0028**	0.0304*	0.056ns	0.0037**	0.0688ns
SS	0.0734ns	0.0049**	0.088ns	0.3317ns	0.0215*	0.1152ns
AGPase	0.0206*	0.0004***	0.1613ns	0.0206*	0.0004***	0.1613ns
AMY	0.0165*	0.0026**	0.1031ns	0.0916ns	0.0018**	0.0478*
BAM	0.0175*	0.0013**	0.0976ns	0.1162ns	0.0125*	0.1215ns
Chlorophyll	0.0214*	<0.0001****	0.0271*	0.0004***	<0.0001****	0.0076**
TN	0.0052**	0.0002***	0.0344*	0.0032**	0.0125*	0.0041**
Pn	0.0214*	<0.0001****	0.0271*	0.0003***	0.00698**	0.0035**
ZmSPS1	0.0017**	<0.0001****	0.0031**	0.0181*	0.0004***	0.0008***
ZmSuSy1	0.0114*	0.0101*	0.0028**	0.0367*	0.0039**	0.0012**
ZmCINV1	0.0259*	<0.0001****	0.0016**	0.0109*	<0.0001****	0.0005***
ZmCWINV1	0.0008***	<0.0001****	0.0137*	0.8211ns	0.0002***	0.0109*
ZmVINV1	0.0441*	0.0001***	0.0172*	0.0017**	<0.0001****	0.0031**
ZmSWEET14	0.8582ns	0.0002***	0.0011**	0.0251*	0.0324*	0.0157*
ZmSUC2	0.0109*	<0.0001****	0.0005***	0.2598ns	<0.0001****	0.0016**
ZmSUT2	0.0151*	<0.0001****	0.0012**	0.2598ns	<0.0001****	0.0016**
ZmSTP2	0.1811ns	0.0004***	0.0008***	0.0109*	<0.0001****	0.0005***
ZmSS1	0.0025**	<0.0001****	0.0011**	0.0043**	<0.0001****	0.0011**
ZmAGPase1	0.0044**	0.0002***	0.0101*	0.0197*	<0.0001****	0.0025**
ZmAMY1	0.0152*	0.0003***	0.019*	0.0027**	<0.0001****	<0.0001****
ZmBAM1	0.0105*	<0.0001****	<0.0001****	0.0081**	<0.0001****	0.0031**

*, **, ***, **** indicate significant differences at the 0.05, 0.01, 0.001, and 0.0001 probability levels, respectively; ns denotes non-significant. H/S ratio: hexose-to-sucrose ratio; SPS/ZmSPS1: sucrose phosphate synthase; SuSy/*ZmSuSy1*: sucrose synthase; CINV/*ZmCINV1*: cytoplasmic invertase; VINV/*ZmVINV1*: vacuolar invertase; AMY/*ZmAMY1*: α-amylase; BAM/*ZmBAM1*: β-amylase; SS/*ZmSS1*: starch synthase; AGPase/*ZmAGPase1*: ADP-glucose pyrophosphorylase; Pn: net photosynthetic rate; TN: total nitrogen; PGS: plant growth stage; NT: nitrogen treatment. *ZmSUC2*, *ZmTP2*, and *ZmSWEET14* denote sucrose transporter genes. PGS × NT: interaction between plant growth stage and nitrogen treatment; df: degrees of freedom.

8.4. Discussion

Nitrogen (N) is a crucial macronutrient, with NO_3^- and NH_4^+ as primary available forms (Peng et al. 2023). While individual N forms have been extensively studied, a significant gap remains in fully elucidating the complex mechanisms by which dynamic shifts between N forms differentially influence plant growth and C metabolism. Our previous study (Amoah and Kaiser, 2025) demonstrated that switching from NO_3^- to NH_4^+ synergistically enhanced maize growth, improved photosynthesis, and optimized carbon metabolism, highlighting its potent metabolic stimulating activity. This study critically builds on that basis by comprehensively evaluating the reverse transition from NH_4^+ to NO_3^-. This provides essential comparative mechanistic insight into the differential efficacy of these distinct N transition strategies in maize, offering a more complete understanding of how plants respond to fluctuating N availability. As hypothesized, our findings suggest that the $NH_4^+ \rightarrow NO_3^-$ transition may have a weaker overall impact on growth and C metabolism compared to the $NO_3^- \rightarrow NH_4^+$ transition observed previously, likely due to the inherent metabolic advantages of NH_4^+ assimilation (Zhang et al. 2019).

8.4.1. NH_4^+ supply promoted superior growth and photosynthetic efficiency in maize

In this study, continuous NH_4^+ treatment significantly enhanced maize seedling growth, as evidenced by increased shoot and root development, larger and well-formed cobs, and greater total biomass accumulation (Fig. S3-4). These improvements were accompanied by elevated photosynthetic activity, increased chlorophyll content, and higher total leaf N levels (Figs. S2–S4, S5A, and 1A–C). These findings align with our previous results, which demonstrated that NH_4^+ treatment promotes plant growth, enhances photosynthetic efficiency, and stimulates C metabolism in maize (Amoah and Kaiser 2025). Moreover, in our previous study, we showed that substituting the N form from NO_3^- to NH_4^+ induces a synergistic effect, enhancing both growth and C metabolism (Amoah and Kaiser, 2025). This suggests that NH_4^+-induced metabolic shifts play a key role in optimizing N remobilization, potentially due to the lower energy cost of NH_4^+ assimilation (2 ATP) compared to the 12 ATP required for NO_3^- assimilation, allowing for more energy-efficient N utilization (George et al. 2016). However, in this study, maize seedlings grown under continuous NH_4^+ supply exhibited superior performance compared to those under other N treatments, including the $NH_4^+ \rightarrow NO_3^-$ and mixed NH_4NO_3 regimes (Figs. S2–S4, S5A, and 1A–C). Here, it is worth noting that plants subjected to the $NO_3^- \rightarrow NH_4^+$ substitution (from our previous work) displayed improved growth, enhanced photosynthesis, and greater C fixation compared to N-free, NO_3^-, and NH_4NO_3 treatments. This underscores the critical role of NH_4^+ in maintaining an optimal C–N balance, achieved through enhanced N assimilation and efficient amino acid biosynthesis (Fig. S7A–B) (Liu et al. 2025). NH_4^+ treatment also had a marked impact on root morphology, significantly increasing root tip number, total root length, root volume, and root surface

area compared to other N treatments (Table S2). These morphological enhancements suggest that NH_4^+ promotes root expansion and improves nutrient acquisition efficiency, thereby facilitating greater N uptake and contributing to enhanced shoot, root, and total biomass accumulation (Fig. 1) (Reddy et al. 2025). Additionally, NH_4^+-treated plants (T3) exhibited significantly higher total protein and amino acid levels compared to those under other N treatments (Figs. S7A–D). This indicates that NH_4^+ directly supports protein biosynthesis via improved N assimilation, reinforcing the metabolic benefits of NH_4^+-based nutrition (Horchani et al. 2010).

8.4.2. NH_4^+ supply promoted growth and enhanced C–N coordination in maize

The physiological adaptations observed in NH_4^+-treated maize seedlings are closely linked to coordinated biochemical and molecular changes in C metabolism, reflecting the central role of N availability in regulating plant growth and development (Nunes-Nesi et al. 2010; Liu et al. 2025). The physiological adaptations observed in NH_4^+-treated maize seedlings are driven by coordinated biochemical and molecular changes in C metabolism in both leaves and roots (Figs. 2 and 3). NH_4^+ treatment induced differential regulation of sugars and starch, with NH_4^+-treated plants accumulated higher carbohydrate levels in leaves than in roots (Figs. 2, 3A–E). This demonstrates that more photosynthetic assimilates are transported to the leaves, serving as an essential energy source for plant growth and adaptation under NH_4^+ treatment conditions (Amoah and Kaiser 2025). Furthermore, NH_4^+-treated plants exhibited significant increases in SPS, SuSy, and INVs (*CINV*, *VINV*, *CWINV*) activity in leaves and roots, aligning with the upregulated expression of sucrose metabolism genes (*ZmSPS1*, *ZmSuSy1*, *ZmSUC2*, *ZmCINV1*, *ZmVINV1*, *ZmCWINV1*) and sucrose transporters (*ZmSWEET14*, *ZmSUT2*, and *ZmSTP2*) (Figs. 4, 5A–F). The enhanced carbohydrate accumulation observed may be attributed to an increased capacity for photosynthetic assimilate unloading, facilitating growth and adaptation in response to N availability. These findings underscore the critical role of N availability in regulating C partitioning and plant development, which is essential for improving NUE (Govindasamy et al. 2023; Amoah and Kaiser 2025; Liu et al. 2025).

Sucrose loading into the phloem at the source (leaf) and its unloading at the sink (root) creates a turgor pressure difference that drives the mass flow of assimilates (Zhao et al. 2020; Xiao et al. 2024). To maintain this pressure gradient and ensure continuous sucrose unloading into the roots, sucrose must be degraded (Xiao et al. 2024). Under NH_4^+ treatment, enhanced maize growth relied on sucrose as a key energy source, evidenced by increased SPS and SuSy activity, along with the upregulation of *ZmSPS1*, *ZmSuSy1*, *ZmCINV1*, *ZmVINV1*, and *ZmCWINV1* (Figs. 9–10A–F), which aligns with previous findings (Zhao et al. 2020; Amoah and Kaiser 2025). Given the role of SuSy as a marker of sink strength, the increased SuSy activity and expression of *ZmSuSy1* suggest a central role in enhancing sink strength under NH_4^+ conditions. Sucrose transporters (*SUTs* and *STPs*) facilitate the movement of

sucrose from source to sink tissues, promoting shoot growth and root development. In this study, *ZmSTP2* and *ZmSUT2* were upregulated in both leaves and roots of NH_4^+-treated plants (Figs. 9–10H–I), indicating strong transcriptional induction and a vital role in facilitating sucrose transport to the roots, thereby ensuring an adequate energy supply for growth. *SUCs* contribute to sucrose allocation, providing both energy and C skeletons for metabolic processes (Zhao et al. 2020; Ravazzolo et al. 2020). Notably, *ZmSUC2* was significantly induced under NH_4^+ treatment (Figs. 9–10C), suggesting its role in sucrose degradation and energy provision for maize growth under NH_4^+ treatment condition.

Furthermore, continuous NH_4^+ treatment significantly increased starch content in the leaves and roots of maize seedlings, indicating a shift in C metabolism under NH_4^+ supply conditions (Fig. 2–3F). Starch serves as a crucial C storage compound, strongly influenced by N availability (Amoah and Kaiser 2025). The higher leaf and root starch content observed in NH_4^+-treated plants reflects enhanced C storage, suggesting that plants under NH_4^+ supply prioritize starch accumulation in both shoots and roots as an adaptive strategy (Amoah and Kaiser, 2025). Additionally, NH_4^+-induced shoot and root growth enhanced assimilate allocation to developing tissues, resulting in greater starch accumulation (Figs. S4 and 1A–D). This buildup may be linked to increased sink strength, facilitating efficient carbohydrate storage and utilization (MacNeill et al. 2017; Wei et al. 2023). NH_4^+ supply also stimulated metabolic activity, particularly by modulating enzyme functions related to C partitioning, thereby enhancing starch metabolism and utilization efficiency (Amoah and Kaiser, 2025). Consistent with increased leaf and root starch accumulation, NH_4^+ treatment elevated SS, AGPase, AMY, and BAM activities, while upregulating the expression of *ZmSS1*, *ZmAGPase1*, *ZmAMY1*, and *ZmBAM1* in maize seedling leaves (Figs. 6, S8A–H). The upregulation of these starch-metabolizing enzymes and their associated genes underscores enhanced starch synthesis, ensuring a stable energy supply for root expansion and adaptation under NH_4^+ supply, as highlighted in previous studies (Li et al. 2018; Amoah and Kaiser 2025).

8.4.3. Diurnal dynamics of sucrose and starch and its regulation by NH_4^+ supply

The diurnal fluctuations in sucrose and starch contents were analysed to identify distinct patterns and regulatory mechanisms influencing N treatments. NH_4^+-treated plants consistently exhibited higher sucrose and starch levels throughout the day, highlighting the role of N availability in modulating key metabolic pathways. Diurnal trends were observed across all treatments (Fig. 7A-D), suggesting that these patterns may not be solely driven by N status but rather reflect a broader regulatory framework modulating C and N metabolism (Amoah and Kaiser, 2025). The rhythmic variation in sucrose and starch, peaking at 17:00, declining at 22:00, and rising again the following morning, may indicate periodic shifts in C uptake and assimilation rates rather than direct fertilization effects (Macduff et al. 1997). Interestingly, NH_4^+-treated plants maintained significantly altered C profiles, characterized by

increased sucrose and starch levels, even after overnight transport. This persistence suggests that the metabolic adjustments induced by NH_4^+ treatment are stable across environmental transitions and are not readily offset by external conditions during transport. The sustained influence of NH_4^+ treatment on N storage and regulation underscores the adaptive capacity of plants under continuous NH_4^+ supply. These findings provide valuable insights into the complex interplay between N and C availability, metabolic regulation, and diurnal rhythms, enhancing our understanding of plant adaptation strategies under NH_4^+ treatment conditions. This study has meticulously mapped the physiological and biochemical changes, alongside identifying key enzyme activities and gene expression patterns related to sucrose and starch metabolism and transport.

NH_4^+-treated plants exhibited significant net accumulation of sucrose and starch, alongside increased degradation of both (Fig. S6C and F). These findings suggest that plants under this treatment not only optimized sucrose storage efficiently but also relied on increased starch and sucrose degradation to sustain metabolic activity (Zhou et al. 2001; Gibon et al. 2004). The dynamic metabolic adjustments observed in NH_4^+-treated plants, characterized by enhanced sucrose and starch synthesis and degradation, indicate a flexible strategy for maximizing energy efficiency under NH_4^+ supply. These results underscore the intricate interplay between N forms and carbohydrate metabolism, reinforcing nitrogen availability as a key determinant of diurnal metabolic patterns. It is also worth noting that at 40 DAT, $NH_4^+ \rightarrow NO_3^-$ -treated plants also exhibited higher net sucrose accumulation when compared to other treatments. While this study primarily examines physiological and molecular responses at 20 and 40 DAT, we acknowledge that short-term dynamics immediately following $NH_4^+ \rightarrow NO_3^-$ treatment may reveal distinct regulatory patterns. Early-phase responses, occurring within hours to a few days, are likely to involve rapid transcriptional shifts, metabolic reprogramming, and signalling cascades that precede the sustained changes observed at later stages. Future studies will incorporate finer temporal resolution post-switch to dissect transient versus sustained regulatory mechanisms, thereby enhancing our understanding of N-induced C reallocation and stress adaptation.

8.4.4. NH_4^+ availability shapes carbohydrate dynamics across maize tissues

In this study, maize plants subjected to continuous NH_4^+ treatment at 40 DAT showed a significant increase in total N content, accompanied by diurnal fluctuations and spatial changes in C distribution. At this stage, C accumulation was particularly pronounced in the leaves (Fig. 2 and 8), and both growth and photosynthetic activity were markedly enhanced (Fig. 1 and S5). Although previous studies have typically linked NO_3^--induced C accumulation more strongly to NO_3^- or mixed N sources rather than NH_4^+ alone (Saiz-Fernández et al. 2017; He et al. 2022; Peng et al. 2023), our recent findings in maize indicate that plants supplied with either continuous NH_4^+ or switched from NO_3^- to NH_4^+ (NFS) also exhibit enhanced C accumulation and photosynthetic capacity. This strongly suggests that NH_4^+

nutrition, particularly when supplied at carefully controlled, lower concentrations designed to avoid toxicity, robustly supports maize growth, as well as N assimilation and metabolism. These metabolic enhancements are attributed to the lower energy cost of NH_4^+ assimilation (2 ATP) compared to the 12 ATP required for NO_3^- assimilation (George et al., 2016). This study also revealed that N treatments, sampling stages, and plant tissues differentially influenced sugar and starch accumulation, consistent with previous findings (Amoah and Kaiser, 2025), further refining our understanding of N management in maize. Specifically: (a) NH_4^+ treatments induced distinct starch and sucrose accumulation patterns across maize growth stages; (b) Starch content in the upper leaves of NH_4^+-treated plants increased significantly compared to other treatments; (c) NH_4^+-treated plants exhibited consistently higher starch and sucrose levels, aligning with previous findings (Amoah and Kaiser, 2025). These results highlight continuous NH_4^+ supply as a key regulator of carbohydrate storage and redistribution in maize. The enhanced carbohydrate retention observed in NH_4^+-treated plants suggests a metabolic strategy to optimize growth and energy reserves.

Although the hydroponic system used in this study allowed precise control of N form and concentration, field-level application of NH_4^+-dominant nutrition may induce rhizosphere acidification, particularly under prolonged or high-rate fertilization. This acidification can impair root function and microbial balance, potentially offsetting the physiological benefits observed under controlled conditions. To mitigate these effects, agronomic strategies such as lime application, split NH_4^+ dosing, or co-supply with NO_3^- may be employed to buffer pH and sustain root-zone health. These approaches are supported by previous findings that highlight the importance of managing rhizosphere pH to preserve microbial balance and nutrient uptake efficiency (Britto and Kronzucker 2002; Guo et al. 2007; Zhu et al. 2018; Xu et al. 2023; Wang et al. 2024).

8.5. Conclusion

This study evaluated the impact of N treatment on growth and C-N coordination in maize. Our findings show that continuous NH_4^+ treatment promoted superior shoot and root development, photosynthetic efficiency, biomass accumulation and also coordinates a finely tuned metabolic strategy. This optimization is driven by the lower energy cost of NH_4^+ assimilation (2 ATP) compared to NO_3^- (12 ATP), enabling a more efficient utilization of N and maximizing energy conservation for maize growth. We show that NH_4^+ actively reshapes carbohydrate dynamics, as evidenced by the enhanced accumulation of sugars and starch in both leaves and roots. This process is intricately linked to the upregulation of key sucrose metabolism enzymes, such as SPS, SuSy, and INVs, and starch-metabolizing enzymes such as SS, AGPase, AMY, and BAM, along with their respective gene expressions. Additionally, the increased capacity for photosynthetic assimilate unloading and efficient sucrose transport, facilitated by upregulated sucrose transporters, such as *ZmSTP2* and *ZmSUT2*

reinforces the sustained energy supply essential for vigorous growth and root expansion. Notably, the stable and increased sucrose and starch levels observed throughout diurnal cycles in NH_4^+-treated plants underscore a robust and adaptive metabolic strategy. This dynamic balance of enhanced carbohydrate synthesis and degradation ensures optimal energy efficiency and resilience across environmental transitions. These insights highlight NH_4^+ as a key regulator of carbohydrate storage and redistribution in maize, advancing our understanding of plant adaptation under NH_4^+ nutrition. The metabolic framework revealed in this study, characterized by optimized C-N balance and energy utilization, is important for improving NUE in maize. Future studies will aim to identify the specific molecular regulators and signalling pathways that mediate the interplay between forms and carbohydrate metabolism. These mechanistic insights will inform sustainable agricultural practices to enhance crop productivity and resilience under diverse environmental conditions.

8.6. Supplementary data

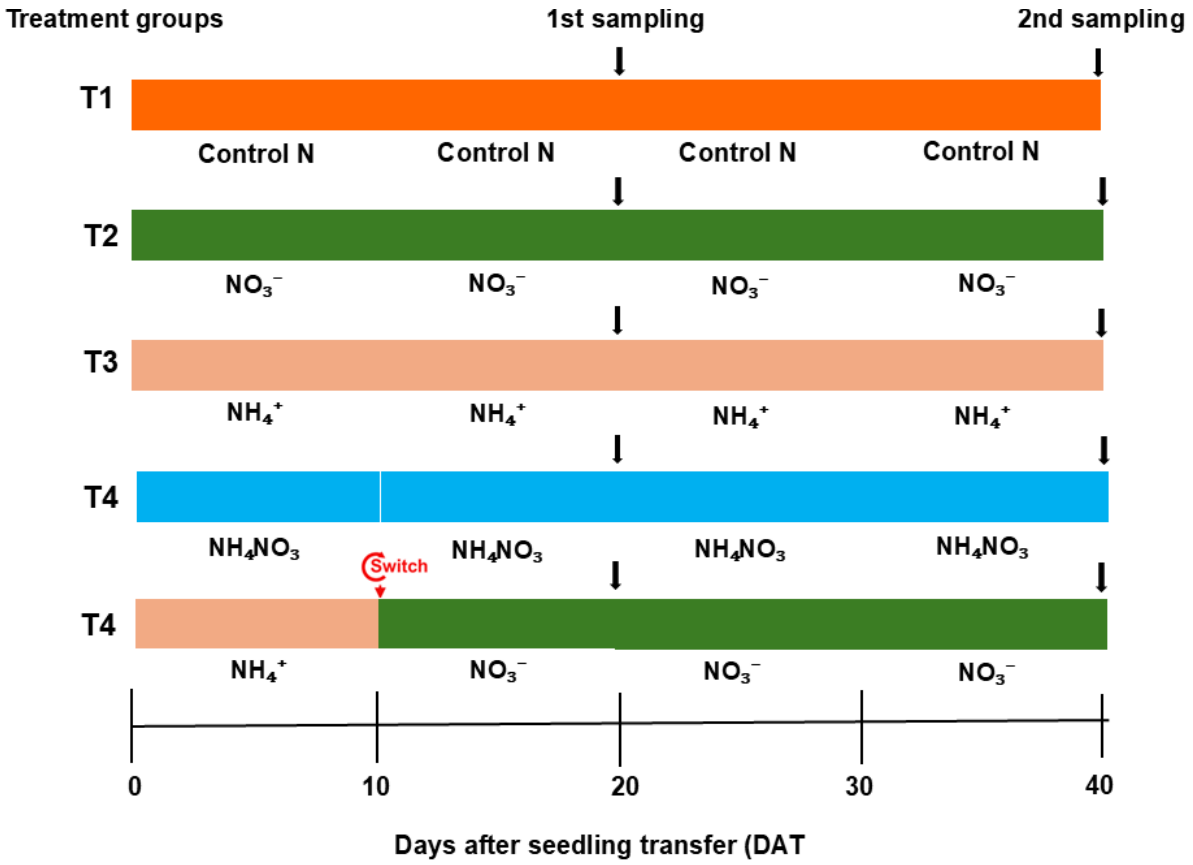

Fig. S8.1 Schematic representation of the experimental setup for the maize inbred line TX-40J. Maize seedlings were assigned to five nitrogen (N) treatment groups (T1 to T5): T1: T1, Control N (N-free); T2: 1 mM NO_3^- (sole NO_3^-); T3: 1 mM NH_4^+ (sole NH_4^+); T4: 0.5 mM NH_4NO_3 (mixed N supply); and T5, substitution of 1 mM NH_4^+ with 1 mM NO_3^- ($NH_4^+ \rightarrow NO_3^-$) at 10 days after seedling transfer (DAT). Plants were subsequently grown for an additional 30 days (up to 40 DAT), with shoot, root, and leaf samples collected at 20 DAT and 40 DAT. In the diagram, orange, green, brown, and blue blocks represent -N, NO_3^-, NH_4^+, and NH_4NO_3, respectively. Red downward arrows indicate the nitrogen form switch (from 1 mM NH_4^+ to 1 mM NO_3^-), while black downward arrows denote tissue sampling time points.

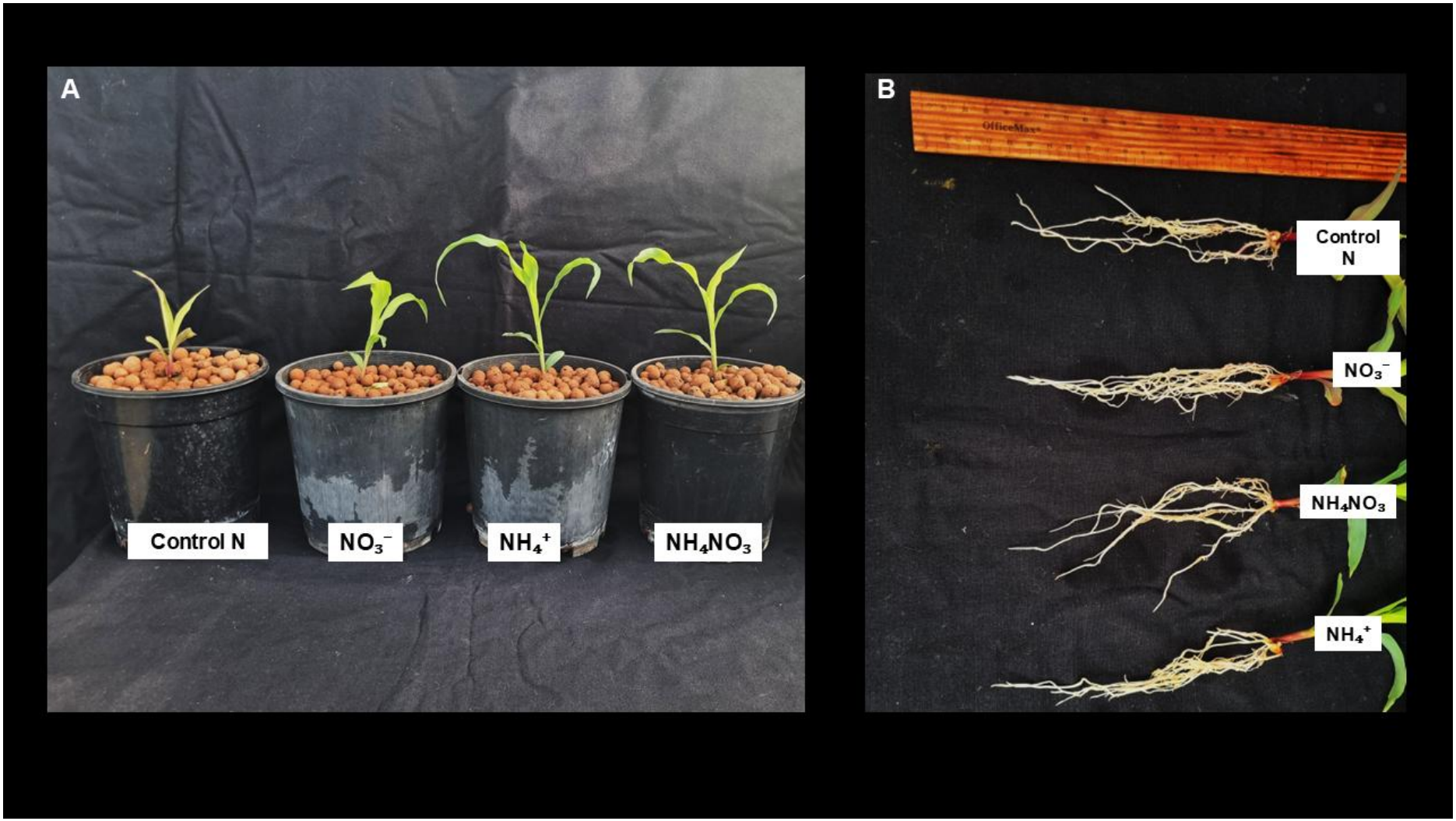

Fig. S8.2 Phenotypic response of the maize inbred line TX-40J to different nitrogen (N) forms. Representative images of shoot morphology at 10 days after nitrogen treatments (DAT).

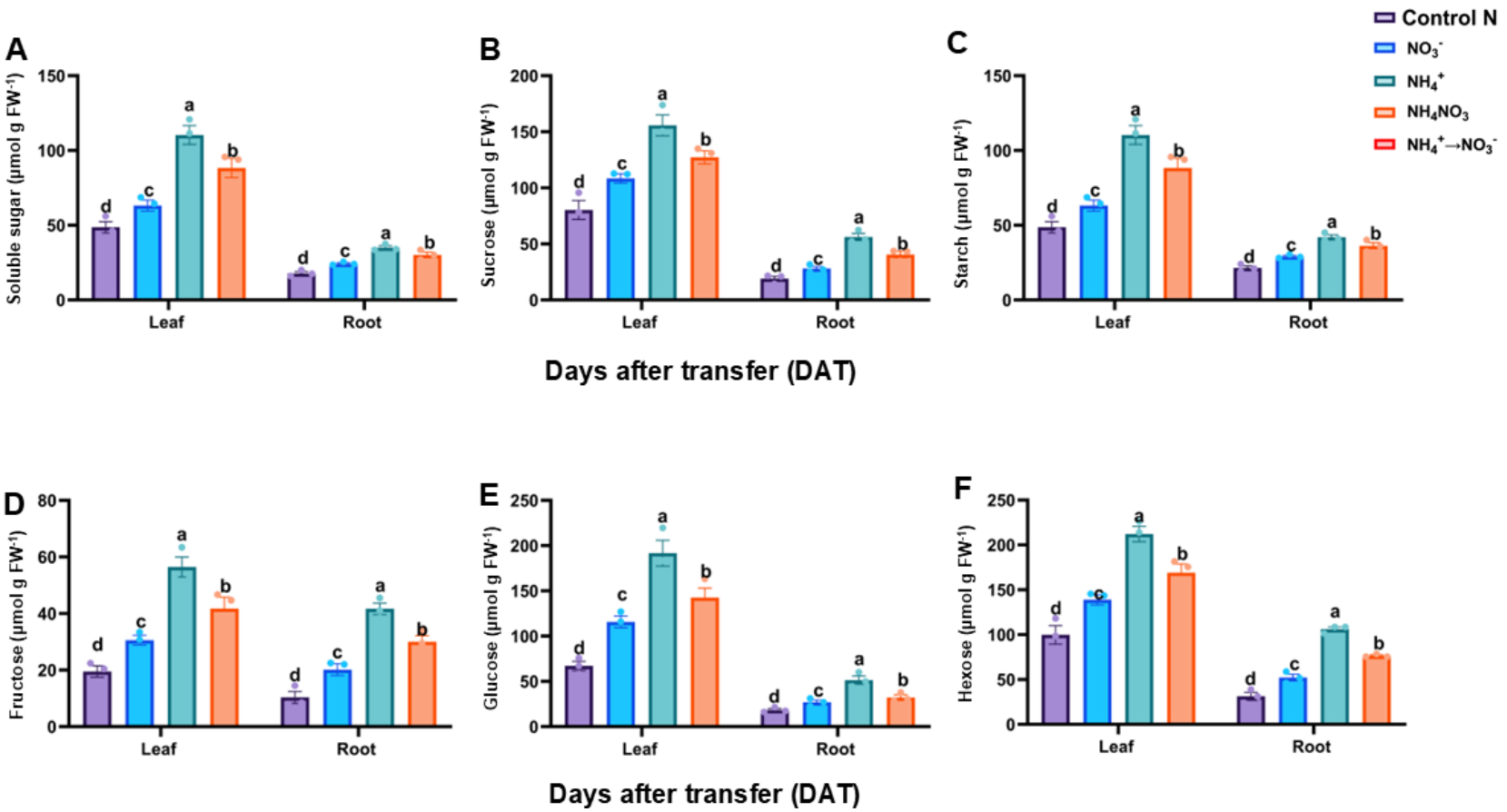

Fig. S8.3 Carbohydrates contents in the leaves and roots of maize seedlings under different nitrogen forms at 10 days after treatment (DAT). Soluble sugar (**A**), sucrose (**B**), starch (**C**), fructose (**D**), glucose (**E**) and hexose (**F**) contents. Data points represent the mean ± standard deviation (SD) of six independent biological replicates (n = 6). Different letters above the error bars indicate statistically significant differences at $P \leq 0.05$. Abbreviations: FW – fresh weight.

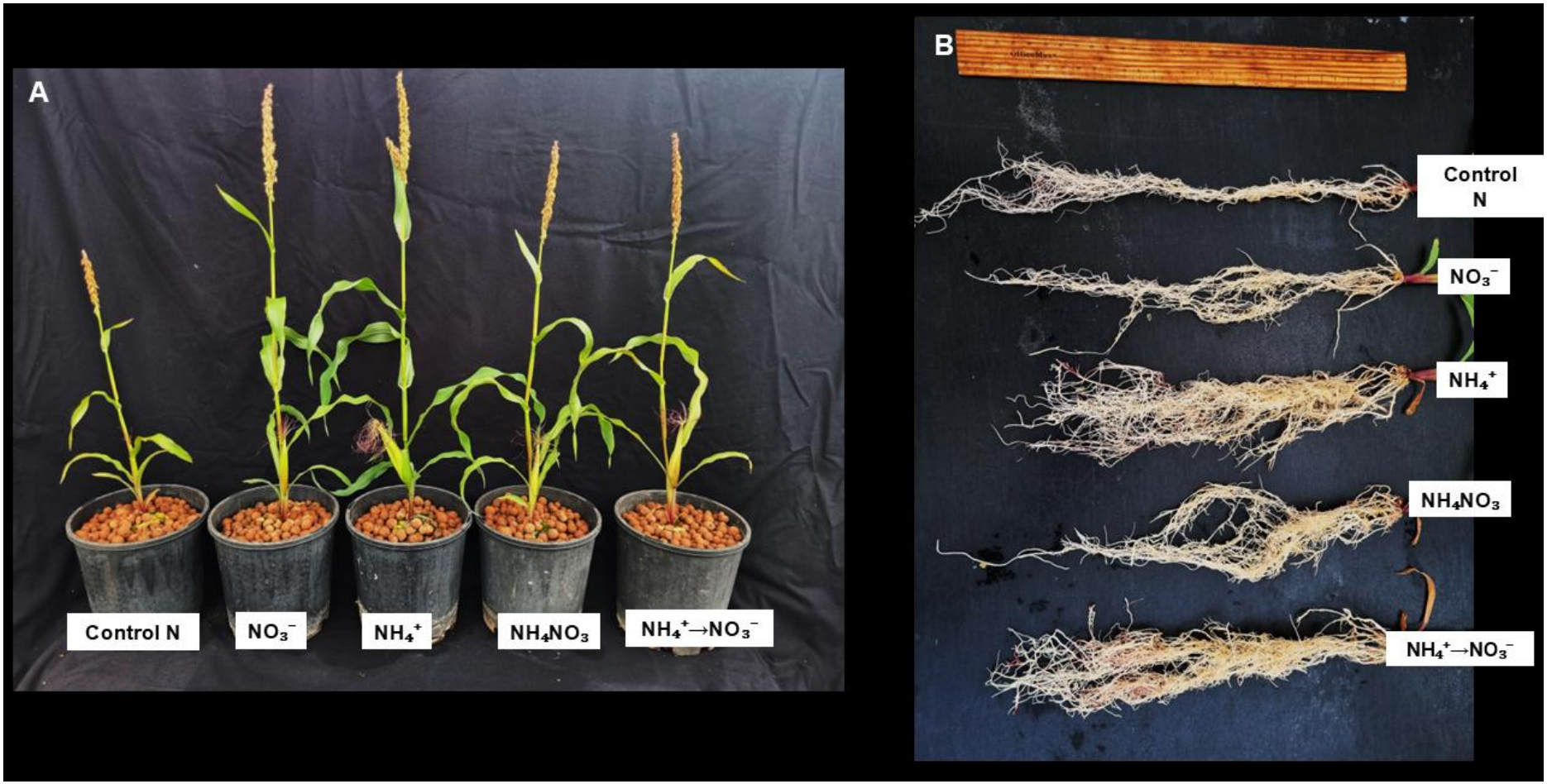

Fig. S8.4 Phenotypic response of the maize inbred line TX-40J to different nitrogen (N) forms. Representative images of shoot morphology (**A**) and root morphology (**B**) at 40 days after nitrogen treatments (DAT).

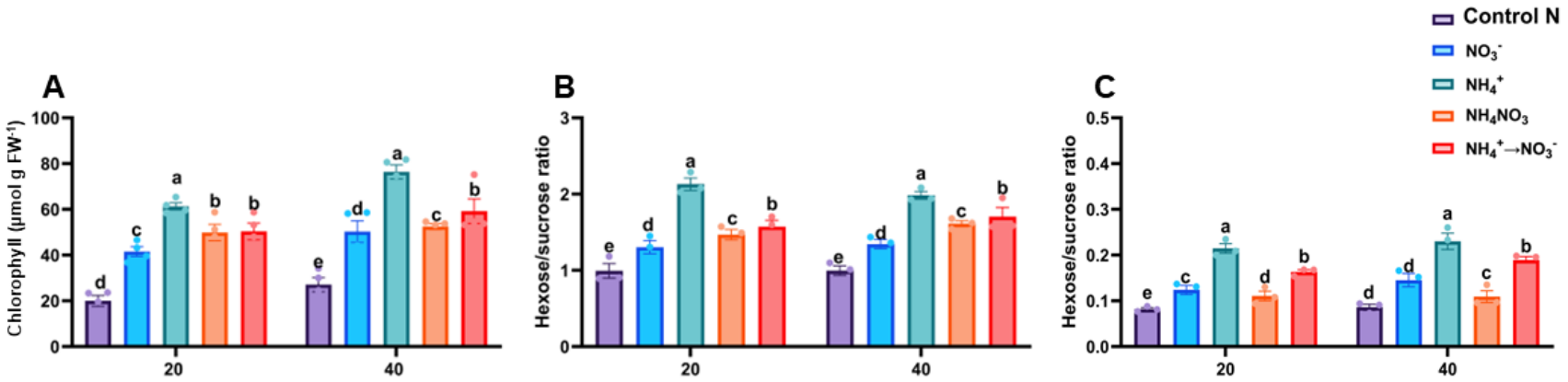

Fig. S8.5 Effect of different N forms on leaf chlorophyll content (A), leaf hexose-to-sucrose ratio (B) and root hexose-to-sucrose ratio (C) at 20 and 40 days after seedling transfer (DAT). Data points represent the mean ± standard deviation (SD) of six independent biological replicates (n = 6). Different letters above the error bars indicate statistically significant differences at $P \leq 0.05$. Abbreviations: FW – fresh weight.

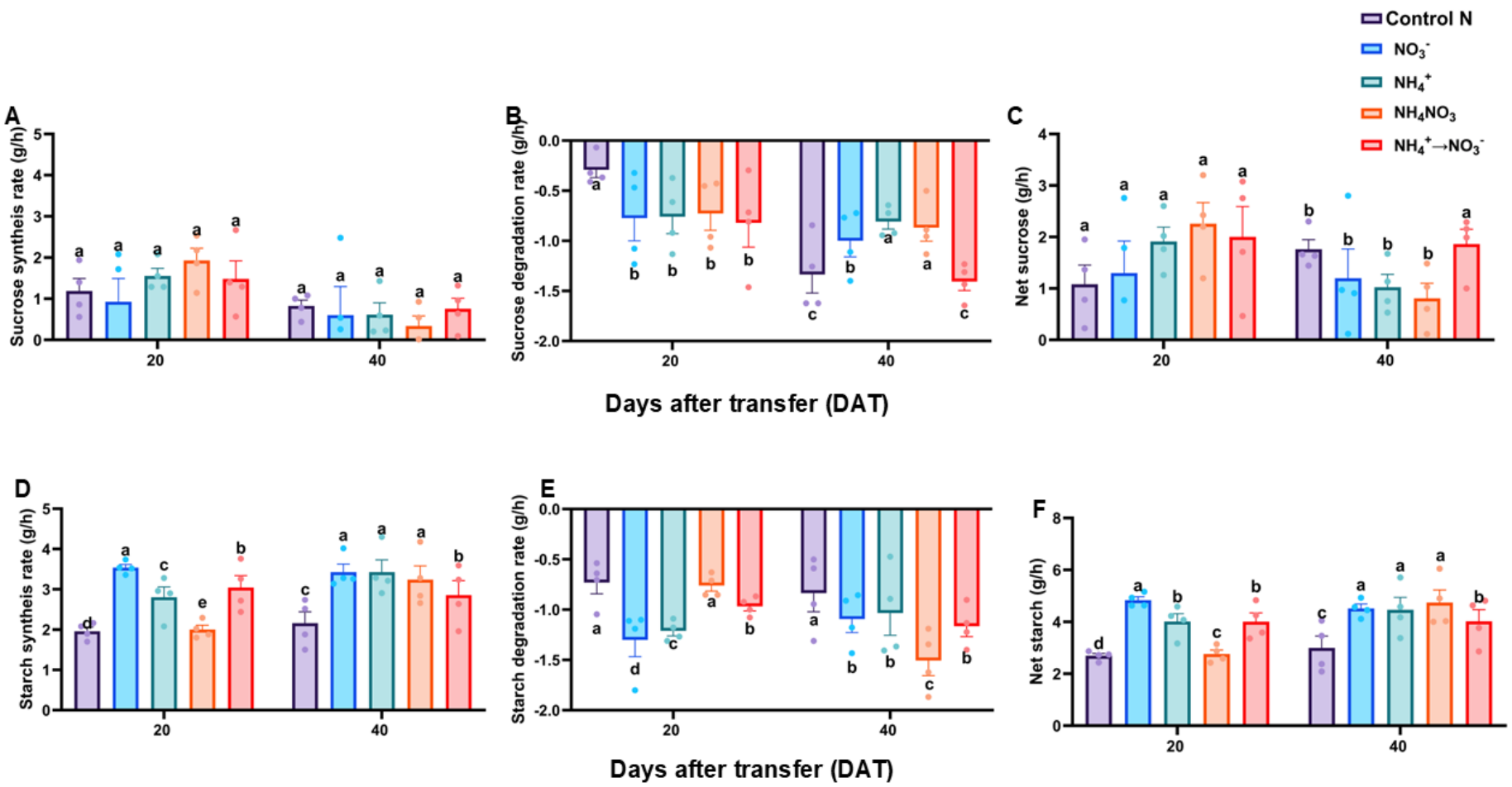

Fig. S8.6 Sucrose synthesis (**A**), sucrose degradation (**B**), net sucrose accumulation rate (**C**), starch synthesis (**D**), starch degradation (**E**) and net starch accumulation rate (**F**) in the leaves of maize seedlings exposed to different nitrogen treatment condition. Data points represent the mean ± standard deviation (SD) of six independent biological replicates (n = 6). Different letters above the error bars indicate statistically significant differences at $P \leq 0.05$. Abbreviations: FW – fresh weight.

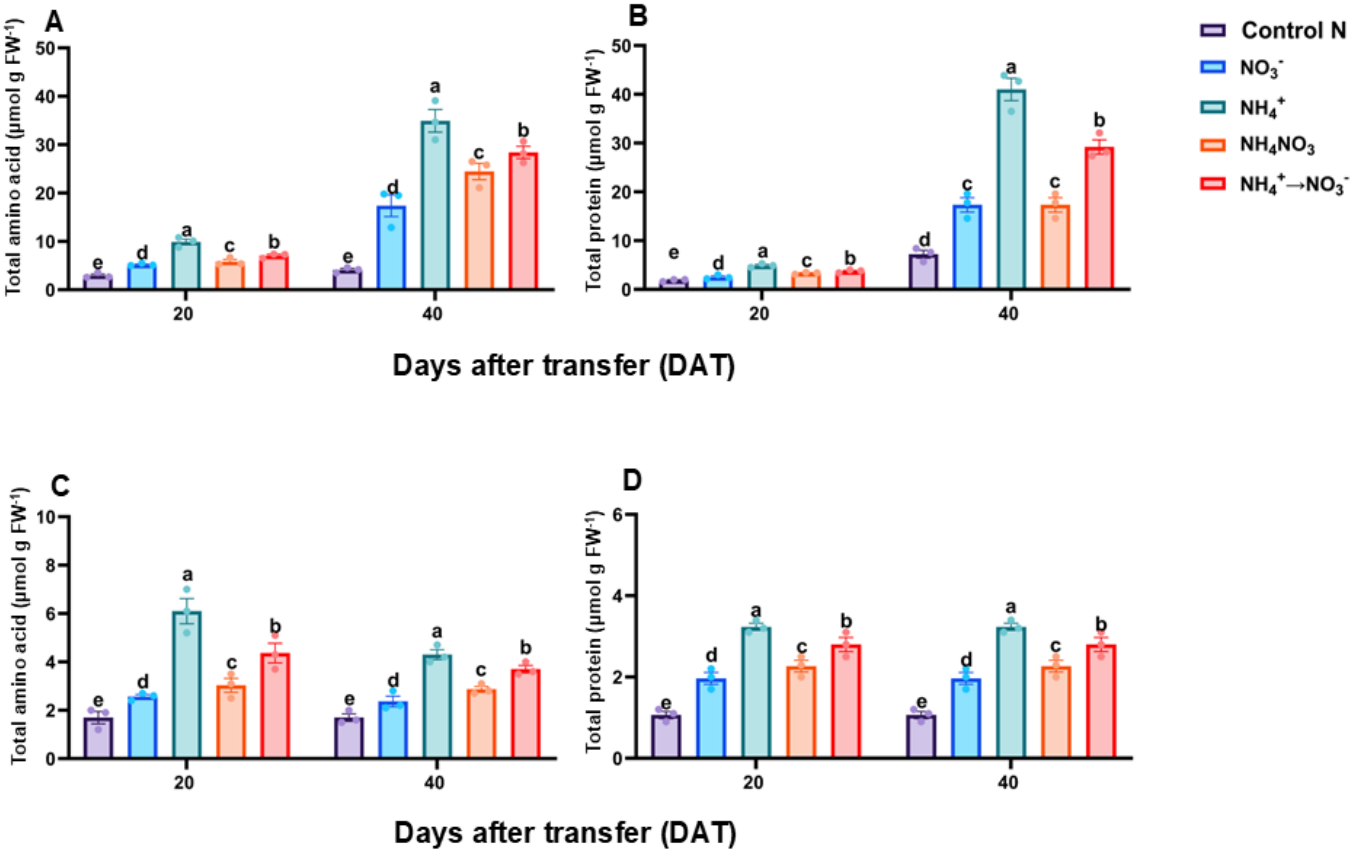

Fig. S8.7 Effect of different nitrogen forms on nitrogen containing compounds. Total amino acid (**A**) and total protein (**B**) content in the leaves and total amino acid (**C**) and total protein (**D**) content in the roots of maize seedlings. Data points represent the mean ± standard deviation (SD) of six independent biological replicates (n = 6). Different letters above the error bars indicate statistically significant differences at $P \leq 0.05$. Abbreviations: FW – fresh weight.

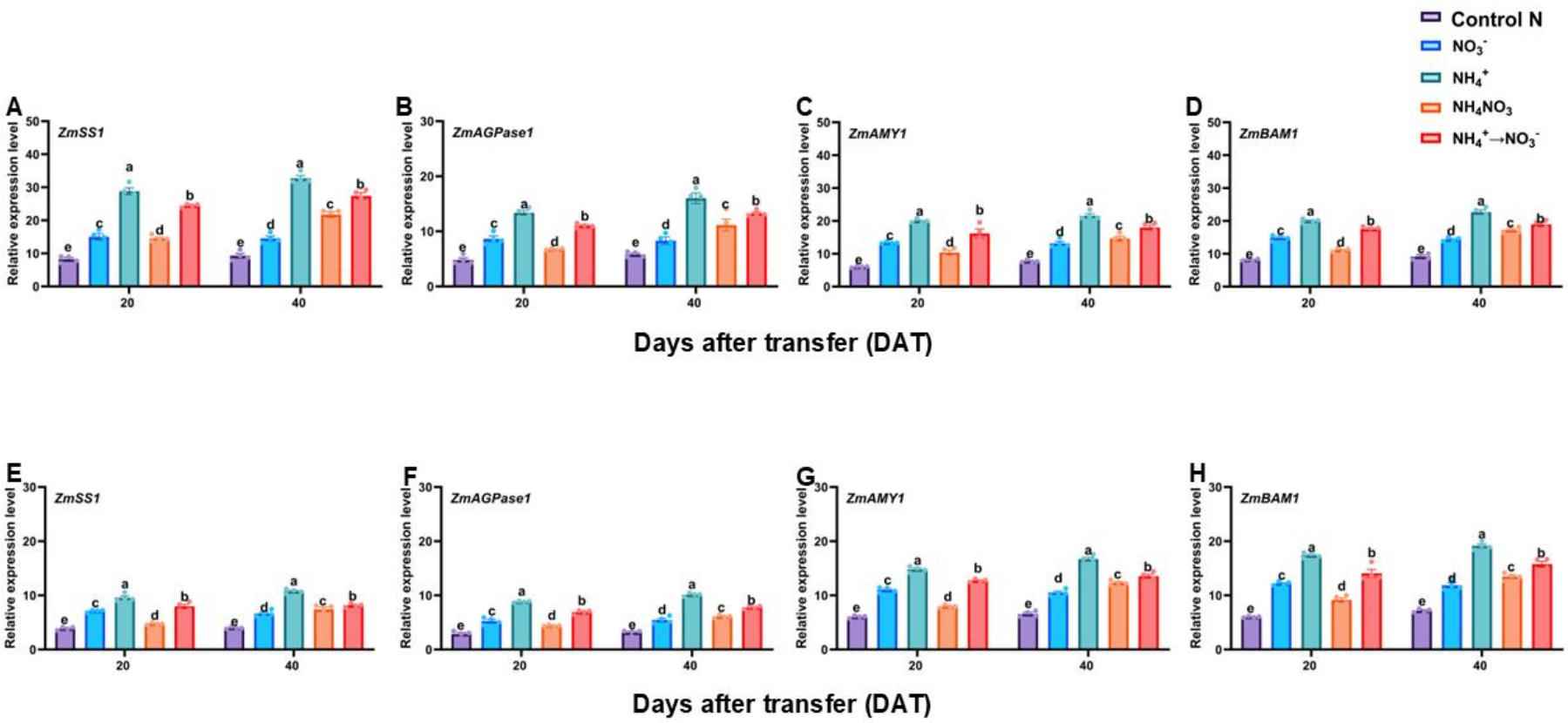

Fig. S8.8 Transcriptional regulation of sucrose metabolism and transporter genes. Expression level of *ZmSS1*, *ZmAGPase1*, *ZmAMY1* and *ZmBAM1* in the leaves (**A-D**) and roots (**E-F**) of maize seedlings subjected to different nitrogen forms. Data points represent the mean ± standard deviation (SD) of six independent biological replicates (n = 6). Different letters above the error bars indicate statistically significant differences at $P \leq 0.05$.

Table S8.1 Effect of different N form on physiological indicators in the shoot, root and leaf of maize

Trait/(plants)	Shoot/leaf				Root			
	Control N	NO_3^-	NH_4^+	NH_4NO_3	Control N	1 mM NO_3^-	NH_4^+	NH_4NO_3
Biomass	0.08 ± 0.01c	0.10 ± 0.01b	0.12 ± 0.01a	0.12 ± 0.01a	0.03 ± 0.01c	0.05 ± 0.01b	0.06 ± 0.01a	0.05 ± 0.01b
Total Biomass	0.18 ± 0.01c	0.15 ± 0.01b	0.19 ± 0.01a	0.17 ± 0.01b	N/A	N/A	N/A	N/A
Pn	17.35 ± 1.23d	22.71 ± 1.64c	27.77 ± 1.20b	31.27 ± 1.55a	N/A	N/A	N/A	N/A
Chlorophyll	21.10 ± 1.22d	29.77 ± 1.54c	39.25 ± 1.52b	34.87 ± 2.30a	N/A	N/A	N/A	N/A
Nitrogen	19.28 ± 0.46d	26.23 ± 1.36c	33.01 ± 0.82b	39.08 ± 1.20a	N/A	N/A	N/A	N/A
R ratio	0.49 ± 0.02a	0.49 ± 0.04a	0.54 ± 0.03a	0.45 ± 0.04a	0.47 ± 0.02a	0.49 ± 0.04a	0.58 ± 0.02a	0.45 ± 0.04a

Data represent the mean ± standard error (SE) of six independent plants (n = 6). Different alphabetical letters on the error bars indicate significant differences at $P \leq 0.05$. Abbreviations: N, nitrogen; R/S ratio, root-to-shoot ratio; Pn, net photosynthetic rate; NA, not applicable.

Table S8.2 Effect of different N form on root morphology at 40 days after seedling transfer (DAT)

Traits/(root)	Control N	NO_3^-	NH_4^+	NH_4NO_3	NO_3^-→NH_4^+
Number of roots	352.31 ± 62.65e	59.12 ± 35.34d	1177.55 ± 61.42a	695.70 ± 52.55c	926.05 ± 65.07b
Total root (m)	89.31 ± 11.7ce	98.16 ± 14.35d	309.42 ± 29.35a	148.07 ± 19.57c	209.30 ± 28.06b
Root volume (cm^3)	36.08 ± 3.28e	43.47 ± 5.23d	169.27 ± 14.16a	78.74 ± 14.88c	118.03 ± 11.30b
Root surface area (cm^3)	291.09 ± 32.59e	440.64 ± 66.61d	1420.44 ± 115.23a	581.79 ± 147.81c	876.25 ± 53.77b

Data represent the mean ± standard error (SE) of six independent plants (n = 6). Different alphabetical letters on the error bars indicate significant differences at $P \leq 0.05$. 'Control N' indicates treatment without nitrogen (N free).

Table S8.3 Composition of the nutrient used for the treatments

Chemical	Final solution (mM)		
	1 mM NO_3^-	**1 mM NH_4^+**	**0.5 mM NH_4NO_3**
$MgSO_4.7H_2O$	1.0000	1.0000	1.0000
KH_2PO_4	1.0000	1.0000	1.0000
		Trace elements	
H_3BO_3	0.0500	0.0500	0.0500
$MnSO_4.H_2O$	0.0050	0.0050	0.0050
$ZnSO_4.7H_2O$	0.0010	0.0010	0.0010
$CuSO_4.5H_2O$	0.0010	0.0010	0.0010
$Na_2MoO_4.2H_2O$	0.0007	0.0007	0.0007
KCl	0.0500	0.0500	0.0500
		Fe-stock	
Fe-Na-EDTA	0.1000	0.1000	0.1000
FeEDDHA	0.1000	0.1000	0.1000
		N stock	
$Ca(NO_3)_2.4H_2O$	0.2500	0.0000	0.0000
KNO_3	1.0000	0.0000	0.0000
$(NH_4)_2SO_4$	0.0000	1.0000	0.0000
NH_4NO_3	0.0000	0.0000	0.5000
		K & Ca (supplement)	
K_2SO_4	0.2500	2.8000	2.7500
$CaCl_2.2H_2O$	0.2500	0.0000	0.2500
$CaSO_4.2H_2O$	1.7500	4.0000	3.8000
KCl	0.1000	0.0000	0.1000

Table S8.4 List of genes studied

NCBI LOCs	Gene name	5' - 3' (Forward primer)	3' - 5' (Reverse primer)
LOC542247	*ZmSuSy*	ACCCATCCATTCCACCTCCG	CACCTGCACCTTCCCCCATT
LOC542711	*ZmSPS*	CCAGCGGCATGTGAATTTGA	AGCATACAATCTTGACAGTCGTA
LOC541615	*ZmSUC2*	CCTCACTACCCGCGCTCTC	TGTGATCGAAATCGAAGGGGAT
LOC542737	*ZmAGPase*	GCGCAATCGATCCATCCGTC	ACCTCCACTGCCTCTCCTCA
LOC541669	*ZmSS*	GAGGAGGCATGCCCTTGACA	CATTGAGGCCCTGTCCACCT
LOC100273083	*ZmSTP2*	CTCCTCTCGTCGTGGTTCAC	AAAAGCACAGCCTGATTCGC
LOC100273029	*ZmAMY1*	TGTACACGGGACTGCATTGAT	TATGCATGGCTCCAATTGCC
LOC542472	*ZmBAM1*	GCTGAGCTCACTGCCGGATA	CCTCAGGTGCACTTTTCGCC
LOC100282708	*ZmSWEET*	CTTGCTGCTGGTCGTGAGCATA	CCTTCATCGTTCTGGCCTCTG
LOC542324	*ZmVINV*	CACTCTGCACCGCAACAAAT	AGAGGCTACACGTCTTCCCA
LOC100382511	*ZmCINV*	GAAGCAACTGCAGAAATGGGC	AGCACTTATGCTTCACAGGGA
LOC100282267	*ZmActin*	CCGTCATAGCAACCCGCATA	GCGAGGAAAAATAGGGGAGC
LOC541665	*ZmUBQc*	CCTGCTCTCCATCTGCTCCC	ATCGCGTACTTCTGCGTCCA
LOC542314	*ZmCWINV*	TGACCGCCTGGGAGATGAAG	TCTCCTTTGGCGGCAGAGAC

CHAPTER 9. GENERAL DISCUSSION AND FUTURE DIRECTIONS

Previous studies have primarily examined the effects of different N forms, such as NO_3^-, NH_4^+, and their combination (NH_4NO_3), on plant growth. While these studies have advanced our understanding of how static N sources influence physiological responses, the impact of a dynamic shift in N forms, referred to as nitrogen form substitution (NFS), remains unexplored. This thesis addresses this gap by examining how changes in N forms, while maintaining a constant total N budget, affect vegetative and reproductive development, as well as C and N accumulation and metabolism in maize.

9.1 Knowledge contribution from this study

The impact of different N forms and levels has been well-documented across various plant species (Wang et al. 2019; Zhao et al. 2020; Wen et al. 2019; Peng et al. 2023a). However, the effects of N deficiency on plant growth remain less understood. In this study, we observed that LN treatment significantly inhibited both shoot and root growth, resulting in an increased root-to-shoot (R/S) ratio. This biomass reduction was accompanied by decreased photosynthetic activity and reductions in total N and nitrate (NO_3^-) levels. The decline in NO_3^- levels was consistent with diel and spatial NO_3^- analyses conducted on different maize tissues, such as the upper, middle, and basal leaves, leaf sheath, and roots. Although LN treatment downregulated the activity and expression of NO_3^- assimilation enzymes such as NR and NiR, it strongly induced the expression of NO_3^- transporter genes, including *ZmNPF6.2*, *ZmNRT2.1*, and *ZmNRT3.1*. Conversely, LN treatment led to increased NH_4^+ accumulation in both leaves and roots of maize seedlings. This was supported by diel and spatial NH_4^+ analyses and correlated with elevated activities of NH_4^+ assimilation enzymes, GS and GOGAT. Furthermore, LN upregulated the expression of NH_4^+ assimilation genes (*ZmGS1* and *ZmGOGAT1*) and NH_4^+ transporter-related genes (*ZmAMT1.*1 and *ZmAMT2.1)*.Similar responses have been reported in apple, where LN significantly altered leaf cell morphology, inhibited chlorophyll synthesis, reduced NO_3^- levels, and downregulated both N assimilation enzyme activities and related gene expression (Wen et al. 2019).

We further explored the impact of low nitrogen (LN) conditions on C metabolism and observed a significant accumulation of soluble sugars and starch in both the leaves and roots of maize seedlings. This increase in carbohydrate reserves mirrored the diurnal and spatial dynamics of sugar and starch distribution across different maize tissues, including upper, middle, and basal leaves. The coordinated rise in soluble sugar and starch levels suggests a compensatory mechanism to buffer the metabolic imbalance caused by nitrogen deficiency. Under LN, the activities of sucrose metabolism, sucrose SPS, SuSy, and INVs, as well as starch metabolism enzymes, SS, AGPase, AMY, and BAM, were markedly elevated. Correspondingly, the expression of their associated genes, such as *ZmSPS1*, *ZmSuSy1*, and *ZmINVs* (*ZmCINV1*, *ZmVINV1*, and *ZmCWINV1*), was significantly upregulated under LN. These

transcriptional and enzymatic changes reflect a robust metabolic shift aimed at enhancing C storage and mobilization to support essential physiological processes during N limitation. Similar responses have been documented in apple roots under LN conditions, where carbohydrate metabolism was notably altered (Zhao et al. 2020). However, our findings in maize reveal a more integrated and tissue-wide response, suggesting that maize may possess a highly dynamic and coordinated regulatory network for managing N and C metabolism under N deficiency condition. The elevated C reserves under LN not only serve as an energy buffer but may also function as signalling molecules that influence nitrogen uptake and assimilation pathways. This intricate crosstalk between C and N metabolism, as detailed in **Chapters 2** and **3**, underscores the complexity of nutrient homeostasis and highlights the adaptive strategies maize employs to sustain growth and development under suboptimal N availability.

In **Chapter 4**, we explored how different N forms, particularly LN, influence maize root development, C fixation, utilization, and distribution. Under LN, maize seedlings exhibited inhibited shoot growth but enhanced root development, leading to a higher root-to-shoot (R/S) ratio. This adaptation involved significant architectural remodelling, including increased root length, tip number, volume, and surface area. LN suppressed the growth of brace, crown, seminal, and primary roots while promoting lateral root proliferation, suggesting a strategic reallocation of resources to maximize nutrient absorption. These morphological changes were supported by coordinated biochemical and molecular shifts in C metabolism. LN roots showed consistently higher accumulation of sugars and starch, indicating increased C translocation from the shoot. Enzymes involved in sucrose (SPS, SuSy, CINV, VINV, CWINV) and starch (SS, AGPase) metabolism were highly upregulated, with corresponding increases in gene expression (*ZmSPS1*, *ZmSuSy1*, *ZmCINV1*, *ZmVINV1*, *ZmCWINV1*, *ZmSS1*, *ZmAGPase1*). This suggests that excess C accumulation under LN may result from inefficient utilization in sink tissues rather than impaired metabolic capacity. While similar responses have been observed in apple (Zhao et al. 2020), the impact of LN on C metabolism across maize root types remains underexplored. Under LN, sugars and starch preferentially accumulated in brace and primary roots, whereas under moderate nitrogen (MN), crown and lateral roots showed greater accumulation. This differential partitioning, reflected in enzyme activity and gene expression, indicates a finely tuned strategy to optimize root function. We propose a coherent model of C–N coordination in maize, where N deficiency triggers root-specific physiological and architectural adaptation, driven by targeted C allocation and tightly regulated metabolism. These insights provide a foundation for improving fertilization strategies and enhancing NUE in sustainable agriculture.

Furthermore, in **Chapter 5 and 6**, we investigated the impact of nitrogen form substitution (NFS) on maize growth and N and C metabolism, a mechanism which is unknown. Here, we observed that the dynamic replacement of NO_3^- with NH_4^+ ($NO_3^- \rightarrow NH_4^+$) enhanced NUE and promoted adaptive physio-biochemical and molecular responses in maize. Comparatively, NFS plants showed superior biomass accumulation, improved photosynthesis and optimized resource allocation than plants grown

under static N regimes. The enhanced accumulation of N metabolites, such as NO_3^-, NO_2^-, and NH_4^+ in the leaves and roots of NFS plants was accompanied by upregulation of N assimilation enzymes activities such as NR, NiR, GS and GOGAT and the expression of their related genes (*ZmNR1*, *ZmNiR1*, *ZmGOGAT1*, *ZmGS1*, *ZmAMT1.1* and *ZmAMT2.1*), demonstrated a coordinated molecular response facilitating efficient NH_4^+ assimilation and mitigating toxicity (Liu and von Wirén 2017). Furthermore, diurnal analyses revealed rhythmic patterns in N metabolite levels and enzyme activities, with NO_3^- peaking during the day and NH_4^+ accumulating at night, reflecting circadian regulation of N metabolism (Shanks et al. 2024). Spatial profiling further showed increased N levels across leaves, sheaths, roots, and developing ears, with roots acting as dynamic nitrogen sinks and leaves serving as temporary storage pools. These findings highlight the plasticity of maize N metabolism under NFS and underscore its capacity to maintain nutrient homeostasis across temporal and spatial scales, offering a biologically relevant strategy for optimizing NUE under variable N environments.

Similarly, in **Chapter 6**, NFS improved growth by improving C allocation and utilization. We observed a significantly increased sugars and starch concentrations in the leaves and roots of NFS plant compared to plants under static N condition. The enhanced sugar and starch levels correlated with the activities of sucrose metabolism enzymes, such as SuSy, CINV, VINV and CWINV. Furthermore, we observed reduction in total sucrolytic activity and hexose-to-sucrose ratio in NFS-treated plants, suggesting restrained sucrose degradation and more efficient assimilate utilization (Shen et al. 2022). The spatial distribution of starch and sucrose, with starch concentrated in leaf tips and sucrose in sheaths, supports the notion that C accumulation resulted from altered sink strength rather than impaired assimilation. Diel analyses revealed efficient remobilization of starch and sucrose overnight, indicating enhanced coordination between source and sink tissues. The reduced root-to-shoot biomass ratio under NFS reflects a balanced growth strategy, likely driven by improved nitrogen assimilation and carbon partitioning (George et al. 2016). These findings highlight NFS as a promising approach for optimizing plant performance in nitrogen-limited environments. By enhancing both source productivity and sink strength, NFS supports synchronized shoot and root development, contrasting with the imbalanced growth often observed under sole NO_3^- or NH_4^+ nutrition. These insights contribute to the development of nutrient-efficient cultivars and precision fertilization strategies for sustainable agriculture.

In Chapter **7** and **8**, we elucidate the influence of low NH_4^+ (LA) supply on growth, N and C metabolism in maize. In chapter 7, Our data showed that LA enhanced maize growth by promoting NUE via coordinated physiological and molecular responses. LA plants showed improved shoot and root biomass, enhanced photosynthetic efficiency and root morphology, supporting energy-efficient N assimilation and robust growth. The increased GS, GOGAT activity, along with upregulation of *ZmGS1* and *ZmGOGAT1*, demonstrates that LA stimulates NH_4^+ assimilation through the GS-GOGAT pathways. This was accompanied by higher protein and amino acid levels, indicating efficient N incorporation and metabolic reprograming under LA (Zhang et al. 2019b). Diel and spatial analyses

revealed sustained NH_4^+ accumulation in leaves and roots, with roots acting as dynamic N sinks and leaves serving as temporary storage pools. These patterns suggest that LA modulates circadian-regulated nitrogen processes, enhancing overnight remobilization and source-sink coordination. These findings underscore the potential of LA regimes to improve NUE and support sustainable maize production. By mimicking natural N fluctuations and minimizing energy costs, LA offers a strategic alternative to conventional NO_3^--based fertilization. These findings highlight the potential of LA regimes to improve NUE and support sustainable maize production.

In **Chapter 8**, we observed that LA plants accumulated higher sucrose and starch in both leaves and roots, which was linked to upregulation of SPS, SuSy, INVs, AGPase, SS, AMY and BAM activities, alongside increased expression levels of *ZmSPS1*, *ZmSuSy1*, *ZmAGPase1* and *ZmBAM1*. These molecular and enzymatic changes facilitated efficient assimilate unloading and redistribution, reinforcing sink strength and supporting maize growth. While similar findings have been reported in apple and maize (George et al. 2016; Zhao et al. 2020), here, the diel and spatial analyses revealed stable sucrose and starch levels across treatment time points and tissue, suggesting robust metabolic regulation under NH_4^+ nutrition. The consistent upregulation of sucrose transporters; *ZmSUT2* and *ZmSTP2*, further support the enhanced capacity for C translocation and utilization. (Ravazzolo et al. 2020). Interestingly, compared to plants grown under reverse NFS ($NH_4^+ \rightarrow NO_3^-$), LA supply yielded enhanced growth and metabolic responses, demonstrating that NH_4^+-based nutrition at lower concentration or when managed carefully to toxicity, offers a strategic benefit for improving NUE and energy conservation (Zhang et al. 2019a). Collectively, low NH_4^+ supply reshapes carbohydrate dynamics and promotes a finely tuned C-N balance in maize. These findings provide a mechanistic basis for developing nutrient-efficient genotypes and precision fertilization strategies to enhance crop resilience under variable N regimes.

9.2. Future research direction

Nitrogen forms, primarily NO_3^- and NH_4^+ had distinct and dynamic effects on growth, C and N metabolism in the maize inbred line TX-40J. As demonstrated in Chapters 2–4, LN supply significantly inhibited shoot growth, photosynthetic efficiency, and N assimilation, while enhancing root development, architectural remodelling C allocation and metabolism. These responses were accompanied by diel and spatial shifts in NO_3^- and NH_4^+ levels, suggesting circadian regulation of nutrient uptake and assimilation. In Chapters 5–6, nitrogen form substitution (NFS), involving a dynamic shift from NO_3^- to NH_4^+, activated a synergistic physio-biochemical and molecular mechanism that improved biomass accumulation, photosynthetic performance, and nutrient homeostasis more effectively than static N regimes. Enhanced source-sink coordination and rhythmic remobilization of starch and sucrose further supported balanced growth and efficient resource utilization. Chapters 7–8

revealed that low NH_4^+ supply promoted robust growth, enhanced photosynthesis, and stimulated coordinated C and N metabolism, outperforming both static NH_4^+ nutrition and reverse NFS ($NH_4^+ \rightarrow NO_3^-$). These findings underscore the plasticity of maize nutrient responses and highlight the potential of dynamic N management strategies to improve nitrogen use efficiency (NUE).

To extend these insights, future research will explore several integrated approaches. (a) Field trials across diverse soil types, environmental condition, and management systems to validate the physiological and metabolic responses observed under controlled conditions and assess the agronomic viability of NFS and LA regimes. (b) Genotypic and species-level comparisons will be conducted to evaluate the broader applicability of these findings, as the current study focused on the maize inbred line TX-40J. Screening diverse genotypes will help identify traits linked to enhanced NUE and C-N coordination. (c) Root-type specific investigations, including transcriptomic and metabolomic profiling of brace, crown, seminal, and lateral roots, will elucidate tissue-specific regulatory networks and C partitioning strategies under variable N regimes. (d) Circadian and spatial regulation of N transporters and assimilation enzymes should be explored using time-course molecular analyses to uncover temporal dynamics in nutrient uptake and metabolism. (e) Energy cost modelling of NH_4^+ versus NO_3^- assimilation will provide insights into the metabolic efficiency of different N regimes, informing low-input fertilization strategies. (f) Integration with precision agriculture, including sensor-based nutrient delivery systems, could enable real-time modulation of N forms based on plant physiological feedback, optimizing resource use and minimizing environmental impact. (g) Examine how mixing the potting medium with soil (at half the amount) shapes root microbiomes, and how these microbiomes affect maize performance. Collectively, these future directions will deepen our understanding of N form-specific regulation, enhance NUE, and support the development of resilient, nutrient-efficient maize cultivars tailored for sustainable agriculture under increasingly variable environmental conditions.

REFERENCES

Afzal S, Chaudhary N, Singh NK (2021) Role of Soluble Sugars in Metabolism and Sensing Under Abiotic Stress. In: Aftab T, Hakeem KR (eds) Plant Growth Regulators: Signalling under Stress Conditions. Springer International Publishing, Cham, pp 305-334. doi:10.1007/978-3-030-61153-8_14

Ahmad N, Jiang Z, Zhang L, Hussain I, Yang X (2023) Insights on phytohormonal crosstalk in plant response to nitrogen stress: a focus on plant root growth and development. International Journal of Molecular Sciences 24 (4):3631

Alam MS, Khanam M, Rahman MM (2023) Environment-friendly nitrogen management practices in wetland paddy cultivation. Frontiers in Sustainable Food Systems Volume 7 - 2023. doi:10.3389/fsufs.2023.1020570

Alami NE, Bourguid M, Kouighat M (2025) Advances in Nitrogen Use Efficiency of 15N-Enriched Fertilizers: A Thirty-Year Review of Research and Innovations for Sustainable Agriculture. Journal of Soil Science and Plant Nutrition:1-23

Ali A, Jabeen N, Chachar Z, Chachar S, Ahmed S, Ahmed N, Laghari AA, Sahito ZA, Farruhbek R, Yang Z (2025a) The role of biochar in enhancing soil health & interactions with rhizosphere properties and enzyme activities in organic fertilizer substitution. Frontiers in Plant Science 16:1595208

Ali A, Jabeen N, Farruhbek R, Chachar Z, Laghari AA, Chachar S, Ahmed N, Ahmed S, Yang Z (2025b) Enhancing nitrogen use efficiency in agriculture by integrating agronomic practices and genetic advances. Frontiers in Plant Science 16:1543714

Aluko OO, Kant S, Adedire OM, Li C, Yuan G, Liu H, Wang Q (2023a) Unlocking the potentials of nitrate transporters at improving plant nitrogen use efficiency. Frontiers in Plant Science 14:1074839

Aluko OO, Kant S, Adedire OM, Li C, Yuan G, Liu H, Wang Q (2023b) Unlocking the potentials of nitrate transporters at improving plant nitrogen use efficiency. Frontiers in Plant Science Volume 14 - 2023. doi:10.3389/fpls.2023.1074839

Amoah J, Ko C, Yoon J, Weon S (2019) Effect of drought acclimation on oxidative stress and transcript expression in wheat (Triticum aestivum L.). J Plant Interact 14: 492–505.

Amoah JN, Adu-Gyamfi MO (2024) Effect of drought acclimation on sugar metabolism in millet. Protoplasma. doi:10.1007/s00709-024-01976-5

Amoah JN, Adu-Gyamfi MO, Kwarteng AO (2023) Effect of drought acclimation on antioxidant system and polyphenolic content of Foxtail Millet (Setaria italica L.). Physiology and Molecular Biology of Plants 29 (10):1577-1589

Amoah JN, Adu-Gyamfi MO, Kwarteng AO (2024) Unraveling the dynamics of starch metabolism and expression profiles of starch synthesis genes in millet under drought stress. Plant Gene 38:100449. doi:https://doi.org/10.1016/j.plgene.2024.100449

Amoah JN, Kaiser BN (2025) Nitrogen Form Substitution Enhances Growth and Carbon Accumulation in Maize. Journal of Plant Growth Regulation. doi:https://doi.org/10.1007/s00344-025-11713-8

Amoah JN, Keitel C, Kaiser BN (2025a) Nitrogen deficiency identifies carbon metabolism pathways and root adaptation in maize. Physiology and Molecular Biology of Plants. doi:https://doi.org/10.1007/s12298-025-01631-0

Amoah JN, Keitel C, Kaiser BN (2025b) Nitrogen deficiency impacts growth and modulates carbon metabolism in maize. Planta 262 (4):94. doi:https://doi.org/10.1007/s00425-025-04814-x

Amoah JN, Seo YW (2021) Effect of progressive drought stress on physio-biochemical responses and gene expression patterns in wheat. 3 Biotech 11 (10):440

Andrews M, Raven J, Lea P (2013) Do plants need nitrate? The mechanisms by which nitrogen form affects plants. Annals of applied biology 163 (2):174-199

Andrews M, Raven J, Sprent J (2001) Environmental effects on dry matter partitioning between shoot and root of crop plants: relations with growth and shoot protein concentration. Annals of Applied Biology 138 (1):57-68

Andrews M, Raven JA (2022) Root or shoot nitrate assimilation in terrestrial vascular plants – does it matter? Plant and Soil 476 (1):31-62. doi:10.1007/s11104-021-05164-9

Ardichvili AN, Loeuille N, Lata J-C, Barot S (2024) Nitrification control by plants and preference for ammonium versus nitrate: positive feedbacks increase productivity but undermine resilience. The American Naturalist 203 (4):E128-E141

Artins A, Martins MC, Meyer C, Fernie AR, Caldana C (2024) Sensing and regulation of C and N metabolism–novel features and mechanisms of the TOR and SnRK1 signaling pathways. The Plant Journal 118 (5):1268-1280

Asibi AE, Chai Q, A. Coulter J (2019) Mechanisms of nitrogen use in maize. Agronomy 9 (12):775

Asim M, Ullah Z, Xu F, An L, Aluko OO, Wang Q, Liu H (2020) Nitrate signaling, functions, and regulation of root system architecture: insights from Arabidopsis thaliana. Genes 11 (6):633

Awasthi P, Laxmi A (2021) Root architectural plasticity in changing nutrient availability. Rhizobiology: Molecular Physiology of Plant Roots:25-37

Baker RF, Leach KA, Boyer NR, Swyers MJ, Benitez-Alfonso Y, Skopelitis T, Luo A, Sylvester A, Jackson D, Braun DM (2016) Sucrose transporter ZmSut1 expression and localization uncover new insights into sucrose phloem loading. Plant Physiology 172 (3):1876-1898

Baki GAE, Siefritz F, Man HM, Weiner H, Kaldenhoff R, Kaiser W (2000) Nitrate reductase in Zea mays L. under salinity. Plant, Cell & Environment 23 (5):515-521

Banik P, Zeng W, Tai H, Bizimungu B, Tanino K (2016) Effects of drought acclimation on drought stress resistance in potato (Solanum tuberosum L.) genotypes. Environmental and Experimental Botany 126:76-89

Baslam M, Mitsui T, Sueyoshi K, Ohyama T (2020) Recent advances in carbon and nitrogen metabolism in C3 plants. International Journal of Molecular Sciences 22 (1):318

Bates LS, Waldren R, Teare I (1973) Rapid determination of free proline for water-stress studies. Plant and soil 39:205-207

Batista-Silva W, Heinemann B, Rugen N, Nunes-Nesi A, Araújo WL, Braun HP, Hildebrandt TM (2019) The role of amino acid metabolism during abiotic stress release. Plant, cell & environment 42 (5):1630-1644

Begam A, Pramanick M, Dutta S, Paramanik B, Dutta G, Patra PS, Kundu A, Biswas A (2024) Inter-cropping patterns and nutrient management effects on maize growth, yield and quality. Field Crops Research 310:109363

Betti M, García-Calderón M, Pérez-Delgado CM, Credali A, Estivill G, Galván F, Vega JM, Márquez AJ (2012) Glutamine synthetase in legumes: recent advances in enzyme structure and functional genomics. International Journal of Molecular Sciences 13 (7):7994-8024

Bilska-Kos A, Mytych J, Suski S, Magoń J, Ochodzki P, Zebrowski J (2020) Sucrose phosphate synthase (SPS), sucrose synthase (SUS) and their products in the leaves of Miscanthus× giganteus and Zea mays at low temperature. Planta 252 (2):23

Bindel N, Neuhäuser B (2021) High-affinity ammonium transport by Arabidopsis thaliana AMT1; 4. Acta Physiologiae Plantarum 43 (4):69

Bloom AJ (1997) Interactions between inorganic nitrogen nutrition and root development. Zeitschrift für Pflanzenernährung und Bodenkunde 160 (2):253-259

Bloom AJ (2015a) The increasing importance of distinguishing among plant nitrogen sources. Current opinion in plant biology 25:10-16

Bloom AJ (2015b) Photorespiration and nitrate assimilation: a major intersection between plant carbon and nitrogen. Photosynthesis Research 123 (2):117-128. doi:10.1007/s11120-014-0056-y

Bloom AJ, Sukrapanna SS, Warner RL (1992) Root respiration associated with ammonium and nitrate absorption and assimilation by barley. Plant Physiology 99 (4):1294-1301

Bollmann A, Bär-Gilissen M-J, Laanbroek HJ (2002) Growth at low ammonium concentrations and starvation response as potential factors involved in niche differentiation among ammonia-oxidizing bacteria. Applied and environmental microbiology 68 (10):4751-4757

Boschiero BN, Mariano E, Azevedo RA, Ocheuze Trivelin PC (2019) Influence of nitrate - ammonium ratio on the growth, nutrition, and metabolism of sugarcane. Plant Physiology and Biochemistry 139:246-255. doi:https://doi.org/10.1016/j.plaphy.2019.03.024

Boudsocq S, Niboyet A, Lata JC, Raynaud X, Loeuille N, Mathieu J, Blouin M, Abbadie L, Barot S (2012) Plant preference for ammonium versus nitrate: a neglected determinant of ecosystem functioning? The American Naturalist 180 (1):60-69

Bradford MM (1976) A rapid and sensitive method for the quantitation of microgram quantities of protein utilizing the principle of protein-dye binding. Analytical biochemistry 72 (1-2):248-254

Braun DM (2022) Phloem Loading and Unloading of Sucrose: What a Long, Strange Trip from Source to Sink. Annual Review of Plant Biology 73 (Volume 73, 2022):553-584. doi:https://doi.org/10.1146/annurev-arplant-070721-083240

Brauner K, Birami B, Brauner HA, Heyer AG (2018) Diurnal periodicity of assimilate transport shapes resource allocation and whole-plant carbon balance. The Plant Journal 94 (5):776-789

Bremner JM, Mulvaney CS (1982) Nitrogen—Total. In: Methods of Soil Analysis. pp 595-624. doi:https://doi.org/10.2134/agronmonogr9.2.2ed.c31

Britto DT, Kronzucker HJ (2002) NH4+ toxicity in higher plants: a critical review. Journal of plant physiology 159 (6):567-584

Britto DT, Kronzucker HJ (2013) Ecological significance and complexity of N-source preference in plants. Annals of Botany 112 (6):957-963. doi:10.1093/aob/mct157

Calderon Flores P, Yoon JS, Kim DY, Seo YW (2021) Effect of chilling acclimation on germination and seedlings response to cold in different seed coat colored wheat (Triticum aestivum L.). BMC Plant Biology 21 (1):252. doi:10.1186/s12870-021-03036-z

Calleja-Cabrera J, Boter M, Oñate-Sánchez L, Pernas M (2020) Root growth adaptation to climate change in crops. Frontiers in plant science 11:544

Cánovas FM, Avila C, Cantón FR, Cañas RA, de la Torre F (2007) Ammonium assimilation and amino acid metabolism in conifers. Journal of Experimental Botany 58 (9):2307-2318. doi:10.1093/jxb/erm051

Cao H, Imparl-Radosevich J, Guan H, Keeling PL, James MG, Myers AM (1999) Identification of the Soluble Starch Synthase Activities of Maize Endosperm1. Plant Physiology 120 (1):205-216. doi:10.1104/pp.120.1.205

Cao H, Liu Z, Guo J, Jia Z, Shi Y, Kang K, Peng W, Wang Z, Chen L, Neuhaeuser B (2024) ZmNRT1. 1B (ZmNPF6. 6) determines nitrogen use efficiency via regulation of nitrate transport and signalling in maize. Plant Biotechnology Journal 22 (2):316-329

Carillo P, Mastrolonardo G, Nacca F, Fuggi A (2005) Nitrate reductase in durum wheat seedlings as affected by nitrate nutrition and salinity. Functional Plant Biology 32 (3):209-219

Cerqueira G, Santos M, Marchiori P, Silveira N, Machado E, Ribeiro R (2019) Leaf nitrogen supply improves sugarcane photosynthesis under low temperature. Photosynthetica 57 (1)

Cetner M, Kalaji H, Goltsev V, Aleksandrov V, Kowalczyk K, Borucki W, Jajoo A (2017) Effects of nitrogen-deficiency on efficiency of light-harvesting apparatus in radish. Plant Physiology and Biochemistry 119:81-92

Chalk P, Smith C (2021) On inorganic N uptake by vascular plants: can 15N tracer techniques resolve the NH4+ versus NO3−“preference” conundrum? European Journal of Soil Science 72 (4):1762-1779

Chanway C, Anand R, Yang H (2014) Nitrogen fixation outside and inside plant tissues. Advances in biology and ecology of nitrogen fixation:3-21

Chaput V, Li J, Séré D, Tillard P, Fizames C, Moyano T, Zuo K, Martin A, Gutiérrez RA, Gojon A, Lejay L (2023) Characterization of the signalling pathways involved in the repression of root nitrate uptake by nitrate in Arabidopsis thaliana. Journal of Experimental Botany 74 (14):4244-4258. doi:10.1093/jxb/erad149

Chen C, Yuan Y, Zhang C, Li H, Ma F, Li M (2017) Sucrose phloem unloading follows an apoplastic pathway with high sucrose synthase in Actinidia fruit. Plant Science 255:40-50

Chen G, Shao D, Gao X, Yuan C, Peng J, Tang F (2019) Genotypic differences in sucrose metabolism with cotton bolls in relation to lint percentage. Field Crops Research 236:33-41

Chen H, Hu W, Wang Y, Zhang P, Zhou Y, Yang L-T, Li Y, Chen L-S, Guo J (2023a) Declined photosynthetic nitrogen use efficiency under ammonium nutrition is related to photosynthetic electron transport chain disruption in citrus plants. Scientia Horticulturae 308:111594

Chen H, Jia Y, Xu H, Wang Y, Zhou Y, Huang Z, Yang L, Li Y, Chen L-S, Guo J (2020) Ammonium nutrition inhibits plant growth and nitrogen uptake in citrus seedlings. Scientia Horticulturae 272:109526

Chen J, Li J, Li W, Li P, Zhu R, Zhong Y, Zhang W, Li T (2024a) The optimal ammonium-nitrate ratio for various crops: A Meta-analysis. Field Crops Research 307:109240

Chen L-H, Xu M, Cheng Z, Yang L-T (2024b) Effects of nitrogen deficiency on the photosynthesis, chlorophyll a fluorescence, antioxidant system, and sulfur compounds in Oryza sativa. International Journal of Molecular Sciences 25 (19):10409

Chen S, Jiang C, Wang H, Bai Y, Jiang C (2023b) Trends in Research on Soil Organic Nitrogen over the Past 20 Years. Forests 14 (9):1883

Chen Wei CW, Luo JinKui LJ, Shen QiRong SQ (2005) Effect of NH4+-N/NO3--N ratios on growth and some physiological parameters of Chinese cabbage cultivars.

Chiasson DM, Loughlin PC, Mazurkiewicz D, Mohammadidehcheshmeh M, Fedorova EE, Okamoto M, McLean E, Glass ADM, Smith SE, Bisseling T, Tyerman SD, Day DA, Kaiser BN (2014) Soybean SAT1 (Symbiotic Ammonium Transporter 1) encodes a bHLH transcription factor involved in nodule growth and NH_4^+ transport. Proceedings of the National Academy of Sciences 111 (13):4814-4819. doi:10.1073/pnas.1312801111

Chiba Y, Shimizu T, Miyakawa S, Kanno Y, Koshiba T, Kamiya Y, Seo M (2015) Identification of Arabidopsis thaliana NRT1/PTR FAMILY (NPF) proteins capable of transporting plant hormones. Journal of plant research 128 (4):679-686

Clarkson D, Hopper M, Jones L (1986) The effect of root temperature on the uptake of nitrogen and the relative size of the root system in Lolium perenne. I. Solutions containing both NH+ 4 and NO3−. Plant, Cell & Environment 9 (7):535-545

Clarkson DT, Warner AJ (1979) Relationships between root temperature and the transport of ammonium and nitrate ions by Italian and perennial ryegrass (Lolium multiflorum and Lolium perenne). Plant physiology 64 (4):557-561

Coleto I, Marín-Peña AJ, Urbano-Gámez JA, González-Hernández AI, Shi W, Li G, Marino D (2023) Interaction of ammonium nutrition with essential mineral cations. Journal of Experimental Botany 74 (19):6131-6144. doi:10.1093/jxb/erad215

Cooke JE, Martin TA, Davis JM (2005) Short-term physiological and developmental responses to nitrogen availability in hybrid poplar. New Phytologist 167 (1):41-52

Corratgé-Faillie C, Lacombe B (2017) Substrate (un) specificity of Arabidopsis NRT1/PTR FAMILY (NPF) proteins. Journal of experimental botany 68 (12):3107-3113

Costa MG, Alves DMR, da Silva BC, de Lima PSR, de Mello Prado R (2024) Elucidating the underlying mechanisms of silicon to suppress the effects of nitrogen deficiency in pepper plants. Plant Physiology and Biochemistry 216:109113

Crawford NM, Glass AD (1998) Molecular and physiological aspects of nitrate uptake in plants. Trends in plant science 3 (10):389-395

Cui B, Lv W, Chen Y, Hou J, Wan H, Song J, Zhang X, Wei Z, Liu F (2025) Biomass Accumulation and CN Partitioning in Soybean Plants in Response to Drought Stress and Elevated Atmospheric CO2 Concentration. Journal of Agronomy and Crop Science 211 (3):e70067

Cui H, Luo Y, Li C, Chang Y, Jin M, Li Y, Wang Z (2023) Effects of nitrogen forms on nitrogen utilization, yield, and quality of two wheat varieties with different gluten characteristics. European Journal of Agronomy 149:126919

da Silva RC, Oliveira HC, Igamberdiev AU, Stasolla C, Gaspar M (2024) Interplay between nitric oxide and inorganic nitrogen sources in root development and abiotic stress responses. Journal of Plant Physiology:154241

de Souza Miranda R, Gomes-Filho E, Prisco JT, Alvarez-Pizarro JC (2016) Ammonium improves tolerance to salinity stress in Sorghum bicolor plants. Plant growth regulation 78:121-131

Dechorgnat J, Francis KL, Dhugga KS, Rafalski JA, Tyerman SD, Kaiser BN (2018) Root Ideotype Influences Nitrogen Transport and Assimilation in Maize. Frontiers in Plant Science 9. doi:10.3389/fpls.2018.00531

Dechorgnat J, Francis KL, Dhugga KS, Rafalski JA, Tyerman SD, Kaiser BN (2019) Tissue and nitrogen-linked expression profiles of ammonium and nitrate transporters in maize. BMC Plant Biology 19 (1):206. doi:10.1186/s12870-019-1768-0

Dechorgnat J, Nguyen CT, Armengaud P, Jossier M, Diatloff E, Filleur S, Daniel-Vedele F (2011) From the soil to the seeds: the long journey of nitrate in plants. Journal of experimental botany 62 (4):1349-1359

Deng Q-Y, Luo J-T, Zheng J-M, Tan W-F, Pu Z-J, Wang F (2023) Genome-wide systematic characterization of the NRT2 gene family and its expression profile in wheat (Triticum aestivum L.) during plant growth and in response to nitrate deficiency. BMC Plant Biology 23 (1):353. doi:10.1186/s12870-023-04333-5

Di D-W (2023) New Molecular Mechanisms of Plant Response to Ammonium Nutrition. Applied Sciences 13 (20):11570

Dong F, Hu J, Shi Y, Liu M, Zhang Q, Ruan J (2019) Effects of nitrogen supply on flavonol glycoside biosynthesis and accumulation in tea leaves (Camellia sinensis). Plant Physiology and Biochemistry 138:48-57

Dong HT, Li Y, Brown P, Akbar D, Xu C-Y (2025) Effects of Nitrogen Application on Soluble Sugar and Starch Accumulation During Sweet Potato Storage Root Formation. Horticulturae 11 (7):837

Dong L, Li Y, Li P, Liu Y, Ma F, Hao X, Guo L (2023a) Growth response of wheat and maize to different nitrogen supply forms under the enrichment of atmospheric CO2 concentrations. Agronomy 13 (2):485

Dong S, Beckles DM (2019) Dynamic changes in the starch-sugar interconversion within plant source and sink tissues promote a better abiotic stress response. Journal of plant physiology 234:80-93

Dong S, Zhou X, Qu Z, Wang X (2023b) Effects of drought stress at different stages on soluble sugar content of soybeans. Plant, Soil & Environment 69 (11)

Du Y, Zhao Q, Chen L, Yao X, Xie F (2020a) Effect of drought stress at reproductive stages on growth and nitrogen metabolism in soybean. Agronomy 10 (2):302

Du Y, Zhao Q, Chen L, Yao X, Zhang W, Zhang B, Xie F (2020b) Effect of drought stress on sugar metabolism in leaves and roots of soybean seedlings. Plant Physiology and Biochemistry 146:1-12. doi:https://doi.org/10.1016/j.plaphy.2019.11.003

Duan Y, Yang H, Wei Z, Yang H, Fan S, Wu W, Lyu L, Li W (2023a) Effects of different nitrogen forms on blackberry fruit quality. Foods 12 (12):2318

Duan Y, Yang H, Yang H, Wei Z, Che J, Wu W, Lyu L, Li W (2023b) Physiological and morphological responses of blackberry seedlings to different nitrogen forms. Plants 12 (7):1480

Duan Y, Yang H, Yang H, Wu Y, Fan S, Wu W, Lyu L, Li W (2023c) Integrative physiological, metabolomic and transcriptomic analysis reveals nitrogen preference and carbon and nitrogen metabolism in blackberry plants. Journal of Plant Physiology 280:153888

Dubey RS, Srivastava RK, Pessarakli M (2021) Physiological mechanisms of nitrogen absorption and assimilation in plants under stressful conditions. In: Handbook of plant and crop physiology. CRC Press, pp 579-616

Éva C, Oszvald M, Tamás L (2019) Current and possible approaches for improving photosynthetic efficiency. Plant Science 280:433-440

Evans JR, Clarke VC (2019) The nitrogen cost of photosynthesis. Journal of Experimental Botany 70 (1):7-15

Fan X, Lu C, Khan Z, Li Z, Duan S, Shen H, Fu Y (2025) Mixed Ammonium-Nitrate Nutrition Regulates Enzymes, Gene Expression, and Metabolic Pathways to Improve Nitrogen Uptake, Partitioning, and Utilization Efficiency in Rice. Plants 14 (4):611

Fan X, Naz M, Fan X, Xuan W, Miller AJ, Xu G (2017) Plant nitrate transporters: from gene function to application. Journal of Experimental Botany 68 (10):2463-2475. doi:10.1093/jxb/erx011

Fang G, Yang J, Sun T, Wang X, Li Y (2021) Evidence that synergism between potassium and nitrate enhances the alleviation of ammonium toxicity in rice seedling roots. Plos one 16 (9):e0248796

Fang XZ, Liu XX, Zhu YX, Ye JY, Jin CW (2020) The K+ and NO3 − Interaction Mediated by NITRATE TRANSPORTER1.1 Ensures Better Plant Growth under K+-Limiting Conditions. Plant Physiology 184 (4):1900-1916. doi:10.1104/pp.20.01229

Fang YY, Babourina O, Rengel Z, Yang XE, Pu PM (2007) Spatial distribution of ammonium and nitrate fluxes along roots of wetland plants. Plant Science 173 (2):240-246

Feng H, Fan X, Miller AJ, Xu G (2020) Plant nitrogen uptake and assimilation: regulation of cellular pH homeostasis. Journal of Experimental Botany 71 (15):4380-4392. doi:10.1093/jxb/eraa150

Feng H, Guo J, Peng C, Kneeshaw D, Roberge G, Pan C, Ma X, Zhou D, Wang W (2023a) Nitrogen addition promotes terrestrial plants to allocate more biomass to aboveground organs: A global meta-analysis. Global Change Biology 29 (14):3970-3989

Feng H, Yan M, Fan X, Li B, Shen Q, Miller AJ, Xu G (2011) Spatial expression and regulation of rice high-affinity nitrate transporters by nitrogen and carbon status. Journal of Experimental Botany 62 (7):2319-2332. doi:10.1093/jxb/erq403

Feng J, Zhu C, Cao J, Liu C, Zhang J, Cao F, Zhou X (2023b) Genome-wide identification and expression analysis of the NRT genes in Ginkgo biloba under nitrate treatment reveal the potential roles during calluses browning. BMC Genomics 24 (1):633. doi:10.1186/s12864-023-09732-4

Figueroa-Bustos V, Palta JA, Chen Y, Siddique KHM (2018) Characterization of Root and Shoot Traits in Wheat Cultivars with Putative Differences in Root System Size. Agronomy 8 (7):109

Filonchyk M, Peterson MP, Zhang L, Hurynovich V, He Y (2024) Greenhouse gases emissions and global climate change: Examining the influence of CO2, CH4, and N2O. Science of The Total Environment:173359

Finzi AC, Berthrong ST (2005) The uptake of amino acids by microbes and trees in three cold-temperate forests. Ecology 86 (12):3345-3353

Follett R, Delgado J (2002) Nitrogen fate and transport in agricultural systems. Journal of Soil and Water Conservation 57 (6):402-408

Forde BG (2002) The role of long-distance signalling in plant responses to nitrate and other nutrients. Journal of experimental botany 53 (366):39-43

Forde BG, Clarkson DT (1999) Nitrate and ammonium nutrition of plants: physiological and molecular perspectives. In: Advances in botanical research, vol 30. Elsevier, pp 1-90

Foyer CH, Ferrario-Méry S, Noctor G (2001) Interactions between carbon and nitrogen metabolism. In: Plant nitrogen. Springer, pp 237-254

Frota JNE, Tucker T (1972) Temperature influence on ammonium and nitrate absorption by lettuce. Soil Science Society of America Journal 36 (1):97-100

Fu Y, Zhong X, Lu C, Liang K, Pan J, Hu X, Hu R, Li M, Ye Q, Liu Y (2023) Growth, nutrient uptake and transcriptome profiling of rice seedlings in response to mixed provision of ammonium-and nitrate-nitrogen. Journal of Plant Physiology 284:153976

Fuertes-Mendizábal T, González-Torralba J, Arregui LM, González-Murua C, González-Moro MB, Estavillo JM (2013) Ammonium as sole N source improves grain quality in wheat. Journal of the Science of Food and Agriculture 93 (9):2162-2171

Gallais A, Coque M (2005) Genetic variation and selection for nitrogen use efficiency in maize: a synthesis.

Gansel X, Muños S, Tillard P, Gojon A (2001) Differential regulation of the NO3–and NH4+ transporter genes AtNrt2. 1 and AtAmt1. 1 in Arabidopsis: relation with long-distance and local controls by N status of the plant. The Plant Journal 26 (2):143-155

Gao K, Chen F, Yuan L, Zhang F, Mi G (2015) A comprehensive analysis of root morphological changes and nitrogen allocation in maize in response to low nitrogen stress. Plant, cell & environment 38 (4):740-750

Gao M, Armin G, Inomura K (2022) Low-Ammonium Environment Increases the Nutrient Exchange between Diatom–Diazotroph Association Cells and Facilitates Photosynthesis and N2 Fixation—a Mechanistic Modeling Analysis. Cells 11 (18):2911

Garnett T, Conn V, Plett D, Conn S, Zanghellini J, Mackenzie N, Enju A, Francis K, Holtham L, Roessner U (2013) The response of the maize nitrate transport system to nitrogen demand and supply across the lifecycle. New Phytologist 198 (1):82-94

Gazzarrini S, Lejay L, Gojon A, Ninnemann O, Frommer WB, von Wirén N (1999) Three functional transporters for constitutive, diurnally regulated, and starvation-induced uptake of ammonium into Arabidopsis roots. The Plant Cell 11 (5):937-947

Geiger DR, Servaites JC, Fuchs MA (2000) Role of starch in carbon translocation and partitioning at the plant level. Functional Plant Biology 27 (6):571-582

George J, Holtham L, Sabermanesh K, Heuer S, Tester M, Plett D, Garnett T (2016) Small amounts of ammonium (NH _4^+) can increase growth of maize (Zea mays). Journal of Plant Nutrition and Soil Science 179 (6):717-725

Ghosh A, Subba V, Roy A, Ghosh A, Kundagrami S (2014) Genetic variability and character association of grain yield components in some inbred lines of maize (Zea mays L.). Journal of Agroecology and Natural Resource Management 1 (2):34-39

Gibon Y, Bläsing OE, Palacios-Rojas N, Pankovic D, Hendriks JH, Fisahn J, Höhne M, Günther M, Stitt M (2004) Adjustment of diurnal starch turnover to short days: depletion of sugar during the night leads to a temporary inhibition of carbohydrate utilization, accumulation of sugars and post-translational activation of ADP-glucose pyrophosphorylase in the following light period. The Plant Journal 39 (6):847-862

Giehl RF, Gruber BD, von Wirén N (2014) It's time to make changes: modulation of root system architecture by nutrient signals. Journal of Experimental Botany 65 (3):769-778

Glass AD, Britto DT, Kaiser BN, Kinghorn JR, Kronzucker HJ, Kumar A, Okamoto M, Rawat S, Siddiqi M, Unkles SE (2002) The regulation of nitrate and ammonium transport systems in plants. Journal of Experimental Botany 53 (370):855-864

González-Hernández AI, Fernández-Crespo E, Scalschi L, Hajirezaei M-R, von Wirén N, García-Agustín P, Camañes G (2019) Ammonium mediated changes in carbon and nitrogen metabolisms induce resistance against Pseudomonas syringae in tomato plants. Journal of Plant Physiology 239:28-37. doi:https://doi.org/10.1016/j.jplph.2019.05.009

Govindasamy P, Muthusamy SK, Bagavathiannan M, Mowrer J, Jagannadham PTK, Maity A, Halli HM, GK S, Vadivel R, TK D (2023) Nitrogen use efficiency—a key to enhance crop productivity under a changing climate. Frontiers in Plant Science 14:1121073

Granot D, David-Schwartz R, Kelly G (2013) Hexose kinases and their role in sugar-sensing and plant development. Frontiers in Plant Science 4:44

Grubb L, Scandola S, Mehta D, Khodabocus I, Uhrig R (2025) Quantitative Proteomic Analysis of Brassica Napus Reveals Intersections Between Nutrient Deficiency Responses. Plant, Cell & Environment 48 (2):1409-1428

Gruber BD, Giehl RF, Friedel S, von Wirén N (2013) Plasticity of the Arabidopsis root system under nutrient deficiencies. Plant physiology 163 (1):161-179

Gu R, Duan F, An X, Zhang F, von Wirén N, Yuan L (2013) Characterization of AMT-mediated high-affinity ammonium uptake in roots of maize (Zea mays L.). Plant and Cell Physiology 54 (9):1515-1524

Guo S, Chen G, Zhou Y, Shen Q (2007a) Ammonium nutrition increases photosynthesis rate under water stress at early development stage of rice (Oryza sativa L.). Plant and Soil 296:115-124

Guo S, Zhou Y, Shen Q, Zhang F (2007b) Effect of ammonium and nitrate nutrition on some physiological processes in higher plants - growth, photosynthesis, photorespiration, and water relations. Plant Biol (Stuttg) 9 (1):21-29. doi:10.1055/s-2006-924541

Hachiya T, Inaba J, Wakazaki M, Sato M, Toyooka K, Miyagi A, Kawai-Yamada M, Sugiura D, Nakagawa T, Kiba T (2021) Excessive ammonium assimilation by plastidic glutamine synthetase causes ammonium toxicity in Arabidopsis thaliana. Nature Communications 12 (1):4944

Hachiya T, Sakakibara H (2017) Interactions between nitrate and ammonium in their uptake, allocation, assimilation, and signaling in plants. Journal of Experimental Botany 68 (10):2501-2512

Hasan MM, Dumbuya G, Alemayehu HA, Matsushima U, Matsunami M, Shimono H (2022) Diurnal regulation of rice N uptake ability under interrupted N supply. Functional Plant Biology 49 (3):219-230. doi:https://doi.org/10.1071/FP21195

Hawkins BJ, Robbins S (2010) pH affects ammonium, nitrate and proton fluxes in the apical region of conifer and soybean roots. Physiologia Plantarum 138 (2):238-247

Hayes KR, Beatty M, Meng X, Simmons CR, Habben JE, Danilevskaya ON (2010) Maize global transcriptomics reveals pervasive leaf diurnal rhythms but rhythms in developing ears are largely limited to the core oscillator. PloS one 5 (9):e12887

He J, Hu W, Li Y, Zhu H, Zou J, Wang Y, Meng Y, Chen B, Zhao W, Wang S, Zhou Z (2022) Prolonged drought affects the interaction of carbon and nitrogen metabolism in root and shoot of cotton. Environmental and Experimental Botany 197:104839. doi:https://doi.org/10.1016/j.envexpbot.2022.104839

Heinemann B, Hildebrandt TM (2021) The role of amino acid metabolism in signaling and metabolic adaptation to stress-induced energy deficiency in plants. Journal of Experimental Botany 72 (13):4634-4645. doi:10.1093/jxb/erab182

Heuermann D, Hahn H, Von Wirén N (2021) Seed yield and nitrogen efficiency in oilseed rape after ammonium nitrate or urea fertilization. Frontiers in Plant Science 11:608785

Hirel B, Lea PJ (2002) The biochemistry, molecular biology, and genetic manipulation of primary ammonia assimilation. In: Photosynthetic nitrogen assimilation and associated carbon and respiratory metabolism. Springer, pp 71-92

Horchani F, Hajri R, Aschi-Smiti S (2010) Effect of ammonium or nitrate nutrition on photosynthesis, growth, and nitrogen assimilation in tomato plants. Journal of Plant Nutrition and Soil Science 173 (4):610-617. doi:https://doi.org/10.1002/jpln.201000055

Hu L, Liao W, Dawuda MM, Yu J, Lv J (2017) Appropriate NH4+: NO3− ratio improves low light tolerance of mini Chinese cabbage seedlings. BMC Plant Biology 17 (1):22

Huang L, Li M, Zhou K, Sun T, Hu L, Li C, Ma F (2018) Uptake and metabolism of ammonium and nitrate in response to drought stress in Malus prunifolia. Plant Physiology and Biochemistry 127:185-193

Huang W-T, Zheng Z-C, Hua D, Chen X-F, Zhang J, Chen H-H, Ye X, Guo J-X, Yang L-T, Chen L-S (2022) Adaptive responses of carbon and nitrogen metabolisms to nitrogen-deficiency in Citrus sinensis seedlings. BMC Plant Biology 22 (1):370

Huanosto Magaña R, Adamowicz S, Pagès L (2009) Diel changes in nitrogen and carbon resource status and use for growth in young plants of tomato (Solanum lycopersicum). Annals of botany 103 (7):1025-1037

Hui D, Ray A, Kasrija L, Christian J (2024) Impacts of climate change and agricultural practices on nitrogen processes, genes, and soil nitrous oxide emissions: a quantitative review of meta-analyses. Agriculture 14 (2):240

Ishiyama K, Inoue E, Watanabe-Takahashi A, Obara M, Yamaya T, Takahashi H (2004) Kinetic Properties and Ammonium-dependent Regulation of Cytosolic Isoenzymes of Glutamine Synthetase in Arabidopsis*. Journal of Biological Chemistry 279 (16):16598-16605. doi:10.1074/jbc.M313710200

Islam MS (2022) Nitrate transport in plant through soil-root-shoot systems: a molecular view. Journal of Plant Nutrition 45 (11):1748-1763

Jakob T, Wagner H, Stehfest K, Wilhelm C (2007) A complete energy balance from photons to new biomass reveals a light-and nutrient-dependent variability in the metabolic costs of carbon assimilation. Journal of experimental botany 58 (8):2101-2112

Jeandet P, Formela-Luboińska M, Labudda M, Morkunas I (2022) The Role of Sugars in Plant Responses to Stress and Their Regulatory Function during Development. International Journal of Molecular Sciences 23 (9):5161

Jia L, Hu D, Wang J, Liang Y, Li F, Wang Y, Han Y (2023) Genome-wide identification and functional analysis of nitrate transporter genes (NPF, NRT2 and NRT3) in maize. International Journal of Molecular Sciences 24 (16):12941

Jian S, Liao Q, Song H, Liu Q, Lepo JE, Guan C, Zhang J, Ismail AM, Zhang Z (2018) NRT1. 1-related NH4+ toxicity is associated with a disturbed balance between NH4+ uptake and assimilation. Plant physiology 178 (4):1473-1488

Jing J, Rui Y, Zhang F, Rengel Z, Shen J (2010) Localized application of phosphorus and ammonium improves growth of maize seedlings by stimulating root proliferation and rhizosphere acidification. Field Crops Research 119 (2-3):355-364

Jones JB (2001) Laboratory guide for conducting soil tests and plant analysis. CRC press,

Khan T, Nadeem F, Gao Y, Yang Y, Wang X, Zeng Z, Hu Y (2019) A larger root system in oat (Avena nuda L.) is coupled with enhanced biomass accumulation and hormonal alterations under low nitrogen. Applied Ecology & Environmental Research 17 (2)

Kiba T, Feria-Bourrellier A-B, Lafouge F, Lezhneva L, Boutet-Mercey S, Orsel M, Brehaut V, Miller A, Daniel-Vedele F, Sakakibara H (2012) The Arabidopsis nitrate transporter NRT2. 4 plays a double role in roots and shoots of nitrogen-starved plants. The Plant Cell 24 (1):245-258

Kiba T, Krapp A (2016) Plant nitrogen acquisition under low availability: regulation of uptake and root architecture. Plant and Cell Physiology 57 (4):707-714

Kishorekumar R, Bulle M, Wany A, Gupta KJ (2020) An overview of important enzymes involved in nitrogen assimilation of plants. Nitrogen metabolism in plants: methods and protocols:1-13

Koch K (2004) Sucrose metabolism: regulatory mechanisms and pivotal roles in sugar sensing and plant development. Current opinion in plant biology 7 (3):235-246

Kojima S, Ishiyama K, Beier MP, Hayakawa T (2021) Ammonium assimilation and metabolism in rice. Progress in Botany Vol 82:211-231

Kong L, Zhang Y, Zhang B, Li H, Wang Z, Si J, Fan S, Feng B (2022) Does energy cost constitute the primary cause of ammonium toxicity in plants? Planta 256 (3):62

Kortstee A, Appeldoorn N, Oortwijn M, Visser R (2007) Differences in regulation of carbohydrate metabolism during early fruit development between domesticated tomato and two wild relatives. Planta 226 (4):929-939

Kovács B, Puskás-Preszner A, Huzsvai L, Lévai L, Bódi É (2015) Effect of molybdenum treatment on molybdenum concentration and nitrate reduction in maize seedlings. Plant Physiology and Biochemistry 96:38-44. doi:https://doi.org/10.1016/j.plaphy.2015.07.013

Kraiser T, Gras DE, Gutiérrez AG, González B, Gutiérrez RA (2011) A holistic view of nitrogen acquisition in plants. Journal of experimental botany 62 (4):1455-1466

Krapp A (2015) Plant nitrogen assimilation and its regulation: a complex puzzle with missing pieces. Current opinion in plant biology 25:115-122

Krapp A, David LC, Chardin C, Girin T, Marmagne A, Leprince A-S, Chaillou S, Ferrario-Méry S, Meyer C, Daniel-Vedele F (2014) Nitrate transport and signalling in Arabidopsis. Journal of Experimental Botany 65 (3):789-798. doi:10.1093/jxb/eru001

Kronzucker HJ, Siddiqi MY, Glass AD (1995a) Compartmentation and flux characteristics of nitrate in spruce. Planta 196:674-682

Kronzucker HJ, Siddiqi MY, Glass AD (1995b) Compartmentation and flux characteristics of nitrate in spruce. Planta 196 (4):674-682

Kronzucker HJ, Siddiqi MY, Glass AD (1996) Kinetics of NH4+ influx in spruce. Plant physiology 110 (3):773-779

Krouk G, Lacombe B, Bielach A, Perrine-Walker F, Malinska K, Mounier E, Hoyerova K, Tillard P, Leon S, Ljung K (2010) Nitrate-regulated auxin transport by NRT1. 1 defines a mechanism for nutrient sensing in plants. Developmental cell 18 (6):927-937

Kumar R, Brar MS, Kunduru B, Ackerman AJ, Yang Y, Luo F, Saski CA, Bridges WC, de Leon N, McMahan C, Kaeppler SM, Sekhon RS (2023) Genetic architecture of source–sink-regulated senescence in maize. Plant Physiology 193 (4):2459-2479. doi:10.1093/plphys/kiad460

Kumar V, Kim SH, Priatama RA, Jeong JH, Adnan MR, Saputra BA, Kim CM, Je BI, Park SJ, Jung KH, Kim KM, Xuan YH, Han C-d (2020) NH4+ Suppresses NO3−-Dependent Lateral Root

Growth and Alters Gene Expression and Gravity Response in OsAMT1 RNAi Mutants of Rice (Oryza sativa). Journal of Plant Biology 63 (5):391-407. doi:10.1007/s12374-020-09263-5

Ladha JK, Pathak H, Krupnik TJ, Six J, van Kessel C (2005) Efficiency of fertilizer nitrogen in cereal production: retrospects and prospects. Advances in agronomy 87:85-156

Lalonde S, Tegeder M, Throne-Holst M, Frommer W, Patrick J (2003) Phloem loading and unloading of sugars and amino acids. Plant, Cell & Environment 26 (1):37-56

Lassaletta L, Billen G, Grizzetti B, Anglade J, Garnier J (2014) 50 year trends in nitrogen use efficiency of world cropping systems: the relationship between yield and nitrogen input to cropland. Environmental Research Letters 9 (10):105011

Lawlor DW (2002) Carbon and nitrogen assimilation in relation to yield: mechanisms are the key to understanding production systems. Journal of experimental Botany 53 (370):773-787

Lea P, Azevedo RAd (2007) Nitrogen use efficiency. 2. Amino acid metabolism. Annals of Applied Biology 151 (3):269-275

Lea PJ, Azevedo RAd (2006) Nitrogen use efficiency. 1. Uptake of nitrogen from the soil. Annals of applied biology 149 (3):243-247

Lee R, Drew M (1989) Rapid, reversible inhibition of nitrate influx in barley by ammonium. Journal of Experimental Botany 40 (7):741-752

Lemaire G, van Oosterom E, Jeuffroy M-H, Gastal F, Massignam A (2008) Crop species present different qualitative types of response to N deficiency during their vegetative growth. Field Crops Research 105 (3):253-265. doi:https://doi.org/10.1016/j.fcr.2007.10.009

Lemoine R, Camera SL, Atanassova R, Dédaldéchamp F, Allario T, Pourtau N, Bonnemain J-L, Laloi M, Coutos-Thévenot P, Maurousset L (2013) Source-to-sink transport of sugar and regulation by environmental factors. Frontiers in plant science 4:272

Leng X, Wang H, Cao L, Chang R, Zhang S, Xu C, Yu J, Xu X, Qu C, Xu Z (2024) Overexpressing PagGS1; 2 maintains carbon and nitrogen balance under high-ammonium conditions and shows increased tolerance to ammonium toxicity in 84K Poplar. Journal of Experimental Botany

Léran S, Varala K, Boyer J-C, Chiurazzi M, Crawford N, Daniel-Vedele F, David L, Dickstein R, Fernandez E, Forde B (2014) A unified nomenclature of NITRATE TRANSPORTER 1/PEPTIDE TRANSPORTER family members in plants. Trends in plant science 19 (1):5-9

Li J, He B, Zhu B, Wang X, Gao J (2021a) Detailed dynamics analysis of net nitrate uptake by wheat roots after sucrose signal molecule treatment. Brazilian Journal of Botany 44 (3):611-615. doi:10.1007/s40415-021-00724-w

Li J, Yang P, Sohail H, Du H, Li J (2023) The impact of short-term nitrogen starvation and replenishment on the nitrate metabolism of hydroponically grown spinach. Scientia Horticulturae 309:111632

Li Y, Liu H, Yao X, Wang J, Feng S, Sun L, Ma S, Xu K, Chen L-Q, Sui X (2021b) Hexose transporter CsSWEET7a in cucumber mediates phloem unloading in companion cells for fruit development. Plant physiology 186 (1):640-654

Li Y, Lu W, Lyu D, Su F, Liu S, Li H, Wang X, Liu Z, Hu L (2018) Effects of different nitrogen application rates on starch accumulation, starch synthase gene expression and enzyme activity in two distinctive potato cultivars. Potato Research 61:309-326

Liang G, Hua Y, Chen H, Luo J, Xiang H, Song H, Zhang Z (2023a) Increased nitrogen use efficiency via amino acid remobilization from source to sink organs in Brassica napus. The Crop Journal 11 (1):119-131. doi:https://doi.org/10.1016/j.cj.2022.05.011

Liang X-G, Gao Z, Fu X-X, Chen X-M, Shen S, Zhou S-L (2023b) Coordination of carbon assimilation, allocation, and utilization for systemic improvement of cereal yield. Frontiers in Plant Science 14:1206829

Liang X-G, Gao Z, Fu X-X, Chen X-M, Shen S, Zhou S-L (2023c) Coordination of carbon assimilation, allocation, and utilization for systemic improvement of cereal yield. Frontiers in Plant Science Volume 14 - 2023. doi:10.3389/fpls.2023.1206829

Liao Y, He T, Wang C, Zheng C, Zhang M (2025) Dissimilatory nitrate reduction to ammonium has a competitive advantage over denitrification under nitrate-limited conditions. Reviews in Environmental Science and Bio/Technology. doi:10.1007/s11157-025-09719-5

Lin S-H, Kuo H-F, Canivenc G, Lin C-S, Lepetit M, Hsu P-K, Tillard P, Lin H-L, Wang Y-Y, Tsai C-B (2008) Mutation of the Arabidopsis NRT1. 5 nitrate transporter causes defective root-to-shoot nitrate transport. The Plant Cell 20 (9):2514-2528

Liu H, Gao X, Fan W, Fu X (2025) Optimizing carbon and nitrogen metabolism in plants: From fundamental principles to practical applications. Journal of Integrative Plant Biology

Liu J, Ma Y, Lv F, Chen J, Zhou Z, Wang Y, Abudurezike A, Oosterhuis DM (2013) Changes of sucrose metabolism in leaf subtending to cotton boll under cool temperature due to late planting. Field Crops Research 144:200-211

Liu X, Wang S, Deng X, Zhang Z, Yin L (2020) Comprehensive evaluation of physiological traits under nitrogen stress and participation of linolenic acid in nitrogen-deficiency response in wheat seedlings. BMC Plant Biology 20 (1):501. doi:10.1186/s12870-020-02717-5

Liu Y, Shen H, Dong S, Xiao J, Zhang R, Zuo H, Zhang Y, Wu M, He F, Ma C (2024) Changes in the Phylogenetic Structure of Alpine Grassland Plant Communities on the Qinghai–Tibetan Plateau with Long-Term Nitrogen Deposition. Plants 13 (19):2809

Liu Y, von Wirén N (2017) Ammonium as a signal for physiological and morphological responses in plants. Journal of Experimental Botany 68 (10):2581-2592

Liu Y, Wang S, Yang H, Chen L, Jiang Q, Ma X, Deng X, Wang H (2023) Effects of nitrogen addition on enzyme activity and metabolites related to nitrogen transformation in Suaeda salsa. Acta Physiologiae Plantarum 45 (10):116

Liu Z, Sha Y, Huang Y, Hao Z, Guo W, Ke L, Chen F, Yuan L, Mi G (2022) Efficient nitrogen allocation and reallocation into the ear in relation to the superior vascular system in low-nitrogen tolerant maize hybrid. Field Crops Research 284:108580

López-Bucio J, Cruz-Ramírez A, Herrera-Estrella L (2003) The role of nutrient availability in regulating root architecture. Current Opinion in Plant Biology 6 (3):280-287. doi:https://doi.org/10.1016/S1369-5266(03)00035-9

Lopez G, Ahmadi SH, Amelung W, Athmann M, Ewert F, Gaiser T, Gocke MI, Kautz T, Postma J, Rachmilevitch S (2023) Nutrient deficiency effects on root architecture and root-to-shoot ratio in arable crops. Frontiers in plant science 13:1067498

Loqué D, Yuan L, Kojima S, Gojon A, Wirth J, Gazzarrini S, Ishiyama K, Takahashi H, Von Wirén N (2006) Additive contribution of AMT1;1 and AMT1;3 to high-affinity ammonium uptake across the plasma membrane of nitrogen-deficient Arabidopsis roots. The Plant Journal 48 (4):522-534. doi:https://doi.org/10.1111/j.1365-313X.2006.02887.x

Lv X, Ding Y, Long M, Liang W, Gu X, Liu Y, Wen X (2021) Effect of foliar application of various nitrogen forms on starch accumulation and grain filling of wheat (Triticum aestivum L.) under drought stress. Frontiers in plant science 12:645379

M'rah Helali S, Nebli H, Kaddour R, Mahmoudi H, Lachaâl M, Ouerghi Z (2010) Influence of nitrate—Ammonium ratio on growth and nutrition of Arabidopsis thaliana. Plant and soil 336:65-74

Ma Y, Wang H, Liu J, Wang R, Che Z (2024) Effects of root trace nitrogen reduction in arid areas on sucrose–starch metabolism of flag leaves and grains and yield of drip-irrigated spring wheat. Agronomy 14 (2):312

Macduff J, Bakken A, Dhanoa M (1997) An analysis of the physiological basis of commonality between diurnal patterns of NH4+, NO3-and K+ uptake by Phleum pratense and Festuca pratensis. Journal of Experimental Botany 48 (9):1691-1701

MacNeill GJ, Mehrpouyan S, Minow MA, Patterson JA, Tetlow IJ, Emes MJ (2017) Starch as a source, starch as a sink: the bifunctional role of starch in carbon allocation. Journal of experimental botany 68 (16):4433-4453

Mahmud K, Panday D, Mergoum A, Missaoui A (2021) Nitrogen losses and potential mitigation strategies for a sustainable agroecosystem. Sustainability 13 (4):2400

Mao J, Wang J, Liao J, Xu X, Tian D, Zhang R, Peng J, Niu S (2025) Plant nitrogen uptake preference and drivers in natural ecosystems at the global scale. New Phytologist 246 (3):972-983

Marino D, Ariz I, Lasa B, Santamaría E, Fernández-Irigoyen J, González-Murua C, Aparicio Tejo PM (2016) Quantitative proteomics reveals the importance of nitrogen source to control glucosinolate metabolism in Arabidopsis thaliana and Brassica oleracea. Journal of Experimental Botany 67 (11):3313-3323

Marmagne A, Masclaux-Daubresse C, Chardon F (2022) Modulation of plant nitrogen remobilization and postflowering nitrogen uptake under environmental stresses. Journal of Plant Physiology 277:153781

Masclaux-Daubresse C, Daniel-Vedele F, Dechorgnat J, Chardon F, Gaufichon L, Suzuki A (2010) Nitrogen uptake, assimilation and remobilization in plants: challenges for sustainable and productive agriculture. Annals of botany 105 (7):1141-1157

Masclaux-Daubresse C, Reisdorf-Cren M, Orsel M (2008) Leaf nitrogen remobilisation for plant development and grain filling. Plant Biology 10:23-36

McCaw ME, Birchler JA (2017) Handling fast-flowering mini-maize. Current Protocols in Plant Biology 2 (2):124-134

McCaw ME, Lee K, Kang M, Zobrist JD, Azanu MK, Birchler JA, Wang K (2021) Development of a transformable fast-flowering mini-maize as a tool for maize gene editing. Frontiers in genome editing 2:622227

McCaw ME, Wallace JG, Albert PS, Buckler ES, Birchler JA (2016) Fast-flowering mini-maize: seed to seed in 60 days. Genetics 204 (1):35-42

Melino VJ, Tester MA, Okamoto M (2022) Strategies for engineering improved nitrogen use efficiency in crop plants via redistribution and recycling of organic nitrogen. Current Opinion in Biotechnology 73:263-269

Mengesha M (2021) Effect and roles of nitrogen supply on photosynthesis. International Journal of Photochemistry and Photobiology 5 (2):19-27

Miflin BJ, Habash DZ (2002) The role of glutamine synthetase and glutamate dehydrogenase in nitrogen assimilation and possibilities for improvement in the nitrogen utilization of crops. Journal of experimental botany 53 (370):979-987

Miller AJ, Fan X, Shen Q, Smith SJ (2008) Amino acids and nitrate as signals for the regulation of nitrogen acquisition. Journal of experimental botany 59 (1):111-119

Miller BD, Hawkins BJ (2007) Ammonium and nitrate uptake, nitrogen productivity and biomass allocation in interior spruce families with contrasting growth rates and mineral nutrient preconditioning. Tree Physiology 27 (6):901-909. doi:10.1093/treephys/27.6.901

Miranda KM, Espey MG, Wink DA (2001) A rapid, simple spectrophotometric method for simultaneous detection of nitrate and nitrite. Nitric oxide 5 (1):62-71

Moreira E, Coimbra S, Melo P (2022) Glutamine synthetase: an unlikely case of functional redundancy in Arabidopsis thaliana. Plant Biology 24 (5):713-720

Mu X, Chen Y (2021) The physiological response of photosynthesis to nitrogen deficiency. Plant Physiology and Biochemistry 158:76-82. doi:https://doi.org/10.1016/j.plaphy.2020.11.019

Mulvaney RL, Khan S, Ellsworth TR (2009) Synthetic nitrogen fertilizers deplete soil nitrogen: a global dilemma for sustainable cereal production. Journal of environmental quality 38 (6):2295-2314

Muratore C, Espen L, Prinsi B (2021) Nitrogen uptake in plants: the plasma membrane root transport systems from a physiological and proteomic perspective. Plants 10 (4):681

Nacry P, Bouguyon E, Gojon A (2013) Nitrogen acquisition by roots: physiological and developmental mechanisms ensuring plant adaptation to a fluctuating resource. Plant and Soil 370:1-29

Naeem A, Deppermann P, Mühling KH (2023) Ammonium fertilization enhances nutrient uptake, specifically manganese and zinc, and growth of maize in unlimed and limed acidic sandy soil. Nitrogen 4 (2):239-252

Navarro-Morillo I, Blasco B, Cámara-Zapata JM, Muñoz-Acero J, Simón-Grao S, Alfosea-Simón M, Plasencia F, García-Sanchez F (2024) Corn Steep Liquor application on pepper plants (Capsicum annum L.) stimulates growth under nitrogen-deficient growing conditions. Scientia Horticulturae 328:112955

Nematpour A, Eshghizadeh HR (2024) Biochemical responses of sorghum and maize to the impacts of different levels of water deficit and nitrogen supply. Cereal Research Communications 52 (2):569-579

Ning P, Peng Y, Fritschi FB (2018a) Carbohydrate dynamics in maize leaves and developing ears in response to nitrogen application. Agronomy 8 (12):302

Ning P, Yang L, Li C, Fritschi FB (2018b) Post-silking carbon partitioning under nitrogen deficiency revealed sink limitation of grain yield in maize. Journal of experimental botany 69 (7):1707-1719

Ninnemann O, Jauniaux J-C, Frommer W (1994) Identification of a high affinity NH4+ transporter from plants. The EMBO journal 13 (15):3464-3471

Noor J, Ahmad I, Ullah A, Iqbal B, Anwar S, Jalal A, Okla MK, Alaraidh IA, Abdelgawad H, Fahad S (2024) Enhancing saline stress tolerance in soybean seedlings through optimal NH4+/NO3− ratios: a coordinated regulation of ions, hormones, and antioxidant potential. BMC Plant Biology 24 (1):572. doi:10.1186/s12870-024-05294-z

Norton J, Ouyang Y (2019) Controls and adaptive management of nitrification in agricultural soils. Frontiers in microbiology 10:1931

Nunes-Nesi A, Fernie AR, Stitt M (2010) Metabolic and signaling aspects underpinning the regulation of plant carbon nitrogen interactions. Molecular plant 3 (6):973-996

Nunes Pires S, Bigolin Teixeira S, Paschoal Silva BE, Espinel Ávila G, Hernke Thiel C, Celente Martins A, Menegatti RD, da Silva Fagundes N, do Amarante L, Avila LAd (2024) Impact of elevated CO2 concentration on carbon and nitrogen metabolism of irrigated rice plants. Journal of Plant Nutrition 47 (10):1613-1629

O'Brien JA, Vega A, Bouguyon E, Krouk G, Gojon A, Coruzzi G, Gutiérrez RA (2016) Nitrate transport, sensing, and responses in plants. Molecular plant 9 (6):837-856

Omara P, Aula L, Oyebiyi F, Raun WR (2019) World cereal nitrogen use efficiency trends: review and current knowledge. Agrosystems, Geosciences & Environment 2 (1):1-8

Ostria-Gallardo E, Bascuñán-Godoy L, Fernández Del-Saz N (2024) Editorial: Nitrogen metabolism in crops and model plant species. Frontiers in Plant Science Volume 15 - 2024. doi:10.3389/fpls.2024.1502273

Ovchinnikova E, Chiasson D, Wen Z, Wu Y, Tahaei H, Smith PMC, Perrine-Walker F, Kaiser BN (2023) Arbuscular-Mycorrhizal Symbiosis in Medicago Regulated by the Transcription Factor MtbHLHm1;1 and the Ammonium Facilitator Protein MtAMF1;3. International Journal of Molecular Sciences 24 (18):14263

Owens LB, Karlen DL (2020) Groundwater: Nitrogen Fertilizer Contamination. In: Managing Water Resources and Hydrological Systems. CRC Press, pp 45-58

Parker JL, Newstead S (2014) Molecular basis of nitrate uptake by the plant nitrate transporter NRT1. 1. Nature 507 (7490):68-72

Pausch J, Holz M, Zhu B, Cheng W (2024) Rhizosphere priming promotes plant nitrogen acquisition by microbial necromass recycling. Plant, Cell & Environment 47 (6):1987-1996

Pearson CJ, Steer BT (1977) Daily changes in nitrate uptake and metabolism in Capsicum annuum. Planta 137 (2):107-112

Pélissier P-M, Motte H, Beeckman T (2021) Lateral root formation and nutrients: nitrogen in the spotlight. Plant Physiology 187 (3):1104-1116. doi:10.1093/plphys/kiab145

Peng W, Wang C-D, Wang X-L, Wu Y-H, Zhang Y, Sun Y-G, Yi S, Mi G-H (2023a) Increasing nitrogen absorption and assimilation ability under mixed NO3− and NH4+ supply is a driver to promote growth of maize seedlings. Journal of Integrative Agriculture 22 (6):1896-1908

Peng W, ZHANG Y, Yi S (2023b) Increasing nitrogen absorption and assimilation ability under mixed NO3− and NH4+ supply is a driver to promote growth of maize seedlings. Journal of Integrative Agriculture 22 (6):1896-1908

Peng Y, Li X, Li C (2012) Temporal and spatial profiling of root growth revealed novel response of maize roots under various nitrogen supplies in the field. PLoS One 7 (5):e37726

Penuelas J, Coello F, Sardans J (2023) A better use of fertilizers is needed for global food security and environmental sustainability. Agriculture & Food Security 12 (1):1-9

Plett D, Holtham L, Baumann U, Kalashyan E, Francis K, Enju A, Toubia J, Roessner U, Bacic A, Rafalski A (2016) Nitrogen assimilation system in maize is regulated by developmental and tissue-specific mechanisms. Plant molecular biology 92:293-312

Podgórska A, Burian M, Gieczewska K, Ostaszewska-Bugajska M, Zebrowski J, Solecka D, Szal B (2017) Altered cell wall plasticity can restrict plant growth under ammonium nutrition. Frontiers in plant science 8:1344

Pokhilko A, Flis A, Sulpice R, Stitt M, Ebenhöh O (2014) Adjustment of carbon fluxes to light conditions regulates the daily turnover of starch in plants: a computational model. Molecular BioSystems 10 (3):613-627

Prathap V, Tyagi A (2020) Correlation between expression and activity of ADP glucose pyrophosphorylase and starch synthase and their role in starch accumulation during grain filling under drought stress in rice. Plant Physiology and Biochemistry 157:239-243

Prescott CE (2022) Sinks for plant surplus carbon explain several ecological phenomena. Plant and Soil 476 (1):689-698

Protto V, Bauget F, Rishmawi L, Nacry P, Maurel C (2024) Primary, seminal and lateral roots of maize show type-specific growth and hydraulic responses to water deficit. Plant Physiology 194 (4):2564-2579. doi:10.1093/plphys/kiad675

Qiang L, Rong J, Wei C, Xiao-lin L, Fan-lei K, Yong-pei K, Hai-chun S, Ji-chao Y (2019) Effect of low-nitrogen stress on photosynthesis and chlorophyll fluorescence characteristics of maize cultivars with different low-nitrogen tolerances. Journal of Integrative Agriculture 18 (6):1246-1256

Qin W, Zhao X, Yang F, Chen J, Mo Q, Cui S, Chen C, He S, Li Z (2023) Impact of fertilization and grazing on soil N and enzyme activities in a karst pasture ecosystem. Geoderma 437:116578

Quesada A, Krapp A, Trueman LJ, Daniel-Vedele F, Fernández E, Forde BG, Caboche M (1997) PCR-identification of a Nicotiana plumbaginifolia cDNA homologous to the high-affinity nitrate transporters of the crnA family. Plant Molecular Biology 34 (2):265-274

Ranjan A, Sinha R, Singla-Pareek SL, Pareek A, Singh AK (2022) Shaping the root system architecture in plants for adaptation to drought stress. Physiologia plantarum 174 (2):e13651

Ravazzolo L, Trevisan S, Forestan C, Varotto S, Sut S, Dall'Acqua S, Malagoli M, Quaggiotti S (2020) Nitrate and ammonium affect the overall maize response to nitrogen availability by triggering specific and common transcriptional signatures in roots. International Journal of Molecular Sciences 21 (2):686

Rayar AJ, Van Hai T (1977) Effect of ammonium on uptake of phosphorus, potassium, calcium and magnesium by intact soybean plants. Plant and Soil 48 (1):81-87

Reay DS, Davidson EA, Smith KA, Smith P, Melillo JM, Dentener F, Crutzen PJ (2012) Global agriculture and nitrous oxide emissions. Nature climate change 2 (6):410-416

Reay DS, Nedwell DB, Priddle J, Ellis-Evans JC (1999) Temperature dependence of inorganic nitrogen uptake: reduced affinity for nitrate at suboptimal temperatures in both algae and bacteria. Applied and Environmental Microbiology 65 (6):2577-2584

Reddy MB, Sravani P, Kumar S, Rajawat MVS, Jaiswal DK, Dhar S, Azman EA, Garg K, Kumar S (2025) Nitrogen use efficiency reimagined: advancements in agronomic, ecophysiological, and molecular strategies. Journal of Plant Nutrition 48 (9):1577-1603

Rengel Z (2015) Availability of Mn, Zn and Fe in the rhizosphere. Journal of soil science and plant nutrition 15 (2):397-409

Rizvi NB, Aleem S, Khan MR, Ashraf S, Busquets R (2022) Quantitative Estimation of Protein in Sprouts of Vigna radiate (Mung Beans), Lens culinaris (Lentils), and Cicer arietinum (Chickpeas) by Kjeldahl and Lowry Methods. Molecules 27 (3):814

Rodríguez-Espinosa T, Papamichael I, Voukkali I, Gimeno AP, Candel MBA, Navarro-Pedreño J, Zorpas AA, Lucas IG (2023) Nitrogen management in farming systems under the use of agricultural wastes and circular economy. Science of The Total Environment 876:162666

Ruan J, Gerendás J, Härdter R, Sattelmacher B (2007) Effect of nitrogen form and root-zone pH on growth and nitrogen uptake of tea (Camellia sinensis) plants. Annals of botany 99 (2):301-310

Ruan Y-L (2014) Sucrose metabolism: gateway to diverse carbon use and sugar signaling. Annual review of plant biology 65 (1):33-67

Ruffel S, Gojon A, Lejay L (2014) Signal interactions in the regulation of root nitrate uptake. Journal of Experimental Botany 65 (19):5509-5517

Saddhe AA, Manuka R, Penna S (2021) Plant sugars: Homeostasis and transport under abiotic stress in plants. Physiologia plantarum 171 (4):739-755

Saiz-Fernández I, De Diego N, Brzobohatý B, Muñoz-Rueda A, Lacuesta M (2017) The imbalance between C and N metabolism during high nitrate supply inhibits photosynthesis and overall growth in maize (Zea mays L.). Plant Physiology and Biochemistry 120:213-222

Salim N, Raza A (2020) Nutrient use efficiency (NUE) for sustainable wheat production: a review. Journal of Plant Nutrition 43 (2):297-315

Santiago JP, Tegeder M (2017) Implications of nitrogen phloem loading for carbon metabolism and transport during Arabidopsis development. Journal of integrative plant biology 59 (6):409-421

Sarasketa A, González-Moro MB, González-Murua C, Marino D (2016) Nitrogen source and external medium pH interaction differentially affects root and shoot metabolism in Arabidopsis. Frontiers in plant science 7:29

Schlüter U, Mascher M, Colmsee C, Scholz U, Bräutigam A, Fahnenstich H, Sonnewald U (2012a) Maize Source Leaf Adaptation to Nitrogen Deficiency Affects Not Only Nitrogen and Carbon Metabolism But Also Control of Phosphate Homeostasis Plant Physiology 160 (3):1384-1406. doi:10.1104/pp.112.204420

Schlüter U, Mascher M, Colmsee C, Scholz U, Bräutigam A, Fahnenstich H, Sonnewald U (2012b) Maize source leaf adaptation to nitrogen deficiency affects not only nitrogen and carbon metabolism but also control of phosphate homeostasis. Plant Physiology 160 (3):1384-1406

Scholberg J, Parsons L, Wheaton T, McNeal B, Morgan K (2002) Soil temperature, nitrogen concentration, and residence time affect nitrogen uptake efficiency in citrus. Journal of Environmental Quality 31 (3):759-768

Seethepalli A, Dhakal K, Griffiths M, Guo H, Freschet GT, York LM (2021) RhizoVision Explorer: open-source software for root image analysis and measurement standardization. AoB PLANTS 13 (6). doi:10.1093/aobpla/plab056

Shah IH, Jinhui W, Li X, Hameed MK, Manzoor MA, Li P, Zhang Y, Niu Q, Chang L (2024) Exploring the role of nitrogen and potassium in photosynthesis implications for sugar: Accumulation and translocation in horticultural crops. Scientia Horticulturae 327:112832

Shanks CM, Rothkegel K, Brooks MD, Cheng C-Y, Alvarez JM, Ruffel S, Krouk G, Gutiérrez RA, Coruzzi GM (2024) Nitrogen sensing and regulatory networks: it's about time and space. The Plant Cell 36 (5):1482-1503. doi:10.1093/plcell/koae038

Shen S, Ma S, Wu L, Zhou S-L, Ruan Y-L (2023) Winners take all: competition for carbon resource determines grain fate. Trends in Plant Science 28 (8):893-901

Shen X, Yang L, Han P, Gu C, Li Y, Liao X, Qin L (2022) Metabolic Profiles Reveal Changes in the Leaves and Roots of Rapeseed (Brassica napus L.) Seedlings under Nitrogen Deficiency. International Journal of Molecular Sciences 23 (10):5784

Shilpha J, Song J, Jeong BR (2023) Ammonium phytotoxicity and tolerance: An insight into ammonium nutrition to improve crop productivity. Agronomy 13 (6):1487

Si C, Shi C, Liu H, Zhan X, Liu Y (2018) Effects of nitrogen forms on carbohydrate metabolism and storage-root formation of sweet potato. Journal of Plant Nutrition and Soil Science 181 (3):419-428

Simons M, Saha R, Amiour N, Kumar A, Guillard L, Clément G, Miquel M, Li Z, Mouille G, Lea PJ (2014) Assessing the metabolic impact of nitrogen availability using a compartmentalized maize leaf genome-scale model. Plant Physiology 166 (3):1659-1674

Sinha SK, Kumar A, Tyagi A, Venkatesh K, Paul D, Singh NK, Mandal PK (2020) Root architecture traits variation and nitrate-influx responses in diverse wheat genotypes under different external nitrogen concentrations. Plant Physiology and Biochemistry 148:246-259. doi:https://doi.org/10.1016/j.plaphy.2020.01.018

Slewinski TL, Braun DM (2010) Current perspectives on the regulation of whole-plant carbohydrate partitioning. Plant Science 178 (4):341-349

Smith AM, Zeeman SC (2020) Starch: a flexible, adaptable carbon store coupled to plant growth. Annual Review of Plant Biology 71 (1):217-245

Smith F, Walker N (1978) Entry of methylammonium and ammonium ions into Chara internodal cells. Journal of Experimental Botany 29 (1):107-120

Sohlenkamp C, Wood CC, Roeb GW, Udvardi MK (2002) Characterization of Arabidopsis AtAMT2, a high-affinity ammonium transporter of the plasma membrane. Plant physiology 130 (4):1788-1796

Stitt M, Zeeman SC (2012) Starch turnover: pathways, regulation and role in growth. Current opinion in plant biology 15 (3):282-292

Suenaga A, Moriya K, Sonoda Y, Ikeda A, Von Wirén N, Hayakawa T, Yamaguchi J, Yamaya T (2003) Constitutive expression of a novel-type ammonium transporter OsAMT2 in rice plants. Plant and Cell Physiology 44 (2):206-211

Sun B, Gao Y, Wu X, Ma H, Zheng C, Wang X, Zhang H, Li Z, Yang H (2020a) The relative contributions of pH, organic anions, and phosphatase to rhizosphere soil phosphorus

mobilization and crop phosphorus uptake in maize/alfalfa polyculture. Plant and Soil 447 (1):117-133

Sun C-H, Yu J-Q, Hu D-G (2017) Nitrate: a crucial signal during lateral roots development. Frontiers in plant science 8:485

Sun H, Zhang Y-Q, Zhang S-B, Huang W (2022) Photosynthetic induction under fluctuating light is affected by leaf nitrogen content in tomato. Frontiers in Plant Science 13:835571

Sun J, Jin L, Li R, Meng X, Jin N, Wang S, Xu Z, Liu Z, Lyu J, Yu J (2023) Effects of Different Forms and Proportions of Nitrogen on the Growth, Photosynthetic Characteristics, and Carbon and Nitrogen Metabolism in Tomato. Plants 12 (24):4175

Sun X, Chen F, Yuan L, Mi G (2020b) The physiological mechanism underlying root elongation in response to nitrogen deficiency in crop plants. Planta 251 (4):84. doi:10.1007/s00425-020-03376-4

Sun X, Ren W, Wang P, Chen F, Yuan L, Pan Q, Mi G (2021) Evaluation of maize root growth and genome-wide association studies of root traits in response to low nitrogen supply at seedling emergence. The Crop Journal 9 (4):794-804

Șuteu D, Băcilă I, Haș V, Haș I, Miclăuș M (2014) Correction: Romanian Maize (Zea mays) inbred lines as a Source of genetic diversity in SE Europe, and Their Potential in Future Breeding efforts. Plos one 9 (1)

Tabuchi M, Abiko T, Yamaya T (2007) Assimilation of ammonium ions and reutilization of nitrogen in rice (Oryza sativa L.). Journal of experimental botany 58 (9):2319-2327

Tang Y, Gao F, Yu Q, Guo S, Li F (2015) The uptake kinetics of NH4+ and NO3− by lettuce seedlings under hypobaric and hypoxic conditions. Scientia Horticulturae 197:236-243

Tegeder M, Masclaux-Daubresse C (2018) Source and sink mechanisms of nitrogen transport and use. New phytologist 217 (1):35-53

Terashima I, Evans JR (1988) Effects of light and nitrogen nutrition on the organization of the photosynthetic apparatus in spinach. Plant and Cell Physiology 29 (1):143-155

The SV, Snyder R, Tegeder M (2021) Targeting nitrogen metabolism and transport processes to improve plant nitrogen use efficiency. Frontiers in Plant Science 11:628366

Tian G, Ren W, Xu J, Liu X, Liang J, Mi G, Gong X, Chen F (2024) Microbiology Combined with the Root Metabolome Reveals the Responses of Root Microorganisms to Maize Cultivars under Different Forms of Nitrogen Supply. Agronomy 14 (8):1828

Tobin AK, Yamaya T (2001) Cellular compartmentation of ammonium assimilation in rice and barley. Journal of Experimental Botany 52 (356):591-604. doi:10.1093/jexbot/52.356.591

Tucker DE, Allen DJ, Ort DR (2004) Control of nitrate reductase by circadian and diurnal rhythms in tomato. Planta 219 (2):277-285. doi:10.1007/s00425-004-1213-x

Tunlid A, Floudas D, Op De Beeck M, Wang T, Persson P (2022) Decomposition of soil organic matter by ectomycorrhizal fungi: mechanisms and consequences for organic nitrogen uptake and soil carbon stabilization. Frontiers in Forests and Global Change 5:934409

Tylova-Munzarova E, Lorenzen B, Brix H, Votrubova O (2005) The effects of NH4+ and NO3− on growth, resource allocation and nitrogen uptake kinetics of Phragmites australis and Glyceria maxima. Aquatic Botany 81 (4):326-342

Ullrich WR, Larsson M, Larsson CM, Lesch S, Novacky A (1984) Ammonium uptake in Lemna gibba G 1, related membrane potential changes, and inhibition of anion uptake. Physiologia plantarum 61 (3):369-376

V P, Ali K, Singh A, Vishwakarma C, Krishnan V, Chinnusamy V, Tyagi A (2019) Starch accumulation in rice grains subjected to drought during grain filling stage. Plant Physiology and Biochemistry 142:440-451. doi:https://doi.org/10.1016/j.plaphy.2019.07.027

Vaast P, Zasoski RJ, Bledsoe CS (1998) Effects of solution pH, temperature, nitrate/ammonium ratios, and inhibitors on ammonium and nitrate uptake by Arabica coffee in short-term solution culture. Journal of Plant Nutrition 21 (7):1551-1564

Van den Ende W (2014) Sugars take a central position in plant growth, development and, stress responses. A focus on apical dominance. Frontiers in Plant Science Volume 5 - 2014. doi:10.3389/fpls.2014.00313

Vessey JK, Henry LT, Chaillou S, Raper Jr CD (1990) Root-zone acidity affects relative uptake of nitrate and ammonium from mixed nitrogen sources. Journal of Plant Nutrition 13 (1):95-116

Viancelli A, Michelon W (2024) Climate change and nitrogen dynamics: Challenges and strategies for a sustainable future. Nitrogen 5 (3):688-701

Vidal EA, Alvarez JM, Araus V, Riveras E, Brooks MD, Krouk G, Ruffel S, Lejay L, Crawford NM, Coruzzi GM (2020) Nitrate in 2020: thirty years from transport to signaling networks. The Plant Cell 32 (7):2094-2119

Vidal EA, Moyano TC, Canales J, Gutiérrez RA (2014) Nitrogen control of developmental phase transitions in Arabidopsis thaliana. Journal of experimental botany 65 (19):5611-5618

von Wirén N, Gazzarrini S, Gojon A, Frommer WB (2000) The molecular physiology of ammonium uptake and retrieval. Current opinion in plant biology 3 (3):254-261

Von Wittgenstein NJ, Le CH, Hawkins BJ, Ehlting J (2014) Evolutionary classification of ammonium, nitrate, and peptide transporters in land plants. BMC evolutionary biology 14 (1):11

Walch-Liu P, Filleur S, Gan Y, Forde BG (2005) Signaling mechanisms integrating root and shoot responses to changes in the nitrogen supply. Photosynthesis research 83:239-250

Wang C, Tillberg JE (1996) Effects of nitrogen deficiency on accumulation of fructan and fructan metabolizing enzyme activities in sink and source leaves of barley (Hordeum vulgare). Physiologia Plantarum 97 (2):339-345

Wang C, Wu G, Wang H, Wang J, Yuan M, Guo X, Liu C, Xing S, Sun Y, Talpur MMA (2024a) Optimizing Tomato Cultivation: Impact of Ammonium–Nitrate Ratios on Growth, Nutrient Uptake, and Fertilizer Utilization. Sustainability 16 (13):5373

Wang F, Wang Q, Yu Q, Ye J, Gao J, Liu H, Yong JW, Yu Y, Liu X, Kong H (2022a) Is the NH4+-induced growth inhibition caused by the NH4+ form of the nitrogen source or by soil acidification? Frontiers in plant science 13:968707

Wang H, Han C, Wang J-G, Chu X, Shi W, Yao L, Chen J, Hao W, Deng Z, Fan M (2022b) Regulatory functions of cellular energy sensor SnRK1 for nitrate signalling through NLP7 repression. Nature Plants 8 (9):1094-1107

Wang L, Ruan Y-L (2015) Shoot–root carbon allocation, sugar signalling and their coupling with nitrogen uptake and assimilation. Functional Plant Biology 43 (2):105-113

Wang P, Wang Z, Pan Q, Sun X, Chen H, Chen F, Yuan L, Mi G (2019) Increased biomass accumulation in maize grown in mixed nitrogen supply is mediated by auxin synthesis. Journal of Experimental Botany 70 (6):1859-1873. doi:10.1093/jxb/erz047

Wang P, Xu D, Lakshmanan P, Deng Y, Zhu Q, Zhang F (2024b) Mitigation strategies for soil acidification based on optimal nitrogen management. Frontiers of Agricultural Science and Engineering 11 (2):229-242

Wang P, Yang L, Sun X, Shi W, Dong R, Wu Y, Mi G (2024c) Lateral root elongation in maize is related to auxin synthesis and transportation mediated by N metabolism under a mixed NO3− and NH4+ supply. Journal of Integrative Agriculture 23 (3):1048-1060

Wang Q, Wang M, Xia AA, Wang JY, Wang Z, Xu T, Jia DT, Lu M, Tan WM, Luo JH (2025a) Natural variation in ZmNRT2. 5 modulates husk leaf width and promotes seed protein content in maize. Plant Biotechnology Journal 23 (4):1039-1052

Wang Q, Zhao Y, Luo W, Li R, He Q, Fang X, Michele RD, Ast C, von Wirén N, Lin J (2013) Single-particle analysis reveals shutoff control of the Arabidopsis ammonium transporter AMT1; 3 by clustering and internalization. Proceedings of the National Academy of Sciences 110 (32):13204-13209

Wang R, Xing X, Crawford N (2007) Nitrite acts as a transcriptome signal at micromolar concentrations in Arabidopsis roots. Plant Physiology 145 (4):1735-1745

Wang S, Zhu Y, Jiang H, Cao W (2006) Positional differences in nitrogen and sugar concentrations of upper leaves relate to plant N status in rice under different N rates. Field Crops Research 96 (2-3):224-234

Wang W, Hu B, Yuan D, Liu Y, Che R, Hu Y, Ou S, Liu Y, Zhang Z, Wang H, Li H, Jiang Z, Zhang Z, Gao X, Qiu Y, Meng X, Liu Y, Bai Y, Liang Y, Wang Y, Zhang L, Li L, Sodmergen, Jing H, Li J, Chu C (2018a) Expression of the Nitrate Transporter Gene OsNRT1.1A/OsNPF6.3 Confers High Yield and Early Maturation in Rice. The Plant Cell 30 (3):638-651. doi:10.1105/tpc.17.00809

Wang Y, Tong L, Liu H, Li B, Zhang R (2025b) Integrated metabolome and transcriptome analysis of maize roots response to different degrees of drought stress. BMC Plant Biology 25 (1):505. doi:10.1186/s12870-025-06505-x

Wang Y, Wang D, Tao Z, Yang Y, Gao Z, Zhao G, Chang X (2021a) Impacts of Nitrogen Deficiency on Wheat (Triticum aestivum L.) Grain During the Medium Filling Stage: Transcriptomic and Metabolomic Comparisons. Frontiers in Plant Science Volume 12 - 2021. doi:10.3389/fpls.2021.674433

Wang Y, Wang Y-M, Lu Y-T, Qiu Q-L, Fan D-M, Wang X-C, Zheng X-Q (2021b) Influence of different nitrogen sources on carbon and nitrogen metabolism and gene expression in tea plants (Camellia sinensis L.). Plant Physiology and Biochemistry 167:561-566

Wang Z, Zhang L, Sun C, Gu R, Mi G, Yuan L (2018b) Phylogenetic, expression and functional characterizations of the maize NLP transcription factor family reveal a role in nitrate assimilation and signaling. Physiologia Plantarum 163 (3):269-281

Wany A, Pathak PK, Gupta KJ (2020) Methods for measuring nitrate reductase, nitrite levels, and nitric oxide from plant tissues. Nitrogen Metabolism in Plants: Methods and Protocols:15-26

Wei C, Jiang J, Liu C, Fang X, Zhou T, Xue Z, Wang W, Zhang W, Zhang H, Liu L, Wang Z, Gu J, Yang J (2023) Effects of Source Strength and Sink Size on Starch Metabolism, Starch Properties and Grain Quality of Rice (Oryza sativa L.). Agronomy 13 (5):1288

Wei J, Chai Q, Yin W, Fan H, Guo Y, Hu F, Fan Z, Wang Q (2024) Grain yield and N uptake of maize in response to increased plant density under reduced water and nitrogen supply conditions. Journal of Integrative Agriculture 23 (1):122-140

Wen B, Li C, Fu X, Li D, Li L, Chen X, Wu H, Cui X, Zhang X, Shen H, Zhang W, Xiao W, Gao D (2019) Effects of nitrate deficiency on nitrate assimilation and chlorophyll synthesis of detached apple leaves. Plant Physiology and Biochemistry 142:363-371. doi:https://doi.org/10.1016/j.plaphy.2019.07.007

Whetton RL, Harty MA, Holden NM (2022) Communicating nitrogen loss mechanisms for improving nitrogen use efficiency management, focused on global wheat. Nitrogen 3 (2):213-246

Whiteside MD, Digman MA, Gratton E, Treseder KK (2012) Organic nitrogen uptake by arbuscular mycorrhizal fungi in a boreal forest. Soil Biology and Biochemistry 55:7-13

Wu Q, Xu J, Zhao Y, Wang Y, Zhou L, Ning L, Shabala S, Zhao H (2024a) Transcription factor ZmEREB97 regulates nitrate uptake in maize (Zea mays) roots. Plant Physiology 196 (1):535-550. doi:10.1093/plphys/kiae277

Wu X, Mubeen S, Luo D, Cao S, Wang C, Yue J, Wu Q, Zhang H, Nie J, Chen C, Wang M, Li R, Chen P (2024b) Function characterization of a soybean sucrose transporter GmSUT4.2 involved in plant growth, development, and crop yield. Plant Growth Regulation 102 (3):529-543. doi:10.1007/s10725-023-01078-x

Xiao Z-D, Chen Z-Y, Lin Y-H, Liang X-G, Wang X, Huang S-B, Munz S, Graeff-Hönninger S, Shen S, Zhou S-L (2024) Phosphorus deficiency promotes root: shoot ratio and carbon accumulation via modulating sucrose utilization in maize. Journal of Plant Physiology 303:154349

Xie L-B, Sun L-N, Zhang Z-W, Chen Y-E, Yuan M, Yuan S (2025) Phenotype Assessment and Putative Mechanisms of Ammonium Toxicity to Plants. International Journal of Molecular Sciences 26 (6):2606

Xu D, Zhu Q, Ros GH, Xu M, Wen S, Zhang F, de Vries W (2023a) Model-based optimal management strategies to mitigate soil acidification and minimize nutrient losses for croplands. Field Crops Research 292:108827

Xu N, Cheng L, Kong Y, Chen G, Zhao L, Liu F (2024a) Functional analyses of the NRT2 family of nitrate transporters in Arabidopsis. Frontiers in Plant Science Volume 15 - 2024. doi:10.3389/fpls.2024.1351998

Xu W, Cui K, Xu A, Nie L, Huang J, Peng S (2015) Drought stress condition increases root to shoot ratio via alteration of carbohydrate partitioning and enzymatic activity in rice seedlings. Acta physiologiae plantarum 37:1-11

Xu Y, Xu R, Li S, Ran S, Wang J, Zhou Y, Gao H, Zhong F (2024b) The mechanism of melatonin promotion on cucumber seedling growth at different nitrogen levels. Plant Physiology and Biochemistry 206:108263

Xu Y, Zhang K, Li S, Zhou Y, Ran S, Xu R, Lin Y, Shen L, Huang W, Zhong F (2023b) Carbon and nitrogen metabolism in tomato (Solanum lycopersicum L.) leaves response to nitrogen treatment. Plant Growth Regulation 100 (3):747-756

Xue Y, Yan W, Gao Y, Zhang H, Jiang L, Qian X, Cui Z, Zhang C, Liu S, Wang H (2021) Interaction effects of nitrogen rates and forms combined with and without zinc supply on plant growth and nutrient uptake in maize seedlings. Frontiers in Plant Science 12:722752

Yamaya T, Oaks A (2004) Metabolic regulation of ammonium uptake and assimilation. In: Nitrogen acquisition and assimilation in higher plants. Springer, pp 35-63

Yan Y, Zhang Z, Sun H, Liu X, Xie J, Qiu Y, Chai T, Chu C, Hu B (2023) Nitrate confers rice adaptation to high ammonium by suppressing its uptake but promoting its assimilation. Molecular Plant 16 (12):1871-1874. doi:10.1016/j.molp.2023.11.008

Yang W, Dong X, Yuan Z, Zhang Y, Li X, Wang Y (2023) Genome-wide identification and expression analysis of the ammonium transporter family genes in soybean. International Journal of Molecular Sciences 24 (4):3991

Yang Z, Yan H, Liu H, Yang L, Mi G, Wang P (2025) Enhancing Crop Nitrogen Efficiency: The Role of Mixed Nitrate and Ammonium Supply in Plant Growth and Development. Biology 14 (5):546

Ye JY, Tian WH, Jin CW (2022) Nitrogen in plants: From nutrition to the modulation of abiotic stress adaptation. Stress Biology 2 (1):4

Yin H, Li B, Wang X, Xi Z (2020) Effect of ammonium and nitrate supplies on nitrogen and sucrose metabolism of cabernet sauvignon (Vitis vinifera cv.). Journal of the Science of Food and Agriculture 100 (14):5239-5250

Yoneyama T, Suzuki A (2019) Exploration of nitrate-to-glutamate assimilation in non-photosynthetic roots of higher plants by studies of 15N-tracing, enzymes involved, reductant supply, and nitrate signaling: a review and synthesis. Plant Physiology and Biochemistry 136:245-254

Yu P, Baldauf JA, Lithio A, Marcon C, Nettleton D, Li C, Hochholdinger F (2016) Root type-specific reprogramming of maize pericycle transcriptomes by local high nitrate results in disparate lateral root branching patterns. Plant Physiology 170 (3):1783-1798

Yuan L, Loqué D, Kojima S, Rauch S, Ishiyama K, Inoue E, Takahashi H, von Wirén N (2007) The organization of high-affinity ammonium uptake in Arabidopsis roots depends on the spatial arrangement and biochemical properties of AMT1-type transporters. The Plant Cell 19 (8):2636-2652

Zadoks JC, Chang TT, Konzak CF (1974) A decimal code for the growth stages of cereals. Weed research 14 (6):415-421

Zayed O, Hewedy OA, Abdelmoteleb A, Ali M, Youssef MS, Roumia AF, Seymour D, Yuan Z-C (2023) Nitrogen Journey in Plants: From Uptake to Metabolism, Stress Response, and Microbe Interaction. Biomolecules 13 (10):1443

Zhang H-Q, Shen R-F, Zhao X-Q (2022) Nitrogen Source Preference in Maize at Seedling Stage Is Mainly Dependent on Growth Medium pH. Agronomy 12 (9):2149

Zhang H, Huang J, Li Y, Zhao J, Mai W, Khan L, Zhang M, Wang W, Zeng C, Chen X (2025) Beyond nitrate transport: AtNRT2.4 responds to local and systemic nitrogen signaling in Arabidopsis. BMC Plant Biology 25 (1):655. doi:10.1186/s12870-025-06695-4

Zhang HQ, Zhao XQ, Chen YL, Zhang LY, Shen RF (2019a) Case of a stronger capability of maize seedlings to use ammonium being responsible for the higher 15N recovery efficiency of ammonium compared with nitrate. Plant and Soil 440 (1):293-309. doi:10.1007/s11104-019-04087-w

Zhang J, Lv J, Dawuda MM, Xie J, Yu J, Li J, Zhang X, Tang C, Wang C, Gan Y (2019b) Appropriate ammonium-nitrate ratio improves nutrient accumulation and fruit quality in pepper (Capsicum annuum L.). Agronomy 9 (11):683

Zhang K, Wu Y, Hang H (2019c) Differential contributions of NO3−/NH4+ to nitrogen use in response to a variable inorganic nitrogen supply in plantlets of two Brassicaceae species in vitro. Plant Methods 15 (1):86. doi:10.1186/s13007-019-0473-1

Zhang L, Sun S, Liang Y, Li B, Ma S, Wang Z, Ma B, Li M (2021) Nitrogen levels regulate sugar metabolism and transport in the shoot tips of crabapple plants. Frontiers in plant science 12:626149

Zhang Z, Tariq A, Zeng F, Graciano C, Zhang B (2020) Nitrogen application mitigates drought-induced metabolic changes in Alhagi sparsifolia seedlings by regulating nutrient and biomass allocation patterns. Plant Physiology and Biochemistry 155:828-841

Zhang Z, Wu Z (2023) CO2 enhances low-nitrogen adaption by promoting amino acid metabolism in Brassica napus. Plant Physiology and Biochemistry 201:107864. doi:https://doi.org/10.1016/j.plaphy.2023.107864

Zhao B, Jia X, Yu N, Murray JD, Yi K, Wang E (2024) Microbe-dependent and independent nitrogen and phosphate acquisition and regulation in plants. New Phytologist 242 (4):1507-1522. doi:https://doi.org/10.1111/nph.19263

Zhao H, Sun S, Zhang L, Yang J, Wang Z, Ma F, Li M (2020) Carbohydrate metabolism and transport in apple roots under nitrogen deficiency. Plant Physiology and Biochemistry 155:455-463

Zhao XQ, Shen RF (2018) Aluminum–nitrogen interactions in the soil–plant system. Frontiers in plant science 9:807

Zhao Y, Liu Z, Duan F, An X, Liu X, Hao D, Gu R, Wang Z, Chen F, Yuan L (2018) Overexpression of the maize ZmAMT1; 1a gene enhances root ammonium uptake efficiency under low ammonium nutrition. Plant Biotechnology Reports 12 (1):47-56

Zheng X, Liu Q, Ji X, Cao M, Zhang Y, Jiang J (2021) How do natural soil NH4+, NO3− and N2O interact in response to nitrogen input in different climatic zones? A global meta-analysis. European Journal of Soil Science 72 (5):2231-2245

Zhou H, Liu Y, Mu B, Wang F, Feng N, Zheng D (2023) Nitrogen limitation affects carbon and nitrogen metabolism in mung bean (Vigna radiata L.). Journal of Plant Physiology 290:154105

Zhou R, Sicher R, Quebedeaux B (2001) Diurnal changes in carbohydrate metabolism in mature apple leaves. Functional Plant Biology 28 (11):1143-1150

Zhu Q, Liu X, Hao T, Zeng M, Shen J, Zhang F, De Vries W (2018) Modeling soil acidification in typical Chinese cropping systems. Science of the Total environment 613:1339-1348

Zhu X, Zhang X, Cao Y, Xin R, Ma Y, Wang L, Xu L, Wang Y, Liu R, Liu L (2022) Genome-Wide identification of sucrose transporter genes and functional analysis of RsSUC1b in Radish (Raphanus sativus L.). Horticulturae 8 (11):1058

Zhu Y, Qi B, Hao Y, Liu H, Sun G, Chen R, Song S (2021) Appropriate NH4+/NO3–ratio triggers plant growth and nutrient uptake of flowering Chinese cabbage by optimizing the pH value of nutrient solution. Frontiers in Plant Science 12:656144

Zoghbi-Rodríguez NM, Gamboa-Tuz SD, Pereira-Santana A, Rodríguez-Zapata LC, Sánchez-Teyer LF, Echevarría-Machado I (2021) Phylogenomic and Microsynteny Analysis Provides Evidence of Genome Arrangements of High-Affinity Nitrate Transporter Gene Families of Plants. International Journal of Molecular Sciences 22 (23):13036

Zsoldos F, Vashegyi Á, Pécsváradi A, Haunold E, Herger P (1999) Nitrate and nitrite transport into cereals affected by low pH and different temperatures. Cereal Research Communications 27 (4):403-409